Dissertation zur Erlangung des Doktorgrades
der Fakultät für Chemie und Pharmazie
der Ludwig-Maximilians-Universität München

Preparation and Analytical Investigation of Amiton and Amiton-like Compounds Closely Related to the Chemical Weapons Convention

"Relevance of Organo(thio)phosphates in the Hazard Defense Sector"

von

Marc André Althoff

aus

Engelskirchen, Deutschland

2018

Erklärung

Diese Dissertation wurde im Sinne von § 7 der Promotionsordnung vom 28. November 2011 von Herrn Prof. Dr. K. L. Karaghiosoff betreut.

Eidesstattliche Versicherung

Diese Dissertation wurde eigenständig und ohne unerlaubte Hilfe erarbeitet.

München, 20.07.2018

.....

Marc André Althoff

Dissertation eingereicht am: 18.05.2018

1. Gutachter: Herr Prof. Dr. K. L. Karaghiosoff

2. Gutachter: Herr Prof. Dr. T. M. Klapötke

Mündliche Prüfung am: 18.07.2018

Die vorliegende Arbeit wurde von Dezember 2013 bis Februar 2017 an der Bundeswehr Dienststelle „Schule ABC-Abwehr und Gesetzliche Schutzaufgaben“ im Dezernat Chemie des Bereich Wissenschaften unter Aufsicht des Dezernatsleiters Chemie, Dr. M. Metzulat, und unter Betreuung von Prof. Dr. K. L. Karaghiosoff des Department Chemie der Ludwig-Maximilians Universität München angefertigt.

To my family

"Success is never the destination, but something that arises when the goal is achieved" unknown author.

Abstract

The recent developments in the Middle East especially, the terroristic acts going on in Syria and Iraq put a new complexion on this work which focusses on the preparation and analytical investigation of Amiton and several homologs thereof and make it even more important.

Amiton is an organophosphate nerve agent, formerly known as a pesticide, and falls under the Chemical Weapons Convention (CWC) whereas the other compounds prepared in the course of this thesis are not covered by the CWC. However, the aim of this thesis was not to identify new chemical warfare agents but to contribute to a better understanding of the existing ones.

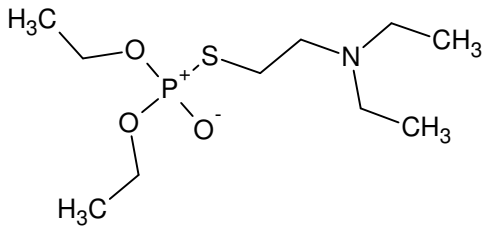

Figure 1: *Chemical structure of Amiton.*

Basically, the work on hand can be divided into five main parts:

Part 1: Preparation of Organophosphates and their Precursors

The synthesis of the Amiton-like compounds was achieved in good yields by the coupling of an appropriate amino alcohol in its enolate form to the respective phosphorylchloride. In the case that the necessary educts were not commercially available the synthesis of the precursors was performed. Finally, nineteen Amiton-like compounds were prepared of which twelve having not been reported in the literature before. Additionally, most of the compounds could be transferred to the corresponding quaternary ammonium salts of which some also yielded single crystals. The latter ones were subjected to X-ray single crystal structure analysis and the structures are described for the first time in this thesis.

A separate study addresses the isomerization of Amitons which are capable of the so called thiono-thiol isomerization. Thus far, no decisive explanation of the mechanism in the literature can be identified so that a new experimental series to describe the facts for Amiton was necessary. It was found that the decay of the thiono educt obeys a first order reaction kinetic which is dependent on the solvent.

Part 2: Characterization by Analytical Instruments

To fully characterize the prepared Amitons and their precursors the most recent and available analytical instruments were used. Especially, these are IR and Raman

spectroscopy, HPLC- and GC- mass spectrometry as well as NMR spectroscopy. Furthermore, the obtained spectra could be uploaded into existing databases of the respective analytical instrument and methods for their recovery were developed.

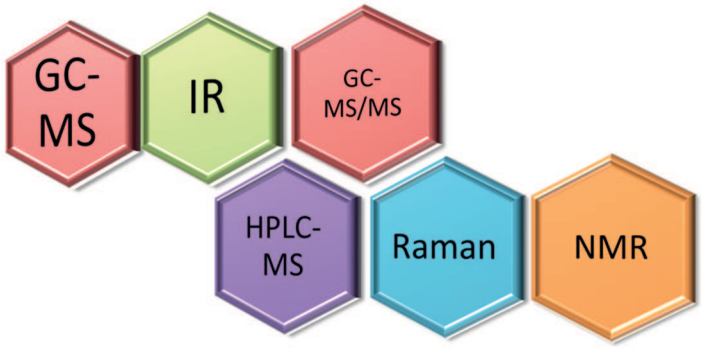

Figure 2: *Analytical methods used for characterization within this thesis.*

In particular, during the measurement of GC-MS spectra it was observed that some of the substances undergo thiono-thiol isomerization while being analyzed and thus are difficult to identify. Still until today this phenomenon is not fully described in literature but could be addressed in a separate part of this work.

Moreover, the mass spectra differ from each other only in a very few peaks due to the very close relationship of the molecules analyzed in this study. Thus, in-depth investigations by two-dimensional mass spectrometry had to be conducted for unambiguous identification. The thus obtained results are reported in a separate part of this thesis.

Part 3: Toxicological Studies

Knowing the toxicological parameters of the prepared compounds is of central importance for safe handling of those compounds. Moreover, an assessment of the toxicity is also crucial in terms of a possible terroristic threat. Organophosphates have the fateful property to inhibit cholinesterases which are essential for the signal transduction in vertebrates.

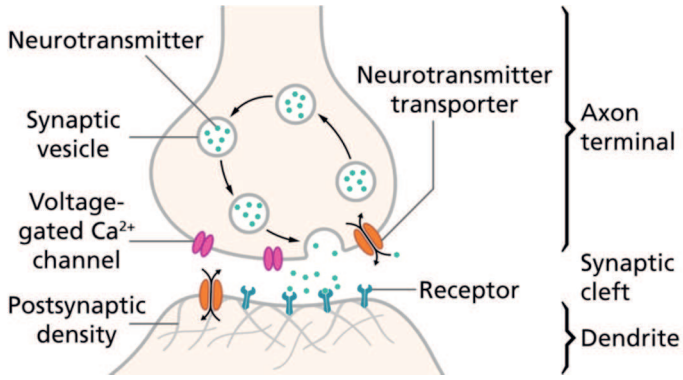

Figure 3: *Graphical depiction of the synaptic cleft of a nervous cell. Graphic is creative commons domain by Thomas Splettstoesser (www.scistyle.com) (Own work) [CC BY-SA 4.0 (https://creativecommons.org/licenses/by-sa/4.0)].*

Most often this process is irreversible and finally leading to breakdown of the organism. For the determination of the inhibitory constants for acetylcholinesterase (AChE) and butyrylcholinesterase (BuChE) activity a classical Ellman-essay was employed. It was found that all compounds but Amiton showed a weak inhibitory potential towards AChE. Additionally, these molecules were found to have a very similar effect towards BuChE. Furthermore, the found results strongly indicate that or prove that the respective inhibitory effect can be tuned very precisely by proper choosing and combining of the substituents of the nitrogen atom as well as the phosphorus atom.

Part 4: Special Investigations

Exceeding the so far described investigations detailed studies on special topics were run.

In a separate series of experiments the vapor pressure data of Amitons prepared in this study were determined by employing the so called transpiration method approach. This involves a controlled gas stream which transports material of the sample under exact control of temperature and measurement time which is proportional to the vapor pressure of the sample.

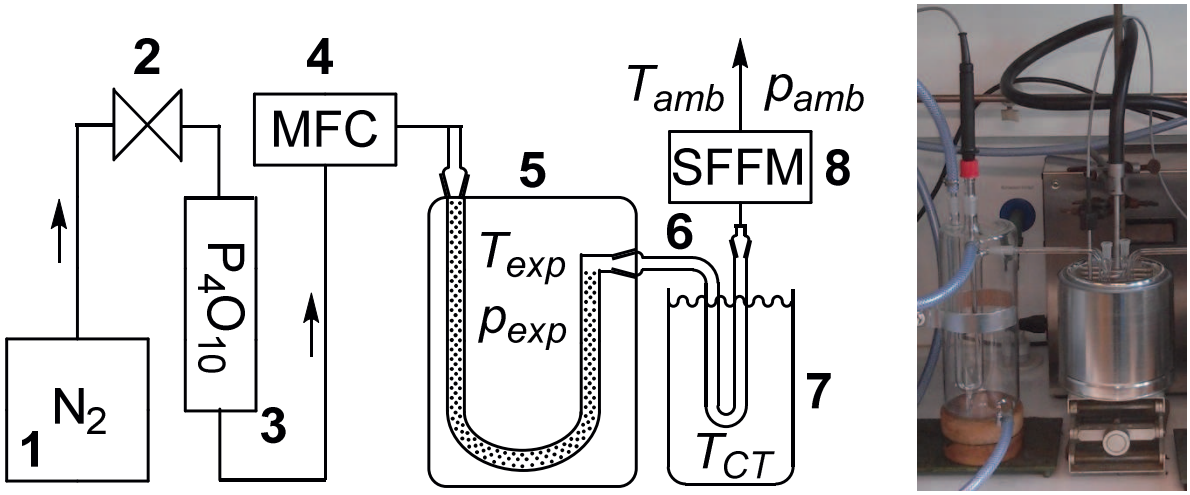

Figure 4: *Schematic representation of the setup used in the transpiration method setup (left) and photography of the original setup (right). 1: nitrogen source, 2: pressure regulator, 3: drying agent, 4: mass flow controller, 5: saturator, 6: cooling trap, 7: cooling bath, 8: soap film flow controller.*

This method was applied for volatile substances so far and was successfully extended in close cooperation with Martin Härtel, LMU, to toxic and thermo-labile compounds like some of the synthesized ones. Knowledge of the vapor pressure and the enthalpy of vaporization allow the estimation of the detectability of a substance from the air. These values are of great importance, because, especially the hand-held and field portable instruments of the Bundeswehr are mainly based on the principle of gas phase detection.

The initially obtained mass spectra are looking very similar to each other and finally were only distinguishable by their respective Kovats indices. The evaluation of the mass spectra

itself results only in very few cases in a clear identification of the compound. For this reason the prepared substances were subjected to a two-dimensional mass spectrometric experiment, to allow an unambiguous assignment. As a major result of these investigations full mass spectrometric fragmentation pathways could be described for the Amiton molecules for the first time.

As a rule these show two main fragmentation pathways. The first one is based on the fragmentation of the nitrogen containing side chain, which is at the same time dominating the mass spectrum. The second pathway is based on the fragmentation of the phosphorus moiety and shows fewer fragments. But, the latter one is at the same time important for the solution of the chalcogen configuration of the central phosphorus atom and thus a complete resolution of the structure by means of mass spectrometry.

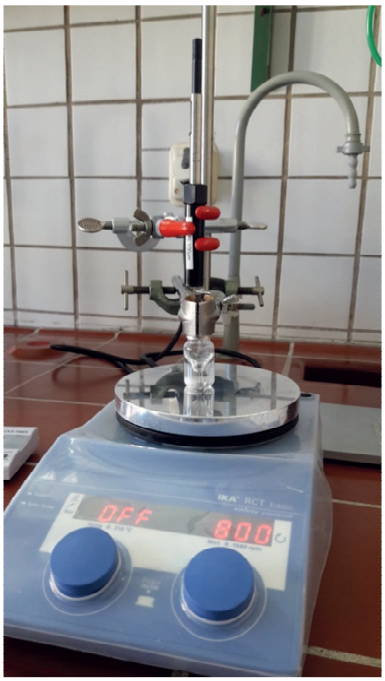

Image 1: *Setup for manually operated SPME for the detection of organophosphates in water.*

Another question was the detection of the substances from different environmental matrices. Usually sampling procedures and samples, like soil or water samples require mostly an intensive sample preparation, e.g. liquid-liquid extraction or solid-phase extraction. Furthermore, in the context of chemical warfare analysis no methods for the work up of so called complex matrices from the environment are described until today. In the conduct of this work a single automated method for solid-phase microextraction (SPME) was developed, which is capable of the extraction and direct processing of phosphororganic compounds from media: air, water and vegetation (foliage and grass) by direct immersion of a PDMS/DVB fiber.

Part 5: Detection and Analysis with Military Detection Equipment and Procedures

A major part of this work was dedicated to the evaluation of the Bundeswehr detection equipment and procedures with respect to the detection and analysis of the compounds prepared in the frame of this thesis. Almost all instruments could be tested. The obtained results very clearly demonstrate that the detection of the compounds is possible but that a distinct identification is tricky, particularly as some results are, but, comprehensible, contrary to others.

Image 2: *Picture of the Fox-Recce vehicle of the Bundeswehr CBRN forces.*

Additionally, two techniques that have not been used so far could be initially tested. First, this was an instrument based on flame photometry and to all challenged compounds correctly responded. Second, a promising benchtop NMR instrument could be used to analyze the compounds. The thus obtained results force the conclusion, that NMR spectroscopy is an absolutely meaningful and necessary supplementation to the so far available instrumentation and offers a fast, affordable and absolutely reliable method to limit the possible compound class of the unknown analyte.

Keywords:

Organophosphate, Amiton, synthesis, vapor pressure, direct immersion, complex matrix, SPME, toxicology, spectrum, isomerization, rearrangement, enthalpy of vaporization, vapor pressure, kinetic study, enzyme inhibition, AChE, BuChE

Zusammenfassung

Die jüngsten Ereignisse im Mittleren Osten, besonders die terroristischen Anschläge und Gräueltaten in Syrien und dem Irak lassen die vorliegende Arbeit, die sich mit der Synthese und analytischen Beschreibung von Amiton beschäftigt, zusätzlich in einem besonderen Licht erscheinen und messen ihr weitere Bedeutung zu.

Amiton selber zählt als Organophosphat zur Gruppe der Nervenkampfstoffe und fällt unter das Chemiewaffenübereinkömmen (CWÜ), wohingegen die anderen Stoffe, die im Rahmen dieser Arbeit hergestellt wurden nicht vom CWÜ erfasst werden. Allerdings war es nicht erklärtes Ziel der Arbeit neue Kampfstoffe herzustellen, sondern vielmehr zum besseren Verständnis der bestehenden beizutragen.

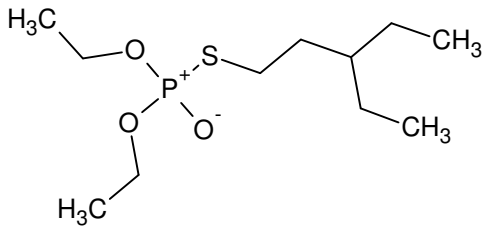

Figure 5: *Strukturformel von Amiton.*

Grundsätzlich kann die vorliegende Arbeit in fünf große Abschnitte eingeteilt werden:

Abschnitt 1: Herstellung der Amitone und ihrer Vorstufen

Die Synthese der Amitone wurde ausgehend von der Kopplung eines entsprechenden Aminoalkohols in Enolatform mit einem Phosphorsäurechlorid in sehr guten Ausbeuten erreicht. Dort wo keine marktverfügbaren Edukte verwendet werden konnten, wurden die benötigten Edukte selbst hergestellt. Als Ergebnis wurden sieben Aminoalkohole und sowie ein Phosphorsäurechlorid als Ausgangsstoffe hergestellt. Schließlich wurden daraus und aus frei erhältlichen Stoffen insgesamt neunzehn Amitone hergestellt. Von diesen sind zwölf bislang nicht in der Literatur beschrieben worden. Zusätzlich ist es gelungen den überwiegenden Teil der Verbindungen in die quartären Ammoniumsalze zu überführen. Von diesen wiederum konnten mehrere Stoffe in einkristalliner Form erhalten werden und mittels Einkristallröntgenbeugung untersucht und erstmalig beschrieben werden.

Eine spezielle Untersuchung betrifft die Isomerisierung der Amitone, die zur sogenannten Thiono-Thiol Umlagerung befähigt sind. Bislang konnte keine eindeutige Erklärung des Mechanismus in der Literatur gegeben werden, sodass eine eigene Versuchsreihe zur Beschreibung des hier zu Grunde liegenden Sachverhalts angefertigt wurde. Es stellte sich heraus, dass die Abnahme des Thiono Edukts einer Reaktion erster Ordnung gehorcht, die abhängig vom Lösungsmittel ist.

Abschnitt 2: Charakterisierung mittels instrumenteller Analytik

Zur Charakterisierung der erhaltenen Amitone und ihrer Vorstufen wurden, soweit verfügbar, alle gängigen Charakterisierungsverfahren herangezogen. Insbesondere sind dies IR und Raman Spektroskopie, HPLC- und GC-Massenspektrometrie sowie NMR Spektroskopie. Weiterhin konnten die erhaltenen Spektren in die Datenbanken der Geräte aufgenommen werden und Methoden zur Wiederfindung der Analyten entwickelt werden.

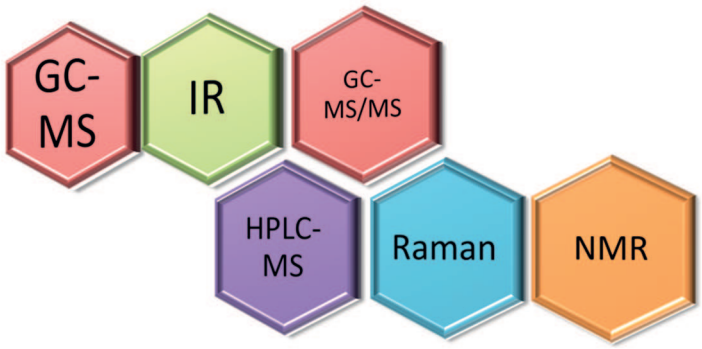

Figure 6: *Übersicht der in dieser Arbeit genutzten Techniken zur Charakterisierung der Moleküle.*

Insbesondere während er Aufnahme von GC-MS Spektren viel auf, dass einige der Stoffe Thiono-Thiol Isomerisierung während der Messung erfahren und somit nur schwer zu identifizieren sind. Dieses bis heute nicht vollständig beschriebene Phänomen der Isomerisierung konnte in einem gesonderten Abschnitt der Arbeit genauer untersucht werden. Weiterhin unterscheiden sich die erhaltenen Massenspektren aufgrund der engen Verwandtschaft der Moleküle nur sehr gering voneinander, sodass weitergehende Untersuchung in Form von zweidimensionalen Massenspektren vorgenommen werden mussten. Die darin erhaltenen Ergebnisse sind einem separaten Kapitel der Arbeit beschrieben.

Abschnitt 3: Toxikologische Untersuchungen

Die Kenntnis der toxikologischen Parameter der hergestellten Verbindungen ist von zentraler Bedeutung für einen sicheren Umgang mit den Stoffen. Darüber hinaus ist eine Bewertung der Giftigkeit auch vor dem Hintergrund einer möglichen terroristischen Bedrohung von großer Wichtigkeit. Organophosphate haben die unangenehme Eigenschaft Cholinesterasen, die für die Signaltransduktion im Körper von in Wirbeltieren essentiell sind, zu hemmen. Zumeist ist dieser Vorgang irreversibel und führt schließlich zum Tod des Organismus.

Zur Bestimmung der Hemmkonstanten wurde ein klassischer Ellman Essay angewendet und die Acetylcholinesterase (AChE)- und Butyrylcholinesterase(BuChE)-Aktivität bestimmt. Es stellte sich heraus, dass alle Stoffe, mit Ausnahme des Amiton selber, nur eine geringer

Hemmwirkung gegenüber AChE aufweisen, aber gegenüber BuChE eine deutlich vergleichbare Wirkung wie das Amiton haben.

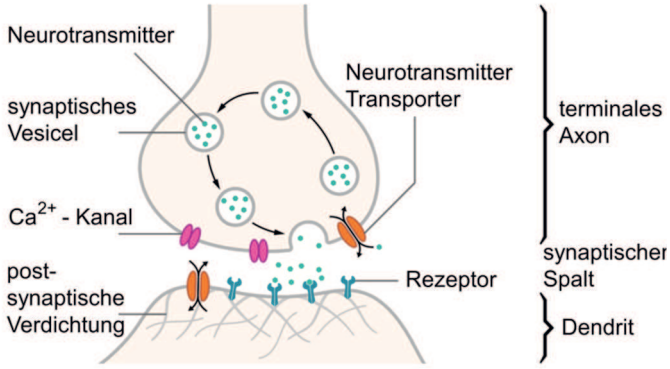

Figure 7: *Schematische Darstellung des synaptischen Spalts einer Nervenzelle. Grafik gehört creative commons domain by Thomas Splettstoesser (www.scistyle.com) (Own work) [CC BY-SA 4.0 (https://creativecommons.org/licenses/by-sa/4.0)].*

Ferner zeigen die erhaltenen Ergebnisse, dass sich die betreffende Hemmwirkung durch geeignete Wahl und Kombination der Substituenten am Stickstoff sowie am Phosphor sehr genau einstellen lässt.

Abschnitt 4: Spezielle Untersuchungen

Über die bisher beschriebenen Untersuchungen hinaus wurden vertiefende Studien zu speziellen Themenbereichen unternommen.

Dies ist zum einen die Bestimmung des Dampfdrucks der hergestellten Amitone mittels der sogenannten Transpirationsmethode, bei der durch einen kontrollierten Gasstrom, Substanz forttransportiert wird, die bei exakter Kontrolle der Temperatur und Messzeit proportional zum Dampfdruck ist.

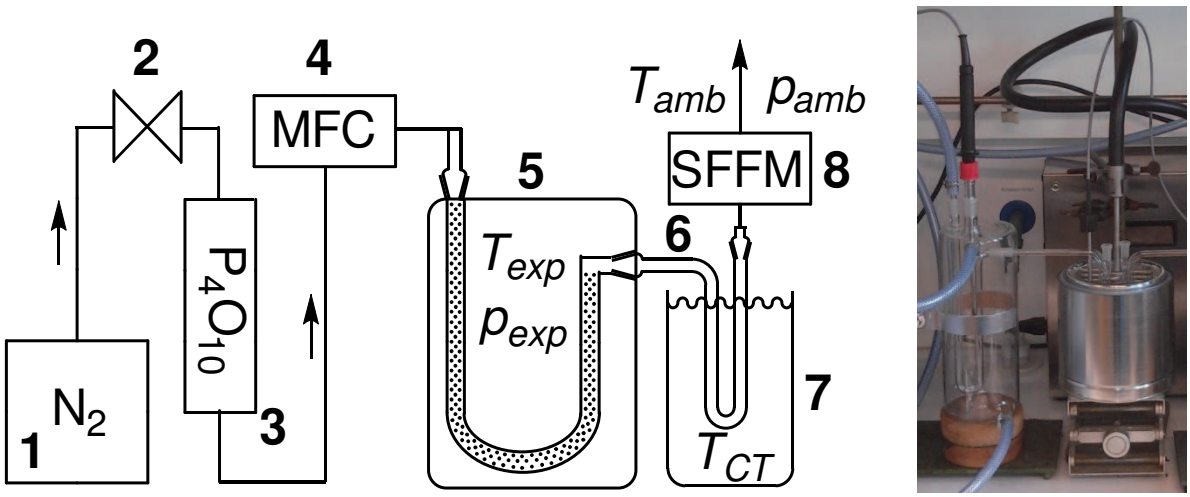

Figure 8: *Schematische Dartsellung des experimentellen Aufbaus für die Transpirationsmethode (links) and Photographie des Originalsetup (rechts). 1: Stickstoffquelle, 2: Druckminderer, 3: Trockenmittel, 4: Massenflusskontrolleinheit, 5: Saturator, 6: Kühlfalle, 7: Kühlbad, 8: Seifenfilm Flussmesser.*

Diese Methode wurde bislang nur für leicht flüchtige Substanzen angewendet und konnte in Zusammenarbeit mit Martin Härtel, LMU München erfolgreich auf toxische und thermolabile Verbindungen wie einiger der hergestellten Amitone übertragen werden. Die Kenntnis des Dampfdrucks und auch der Verdampfungsenthalpie ermöglicht es eine Abschätzung bezüglich der Detektierbarkeit eines Stoffes aus der Luft vorzunehmen. Da insbesondere die handgehaltenen und Feldtauglichen Instrumente der Bundeswehr auf dem Prinzip der Gasphasendetektion beruhen kommt diesen Werten eine große Bedeutung zu.

Die anfänglich erhaltenen Massenspektren wiesen eine sehr große Ähnlichkeit zueinander auf und waren schließlich nur noch anhand ihrer unterschiedlichen Kovastindizes den einzelnen Substanzen zuzuordnen. Eine Auswertung der Spektren allein führt in den seltensten Fällen zu einer eineindeutigen Lösung. Aus diesem Grund wurden die hergestellten Substanzen erneut mittels zweidimensionaler Massenspektrometrie untersucht, um eindeutige Zuordnungen vornehmen zu können. Als wesentliches Ergebnis dieser Untersuchungen konnten zum ersten Mal vollständige Fragmentierungswege der Amitone beschrieben werden. Diese weisen in der Regel zwei Hauptzerfallswege auf. Der erste basiert auf der Fragmentierung der Stickstoff enthaltenen Seitenkette welche zugleich das Massenspektrum dominiert und der zweite Weg basiert auf dem Zerfall des Phosphor tragenden Restes und besitzt in der Regel weniger Fragmente. Der letztere ist aber gelichzeitig entscheidend für die Lösung der Chalcogen-Konfiguration des zentralen Phosphors und damit für die vollständige Lösung der Struktur mittels Massenspektrometrie.

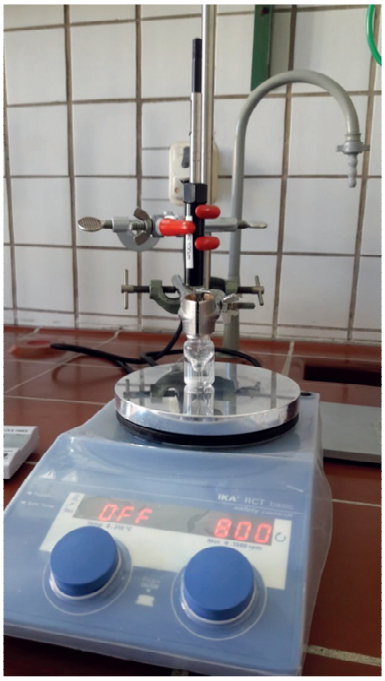

Image 3: *Aufbau für manuelle SPME zum Nachweis von Organophosphaten aus Wasser.*

Eine weitere Fragestellung war der Nachweis der Substanzen aus verschiedenen Umweltmedien. Klassische Probennahme Verfahren und Probenarten, wie z.B.

Bodenproben oder auch Wasserproben bedingen zumeist eine intensive Probenaufbereitung, z.B. durch Flüssig-Flüssigextraktion oder Festphasenextraktion. Darüber hinaus werden im Bereich der Kampfstoffanalytik von Umweltproben bis heute keine Verfahren zur Aufbereitung von sogenannten komplexen Matrices beschrieben. Im Rahmen dieser Arbeit konnte eine einzige automatisierte Methode zur Festphasenmikroextraktion (SPME) entwickelt werden, welche es ermöglicht phosphororganische Verbindungen aus den Medien: Luft, Wasser und Vegetation (Blätter und Grass) durch direkte Immersion einer PDMS/DVB Faser zu extrahieren und unmittelbar mittels GC-MS zu untersuchen.

Abschnitt 5: Nachweis mit militärischen Detektionsgeräten und -verfahren

Ein wesentlicher Teil der Arbeit bestand darin, die bei der Bundeswehr eingeführten Spür- und Messverfahren und zugehörigen Geräte hinsichtlich ihrer Eignung zur Detektion und Nachweis der hergestellten Stoffe zu untersuchen. Im Rahmen dieser Arbeit konnten nahezu alle genutzten Geräte verwendet werden. Die erhaltenen Ergebnisse zeigen sehr deutlich, dass mit den vorhandenen Equipment ein Nachweis gelingen kann, eine eineindeutige Identifizierung aber schwierig ist; zumal sich erhaltene Ergebnisse zum Teil, allerdings nachvollziehbar, wiedersprechen.

Image 4: *Spürpanzer Fuchs der ABC-Abwehrkräfte der Bundeswehr.*

Zusätzlich konnten zwei bislang nicht eingeführte Messverfahren untersucht werden. Dies ist zum einen ein Gerät, welches auf Flammenphotometrie basiert und alle erhaltenen Stoffe korrekt angezeigt hat. Zum anderen konnte ein vielversprechendes Benchtop NMR Spektrometer genutzt werden, um die Stoffe zu untersuchen. Die dabei erhaltenen Ergebnisse legen den Schluss nahe, dass die NMR Spektroskopie eine absolut sinnvolle und notwendige Ergänzung zu dem bislang verfügbaren Instrumentarium darstellt und eine schnelle, kostengünstige und zuverlässige Eingrenzung der möglichen Substanzklasse erlaubt.

Schlagwörter:

Organophosphat, Amiton, Synthese, Dampfdruck, direkte Immersion, komplexe Matrix, SPME, Toxikologie, Spektrum, Isomerisierung, Umlagerung, Verdampfungsenthalpie, Dampfdruck, kinetische Untersuchung, Enzym Inhibition, AChE, BuChE

Abbreviations

°C	degree Celsius
AC	hydrogen cyanide
Ach	acetylcholine
AChE	acetylcholine esterase
ATChI	acetylthiocholine iodide
AED	atomic emission detector
amu	atomic mass unit
ATR	attenuated total reflection
b.p.	boiling point
BuChE	butyrylcholine esterase
BuTChI	S-butyrylthiocholine iodide
CBRN	chemical, biological, radiological and nuclear
CDSEP	Chemical Defense, Safety and Environmental Protection
CI	chemical ionization
CLX	chlororganic compound
CWC	Chemical Weapons Convention
CY	cyanide
d	doublet
DAD	diode array detector
DIBAL-H	diisobutylaluminium hydride
DPM	dipropylenglycol methylether
DTNB	5,5'-dithiobis-(2-nitrobenzoic acid)
DVB	divinylbenzene
EA	elemental analysis
ECBC	Edgewood Chemical Biological Center
EI	electronic ionization
EOD	explosive ordnance disposal
EPA	Environmental Protection Agency
ESI	electron spray ionization
eV	electron Volt
FID	flame ionization detector
GA	Tabun, ethyl dimethylphosphoramidocyanidate
GB	Sarin, (*RS*)-*O*-isopropyl methylphosphonofluoridate
GC	gas chromatography
GD	Soman, 3,3-dimethylbutan-2-yl methylphosphonofluoridate
HD	sulfur mustard, bis(2-chloroethyl) sulfide
HDPE	high density polyethylene
HN	nitrogen mustard
HPLC	high performance liquid chromatography
IMS	ion mobility spectrometry

IR	infrared
ISIS	Islamic State in Iraq and Syria
KI	Kovats index
L	Lewisite, 2-chloroethenylarsonous dichloride
LCD	lightweight chemical detector
LMU	Ludwig-Maximilian University
LOD	limit of detection
LOQ	limit of quantification
MBTFA	N-methyl-bis-trifluoroacetamide
m	multiplet
MM 1	Mobil Mass Spectrometer 1
MM 2	Mobil Mass Spectrometer 2
MS	mass spectrometry
MS	methyl salicylate, methyl 2-hydroxybenzoate
NATO	North Atlantic Treaty Organization
NMR	nuclear magnetic resonance
NSN	NATO stock number
o	octet
OP	organophosphate
OTP	organothiophosphate
PA	polyamide
PDMS	polydimethylsiloxane
PTV	programmed temperature vaporizing
q	quartet
qui	quintet
RI	refractive index
Raid-M	rapid alarm and identification device monitor
RSH	rapid sample handling
s	singlet
sep	septet
sex	sextett
SPME	solid-phase micro extraction
t	triplet
TIC	toxic industrial chemical
TDI	toluene diisocyanate
UV	ultraviolet
vis	visible
VG	NATO code for Amiton
VX	*O*-ethyl *S*-[2-(diisopropylamino)ethyl] methylphosphonothioate
VXR	*O*-isopropyl *S*-[2-(diethylamino)ethyl] methylphosphonothioate

Table of Contents

1 Introduction

The work described in this thesis is highly motivated by the content of the article entitled "Organophosphates: A Common But Deadly Pesticide"-recently published by National Geographic.[1] The article gives a short but detailed description that the use of organophosphate (OP) pesticides is comparable to walk a fine line; and blessing or curse of their development are two sides of the same medal. Regardless of the known potential health risks and actual fatalities, either by purpose or by chance, these compounds have been and are continued to be widely used as pesticides throughout the world. However, people become more aware about the potential negative side effects connected with the use of OPs. Discussions for example about the prolongation of the permission to use Glyphosate® have been put on the agenda since the population becomes more sensitive for health issues than this was the case about 20-30 years earlier.[2] On the other hand reports about the misuse of organophosphates by terrorist organizations, such as the attack by the Aum-cult in the Tokyo subway with Sarin, exacerbate the dispute between opponents and supporters of the use of OP's as pesticides.[3] Whereas the use of chemicals as weapons of fear (not chemical warfare agents, which fell under the CWC) by the Taliban in Afghanistan is only reported in the international news and not in the local German news. This is somewhat irritating since this exemplary incident in which 74 girls were poisoned with Malathion, a pesticide nowadays banned in the EU, while they were attending school, was not the first of this kind and unfortunately not the last.[4-6]

Things got even worse during the rise of the so called Islamic State or short: IS. The Syrian regime started to use chemical weapons in the internal conflict against unprotected civilians with large numbers of casualties under the blanket of fighting terrorists. Luckily, the OPCW got the chance to proof this officially.[7] Ignoring this official statement the Syrian Regime did not stop to use CWA's in the internal conflict, neither did IS.[8] For the outstanding job, later in the year, the OPCW was awarded the Nobel Peace Prize 2013.[9]

Finally (officially), Syria was forced to hand over the declared chemical weapons stockpile which than was destroyed on board the MV Cape Ray (Image 5) in the Mediterranean Sea in a world-wide and once in a lifetime happening event.[10] The chemicals being destroyed were mainly mustard gas and precursors for the production of sarin. The process was performed by the field deployable hydrolysis system, a specialized setup originating from and developed by the US Army Edgewood Chemical Biological Center (ECBC)[1][11]. The hydrolysis products were afterwards shipped to different member states of the CWC for further treatment.[12]

[1] www.ecbc.army.mil

Image 5: *MV Cape Ray (right) on board which the declared Syrian chemical weapons were destroyed. (Image released by the United States Navy with the ID 140110-N-XB010-088.)*

This absolute positive development is drawn back by the fact that the IS is still motivated to use chemical weapons on their own since they allegedly found and got control over some of the Syrian CWA arsenals.[13] Additionally, it has to be assumed that members of the IS are also capable to produce chemicals and chemical warfare agents on their own.[14] According to the news on the internet and the report of the OPCW the CWA's and chemicals used in Syria and Iraq were, until today, chlorine, mustard as well as sarin. Furthermore, in a book by *Ackermann* the aim of terrorist groups, namely Jihadist, to achieve chemical weapons by their own is clearly stated and was still emphasized to be so today by numerous speakers during the 2016 CBW-Symposium in Stockholm[2].[15]

By having a closer look at the annexes of the CWC, one can easily conclude that not all chemicals are banned and that of some even potent OPs and organothiophosphates(OTPs) can be thought of, which are not covered by this convention. (Figure 9)

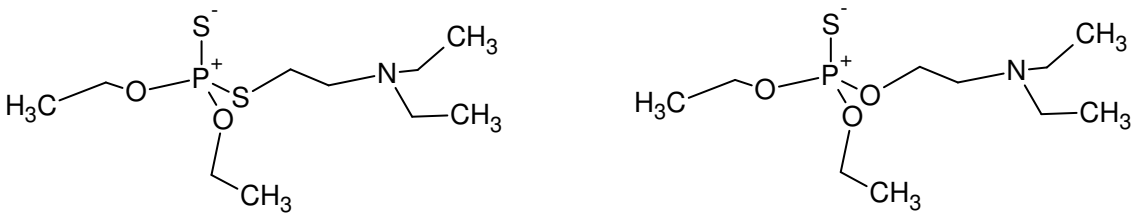

Figure 9: *Possible structures for molecules which do not fell within the scope of the CWC, but which can be easily turned into Amiton by applying heat to the molecule on the right (isomerization) or by the cytochrome P450 enzyme in the human liver (oxidation).*

From a military point of view it is reasonable to conceal details about these topics which is why that information only slightly breaks through the surface. One reason probably is to not irritate the population. Moreover, the economic factor as well as lobbying must certainly not

[2] www.cbw.se

be neglected, since companies make much profit with the sales of OPs in the agriculture sector.[16]

However, also in other countries, which are not on the breaking news of today's TV-channels, chemicals are employed to threaten the population in open conflicts like in Darfur.[17] Moreover, some countries seek to obtain chemical weapons and atomic bombs as a threat potential not to be attacked by other countries as is the case for North Korea.[18] Finally, also countries having ratified the CWC, namely Russia, are allegedly seeking to find new ways of bypassing international law by development of new even more potent, so called Novichok agents.[19-21] Against the backdrop of these facts, the statement of US-American General J.J. Pershing under the impression of the first World War in 1919: "Whether or not gas will be employed in future wars is a matter of conjecture, but the effect is so deadly to the unprepared that we can never afford to neglect the question." holds still true today.[22]

Despite this intense and controversy discussion about the use of OPs and other chemicals as well, the chemistry of this substance class is still not fully explored. In particular, a lot of chemical and physical data about even well-known and old OPs are still missing or are not publically available. This may be due to the fact that the analytical methods and equipment available during their development period in the 1950's to 1970's lack the required accuracy and detection limit for complete characterization of these compounds as state-of-the-art technology offers nowadays.

Although, a lot of different methods for the investigation of OP's are available the applicability of these methods in field test under real life conditions or case studies have not yet been reported on. Most investigations deal with so called simulant substances which more or less model the original V-series compounds.[23] By comparison of the chemical structures of those simulants and the original CWA molecule one can easily see that physical and chemical properties and therefore the behavior must be different. Thus, most often so called simulant libraries are emplaced to give the desired results on the instruments display for field training exercises. But, still today efficient simulants which model the chemical and physical behavior of the CWA's are not available.

Due to the high number of poisonings and even deaths as well as the development of unambiguous and reliable detection methods for easy and unambiguous identification of this substance class in the field is of high importance, or from a military point of view: "It's best to know ones opponent.".[24]

2 Objective of this Thesis

The work of this thesis focusses on the characterization and investigation of Amiton-like OPs. For this purpose several structurally slightly different molecules were synthesized and tested towards their toxicity for AChE and BuChE. Mainly up to date analytical laboratory equipment is used to fully describe the synthesized molecules and to obtain spectra to be integrated into existing databases. Moreover, the hand-held and field deployable instruments of the Bundeswehr are challenged with the obtained substances to prove whether existing investigation principles are capable of dealing with these substances. Furthermore, a kinetic study of the still unresolved thiono-thiol rearrangement of this compound class is performed by the use of different solvents, temperatures and chiral molecules to unravel the mechanism of this phenomenon. To date, no fast and reliable methods for the detection and analysis of chemical warfare agents from complex matrices, e.g. grass or foliage, in the CBRN sector exists. For this reason solid-phase micro extraction (SPME) is tested towards the applicability as high speed extraction and sample preparation method. Besides this, the obtained molecules are evaluated to their applicability as simulant substances modeling the real behavior of V-series chemical warfare agents.

The systematic investigation of Amiton-related OP's and OTP's includes the following steps:

- Preparation of the target molecules partly including the synthesis of non-commercially available precursor molecules.
- Determination of the inhibiting capacity of these molecules, since only few values are reported in literature, which are hardly comparable to each other because of the different origin of the target enzymes. Furthermore, these studies will allow the estimation of toxicity values for the respective substance and help to determine the necessary precautions regarding occupational health measures in the lab.
- Complete characterization by state-of-the-art laboratory instrumentation methods like IR, Raman, GC-MS, HPLC-MS and NMR. Furthermore, the determination of vapor pressure values is of significant interest since most portable instruments are based on the detection in the vapor state.
- Additionally, the elucidation of the fragmentation pathways in the mass spectrometer is to be investigated since this is the method of choice for the Bundeswehr to identify and characterize unknown compounds in the field by the field deployable chemistry lab.
- Investigation of the detectability with the established hand-held detection devices of the Bundeswehr, to prove the capability of available methods and instruments.
- Finally, a test regarding the recovery from environmental samples shall be developed. Especially, the applicability of SPME for the extraction from complex matrices like grass or foliage should be proved.

3 Fundamentals and Theory

3.1 Organophosphates (OPs) Now and Then

The first OP with AChE inhibiting capacity was tetraethyl phosphate which was synthesized by *Philippe de Clermont* in France in 1854.[25] At this time their strong toxicity was unknown and increased safety measures for safe handling of chemicals had not been implemented. The first incident which clearly connects the negative implications observed with the use of OPs was reported 80 years later by *Lange and Krüger*.[26] In their study they described the odor of the synthesized dimethyl phosphorofluoridate as strong aromatic and pleasant. Some minutes later they complained about pain in the larynx and headache and breathlessness. Due to these toxicological implications, the safety standards, especially for handling of trial products have been increased tremendously.

The pointed development of the substance class of organophosphates begun with *Alexander Arbusov's* and *August Michaelis'* first experiments in the early 19th century, whereas *Gerhard Schrader* was the first to discover their toxic potential in the mid 1930's when he was searching for new insecticides at I.G. Farben in Leverkusen and later on at Bayer.[27] By chance he discovered the later well-known chemical warfare agents Tabun (1936) and Sarin (1939) which he had to report to the German Reich due to their strong toxic effects.[28] Dating back to that time the nowadays well known Schrader-formula (Figure 10) was born which is even reported in a famous German "semi-scientific" journal.[29]

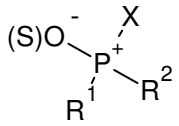

Figure 10: *Drawing of the Schrader formula where R^1 represents for an alkoxy group, R^2 stands for an alkoxy, alkyl or dialkylamino group which is of basic character and X indicates an acidic moiety like halogen, cyanid, phenoxy or disubstituted pyrophosphate.*

Later on other researches in Great Britain, *R. Ghosh* from Imperial Chemical Industries, and Sweden, *L.E. Tammelin* from the Swedish National research Institute, successfully developed new phosphor organic compounds. Due to the tense situation in the world policy no contact of this three research groups was established and they ended up with the same compound class bearing the most toxic molecules.[30] In 1952 it was *R. Ghosh* of the British Imperial Chemical Industries (ICI) who claimed a patent for the synthesis of Amiton and related compounds.[31] Especially Amiton was intensively studied, e.g. by *Baldit* and *Cadogan et al.*[32-34] Today, those substances are known as Tammelin-esters (Figure 11). During his studies in the 1950's, the researcher *Tammelin* also identified the basicity of the

nitrogen atom within the molecule as the most critical factor for its toxicity.[35, 36] Two text books high-lighting the historic development and use of CWA's and especially nerve agents throughout the world were written by *Tucker* and *Harris et al*.[37, 38] A review by *Delfino et al.* gives an overview on the OPs used as chemical warfare agents.[39]

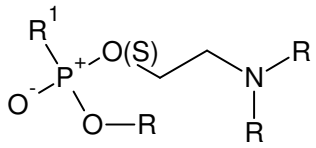

Figure 11: *Drawing of the basic structure for Tammelin's esters where R represents an alkyl moiety and R^1 stands for fluorine, an alkyl or an alkoxy moiety.*

Based on the findings of *Schrader* and *Tammelin* the "modern" nerve agent VX and others were synthesized in the following years. Simultaneously postulations where VX was one of the most toxic chemical warfare agents were substantiated. Noteworthy, the structure of VX was already patented by the German company Bayer in 1957 in Germany and later on in 1961 in the USA.[40]

Besides this military-focused research a lot of research was done to come up with a lot of different organophosphorus compounds with tunable properties towards the toxicity and efficiency towards pest as the desired target class without being harmful to mammals. Due to the large number of existing literature resources for the particular research a complete overview of this topic would be out of scope of this thesis. Therefore, cross-references to the most important text books to this field shall be given at this point: The most important book was written by *Satoh et al*, which focusses on AChE-inhibiting enzymes[41], another comprehensive reference work is the book written by *Fest et al*.[42]

Besides their use as pesticides and CWA's, OPs are also used as flame retardants, plasticizers and auxiliaries in the fabrication of paper and textiles, hydraulic liquids, and many more.[43-46] Moreover, life is based on organophosphates i.e. OPs are one important building block of our genome: DNA and RNA.[47]

The recent research in the field of hazard defense mainly focusses on the detection of the classical CWA's, medical treatment to overcome the toxic effects and on the development of new detection methods.[48-52] Due to the strong toxic action of the analyte molecules this research is most often based on simulant substances and analogues which shall model or mimic the chemical behavior of the original target analyte.[23]

3.2 Legal and Regulatory Aspects

Since the Chemical Weapons Convention is in place and valid for the member states, trading and dealing with substances which fell within the scope of its annexes is limited and only a few authorities are allowed to work with these substances per se.[53] The German Bundeswehr runs three institutions which are authorized to perform research with those compounds for protective purposes. Those are the Defence Scientific Institute for CBRN-Defence in Munster, the Institute for Pharmacology and Toxicology of the Bundeswehr in Munich and the Chemistry Section of the CBRN Defence Safety and Environmental Protection School in Sonthofen at which most of this thesis' work was done.

Moreover, not all OPs comply with the CWC but also a lot of them apply to national and international law and regulations since some of them are used as pesticides or plasticizers. Many of the pesticides, especially the highly toxic organophosphate and carbamate anticholinesterase agents, can cause serious health issues and symptoms, even fatalities to exposed humans, and thus the strict regulation of exposure to these compounds is highly justified.[54] To keep track of all those regulations for the different countries is nearly impossible since regulations are altered frequently by national legislation. Several institutions for instance the U.S. Environmental Protection Agency[3] or the European Food Safety Authority[4] are empowered to act as an advisory board and conduct risk assessments for the respective legislative authorities.

[3] https://www3.epa.gov/
[4] http://www.efsa.europa.eu/en/topics/topic/pesticides

3.3 Thiono-Thiol Rearrangement

OTP's can readily be isomerized to OP's by applying heat. This reaction is called thiono-thiol rearrangement and was first discussed by *Emmett et al*. as early as 1911.[55] By thermal treatment of O,O,O-trimethyl thionophosphate in a sealed tube at 100°C for two hours O,O,S-trimethyl thiophosphate was obtained in about 50% yield.[56] This reaction was then applied in the industry for the preparation of Amiton from its thiono analogue in bulk.[31] The mechanism behind the reaction was later discussed in more detail by several well-known researchers like *Fukuto, Tammelin* or *Hilgetag*; they came to different conclusions with experimental evidence for their theories.[57-60] Until the late 1990's several researchers found evidence for either the one or the other hypothesis but could not isolate an intermediate structure to completely prove their theory.

Additionally, also discussed are several influences by catalyst molecules like acids or bases as well as metal atoms.[61-63]

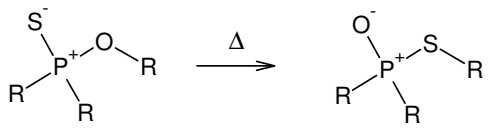

Figure 12: *Shown are the minimum structurally prerequisites for the thiono-thiol rearrangement.*

In Figure 12 the structural unit of the OTP is shown which is involved in the rearrangement reaction. The latest study available, by *Kuntsivich et al*., came to the conclusion that it is best to do some calculations to prove one of the theories right, ending up in a third possible reaction pathway.[64] However, the real nature of this rearrangement is still undiscovered until today and some proposed mechanisms with more or less hard evidence can be found in the literature. Moreover, other rearrangements like the Miyazaki-Neewman-Kwart rearrangement or the Smiles rearrangement are also feasible reaction pathways which do not even require a phosphorus atom at all and show the tendency of sulfur to switch places with oxygen.[65, 66]

Based on the several experimental data basically two proposed mechanisms are discussed: first an ionic process with contacting ion pairs for which two different pathways (intermolecular or intramolecular) are discussed and second a cyclic intramolecular process shall be the true reaction pathway (Figure 13).[58, 59, 67-69]

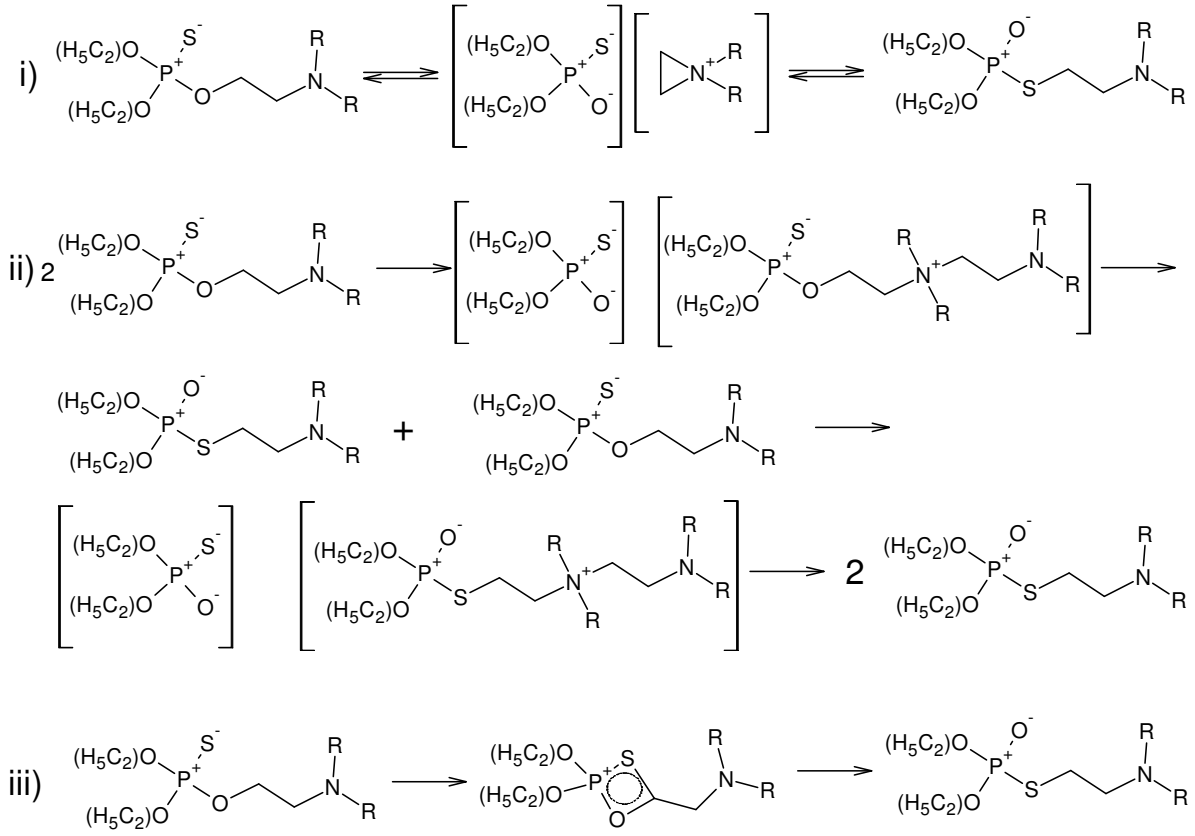

Figure 13: *Proposed mechanisms for the thiono-thiol rearrangement of OTPs. i.) and ii) represent the idea of the ionic mechanisms involving contacting ion pairs. Iii) Exemplifies the idea of a cyclic transition state (four-membered ring).*

All the above hypotheses do have in common that they run smoothly for the system under investigation, however, a general mechanism is not clearly noticeable. From the literature studies it is most likely that one of the proposed mechanisms would also suit for the analyte molecules under investigation.

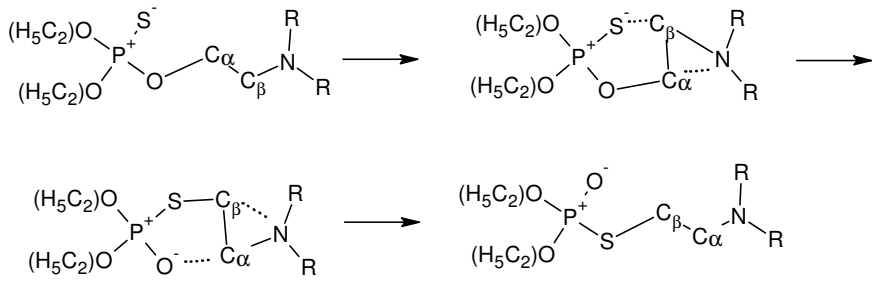

Figure 14: *Depiction of the proposed isomerization mechanism after Kuntsivich et al. during which the C_α and C_β are proposed to switch places and a five-membered ring is formed in the transition state.[64]*

One aim of this thesis is to identify the mechanism for the isomerization of Amiton-like systems under investigation. This is done by establishing a stable transition state by blocking the isomerization reaction or by detecting and isolating the intermediate. Furthermore, the aim was to investigate the kinetic order of the isomerization reaction. The following molecules were identified to be needed for this work:

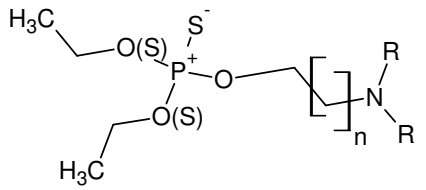

R = Me, Et, *i*-Pr, *t*-Bu and Ph

R-R = $(CH_2)_4$ and $(CH_2)_5$ as ring

n = 1, 2, 3 and 4

Figure 15: *Basic structure of the target molecules to prove the pathway of the thiono-thiol rearrangement of Amiton and Amiton-like structures, where R can be an alkyl (methyl, ethyl, i-propyl, t-butyl) or phenyl moiety or mimic the beginning and ending of a hydrocarbon chain resulting in a pyrrolidine or piperidine ring; n ranges from one to four.*

Theoretically, the stability of the transition state can be increased by chemical design of the starting material: i) Increasing the steric hindrance through more bulky alkyl moieties at the nitrogen atom, should slow down or best prevent the overall rearrangement process; ii) Enhancing the “bridge”-length between oxygen and nitrogen should increase the stability of the proposed transition states, i.e., the quaternary ammonium ion, even to this extent that rearrangement is prevented; iii) proving the calculated transition state of *Kuntsivich et al*.[64] (Figure 14), where C_α and C_β are proposed to switch places a sidechain would have to be introduced in the “O-N-bridge” to make the isomerization visible by NMR-measurements. A different approach could also be to label the carbon or hydrogen atoms selectively to see a difference in the chemical shift values of the participating atoms.

Since none of the molecules is available from any supplier due to strict trade restrictions it was necessary to synthesize them.

There are different methods available to study the thiono-thiol rearrangement of the isomerization reaction. *Tammelin* followed the isomerization by observing the decay of the P=S band in the IR spectrum and the evolution of the P=O band in the same spectra, which is a very rough method.[59] Others followed the reaction later by NMR spectroscopy. The observed reaction orders for the Amiton formation from its thiono form were determined to be first order in 1955 by *Henglein and Schrader*.[70, 71] Later it was reported by *Muller and Goldenson* that the reaction order is not to be of first order but to be in between zero and first order.[72] Only one year later new evidence was found again for the reaction being of first order and a way to indirectly prove the postulated intermediate structure to be a contacting ion pair.[58]

3.4 Basics of Reaction Kinetics

To determine the law of the rate order and the overall reaction kinetics experimentally, basically two methods can be employed: one is the isolation method in which all but one reactant is employed in excess so they can be claimed constant, or the method of initial rates in which the influence of different initial concentrations is investigated. The first method cannot be employed for the thiono-thiol rearrangement since it is an intramolecular process. The rate of the reaction for the conversion of one compound is generally given by the following equation:

$$v = \frac{1}{\nu_A}\frac{d[A]}{dt} \tag{3.1}$$

with: v = reaction rate [mol $L^{-1}s^{-1}$],
[*A*] = concentration of substance A [mol L^{-1}],
t = time [s],
ν_A = molecularity with respect to substance *A* [ ].

The reaction order can be determined if the reaction rates are proportional to the concentration of the respective reactant and can be expressed by the following equation:

$$v = kc_A^{\alpha}\, c_B^{\beta} \ldots, \tag{3.2}$$

with: v = reaction rate [mol $L^{-1}s^{-1}$],
k = rate constant [*dependent of the order of the reaction*],
c = concentration of the respective compound [mol L^{-1}],
A = index for compound A,
B = index for compound B,
α = order of reaction for compound A,
β = order of reaction for compound B.

The power of the concentration of a compound in the rate law is the reaction order of the respective compound. The sum of all powers is the overall reaction order:

$$n = \alpha + \beta + \cdots, \tag{3.3}$$

with: *n* = reaction order
α = order of reaction for compound A
β = order of reaction for compound B.

Strictly, the method of the initial rates is only valuable for simple reactions. For more complicated reactions and forming transition states the kinetics has to be followed over a wider range of the overall reaction and has to be compared to the initial values. To obtain the concentration of a given compound the rate laws need to be integrated since they are differential equations. The solutions of the integrations for reactions of zero, first and second order reaction kinetics are given in Table 1. From these solutions it is possible to obtain relationships of the variables towards time and to give linear plots in which the respective slope yields the rate constant of the reaction.[73]

Additionally, the half-life time of a given compound in the reaction can be used for the determination of the reaction order. Therefore, the initial concentration of the compound of interest is varied and the results are compared with each other.[74]

In most cases the temperature dependence of the rate constant can be modelled by the Arrhenius equation:[75]

$$\ln k = \ln A - \frac{E_A}{RT} \tag{3.4}$$

with: k = rate constant [*dependent of the order of the reaction],*
A = pre-exponential factor,
E_A = energy of activation [J mol^{-1}],
R = gas constant [J K^{-1} mol^{-1}],
T = temperature [K].

By plotting ln k versus $1/RT$ a linear correlation can be obtained in which $-E_A$ is the slope and the y-intercept represents ln A. Therefore, the reactions have to be monitored at different temperatures.

Furthermore, the two Arrhenius parameters A and E_A can be condensed in a single expression, the so called Gibbs energy of activation $\Delta^{\ddagger}G$ which links chemical kinetics with thermodynamics, leading to the following equations:

$$K = e^{-\frac{\Delta^{\ddagger}G}{RT}} \quad \text{or} \quad \Delta^{\ddagger}\mathrm{G} = -RT\ ln\ K \tag{3.5}$$

with: K = equilibrium constant [ ],
$\Delta^{\ddagger}G$ = Gibbs energy of activation [J],
R = gas constant [J K^{-1} mol^{-1}],
T = temperature [T].

Table 1: *Overview of some integrated rate laws according to [73] with v = d[P]/dt.*

reaction order	reaction	rate law	t1/2
0	A → P	$v = k$ $kt = [P]$	$\frac{[A]_0}{2k}$
1	A → P	$v = k[A]$ $kt = ln\frac{[A]_0}{[A]_0 - [P]}$	$\frac{ln2}{k}$
2	A → P	$v = k[A]^2$ $kt = ln\frac{[P]}{[A]_0([A]_0 - [P])}$	$\frac{1}{k[A]_0}$
2	A + B → P	$v = k[A]\,[B]$ $kt = \frac{1}{[B]_0 - [A]_0} ln\frac{[A]_0([B]_0 - [P]}{([A]_0 - [P])[B]_0}$	$\frac{1}{k[A]_0}$

3.5 Synthesis

A lot of different synthesis routes to organo(thio)phosphates and their precursors exist in literature.[76-78] Here, only a brief overview of the different approaches used in this thesis will be given, without claiming completeness to cover the whole literature available to date.

3.5.1 Organo(thio)phosphates

The main synthetic approach used was to couple an amino (thio)alcohol with a dialkylchloro(thio)phosphate (Figure 16) starting from commonly available educts. However, some educts had to be synthesized as they were not available from standard suppliers. Actually, the focus of this work was not to prove whether it is possible to yield an OP or OTP from absolute legal available educts, which would not be traced by any government or would be banned by any law. For sure it is possible to synthesize even the educts used in this thesis from the very raw material like phosphorus or ammonia itself but this would mean quite a laborious work to be done. As an example, $POCl_3$ can be obtained by the reaction of white or red phosphorus with chlorine gas, giving PCl_3 which can be further reacted with oxygen gas to give the desired product. Also other routes exist which are described in a textbook by *Patniak et al.*[79]

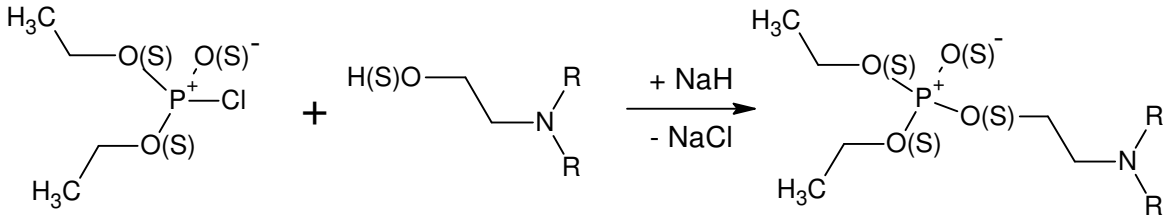

Figure 16: *Basic reaction scheme for the synthesis of OP's and OTP's. A dialkylchloro-(thio)phosphate is reacted with a tertiary amino-alcohol to give the desired O(T)P. R stands for any alkyl group or rings.*

When the desired product is an OP having the sulfur in the thiol form a somewhat 'easier' approach can be chosen since higher temperatures are not affecting the outcome of the reaction. Furthermore drying of the solvent is not necessary since moisture sensitive compounds such as hydride is not needed for the reaction used, but only water. (Figure 17) The desired target compounds can be yielded by the general reaction scheme according to Figure 16. At first glance, the synthesis looks straight forward. However, the formed product heavily depends on the chosen reaction conditions. To yield an OTP with thiol configuration in the amino functionalized moiety or on OP, the reaction can be performed in water, since the higher reaction temperature has no influence on the later chemical constitution at the phosphorus atom. In case of synthesizing the OTPs with thiono configuration the reaction

temperature has to be controlled carefully, since higher temperatures will favor the thiono-thiol-rearrangement and thus result in a mixture of the two compounds instead of a pure product.

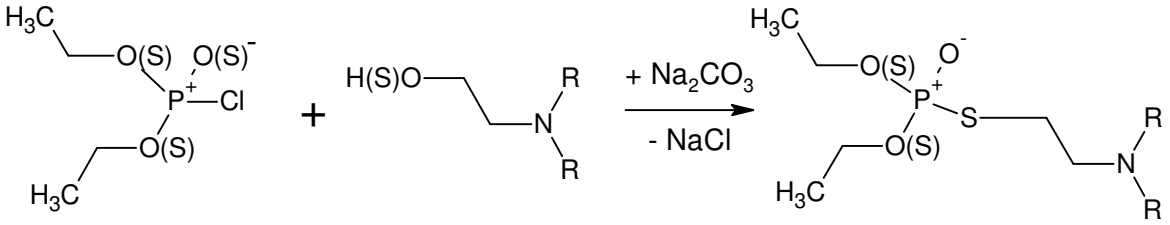

Figure 17: *Basic reaction scheme for the synthesis of OP's and OTP's with the thiol functionality in the amino functionalized moiety. A dialkylchloro-(thio)phosphate is reacted with a tertiary amino-alcohol to give the desired OTP. Of course only one educt has to bear a sulfur atom, either thio alcohol or O(S),O(S)'-diethyl phosphorochloridothioate.*

Amiton itself as the starting OTP from which all the other compounds chemical structures in this thesis are derived was first described by *Ghosh* in 1952.[31] From this publication and later ones by *Gupalo et al*. and *Baldit* the basic reaction pathway was available and promising to yield enough product in one batch for the further investigations planned.[32, 80] Not any hydride can be used in the first reaction step, the formation of the (thio)ethanolate anion. This was examined by *Kashima et al*. who found that in the methylation process of 2-aminoethanol sodium hydride is required to form the ethanolate anion to alkylate the oxygen and therefore forming an ether. In contrast, lithium hydride or calcium hydride is used to 100% alkylate the nitrogen moiety.[81]

Other reaction pathways can be found, e.g. in the text books by *Timperle*y or by *Hartley*.[76, 77] Another comprehensive source of information is the dictionary of organophosphorus compounds.[78] Additionally, a lot of semi-scientific protocols exist in more or less reliable literature resources from the internet, which have its origin from a somewhat questionable background.[82-84]

3.5.2 Amino-alcohol Precursors

From the numerous papers available in the literature two main approaches for the synthesis of amino-alcohols can be identified: The first reaction pathway, which is the preferred one, starts from an amino alcohol with a primary or secondary amine moiety which is reacted with one or two equivalents of an alkyl halide (Figure 18 upper right side).[85] The alkyl halide(s) is/are chosen accordingly to the desired product of the reaction, may it be a symmetrically or unsymmetrically substituted amino alcohol. In the second route secondary amines are converted with ethylene oxide or ethylene sulfide to yield tertiary ethanol amines (Figure 18 upper left side).[86-88] To yield the desired amino thio alcohols a third reaction

pathway can be employed which exchanges the hydroxyl-group *via* a chlorine intermediate with a thiol-group (Figure 18 lower part).[89]

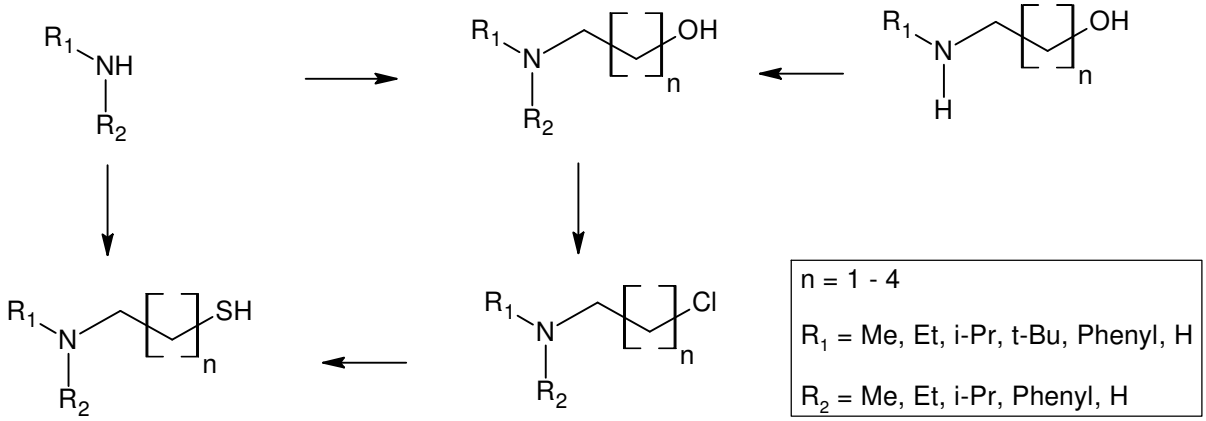

Figure 18: *Different reaction pathways to the synthesis of amino alcohol precursors starting from commonly available educts.*

Larger amino alcohols, like 4-(diethylamino) butan-1-ol, can also be obtained from lactone esters with the use of DIBAL-H.[90] Aminoalcohols having a longer alkyl chain between the alcohol functional group and the nitrogen atom and branched side chains on the alkyl backbone have been patented in 2008 by the Kuraray Co. Ltd.[91] Another elegant route is the use of ethyl diethylaminoacetate being converted to the respective amino alcohol by using lithium aluminium hydride and water to hydrolyze the intermediate.[92] The advantage of this approach is the less laborious work up compared to the other routes described so far. Last but not least to introduce aryl groups at the nitrogen a copper catalyst has to be used since those substituents are large compared to regular alkyl groups.[93]

Moreover, the syntheses on a larger technical scale is described in patent literature dating back up to 1945 and involve high pressure or are modern and need complex catalytic systems and are thus also not applicable for syntheses with standard glass ware.[94-100]

3.5.3 Dialkylchlorothiophosphate Precursors

The synthesis of this compound class was reported for the first time by *Carius* in 1861.[101] Nearly one hundred years later a review on the preparation was published by *Fletcher* in 1950.[102] Generally two main routes exist in literature for the preparation of dialkylchloro(thio)phosphates. An approach by *Mastin et al.* (Figure 19) can be used to prepare S,S-diethyl phosphorochloridodithioate and diethyl phosphorochloridotrithioate. [103, 104] Unfortunately the reported yields of about 22% are very poor.

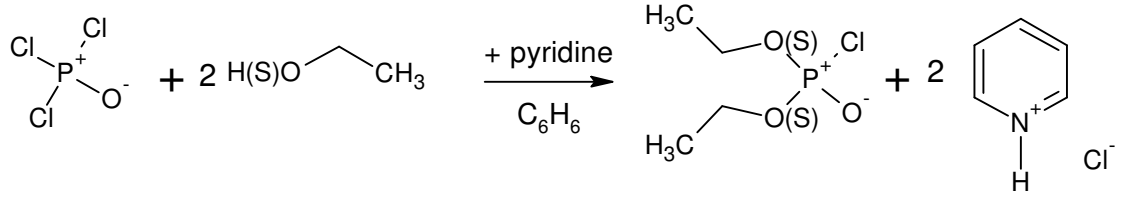

Figure 19: *Reaction pathway for the synthesis of dialkylchlorodithiophosphates according to Fletcher.[103, 104] $POCl_3$ is reacted with two equivalents of thio ethanol in benzene to which 2 equivalents of pyridine are added to catch the forming hydrochloric acid.*

A second reaction pathway is given by *Regel et al*. (Figure 20) which yields about 60 to 70% depending on the used (thio) alcohol precursors.[105, 106]

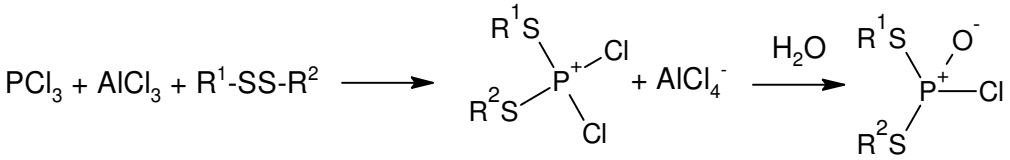

Figure 20: *Reaction pathway for the synthesis of dialkylchlorodithiophosphates according to Regel et al.[106] Aluminium chloride is dispersed in phosphorus trichloride and reacted with the respective dialkyl disulfide. In a second step water is added and the desired product can be obtained.*

For the preparation of O,S-dialkyl phosphorochloridothioate and O,S-dialkyl phosphorochloridodithioate either the mono alkylated byproducts of the above synthesizes can be 'reused' and reacted a second time with the respective (thio) alcohol or a reaction pathway offered by *Lippman et al.* can be employed.[107]

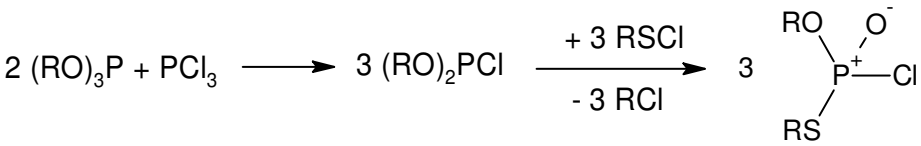

Figure 21: *Reaction pathway for the synthesis for mixed dialkylchlorothiophosphates according to Lippman et al.[107]. Phosphorus trichloride is reacted with trialklyphosphite in the first place. In the second step the yielded dialkyl phosporochloridoite is reacted with an alkyl sulfenyl chloride to give the mixed dialkyl phosphorochloridothioate.*

3.5.4 Quaternary Ammonium Salts

The advantage to use quaternary ammonium salts for many pesticides is that those salts are usually very stable, prevent aging of the molecules and makes them water soluble. All these properties are useful for the application of pesticides within the frame of the desired purpose. Another aspect of preparing those salts can be the purification of a crude product or the possibility to add other substances to the now solidified molecule like dyes or other auxiliaries. The procedures for preparation are widely published, starting off with patents for historical reasons.[108, 109] Mainly oxalic acid (*cf*. Figure 22) was used to form those salts.[32] Other possibilities are to use dry hydrogen chloride or *p*-toluoenesulfonic acid.

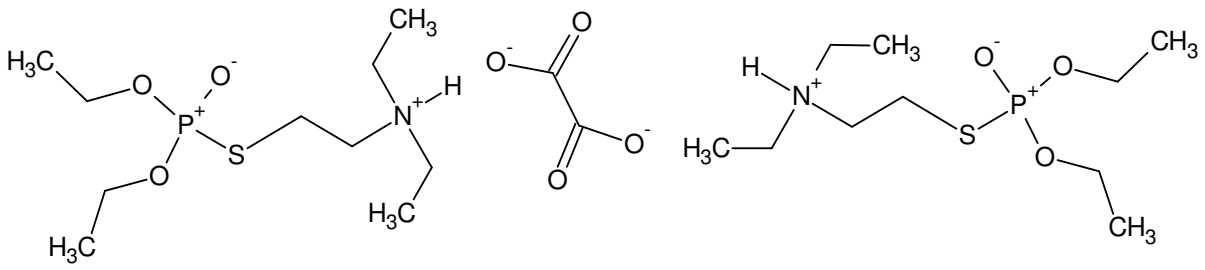

Figure 22: *Example for a quaternary ammonium salt for Amiton with oxalic acid as it was prepared by Baldit et al.[32]*

A general aspect in the preparation of these salts, especially for OPs bearing a basic moiety, is that water and even moisture complicates the formation of these salts. But, once formed they are quite stable for a while.[110] Basically, they are easily formed by adding equivalent amounts of the respective OP or OTP to an acid or acidic compound. The formation can generally be assisted by applying heat over a longer period of time and small amounts of solvent. For the compounds under investigation in this thesis heating has to be minimized since the OTP readily tend to isomerize.

A second reaction pathway which can be used is the direct alkylation of the tertiary ammonium compound by an alkyl halide, where the halide is most often iodide or bromide. Also this reaction pathway was patented very early by some American researchers from Campbell Pharmaceuticals (Figure 23) which shows that this technique was and still is of great importance for this industry branch since many pharmaceuticals have to be delivered into the body system of the patient.[111-114]

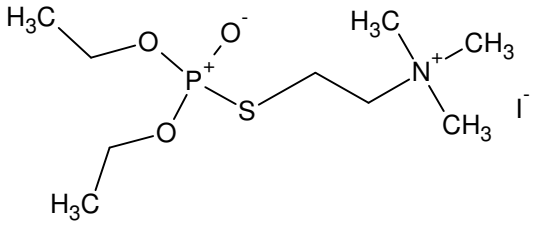

Figure 23: *Example for the alkylation of an OTP, namely Echothiophate, which is a drug used as an ocular antihypertensive.[114]*

The resulting quaternary ammonium salts are many-fold more soluble in water then the tertiary ammonium compounds which makes them even more toxic since the human body system is mainly consisting of water. Today the preparation of quaternary ammonium salts is a basic preparative skill of any chemist and general procedures can be found in a lot of text books.[115-118]

For all the possible salts of V-agents, yielded by the above reactions, no single crystal structure has been reported yet.

3.6 Biological Effects of Organophosphates

Amiton as an organophosphate is known to be a strong AChE inhibitor and therefore also the derivatives investigated in this thesis could possibly have an unneglectable inhibiting capacity themselves for this enzyme.[119] Additionally, the interaction with BuChE, which also belongs to the family of α/β-hydrolases, is of great importance since this enzyme is more ubiquitous in the human body and is chosen as a therapeutic for organophosphate poisoning.[120] However, the inhibition of the AChE causes a cholinergic crisis of the nervous system and therefore results in acute and even chronic toxicity. Hence, the measurement of this inhibition capacity is crucial for evaluation and estimation of mammalian toxicity.

For their investigations on the mechanism of the chemical transmission of nerve impulses *Dale and Loewi* were awarded the Nobel Prize in physiology or medicine in 1936.[121]

3.6.1 Enzyme Inhibition

The commonly accepted mechanism for organophosphate poisoning is the binding to a serine moiety in the active site of the enzyme.[122]

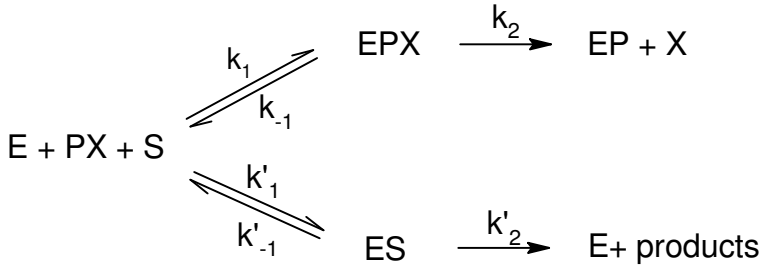

Figure 24: *Depiction of the possible reaction pathways for the enzyme (E) with substrate (S) and phosphor organic substance (PX) The upper pathway competes with the lower pathway which is the usual reaction when no inhibitor is present.[123]*

A measure for the first reaction step is the dissociation constant K_D which depends on the affinity of the inhibitor or substrate for the active site of the enzyme: smaller values of the constant indicate higher affinity of the inhibitor/substrate to the active site. The second step is determined by the phosphorylation ability of the inhibitor, which is measured by the phosphorylating constant k_2, which is a monomolecular rate constant.

Since in the last step of the upper reaction pathway in Figure 24 the enzyme is irreversibly bound to the products, more and more enzyme molecules are used up if the concentration of the OP-substance is large enough. Additionally, the second reaction step, which frees the

leaving group X, is faster than the reaction leading backwards to the educts. Thus the upper reaction is a quasi-irreversible reaction. Whereas the lower reaction pathway in Figure 24 represents the classical enzyme reaction model, in which the enzyme is freed again after the reaction to start a new reaction cycle.

3.6.1.1 Mode of Action of OP's and OTP's

Regularly, the ACh molecules are located in the synaptic vesicles in the cytoplasm of cholinergic nerve terminals. The release is triggered by nerve impulses and the molecule is entering the synaptic cleft. Therein the molecules immediately bind to the membrane upon which they are instantaneously hydrolyzed by AChE into choline and acetic acid.[124] Any delay in this process causes a prolonged excitation and thus permanent transmission of nervous impulses. OPs as well as carbamates have the potential of inhibiting the AChE molecule. The Inhibition occurs as a result of the phosphorylation of a serine moiety in the active center of the enzyme.[125] Moreover, the mode of action is a combination of the phosphorylation process and the binding affinity at the active site.[126] The overstimulation of the released neurotransmitter ACh causes a so called cholinergic crisis and results in an end-organ overstimulation.[127]

Compared to AChE the BuChE is more widely available in the body. It is synthesized in the liver and secreted into the blood system. Thus it is easier to extract and better available for testing outside the body. It is also a serine esterase and its activity can also be hampered by OPs. Hence, it is used and stockpiled by the US government for protection against nerve agents. It has the function of a scavenger molecule in this sense of use.[41] AChE would also be possible to use for this purpose but the half-live time in the body and the non-availability in large quantities make it rather unattractive for this purpose.[128] Moreover, it was found out that BuChE acts as detoxifying agent of the body and protects the neurotransmitter function of AChE.[129]

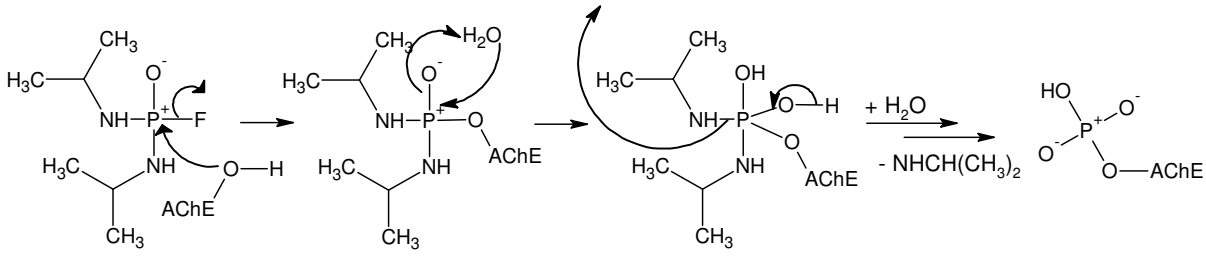

Figure 25: *"Proposed mechanism of inhibition and aging of MIP on AChE proceeds by net loss of isopropylamine groups. The exact mechanism (SN1 or SN2) of aging is not known but is shown here as SN2. The aged moiety is shown in its expected ionization state at pH 8.0."[130]*

However, in some cases the inhibition is reversible by the treatment with BuChE, certain oximes or atropine. In some cases this treatment is not successful, since the hydrolysis of

the inhibited enzyme is that fast that no more leaving groups are available at the inhibitor and thus an aged complex is formed which can no longer be reactivated (*cf.* Figure 25).

3.6.1.2 Structure-Activity-Relationship

The described toxicity towards the inhibition of AChE and BuChE does also play a major role in the poisonous action against insects. Phosphorylating agents have been synthesized in a huge number with the objective of minimizing the mammalian toxicity problem while maintaining high toxicity to insects.[131]

Toy and Walsh published a summary on major phosphorus insecticides commercially produced and discussed the structural requirements for useful activities.[132]

Mainly the compounds have to be a methyl or ethyl ester and the phosphorus has to bear either a phosphoryl or thiophosphoryl group. Additionally, a good leaving group has to be present as well, which can be aryloxy like in Parathion or heteroaryloxy like in Diazinon.[133] Other good leaving groups include phosphate as in Schradan or thioxy as in Amiton.[42, 131, 134, 135]

A comprehensive overview on the structure-activity-relationship and the use of OPs as also therapeutics was given by *Čolović et al.*[136] Therein it is shown that for example fluorine is a very good leaving group as is the case in the chemical warfare agents Sarin or Tabun. However, also the alkyl substituents of the thioxy group do have an influence since they mainly direct the interaction of binding.[137, 138] The diisopropyl substituent, e.g. of VX, has a higher binding affinity as the diethyl substituent in Amiton.[39] Last but not least the phosphorus coordination being a phosphonic acid derivative does have a stronger interaction than a phosphoric acid derivative. Numerous investigations on these structure-activity-relationships can be found in the literature.[139-142] For example the study by *G. Schrader* can be named in which a lengthy variation of the chlorine substituents position on a benzene-ring in case of the insecticide Chlorthion is discussed.[143]

3.6.2 Inhibition Kinetic Studies

Whether or not an organophosphorus substance is of relevance regarding its toxicity value can only be determined by investigating the interaction with an isolated enzyme, whole blood serum from the species of interest or by *in vivo* experiments. Since the Chemistry Section of the CDSEP School is not allowed to handle whole blood serum or to execute experiments, because it is not a medical facility, all investigations were performed with isolated enzymes. In this case the toxicity values can be compared with each other to give an indication of the i*n vivo* toxicity by correlating them *via* known substances to *in vivo*

studies results from other investigators. Moreover, the determined values can be compared to literature values.

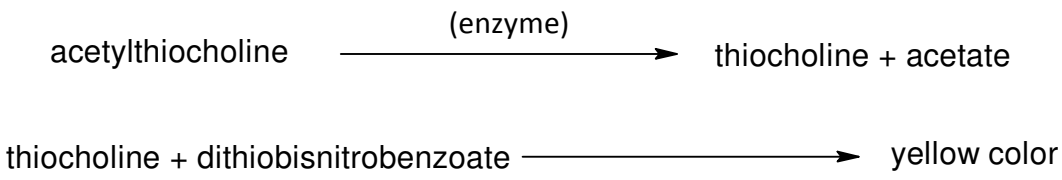

Figure 26: *2-Step reaction pattern for the colorimetric determination of the enzyme activity according to the Ellman essay. The expression yellow color stands for 2-nitro-5-thiobenzoate which is deprotonated in basic and neutral media and in these conditions is giving a yellow color impression (cf. Image 6).*

For inhibition kinetic studies a classical Ellman essay can be used.[144] A good summary of this state of the art technique and its application towards inhibition kinetic studies can be found in the work of *Worek et al*.[145] The enzymes of interest are AChE and BuChE, especially AChE form electric eel and BuChE from equine serum. Noteworthy, the structure and catalytic activity of enzymes vary from species to species and might even depend on the extracted tissue of one species, such as liver, heart or kidneys. For this reason the enzymes used in this study were chosen according to the available literature studies to compare the results with already existing values from literature.[146-150] Moreover, the price of AChE and BuChE increases dramatically the more likely the species, they were isolated from, is to humans.

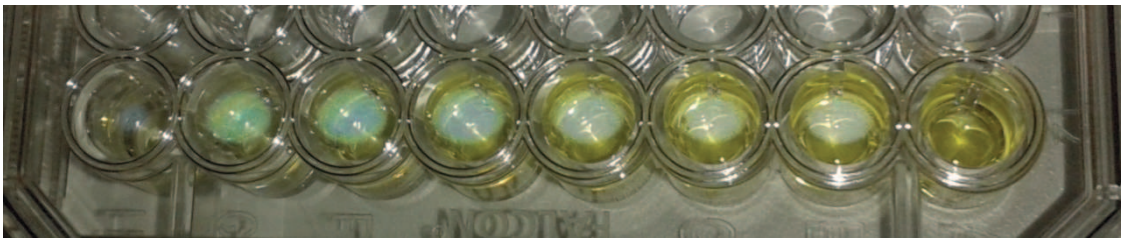

Image 6: *Shown is the typical yellow color of the Ellman essay from the reaction of thiocholine with dithiobisnitrobenzoate on a 96-well plate. Each well was spiked with a different amount of organophosphate inhibitor. Amounts decrease from left to right.*

In principle the enzyme reacts with its substrate acetylcholine or acetylthiocholine to yield acetate and the respective choline as the reaction products (Figure 26). In a second step the choline fragment is reacting with dithiobisnitrobenzoate to result in a yellow color impression (Image 6) which has an absorption maximum at 412nm.[151] Since this second step is fast, this reaction pattern can be easily used to monitor the enzyme reaction. Besides this well-established procedure also other techniques, e.g. microdensitometry or microphotometry, can be used to monitor AChE activity in tissue sections.[152]

For the determination of the relevant data, like the molar inhibition constant k_i, a continuous or a discontinuous method can be employed. In the discontinuous method two data points are used to determine the slope of the curve. Therefore a certain amount of enzyme and a certain amount of OP/OTP are reacted with each other and two samples at different reaction times are taken and the absorption values are determined. The resulting slope represents the inhibition constant at the given OP/OTP concentration. To yield the molar inhibition constant the following equation can be used:[153]

$$k_i = \frac{1}{[OP]t} ln \frac{v_0}{v_t} \qquad \textbf{(3.6)}$$

with: k_i = molar inhibition constant,
[OP] = concentration of OP/OTP,
v_0 = reaction velocity at time 0,
v_t = reaction velocity at time t.

In general it can be said that larger k_i-values represent stronger inhibition of AChE, i.e. analytes with large k_i-values are more poisonous than compounds with lower inhibition constants. If it is possible to monitor the reaction pathway over a larger period of time the absorption curve reaches a plateau and the calculation is somewhat more laborious but results in more precise numbers. This is due to the fact that the plateau consists of more data points and thus has a smaller error compared to the slope of the initial data points of the absorption curve. Actually, more than one OP/OTP concentration has to be measured no matter which method is employed. The data evaluation for the continuous method has to be done according to the theory of *Forsberg and Puu*:[146]

$$\frac{\Delta t}{\Delta \ln v} = \frac{K_d}{k_2} \frac{1}{[OP](1-\alpha)} + \frac{1}{k_2} \qquad \textbf{(3.7)}$$

with: K_d = dissociation constant,
k_2 = unimolecular phosphorylating constant,
[OP] = concentration of OP/OTP,
α = $[S]/(K_M - [S])$ *where:*
[S] is the substrate concentration and
K_M is the Michaelis-Menten constant.

Thus, from a plot of $\Delta t/\Delta \ln v$ against $1/[OP](1-\alpha)$ (secondary plot), K_d is determined as the reciprocal value of the intercept on the abscissa and k_2 as the reciprocal value of the intercept on the ordinate.[146]

3.7 Analytics and Detection

The most important information about organophosphates is their toxicity. Therefore the determination of the inhibiting capacity of AChE or BuChE is of great relevance. Knowing these values makes the handling of the compounds not saver but gives a somewhat better feeling about the potential risk of the compound. Furthermore it is of great value for the medical staff which has in worst case to deal with poisoning.

Additionally the full characterization of the molecules, which was not always done in the past, or better to say not always made publically available, is essential to have, since only then an exact recovery and clear identification can be successful. To achieve this goal, also sample preparation techniques for example for the recovery of the analyte from the environment should be available.

A lot of methods and procedures are known from the literature which focuses especially on the analytics and detection of chemical warfare agents and their degradation products. They can roughly divided into several groups of analytical tasks: literature on the detection in food samples [154, 155], field portable instrumentation and methods [156-158] or literature dealing with individual compounds [159, 160] or individual methods [52, 161] and last but not least the identification of adducts in the human body [162, 163].

3.7.1 Vapor Pressures

3.7.1.1 General Considerations

The vapor pressure is the physico-chemical parameter that is linked to the saturation equilibrium concentration of the analytes to be detected. The knowledge of the gas phase concentration of the analyte is essential for the definition of the air volume that needs to be sampled for exceeding the limit of detection (LOD) of the applied detector system. In case of substances being toxic or harmful by inhalation or direct contact with the skin, the early detection is of great importance for obvious reasons.

The today's standard mobile analytical instruments of civilian and military action forces are based on technologies like ion mobility spectroscopy or gas chromatography coupled to mass spectrometry and can thus only detect airborne substances without laborious sampling and sample pretreatment procedures.[156, 157] Moreover, if the vapor pressure of a substance is very low, the compound poses only little threat to living beings by inhalation but is therefore more persistent in the environment and causes a severe threat upon direct contact. However, the vapor pressure data can also help to estimate a hazardous area and time frame after the release of such substances. For OTPs only a small number of values

on the vapor pressure of pesticides and especially chemical warfare agents are reported in literature so far [32, 164] and their detectability is thus hard to predict. Using the ideal gas equation the saturation concentration c_{sat} of an analyte can be calculated from its vapor pressure:

$$c_{sat} = \frac{p_{sat} \times M}{R \times T} \quad \textbf{(3.8)}$$

with: c_{sat} = saturation concentration [mg L^{-1}],
p_{sat} = saturation vapor pressure [Pa],
M: = molecular weight of the analyte [kg/mol],
R: = ideal gas constant (8.31446 J mol^{-1} K^{-1}),
T: = temperature [K].

The vapor pressure is also an essential parameter in a multitude of models for evaporation of droplets.[165-167] However, the described thiono-thiol rearrangement of organo(thio)phosphates can have an impact on the determination of the vapor pressure data since the isomers have different vapor pressure values. Thus, measurements with isomer mixtures will result in mixed vapor pressures weighed by the molar ratio of the isomers according to Dalton's Law of partial pressures for a binary mixture.

3.7.1.2 Transpiration Method Setup

The transpiration experiment has been newly established in the research group of Prof. Klapötke at the University of Munich. The method was adapted from the existing experimental setup of Prof. S. Verevkin from the University of Rostock.[168-170] The basic principle of the transpiration experiment is to saturate a well-defined carrier gas stream at a temperature T_{exp} and to measure the concentration of the analyte within. Additionally, this method has not yet been approved for the general applicability for the investigation of highly toxic and thermo-labile compounds.

The transpiration method setup is also suitable for the purification of the analytes during the experiment. Prior to the experiment the analyte is conditioned by subjection to the carrier gas stream at elevated temperatures for the removal of impurities.

3.7.2 Field Detection with Military Equipment and Instruments

Amongst the forces in the security sector around the world a large variety of different equipment for the fast detection and monitoring of hazardous substances can be found.[171, 172] These can range from a simple detector paper over hand-held devices to the most complex instruments. In the Bundeswehr CBRN-forces the hand-held devices and

methods used are: the chemical agent detector paper, the Dräger test tubes, the IMS-technique which can be found in the LCD 3.3 and the RAID-M 100 and the First Defender RMX based on Raman spectroscopy as well as the Hazmat ID IR spectroscopy instrument. Additionally, the Inficon Hapsite ER mobile GC-MS system is used within the Bundeswehr which has unfortunately strong limitations regarding the detectability of molecules heavier than mustard since neither the GC-inlet nor the interior of the instrument, e.g. valves and ion source, can be heated to higher temperatures and therefor prevention of inside contamination is nearly impossible. The bigger instrumentation devices are mounted inside the FOX recce vehicle and are the mobile mass spectrometer MM1 and MM2 and were both built by Bruker Daltronik GmbH. In the following section the different instruments and analytical methods are briefly described for a better understanding of the underlying measurement principle.

3.7.2.1 Chemical Agent Detector Paper

The chemical agent detection paper allows the fast detection of chemical warfare agents. This is due to a reaction of the target molecules with one or more of the three different dyes immobilized on the paper.[173] Depending on the type of chemical agent (blister or nerve agent) a different color occurs after contact (Image 7).[171] This kind of detector paper is provided to NATO by the Canadian authorities and is able to detect CWA's as liquids and vapors, whereas the commercially available detector paper is not capable of the detection of vapors.[174]

Image 7: *3-Way chemical agent detector paper booklet: The three colored bars on the left hand side are for referring the color indication to the chemical agent substance class. G = G-type nerve agents (yellow), H = blister agents (red) and V = V-type nerve agents (dark green).*

There also exists a chemical agent detector paper for training purposes which is designed to give a color reaction with the Bundeswehr chemical agent simulant substance which mainly consists of glycerin and citric acid and therefore is nothing else as regular pH-paper. Since all synthesized substances are of light basic character no color reaction is expected to occur on this type of detector paper.

3.7.2.2 Dräger Test Tubes

The Dräger test tubes are fast and reliable in detecting air borne substances. A lot of different substances can be detected by the appropriate test tube. The reaction scheme of the test-tube for phosphoric acid esters, according to the manufacturer, is as follows:

a) 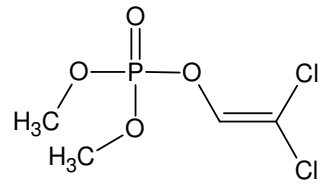 + cholinesterase ⟶ inactive enzyme

b) butyrylcholine iodide + H_20 ⟶ butyric acid

c) butyric acid + phenol red ⟶ red reaction product

The phosphoric acid ester 0.05/a test tube (Image 8) which is calibrated towards dichlorvos (2,2-dichlorovinyl dimethyl phosphate), is used in the Bundeswehr for the detection of G- and V-type nerve agents since the test tube has a broad cross sensitivity for other phosphoric acid esters.[175]

If phosphoric acid esters are present the enzyme is inactivated and butyric acid will not form, thus the weak alkali solution colors the indicating layer red and must be stable for one minute. If the enzyme remains active, phosphoric acid esters are not present, and the indicating layer remains yellow because of butyric acid formation.[175]

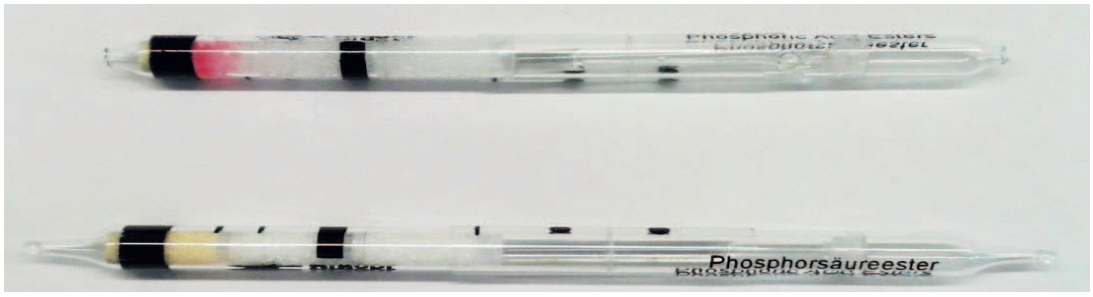

Image 8: *Depiction of the Dräger test tube for phosphoric acid esters detection: The Upper test tube shows a positive reaction result indicated by the red color on the left hand side of the test tube. In the lower part of the picture a new and sealed test tube is shown as a reference.*

However, the standard deviation of the above reaction sequence in the test tube is quite large. The error for quantification by this method is about 30%![175] With this large uncertainty the method is very unreliable and false negative results could lead to fatalities amongst the people feeling save due to the incorrect response. Therefore, there is an urgent need to improve the hand-held detection methods

3.7.2.3 Ion Mobility Spectrometry

Ion mobility spectrometry was originally invented as a laboratory instrumentation setup but has become nowadays an import field applicable technique which can be found at almost

every airport in the world for the detection of explosives. Moreover this technique is widely used amongst security sector forces like fire fighters, police and the military.[176] Within the military these technique is used for the detection and monitoring of chemical warfare agents. For this fast growing community of users and numerous applications Springer launched the publication of the International Journal of Ion Mobility Spectrometry in 1997.[5]

In the Bundeswehr two devices are implemented for the detection of chemical warfare agents using the IMS technology. These are the Smiths Detections' light weight chemical detector, LCD 3.3, and the Bruker Raid-M 100 (Image 9). These instruments were deigned to detect several CWA's but do also have a large cross sensitivity towards other chemical compounds and thus can easily lead to false positive results or misinterpretations since the underlying databases are limited in the number of entries. A critical evaluation of the Raid-M 100 for the detection of CWA'S was performed by the Edgewood Chemical Biological Center in 2003.[177]

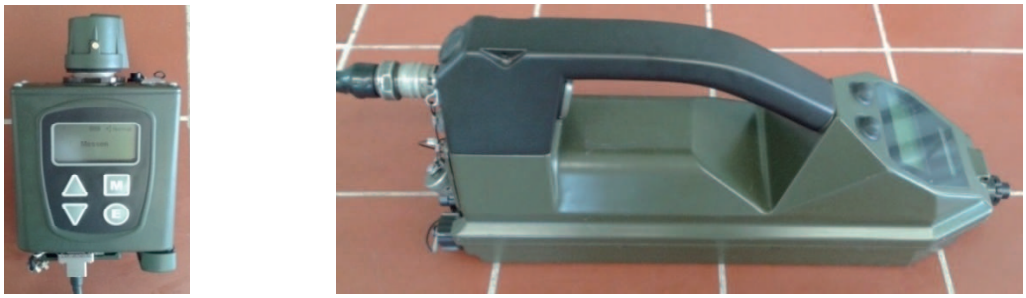

Image 9: *Depiction of the Smiths Detection LCD 3.3 (left) and the Bruker Raid-M 100 IMS instruments which are used in the Bundeswehr. Both can be connected to a Laptop PC for remote control and data recording.*

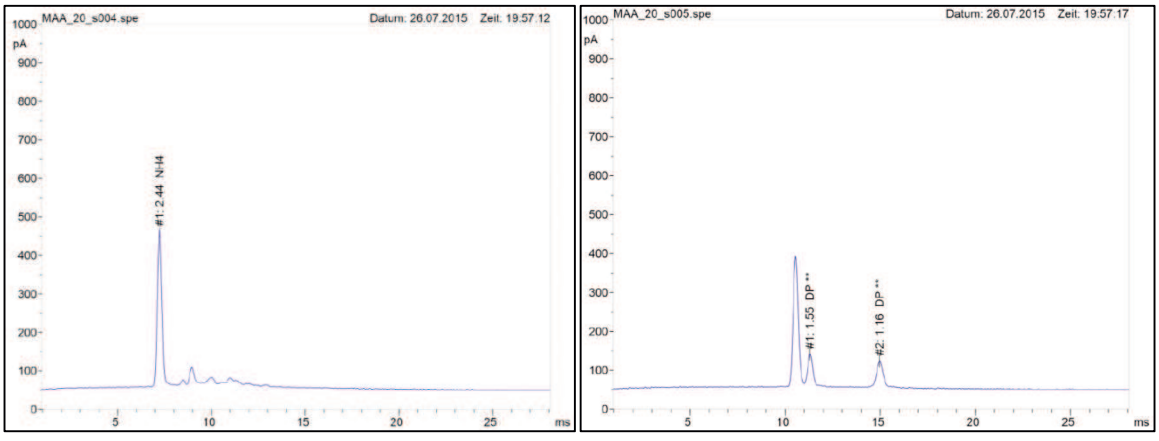

Figure 27: *Examples of IMS-chromatograms for a blank measurement (left) with the dopant peak of ammonia and that of the measurement of compound* ***XXII*** *(right) where the dopant peak is gone, because the concentration of the analyte is high enough that several clusters could be formed.*

[5] http://link.springer.com/journal/12127

A basic construction scheme for the elucidation of the measurement principle of these instruments is depicted in Figure 28.Molecules entering the ionization chamber collide with the reactant ion cluster molecules to form positively or negatively charged clusters. Depending on the concentration of the analyte, monomer or dimer clusters can be formed resulting in two or more peaks in the respective IMS chromatogram (Figure 27)[178].

When the gate to the drift tube is opened the clusters and other molecules can enter and thus are exposed to an electric field which accelerates the cluster ions. To assist the separation process a so called drift gas is flushed in the opposite direction of the drift path. The corresponding drift time directly correlates with the mass of the ion clusters formed during the ionization process, their cross-section and electric charge[179]. A full scientific description of the main chemical processes in the instruments and different methods of coupling this method with other detectors can be found in various text books and review articles.[180-183]

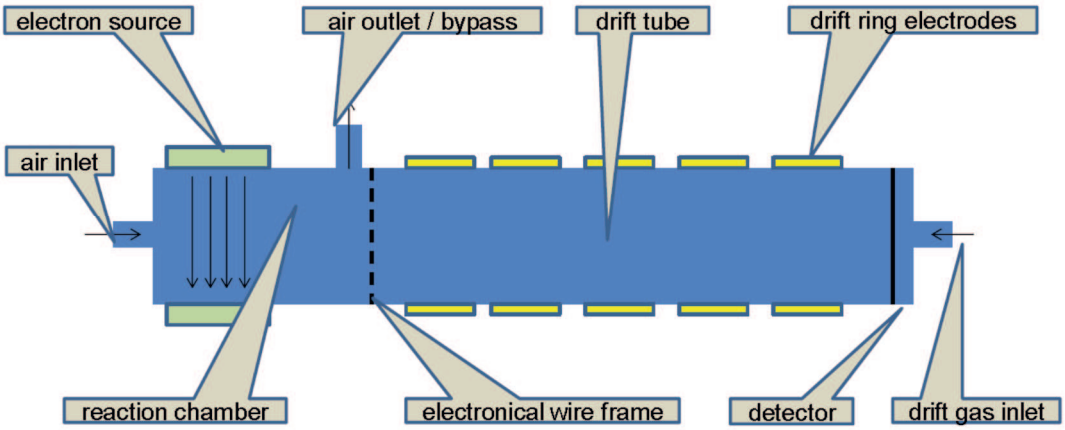

Figure 28: *Schematic drawing of a typical IMS drift tube.*

According to the Mc Daniel – theory the ion-mobility is given by [184, 185]:

$$K = \frac{3e}{16N} \cdot \sqrt{\left(\frac{1}{m} + \frac{1}{M}\right) \cdot \sqrt{\frac{2\pi}{kT}} \cdot \frac{1}{\omega_D}} \qquad \textbf{(3.9)}$$

with:

	K	= ion-mobility
	M	= mass of neutral drift-gas molecules,
	m	= mass of the respective cluster ion
	ω_D	= average collision diameter
	e	= electron charge
	T	= temperature
	k	= Boltzmann-constant
	N	= gas density

The resulting detector signals can be correlated from one instrument to another by the comparison of their reduced mobility constant K_0 which is given by [186]:

$$K_0 = \frac{d \cdot T_0 \cdot p}{E \cdot T \cdot p_0 \cdot t_D} \quad \textbf{(3.10)}$$

with:
- K_0 = reduced mobility in [$cm^2 \cdot V^{-1} \cdot s^{-1}$],
- d = length of the drift-tube [cm]
- T_0, p_0 = temperature at standard conditions (273,15K and 760torr) and pressure respectively
- p = atmospheric pressure at recording time [torr]
- E = electric field inside the drift-tube [$V\ m^{-1}$]
- t_D = measured drift time [s]
- T = temperature inside the drift-tube [K]

The main differences of both devices are the different limit of detection and the ionization source used. The LCD 3.3 uses a corona discharge device, whereas the Raid-M 100 uses a radioactive β-source (100 MBq ^{63}Ni). In the corona discharge device the electrons are accelerated by an electric filed to reach the energy levels needed for ionization, whereas in the β-source device the electrons have high energy levels and thus need to be moderated to reach the needed energy levels. Hence, different energy level distributions are found in the two devices and therefore the ionization processes can be different. The Ni^{63}-source has an average energy level of about 17 keV and a maximum energy reached by the β-emission of about 67 keV.[187]

Moreover, the LCD 3.3 is comprised of two separate drift tubes, one for positive mode and one for negative mode to be measured at the same time. Although the RAID-M 100 is larger compared to the LCD 3.3 it has only one drift tube, which is longer and hence is supposed to have a better resolution. However, it has the disadvantage that it has to be switched between positive and negative mode for the detection of the respective positive and negative clusters.

Due to the enormous number of possible molecules being detectable in the vapor state the number of false positive as well as of false negative results is rather high. Therefore, it is of great importance to know for which scenario the library of the instrument was set up for.

Both instruments display incremental bar-levels during a measurement if there is a hit in the library. According to the manufacturers these bar-level readings can be used for quantification. Since these bar-levels differ from substance to substance and are dependent on several other effects like temperature and outside air pressure a reliable quantification result is hard to obtain. Moreover, the performance of the instrument cannot be checked in

the field, because special software is needed to have a look at the originating IMS-chromatogram and check for the amount of reactant ion peak present. The recovery of this reactant ion peak after the first measurement is crucial for a trustworthy result in the next measurement for the reason that, if there are no reactant ions in the system, hardly no target molecule clusters can form. The effect of an “overdose” by the analyte can be seen in Figure 27. There the dopant peak in the chromatogram on the left hand side is totally gone (exhausted) by interaction with the analyte molecules, as can be seen on the right hand side. The total recovery takes several minutes meaning that only a smaller number of dopant molecules is able to interact with another or a different substance shortly after. Additionally the calibration of the instrument will totally fail and no alert will be reported at all. Moreover, the limiting property for the detection of a specific substance is its concentration in the air which is directly related to the vapor pressure of the substance.

Table 2: *Compilation of the library entries regarding the detection of chemical warfare agents for the IMS-instruments used by the Bundeswehr.*

instrument	library entries
LCD 3.3	VX, VXR, GA, GB, GD, HD, HN, CY
RAID M 100	VX, GD, GB, GA, HD, L, AC, HD, HN

In general the Bundeswehr instruments were developed to detect CWA’s. Since the Chemistry Section of the CDSEP School has advanced software packages for each instrument it is possible to compare the results displayed on the instruments with the originating ion mobility spectra and the determination of the non-instrument specific K_0-values.

3.7.2.4 Flame Spectrophotometry

A flame spectrometry detector offers a different approach towards the detection of airborne substances like gases, aerosols dust and particles. As a rule atomic elements give specific light emitting spectra if they are burned in a hydrogen flame. This attitude is especially useful for the detection of sulfur, phosphorus, potassium, sodium and many other elements.

Since chemical warfare agents mainly bear either one or two atoms of a kind in their molecular structure the presence of such compounds will be easily detectable by the appearance of the respective characteristic emitted light. The AP4C from Proengin (Image 10) is such an instrument which will be mounted on a new detection vehicle of the Bundeswehr and thus will be capable of the detection of many different chemical compounds. Since the instrument has no specific database it cannot be used as an identification device, but as a warning and alerting instrument, which gives a hint to the compound class. However, all nerve agents such as Sarin, Soman, Tabun or VX contain

phosphorus; all blister agents, such as mustard gas and lewisite contain either arsenic of sulfur, all blood agents contain arsenic or emit a HNO molecule when burned in a hydrogen flame.[188]

Image 10: *Photography of the AP4C from Proengin.*

Thus, this technique seems to be quite comparable to an atomic emission detector which can be coupled with a GC system. The difference is that the AED device uses helium plasma instead of a hydrogen flame to generate the element specific emissions.

The AP4C is set up that way that way that the warning and alerting limits are set to the individual exposure guideline levels of the compounds containing sulfur, phosphorus and the other detectable elements. A basic scheme of the display and the different detection channels is given in Figure 29.

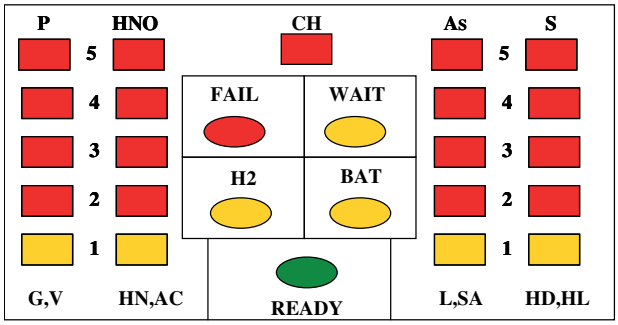

Figure 29: *Basic scheme of the display of the AP4C from Proengin showing the different detection channels and the status signals. The schema was provided by Proengin company and allowed to be reproduced in this thesis.[188]*

In general the instrument does not need a purge after performing the measurement since all parts of the system are heated by the burning hydrogen flame and thus a steady cleaning is performed. Moreover, it is possible to not only measure substances which are airborne by themselves but to use a little heating device, called liquid agent device (Image 11), which can be dipped into liquids or onto surfaces and from which the adsorbed substances are evaporated and thus introduced into the instrument. This special feature seems to be superior compared to the LCD 3.3 or the Raid M since they have so called cold zones inside onto which the non-volatile compounds get adsorbed and therefore will always produce artefacts.

Image 11: *Photography of the liquid agent device (rigth) to be used with the AP4C from Proengin and the pipe bowl (left) to use with it.*

3.7.2.5 IR and Raman Spectroscopy

IR and Raman spectroscopy are both not new techniques but they have found their way into the security sector since the instruments used seem to get more compact during the time. The hand-held Raman spectrometer First Defender RMX (Image 13) is such an instrument and is widely used amongst the military. The Bundeswehr employs these instruments mainly in the field of explosives detection with the EOD-forces as well as in CBRN related situations with the CBRN forces.

Image 12: *Photography of the Hazmat ID from Smith Detection.*

The CDSEP School in Sonthofen is one of the two training facilities amongst the Bundeswehr for EOD specialists and responsible for the database development. Hence, the measured spectra can directly be used for building these databases. The same holds true for the HazMat ID 360 IR spectrometer from Smiths Detection (Image 12), which cannot really said to be handheld since it comes in a quite large box compared to the First

Defender RMX. However, it has a big advantage, since the instrument itself can be directly used in the “hot-zone” and easily dipped into a decontamination solution after the job is finished.

The use of Raman spectroscopy with the First Defender RMX is some cases superior to the IR spectroscopy due to its “gooseneck” with which it is possible to measure substances from a distance and through containments. This advantage is of great use because it is not necessary to open closed or sealed containments to perform sampling prior to the measurement.

Both techniques, IR and Raman, do have a big disadvantage in situations where non-pure substances need to be investigated. Mixtures or substances comprising more than one compound most often lead to false or even no useful results if a database check is performed. To overcome this issue, databases can be built up from predefined mixtures in different ratios of the target compounds. Nevertheless, as a precondition it has to be known which other compound(s) come along with the analyte in the analytical task. This elegant technique can be mainly used in the field of process control, or in drug analytics, since the measurement conditions do not change in, as is true for military asymmetric scenarios.

Image 13: *Photography of the Thermo Fisher Scientific First Defender RMX. An important feature of this instrument is the “gooseneck” through which the laser beam is guided to the sample and makes it possible to measure substances in bulk without transferring them into a sample vial.*

3.7.2.6 Gas Chromatography - Mass Spectrometry

The only two mobile GC-MS instruments of consideration in this thesis are the MM1 (Image 15) and MM2 (Image 14) from Bruker Daltronik GmbH. The basic measurement principle of these instruments does not differ from a regular GC-MS instrument. The most important

feature is the non-usual sample inlet system. Both instruments have a flexible GC-column on top of which is a simple probe head which evaporates samples by maintaining a temperature of 260°C upon contact with the sample or easily sucks vapor phase samples into the GC-column. Additionally, the MM1 instrument can be equipped with a GC-oven which extends the chromatographic column of the system and therefore enhances the analytical capability of the device.

Image 14: *Photography of the mobile mass spectrometer MM2 from Bruker Daltronik, dismounted from the FOX-CRN-Recce vehicle (green box) and the GC-column (black tube) at which end the inlet head of the GC-column can be seen (silver port above the lab boy) and the command laptop (left).*

The underlying database of the MM1 is comprised of carefully selected compounds of the different classical chemical warfare agents and their precursors and degradation products as well as toxic industrial chemicals, so called TIC's. The detection of the compounds is mainly automated and is done by the comparison of the four most prominent and characteristic masses of the compounds which are loaded into the systems detection list with the measured spectra. This procedure seems to be limited but the opposite is true and the systems run very well for the scenarios the MM1 was originally build for.

Moreover, both instruments are capable for the use of Tenax®-tubes from which adsorbed analytes can be introduced into the analytical system *via* thermo desorption (Image 16). Usually, these instruments are not laboratory equipment rather then they are mounted on the CRN recce vehicles FOX of the Bundeswehr. The depicted instruments are dismounted since they are used to maintain and expand the databases for the missions of the vehicles.

Image 15: *Photography of the control panel of the mobile mass spectrometer MM1 from Bruker Daltronik in the enhanced version of the mass spectrometer system.*

The also available Hapsite ER (no picture shown) is not capable of the measurement of the analyte molecules under investigation of this thesis since they are not volatile enough to enter the instrument and are almost at the upper limit of detection with respect to their molecular mass. Furthermore, the chromatographic column of the instrument cannot be heated on a regular basis and thus a contamination of the system is most likely to happen and was not wanted.

Image 16: *Photography's of the Tenax®)-tube (left),the introduction port for the Tenax® tube of the GC-oven of the mobile mass spectrometer MM1 and the view inside the GC-oven of the mobile mass spectrometer MM1 (right).*

3.7.3 Analytics with Laboratory Equipment and Instruments

In general terms the characterization of newly prepared molecules is performed by the analytical study with different instrumentation methods. In the following section the available laboratory instrumentation methods used in this thesis are very briefly described since the methods are well known and belong to routine analytics. Additionally, the individual features of the respective analytical method are highlighted. For a detailed description of the employed techniques several well-known text books can be used.

3.7.3.1 Gas Chromatography - Mass Spectrometry

Since gas chromatographs can be coupled to a lot of different detectors they are versatile tools to be applied in the separation and analytics of pesticides and CWA's. In the following chapter the main features of the available instrumental methods used in this thesis will be explained briefly. In-depth insight into the different techniques and its applications can be found in several textbooks.[189-191]

To keep gas chromatographic results comparable the so called Kovats index can be calculated according to the following equation for temperature programmed gas chromatographs:[192, 193]

$$K_i = 100 \left[n + (N - n) \frac{t_{r(analyte)} - t_{r(n)}}{t_{r(n)} - t_{r(N)}} \right] \qquad \textbf{(3.11)}$$

with: K_i = Kovats index,
n = number of carbon atoms of the smaller alkane,
N = number of carbon atoms of the larger alkane,
$t_{r(x)}$ = retention time of the respective compound.

An important factor to be aware of is the relative abundance of isotopes for the atoms included in the molecules under investigation since from this so called isotope pattern important information on the structure and composition can be obtained (Table 3).

Table 3: *Compilation of the isotope pattern for different atom species important for mass spectrometry and NMR experiments.[194]*

Atom	C	O	S	N
Isotope 1	^{12}C = 98.90	^{16}O = 99.76	^{32}S = 95.02	^{14}N = 99.64
Isotope 2	^{13}C = 1.10	^{17}O = 0.04	^{33}S = 0.75	^{15}N = 0.34
Isotope 3		^{18}O = 0.20	^{34}S = 4.21	
Isotope 4			^{36}S = 0.02	

Gas chromatography itself is used as a separation technique of the injected sample under investigation. Influencing factors of the separation of the different components of the injected sample are: length and inner diameter of the column, film thickness of the column, carrier gas flow and temperature ramp parameters. After the separation the compounds elute from the column in an order similar to their boiling points, unless a reversed phase column is used. The sample is then transferred to the detector which is coupled to the GC.

3.7.3.1.1 Flame Ionization Detector (FID)

Coupling of gas chromatographs to flame ionization detectors (FID) results is one of the most often used detector types since the FID is a universal tool for the detection of carbon containing molecules which are the most common ones in organic chemistry. The basic principle is the observation of the change in the electric field of a hydrogen flame under pyrolysis of the analytes by addition of oxygen. FID's are known to have a low limit of detection and a large linear response.[195] Due to this feature FID's are used for purity determinations of organic reaction products.

3.7.3.1.2 Electron Impact Ionization (EI)

The generation of positive charged ions by electronical ionization is the classical ionization technique in mass spectrometry. It was first used and described by *Dempster* in 1918.[196] The process of fragmentation by this method is called the concept of localized charge and was established by *Budzikiewicz*.[197] The energy needed to extract an electron from a molecule is above 10 eV and is comparable to the first ionization energies. The highest ion yield is achieved at 70 eV. This energy level is high enough to not only remove electrons from molecules but also to break up bonds between atoms within the molecule and produces therefore charged fragments. Today 70 eV is the standard ionization energy on all commercial available instruments for comparability reasons of the different mass spectra. It also results in fragment rich mass spectra in which the molecular peak is most often missing.[191]

3.7.3.1.3 Chemical Ionization (CI)

For the observation of the molecular fragment peak a softer ionization technique as electronical ionization is needed. Developed in the 1960's by *Munson and Field* the ionization is achieved by the reaction of molecules with ions transferring protons to the analyte molecules.[198] The reactant gas itself gets ionized by electron impact ionization and is most often methane. The resulting ions are usually $M\text{-}H^+$-ions and fragmentation is suppressed since the ionization is a soft ionization process.[199]

3.7.3.2 Tandem-MS Fragmentation Studies of CWA's

The development of triple-quadrupole mass spectrometer was originally aimed at the use for better quantification experiments in complex analyte chromatograms, since the tandem-

MS extends the chromatography-MS experiment to a fourth dimension and thus allows to observe the fragmentation of a distinct ion generated by the target analyte. Those target ions have to be identified beforehand in a separate analysis. The experiment is called Selected Reaction Monitoring (SRM) whereas consequently the observation of more than one target ion at a time is called Multiple Reaction Monitoring (MRM).

Moreover, this technique can be used to study fragmentation pathways of chemical substances and thus gives access to experimental evidence for the assumed fragment ions and a better understanding of the fragmentation pattern of the analytes.

In general three different scan modes can be employed by this tandem-MS method:

i) product ion scan,
ii) precursor ion scan and
iii) neutral loss scan.

Within all three modes quadrupole Q2 is used for the fragmentation of the ions, whereas Q1 and Q3 are either in scan mode or in constant m/z mode or both in scan mode for the detection of neutral loss reactions. A detailed description of the MS/MS technique and other instrumental setups can be found in a review article by de Hoffmann.[200]

Until today only few studies elucidating the fragmentation pathways of chemical warfare agents are available, all of them employ electrospray ionization (ESI) tandem MS so far.[201-205]. However, one study on the fragmentation of Amiton exists which was done by *Ellis-Steinborner et al* in 2006.[206] None of the mentioned studies offers information on the fragmentation mechanism regarding the supposed fragmentation pattern, e.g. α-fragmentation or Mc-Lafferty rearrangement, but do report the identified m/z ions and the lost fragments. Also studies on pesticides which are structurally comparable to CWA's have only be performed by ESI-MS studies.[207]

The comparability of these reported fragmentation pathways obtained from ESI-MS towards those gained by a triple quadrupole instrument, has yet to be proved. The only publically available studies on a chemical warfare agent, namely VX, using a triple quadrupole instrument were done by the ECBC in 2008 and lately by *Saeidian et al*. in 2016.[160, 208] Additionally, compiled mass spectra of organophosphorus compounds can be found in the series entitled "Topics in Phosphorus Chemistry".[209]

For the performed fragmentation studies of this thesis a three step approach was used, which was offered by the Auto SRM software by Thermo Fischer Scientific. In the first step a full scan spectrum of the sample is taken. From this "study" the compounds for the second step have to be identified by their retention times in the GC and fragments have to be

chosen to be further fragmented. Finally, in the third step an energy optimization of the applied collision energy is performed resulting in optimum values of the ionization energy to maximize the yield of the individual daughter fragments.

3.7.3.3 High-Performance Liquid Chromatography – ESI-Mass Spectrometry

Amongst the separation techniques liquid chromatography is one of the oldest and best known. Advantageous of high-performance liquid chromatography is that thermolabile, polar or high molecular weight compounds can be investigated. Comparable to gas chromatography at the end of the separation process the analytes are transferred to a detector system, in this case a mass spectrometer.[210]

The principle of electron-spray ionization is to nebulize liquid samples and thus gaining positive and negatively charged ions. The ions undergo a phase transition from liquid to vapor state und are introduced into the high vacuum of the mass spectrometer by a collimator system. The advantage of this technology is that molecules up to a molecular weight of 1000 g/mol are single charged and rarely undergo fragmentation reactions.[211]

3.7.3.4 NMR-Spectroscopy

NMR spectroscopy offers a versatile tool for the structure elucidation of organic molecules. Especially the ^{31}P-NMR technique coupled or decoupled to protons can be very useful in the determination of the coordination of the phosphorus.[212] The chemical shift values for the phosphorus cover a wide range. Pure phosphorus as in P_4 shows a chemical shift of -461 ppm whereas PH_3 is reported at -240 ppm and PBr_3 with +227 ppm appears on the complete opposite site of the chemical shift scale referenced to phosphorus acid (H_3PO_4, 85%). Thus, it is expected to differentiate the thiono-thiol isomers and to tell the degree of isomerization by this technique. Additionally, also the coupling constants of phosphorus can be found over a wide range. This can be demonstrated very impressively by a molecule where a fluorine atom is directly bond to the phosphorus: the range is from 500 to 1400 ppm.[213]

Additionally, only two citations can be found for a ^{31}P NMR of Amiton. The first one by the Ministry of Foreign Affairs of Finland is not to find in the open source literature, but is cited by the second one by *Borrett et al*. which is only giving the chemical shift value of the phosphorus being 28.4 ppm.[214] Thus, an urgent need in gathering information on NMR properties of the compound class under investigation is obvious. Furthermore, the application of additional ^{1}H, ^{13}C and two dimensional experiments for this compound class will lead to a better understanding of the chemistry behind.

Generally, NMR-spectrometers are known to be big machines, need a high filed strength for good resolution, consume lots of energy and need a cryogen for maintaining a

homogeneous magnetic field. In recent years several companies, like Oxford instruments[6], Thermo Fisher[7] or Magritek[8] (Image 17) and others developed a new series of so called benchtop NMR spectrometers.

Image 17: *Photography of the Magritek SpinSolve benchtop NMR-spectrometers. The picture was kindly provided by the Magritek company, Aachen, Germany.*

Those small instruments, where the heaviest are of < 60 kg weight, are operated at magnetic fields of 45 to 80 MHz which is almost 1/10th of the regular field strength of classical instruments. Furthermore these instruments are equipped with permanent magnets, need almost no shimming of the magnetic field and can be operated without deuterated solvents. The resolution is varying from 2 to < 0.5 Hz. This means those instruments are not high resolution instruments but may have a certain value for routine analyses or applications in the field due to their compact and robust appearance.

3.7.3.5 Single Crystal X-ray Diffraction

A lot of pesticides as well as Amiton are frequently described as salts formed by the addition of an organic acid, e.g. oxalic acid.[[215, 216] However, still until today no single crystal structure of any of these compounds can be found in the literature. Just recently *A. Danner* was able to isolate a single crystal from Amiton treated with oxalic acid during the course of his master thesis in our labs.[217]

Information about the crystal structure is advantageous for a deeper insight of the molecules actual structure, allows calculating densities of the compounds and finally shows whether or not a substituent is for example adding sterically hindrance to a certain proposed mechanism as is for the until today unresolved thiono-thiol rearrangement of OTP's.

[6] https://oxford-instruments.de/produkte/spektrometer/nmr-spektrometer/benchtop-nmr-mqc
[7] https://www.thermofisher.com/order/catalog/product/912A0832
[8] http://www.magritek.com/products/spinsolve/

However, the critical step in the performance of single X-ray experiment is the formation and growth of a single crystal.

3.7.4 Application of Solid-phase Microextraction

3.7.4.1 Introduction

The theories and experimental aspects presented within this chapter are mainly based on the personal experience, a special training provided by *Pawliszyn* and his group at the University of Waterloo, Canada, during the development of this thesis and the handbook of solid-phase microextraction.[218] Furthermore, a close collaboration has been established in the meantime. Since the invention of solid-phase micro extraction by *Pawliszyn* in 1990 this technique has rapidly entered the field of sample preparation and has become a versatile tool amongst other available sample preparation techniques.[219, 220]

The basic principle of solid-phase microextraction is the use of a fused silica fiber coated by a liquid (polymeric extraction medium) or solid (sorbent) to extract analytes from different types of sample matrices (liquids or gases).[221] Therefore, these two extraction modes are called direct immersion extraction and headspace extraction. Furthermore, it is possible to extract analytes from so called complex matrices like fruits, vegetables or even living tissue (*in vivo* extraction) in which the liquid contains particles in the widest meaning of the word.[222, 223] Moreover, the SPME experiment is a powerful sampling and sample preparation technique at the same time which allows to directly introduce the SPME fiber after the extraction process into the injector of a GC-MS system and to perform the analysis without further treatment of the extract. Thus this technique is called solvent free extraction.

However, SPME is a multiphase equilibration process in which the fiber coating, the gas phase or headspace, a homogenous matrix and matrix particles are present. In complex matrices this multiphase system is hard to describe by simple equations and thus mainly the response of the detector signal is reported by many researchers instead of the amount (in ng) extracted by the fiber, which is not suitable according to Prof. Pawliszyn. A reproduction of an easy schema presented by Prof. Pawliszyn at the ExTech Symposium 2016 in Torun, Poland, to elucidate the different equilibria for both extraction techniques is given in Figure 30. The main difference between a headspace and a direct immersion extraction is that three instead of two equilibration processes have to take place for a headspace extraction and thus the extraction efficiency is lower compared to the direct immersion method. On the other hand in the direct immersion process the matrix can also be adsorbed by the polymeric fiber coating and thus have an influence on the extraction capacity as well as on the reproducibility of the extraction experiment due to a decreased extraction surface which is blocked by the matrix.

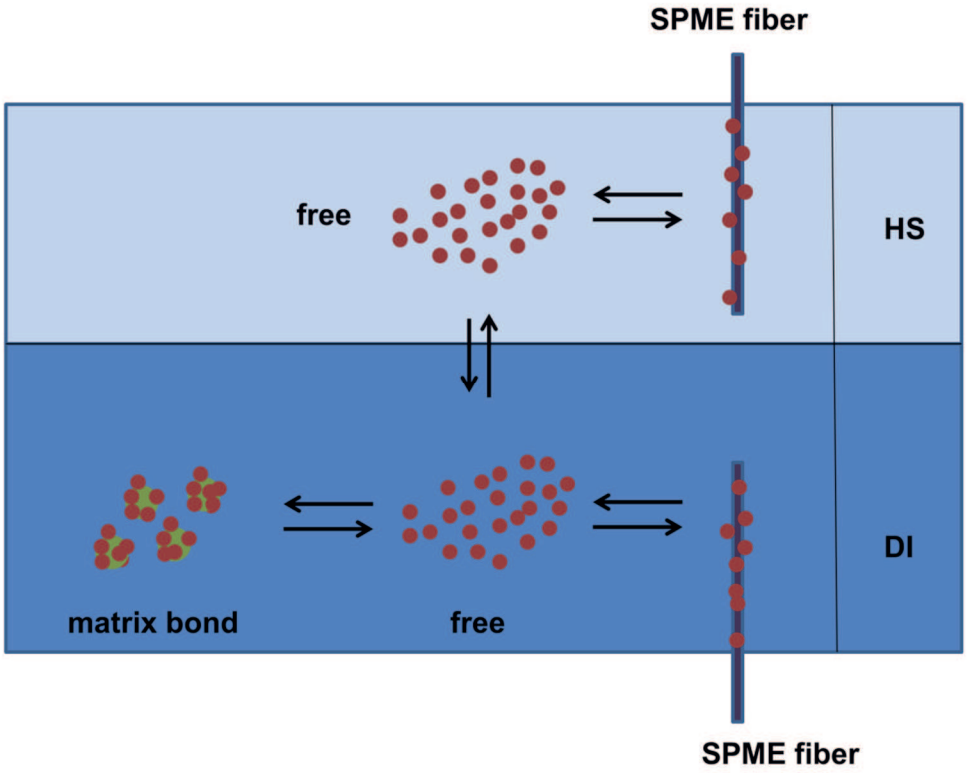

Figure 30: *Representation of the different equilibrium processes in complex mixtures for headspace (HS) and direct immersion (DI) SPME techniques.*

In a standard SPME setup, a fiber which can have basically six different commercial available coatings: PDMS, PA, Carbowax, PDMS/DVB, DVB/Carboxen-PDMS, Carboxen-PDMS, is exposed to the analyte containing sample for a precisely controlled period of time. Additionally, two extraction conditions can be applied, first a partitioning equilibrium extraction between the sample and the matrix and the extraction phase, second a pre-equilibrium extraction approach in which the extracted amount directly correlates to the extraction time.

Crucial variables to keep control of in a SPME experiment are: temperature, pH value, salt concentration/ionic strength, agitation speed, extraction time, polarity of sample matrix and coating material.[224]

3.7.4.2 Notes on Solid-phase Microextraction Method Development

For the successful development of a reliable SPME method it is of great importance to know the target analyte and its chemical/physical properties. The parameters given in section 3.7.4.1 are varied one by one until the amount extracted is maximized for the individual parameter. Then the optimized conditions are applied to the sample and the amount extracted should be at the optimum.[224, 225]

To set this up, so called extraction time curves have to be measured and plotted, to decide in which equilibrium regime one has to operate. In this extraction time profiles the response

(area) of the instrument is plotted against the extraction time. Beforehand, an analogue curve for calibration reasons has to be measured by regular liquid injection in split less mode to determine the absolute response of the instrument for the target analyte. By comparing the obtained response (area) of the liquid injection to the SPME extraction it is possible to determine the amount of nanogram extracted on the fiber.[226] An absolute determination of the concentration of the analyte can only be done by a partitioning experiment at prolonged times, where an absolute equilibrium between fiber and sample is reached.[227, 228]

$$n_\infty = \frac{V_f \cdot V_s \cdot K_{fs} \cdot c_0}{V_s + V_f \cdot K_{fs}} \qquad \textbf{(3.12)}$$

with:
- n_∞ = amount extracted at equilibrium
- V_f = volume of the fiber
- V_s = volume of the sample
- K_{fs} = fiber/sample distribution constant
- c_0 = initial concentration of the sample

This equation can be simplified if the sample volume can be considered being very large:

$$n_\infty = K_{fs} \cdot V_f \cdot c_s \qquad \textbf{(3.13)}$$

By further applying basic equations of molecular diffusion and thermodynamics it is possible to derive a relationship between the extraction and the distribution coefficients of the analyte for the individual phases in the sample.[229]

3.7.4.3 Direct Immersion vs. Headspace SPME

A headspace extraction is the easiest extraction process since only the equilibrium between the fiber and the headspace and that of the headspace and the liquid phase has to be taken into account and the fiber has no direct contact to the matrix. It gets more complicated if the analyte has to be extracted from a liquid phase other than pure water but which is for a fruit juice for example. In this case a third equilibrium (matrix-liquid) has to be considered and the matrix usually tends to stick to the fiber and blocks adsorption sites making the reproducibility of the experiment difficult.[230] To overcome the described disadvantages a washing step could be introduced which on the other hand poses the risk of losing analyte to the washing solution. Recently a new fiber type was developed by Pawliszyn group in cooperation with Supleco which has an additional over-coating to prevent matrix adsorptions on the fiber.[231]

3.7.4.4 Applicability towards the Analysis of Chemical Warfare Agents

Today's challenge is to keep track of the molecules banned by the CWC and to have fast and reliable detection and analytical methods available. In the vast literature on SPME some papers can be found which deal with the extraction of chemical warfare agents from different matrices. In recent years SPME has been introduced to an ever growing field of different applications stressing the versatility of this technique for different analytical tasks. In particular, SPME has been adapted for the fast and reliable detection of CWA's.[232, 233] The first example on the applicability was given by *Lakso et al*. in 1997 on the extraction from water samples.[233] He found that a combinational fiber of PDMS and DVB was most effective. Other publications focus on the extraction of single compounds like VX or GB from a single extraction matrix like soils, meaning headspace extractions.[234, 235]

In 2007 *Zygmunt et al* in 2011 *Popiel and Sankowska* each published a review for the different chemical warfare agents and procedures to extract them.[161, 236] However, no direct immersion extraction methods from complex matrices of this compound class could be found. Although studies combining SPME with IMS technology for the analysis of chemical warfare agent's precursors and degradation products from soil samples was done, no reference was found which concentrates on the analysis of the pure agents from soil samples.[237] Additionally, no direct immersion SPME method, which is recommended for low volatile molecules, has yet been reported for the analysis of any OP related to the CWC from complex matrices.[161] This fact seems surprising since a lot of work has been done to extract analytes from vegetables or fruits and most parts of the environment are covered by vegetation which is more or less comparable to the latter ones mentioned.[231] Also the well-known handbook of *Vanninen* on operating procedures in the verification of chemical disarmament does only give procedures on extraction from headspace for soil and environmental samples (water).[232] However, a review on different SPME methods for environmental samples for organic pollutants was given by *Zygmunt* in 2001.[238]

3.7.4.5 Extraction from Complex Matrices

In the analysis by direct immersion of complex matrices (liquid) the SPME technique has been widely used and has proved itself as a powerful tool. The first report on a direct immersion method was given by *Zhang et al*. in 1996, who showed that it was possible to protect the fiber from humic acids and thus from matrix interferences.[239] Nowadays, also biocompatible fibers are available as well as inert fibers towards certain matrices of general interest.[231, 240] In 2001 *Volante et al.* brought it to the extreme to analyze pesticide residues from honey by immersing the fiber in a water honey solution for 60 minutes and processed it by GC/MS which is the most frequently used technique amongst SPME.[241] Other researchers focus on the extraction from fruits or food in general in which the matrix plays an important role and can have a severe influence on the extraction process and thus

on the extraction itself.[242] Just recently one group even reported on a SPME experiment involving spaghetti Bolognese sauce.[243] These reports and many others more seem to help to extend the existing verification methods towards the application of direct immersion SPME for complex matrices.[231, 244-246] Additionally, specialized over-coated fibers were recently developed by the Pawliszyn group and commercialized by Supelco to prevent matrix particles from attaching to the fiber surface.

4 Results and Discussion

In this chapter all results are presented in individual subsections which thematically fit to each other.

In the first chapters of this section the results of the syntheses and characterization by different analytical methods are summarized and discussed. The full set of analytical data obtained from the different methods that have been used for characterization are compiled in the annex of this thesis.

Second, special investigations like studies on the thiono-thiol rearrangement, vapor pressure determinations, survey of mass spectral fragmentation pathways in the GC-MS/MS and toxicological studies are presented. However, not all compounds could be investigated by all of the mentioned methods within the scope of this thesis.

Finally, the application of field sampling methods like SPME for the recovery of the analytes from the environment are presented along with test results from investigations with military equipment such as hand-held test tubes or other field portable instruments.

4.1 Amino Alcohol Precursors

4.1.1 Synthesis

In total seven different symmetrically substituted amino alcohols (**I** –**VII**) were synthesized (Figure 31). However, only four compounds (**I**, **II**, **III** and **VII**) were employed for further synthesis of Amiton-derivatives.

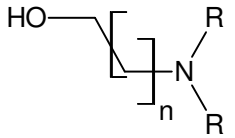

Figure 31: *Basic structural motif of the prepared amino alcohols.* ***I****: n = 2, R = Et;* ***II****: n = 3, R = Et;* ***III****: n = 4, R = Et;* ***IV****: n = 2, R = isoPr,* ***V****: n = 3, R = isoPr;* ***VI****: n = 4, R = Me,* ***VII****: n = 1, R = Ph.*

The tertiary amino alcohols were prepared according to the following procedure: The primary amino alcohol was dissolved in tetrahydrofuran and allowed to react with lithium hydride, which selectively removes the amine hydrogen atoms and yields the di-alkylated product.[81] Further treatment with the required alkyl iodide resulted in the desired product. Purification was done by liquid-liquid extraction since the boiling points of most of the alcohol educts almost coincides with those of the products, and thus a successful distillation was impossible to perform. The only exception to this reaction pathway is the synthesis of

compound **VII**, as no product could be obtained by this method. Moreover, a reaction involving Cu(I)Cl and potassium hydroxide instead of lithium hydride was successful and yielded a very high amount of product (76.2%).

Noteworthy, all of the synthesized amino alcohols are known from literature. However, these compounds were either commercially not readily available or only offered in tiny quantities (mg-scale) from standard suppliers. Thus, all starter molecules were synthesized in a 40 mmol lab scale to have enough material for the following synthesis steps. Moreover, most of the analytical data presented in this thesis was not yet reported for the compounds.

The yields are reported and summarized in Table 4. Obviously the yields of about 50% in average are very low. Considering the moderate efficiency of the hydride agent of about 53%, as reported by *Kashima et al.*, the reported values are reasonable and nearly the maximum yields that can be obtained by this synthesis route are matched.[81] Only in case of compound **III** the yield is greater than reported in the literature. Compound **VII** was synthesized by a different reaction pathway and thus the yield cannot directly be compared to the others. The in average missing 3-10% in yield can be mainly linked to the existence of mono-alkylated byproducts. This is especially true for compounds **II** and **VII**. Additionally, this can also be seen from the elemental analysis data which confirms the presence of mono- and di-alkylated products in the mixture. The same holds true for the refractive index values, which all have noticeable deviations from the given literature values. (Table 4) However, no efficient separation method for the differently substituted amino alcohols is available or could be found in literature.

Table 4: *Summary of the experimental yields and index of refraction of the amino alcohol precursors. Ratio of mono and di-alkylated product was obtained by GC-MS analysis of derivatized compound.*

Compound	CAS-No.	Yield [%]	Ratio [%] (di/mono)	n_D^{20}	n_D^{20}Lit.
I	622-93-5	45.9	90.4	1.4409	1.4439 [247]
II	2683-56-9	45.0	38.3	1.3907	1.4475 [248]
III	2683-57-0	74.9	85.4	1.4432	1.4546 [249]
IV	7539-61-9	42.3	86.7	1.4641	1.4447 [247]
V	103859-38-7	43.7	45.9	1.4698	1.4541 [250]
VI	27384-58-3	49.5	61.2	1.4490	1.4447 [251]
VII	6315-51-1	76.2	18.6	1.5621	1.6225 [252]

This fact indeed can be identified for future work to be conducted. The refractive index values from literature references, as reported in Table 4, are related to different synthetic

routes involving catalysts or were findings during the study of other compounds. However, it was not the aim of this thesis to obtain ultra-pure compounds but to prove the possibility of getting access to these molecules by rather simple reaction pathways. This for sure cannot involve the use of rare catalysts. Purification by distillation is almost impossible, since according to literature, the boiling point of mono- and di-alkylated products only differs by two degree centigrade. The classical Hinsberg-procedure for the separation of primary and secondary amine bases is inapplicable in the presence of the alcohol function of the molecule.[253, 254] This means that a protection and de-protection of the alcohol functional group would be necessary for quantitative separation by this means.

The ratio of mono- and di-alkylated product is also given in Table 4. Only in case of compounds **II** and **VII** the mono alkylated product is present in excess which can be clearly seen from the large mismatch of the refractive index. The measured one is very close to the one for the mono-alkylated product of 1.5749 reported in literature[255]. It has also be taken into account that the reported literature values date bake to the 1940's- 50's and thus the accuracy of the instruments might be different to the one of modern instruments.

However, the presence of byproducts is not critical for the further use of the amino alcohols in this study, since the work up of the (thio)phosphates only works for the di-alkylated products and thus the separation from the mono-alkylated product is indirectly achieved. However, this of course decreases the yield for the Amiton-derivatives. Furthermore, no mono-alkylated byproduct was observed in any of the (thio)phosphate GC-MS, HPLC-MS or NMR spectra.

4.1.2 Characterization

Characterization of the prepared amino alcohols could be performed by the use of infrared and Raman spectroscopy and derivatization GC-MS with MBTFA as derivatization reagent. Furthermore, HPLC-MS analyses were conducted to prove for yielding the mono- or di-alkylated product, respectively.

4.1.2.1 Vibrational Spectroscopy

As examples the IR spectra of 3-(diethylamino)propan-1-ol (**I**) as shown in Figure 32, 2-(diphenylamino)ethan-1-ol (**VII**) (Figure 33) and the Raman spectrum of the same molecule (Figure 34) are discussed in detail. The spectra of the other molecules are reported in section A.1 (IR spectra) and A.2 (Raman spectra) of the supplement.

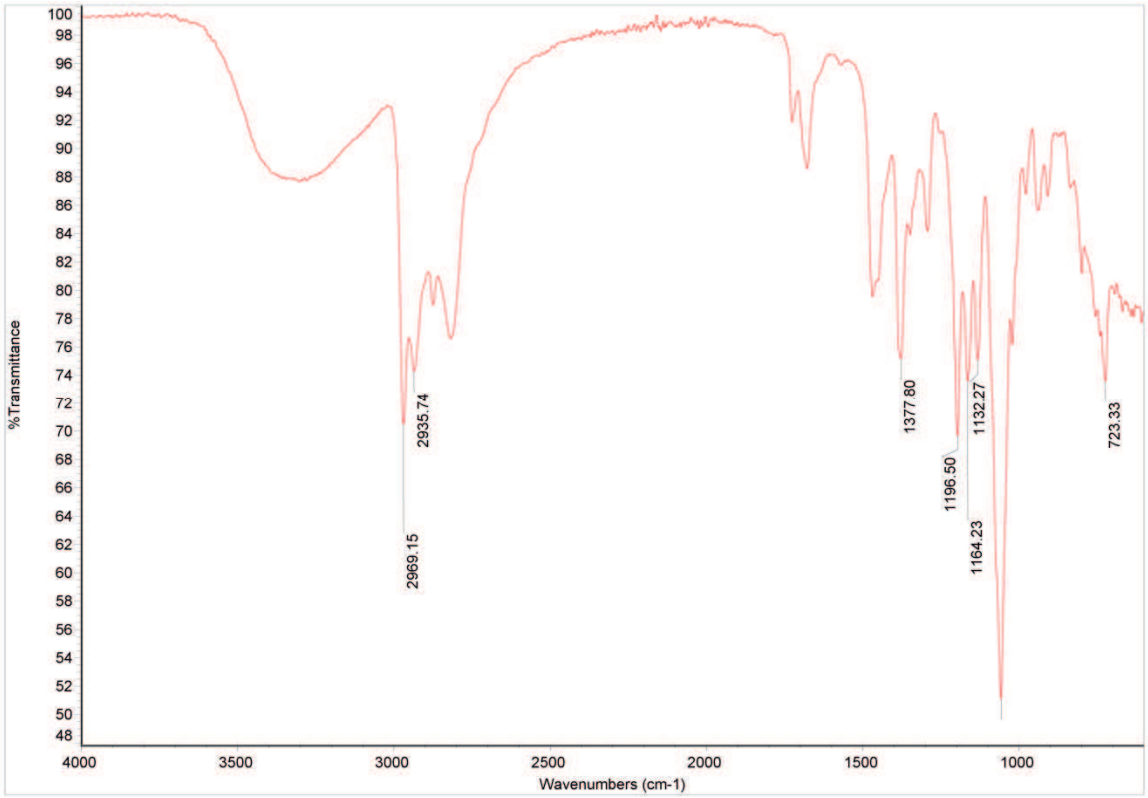

Figure 32: *IR spectrum of 3-(diethylamino)propan-1-ol. (**I**)*

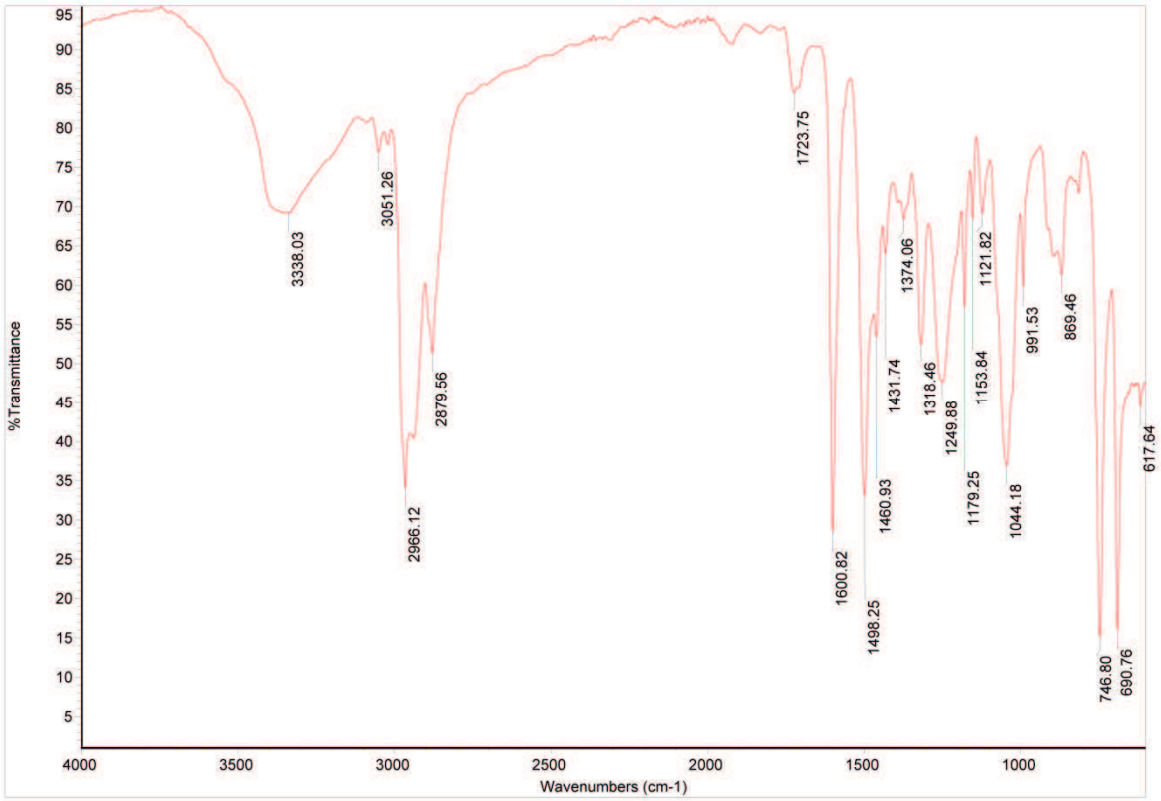

Figure 33: *IR spectrum of 3-(diphenylamino)ethan-1-ol. (**VII**)*

In all IR spectra the broad OH-band at about 3300 cm^{-1} is clearly visible, which is in very good agreement with the literature.[256] The broadening of the peak arises from the high concentration of the sample and therefore from strong intermolecular bonding. Furthermore, the CH_3 and CH_2 asymmetric vibrations can be observed at about 2970 cm^{-1} and 2935 cm^{-1}, respectively. The stretching vibration of the N-C-H groups of the tertiary amine can be found at 2820 cm^{-1}. Additionally, the signals in the region of about 1210-1150 cm^{-1} can be accounted to the tertiary aliphatic amine moiety. The same motives can be found in the IR spectra of the other amino alcohols. Again, only compound **VII** shows different features due to the two aromatic substituents at the nitrogen atom.

Thus, in several regions typical of aromatic compounds peaks can be observed resulting from ring carbon-carbon stretching vibrations (1600 cm^{-1}) and the strong C-H out of plane vibrations (900-650 cm^{-1}). The stretching vibrations of the ring CH bonds within the region of 3080-3010 cm^{-1} are very weak and are partly overlapped by the broad OH-band at 3336 cm^{-1}.

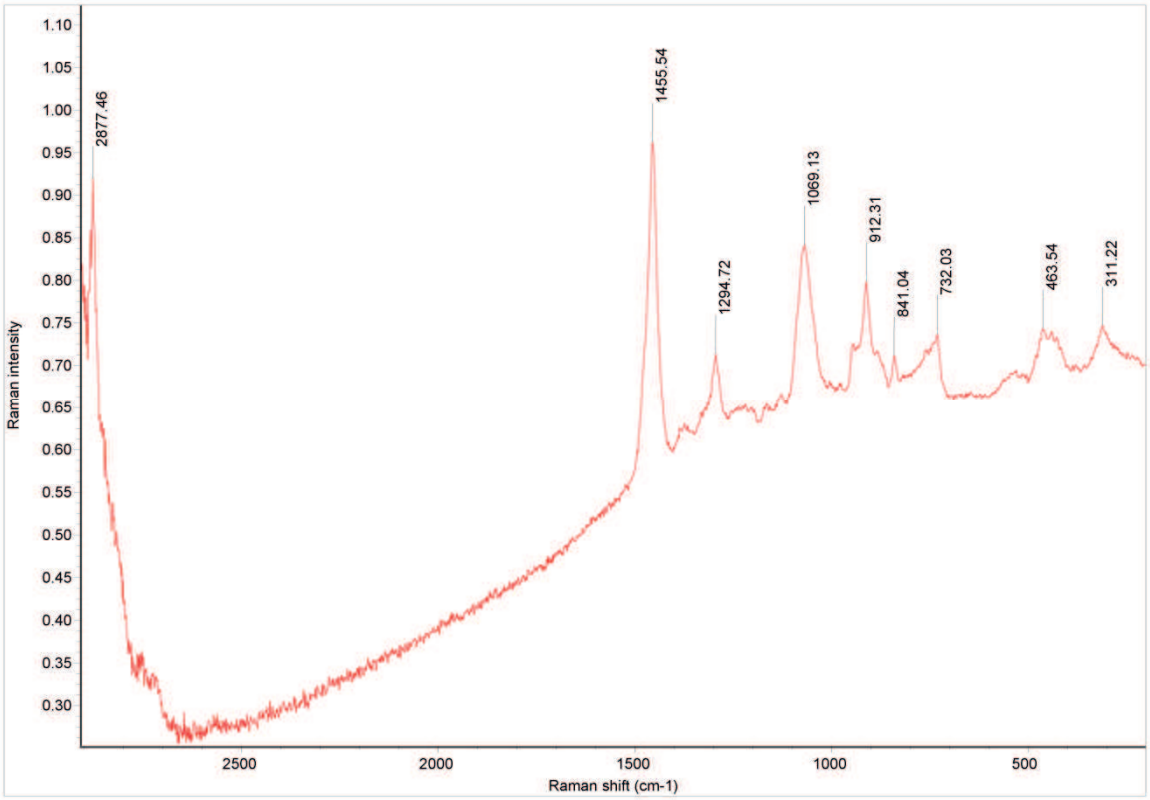

***Figure 34**: Raman spectrum of 3-(dimethylamino)propan-1-ol (**I**).*

However, IR and Raman spectroscopy are rather insensitive towards the presence of mono alkylated product and di-alkylated product at the same time. IR and Raman spectroscopy are complementary instrumental methods: however the appearance of bands in both IR and Raman spectroscopy depends on the elements of symmetry of a molecule, i.e. on the

change of the dipole moment or polarizability, which is why the IR and Raman spectra do show some similarities but do also differ largely as can be seen from Figure 34. Especially the symmetric vibrations of the aliphatic CH_3 and CH_2 group can be found in the Raman spectra at about 2880 cm^{-1} but are missing in the respective IR spectrum. Additionally, signals at 1455 cm^{-1} can be accounted to the asymmetric CH_3 vibration which was also not observed in the IR. The signal at about 1070 cm^{-1} is assigned to the tertiary amine moiety of the molecule which is in agreement with the IR spectra. Unfortunately, no Raman spectra could be obtained for compounds **III, IV, V** and **VII** since the instrument reported a high fluorescence of the sample and aborted the measurement. This phenomenon is sometimes a problem in the application of this otherwise useful technique.

Additionally, it has also to be noted that the Raman spectrometer (First Defender) has a smaller effective range towards lower frequencies and thus is not able to resolve some of the bands observed in IR spectra. This makes it hard to tell whether a molecule has OH or NH functionality or is comprised of a larger alkyl groups. For this reason all IR and Raman spectra are shown in the Annex of this thesis and a lengthy tabular report of the observed signals is not given at this point.

4.1.2.2 GC-MS and HPLC-MS

HPLC-ESI-MS offers a straightforward method to confirm the outcome of the reaction whereas the determination of amino alcohols with GC-MS, needs a derivatization step in advance of the measurement due to their high polarity and therefore very strong interaction with the capillary column. *N*-methyl-bis(trifluoroacetamide) (MBTFA) was used as the derivatizing agent and thus the recorded mass spectra show a shift in the m/z value of +96 amu for the molecular peak as this reagent interacts with the alcohol functional group (Table **5** and Figure 35).

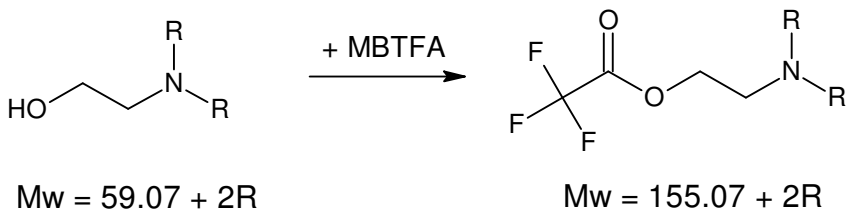

Figure 35: *Basic reaction scheme for the derivatization of an amino alcohol with MBTFA to give a new product having a molecular weight 96 amu heavier than the educt per hydrogen atom of either an OH or NH or, NH_2 moiety. R in this case represents a non-hydrogen atom.*

Table 5 also compares the calculated mass values with the determined values of the HPLC experiment. As can be seen these values match quite good. This comparison was done to figure out whether the product was mono- or di-alkylated. Only slight amounts of mono-alkylated educts were found in the obtained products (Table 4) which proves the established liquid-liquid extraction method as very effective.

Table 5: *Comparison of the experimental HPLC molecular peak values (MH^+) and those of the derivatized adducts of MBTFA measured by GC-MS(EI) with the calculated molecular masses for the amino alcohol precursors. Given are also the Kovats index data for the GC-MS (EI) investigation of the derivatized molecules.*

Compound	Calculated mass [g/mol]	MH^+ HPLC	M^++MBTFA	KI
I	131.22	132.2	228	1446
II	145.24	146.2	242	1147
III	159.27	160.2	256	1260
IV	159.27	160.2	256	1156
V	173.30	174.3	270	1444
VI	131.26	132.2	227	1258
VII	213.26	214.1	310	1808

Compound **VII** was the sole molecule which could also be analyzed without derivatization due to the fact that the phenyl substituents at the nitrogen atom strongly add to the more nonpolar character of the molecule compared to the relatively small alkyl groups of the other substituents.

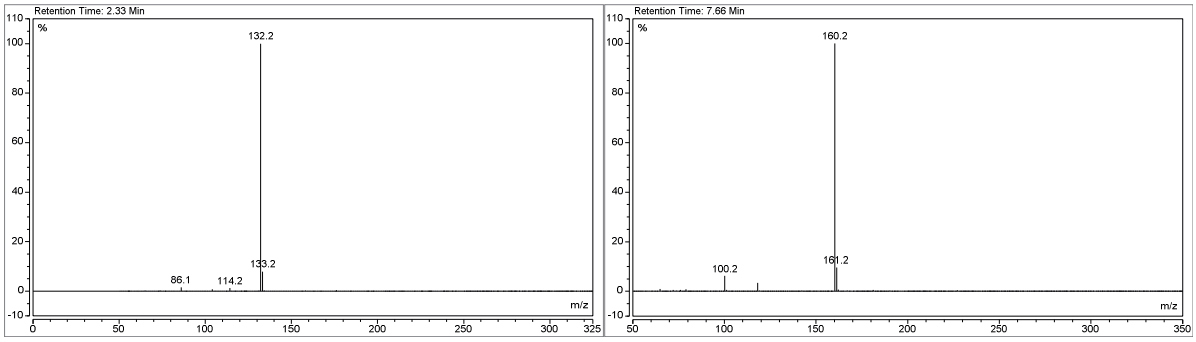

Figure 36: *Shown are the HPLC-ESI-MS spectra of compounds **I** (left) and **IV** (right).*

The full set of GC-MS and HPLC-ESI-MS spectra can be found in chapters A.3 and A.4 of the annex. All HPLC-ESI-MS spectra show a very strong molecule peak whereas fragments are very rare and are in maximum 5% of the height of the base peak. As an example the ESI-MS spectra of compounds **I** and **IV** are given in Figure 36. Thus, a discussion of the fragmentation pathways in the ESI MS is not helpful at this point.

In contrast to the ESI-MS spectra, the derivatized GC-MS spectra show some interesting features that are mentioned and discussed in the following. Besides the expected molecular peak, which is 96 amu higher than the expected molecular peak per free proton bond to a nitrogen or oxygen atom, two very prominent peaks can be observed. The first one is of a m/z ratio 14 amu smaller than the expected molecular peak indicating the loss of a methyl

group. The second one most likely also arises from bond scission in proximity of the nitrogen atom. This general pattern is illustrated in Figure 37 for compound **I** and can be adopted for all the other molecules, including the mono alkylated, but besides compound **VII**. In case of compound **VII** only the mechanism shown on the right-hand side of Figure 37 can be applied. The frequently occurring formation a cycloheptatrien system from benzene rings is not observed in this case, since this would involve the incorporation of the amine and thus a complete break-down of the molecule. The latter is actually not the case.

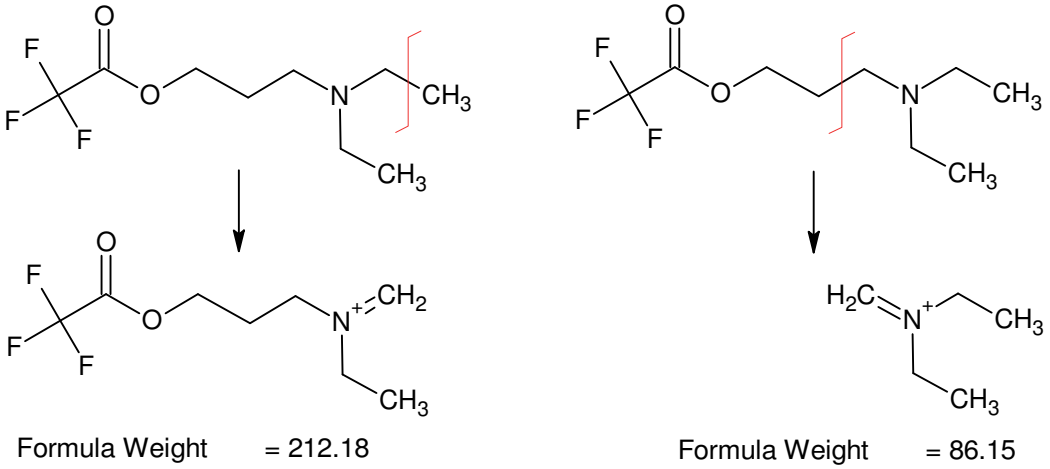

Figure 37: *Depiction of the most likely fragmentation sites to explain the observed fragments for the derivatized amino alcohols; in this example for compound **I**. The red lines indicate the possible fragmentation sites. The pattern on the right side holds true for all other amino alcohols of this thesis.*

4.1.2.3 NMR-Spectroscopy

The ^{1}H and ^{13}C NMR data which were derived from ^{1}H, ^{13}C, and the corresponding ^{1}H, ^{1}H COSY, ^{1}H, ^{13}C HMBC and ^{1}H, ^{13}C HSQC spectra are summarized in Table 6 for the ethyl functionalized amino alcohols and in Table 7 for the methyl and phenyl functionalized compounds. Additionally, the chemical shift values for the mono-alkylated compounds are also given, in cases where signals could be observed and clearly identified in the respective NMR spectra. However, spectra for compounds **IV** and **V** were not measured.

In general it can be stated that the longer the alkyl chain between the nitrogen and the oxygen becomes the more difficult it is to resolve the coupling constants, resulting in the report of multiplets. Furthermore two individual spin systems can be identified in the molecules. The nitrogen atom divides the molecule into two independent spin systems; coupling *via* the nitrogen atom could not be observed. However, $CDCl_3$ as the standard solvent used in the NMR experiments prevents the exchange of the hydroxyl proton and thus the chemical shift value can be observed in all the molecules. Unfortunately, no coupling constants of this proton could be observed. The chemical shift values observed for the OH protons of the synthesized amino alcohols ranges from 1.14 to 3.09 ppm, which is in good agreement with literature values of 0.5 to 4.0 ppm.[257]

Also the NH proton of the mono-alkylated compounds can be assigned to a broad singlet signal. Couplings to the adjacent CH_2-groups could not be detected and thus the NH exchange rate is estimated to be of intermediate velocity.[257]

Table 6: *Results of the NMR spectroscopy studies of the amino alcohols bearing ethyl groups at the nitrogen atom. Given are the chemical shift values for ^1H and ^{13}C as well as the coupling constants and the multiplicity of the proton coupling signals.*

Compound	δ C [ppm]		δ H [ppm]		*J* [Hz]	
I 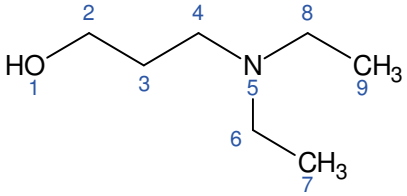			H1	1.14, t, 1H	$^3J_{H1H2}$	3.1
	C2	64.6	H2	3.73, m, 2H		
	C3	27.7	H3	1.62, p, 2H	$^3J_{H3H4,}$	5.6
					$^3J_{H3H2}$	5.6
					$^4J_{H3H1}$	5.6
	C4	53.8	H4	2.58, t, 2H	$^3J_{H5H4}$	5.8
	C6, C8	46.8	H6, H8	2.47, q, 4H	$^3J_{H6H7}$	7.1
	C7, C9	11.6	H7, H9	0.99, t, 6H	$^3J_{H7H6}$	7.2
II 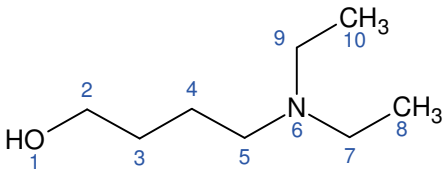	C2	62.4	H2	3.48, t, 2H	$^3J_{H2H3}$	3.1
	C3	32.5	H3	1.58, tt, 2H	$^3J_{H3H4}$	5.5
	C4	26.1	H4	1.58, tt, 2H	$^3J_{H4H5}$	5.5
	C5	53.2	H5	2.34,m, 2H	-	-
	C7, C9	46.1	H7, H9	2.49, q, 4H	$^3J_{H7H8}$	7.2
	C8, C10	10.6	H8, H10	0.98, t, 6H	$^3J_{H7H8}$	7.2
II-mono-alkylated 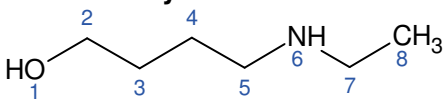			H1	4.79, s, 1H		
	C2	62.3	H2	3.48 t, 2H	$^3J_{H2H3}$	3.1
	C3	32.1	H3	1.58, m, 2H	-	-
	C4	25.5	H4	1.79, m, 2H	-	-
	C5	49.1	H5	2.57, t,2H	$^3J_{H4H5}$	5.7
			H6	4.79, s, 1H	-	-
	C7	43.3	H7	2.59, q, 2H	$^3J_{H7H8}$	7.2
	C8	14.7	H8	1.05, t, 3H	$^3J_{H7H8}$	7.2
III 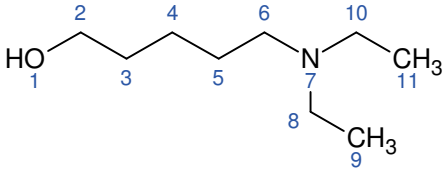			H1	1.14, s, 1H	$^3J_{H1H2}$	7.0
	C2	62.1	H2	3.53, t, 2H	$^3J_{H2H3}$	6.5
	C3	32.4	H3	1.50, m, 2H	-	-
	C4	26.3	H4	1.42, m, 2H	-	-
	C5	23.8	H5	1.29, m, 2H	-	-
	C6	52.7	H6	2.35, m, 2H	-	-
	C8, C10	46.6	H8, H10	2.45, dq, 4H	$^3J_{H8H9}$	7.2
					$^4J_{H8H10}$	2.2
	C9, C11	11.2	H9, H11	0.95, t, 6H	$^3J_{H8H9}$	7.2
III-mono-alkylated 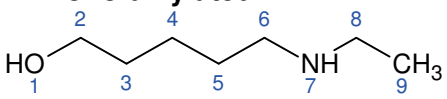			H1	3.34, s, 1H		
	C2	65.8	H2	3.41, q, 2H	$^3J_{H2H3}$	7.0
	C3	29.4	H3	1.46, m, 2H	-	-
	C4	15.2	H4	1.14, t, 2H	$^3J_{H3H4}$	7.0
	C5	23.4	H5	1.30, m, 2H	-	-
	C6	49.4	H6	2.56, q, 2H	$^3J_{H8H9}$	6.4
			H7	3.02 s	-	-
	C8	44.0	H8	2.58, q, 2H	$^3J_{H8H9}$	7.2
	C9	14.9	H9	1.04, t, 3H	$^3J_{H8H9}$	7.2

Table 7: *Results of the NMR spectroscopy studies of the amino alcohols bearing other than ethyl groups at the nitrogen atom. Given are the chemical shift values for ^{1}H and ^{13}C as well as the coupling constants and the multiplicity of the coupling signals.*

Compound	δ C [ppm]		δ H [ppm]		*J* [Hz]	
VI 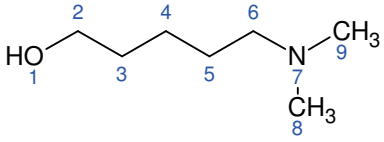	C2	62.2	H2	3.57, t, 2H	$^{3}J_{H2H3}$	6.5
	C3	27.1	H3	1.46, m, 2H		
	C4	23.4	H4	1.36, m, 2H		
	C5	32.4	H5	1.53, m, 2H		
	C6	59.5	H6	2.25, t, 2H	$^{3}J_{H6H5}$	7.3
	C8, C9	45.2	H8, H9	2.18, s, 6H		
VII 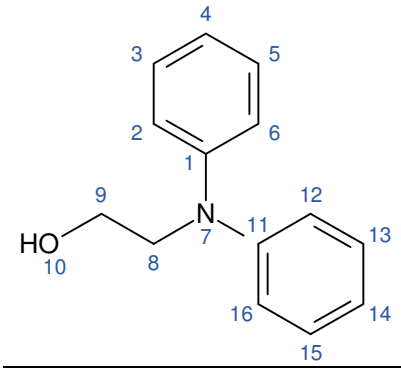			H10	1.96, s, 1H		
	C9	61.3	H9	4.04, q, 2H	$^{3}J_{H9H8H10}$	7.2
	C8	54.3	H8	3.83, t, 2H	$^{3}J_{H8H9}$	7.2
	C1, C11	148.2				
	C2, 6, 12, 16	113.6 129.3	H3, 5, 13, 15	6.58, m 7.11, m		
	C3, 5, 13, 15	118.3	H2, 6, 12, 16	6.67, m		
	C4, C14					

Generally, it can be stated, that the closer a CH_2-group is attached to an electronegative hetero atom the higher are its ^{13}C chemical shift values. The influence on the chemical shift value is greater for the oxygen atom than for the nitrogen atom. Additionally, this influence is greater for CH_2 groups than for CH_3-groups. Moreover, the presence of further alkyl groups attached to the nitrogen atom leads to further de-shielding of C-atoms in alpha and beta position. The resolved coupling constants of the protons fit very nicely to each other, since the corresponding coupling constant could be found on both coupling signals and are of the same value which makes the obtained results trustworthy. Unfortunately, the proton spectrum of compound **VII** is too crowded that a clear identification of the phenyl proton couplings was not possible.

4.1.3 Conclusion

Seven symmetrically substituted amino alcohols of which four were used for further syntheses, could be successfully synthesized. In general it can be said that the synthesis of tertiary amino alcohols can be performed in a moderate yield without great effort. In average the yield was greater than 50%, which is quite close to the reported value of 53% from literature. The purification is not possible by distillation since the boiling points of the educts and products are too close together. New methods for the separation of mono- and di-alkylated products are still needed to be found. However, the separation at this point is not crucial since in the further use of these educts only the di-alkylated species will remain. The characterization can easily be done by HPLC-MS measurement. With the aid of the

MH^+-signal in the spectra it can clearly be determined whether the alkylation with alkyl iodide was successful regarding the di-alkylation or mono-alkylation of the primary amino alcohol. Furthermore, derivatization GC-MS offers also a simple way to clearly distinguish between mono- or di-alkylation of the educt.

A major finding of the measured NMR spectra is that the amino alcohols consist of two non-interacting spin systems which are separated by the ‘central’ nitrogen atom.

Additionally, IR and Raman spectroscopy methods are also suitable methods which can be used to identify the basic features of an amino alcohol. However, both methods are limited with regards of distinguishing between hydroxyl and primary and secondary amine functional groups since the vibrational modes fall in the same region of the spectra. Moreover, for four of the molecules it was not possible to record a Raman spectrum since the instrument reported a high fluorescence level and aborted the measurement.

4.2 Dialkylchloro(thio)phosphate Precursor

4.2.1 Synthesis

In the course of this thesis it was required to prepare a dithioethoxy isomer of the O,O'-diethyl phosphorochloridothioate as starting molecule to evaluate the toxicity of the resulting Amiton derivate and to evaluate any other influence resulting from the chalcogen exchange. Due to the lack of commercial availability this molecule was also not available from regular suppliers. It had to be synthesized as well.

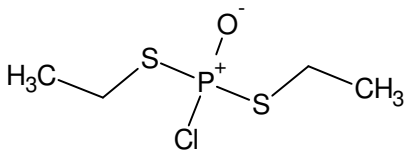

Figure 38: *Chemical structure of the prepared S,S-diethyl phosphorochloridodithioate (**VIII**).*

The relatively low yield of about 6% of the synthesized of *S,S*-diethyl phosphorochloridodithioate (**VIII**, Figure 38) *via* reaction pathway A (Figure 19) was less than half of the amount given in the article by *Mastin et al.*[103] Moreover, the given boiling point could not be found for the title compound. The given boiling point of 110-113°C at 2 mmHg was that observed for the mono thiolated isomer instead of the desired product which actually boils at 105-112°C at 0.2 mbar. This may also explain the deviation in the refractive index in the reported citation. Furthermore, it was observed that the product forms smoke in contact with ambient air (moisture). Reaction pathway B (Figure 20), according to a patent by *Regel et al.*, offered a very suitable option to gain the desired product in a ten-fold higher yield compared to reaction pathway A.[106] Moreover, pathway B involves only few basic preparation steps and does not require trained experimental skills.

Table 8: *Summary of the experimental yield, calculated mass and index of refraction for the dialkylchloro(thio)phosphate precursor.*

Compound	Yield [%]	Calc. mass [g/mol]	n_D^{20}	n_D^{20} Lit
VIII (*via* path A)	6.1	204.67	1.5517	1.5485 [106]
VIII (*via* path B)	62.0	204.67	1.5522	1.5485 [106]

4.2.2 Characterization

4.2.2.1 Vibrational Spectroscopy

A strong band occurs at 1225 cm^{-1} in the IR spectrum of compound **VIII** which is assigned to the P=O stretching vibration of the molecule. Furthermore the alkyl sidechains show CH_3

and CH_2 asymmetric vibrations that can be observed at about 2970 cm^{-1} and 2930 cm^{-1}, respectively. The strong band at 899 cm^{-1} can be identified as the C-S stretching vibrations of the molecule. Other stretching vibrations, e.g. P-S or P-Cl (400 – 500 cm^{-1}), known in literature are not observable with the IR-ATR instrument used, since they occure below the lower detection limit of this instrument which is 600 cm^{-1}.[213]

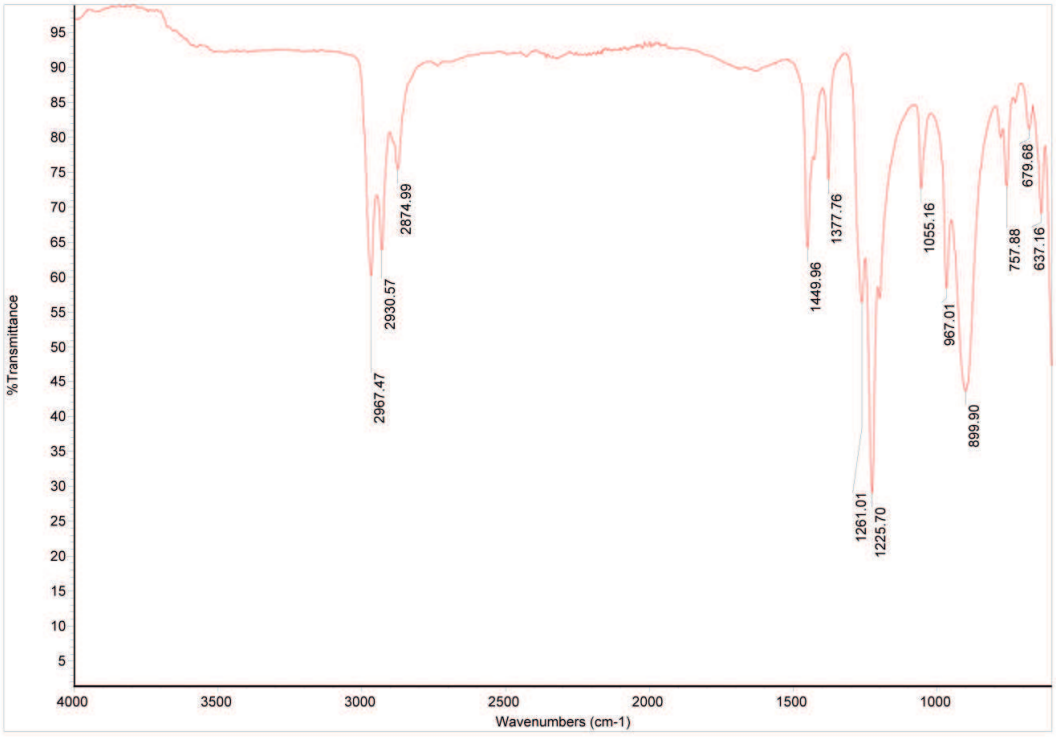

Figure 39: *IR spectrum of compound* ***VIII****.*

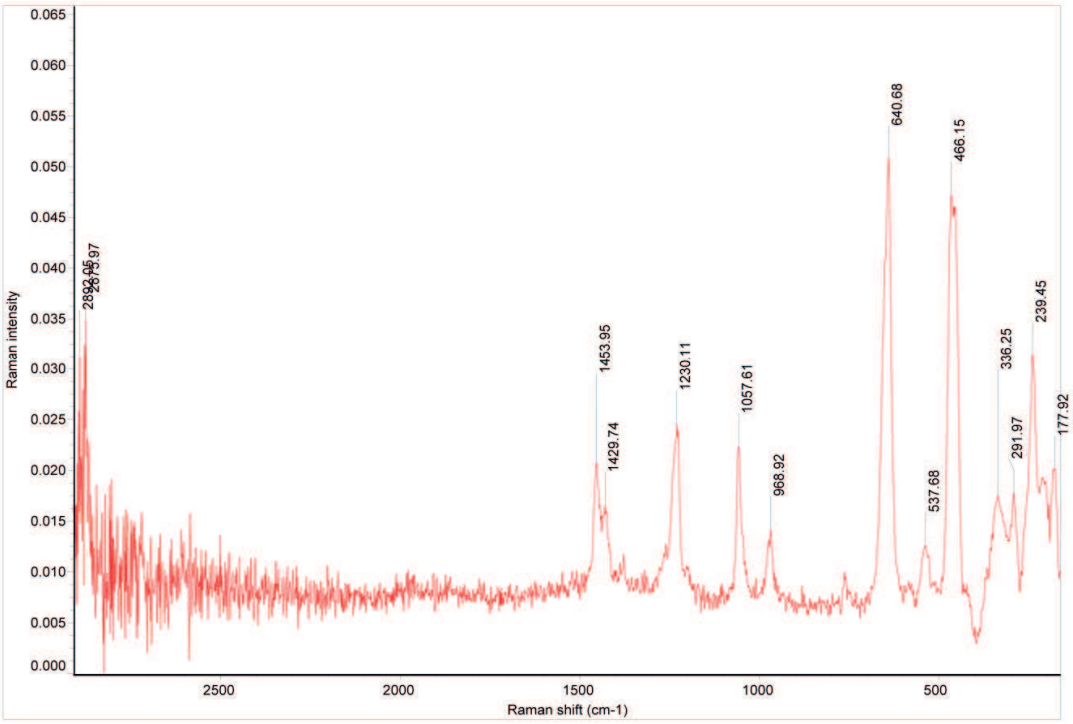

Figure 40: *Raman spectrum of compound* ***VIII****.*

The Raman spectrum of compound **VIII** shows generally weaker signals than the IR spectra. As is true for Raman spectrum of the respective amino alcohol analogue fingerprints dominate the Raman spectrum of **VIII**: the non-observed symmetric vibrations of the aliphatic CH_3 and CH_2 group in the IR spectra can be found in the Raman spectra at about 2880 cm^{-1}. Additionally, signals at 1455 cm^{-1} can be accounted to the asymmetric CH_3 vibration which was also not observed in the IR.

4.2.2.2 GC/MS and HPLC-ESI/MS spectrometry

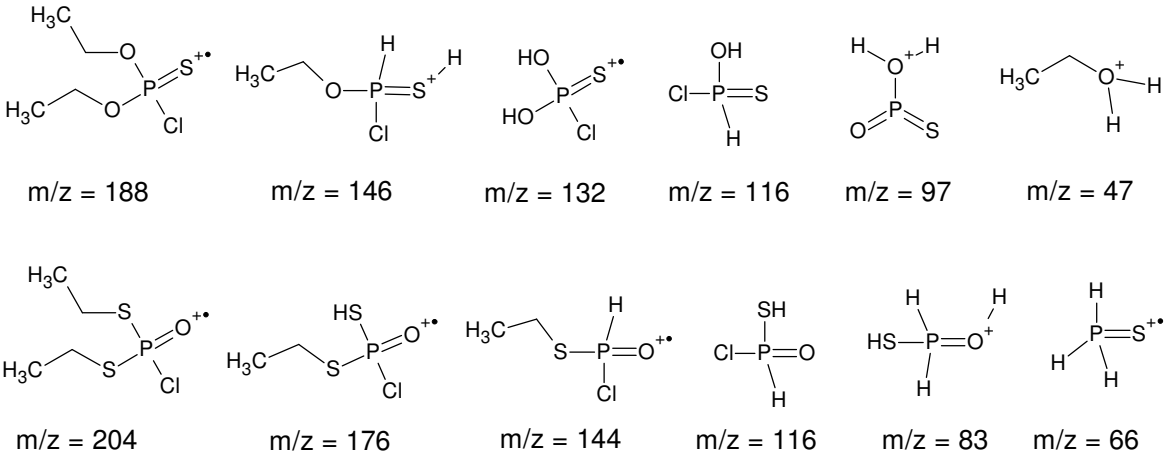

Figure 41: *Illustration of the main mass spectrometric fragments for O,O'-diethyl phosphorochloridothioate (upper row) and S,S-diethyl phosphorochloridodithioate (**VIII**) (lower row).*

The characterization by GC-MS methods showed, non-surprisingly, the same molecular fragmentation motif as the O,O'-diethyl phosphorochloridothioate. This is illustrated in Figure 41. Interestingly, the fragmentation pattern is slightly different for both molecules although they have the same chemical structure. However, both compounds have six main observable fragments. The ethanol fragment from the O,O'-diethyl phosphorochloridothioate is observed whereas the mercapto ethanol fragment of compound **VIII** is not observed. Additionally both molecules show a fragment of m/z of 116 which again is due to the isomeric structure of the molecules.

Unfortunately, no HPLC-MS spectra could be obtained since no proper instrumental setup was found for the detection of this compound class.

4.2.2.3 NMR Spectroscopy

Results from NMR spectroscopy are given in Table 9. The interpretation is straightforward. Interestingly, the vicinal coupling of the CH_2 protons to the methyl protons and the phosphorus is of the same order and could not be resolved. The proton-proton couplings are split into a doublet each due to the coupling with the phosphorus atom and are in the expected range of 0.5 to 20 Hz.[257]

Table 9: *Results of the NMR spectroscopy studies of the dialkylchloro(thio)phosphate precursor molecule (**VIII**). Given are the chemical shift values for ^{31}P, ^{1}H and ^{13}C as well as the coupling constants and the multiplicity of the signals.*

Compound	δ P [ppm]	δ C [ppm]	*J* [Hz]	δ H [ppm]	*J* [Hz]
VIII	P2	C4, C6	$^{1}J_{CH}$ 144.6	H4, H6	$^{3}J_{H4H5}$ 7.5
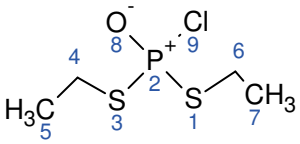	58.6	28.6, dp	$^{2}J_{CH5}$ 4.5 $^{2}J_{PC}$ 4.5	3.04, dq, 4H	$^{3}J_{HP}$ 4.7
		C5, C 7	$^{1}J_{CH}$ 129.1	H5, H 7	$^{3}J_{H4H5}$ 7.5
		15.7, qdt	$^{2}J_{CH4}$ 3.5 $^{3}J_{PC}$ 6.9	1.40, td, 6H	$^{4}J_{HP}$ 0.7

4.2.3 Conclusion

The two possible reaction pathways vary widely with respect to the experimental yields. The reaction pathway *via* the use of $AlCl_3$ offers a very easy access to this molecule, which additionally can be very well separated from the mono thiolated isomer by vacuum distillation. Unfortunately, the HPLC-MS method could not be optimized to detect and characterize the molecule. All other reported spectra are in very good agreement with previously reported results or match, e.g. with the theoretical assignment of chemical groups, to typical vibrational bands in the IR and Raman spectrum.

4.3 Organo(thio)phosphates

This chapter focusses on the synthesis and characterization of the different organo(thio)phosphates. Due to the considerable large number of synthesized molecules the results are presented according to structurally related motifs of the different compounds to show relations between the different molecules and to evaluate the influence of certain alterations in the molecular structure on for instance the chemical shift values.

4.3.1 Synthesis

A total of 19 different OP's and OTP's (Figure 42) could be successfully synthesized of which twelve of them have not yet been reported in literature before. Those are marked by an asterisk (*) in Table 10. Additionally, it is the case that besides Amiton (**X**) the other derivatives are only generally covered by mainly patent literature but no special procedure of synthesis or analytical data for the individual molecules are given so far.

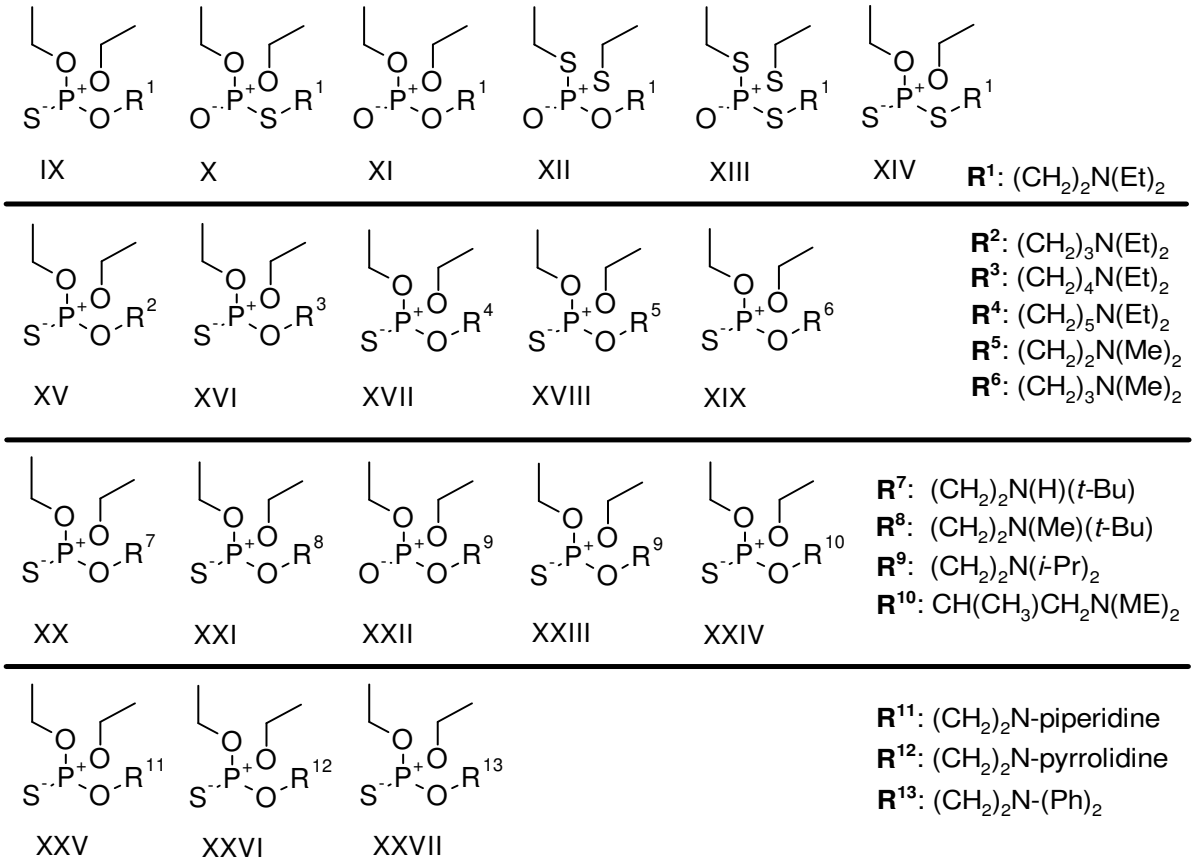

Figure 42: *Overview of the synthesized Amiton (**XXIII**) derivatives. The alterations are i) the chalcogen configuration at the phosphorus atom ii) the distance between phophorus and nitrogen iii) variation of the substituents of the nitrogen and iv) the inclusion of nitrogen in a ring structure.*

The general procedure of the synthetic route employed was according to Figure 43. In the first step an amino alcohol is allowed to react with 1.05 equivalent amounts of sodium hydride to form the respective alcoholate anion under reflux. In the second step the reaction mixture is cooled on an ice bath and the corresponding (thio) phosphoryl chloride is added. The mixture is allowed to warm to room temperature and is purified by a two-step process. The first step of the liquid-liquid extraction work-up involves the acidification of the solution with aqueous hydrogen chloride and thereby the destruction of the unreacted sodium hydride. Thus the target compound forms a quaternary ammonium salt and becomes water soluble. The two phases are separated and the unreacted (thio) phosphoryl chloride remains in the benzene layer. The forming by product sodium chloride which also is dissolved in the water phase is useful in the second step. This step begins with the neutralization of the hydrogen chloride with ammonia and again setting free the tertiary amine. In the last step the desired product is transferred into diethyl ether. Sometimes it could be observed that upon the neutralization reaction a second layer of pure product already forms as droplets on top of the water layer. The ether extract is dried over sodium sulfate and rotary evaporated. The presence of the sodium chloride from the reaction and the ammonium chloride from the neutralization process increases the salt concentration and ionic strength of the water phase and thus supports the phase transfer of the product from the water phase into the organic phase ("salting-out-effect"). The amino alcohol educt remains mainly in the water phase. Otherwise it can get separated during the rotary evaporation process since it has a lower boiling point compared to the respective products. On the other hand excessive rotary evaporation, also performed at moderate temperatures of 40°C, promotes the formation of the undesired thiol isomers of the organothiophosphate compounds. This means that it is nearly impossible to obtain a 100% pure product by using these standard purification methods. A solution to this issue could be the use of a Kugelrohr distillation apparatus, which was not available in the lab.

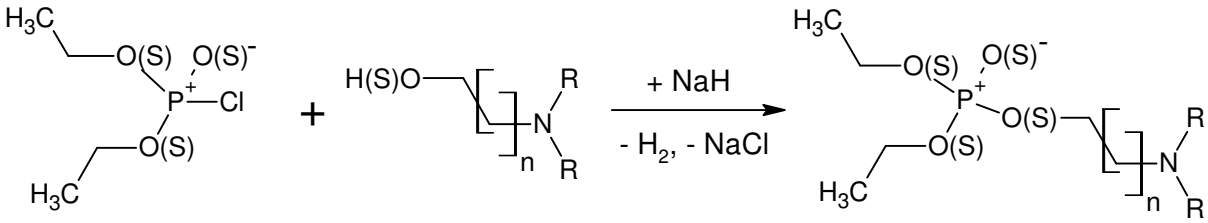

Figure 43: *Depiction of the general reaction schema for the synthesis of the O(T)P's in this study. R can be any alkyl, aryl or a ring closure with CH_2 groups; n can run from 1 to 4.*

Since the separation by the liquid-liquid extraction yielded very pure substances this procedure was also applied to those not capable of thiono-thiol rearrangement, instead of distilling them under reduced pressure. This also was found to be very convenient to prove the accessibility of these compounds without the use of specialized chemistry equipment. However, a major disadvantage of this procedure is in fact the liquid-liquid extraction itself,

because one has to be very careful in handling the separatory funnel and not to cause spill of a highly toxic substance.

Table 10: *Compilation of the yields and index of refraction for the synthesis of the organothiophosphate compounds compared to literature known refractive index values.* marks those compounds which have not yet been reported in literature by other authors and thus can be claimed to be reported for the first time.*

Compound	CAS-No.	Yield [%]	n_D^{20}	n_D^{20} Lit.
IX	5823-21-2	90.3	1.4611	1.4593 (nD25) [58]
X	78-53-5	61.0	1.4668	1.4666 (nD25) [258]
XI	4015-46-7	52.8	1.4280	1.4288 [33]
XII*	-	42.3	1.4596	-
XIII*	-	56.8	1.5399	-
XIV	23713-11-3	54.9	1.4993	-
XV*	-	64.7	1.4629	-
XVI*	-	52.7	1.4478	
XVII*	-	45.4	1.4641	-
XVIII	93375-37-2	65.8	1.4394	1.459 [59]
XIX*	-	88.3	1.4632	-
XX*	-	74.4	1.4502	-
XXI*	-	99.1	1.4567	-
XXII*	-	70.9	1.4480	-
XXIII*	-	69.6	1.4650	-
XXIV	108754-00-3	58.5	1.4551	-
XXV*	-	78.4	1.4808	-
XXVI	66932-73-8	75.0	1.4785	-
XXVII*	-	53.6	1.5650	

The obtained yields are compiled in Table 10. The purities range from 95 to 99% with the major side products being the respective disulfide of the amino alcohol or the thiol isomer. The formation of disulfides as side products is a common side reaction and is described in text books of organic synthesis.[76, 259] The formation of the isomeric by-products is

favored in case of long evaporation times of the ether during the purification using the rotational evaporator or if the (thio)phosphoryl educt was added too fast.

As a main outcome of the syntheses the yields range from values above 90 % to as low as 42 % of the theoretical yield. This wide range is not surprising since a lot of different precursors had to be coupled with each other and thus not always the same chemical reactivity can be expected. Former experiments by *A. Danner*, during his Master's thesis, prevailed that the use of solid metallic sodium as the reagent to form the ethanolate anion of the amino alcohol precursors resulted only in yields of a maximum of 40 percent of the theoretical possible amount.[217] Hence, in this thesis sodium hydride was used in an inert solvent (benzene) instead of metallic sodium. For the scale of the performed reactions of about 40 mmol, this method is very convenient for the use in the lab. Certainly for an industrial scale process synthesis, this method would be too expensive to be employed.

Furthermore, a complete set of refractive indexes is now available which can be used to distinguish the compounds from one another very precisely although these values have narrow range.

4.3.2 Characterization

For the characterization of the different molecules only a few literature resources are available for comparison since this compound class was developed in the mid-20th century and available instrumentation methods were mainly limited to IR. Mostly, the characterization was also done by thin layer chromatography or other early easy to determine parameters. However, a full characterization could be achieved by also IR and other up to date techniques. Regarding reported experimental values performed with more modern instruments research has lost focus on this compound class due to its ban by the CWC and more advantageous, tailor-made compounds were developed in the meanwhile as effective pesticides lacking high vertebrate toxicity. Only one study on the Amiton molecule by *Borrett et al.* could be found dating back to the year 2000.[214]

4.3.2.1 Vibrational Spectroscopy

As is true for the precursor molecules, all substances could be analyzed by IR spectroscopy but for most of the compounds no Raman spectra could be obtained due to high fluorescence of the samples or the recorded signal intensity being too weak to allow a clear assignment of the bands. In general most compounds show the same spectroscopic feature around 2970 cm^{-1} and 2935 cm^{-1}, two to three strong bands can be assigned to the CH_3 and CH_2 asymmetric vibrations, respectively. This fact is non-surprising since those signals can mainly be denoted to the substituents on the phosphorus and/or additionally belong to the alkyl substituents on the nitrogen atom, which in some cases are the same (**IX** - **XVII**).

Additionally, the stretching vibration of the N-C-H groups of the tertiary amine can be found at 2820 cm^{-1}. Moreover, the signals in the region of about 1210-1150 cm^{-1} can be accounted to the tertiary aliphatic amine moiety.

However, the IR spectra can be used to determine the phosphorus coordination regarding being phosphoryl or thiophosphoryl, since these two groups do have a very significant influence on the position of the bands in the respective spectrum. Furthermore, early researchers on this compound class, like *G. Schrader et al.*, exploited this feature to follow the thiono-thiol isomerization process of the insecticides “Systox” and “Metasystox” *via* IR spectroscopy.[70] They observed the P=O valence vibration at 1250 cm^{-1}.

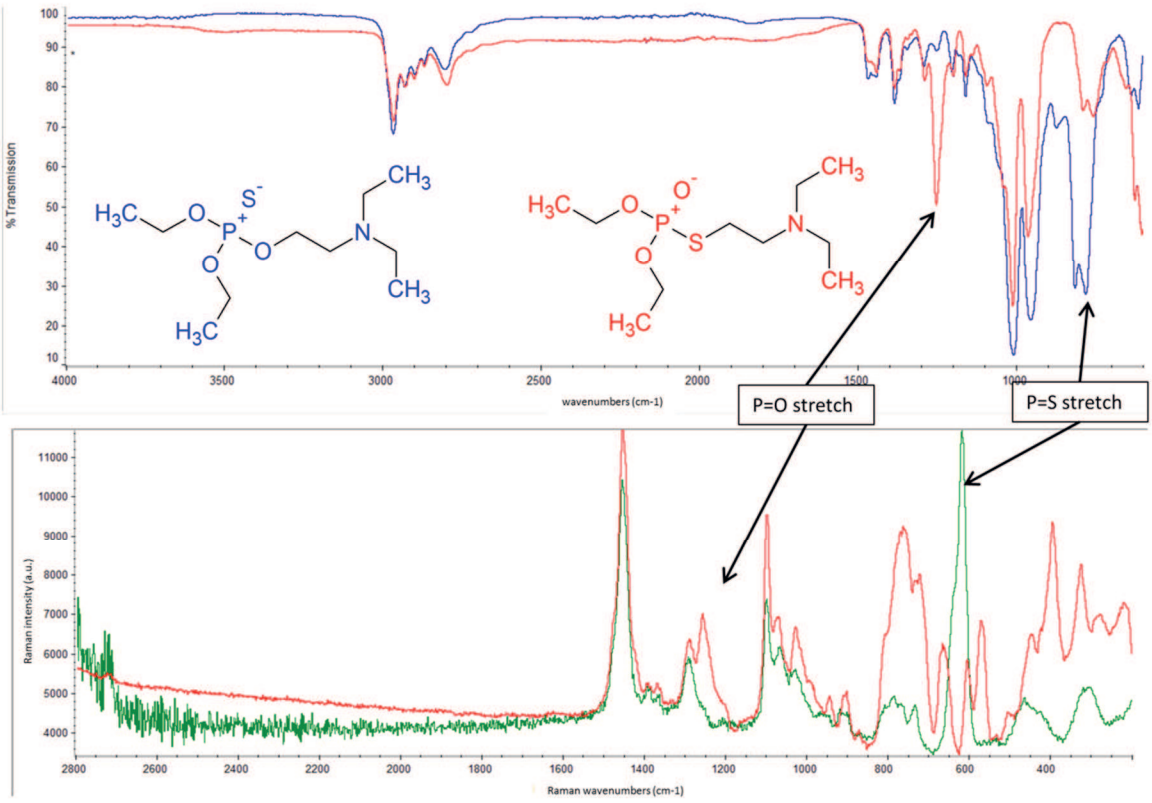

Figure 44: *Comparison of IR (top) and Raman spectra (bottom) of compounds* ***IX*** *(blue in IR and green in Raman) and* ***X*** *(Amiton, red).*

By comparison of the IR spectra of compounds **IX** and **X** (top of Figure 44) the same vibrational pattern can be found for the Amiton molecule. The P=S valance vibrations of the thiol isomer can be found at about 800 cm^{-1}. However, both molecules show the same pattern for the CH_3 and CH_2 vibrations in the region of 2900-3000 cm^{-1} as well as some weak CH deformation vibrations in the region of 1430 cm^{-1}. These findings are in very good agreement with common literature values.[256] The same differentiation of the molecules can be achieved by comparison of the respective Raman spectra (bottom of Figure 44). However, the P=O stretching vibration is less pronounced in comparison with the one detected in the IR spectra whereas the P=S stretching vibration is of the same order of

magnitude. Additionally, the doublet structure of the P=S stretching vibration absorption maxima in the IR can be accounted to the presence of two rotational isomers of the molecule.[213]

These two vibrational bands are the only two features of almost all IR and Raman spectra which can be usefully applied in the characterization of the molecules. A differentiation by other spectral properties for these structurally very close related compounds is almost impossible with these rather insensitive analytical techniques. However, phosphor organic compounds containing one or more alkoxy groups can be very easily identified by detecting the presence of strong vibrational bands in the region of 1000 to 1100 cm^{-1}. Those vibrations can be accounted to the P-O-C in-phase and out-of-phase vibrations. However, the proportion of the C-O and P-O stretching vibration alters depending on the other substituents and most often gives rise to a very strong double signal in this region.[213] On the contrary the same vibrations for the respective thiono derivative would be observable in the region of about 500-550 cm^{-1} which is not detectable with the IR instruments used in this study. For completeness, all IR and Raman spectra are shown in the Annex A.1.

4.3.2.2 GC/MS and HPLC-ESI/MS Spectrometry

This section concentrates on the main analytical results of the characterization of OPs and OTPs by mass spectrometry. A more detailed description of the formation of the individual fragments in the GC-MS (EI) is given in chapter 4.9 Mass Spectrometric Fragmentation Pathways. However, the Kovats indices determined for the different GC-MS instruments available during this thesis are given in Table 11 as well as the HPLC retention times and the basic information from the HPLC-ESI-MS experiments.

For the determination of the Kovats index the following n-alkanes were used to cover the retention times of the analytes: undecane, dodecane, tridecane, hexadecane,octadecane, icosane and docosane. Additionally, for better comparison the obtained Kovats indices are plotted in Figure 45. This plot shows that for all the instruments the retention index data are in very good agreement with each other and the molecules can be separated according to these values. Only for Amiton (**X**) and its thiono isomer (compound **IX)** the values do differ to a larger extent. An explanation for this observation could not be found so far. The KI-data for a single instrument is reproducible within a very small range and differs only by 5 to 10 points over 5 consecutive injections, which is in very good agreement with the theoretically expected deviation.[192]

Moreover, a very important result from this analysis is the inability of the mass spectrometer MM1 to detect compounds of KI's higher than ~2000. Additionally, it was found that the systems library in almost all cases resulted in false positive alerts for different CWA'S like VX. This is because the library does not have the full mass spectrum of the compounds

available but is matching the four most prominent fragment ions of the current chromatogram with respective entries in the library.

Table 11: *Compilation of the calculated mass in g/mol and comparison with $[MH]^+$ values from HPLC-ESI-MS for organ(thio)phosphates. Additionally, the m/z values of the most prominent fragments of ESI MS studies are given. Furthermore, the Kovats indices determined for the different GC-MS instruments used in this study are also reported. Numbers in brackets represent values for the respective thiol isomers of the initial compound as far as observed in the HPLC from samples that were stored >6 month and < 4°C in the fridge. #compounds have not been reported in literature before. *compounds did not successfully pass the GC-column of the instrument. &compounds were not available for measurement.*

Compound	mass [g/mol]	$[MH]^+$	main fragm.	R_t HPLC	KI TSQ	KI iontrap	KI MSD	KI MM1
IX	269.34	270.1	100.1	9.16 (7.60)	1664	1762	1590	1599
X	269.34	270.1	100.1	7.61	1792	1831	1710	1819
XI	253.27	254.2	100.1	6.44	1561	1546	1537	1601
XII	285.40	286.1	100.1	8.61	2268	2299	2314	*
XIII	301.47	302.1	100.1	9.28	2163	2200	2125	*
XIV	285.40	286.1	100.1	9.61	1816	1790	1780	1784
XV	283.36	284.2	114.2	9.28 (8.20)	1719	1748	1686	1701
XVI	297.39	298.1	128.2	9.60	1696	&	1695	&
XVII	311.42	312.1	142.2	9.78 (9.06)	2018	2022	2019	*
XVIII	241.28	242.1	72.0	8.73 (7.53)	1411	1447	1441	1505
XIX	255.31	256.1	86.0	8.96 (7.56)	1568	1545	1536	1603
XX	269.34	270.1	100.1	9.31 (8.39)	1610	1578	1573	1614
XXI	283.36	284.1	228.1	8.16	1678	1680	1706	1689
XXII	281.32	282.2	128.1	7.12	1789	1681	1669	1708
XXIII	297.39	298.2	128.2	9.44 (8.37)	1880	1818	1812	1828
XXIV	255.31	256.1	86.1	9.01	1352	1593	1431	1603
XXV	281.25	282.2	112.1	9.23 (7.79)	1886	1829	1792	1819
XXVI	267.32	268.1	98.1	8.92 (7.75)	1740	1720	1715	1719
XXVII	365.42	388.1	196.3	18.29	2074	2069	2071	*

This finding leads to the final conclusion that in case of a prolonged operating life of the MM1 instruments the database entries have to be modified in that way that the alert on the users screen reads like: “Alert for phosphorus organic compound, possible CWA.” It is important to do so, otherwise a lot of non-lethal scenarios will fall prey to the incorrect matching of the ‘out-dated’ libraries.

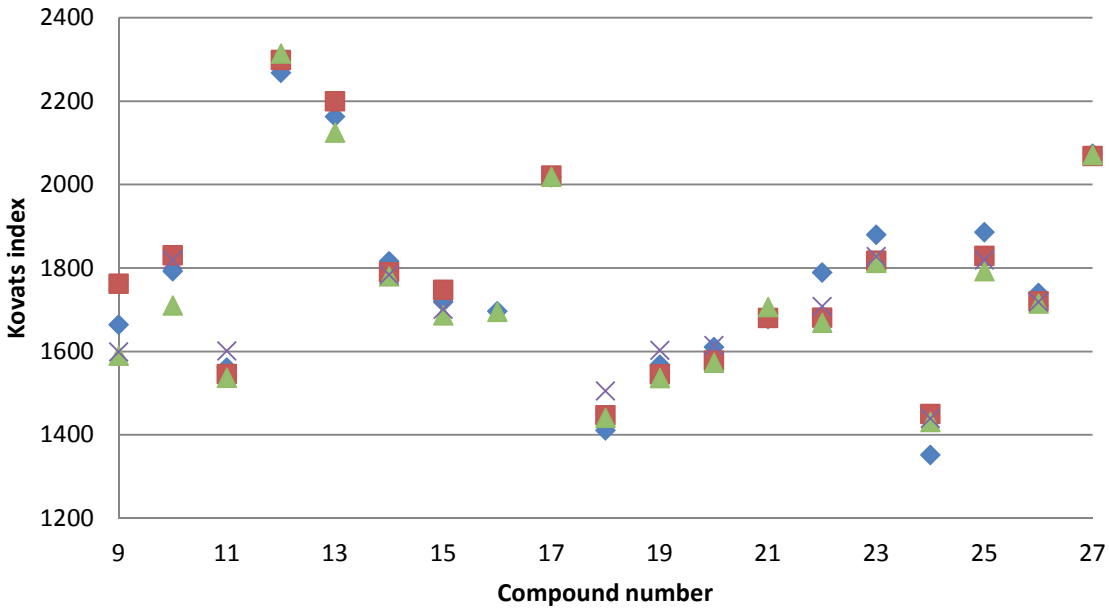

Figure 45: *Comparison of the Kovats index values (Table 11) obtained for the different detector systems coupled to gas chromatography. ◆ data from TSQ instrument, ■ data from ion trap instrument, ▲ data from MSD instrument, × data from mobile mass spectrometer of the FOX recce vehicle.*

Generally, no molecular mass peak is found in the respective GC-MS mass spectra of all compounds due to its low intensity compared to the signal-to-noise ratio. For this reason the expected mass peak might be identified if the total mass of the molecule is known. Otherwise it would be accounted to be background noise in most of the cases. However, the molecular mass peak of unknown species can be obtained by the application of the chemical ionization technique of the iontrap instrument. Thus, the combination of this additional experiment with the respective KI enables a clear identification of the molecular mass peak of each molecule.

It is important to emphasize that thiono-thiol isomerization of the OTPs already takes place inside the GC-MS system. This fact might be misinterpreted at first glance since one might conclude that isomerization always takes place during synthesis leading to isomeric mixtures and not to pure thiono isomers. The gas-chromatogram of the isomerizable compound, compound **XXV**, shows this behavior more pronounced than the others. By first injecting ‘standard’ amounts of sample a chromatogram with a single signal was obtained, which was believed to be the desired compound. However, by the analysis of compounds **IX** and **X** which are thiono-thiol isomers it was detected that isomerization was progressing

during the analytical process in the instrument. The injection of higher concentrated samples resulted in a strange two peak chromatogram in which the signals are connected by a 'cat's arched back' (Figure 46). The most interesting fact here is that the mass spectra at each point of the chromatogram looks the same and thus belongs to the same molecule. All underlying mass spectra are comprised of the following ions: 98 and 111, only in the case of a signal above 20 MCounts and at a retention time of 20 minutes, the molecular base mass peak of 281 with its isotopic masses 282 and 283 is also present.

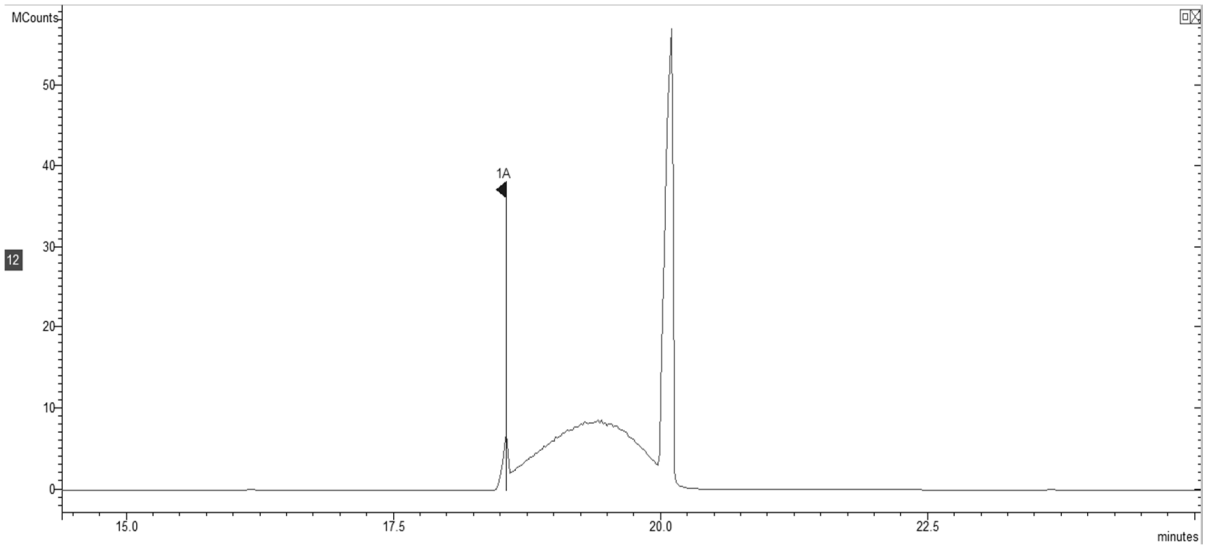

Figure 46: *Excerpt of the gas chromatogram of a saturated injection of pure compound* ***XXV*** *resulting in two peaks for a pure compound which was proved by ^{31}P-NMR measurement of the same sample.*

However, the different retention times of the first signal and the second signal clearly indicates that two different compounds are present. The first signal can be matched with the thiono isomer and the second one can be accounted to the thiol isomer. This could be proved by comparison of compounds **IX** and **X** which are the thiono-thiol forms of one another. Additionally, it has to be mentioned that only in case of compound **XXV** the second signal peak is higher and very well pronounced compared to the one belonging to the thiono isomer. For all other compounds the opposite is true.

Moreover, the assumption can be made that this behavior goes along with the isomerization tendency and it should be possible to prove this by separate experiments. In comparison, in the respective HPLC chromatogram and in the ^{31}P-NMR spectrum only one single peak is observed for the same sample. The reason for this is that as opposed to a GC-MS system in the NMR-spectrometer and in the HPLC system almost no energy is applied on the analyte during the injection and separation process which would then favor the isomerization process. Consequently, this systematic comparison of different analytical methods clearly proves that this phenomenon is either happening in the injector of the GC instrument or taking place during the ramped oven temperature program. The observation of the formation of the 'hill' between two signals would usually prompt the analyst to reduce

the concentration of the sample. Doing so can lead to fatal errors since small amounts of analyte get totally converted to the respective thiol isomers since there are too little molecules remaining in the sample to be detected as the thiono isomer and thus making the analysis result absolutely useless or even false.

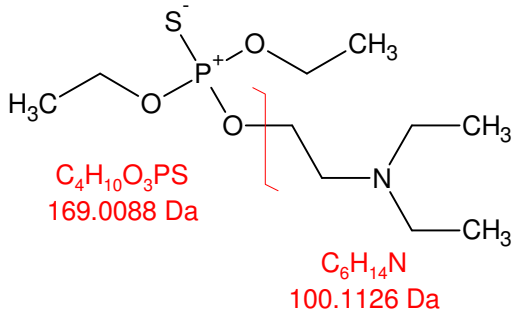

Figure 47: *Elucidation of the most possible fragmentation site in the molecules regarding the HPLC-ESI-MS experiment, resulting in the observed fragment m/z 100.1 for compounds bearing the ethyl-N,N'-diethylamino moiety.*

In comparison the HPLC-ESI-MS spectra are quite different. As depicted in Figure 47 for the HPLC-MS experiment, the main fragmentation site of the molecule, which breaks down the compound into more or less the two educts of the used synthesis route, gives only rise to two fragments. One fragment always is the molecular mass peak [MH^+] and the other peak belongs to the most prominent fragment of the amine part of the molecule. This fragmentation pattern is also true for the GC-MS experiments, additionally resulting in only a few higher mass peaks and a lot of smaller fragments usually showing m/z ratios smaller than 100. These two features i) no observable molecular mass peak in the GC-MS and ii) small fragments, which for a large number of molecules are almost identical makes it extremely challenging to clearly identify the correct molecule only by its EI mass spectra obtained from gas chromatographic separation.

In the HPLC-ESI/MS all compounds could be identified by the formation of the $[MH]^+$ ion. The only exemption to this is compound **XXVII** which is forming the respective sodium-adduct and thus shows a mass 23 amu higher than the actual molecular weight. Additionally, to the base peak, representing the molecular peak +1 amu, in most cases a very prominent second peak could be observed. Additionally, both peaks show the typical satellite signals of the different isotopes in the molecule. For instance, the base peak in the sulfur containing compounds is showing two additional signals arising from the natural isotopes of sulfur and carbon. On the contrary the most prominent fragment peak only shows one additional satellite signal resulting from carbon, since in the fragment no sulfur is found.

From the HPLC ESI-MS experiments at a cone voltage of 30 eV it can be concluded that most likely the bond between the CH_2 group of the nitrogen moiety and the heteroatom

(oxygen or sulfur) bonded to the phosphorus is broken. This can be explained by the very good stabilization of the positive charge of the resulting fragment on the nitrogen atom. Noteworthy, the relative peak intensity for the fragments formerly bonded to an oxygen atom is much higher than those of the fragments formerly bonded to a sulfur atom (Figure 48).With respect to the dissociation energies for the respective bonds it would be expected that it is more likely to cleave the C-S (ΔE = 259 kJ mol^{-1}) bond instead of the C-O (ΔE = 360 kJ mol^{-1}) bond.[73] The pattern for the formation of the second largest peak is depicted in Figure 47. The only exemption to this rule is compound **XXI** in which it is more likely to set free the *tert*-butyl group instead of the whole amino functionalized sidechain. This can be explained by the large sterically hindrance of the *tert*-butyl group and the anyway positive character of this substituent which thus weakens the N-C bond upon gaining a positive charge during the ionization spraying process in the instrument.

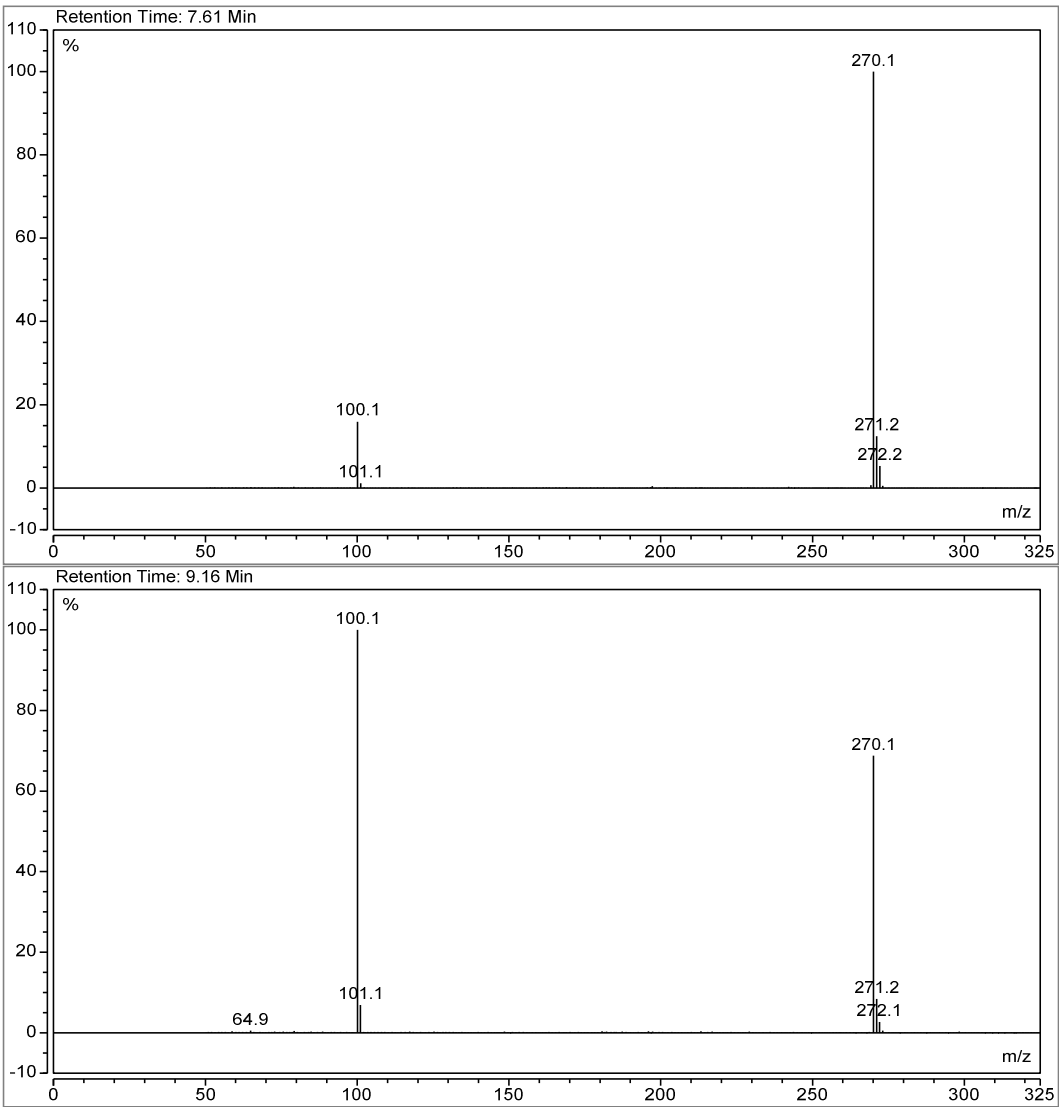

Figure 48: *Comparison of the HPLC-ESI-MS spectra of compounds **IX** (bottom) and **X** (top). It has to be noted that compound **X** is the thiol isomer of compound **IX**.*

4.3.2.3 NMR Spectroscopy

In the Amiton derivatives in total five different NMR active nuclei can be observed: ^{1}H, ^{13}C, ^{14}N, ^{15}N and ^{31}P. Hence the nitrogen ^{15}N nuclei is insensitive and the ^{14}N nuclei is unfavorable because of its quadrupole nature resulting in broad signals, no nitrogen NMR experiments were performed. Because of the expected numerous coupling interactions the interpretation of the non-decoupled spectra can become quite laborious and a proper strategy in order to discover the full set of information of the spectra has to be used.[260]

First, the spectra of ^{31}P are evaluated and the chemical shift values as well as the coupling constant(s) of phosphorus with the adjacent hydrogen atoms of the CH_2 groups next to the oxygen or sulfur are determined. In the next step the $^{13}C\{^{1}H\}$ spectra are used to determine the chemical shift values of the carbon atoms and the coupling constants of carbon with phosphorus, usually resulting in doublets. The same can be done with the ^{1}H spectra, where in addition also the couplings derived from ^{31}P can be cross checked and the couplings between the protons are detected. From the two dimensional ^{1}H, ^{13}C HMBC and ^{1}H, ^{13}C HSQC spectra the connectivity of proton to carbon atoms can be identified and thus with the help of ^{1}H, ^{1}H COSY spectra the total connectivity of the molecule be discovered. Finally, the ^{13}C spectra can be evaluated to cross-check the results and obtain further information on coupling relationships.[261]

For simplicity, abbreviations and combinations thereof are used for the description of the coupling patterns; multiplets are reported by their center instead of their ranges.

Since the complexity of the obtained results is overwhelming, they are summarized in several tables in the following chapter and are discussed in the main text between the individual tables to derive relationships with each other or to discuss changes in chemical shifts and coupling constants from one molecule to another.

Obviously, the most important information can be gained from the ^{31}P-NMR spectra, since the chemical shift values are strongly dependent on the substituents of the phosphorus atom (Table 13). Especially, for the second motif in Table 13 the range is quite narrow as can be seen from the more detailed results in Table 12. The deviation is less than 3 ppm. Interestingly seems to be the fact that a thiono configuration with otherwise three oxygen atoms bonded to the central phosphorus, e.g. **XIX**, exhibits almost the same chemical shift value as in the exact opposite case (**XIII**).

Another common feature is that the $^{3}J_{PH}$ coupling to the prochiral CH_2 groups, each bonded to a hetero atom (oxygen or sulfur) next to the phosphorus, is of the same order for all such CH_2-groups and thus mostly results in a septet.

Table 12: *^{31}P chemical shifts and the corresponding $^{3}J_{PH}$-coupling constants. Compounds **XXXIII-iso** and **XXXIII-oxo** were additionally found in the ^{31}P NMR spectra of compound **XXXIII** which was taken after one year of storage in the fridge (< 4 °C).*

Compound	δ ^{31}P [ppm]	$^{3}J_{PH}$ [Hz]	$^{3}J_{PH}$ [Hz]
IX	69.0	sep 9.6	sep 9.6
X	29.6	qui 15.4	t 8.7
XI	0.3	sep 7.9	sep 7.9
XIII	65.4	sep 15.0	sep 15.0
XIV	96.8	qui 16.5	t 9.9
XV	68.9	sep 9.5	sep 9.5
XVI	68.9	sep 9.5	sep 9.5
XVII	69.0	sep 9.5	sep 9.5
XVIII	67.7	sep 9.5	sep 9.5
XIX	67.9	sep 9.7	sep 9.7
XX	0.4	m	m
XXII	69.0	sep 9.6	sep 9.6
XXIII-iso	30.3	qui 17.1	t 8.6
XXIII-oxo	0.6	m	m
XXIV	67.4	sep 9.5	sep 9.5
XXV	69.0	sep 9.6	sep 9.6
XXVI	68.9	sep 9.5	sep 9.5
XXVII	69.5	sep 9.4	sep 9.4

This means that the six protons are magnetically equivalent. Although the CH_2 protons are prochiral themselves no geminal coupling could be observed in any of the spectra. Only in case of compounds **X**, **XIV** and **XXIII-iso** another coupling, giving a triplet motif, can be resolved. For compound **XXII** this coupling vanishes into a multiplet. This shows that the ethoxy moieties are still equivalent to each other, but now the CH_2-group of the N-moiety is different to them.

Table 13: *Comparative summary of the effect on ^{31}P chemical shifts of the different chalcogen configurations of the phosphorus atom of the compounds prepared.*

Configuration	δ ^{31}P [ppm]	Configuration	δ ^{31}P [ppm]
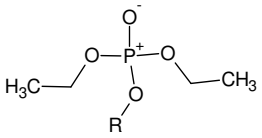	0.2-0.7	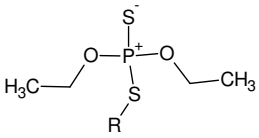	96.8
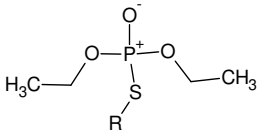	29.6-30.3	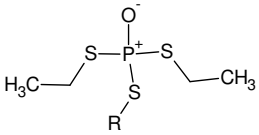	65.4
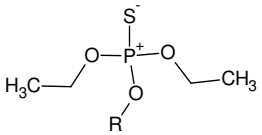	67.7-69.5	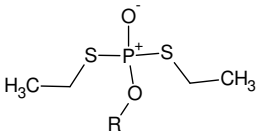	0.5

The difference in the resulting ^{31}P spectra can be nicely seen in Figure 49. Here the septet of the six equivalent CH_2-protons of the compound **IX** clearly differs from the triplicated quintet of the two different set of CH_2-groups in compound **XIV**. Although the low resolution does not allow resolving all of the expected 15 lines for compound **XIV** it is quite obvious that the configuration of the phosphorus plays a major role in the coupling system.

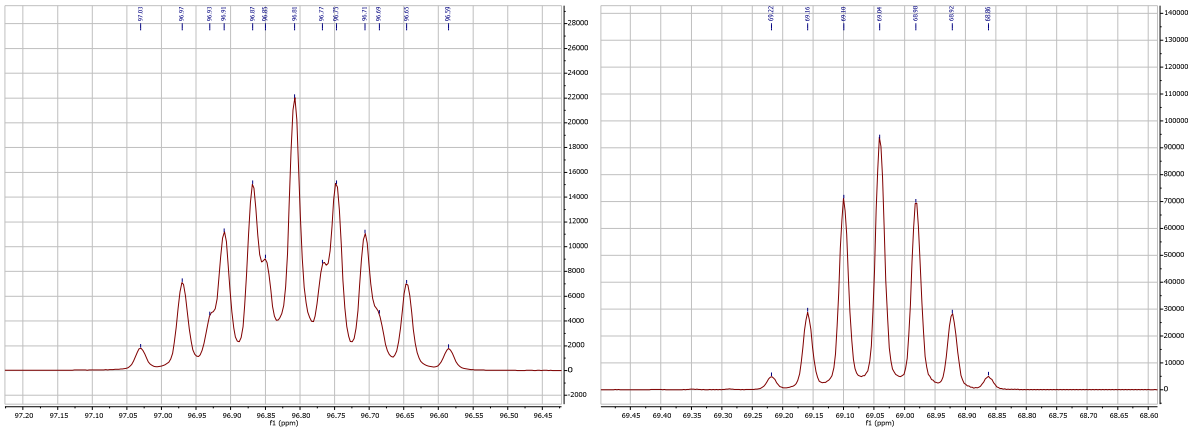

Figure 49: *^{31}P spectrum of compounds **IX** (right) and **XIV** (left) to illustrate the effect of the differently chalcogen coordinated phosphorus atom on the splitting pattern in the ^{1}H coupled spectra.*

Even with the help of the MestreNova embedded Resolution Booster tool a complete set of the expected 15 lines is not obtained. Thus, an algorithm for the deconvolution of FID-data was used to better resolve the obtained spectra. This algorithm is based on a Lorentz-Gauss transformation of the FID signal with a tunable weighing of the two mathematical functions until the best resolution is achieved. A full implementation and application of this algorithm, which was invented and is still under development and optimization for NMR experiments by Prof. Dr. Kalthoff of the Hochschule Heilbronn, Germany[9], was at this early stage not possible. However, the impressive potential of this algorithm is demonstrated in Figure 50. It can be seen that the MestreNova Resolution Booster improves the resolution

[9] https://www.hs-heilbronn.de/oliver.kalthoff

of the 13 lines of the ^{31}P spectra of compound **XIV** (*cf.* left part of Figure 49) in that way that they get baseline separated. Compared to this, the Lorentz-Gauss deconvolution algorithm applied by Prof. Dr. Kalthoff resolves two additional small but important signals next to the central peak of the multiplet, which now completes the triplicated quintet and makes an exact interpretation possible.

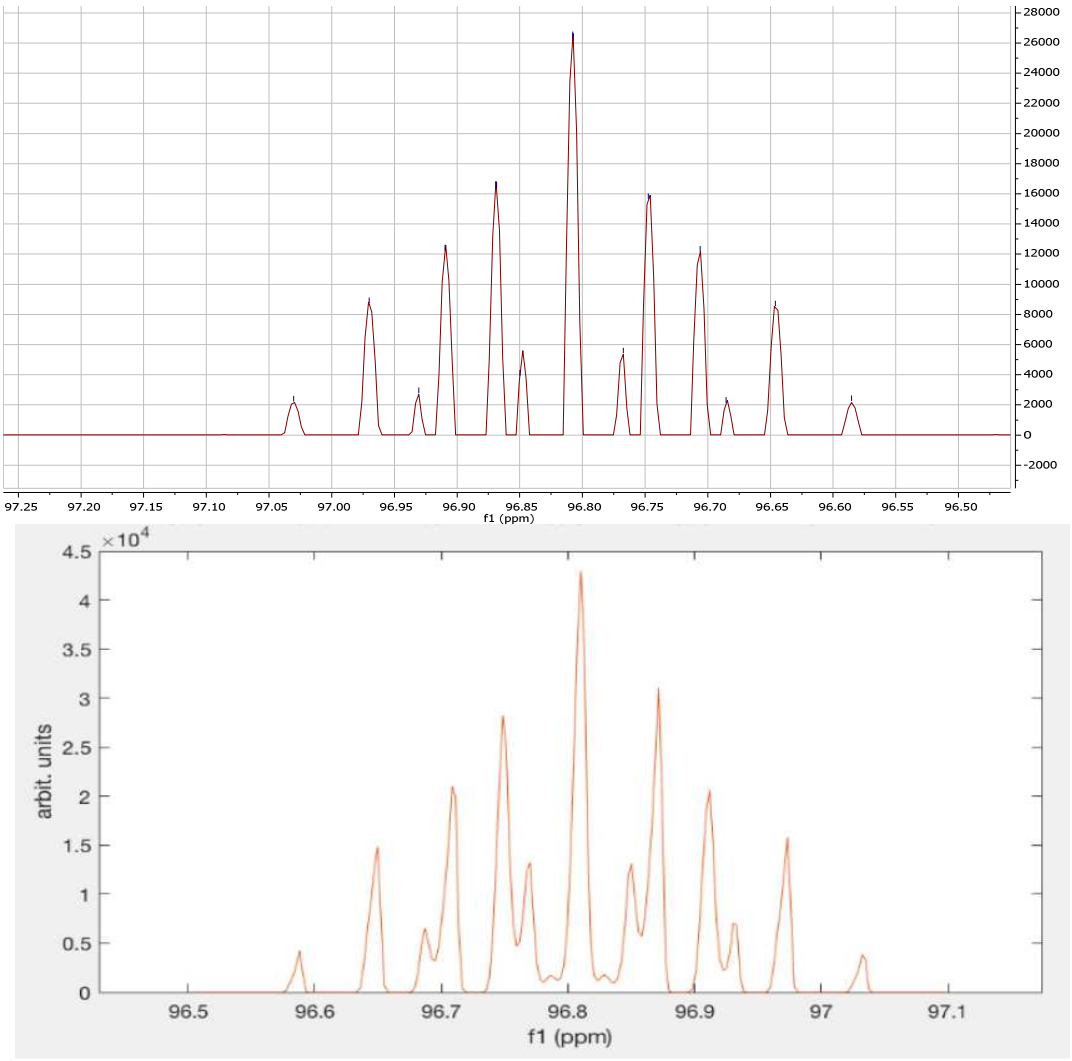

Figure 50: *Comparison of the application of the MestreNova Resolution Booster (top) versus the result of the Lorentz-Gauss deconvolution algorithm from Prof. Dr. Kalthoff (bottom) on the same ^{31}P NMR FID data for compound* ***XIV****.*

The presented solution of the deconvolution issue is also superior to the MestreNova Resolution Booster in terms of the conservation of relative signal intensities, which is not the case for the MestreNova algorithm.[262] Regarding the discussion of the obtained data it seems to be helpful to have a closer look at the basic structural features of the molecules under investigation: All of them have phosphorus as the central atom to which four hetero atoms, oxygen and/or sulfur in varying ratios, are directly attached. In all cases two of the chalcogen atoms bear an alkyl side chain with is a CH_2-CH_3-group. A third oxygen or sulfur atom is linking the nitrogen moiety side chain to the central phosphorus atom and in all but

one case has at least two CH_2-groups as spacers to the nitrogen. The remaining chalcogen atom is only bond to the phosphorus atom itself. This part of the molecule forms a complex interacting spin system due to couplings of the phosphorus to all of the previously mentioned nuclei, generally resulting in doublets.

Additionally, the protons of each sidechain couple with each other and form sub spin systems. Thus, the resulting spin system for the protons of the two CH_2-groups connected to the CH_3-groups can be denoted as an ABM_3X-spin system. A and B represent the two protons of the CH_2-group, M the methyl protons and X the central phosphorus atom. In most cases A and B do not show their diasterotopic properties and thus can be written as A_2. A similar description can be found for the respective carbon atoms, which do show ^1J-couplings to the directly bonded protons, ^2J-couplings to the neighboring protons and ^2J and ^3J-couplings, respectively, to the phosphorus.

The protons of the two CH_2-groups of the nitrogen containing side-chain always show a coupling to the phosphorus as well, resulting in a doublet, and do show vicinal couplings with each other. The carbon atoms do show geminal couplings to the respective protons as well as couplings with the central phosphorus atom and couplings to the directly bonded protons.

However, it seems to be the case that no interaction of the atoms “behind” the nitrogen from the viewing direction of the phosphorus, in terms of identifiable coupling constants, can be observed.

For the correlation of the found coupling constants and chemical shift values the work of *Williamson et al*. from 1968 on the coupling of phosphorus and hydrogen over three and four bonds and text book of Halmann on phosphorus compounds as well as the one of Quin are of great value since the last two have many cross referencing to a large numbers of original literature.[131, 213, 263] Additionally, the Karplus correlation which links the vicinal coupling constants of protons to their dihedral angles is helpful in terms of detecting rigid parts of the molecules versus those parts which can freely rotate along carbon-carbon bonds and thus making the attached protons at least chemically equivalent and the resulting spectrum easier to interpret.[264] in case of a free rotation the coupling constants are expected to show mean values of about 7 to 8 ppm.

Table 14 compares Amiton (**X)** with its thiono isomer (**IX**). Expectedly, the coupling constants have only slightly changed. The most prominent differences can be found in the coupling constants involving the central phosphorus atom. Thus, for the ethoxy groups it could be found that $^2J_{PC}$ coupling increases from thiono to thiol isomer and the $^3J_{PC}$ coupling decreases. Exactly the opposite is found for the corresponding $^3J_{PH}$ coupling. Moreover, the influence of the sulfur instead of the oxygen within the sidechain is very large and has a

dramatic effect on the chemical shift of the adjacent methylene group, resulting in an upfield shift of about 30 ppm. The influence of the sulfur atom on the carbon atom (C7) in the molecule is less pronounced. No effect on the vicinal couplings of the protons is observed. The methyl protons show vicinal couplings of 7.1 Hz respectively, meaning that these groups are freely rotating along the C-C axis.

The same holds true for the two methylene groups in the nitrogen side chain in the thiono isomer. The sulfur seems to exhibit a very strong shielding towards the coupling of the protons to phosphorus and amongst each other resulting in a multiplet structure which could not be further resolved.

Table 14: *Results of the NMR spectroscopic studies of Amiton (**X**) and its thiol isomer (**IX**). Given are the chemical shift values for ^{1}H and ^{13}C as well as the coupling constants and the multiplicity of the signals.*

Compound	δ C [ppm]	*J* [Hz]	δ H [ppm]	*J* [Hz]
IX 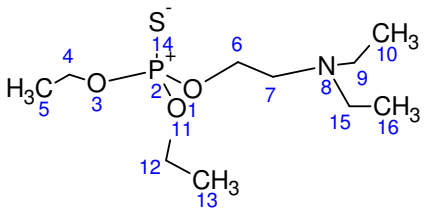	C4, C12 64.1, tdq	$^{1}J_{CH}$ 148.3 $^{2}J_{CH5}$ 4.4 $^{2}J_{PC}$ 5.6	H4, H12 4.06, dq, 4H	$^{3}J_{H4H5}$ 7.1 $^{3}J_{PH}$ 10.1
	C5, C13 15.8, qdt	$^{1}J_{CH}$ 127.5 $^{2}J_{CH14}$ 2.6 $^{3}J_{PC}$ 7.53	H5, H13 1.26,td, 6H	$^{3}J_{H4H5}$ 7.1 $^{4}J_{PH}$ 0.8
	C6 66.0, tdt	$^{1}J_{CH}$ 148.0 $^{2}J_{PC}$ 6.0 $^{2}J_{CH7}$ 3.5	H6 4.01, dt, 2H	$^{3}J_{H6H7}$ 6.6 $^{2}J_{PH}$ 9.6
	C7 52.2, tdt	$^{1}J_{CH}$ 133.0 $^{2}J_{CH6}$ 4.6 $^{3}J_{PC}$ 7.8	H7 2.67, t, 2H	$^{3}J_{H6H7}$ 6.7
	C9, C15 47.6, to	$^{1}J_{CH}$ 132.5 $^{2}J_{CH10}$ 4.4 $^{3}J_{C9H15}$ 4.4	H9, H15 2.51, q, 2H	$^{3}J_{H9H10}$ 7.1
	C10, C16 11.9, qt	$^{1}J_{CH}$ 125.5 $^{2}J_{CH14}$ 3.1	H10, H16 0.96,t, 6H	$^{3}J_{H9H10}$ 7.1
X 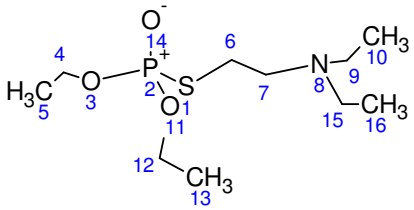	C4, C12 63.4, tdq	$^{1}J_{CH}$ 148.2 $^{2}J_{CH5}$ 4.4 $^{2}J_{PC}$ 6.1	H4, H12 4.10, dq, 4H	$^{3}J_{H4H5}$ 7.1 $^{3}J_{PH}$ 8.9
	C5, C13 16.0, qdt	$^{1}J_{CH}$ 127.4 $^{2}J_{CH14}$ 2.6 $^{3}J_{PC}$ 7.2	H5, H13 1.30,td, 6H	$^{3}J_{H4H5}$ 7.1 $^{4}J_{PH}$ 0.8
	C6 28.4, tdt	$^{1}J_{CH}$ 143.1 $^{2}J_{PC}$ 3.6 $^{2}J_{CH7}$ 3.3	H6 2.83, m, 2H	
	C7 53.1, tdt	$^{1}J_{CH}$ 135.7 $^{2}J_{CH6}$ 4.5 $^{3}J_{PC}$ 5.3	H7 2.68, m, 2H	
	C9, C15 46.2, to	$^{1}J_{CH}$ 132.3 $^{2}J_{CH10}$ 4.4 $^{3}J_{C9H15}$ 4.4	H9, H15 2.50, q, 2H	$^{3}J_{H9H10}$ 7.2
	C10, C16 11.8, qt	$^{1}J_{CH}$ 125.5 $^{2}J_{CH14}$ 3.0	H10, H16 0.97,t, 6H	$^{3}J_{H9H10}$ 7.2

Table 15: *Results of the NMR spectroscopic studies of the Amiton derivatives bearing ethyl groups at the nitrogen atom but having a different chemical surrounding of phosphorus. Given are the chemical shift values for ^{1}H and ^{13}C as well as the coupling constants and the multiplicity of the signals.*

Compound	δ C [ppm]	*J* [Hz]	δ H [ppm]	*J* [Hz]
XI 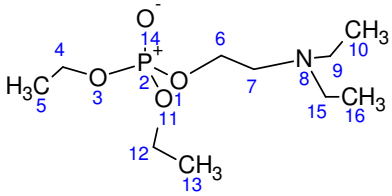	C4, C12 63.6, tdq	$^{1}J_{CH}$ 147.8 $^{2}J_{CH5}$ 4.4 $^{2}J_{PC}$ 5.9	H4, H12 4.05, dq, 4H	$^{3}J_{H4H5}$ 6.9 $^{3}J_{PH}$ 7.7
	C5, C13 16.1, qdt	$^{1}J_{CH}$ 127.1 $^{2}J_{CH14}$ 2.6 $^{3}J_{PC}$ 6.7	H5, H13 1.28,td, 6H	$^{3}J_{H4H5}$ 7.1 $^{4}J_{PH}$ 1.0
	C6 65.6, tdt	$^{1}J_{CH}$ 147.5 $^{2}J_{PC}$ 6.1 $^{2}J_{CH7}$ 3.4	H6 3.98, dt, 2H	$^{3}J_{H6H7}$ 6.5 $^{2}J_{PH}$ 7.4
	C7 52.5, tdt	$^{1}J_{CH}$ 135.7 $^{2}J_{CH6}$ 4.5 $^{3}J_{PC}$ 5.3	H7 2.68, td, 2H	$^{3}J_{H6H7}$ 6.5 $^{3}J_{PH}$ 0.6
	C9, C15 47.6, to	$^{1}J_{CH}$ 132.6 $^{2}J_{CH10}$ 4.4 $^{3}J_{C9H15}$ 4.4	H9, H15 2.51, q, 2H	$^{3}J_{H9H10}$ 7.1
	C10, C16 11.8, qt	$^{1}J_{CH}$ 125.4 $^{2}J_{CH14}$ 3.0	H10, H16 0.94,t, 6H	$^{3}J_{H9H10}$ 7.1
XIV 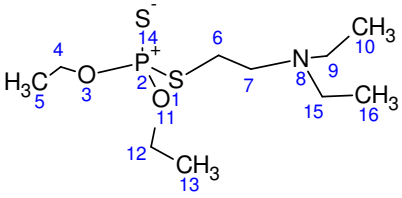	C4, C12 63.8, tdq	$^{1}J_{CH}$ 148.0 $^{2}J_{CH5}$ 4.4 $^{2}J_{PC}$ 6.1	H4, H12 4.05, dq, 4H	$^{3}J_{H4H5}$ 7.1 $^{3}J_{PH}$ 7.7
	C5, C13 15.8, qdt	$^{1}J_{CH}$ 127.6 $^{2}J_{CH14}$ 2.6 $^{3}J_{PC}$ 8.3	H5, H13 1.23,td, 6H	$^{3}J_{H4H5}$ 7.1 $^{4}J_{PH}$ 0.7
	C6 36.7, ttd	$^{1}J_{CH}$ 139.7 $^{2}J_{PC}$ 0.6 $^{2}J_{CH7}$ 3.5	H6 2.81, m, 2H	
	C7 52.3, t	$^{2}J_{CH6}$ 4.2	H7 2.59, m, 2H	
	C9, C15 47.0, to	$^{1}J_{CH}$ 132.8 $^{2}J_{CH10}$ 4.4 $^{3}J_{C9H15}$ 4.4	H9, H15 2.43, q, 2H	$^{3}J_{H9H10}$ 7.1
	C10, C16 12.0, qt	$^{1}J_{CH}$ 125.4 $^{2}J_{CH14}$ 3.0	H10, H16 0.92,t, 6H	$^{3}J_{H9H10}$ 7.2

Additionally, the C9 carbon atom is also influenced by the different chalcogen configurations on phosphorus. This can be observed as a slight deshielding of the carbon atom. However, no further effects on the A_2M_3-spin system of the nitrogen substituents can be observed. The same holds true for compound **XIV** (Table 15) in which also a sulfur atom is introduced in the amino functionalized side chain. Here the strongest effect of the second sulfur atom can be found to be a stronger deshielding of the C6 atom compared to Amiton (**X**) itself. The rest of the molecule of course exhibits the same coupling patterns but different coupling constants. Another change can be observed regarding the $^{3}J_{PH}$ coupling of the ethoxy sidechain, which is the weakest of the three molecules discussed so far. Interestingly, this does not change for the fourth possible chalcogen configuration of compound **XI** (Table 15)

in which the phosphorus is surrounded by four oxygen atoms. Additionally, this configuration is more or less very well comparable with the values found for compound **IX**.

Table 16: *Results of the NMR spectroscopic studies of the Amiton derivatives having two mercaptoethanol groups instead of ethoxy groups bound to phosphorus. Given are the chemical shift values for ^{1}H and ^{13}C as well as the coupling constants and the multiplicity of the signals.*

Compound	δ C [ppm]	*J* [Hz]	δ H [ppm]	*J* [Hz]
XII 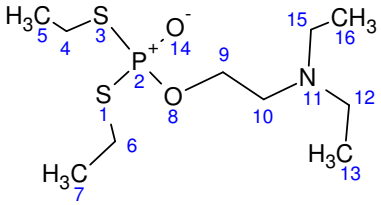	C4,C6	$^{2}J_{PC}$ 3.8	H4,H6	
	25.4, dm		2.67, m,2H	
	25.2, dm			
	C5,C7	$^{3}J_{PC}$ 5.8	H5,H7	
	16.6, dm		1.30, ,2H	
	16.3, dm			
	C9	$^{1}J_{CH}$ 125.3	H9	$^{3}J_{PH9}$ 7.6
	65.8, td, 1C	$^{2}J_{PC}$ 6.2	4.01, dt, 2H	$^{3}J_{H9H10}$ 6.6
	C10	$^{1}J_{CH}$ 132.5	H10	$^{3}J_{H9H10}$ 6.8
	52.5, tm		2.67, t, 2H	
	C12, C15	$^{1}J_{CH}$ 132.4	H12, H15	$^{3}J_{H12H13}$ 7.1
	47.7, tm		2.50, q, 4H	
	C13, C16	$^{1}J_{CH}$ 125.3	H13, H16	$^{3}J_{H12H13}$ 7.1
	11,9, qt	$^{2}J_{C12H13}$ 3.1	0.95, t, 6H	
XIII 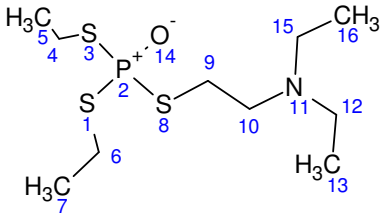	C4, C6	$^{1}J_{CH}$ 143.9	H4=H6	$^{3}J_{PH4}$ 15.4
	27.5,tqd	$^{2}J_{PC}$ 4.0	2.94,dq, 4 H	$^{3}J_{H4H5}$ 7.4
		$^{2}J_{CH5}$ 4.5		
	C5, C7	$^{1}J_{CH}$ 128.5	H5=H7	$^{4}J_{PH5}$ 0.3
	16.1, qdt	$^{2}J_{C4H5}$ 3.5	1.38, td, 6H	$^{3}J_{H5H4}$ 7.4
		$^{3}J_{PC}$ 5.4		
	C9	$^{1}J_{CH}$ 142.3	H9	$^{3}J_{PH9}$ 7.0
	30.6, td	$^{2}J_{PC}$ 3.4	2.99, td, 2H	$^{3}J_{H9H10}$ 8.0
	C10	$^{1}J_{CH}$ 135.8	H10	
	52.8, td	$^{3}J_{PC}$ 4.7	2.76, s, 2H	
	C12, C15	$^{1}J_{CH}$ 132.5	H12=H15	$^{3}J_{H12H13}$ 7.2
	50.0, tq	$^{2}J_{C12H13}$ 3.1	2.51, q, 4H	
	C13, C16	$^{1}J_{CH}$ 125.6	H13=H16	$^{3}J_{H12H13}$ 7.2
	11.9, qt	$^{2}J_{C12H13}$ 3.1	0.97, t, 6H	

Compound **XIII** (Table 16) has three sulfur atoms coordinated to the phosphoryl group of the otherwise unchanged molecule. Furthermore, compound **IX** has the exact opposite chalcogen configuration than compound **XIII**. Again, the influence of the sulfur atom in the nitrogen containing side chain is very strong on the chemical shift value of the neighboring carbon atom and can be compared to compounds **X** and **XIV.** It amounts at about 30 ppm.

In conclusion of these different chalcogen configurations it can be said, that the sulfur atom, in addition to its effect on the chemical shift values and coupling constants of the phosphorus atom, also has a strong effect on the adjacent carbon atom and the hydrogen atoms bonded to the latter one.

The next compounds being described show all the same thiono configuration of the phosphorus with the side chains being attached *via* oxygen atoms to phosphorus. First the

effect of the elongation of the nitrogen bearing side chain is described while the nitrogen still bears two ethyl substituents (Table 17). In compound **XV** three CH_2 groups instead of two are present and in compound **XVII** five CH_2 groups are introduced between the respective oxygen and nitrogen atom of the nitrogen containing side chain. As expected, the chemical shift values and coupling constants of the ethoxy sidechains do not change compared to those molecules described so far and having the same phosphorus-chalcogen surrounding.

Additionally, also the chemical shift values and the observed coupling patterns of the ethyl substituents at nitrogen have not changed. In comparison of compounds **IX**, **XV** and **XVII** the carbon atom next to oxygen is shifted further downfield the more CH_2 groups are attached next to it. Moreover, in compound **XV** for all CH_2 carbon atoms the expected coupling constants could be resolved giving each a triplicated ($^2J_{CH}$) doublet ($^{2\text{-}4}J_{PC}$) of triplets ($^1J_{CH}$). Interestingly, also for the middle carbon atom C7 only a tdt is observed instead of the expected tdtt. This means that the hydrogen atoms at C6 and C8 are chemically and magnetically equivalent to each other and do not cause additional splitting.

Additionally, for the hydrogen atoms in this side chain the chemical and magnetical equivalence of H6 and H8 atoms is clearly demonstrated by the coupling pattern of H7 which is a duplicated quartet. However, the H8 atoms do not show a coupling to phosphorus anymore, which is explained by the long coupling path over five bonds that is too long. Having a closer look at compound **XVII** (Table 17) the observable coupling parameters change quite a lot in that sense that the normally observed doublet structure caused by the coupling of carbon to phosphorus can only be observed for C6 and C8. Also the coupling pattern of C6 is different being a dtq instead of a tdt meaning that it couples not only with the H7 but also with the H8 hydrogen atoms, which again are chemically and magnetically equivalent.

Additionally, C7, C9 and C10 neither show a coupling interaction to phosphorus nor a coupling interaction with the hydrogen atoms of the neighboring carbon atoms, respectively. Regarding the coupling parameters of the hydrogen atoms, only H6 and H10 show the same pattern and allow the determination of coupling constants as do the respective atom positions in other molecules. Those hydrogen atoms bonded to the middle carbon atoms C7, C9 and C10 have a higher order multiplet structure which could not be resolved at this point.

Table 17: *Results of the NMR spectroscopic studies of the thiol-Amiton derivatives with O-N chain length of 3, 4 and 5 CH_2-groups. Given are the chemical shift values for ^1H and ^{13}C as well as the coupling constants and the multiplicity of the signals.*

Compound	δ C [ppm]	*J* [Hz]	δ H [ppm]	*J* [Hz]
XV 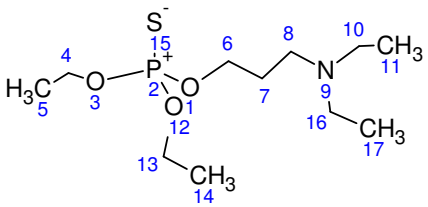	C4, C13 64.1, tdq	$^1J_{CH}$ 147.9 $^2J_{PC}$ 5.6 $^2J_{CH10}$ 3.8	H4, H13 3.98, dq, 4H	$^3J_{H4H5}$ 7.1 $^3J_{PH}$ 9.7
	C5, C14 15.9, qdt	$^1J_{CH}$ 127.2 $^2J_{C9C10}$ 2.6 $^3J_{PC}$ 7.5	H5, H14 1.19, td, 6H	$^3J_{H4H5}$ 7.1 $^4J_{PH}$ 0.8
	C6 66.7, tdt	$^1J_{CH}$ 148.2 $^2J_{PC}$ 5.7 $^2J_{CH7}$ 3.8	H6 3.96, dt, 2H	$^3J_{H6H7}$ 6.4 $^2J_{PH}$ 8.8
	C7 27.8, tdq	$^1J_{CH}$ 127.2 $^2J_{CH6}$ 2.8 $^3J_{PC}$ 7.5	H7 1.69, qd, 2H	$^3J_{H6H7}$ 6.4 $^4J_{PH}$ 0.9
	C8 49.0, tdt	$^1J_{CH}$ 132.0 $^4J_{PC}$ 4.5 $^3J_{CH6}$ 8.9	H8 2.39, t, 2H	$^3J_{H7H8}$ 7.5
	C10, C16 46.9, to	$^1J_{CH}$ 132.1 $^2J_{CH11}$ 4.4 $^3J_{CH16}$ 8.4	H10, H16 2.38, q, 4H	$^3J_{H10H11}$ 7.2
	C11, C17 11.7, qt	$^1J_{CH}$ 125.4 $^2J_{CH10}$ 3.1	H11, H17 0.88, t, 6H	$^3J_{H10H11}$ 7.2
XVII 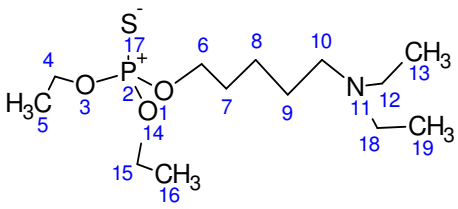	C4, C15 64.1, tdq	$^1J_{CH}$ 147.8 $^2J_{PC}$ 5.7 $^2J_{CH10}$ 4.4	H4, H15 4.05, dq, 4H	$^3J_{H4H5}$ 7.1 $^3J_{PH}$ 9.1
	C5, C16 15.8, qdt	$^1J_{CH}$ 127.4 $^2J_{C9C10}$ 2.6 $^3J_{PC}$ 7.6	H5, H16 1.26, td, 6H	$^3J_{H4H5}$ 7.1 $^4J_{PH}$ 0.8
	C6 67.9, dtq	$^1J_{CH}$ 147.1 $^2J_{PC}$ 6.0 $^3J_{CH7/8}$ 5.8	H6 3.97, dt, 2H	$^3J_{H6H.7}$ 6.7 $^2J_{PH}$ 8.7
	C7 23.5, t	$^1J_{CH}$ 126.5	H7 1.30, hom, 2H	
	C8 29.9, dt	$^1J_{CH}$ 126.5 $^4J_{PC}$ 7.7	H8 1.61, hom, 2H	
	C9 26.4, t	$^1J_{CH}$ 125.5	H9 1.42, m, 2H	
	C10 52.6, t	$^1J_{CH}$ 141.9	H10 2.36, t, 2H	$^3J_{H10H9}$ 7.8
	C12, C18 46.8,tq	$^1J_{CH}$ 132.4 $^2J_{CH13}$ 3.9	H12, H18 2.47, q, 4H	$^3J_{H13H12}$ 7.1
	C13, C19 11.5, q	$^1J_{CH}$ 125.3	H13, H19 0.95, t, 6H	$^3J_{H13H12}$ 7.1

In case of compounds **XVIII** and **XIX** (Table 18) in which the nitrogen substituents are methyl groups instead of ethyl groups and the number of CH_2 groups between oxygen and nitrogen is two and three, respectively, slight differences can be observed amongst the two molecules. The ethoxy side chains of course are not affected by these alterations. The doublet coupling of the phosphorus is still observable for C5 in compound **XVIII** whereas it is not observable for C6 in compound **XIX**.

Table 18: *Results of the NMR spectroscopic studies of the Amiton derivatives bearing methyl groups at the nitrogen atom. Given are the chemical shift values for ^{1}H and ^{13}C as well as the coupling constants and the multiplicity of the signals.*

Compound	δ C [ppm]	*J* [Hz]	δ H [ppm]	*J* [Hz]
XVIII 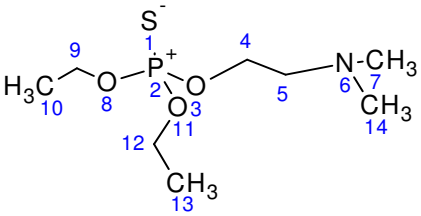	C9, C12 65.6, tdq	$^{1}J_{CH}$ 148.1 $^{2}J_{PC}$ 5.6 $^{2}J_{CH10}$ 4.4	H9, H12 4.03, dq, 4H	$^{3}J_{PH9}$ 9.6 $^{3}J_{H9H10}$ 7.1
	C10, C13 15.8, qdt	$^{1}J_{CH}$ 127.2 $^{2}J_{C9C10}$ 2.6 $^{3}J_{PC}$ 7.5	H10, H13 1.23, dt, 6H	$^{4}J_{PH10}$ 0.8 $^{3}J_{H9H10}$ 7.1
	C4 65.7, tdt	$^{1}J_{CH}$ 147.5 $^{2}J_{PC}$ 5.8 $^{2}J_{CH5}$ 3.0	H4 4.03, dt, 2H	$^{3}J_{PH4}$ 9.3 $^{3}J_{H4H5}$ 6.0
	C5 58.7, tdqt	$^{1}J_{CH}$ 132.6 $^{2}J_{CH4}$ 2.7 $^{3}J_{PC}$ 8.0 $^{3}J_{CH7}$ 5.1	H5 2.51, dt, 2H	$^{3}J_{H5H4}$ 6.0 $^{4}J_{PH5}$ 0.6
	C7, C14 45.6, qtt	$^{1}J_{CH}$ 133.0 $^{3}J_{CH5}$ 5.5 $^{4}J_{CH4}$ 0.9	H7, H14 2.18, s, 6H	
XIX 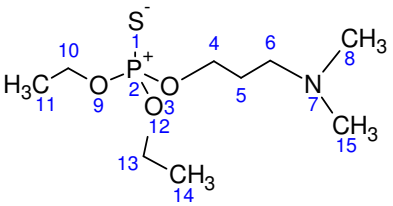	C10, C13 64.1, tdq	$^{1}J_{CH}$ 147.9 $^{2}J_{PC}$ 5.6 $^{2}J_{CH11}$ 4.4	H10, H13 4.05, dq, 4H	$^{3}J_{PH10}$ 9.7 $^{3}J_{H10H11}$ 7.1
	C11, C14 15.8, qdt	$^{1}J_{CH}$ 127.2 $^{2}J_{C10H11}$ 2.6 $^{3}J_{PC}$ 7.4	H11, H14 1.25, td, 6H	$^{4}J_{PH11}$ 0.8 $^{3}J_{H10H11}$ 7.1
	C4 66.4, tdtt	$^{1}J_{CH}$ 147.8 $^{2}J_{PC}$ 5.7 $^{2}J_{CH5}$ 4.4 $^{3}J_{CH6}$ 4.5	H4 4.03, dt, 2H	$^{3}J_{PH4}$ 9.0 $^{3}J_{H4H5}$ 6.5
	C5 28.2, tdt	$^{1}J_{CH}$ 127.5 $^{3}J_{PC}$ 7.5 $^{2}J_{CH}$ 2.6	H5 1.77 ttd, 2H	$^{3}J_{H5H6}$ 7.1 $^{3}J_{H4H5}$ 6.5 $^{4}J_{PH5}$ 0.8
	C6 55.7, ttt	$^{1}J_{CH}$ 132.1 $^{2}J_{CH5}$ 4.9 $^{3}J_{CH4}$ 9.8	H6 2.29, t, 2H	$^{3}J_{H5H6}$ 7.1
	C8, C15 45.4, tqq	$^{1}J_{CH}$ 132.9 $^{3}J_{CH6}$ 5.5 $^{3}J_{CH15}$ 4.5	H8, H15 2.15, s, 6H	

For the methyl protons H7 and H14 no coupling constants can be found resulting in a strong singlet signal for the methyl substituents. This can also be observed in compound **XIX**. Moreover, in compound **XV** (Table 17), which bears two ethyl groups on the nitrogen instead of methyl groups, all CH_2 groups between the oxygen and the nitrogen atom show a doublet coupling with the phosphorus which is not observed for the C6 carbon in compound **XIX**. Additionally, the methyl carbon atoms of compound **XIX** do undergo coupling interactions with the C6 hydrogen atoms. The C4 carbon atom shows couplings to all hydrogen atoms of the CH_2 groups and phosphorus giving a tdtt coupling pattern. The C6 carbon atom is not coupled to phosphorus which is different again compared to compound **XV** (C8 carbon).

Table 19: *Results of the NMR spectroscopic studies of the Amiton derivatives with mono-alkylated nitrogen atom. Given are the chemical shift values for ^{1}H and ^{13}C as well as the coupling constants and the multiplicity of the signals.*

Compound	δ C [ppm]	*J* [Hz]	δ H [ppm]	*J* [Hz]
XX 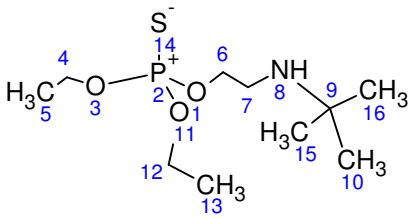	C4, C12 64.1, tdq	$^{1}J_{CH}$ 148.0 $^{2}J_{PC}$ 5.5 $^{2}J_{C4H5}$ 4.5	H4, H12 4.01, dq, 4H	$^{3}J_{PH4}$ 9.7 $^{3}J_{H4H5}$ 7.0
	C5, C13 15.8, qdt	$^{1}J_{CH}$ 127.2 $^{3}J_{PC}$ 7.5 $^{2}J_{C5H4}$ 2.6	H5, H13 1.21, td, 6H	$^{4}J_{PH5}$ 0.9 $^{3}J_{H4H5}$ 7.1
	C6 68.5, tdt	$^{1}J_{CH}$ 148.5 $^{2}J_{PC7}$ 5.9 $^{2}J_{CH7}$ 3.7	H6 4.02, dt, 2H	$^{3}J_{PH4}$ 9.4 $^{3}J_{H6H7}$ 5.5
	C7 42.5, tdt	$^{1}J_{CH}$ 133.7 $^{2}J_{CH6}$ 2.2 $^{3}J_{PC}$ 7.5	H7 2.72, dt, 2H H8 1.08, t, 1H	$^{2}J_{PH4}$ 5.5 $^{3}J_{H6H7}$ 0.7 $^{3}J_{H7H8}$ 7.0
	C9 50.0, qt	$^{1}J_{CH}$ 125.8 $^{3}J_{CH10}$ 2.7		
	C10, C15, C16 28.8, qsep	$^{1}J_{CH}$ 124.7 $^{3}J_{CH15}$ 4.2	H10, H15,16 0.99, s, 9H	

When changing the alkyl substituents of the nitrogen atom by a hydrogen atom and a tertiary butyl group, compound **XX** (Table 19) again the ethoxy substituents of the phosphorus are not affected by this exchange. However, the C6 carbon atom is shifted further down field having a chemical shift value of 68.5 ppm. The CH_3 protons of the tertiary butyl group themselves are chemically and magnetically equivalent giving a strong singlet signal in the proton spectrum. The chemical shift value of the methyl carbon atoms (C10, C15 and C16) is comparably higher than for methyl groups of the ethyl substituents as in compounds **XV** or **XVII**. This can be explained by inductive effects of the other methyl groups attached to the C9 carbon atom, which each results in about 9 ppm of paramagnetic deshielding on the chemical shift value.[265]

Compounds **XXII** and **XXIII** are described next (Table 20). Both molecules have the same nitrogen containing side chain structure as has the deadly nerve gas VX. Thus, both compounds are of great interest, since only a few ^{13}C and no ^{1}H spectra could be found in the publically available literature so far. On the contrary a lot of ^{31}P studies are available for VX.[266] The found chemical shift values are in good agreement with the cited literature. Moreover, compound **XXII** consists of a central phosphorus atom completely coordinated by oxygen, whereas compound **XXII** is the thiono isomer of **XXIII**. This feature has only a minor effect on the chemical shifts of the ethoxy groups as well as on the CH_2 group of C4. The strongest effect of this change is the influence on the $^{3}J_{PH}$ coupling constant, which is with a value of 17.53 Hz the highest one of all described compounds. The isopropyl substituents at the nitrogen interact with each other. This can be seen from the coupling pattern of the carbon atoms and the respective hydrogen atoms.

Table 20: *Results of the NMR spectroscopic studies of the Amiton derivatives bearing isopropyl groups at the nitrogen. Given are the chemical shift values for ^{1}H and ^{13}C as well as the coupling constants and the multiplicity of the signals.*

Compound	δ C [ppm]	*J* [Hz]	δ H [ppm]	*J* [Hz]
XXII 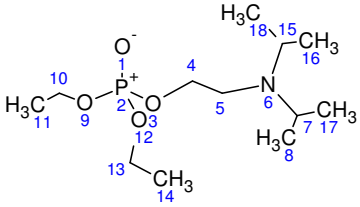	C10, C13 63.6, tdq	$^{1}J_{CH}$ 147.8 $^{2}J_{PC}$ 5.8 $^{2}J_{CH11}$ 4.4	H10, H13 4.05, dq, 4H	$^{3}J_{PH}$ 7.9 $^{3}J_{H10H11}$ 7.1
	C11, C14 16.2, qdt	$^{1}J_{CH}$ 126.9 $^{3}J_{PC}$ 6.7 $^{2}J_{C11H10}$ 2.6	H11, H14 1.27, dt, 6H	$^{4}J_{PH}$ 1.0 $^{3}J_{H10H11}$ 7.1
	C4 67.9, tdt	$^{1}J_{CH}$ 149.3 $^{2}J_{PC}$ 6.4 $^{2}J_{CH5}$ 4.1	H4 3.83, dt, 2H	$^{3}J_{PH}$ 7.0 $^{3}J_{H10H11}$ 8.0
	C5 45.0, tdt	$^{1}J_{CH}$ 132.3 $^{2}J_{CH}$ 3.1 $^{3}J_{PC}$ 7.5	H5 2.64, m, 2H	
	C7, C15 49.5, ddq	$^{1}J_{CH}$ 133.1 $^{2}J_{CH8}$ 4.0 $^{3}J_{CH17}$ 8.1	H7, H15 2.92, sep, 2H	$^{3}J_{H7H8}$ 6.5
	C8, C16-C18 20.8, qqd	$^{1}J_{CH}$ 124.9 $^{2}J_{CH7}$ 3.3 $^{3}J_{CH17}$ 4.9	H8, H16-H18 0.93, d, 12H	$^{3}J_{H7H8}$ 6.5
XXIII 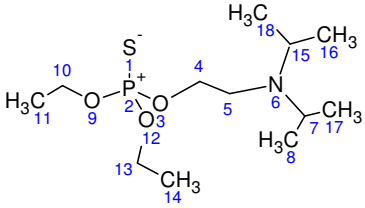	C10, C13 63.3, tdq	$^{1}J_{CH}$ 147.9 $^{2}J_{PC}$ 6.0 $^{2}J_{CH11}$ 4.4	H10, H13 4.10, dq, 4H	$^{3}J_{PH}$ 17.5 $^{3}J_{H10H11}$ 7.1
	C11, C14 16.1, qdt	$^{1}J_{CH}$ 127.3 $^{2}J_{CH10}$ 2.6 $^{3}J_{PC}$ 7.2	H11, H14 1.30, dt, 6H	$^{4}J_{PH}$ 0.8 $^{3}J_{H10H11}$ 7.1
	C4 68.3, tdt	$^{1}J_{CH}$ 149.5 $^{2}J_{PC}$ 6.4 $^{2}J_{CH5}$ 4.4	H4 3.84, dt, 2H	$^{3}J_{PH4}$ 10.2 $^{3}J_{H4H5}$ 8.0
	C5 46.1, tdt	$^{1}J_{CH}$ 134.8 $^{2}J_{CH4}$ 4.4 $^{3}J_{PC}$ 5.4	H5 2.63, m, 2H	
	C7, C15 48.9, dsept	$^{1}J_{CH}$ 132.8 $^{2}J_{CH8}$ 3.9	H7, H15 2.92, sep, 2H	$^{3}J_{H7H8}$ 6.5
	C8, C16-C18 20.9, qm	$^{1}J_{CH}$ 125.2	H8, H16-H18 0.94, d, 12H	$^{3}J_{H7H8}$ 6.6

Also for compounds **XXV** and **XXVI** (Table 21) only the coupling of the nitrogen bearing side chain is of interest since the rest of the molecule is unchanged regarding its chemical constitution as compared to for example compound **IX**. Both molecules have the nitrogen atom embedded in a ring system of five or four CH_2 groups, respectively. For both molecules a mirror plane as symmetry element in the nitrogen containing ring can be identified which leads to a simplification of the signals for the carbon atoms. As expected the direct neighbors of the nitrogen atom are deshielded and have comparable chemical shift values. Only the CH_2 group of the side chain is further deshielded by the influence of the electronegative oxygen atom. In comparison of compound **XXV** and **XXVI** the two next neighboring and also equivalent CH_2 groups are stronger deshielded in compound **XXV** due to an extra CH_2 group in the six-membered ring system. For compound **XXVI** at least the

direct coupling of the carbon atoms and the respective hydrogen atoms could be resolved whereas other coupling parameters are hidden in a multiplet structure of the signal. However, in both cases the signals could be partially resolved for the direct neighbors of the nitrogen atom but remained unresolved for the hydrogen couplings of the ring system. Anyway, the resolution of the signals for compound **XXV** was better than those of compound **XXVI** and thus more details could be extracted from the spectrum.

Table 21: *Results of the NMR spectroscopic studies of the Amiton derivatives with the nitrogen atom embedded in a ring system. Given are the chemical shift values for ^{1}H and ^{13}C as well as the coupling constants and the multiplicity of the signals.*

Compound	δ C [ppm]	*J* [Hz]	δ H [ppm]	*J* [Hz]
XXV 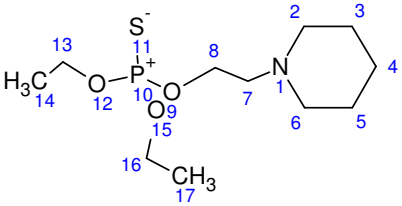	C13, C16	$^{1}J_{CH}$ 148.2	H13, H16	$^{3}J_{PH13}$ 9.6
	64.1,tdq	$^{2}J_{PC}$ 5.5	4.04, dq, 4H	$^{3}J_{H13H14}$ 7.1
		$^{2}J_{CH14}$ 4.4		
	C14, C17	$^{1}J_{CH}$ 127.2	H14, H17	$^{4}J_{PH14}$ 0.8
	15.8, qdt	$^{2}J_{C14H13}$ 2.6	1.25, td, 6H	$^{3}J_{H13H14}$ 7.1
		$^{2}J_{PC}$ 7.6		
	C8	$^{1}J_{CH}$ 147.7	H8	$^{3}J_{PH8}$ 9.4
	65.4, tdt	$^{2}J_{PC}$5.8	4.06, dt, 2H	$^{3}J_{H8H7}$ 6.3
		$^{2}J_{CH7}$ 3.4		
	C7	$^{1}J_{CH}$ 133.2	H7	$^{3}J_{H7H8}$ 6.3
	58.3, tdt	$^{2}J_{CH8}$ 2.2	2.56, td, 2H	$^{4}J_{PH7}$ 0.6
		$^{3}J_{PC}$ 8.0		
	C2, C6	$^{1}J_{CH}$ 132.1	H2, H6	$^{3}J_{H2H3}$ 5.4
	54.7, tsep	$^{2,3}J_{CH3,4}$ 4.4	2.38, t, 4H	
	C3, C5	$^{1}J_{CH}$ 128.2	H3, H5	$^{3}J_{H2H3}$ 5.4
	25.9, m		1.49, tt, 4H	$^{3}J_{H3H4}$ 5.8
	C4	$^{1}J_{CH}$ 123.9	H4	
	24.1, m		1.35, m, 2H	
XXVI 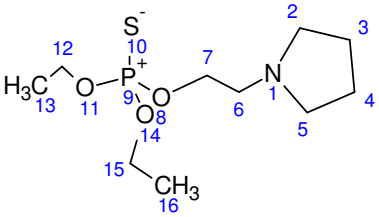	C12, C15	$^{1}J_{CH}$ 148.0	H12, H15	$^{3}J_{PH12}$ 9.6
	64.1, tdq	$^{2}J_{PC}$ 5.6	4.06, dq, 4H	$^{3}J_{H12H13}$ 7.1
		$^{2}J_{CH12}$ 4.4		
	C13, C16	$^{1}J_{CH}$ 127.2	H13, H16	$^{4}J_{PH13}$ 0.8
	15.8, qdt	$^{2}J_{PC}$ 7.5	1.26, td, 6H	$^{3}J_{H12H13}$ 7.1
		$^{2}J_{C13H12}$ 2.6		
	C7	$^{1}J_{CH}$ 147.7	H7	$^{3}J_{PH7}$ 9.2
	66.2, tdt	$^{2}J_{PC}$ 5.7	4.09, dt, 2H	$^{3}J_{H7H6}$ 6.1
		$^{2}J_{CH6}$ 3.4		
	C6	$^{1}J_{CH}$ 132.5	H6	$^{4}J_{PH7}$ 0.6
	55.3, tdm	$^{2}J_{PC}$ 8.2	2.70, td, 2H	$^{3}J_{H7H6}$ 6.2
	C2, C5	$^{1}J_{CH}$ 137.2	H2, H5	
	54.3, tm		2.50, m, 4H	
	C3, C4	$^{1}J_{CH}$ 131.3	H3, H4	
	24.2, tm		1.70, m, 4H	

The next two molecules (Table 22) are different since they do not fit into the systematic structures of the so far discussed ones. Compound **XXIV** is best comparable to compound **XVIII**. In addition to this molecule a methyl group is attached to the carbon atom next to the oxygen of the amino functionalized side chain in both possible stereo isomeric forms.

Table 22: *Results of the NMR spectroscopic studies of the Amiton derivatives having different structure compared to the other Amiton molecules. Given are the chemical shift values for ^{1}H and ^{13}C as well as the coupling constants and the multiplicity of the signals.*

Compound	δ C [ppm]	*J* [Hz]	δ H [ppm]	*J* [Hz]
XXIV 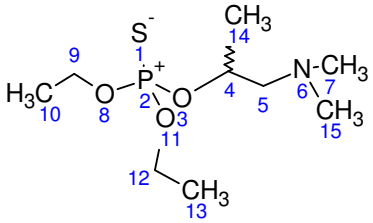	C9 64.1, tdq	$^{1}J_{CH}$ 147.9 $^{2}J_{PC}$ 5.5 $^{2}J_{CH10}$ 4.4	H9 4,05, m, 2H	
	C12 64.0, tdq	$^{1}J_{CH}$ 147.9 $^{2}J_{PC}$ 5.7 $^{2}J_{CH10}$ 4.5	H12 4,05, m, 2H	
	C10, C13 15.9, qdt	$^{1}J_{CH}$ 127.3 $^{2}J_{C10H9}$ 2.6 $^{3}J_{PC}$ 8.1	H10, H13 1,27, t, 6H	$^{3}J_{H10H9}$ 7.2
	C4 74.1, dm	$^{1}J_{CH}$ 147.1	H4 4.60, dsex, 1H	$^{3}J_{PH14}$ 10.5 $^{3}J_{H4H14}$ 6.3 $^{3}J_{H4H5}$ 6.3
	C5 65.0, t	$^{1}J_{CH}$ 148.1	H5 2.43, d, 2H 2.49, d, 2H	$^{3}J_{H4H5}$ 6.4
	C14 19.9, qdtd	$^{1}J_{CH}$ 127.5 $^{2}J_{C14H4}$ 1.4 $^{3}J_{PC}$ 3.5 $^{3}J_{C14H5}$ 3.4	H14 1.27, m, 3H	
	C7, C15 46.0, qqt	$^{1}J_{CH}$ 133.3 $^{3}J_{C7H15}$ 5.5 $^{3}J_{C7H5}$ 0.9	H7, H15 2.21, s, 6H	
XXVII 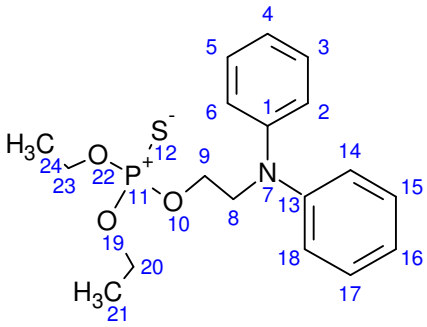	C20, C23 64.6, tdq	$^{1}J_{CH}$ 148.1 $^{2}J_{PC}$ 5.6 $^{2}J_{CH21}$ 4.4	H20, H23 4.04, dqd, 4H	$^{3}J_{PH20}$ 9.7 $^{3}J_{H21H20}$ 7.1 $^{2}J_{H20H20}$ 0.9
	C21, C24 15.9, qdt	$^{1}J_{CH}$ 127.3 $^{2}J_{C4H20}$ 2.2 $^{3}J_{PC}$ 7.5	H21, H24 1.24, dt, 6H	$^{4}J_{PH21}$ 0.3 $^{3}J_{H5H4}$ 7.1
	C9 66.4, tdt	$^{1}J_{CH}$ 148.5 $^{2}J_{PC}$ 5.7 $^{2}J_{CH8}$ 2.7	H9 4.17, dt, 2H	$^{3}J_{PH9}$ 9.6 $^{3}J_{H9H8}$ 5.2
	C8 43.9, tdt	$^{1}J_{CH}$ 136.7 $^{3}J_{PC}$ 7.3 $^{2}J_{CH9}$ 2.2	H8 3.24, dt, 2H	$^{3}J_{H9H8}$ 5.4 $^{4}J_{PH9}$ 0.9
	C4, C16 118.5, dtt	$^{1}J_{CH}$ 160.9 $^{3}J_{CH3}$ 7.4 $^{4}J_{CH2}$ 0.9	H4, H16 6.78, tt, 2H	$^{3}J_{H4H3}$ 7.3 $^{4}J_{H4H2}$ 1.1
	C2, C6, C14, C18 113.7, ddtm	$^{1}J_{CH}$ 150.5 $^{3}J_{CH3}$ 7.8 $^{4}J_{CH6}$ 1.5	H2, H6, 14, 18 6.69, dtm, 4H	$^{3}J_{H2H3}$ 7.7 $^{4}J_{H4H2}$ 1.1
	C3, C5, C15, C17 129.4, dddd	$^{1}J_{CH}$ 157.5 $^{3}J_{CH4}$ 7.8 $^{3}J_{CH2}$ 7.4 $^{4}J_{CH5}$ 1.8 $^{5}J_{CH6}$ 0.9	H3, H5, 15, 17 7.23, dm, 4H	$^{3}J_{H4H3}$ 7.3
	C1, C13 147.6, tm	$^{3}J_{CH3}$ 8.7 $^{2}J_{CH2}$ 1.3		

This feature gives rise to some additional observations in the respective ^{1}H NMR spectra of the H5 hydrogen atoms. However, the most convenient information to start with is the carbon NMR spectrum. The described substitution has a strong effect on the chemical shift value of the C4 carbon atom to which the methyl group is attached. Its chemical shift value in compound **XVIII** is 118.5 ppm, which is in very good agreement with available increment table data.[265] For the C5 carbon atom a comparable value is observable. Additionally, the two hydrogen atoms H5 are diastereotopic. This can be observed from the respective proton NMR spectrum. Interestingly, only for the methyl group a coupling to phosphorus could be resolved while for C5 only the direct coupling with the protons bonded to the carbon atom could be resolved.

The last compound of the Amiton derivatives has two phenyl rings as substituents on the nitrogen atom and thus has also a symmetry element which makes the two substituents chemically and magnetically equivalent. Since the carbon atoms of the phenyl ring are aromatic they are shifted towards higher ppm values and range between 118 ppm for the C4 carbon atom furthest away of the nitrogen and 147 ppm for the carbon directly attached to the nitrogen atom. Furthermore, the respective carbon and proton chemical shifts very nicely match with the values found for the diphenylamine molecule in the spectral database of organic compounds which ideally models this part of the molecule.[10] However, it was not possible to obtain all information about the coupling constants of the ring system since the signals are split up into complex multiplets.

4.3.3 Conclusion

A total of 19 different Amiton derivatives could be successfully synthesized. Twelve of them have not yet been reported in the public literature. Besides the Amiton molecule itself little to no spectroscopic or spectrometric data can be found in the literature for the other compounds. This gap of information could now successfully be closed since all missing IR spectra were recorded on recent analytical instruments. Where possible, also the corresponding Raman spectra were measured and evaluated as well. Additionally, the refractive index values were measured.

Furthermore, a general fragmentation pattern for the Amiton derivatives, under investigation with HPLC ESI-MS, could be identified. Additionally, for the majority of the compounds also the thermodynamically more stable thiol-isomers, could be detected during the standard GC/MS experiment and can thus now be distinguished by the corresponding Kovats index for several available detector systems, e.g. ion trap or quadrupole detectors. Molecules with Kovats indices of values higher than 2000, are no more detectable by the mobile mass

[10] http://sdbs.db.aist.go.jp/sdbs/cgi-bin/direct_frame_top.cgi

spectrometer MM1 of the FOX Recce vehicle. Furthermore, it has to be noted that the experimental setup of a GC-MS instrument is not optimized for the detection of low quantities of the thiono isomers since these are completely converted to the corresponding thiol isomer during the measurement.

It was also found that ^{31}P NMR spectroscopy offers an ideal methodology for the determination of the phosphorus surroundings with respect to the coordination of oxygen and sulfur to the phosphorus central atom. The basic identified feature is that the more sulfur instead of oxygen is bonded to phosphorus the more de-shielding takes place and thus leads to a downfield shift of almost 30ppm per sulfur atom. Alterations in substituents bonded next to the sulfur atom do only have a minor influence resulting in a maximum deviation of 3ppm. However, some compounds show additional coupling constants in the ^{31}P $\{^{1}H\}$ NMR spectra which could not be totally resolved by standard NMR evaluation software. Thus, a deconvolution algorithm developed by Prof. Kalthoff, a cooperation partner from the Hochschule Heilbronn, could be successfully employed to address this issue. Hence, it is possible to fully describe the coupling pattern of the ^{31}P $\{^{1}H\}$ NMR measurements. Moreover, a complete set of NMR data was recorded including important 2D-experiments like ^{1}H-^{1}H-COSY, HMQC and HMBC.

By comparison of the different analytical results with each other it seems to be clear that NMR spectroscopy is somewhat superior to GC-MS and HPLC-MS measurements since a lot of information can be gathered and derived from the different spectra. Additionally, it can be clearly identified which structural motifs, especially of the phosphorus atom are present. Also recent research of analytical laboratories in the verification regime of chemical warfare agents are on the way to develop new NMR pulse sequences and new experiments to enhance sensitivity and clarify the obtained results.[267, 268]

4.4 Investigation of the Thiono-Thiol Rearrangement

All experiments were performed by the experimental use of an HPLC system in which the isomerization reaction (*cf.* Figure 52) was observed directly up to a maximum temperature of 45°C, the upper limit of the autosampler. An example of the change in concentration over time can be seen in Figure 51 for the isomerization of compound **IX** into compound **X** at 45°C in methanol and an initial concentration of compound **IX** of 1 ppm.

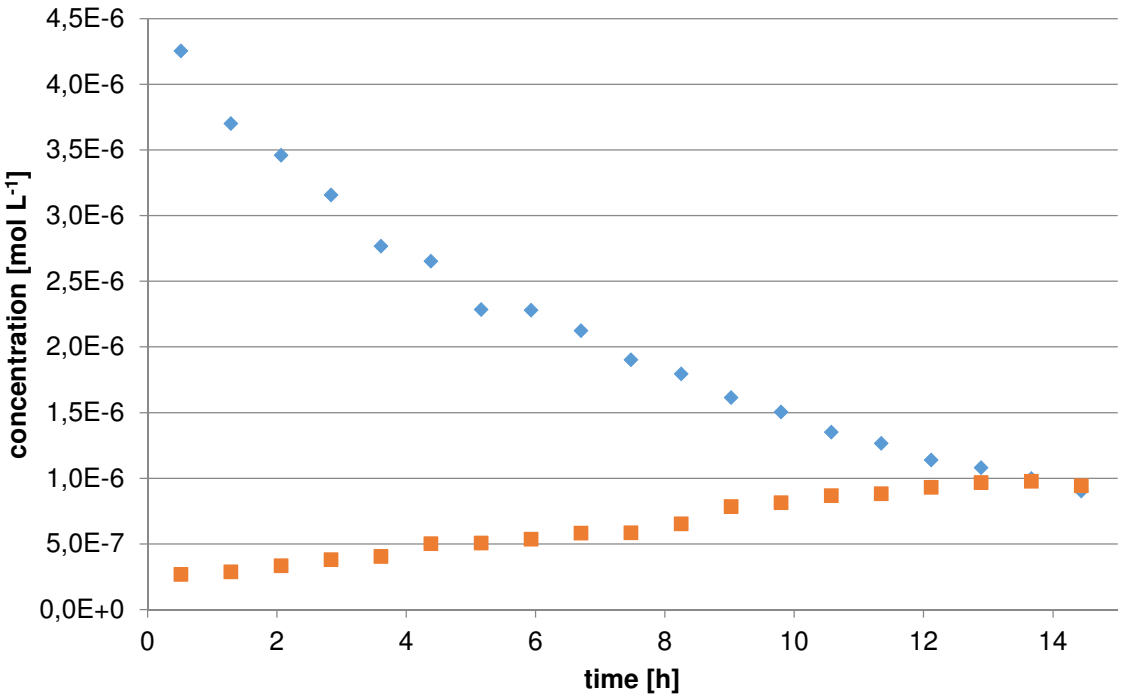

Figure 51: *Graphical representation of the isomerization experiment results: The decay of compound* ***IX*** *(◆) and the formation of compound* ***X*** *(■) in methanol at 45°C.*

Experimental results presented above this temperature regime were obtained by heating diluted samples of the substances in a heating block and taking aliquots at the given time intervals. Figure 51 shows that different rate laws apply for the decomposition and the formation.

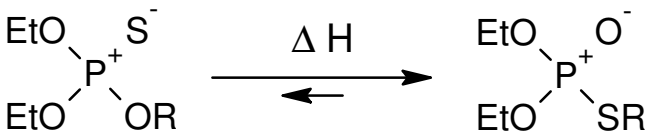

Figure 52: *Graphical depiction of the thermal isomerization reaction.*

Basically the following compounds were subjected to the isomerization studies: **IX**, **XVIII**, **IXX**, **XXIII**, **XXV** and **XXVI**. All were investigated in methanol as a protic polar solvent and

acetonitrile as an aprotic solvent of medium polarity. The isomerization of compound **IX** was additionally followed in acetone which is even more polar compared to acetonitrile and also aprotic. During the preliminary experiments to optimize the HPLC method it was found that the linear regime of the detector is best met with concentrations in the low ppm regime, typically one to ten ppm.

4.4.1 Reaction Order and Kinetic Constants for the Thiono-Educt Depletion

First of all the reaction order of the isomerization needs to be identified to further investigate the rearrangement. Therefore, the initial concentration of the molecule under investigation was altered and the reaction solution heated at the given temperature for a longer period of time; typically 12-16 hours. The resulting data, e.g. Figure 51, were analyzed and the reaction order was determined through linearization methods of the plot of the concentration versus reaction time. The example given in Figure 51 clearly shows that the decay of compound **IX** in methanol follows a different reaction order than that of compound **X** for its formation.

According to Table 1 three cases can be distinguished:

a) zero order: concentration versus time is linear
b) first order: ln of the concentration versus time is linear
c) second order: reciprocal concentration versus time is linear
d) third order: double reciprocal concentration versus time is linear

If none of the three options results in a linear behavior, the reaction is of higher order or broken order. From the known literature these cases are unlikely to be expected for the isomerization process.

The reactions investigated in most detail are those of compounds **IX** and **XXIII** which readily isomerizes into Amiton (**X**) and compound **XXIII-iso**, respectively. These are of greatest importance since Amiton is the most toxic compound used for this thesis and compound **XXIII** and its isomer are the second most toxic ones. The reaction in methanol at 45°C is of first order with respect to the decay of compound **IX** as can be seen from Figure 53.

Table 23: *Data of the linear regression parameters of compound **IX** at 45°C in methanol calculated from the plot in Figure 53.*

concentration	slope	y-intercept	R^2
0.5 ppm	-0.1095	-13.06	0.997
1 ppm	-0.1075	-12.36	0.997
2 ppm	-0.1081	-11.84	0.995

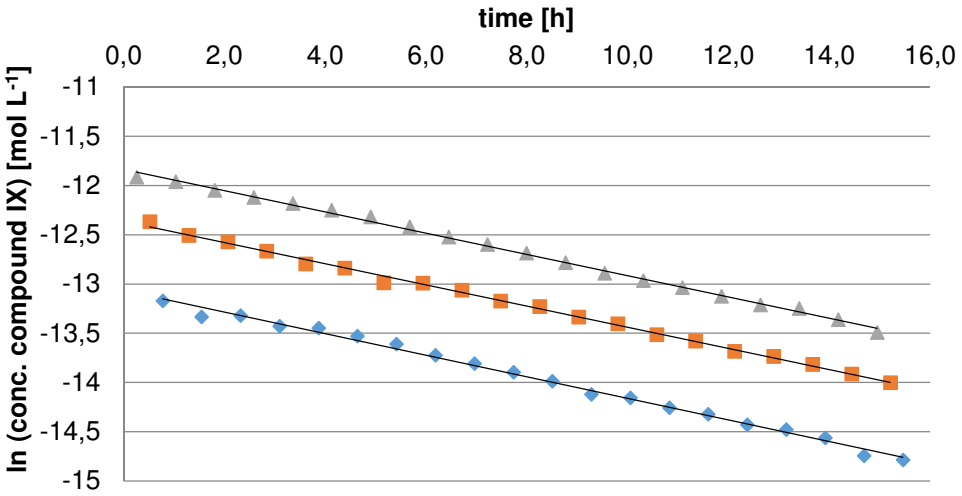

Figure 53: *Plot of the linearized reaction diagrams of compound **IX** at 45°C in methanol. ◆ = 0.5 ppm, ■ = 1.0 ppm, ▲ = 2.0 ppm.*

For a first order reaction the reaction rate constant *k* can be determined as the negative value of the slope from plotting ln [*A*] vs. time according to the rate law given in Table 1. Additionally, the y-intercept represents the ln $[A]_0$ value. Respective regression parameters are given in Table 23. As can be seen from Figure 53 the slope and thus the reaction rate constant is independent of the initial concentration (zero order kinetics). Furthermore, the reaction conditions and parameters determined thereof are given in Table 24 along with values for additional investigations in different solvents for compound **IX**.

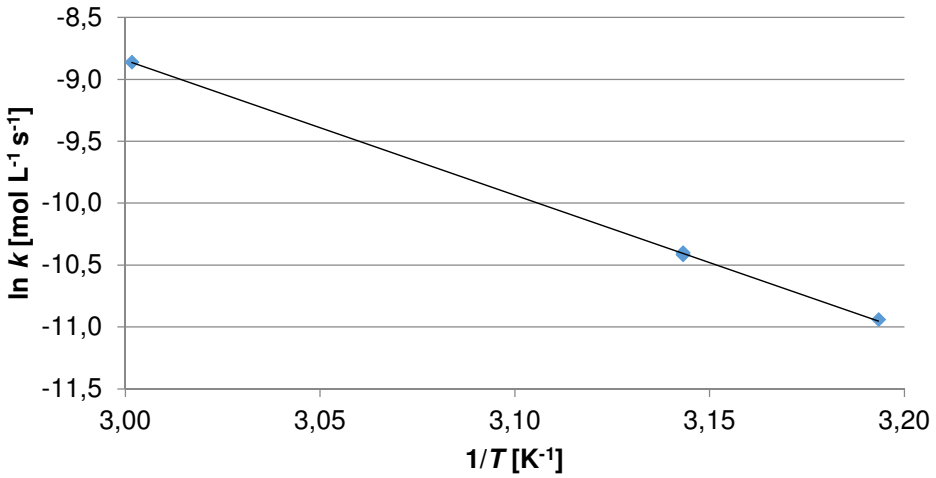

Figure 54: *Arrhenius plot of ln k versus 1/T of the isomerization of compound **IX** to Amiton (**X**) with linear regression curve. The slope equals $-E_A/R$ and the y-intercept is the pre-exponential factor A.*

Moreover, the data were tested to obey the Arrhenius-equation (equation (3.4)) by plotting ln *k* versus 1/*T* in Figure 54. From this plot the pre exponential Arrhenius-factor *A* (y-intercept = ln *A*) and the activation energy E_A (slope = $-E_A/R$) of the isomerization reaction of compound **IX** can be determined. Additionally, the free enthalpy of activation $\Delta^{\ddagger}G$. can be

determined by applying the Eyring theory which gives access to the calculation of the activation enthalpy $\Delta^{\ddagger}H$ and activation entropy $\Delta^{\ddagger}S$.[73, 269] The determined values are reported in Table 25.

Table 24: *Summary of the experimental conditions and determined kinetic parameters for the isomerization of compound* ***IX*** *in different solvents. Unit of the reaction rate is mol L^{-1} s^{-1} for a zero order reaction and s^{-1} for a first order reaction, respectively.*

Solvent	Temp. [°C]	Initial conc. [ppm]	Reaction order	Reaction rate *k* [s^{-1}]	$t_{½}$ [h]
methanol	40	10	1st	1.77E-5	10.87
	45	0.5	1st	3.04E-5	6.33
	45	1	1st	2.99E-5	6.45
	45	2	1st	3.00E-5	6.41
	60	1	1st	1.42E-4	1.36
acetonitrile	40	10	1st	4.90E-6	2356.04
	45	1	1st	2.64E-5	437.20
	50	1	1st	1.70E-6	113.06
acetone	45	1	1st	4.38E.6	45.19
	50	1	1st	1.49E-6	43.93
	60	1	1st	2.37E-5	8.13

To obtain the Eyring results a plot of $\ln(k\,h/(k_B\,T))$ versus $1/T$, which results in a straight line with the slope being $-\Delta^{\ddagger}H/R$ and a y-intercept of $\Delta^{\ddagger}S/R$, was used. From these values the Gibbs free energy of the transition state can be determined by the basic thermodynamic equation:[270]

$$\Delta^{\ddagger}G = \Delta^{\ddagger}H - T\,\Delta^{\ddagger}S \qquad \textbf{(4.1)}$$

with: $\Delta^{\ddagger}G$ = Gibbs free energy of the transition state [J/mol],
$\Delta^{\ddagger}H$ = enthalpy of the transition state [J/mol],
T = temperature [K],
$\Delta^{\ddagger}S$ = entropy of the transition state [J/mol].

As can be seen form Table 25 the activation energy and the activation enthalpy can be determined from both approaches by making use of the relation:[271]

$$E_A = RT - \Delta^{\ddagger}H \qquad \textbf{(4.2)}$$

with: E_A = activation energy [J/mol],
R = ideal gas constant [J/(K mol)],

T = temperature [K],

$\Delta^{\ddagger}H$ = enthalpy of the transition state [J/mol].

Furthermore, the calculated values are in very good agreement with each other. Actually, only for the determination of $\Delta^{\ddagger}G$ the Eyring equation needs to be applied or (4.1) with known values for $\Delta^{\ddagger}H$ and $\Delta^{\ddagger}S$. Moreover, by knowing this number a calculation of the equilibrium constant of the transition state can be done by making use of equation (3.5).

Quite obviously the kinetic parameters for the depletion reaction in methanol are very comparable to each other for compound **IX** and compound **XXIII**. On the contrary, in non-polar aprotic solvents differences are observed. However, the individual molecules do show almost no difference in their kinetic parameters by changing from acetonitrile to acetone. It was found that compound **XXIII** has lower activation energy in all cases compared to compound **IX**. Moreover, the necessary activation energy increases for compound **IX** from protic to aprotic media whereas it drops for compound **XXIII**. The entropy for the isomerization of compound **XXIII** is about double the value in acetonitrile and acetone as it is in methanol. For compound **IX** it is exactly the opposite.

Table 25: *Summary of the Arrhenius parameters and kinetic constants of the transition state for the decay of the educts of the different isomerization reactions in acetonitrile (MeCN), methanol (MeOH) and acetone, respectively. [a)]evaluation according to the Arrhenius equation, [b)]evaluation according to the Eyring equation.*

Compound	Solvent	A [s^{-1}]	E_A [kJ mol^{-1}]	$\Delta^{\ddagger}G$ [kJ mol^{-1}]	$\Delta^{\ddagger}H$ [kJ mol^{-1}]	$\Delta^{\ddagger}S$ [J $mol^{-1}K^{-1}$]
IX[a)]	MeCN	8.51E11	107.80	-	105.16	-25.38
IX[b)]	MeCN	-	107.76	109.15	107.76	-12.70
IX[a)]	MeOH	2.22E10	90.54	-	87.89	-55.67
IX[b)]	MeOH	-	90.49	105.62	87.85	-55.87
IX[a)]	acetone	1.93E12	107.46	-	104.82	-18.58
IX[b)]	acetone	-	107.40	111,43	104.76	-20.99
XXIII[a)]	MeCN	4.83E7	67.23	-	64.59	-107.40
XXIII[b)]	MeCN	-	67.11	99.45	64.46	-109.97
XXIII[a)]	MeOH	3.04E10	81.24	-	78.59	-53.10
XXIII[b)]	MeOH	-	81.20	97.14	78.55	-58.43
XXIII[a)]	acetone	1.08E9	78.21	-	75.56	-80.87
XXIII[b)]	acetone	-	78.17	104.58	75.52	-91.34

Over-all, from the observed half-life times reported in Table 24 and Table 26 it can be stated that the depletion reaction is fastest in methanol and slowest in acetonitrile. Moreover, the half-life time is dependent on the substituents of the nitrogen. Although the isopropyl groups of compound **XXIII** are sterically demanding more space as the ethyl groups of compound

IX the reaction is finished within minutes in methanol. Even for the methyl substituted compound **XVIII** reaction times of several days under the same reaction conditions are observed.

Table 26: *Summary of the experimental conditions and determined kinetic parameters for compounds **XVIII**, **XXIII** and **XXV**. Unit of the reaction rate is mol L^{-1} s^{-1} for a zero order reaction and s^{-1} for a first order reaction, respectively.*

Solvent	Compound	Temp. [°C]	Initial conc. [ppm]	Reaction order	Reaction rate *k*	$t_{½}$
methanol	**XVIII**	40	10	0^{th}	9.43E-7	8.5 d
	XVIII	45	1	0^{th}	1.38E-6	5.8 d
	XXIII	40	10	1^{st}	4.24E-4	27.2 min
	XXIII	50	1	1^{st}	1.40E-3	8.2 min
	XXIII	60	1	1^{st}	2.75E-3	4.2 min
	XXV	45	1	1^{st}	3.04E-6	63.4 h
	XXV	45	2	1^{st}	2.96E-6	65.0 h
acetonitrile	**XVIII**	40	10	0^{th}	8.54E-7	9.4 d
	XVIII	45	1	0^{th}	1.41E-6	5.67 d
	XXIII	50	1	1^{st}	4.05E-4	28.5 min
	XXIII	60	1	1^{st}	1.28E-3	9.0 min
	XXIII	70	1	1^{st}	1.73E-3	6.7 min
acetone	**XXIII**	40	10	1^{st}	2.33E-5	8.27 h
	XXIII	45	1	1^{st}	5.50E-5	3.50 h
	XXIII	50	1	1^{st}	7.75E-5	2.54 h
	XXIII	60	1	1^{st}	1.55E-4	1.24 h

For compounds **XV**, **XIX** and **XXVI** no kinetic evaluation regarding the depletion of the thiono isomer was performed. However, the overall observed time scale of the reaction for these compounds was comparatively longer than for compounds **IX**, **XVIII** and **XXIII** in aprotic solvents. Only for compound **XXV** an evaluation of the reaction in methanol was done; it decreases linear.

4.4.2 Reaction Order and Kinetic Constants for the Thiol-Product Formation

In the same manner as for the thiono decay reaction kinetic, data were obtained at the same time of the experiment for the formation of the favored thiol product. In Figure 55 the formation of the respective isomers for the compounds studied is plotted versus time for the reaction in acetonitrile at 45°C. It can be very nicely seen that the initial increase in

concentration follows a linear relationship over time. Only in proximity of the equilibrium the slope alters and approaches a linear asymptote to the final concentration plateau. The reaction is fastest for the formation of compound **XXIII-iso** (not plotted in Figure 55) and fully observable for compound **IX-iso**. It is slowest for compound **XIX-iso**. Basic kinetic parameters are given in

Table 27 for compound **IX-iso** and in Table 30 for further molecules and isomerization reactions studied. Half-life times were not calculated since they refer to the decay of a substance, whereas the isomers are forming.

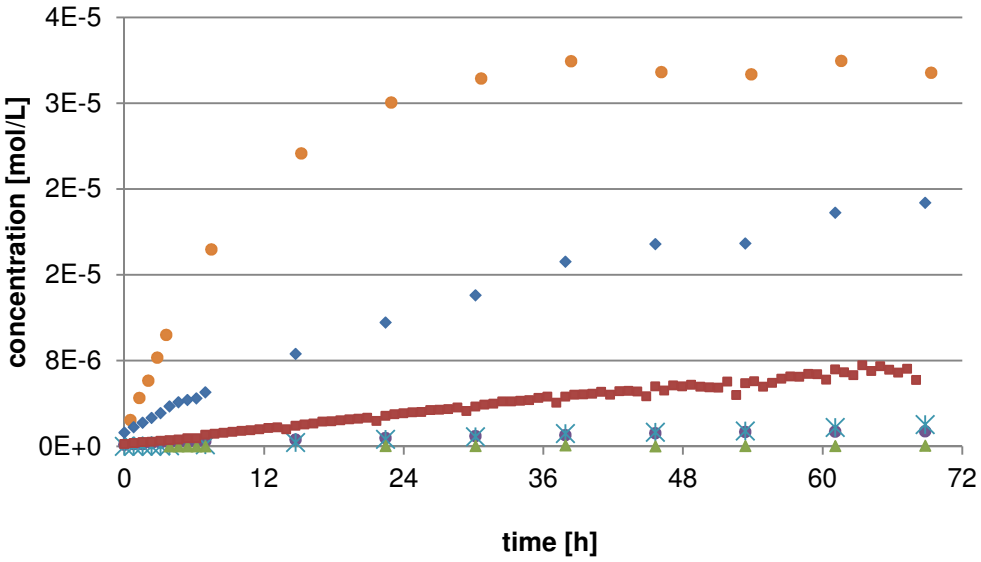

Figure 55: *Plot of the change in concentration of thiol isomers of compounds **XI** (●), **XV** (●), **XVIII** (✳) **XIX** (▲), **XXV** (◆) and **XXVI** (■) versus reaction time in acetonitrile at 45°C. Initial concentration was 1E-5 mol/L.*

In analogy to Figure 53 the formation of compound **IX-iso** is presented in Figure 56. It can be seen that the formation of the respective isomer is strongly concentration dependent. Furthermore, from the data in Table 27 it can be seen that for each increase in concentration no comparable increase in the reaction rate can be observed. Thus, it must be concluded that the reaction must be of some pseudo reaction order or of a broken order, although the change in concentration over time results in a linear relationship.

Table 27: *Data of the linear regression parameters of compound **IX** at 45°C in methanol calculated from the plot in Figure 53.*

concentration	slope	y-intercept	R^2
0.5 ppm	3.95E-8	2.31E-7	0.997
1 ppm	5.54E-8	3.63E-7	0.997
2 ppm	1.44E-7	4.52E-7	0.995
10 ppm	1.62E-6	5.21E-7	0.995

Table 28: *Summary of the experimental conditions and determined kinetic parameters for the isomerization of compound **IX** in different solvents. Unit of the reaction rates would be mol L^{-1} s^{-1} for a zeroth order reaction and s^{-1} for a first order reaction, respectively.*

Solvent	Temp. [°C]	Initial conc. [ppm]	Reaction order	Reaction rate k
methanol	40	10	?	1.57E-10
	45	0.5	?	3.95E-8
	45	1	?	5.54E-8
	45	2	?	1.44E-7
	45	10	?	1.62E-6
	60	1	?	1.01E-7
acetonitrile	40	10	?	4.32E-6
	45	1	?	4.13E-7
	45	10	?	5.48E-5
	50	1	?	4.53E-6
	60	1	?	6.10E-6
acetone	45	1	?	9.85E-8
	50	1	?	9.55E-7
	60	1	?	1.20E-6

However, from Figure 55 it can be assumed that the complete reaction curve for compound **IX-iso** could be linearized by applying a logarithmic function. This is actually not the case. Moreover, with respect to the concentration dependence, only those measurement sets of Table 28 can be subjected to a detailed study by applying the Arrhenius and Eyring equations, which are of the same initial concentration. The results of these investigations are reported in Table 29 and are generally not dependent on the reaction order as long as a linearized relationship of the concentration change with reaction time is given. Since the decay of the thiono isomers follows a first order reaction kinetics it can be assumed the basic underlying reaction can be abbreviated by: A → B + C, which would be typical for a first order reaction. The determined thermodynamic data summarized in Table 29 show only a positive value for the transition state entropy for compound **IX-iso** in acetonitrile, whereas in comparison to the decay reaction always negative values were found. Moreover, the activation energy is higher for compound **XXIII-iso** compared to compound **IX-iso** in case of methanol as the solvent. On the other hand it is only half the energy for acetonitrile and acetone. The same is true for the enthalpy of the transition state.

In Table 30 further parameters of other reactions followed over time are given. As can be seen the reaction rate is dependent on the concentration for all the compounds.

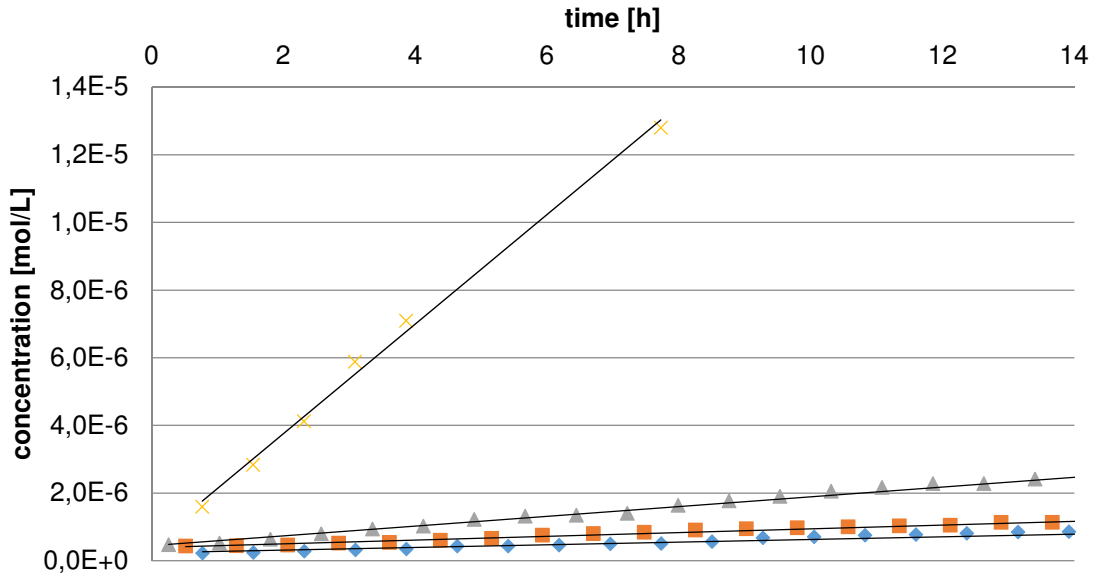

Figure 56: *Plot of concentration increase (formation) of compound **IX-iso** from compound **IX** at 45°C in methanol at varying starting concentrations: ◆ = 0.5 ppm, ■ = 1.0 ppm, ▲ = 2.0 ppm and × = 10.0 ppm. Compare Figure 53 for the decay of compound **IX**.*

Table 29: *Summary of the Arrhenius parameters and kinetic constants of the transition state for the decay of the educts of the different isomerization reactions in acetonitrile (MeCN), methanol (MeOH) and acetone, respectively. [a]evaluation according to the Arrhenius equation, [b]evaluation according to the Eyring equation.*

Compound	Solvent	A [s^{-1}]	E_A [kJ mol^{-1}]	$\Delta^{\ddagger}G$ [kJ mol^{-1}]	$\Delta^{\ddagger}H$ [kJ mol^{-1}]	$\Delta^{\ddagger}S$ [J $mol^{-1}K^{-1}$]
IX[a]	MeCN	1.57E14	140.68	-	138.03	18.00
IX[b]	MeCN	-	140.61	136.99	137.97	3.07
IX[a]	MeOH	84.41	73.08	-	70.44	-216.90
IX[b]	MeOH	-	73.02	140.59	70.38	-220.71
IX[a]	acetone	6.53E11	130.29	-	127.64	-27.58
IX[b]	acetone	-	130.23	140.85	127.58	-41.70
XXIII[a]	MeCN	9.46	55.65	-	53.01	-253.09
XXIII[b]	MeCN	-	55.53	128.96	52.88	-239.13
XXIII[a]	MeOH	1.18E6	87.61	-	84.96	-133.52
XXIII[b]	MeOH	-	87.57	128.54	84.92	-137.10
XXIII[a]	acetone	1.40E-7	68.47	-	65.83	-116.95
XXIII[b]	acetone	-	62.91	105.27	60.27	-141.46

Table 30: *Summary of the experimental conditions and determined kinetic parameters for compounds other than* ***IX****.*

Solvent	Compound	Temp. [°C]	Initial conc. [ppm]	Reaction order	Reaction rate *k* [mol $L^{-1}s^{-1}$]
methanol	**XVIII**	40	10	?	2.80E-7
	XVIII	45	1	?	8.31E-9
	XVIII	50	1	?	1.08E-8
	XVIII	60	1	?	2.03E-8
	XIX	45	10	?	1.88E-8
	XXIII	40	10	?	5.04E-9
	XXIII	50	1	?	7.29E-9
	XXIII	60	1	?	2.44E-8
	XXV	40	10	?	8.08E-6
	XXV	45	0.5	?	1.06E-7
	XXV	45	1	?	5.55E-7
	XXV	45	2	?	7.15E-7
	XXV	45	10	?	1.11E-5
	XXV	60	1	?	4.70E-7
acetonitrile	**X**	45	10	?	7.55E-8
	XV	45	10	?	9.71E-7
	XVIII	40	10	?	5.25E-7
	XVIII	45	1	?	4.67E-8
	XVIII	45	10	?	5.44E-7
	XIX	45	10	?	3.06E-7
	XXIII	50	1	?	3.62E-7
	XXIII	60	1	?	1.89E-7
	XXIII	70	1	?	1,39E-6
	XXV	45	10	?	1.28E-5
	XXV	50	1	?	4.73E-7
	XXV	60	1	?	6.06E-7
	XXVI	45	10	?	2.87E-6
acetone	**XXIII**	40	10	?	1.03E-5
	XXIII	45	1	?	3.85E-7
	XXIII	50	1	?	9.55E-7
	XXIII	60	1	?	6.73E-6

Furthermore, compound **XXIV** does not show any isomerization at all. Even at elevated temperatures of 60°C and over several days no thiol isomer is found in the reaction mixture.

This could be an indication for the sterically demanding transition state. In the beginning it was thought of using this molecule to prove the theoretically postulated reconfiguration mechanism by *Kuntsivich et al.*[64] by isomerizing the molecule and finally have experimental evidence. A more convenient approach could be to exchange the hydrogen atoms by deuterium atoms and check the isomerization results by NMR-spectrometry.

4.4.3 Comparison to Literature-known Studies of the Thiono-Thiol Rearrangement

The four discussed mechanisms in literature were already reported in Chapter 3.3 in Figure 13 and Figure 14. Here they are represented in a reduced form to see differences or common features to the data obtained in the isomerization study of this thesis.

The derived reaction pathways are as follows:

i.	P=S	→	IM1 + IM2	→	P=O
ii.	P=S + P=S	→	IM1 + IM2	→	P=S + P=O
iii.	P=S	→	four-membered ring	→	P=O
iv.	P=S	→	five-membered ring and re-configuration	→	P=O

Table 31: *Collocation of found literature values for the isomerization of Amiton and Amiton-like compounds.*

Compound	T [°C]	Solvent	Reaction order	Reaction rate *k*	E_A [kJ/ mol^{-1}]	Source
IX	73.8	-	1st	4.5E-5 s^{-1}	-	[58]
Systox	37.2	-	1st	1.8E-8 s^{-1}	117	[57]
	37.2	ethanol	1st	6.1E-7 s^{-1}	-	[57]
	37.2	chloroform	1st	8.0E-8 s^{-1}	-	[57]
XVIII	100	-	0	-	-	[59]
$(EtO)_3P=S$	80.1	$CH_3CONHCH_3$	pseudo1st	7.4E-4	-	[272]
Methyl Parathion	60	acetonitrile	2nd	4.82E-4	-	[67]
O-methyl dimethyl-aminoethymethyl-thionophosphonate		cyclic transition state			209	[64]
		ionic transition state			272	[64]
		contacting ion-pair transition state			146	[64]

Furthermore, a comprehensive collocation on available literature studies containing explicit kinetic parameters is given in Table 31. Additionally, a lot of semi-quantitative resources can be found on thiono-thiol rearrangement investigations, which unfortunately do not contain any kinetic constants at all.[61-63, 68] A direct search in SciFinder resulted in two papers for the parameter ‘thiono thiol isomerization kinetic’, as well as for ‘thiono thiol

rearrangement'. However, the parameter 'thiono thiol rearrangement' resulted in 98 hits and 'mechanism thiono thiol' gave only ten hits. Unfortunately, most of the investigations focus on the synthesis of new compounds taking advantage of the thiono-thiol rearrangement but do rarely present more than the conversion efficiency of the chosen reaction conditions.

According to *Fukuto et al*. the isomerization of P=S-Amiton (**IX**) and Systox is faster in more polar solvents and almost inhibited in 2,2,4-trimethylpentane and thus the isomerization must be of ionic character.[57, 58] This postulate is in good agreement with the calculations of *Kuntsivich et al*.[64] Interesting seems also the fact that the reaction order ranges from zero to second order for the isomerization reactions described in literature.

4.4.4 Conclusion

In this part of the thesis the isomerization reaction of two compounds (**IX** and **XXIII**) was studied in detail and the parameters E_A, $\Delta^{\ddagger}G$, $\Delta^{\ddagger}H$ *and* $\Delta^{\ddagger}S$ could be determined. Additionally, some other compounds were studied regarding the reaction rate. In summary, it was found that the reaction order is different for the decay and the formation reaction. Thus, they follow two different rate laws. This has to the best of our knowledge not yet been reported in literature and is independent of the solvent employed. Generally, the reaction rate is depending on the concentration of the sample as well as it is faster in more polar and protic solvents.
Interestingly, the reaction order is different for different compounds, which is in good agreement with the known literature date (*cf*. compound **XVIII**). Additionally, the half-life time of the educt is varying amongst different compounds from a couple of minutes to several days under otherwise unchanged reaction conditions.

For future work it is suggested to use a different experimental setup. Especially, faster analysis methods have to be applied to look into the very beginning of the reaction and get detailed insight in the initial slopes of the decay as well as the formation. This was not possible to be achieved with the given HPLC-MS setup. Another drawback of the HPLC-MS setup is that it is on the one hand very sensitive for the analyte of interest but on the other hand is insensitive towards the detection of intermediates or side products.
Furthermore, it would be of interest what the kinetic parameters would look like in bulk solution and under the influence of a Lewis-acid catalyst like $FeCl_3$.

4.5 Quaternary Ammonium Salts

The main advantage of the preparation of quaternary ammonium salts lies in the hindrance of decomposition and prevention of the thiono-thiol rearrangement of the respective compound. In addition, compared to materials in their liquid state, solids are easier in handling. Although in the literature several general procedures for the preparation of quaternary amines are described, it was only possible to grow single crystals for compounds for which a cation is listed in Table 32. An explanation for this might be (i) the steric hindrance by the substituents at the nitrogen and (ii) the strong hygroscopicity of the forming compound.

4.5.1 Synthesis

In the available literature which focusses on procedures for the synthesis of OP's and OTP's it was always stated that the formation of quaternary salts is very straight forward. Thus, it was the idea to prove the given basic reactions and to collect missing data of the different molecules. The main goal was not to have an optimum yield but to characterize the salt by the determination of its melting point (Table 32). Some of the compounds yielded very pure single crystals which could be additionally characterized by single crystal X-ray diffraction.

Image 18: T*he oxalate of compound* ***XVIII*** *= compound* ***XXX****, which forms thin platelet like structures, after recrystallization and drying from methanol.*

Basically two different routes were applied for the preparation of the salts (*cf.* Figure 57). The first one involves the reaction of the OP with methyl iodide in stoichiometric ratio of 1:1

in tetrahydrofuran as solvent, according to well-known procedures of basic preparative organic text books, e.g. *Organikum*.[115] The second approach was to react the respective OP with an organic acid. The two acids used here were citric acid and oxalic acid hence the OPs are of basic character.

Table 32: *Summary of the prepared quaternary ammonium salts. Given is the parent compound (cation) and corresponding counterion (anion) [Pairs in* ***bold*** *could be characterized by single X-ray crystallography.], crystals appearance, experimental melting point as determined by DSC and available literature values. * indicates compounds not reported in literature so far.*

Compound	Cation	Anion	Appearance	Melting Point [°C]	Melting Point Lit. [°C]
XXVIII*	IX	citric acid	needle like	103.7	-
XXIX	**IX**	**oxalic acid**	plates	87.7	87-88 [108, 273]
XXX	**XIV**	**oxalic acid**	plates	127.9	126.5 [108]
XXXI	XVIII	MeI	cube-like	81.5 /114.8	92 [274] 114-117 [112] 117-119.5 [112]
XXXII*	XVIII	citric acid	white powder	89.3	-
XXXIII	**XVIII**	**oxalic acid**	flat needles	89.8 149.1 (decomp.)	132 [59] 131-132 [112] 148-149 [111, 112]
XXXIV	**XVIII**	**XVIII**	needles	180.2	-
XXXV*	XIX	oxalic acid	flat needles	106.1	-
XXXVI *	**XX**	**MeI**	powder	93.1	-
XXXVII	XXIV	oxalic acid	plates	118.2	114-115 [112]
XXXVIII*	**XXV**	**MeI**	plates	112.4	-
XXXIX	**XXV**	**oxalic acid**	plates	119.3	-
XL*	**XXVI**	**MeI**	plates	49.1	-
XLI	**XXVI**	**oxalic acid**	needles	117.6 143.2-148.2 (decomp.)	120-121 [111, 112]
XLII*	XXVII	oxalic acid	powder	138.9	-

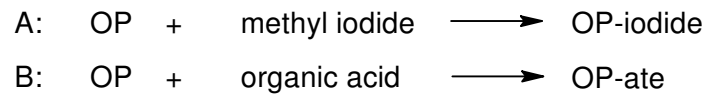

Figure 57: *Synthetic routes for the preparation of the quaternary ammonium salts of the respective organophosphate (OP).*

All compounds listed as cation in Table 32 could be obtained in crystalline solid form by reaction with the given anion. For the other Amiton-like compounds prepared in this thesis all efforts to crystallize those, including systematic screening of solvent molecules of different polarity failed so far. Especially, compounds **XXII** and **XXIII** could not be prepared in crystalline form. This is most likely due to strong sterical shielding of the nitrogen atom by the two isopropyl substituents. The reactions always resulted in pasty melts which immediately cleared upon the addition of new dry solvent.

In total, fifteen different quaternary ammonium salts could be prepared of which eight have not been reported in literature so far. Additionally, for nine compounds also single crystals could be isolated. It has to be noted that none of the obtained single crystal structures has been reported in literature before.

Besides the determination of the respective crystal structure, further characterization of the prepared compounds was done by IR spectroscopy in addition to the determination of the compounds melting points (*cf.* Table 32).

4.5.2 Characterization by Vibrational Spectroscopy

In general, it can be noted that the IR signals of the pure (non-quaternized) parent compound can also be found and identified in the IR spectrum of the respective salt. This is illustrated in Figure 58 with the IR spectra obtained for compound **IX** and its salts (**XXIX** and **XXVIII**).

Compared to the parent compound's IR spectra an additional broad and strong band at 1718 cm^{-1} can be found. This one can be referred to the carboxylic acid C=O stretching vibration, which would be expected in the region of 1700 - 1740 cm^{-1}. The very pronounced broadening in the region of 2500 cm^{-1} to 3000 cm^{-1} can be associated with the additional presence of O-H stretching vibrations from the oxalic and citric acids anions in the crystal.

Additional discussion of the vibrational spectra can be found in Section 4.5.3.3, which focusses on crystalline compounds derived from compound **XXVIII**.

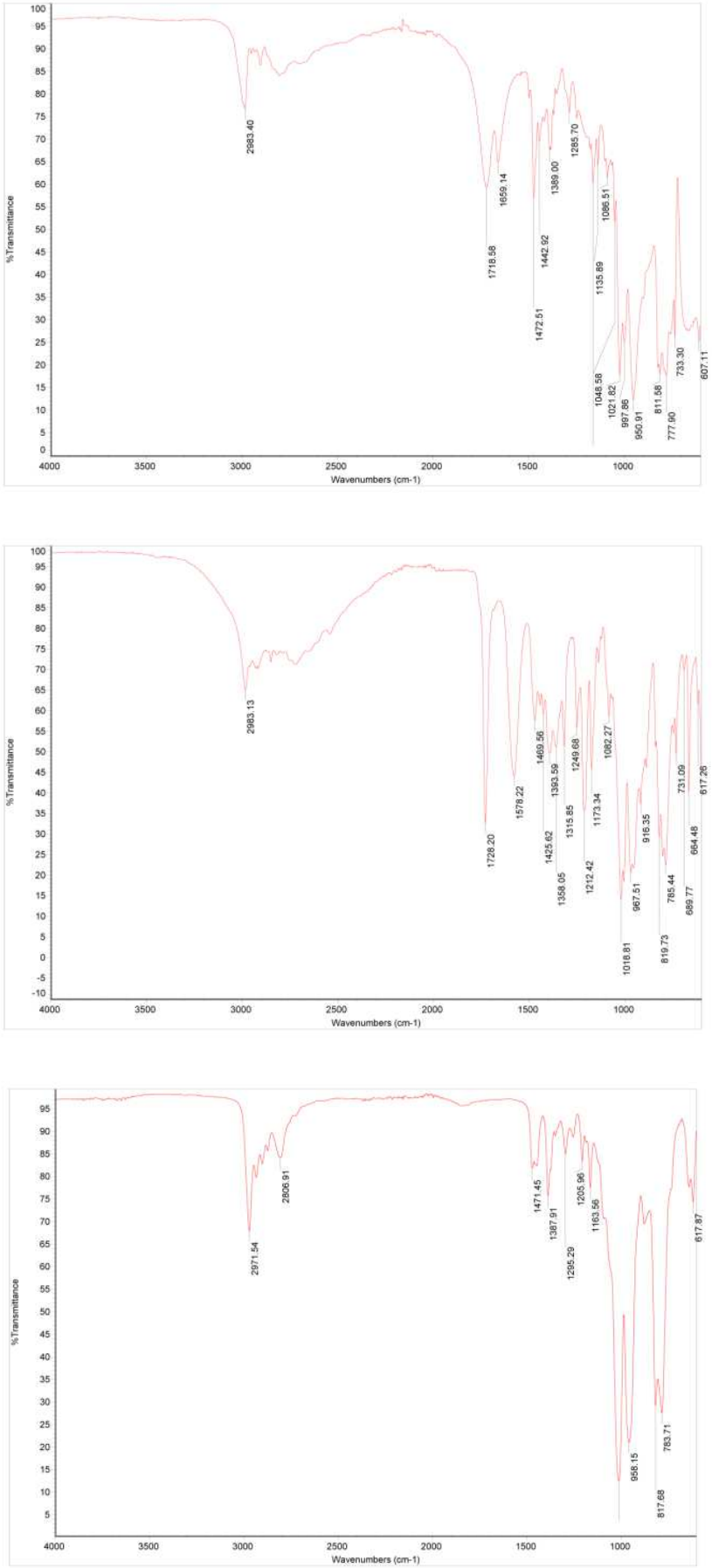

Figure 58: *IR Spectra of compounds* ***XXIX*** *(top left),* ***XXVIII*** *(middle) and* ***IX*** *(bottom).*

4.5.3 Characterization by Single Crystal X-ray Diffraction

Details for X-ray data collection and structure refinements are summarized in Chapter A.5.

4.5.3.1 2-[(Diethoxyphosphorothioyl)oxy]-*N,N*-diethylethanaminium oxalate (XXIX)

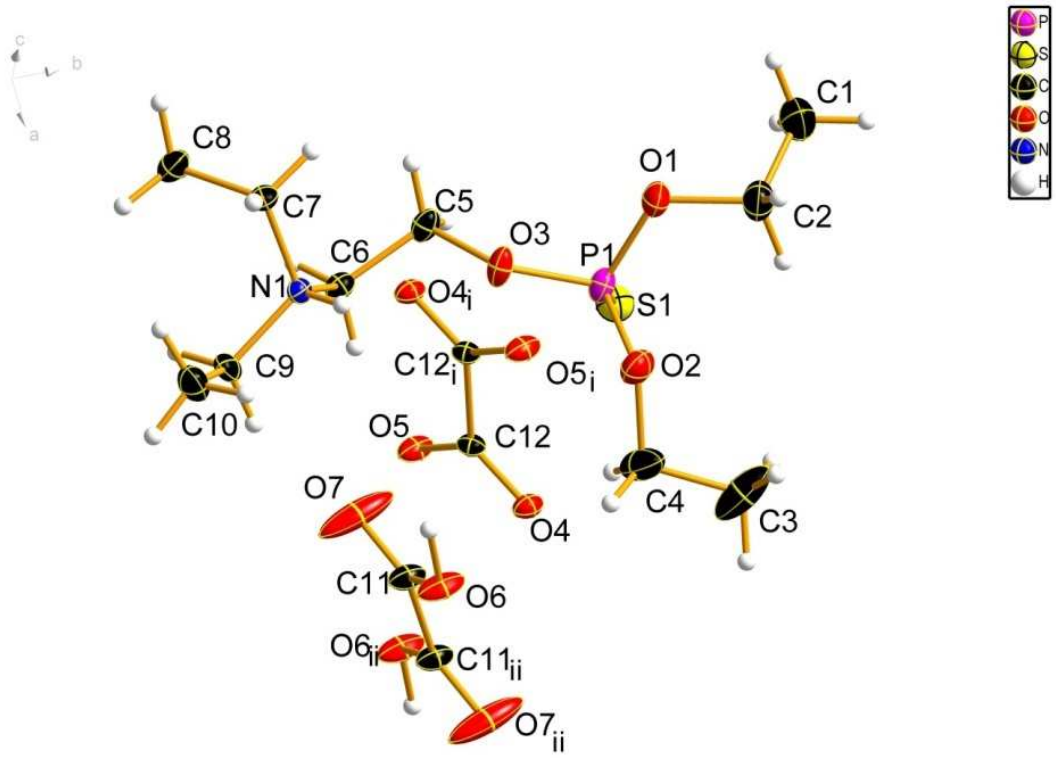

Figure 59: *Molecular structure of the oxalate salt of* ***IX*** *(**XXIX)** in the crystal (asymmetric unit with grown fragments indicated by the letter i), DIAMOND [275] representation; thermal ellipsoids are drawn at 50 % probability level. Symmetry code: (i) 1-x, -y, 2-z; (ii) 1-x, -y, 1-z.*

The title compound crystalizes in the monoclinic space group $P2_1/n$. The asymmetric unit contains one protonated molecule of compound **IX** (cation) which is coordinated by one molecule of oxalic acid (anion) (*cf.* Figure 59). The unit cell is comprised of four molecules of each species. The oxalic acid is coordinated to the molecule *via* hydrogen bonds formed between the protonated nitrogen and O4. Oxalic acid itself is aligned in a chain like structure again by hydrogen bridges between two oxalic acid anions. Structural parameters of the hydrogen bonds are reported in Table 34. Details on bond length, bond and torsion angles are reported in Table 33. All bond lengths are as expected. The coordination sphere of the phosphorus atom is a tetrahedron with all O-P-S bond angles being 116°, whereas the respective O-P-O angles are about 15° smaller. In Figure 60 and Figure 61 the unit cell of compound **XXIX** is shown in two different views. Along the *c*-axis it can be very nicely seen that the oxalic acid molecules are sitting on the centers of the *a*- and *b*-axis. They are twisted against each other. The cations of compound **IX** are ordered from head to tail along the *b*-axis but every second molecule is rotated by 180° along this axis. The same is true for the viewing direction along the *c*-axis. The oxalic acid molecules themselves are forming chain-like structures along the *c*-axis.

Table 33: *Selected bond lengths (Å), bond angles (°) and torsion angles for compound* ***XXIX****. Symmetry code: (i) 1-x, -y, 2-z; (ii) 1-x, -y, 1-z.*

bond length (Å)		bond angles (°)		torsion angles (°)	
P1—O3	1.568(2)	O3—P1—O2	103.2(1)	O2—P1—O3—C5	-154.7(2)
P1—O2	1.572(2)	O3—P1—O1	101.1(1)	O1—P1—O3—C5	100.9(2)
P1—O1	1.575(2)	O2—P1—O1	101.1(1)	S1—P1—O3—C5	-26.4(2)
P1—S1	1.920(1)	O3—P1—S1	116.3(1)	O3—P1—O2—C4	102.5(2)
C12—O4	1.239(2)	O2—P1—S1	116.1(1)	O1—P1—O2—C4	-153.1(2)
C12—O5	1.270(2)	O1—P1—S1	116.6(1)	S1—P1—O2—C4	-25.9(2)
O3—C5	1.459(2)	O4—C12—O5	126.7(2)	O3—P1—O1—C2	163.1(2)
O6—C11	1.272(2)	O4—C12—C12^{i}	118.8(2)	O2—P1—O1—C2	57.0(2)
N1—C6	1.504(2)	O5—C12—C12^{i}	114.5(2)	S1—P1—O1—C2	-69.8(2)
N1—C9	1.505(2)	C5—O3—P1	124.3(2)		
C12—C12^{i}	1.555(3)	C6—N1—C9	109.8(2)		
N1—C7	1.508(2)	C6—N1—C7	113.5(2)		
O2—C4	1.453(3)	C9—N1—C7	113.2(2)		
O1—C2	1.469(2)	C4—O2—P1	124.3(2)		
C11—O7	1.211(2)	C2—O1—P1	120.0(2)		
C7—C8	1.521(3)	O7—C11—O6	125.6(2)		
C6—C5	1.506(3)	O7—C11—C11^{ii}	121.0(2)		
C9—C10	1.513(3)	O6—C11—C11^{ii}	113.3(2)		
C1—C2	1.494(3)	N1—C7—C8	114.0(2)		
C4—C3	1.495(4)	N1—C6—C5	114.4(2)		
C11—C11^{ii}	1.547(4)	O3—C5—C6	108.7(2)		
		N1—C9—C10	111.8(2)		
		O2—C4—C3	109.1(2)		
		O1—C2—C1	109.6(2)		

Table 34: *Parameters of the hydrogen bonds of compound* ***XXIX****. Symmetry code: (i) 1-x, -y, 2-z.*

D---H...A	D--H [Å]	H--A [Å]	D--A [Å]	D--H-----A
N1---H1...O4^{i}	0.83	2.03	2.795	152.3°
O6---H6...O5	1.04	1.43	2.465	178.0°

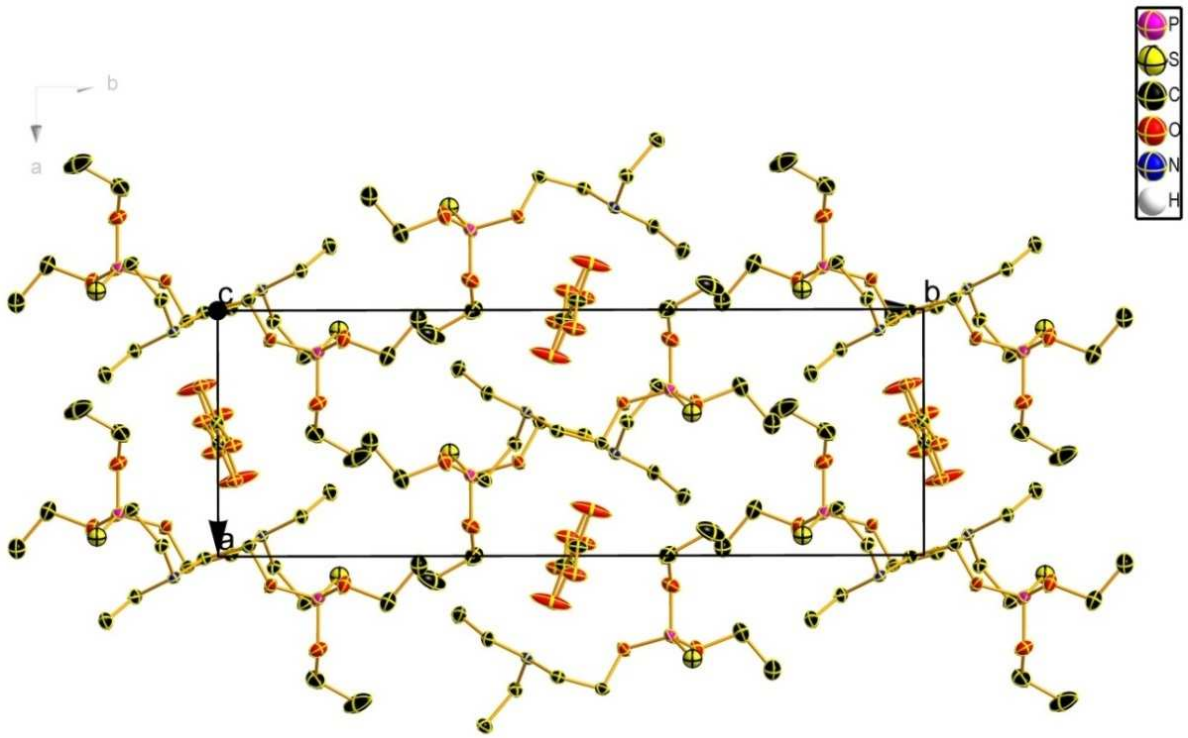

Figure 60: *Crystal structure of compound* ***XXIX****, DIAMOND [275] representation along the c-axis of the unit cell; thermal ellipsoids are drawn at 50 % probability level. Hydrogen atoms and split positions are omitted for clarity.*

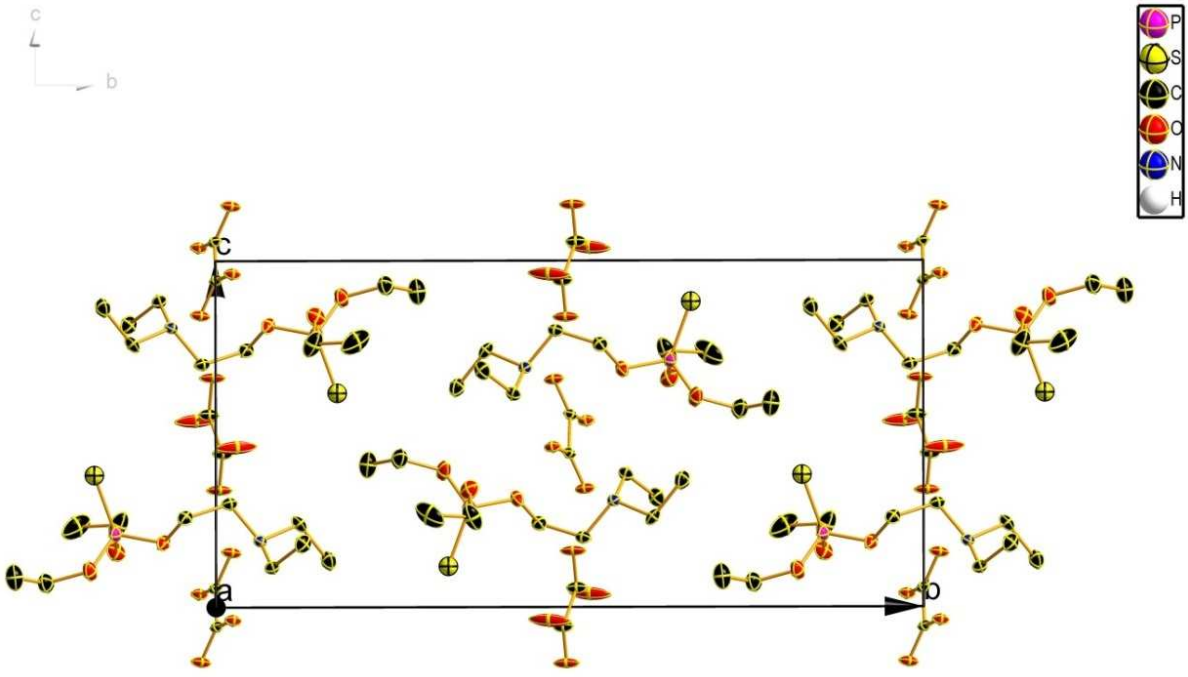

Figure 61: *Crystal structure of compound* ***XXIX****, DIAMOND [275] representation along a-axis of the crystal lattice; thermal ellipsoids are drawn at 50 % probability level. Hydrogen atoms and split positions are omitted for clarity.*

4.5.3.2 2-[(Diethoxyphosphorothioyl)sulfanyl]-*N*,*N*-diethylethanaminium oxalate (XXX)

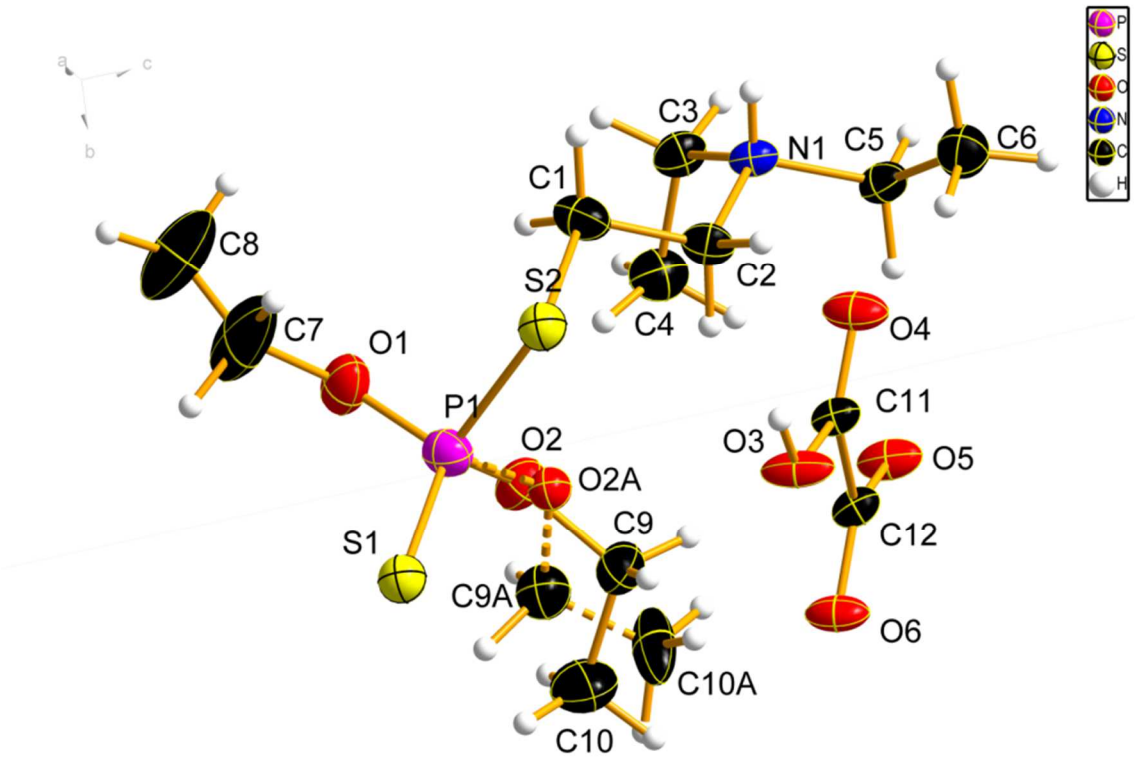

Figure 62: *Molecular structure of the oxalate salt of* ***XIV*** *(****XXX****) in the crystal (asymmetric unit), DIAMOND* ***[275]*** *representation; thermal ellipsoids are drawn at 50 % probability level. The broken bonds indicate a split position of the respective atoms.*

The oxalate of compound **XIV** crystallizes in the orthorhombic space group *Pbca* and has a total of eight formula units in the unit cell. The asymmetric unit is shown in Figure 62. It comprises one molecule **XIV** (cation) and one molecule of oxalic acid (anion). Again the two compounds are coordinated by hydrogen bonds with each other (*cf.* Table 35). Compared to compound **XXIX** one of the ethoxy moieties is disordered into a second position, which is indicated by the letter A. The unit cell is shown in Figure 63. As can be seen the oxalic acid anions are forming a chain-like structure along the *a*-axis. Every second molecule is orientated the same way but is slightly twisted towards the adjacent one. Always two compound **XIV** molecules are aligned tail-to-tail and are stacked along the *b*-axis of the crystal. A second set of molecules **XIV** is turned by 180° around the *a*-axis and is occupying the second half of the crystal lattice.

Table 35: *Parameters of the hydrogen bonds of compound* ***XXX****. Symmetry code: (i) 1/2+x, +y, 3/2-z (ii) 1/2-x, -1/2+y, +z.*

D---H...A	D--H [Å]	H--A [Å]	D--A [Å]	D--H-----A
O3---H3...O5^{i}	0.86	1.63	2.475	168.8°
N1---H1...O6^{ii}	0.82	2.01	2.805	165.4°

Table 36: *Selected bond lengths (Å), bond angles (°) and torsion angles of compound* ***XXX****. Symmetry code: (i) 1/2+x, +y, 3/2-z (ii) 1/2-x, -1/2+y, +z.*

bond length (Å)		bond angles (°)		torsion angles (°)	
P1—O1	1.566(2)	O1—P1—O2A	110.9(2)	O2A—P1—O1	110.9(2)
P1—O2	1.578(3)	O1—P1—O2	95.0(2)	O1—P1—O2	95.0(2)
P1—O2A	1.56(4)	O2A—P1—S1	113.3(2)	O2A—P1—S1	113.3(2)
P1—S1	1.917(2)	O1—P1—S1	117.5(1)	O1—P1—S1	117.5(1)
P1—S2	2.071(2)	O2—P1—S1	119.0(2)	O2—P1—S1	119.0(2)
S2—C1	1.842(3)	O2A—P1—S2	97.5(2)	O2A—P1—S2	97.5(2)
O4—C11	1.203(3)	O1—P1—S2	107.4(1)	O1—P1—S2	107.4(1)
O3—C11	1.293(3)	O2—P1—S2	108.8(2)	O2—P1—S2	108.8(2)
O6—C12	1.232(3)	S1—P1—S2	108.1(1)	S1—P1—S2	108.1(6)
O5—C12	1.255(3)	C1—S2—P1	101.7(2)	C1—S2—P1	101.7(2)
O2—C9	1.468(5)	C2—N1—C5	110.2(2)	C2—N1—C5	110.2(2)
O2A– C9A	1.41(6)	C2—N1—C3	113.8(2)	N1—C3—C4	114.3(2)
C4—C3	1.515(4)	C5—N1—C3	111.9(2)	N1—C5—C6	112.1(2)
C6—C5	1.516(4)	C2—C1—S2	107.6(2)	C8—C7—O1	112.8(4)
C8—C7	1.377(7)	N1—C2—C1	113.4(2)	C7—O1—P1	119.2(3)
N1—C5	1.503(4)	N1—C3—C4	114.3(2)	O4—C11—O3	126.0(3)
N1—C3	1.510(4)	N1—C5—C6	112.1(2)	O4—C11—C12	121.8(2)
N1—C2	1.500(3)	O1—C7—C8	112.8(4)	O3—C11—C12	112.2(2)
O1—C7	1.464(5)	N1—C2—C1	113.4(2)	O6—C12—O5	127.6(3)
C2—C1	1.506(4)	C7—O1—P1	119.2(3)	O6—C12—C11	118.1(2)
C12—C11	1.566(4)	C9—O2—P1	120.7(4)	O5—C12—C11	114.3(2)
C9—C10	1.481(7)	C9A—O2A—P1	122(3)	O2—C9—C10	110.5(4)
C9A—C10A	1.37(7)			C2—N1—C3	113.8(2)
				C5—N1—C3	111.9(2)
				C2—C1—S2	107.6(2)
				N1—C2—C1	113.4(2)
				C9—O2—P1	120.7(4)
				C10A—C9A—O2A	110.(4)
				C9A—O2A—P1	122.(3)

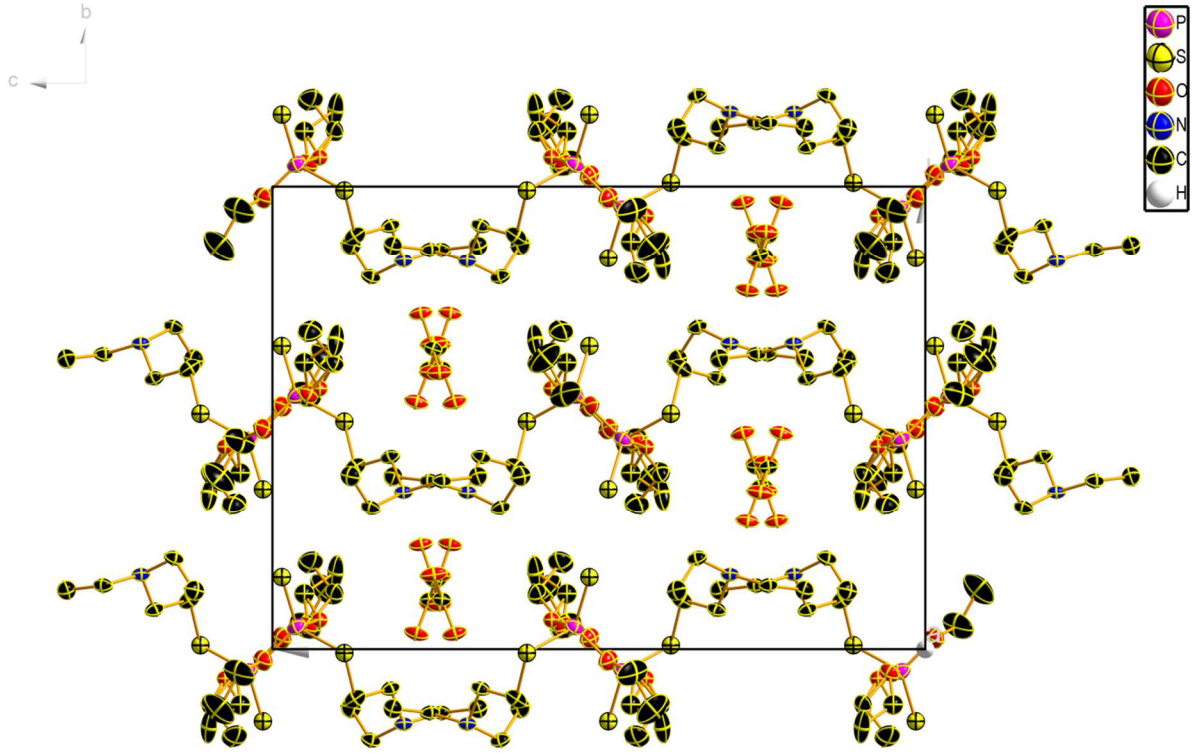

Figure 63: *Crystal structure of the oxalate salt of **XIV** (**XXX**) view of the unit cell along the a-axis, DIAMOND [275] representation; thermal ellipsoids are drawn at 50 % probability level. The broken bonds indicate a split position of the respective atoms. Hydrogen atoms are omitted for clarity.*

4.5.3.3 Crystalline Compounds Derived from and Related to Compound XVIII

4.5.3.3.1 Oxalate and 'Hard' Evidence of the Decomposition Product of Compound XVIII

During the storage of pure Amiton and comparable compounds it was noted that degradation products were forming.[33, 59] The investigation of those compounds was done by means of IR spectroscopy and synthesis of the postulated molecules.[33, 258]

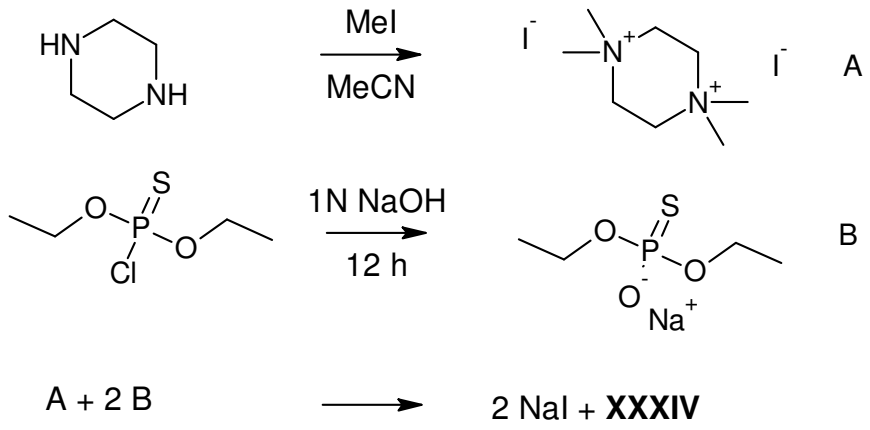

Figure 64: *Synthesis pathway for the preparation of compound **XXXIV**.*

The here described degradation product of compound **XVIII** was found in a long stored NMR tube. To prove this degradation process the postulated decomposition product (compound **XXXIV**) was synthesized (*cf.* Figure 64) and single crystals suitable for X-ray crystallography were grown. Furthermore, the reaction of compound **XVIII** with oxalic acid yielded single crystals suitable for X-ray crystallography (**XXXIII**), which are also described in the following.

4.5.3.3.2 Vibrational Spectroscopy

In the IR spectra of all three compounds (**XVIII**, **XXXIII** and **XXXIV**) a strong band can be assigned to the CH_3 asymmetric vibration at 2966-2979 cm^{-1}. In the spectrum of compound **XVIII** also the respective CH_2 vibration at 2822 and 2771 cm^{-1} can be identified. Some weak CH deformation vibrations in the region of 1448 cm^{-1} to 1476 cm^{-1} can also be found along all three compounds. Additionally, the stretching vibration of the N-C-H groups of the tertiary amine is observed at 2771 $cm^{-1}$for compound **XVIII**. Moreover, the band at 1162 cm^{-1} can be assigned to the tertiary aliphatic amine moiety. These findings are in very good agreement with literature values.[256] The P=S valance vibrations can be found in the region of 820 cm^{-1} and 780 cm^{-1} as a strong doublet band for all three compounds. The doublet structure of the P=S stretching vibration absorption maxima in the IR can be accounted to the presence of two rotational isomers of the molecule.[213]. An additional strong signal at 1703 cm^{-1} can be found in the IR spectrum of compound **XXXIII** which can be clearly assigned to the carbonyl stretching vibration of the oxalic acid part of the crystal.[195]

Due to the strong fluorescence of compounds **XVIII** and **XXXIII** no Raman spectra could be obtained. The Raman spectrum of compound **XXXIV** shows fewer vibrational modes compared to its IR spectrum. The CH deformation vibrations of the piperazine ring can be found at 1435 cm^{-1} and the CH_3 rocking vibrations of the P-OCH_2CH_3 moiety at 1186 cm^{-1}, respectively. Finally, at 1037 cm^{-1} the respective P-O-C stretching vibrations can be identified and at 809 cm^{-1} the C-C vibrations of the piperazine ring occur.

4.5.3.3.3 Molecular and Crystal Structure of the decomposition product of compound XVIII (XXXIV)

The molecular structure of the asymmetric unit of the decomposition product of compound **XVIII** (**XXXIV**) is presented in Figure 65. It crystallizes in the monoclinic space group $P2_1/n$. As can be seen, the structure is comprised of two individual fragments of the parent molecule (**XVII**) being the respective counterion of one another. The positive charge is located on the nitrogen atom, although it is only showing three bonds to carbon atoms. This is because a symmetry operation (180° rotation) of the unit cell has to be performed to see the actual appearance of the crystal structure (*cf.* Figure 66). The former bond between C5 and O2 of the parent molecule (**XVIII**) has been cleaved and instead the nitrogen moiety has formed a 1,1,4,4-tetra-methyl-substituted piperazine cation by joining a second nitrogen

moiety of another molecule. The N-C bond lengths in the ring seem to be slightly larger than those to the methyl groups but are still in the same range with respect to the calculated standard deviation. However, with about 1.50 Å they are slightly longer compared to tabulated values of a standard C-N bond being 1.47 Å.[194] Compared to an unsubstituted piperazine molecule those bond lengths are shorter by about 0.02 Å.[276] The ring formed has chair configuration. The nitrogen atom exhibits a distorted tetrahedral configuration with bond angles in the range of 108.5 to 111.7° which can be explained by the two different sets of substituents (methyl and methylene). The anionic part of the crystal is formed by the *O,O*-diethyl-thio-phosphate moiety. The phosphorus as the central atom of this part has also a distorted tetrahedral configuration. The S1-P1-O2 angle is with 119.2(1)° is significantly larger as compared to the other S-P-O angles of 104.4(3)° and 111.3(1)°. The bond lengths of the respective atoms are also of significant importance. As known from compound **XVIII** the oxygen atom O2 was bound to a CH_2-group (C5) before the decomposition and thus the P-O2 bond would be expected to have the length of a single bond.

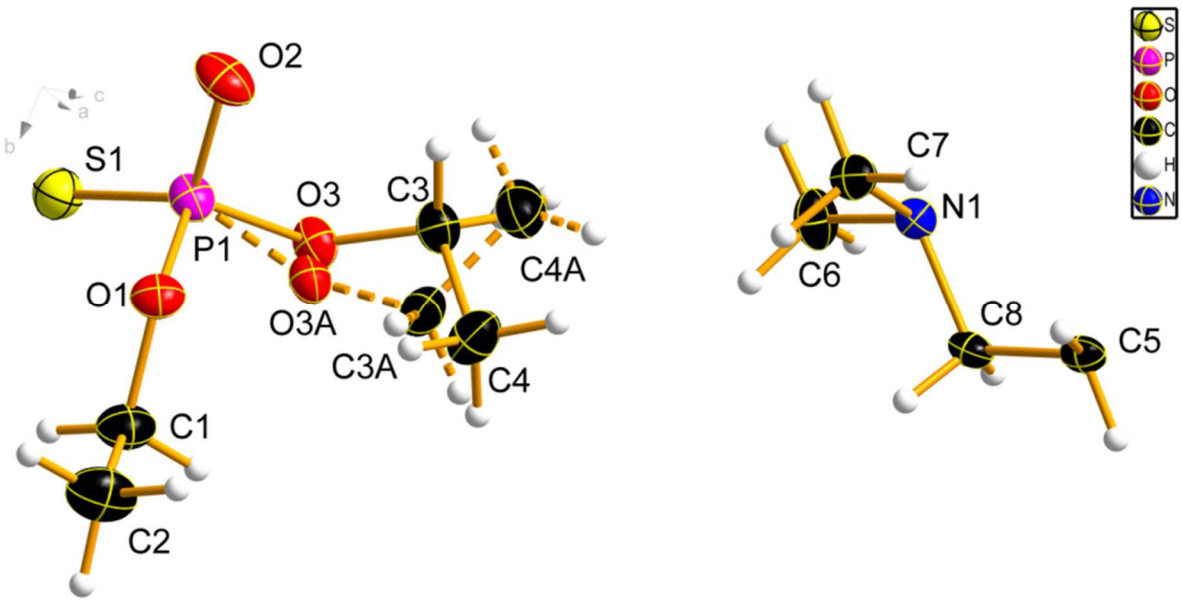

Figure 65: *Molecular structure of the decomposition product of* ***XVIII*** *(****XXXIV****) in the crystal (asymmetric unit), DIAMOND [275] representation; thermal ellipsoids are drawn at 50 % probability level. The broken bonds indicate a split position of the respective atoms.*

On the contrary the P1-O2 bond has the length of a classical P-O double bond with 1.483(4) Å, whereas the P1-S1 bond length of 1.967(5) Å lies in between that of a single and a double bond (2.11 Å and 1.91 Å, respectively).[194] Additionally, the P1-O1 and P1-O3 bonds are also shorter as expected for a single bond and have rather comparable values of 1.606(3) Å and 1.585(9)Å, respectively. The carbon-carbon bonds are shorter than expected. This can be accounted to the strong electron withdrawing properties of the neighboring oxygen atom.

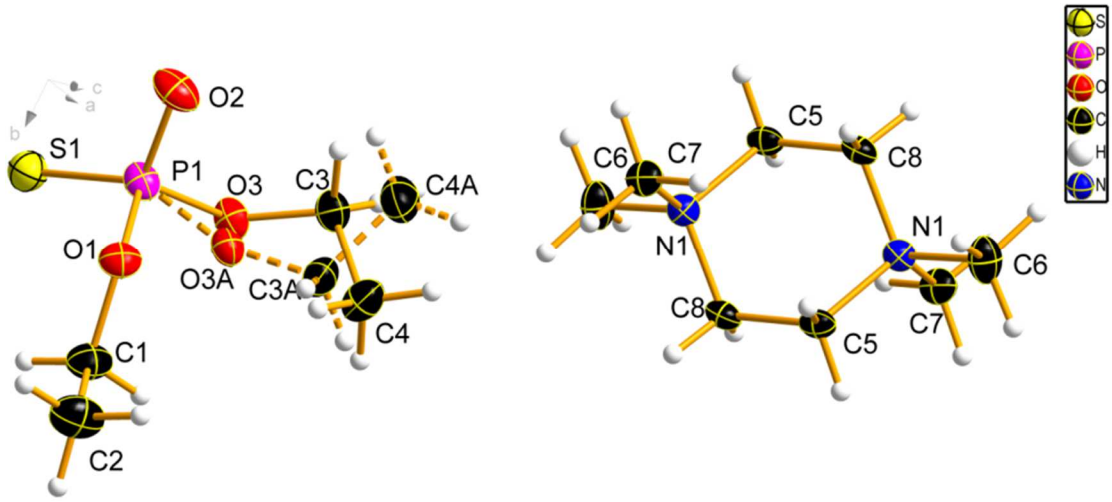

Figure 66: *Crystal structure of the decomposition product of* ***XVIII*** *(****XXXIV****), DIAMOND [275] representation; thermal ellipsoids are drawn at 50 % probability level. The second anion moiety is omitted for better clarity. Broken bonds indicate a split position of the respective atoms.*

Moreover, one ethoxy moiety (O3-C3-C4) bonded to the phosphorus atom is disordered over two positions. By growing the unit cell one can see that each of the nitrogen containing ring sits on the corners as well as in the center of the unit cell. Figure 67 also shows that four formula units are the content of the unit cell. The six-membered piperazine ring itself forms a sub-lattice comparable to tungsten in the body-centered cubic (A2) structure.[277] The four negatively charged counterions can be easily identified in Figure 67. No hydrogen bonds could be found in the crystal structure.

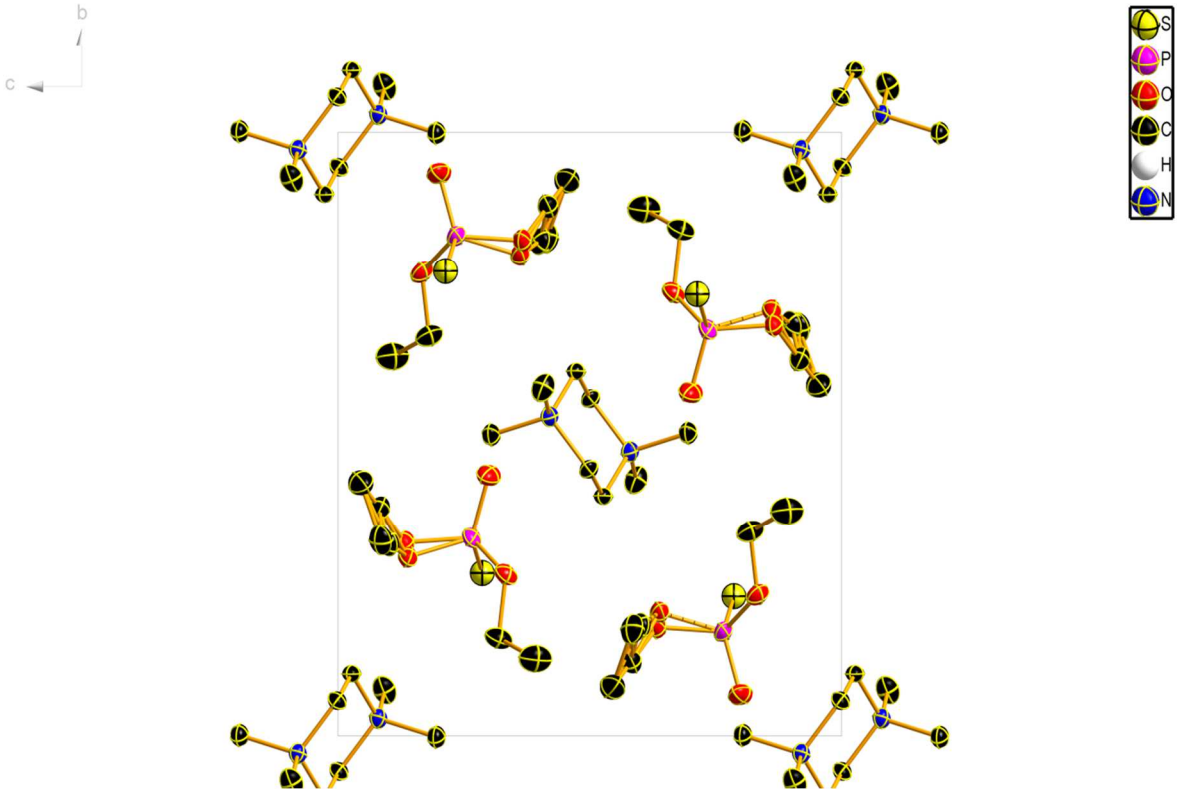

Figure 67: *Crystal structure of compound* ***XXXIV,*** *view of the unit cell along the a-axis, DIAMOND [275] representation; thermal ellipsoids are drawn at 50 % probability level. The broken bonds indicate a split position of the respective atoms. Hydrogen atoms are omitted for better clarity.*

4.5.3.3.4 Molecular and Crystal Structure of compound XXXIII

The molecular structure of the asymmetric unit of the oxalatesalt of compound **XVIII** (**XXXIII**) is presented in Figure 69. It crystallizes in the triclinic space group *P*-1. The asymmetric unit is containing one molecule of compound **XVIII** (anion) and one molecule oxalic acid (cation). First, they are connected *via* two hydrogen bridges form the oxalic acid (O4 and O6) towards the hydrogen atoms of methyl groups bound to the nitrogen atom of compound **XVIII**; and second, by a shorter and thus stronger hydrogen bridges between H1, located on the nitrogen atom N1, and O5 and O7 of the oxalic acid molecule (*cf*. Figure 68 and Table 38). Selected bond length and bond angles are given in Table 37. The bond lengths are all in the expected range and do agree with reported literature values.[194] According to the observed bond angles it can be seen that the sulfur atom is demanding in space and thus forces the three oxygen atoms, which are bound to the phosphorus atom, to get closer to each other. The S – P – O angles range from 113° to 117°, whereas the respective O – P – O angles vary from 102° to 104°. Additionally, the crystal structure shows several hydrogen bonds. The shortest ones were found in between the oxalic acid anions (O4 – H7), which results in the formation of flat layered structure (chains) of the anions in the *a*-*b*-plane (*cf*. Figure 68 and Figure 70). The shortest hydrogen bond is the latter one with a distance of 1.36 Å, being almost a true bond between the participating atoms.

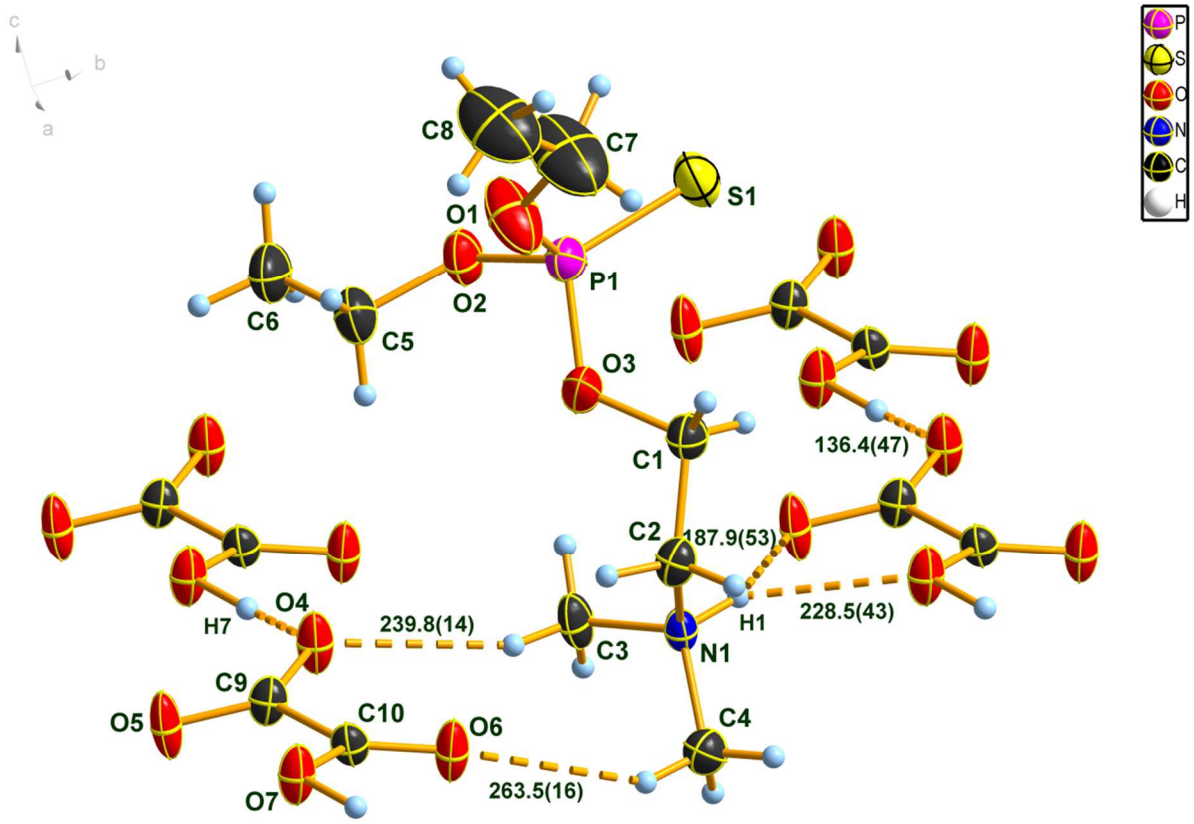

Figure 68: *Hydrogen bonding of the crystal structure of* ***XXXIII****, DIAMOND [275] representation; thermal ellipsoids are drawn at 50 % probability level. The broken bonds indicate hydrogen bonds.*

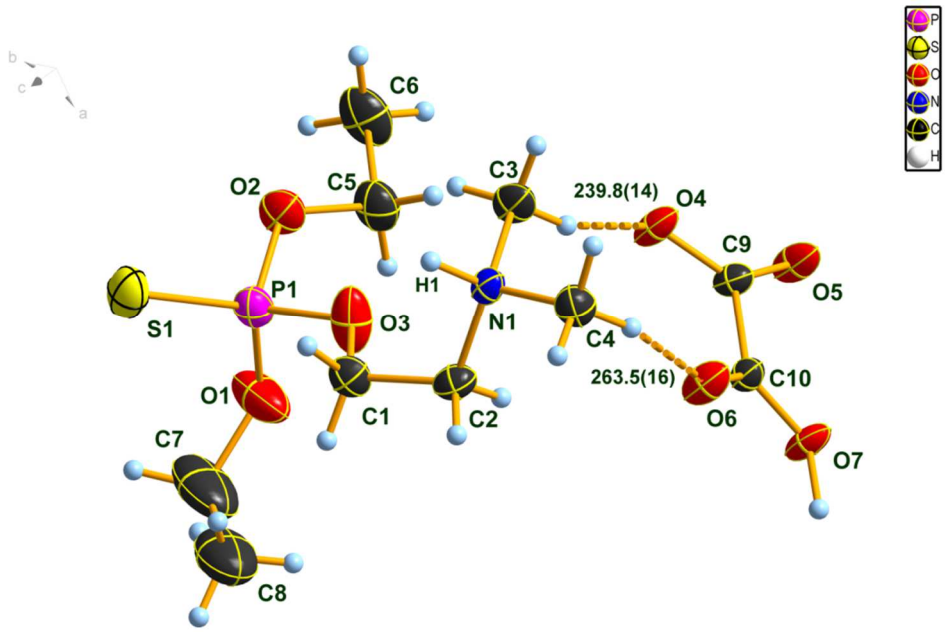

Figure 69: *Molecular structure of* ***XXXIII*** *in the crystal (asymmetric unit), DIAMOND* ***[275]*** *representation; thermal ellipsoids are drawn at 50 % probability level. The broken bonds indicate hydrogen bonds.*

Table 37: *Selected bond lengths (Å), bond angles (°) and torsion angles of compound* ***XXXIII****.*

bond length (Å)		bond angles (°)		torsion angles (°)	
P1—O1	1.558(2)	O1—P1—O2	103.5(1)	O1—P1—O2—C5	-54.4(2)
P1—O2	1.564(2)	O1—P1—O3	103.8(1)	O3—P1—O2—C5	53.0(2)
P1—O3	1.570(2)	O2—P1—O3	101.7(1)	S1—P1—O2—C5	178.1(2)
P1—S1	1.913(1)	O1—P1—S1	116.8(1)	O1—P1—O3—C1	-92.5(2)
O4—C9	1.263(3)	O2—P1—S1	113.3(1)	O2—P1—O3—C1	160.3(2)
O5—C9	1.232(3)	O3—P1—S1	115.8(1)	S1—P1—O3—C1	37.0(2)
O2—C5	1.465(3)	C5—O2—P1	122.7(2)	C4—N1—C2—C1	162.4(2)
O6—C10	1.217(3)	C4—N1—C3	109.9(2)	C3—N1—C2—C1	-73.8(2)
O7—C10	1.304(3)	C4—N1—C2	110.3(2)	O6—C10—C9—O5	160.3(2)
O1—C7	1.390(4)	C3—N1—C2	113.4(2)	O7—C10—C9—O5	-18.4(3)
C5—C6	1.499(4)	C1—O3—P1	121.9(2)	O6—C10—C9—O4	-19.7(3)
C8—C7	1.417(5)	O5—C9—O4	126.6(2)	O7—C10—C9—O4	161.6(2)
N1—C4	1.486(3)	O5—C9—C10	118.8(2)	P1—O3—C1—C2	176.1(2)
N1—C3	1.490(3)	O4—C9—C10	114.6(2)	N1—C2—C1—O3	76.5(3)
N1—C2	1.495(3)	O3—C1—C2	110.3(2)	O2—P1—O1—C7	-149.8(4)
O3—C1	1.443(3)	C7—O1—P1	127.4(2)	O3—P1—O1—C7	104.3(4)
C2—C1	1.498(4)	O2—C5—C6	106.9(2)	S1—P1—O1—C7	-24.5(4)
		O1—C7—C8	115.8(4)	P1—O2—C5—C6	166.9(2)
		N1—C2—C1	113.7(2)	P1—O1—C7—C8	179.1(3)
		O6—C10—O7	125.5(2)		
		O6—C10—C9	121.9(2)		
		O7—C10—C9	112.7(2)		

The oxalate anions are connected by weaker hydrogen bonds with the respective cations. (*cf.* Table 38 and Figure 68). Two oxygen atoms (O5 and O7) of the oxalic acid are connected with the NH hydrogen atom of the next neighboring molecule **XVIII.** The remaining oxygen atoms (O4 and O6) of the oxalic acid anion interact with the two methyl groups bonded to the protonated nitrogen atom of another cation of **XVIII**.

Table 38: *Parameters of the hydrogen bonds of compound **XXXIII**. Symmetry codes: (i) 1+x, +y, +z, (ii): 1+x, +y, +z, (iii): -x, 1-y, 1-z, (iv) 1-x, 1-y, 1-, z, (v) 1+x, 1+y, +z, (vi) -x, -y, 1-z, (vii) -x, 1-y, 1-z.*

D--H...A	D--H [Å]	H--A [Å]	D--A [Å]	D--H-----A
O7---H7...O4^{i}	1.10	1.36	2.459	174.1°
N1^{ii}---H1^{ii}...O5^{v}	0.94	1.88	2.759	154.2°
N1^{iii}---H1^{iii}...O5^{vi}	0.94	1.88	2.759	154.2°
O7^{iv}---H7^{iv}..O4^{vii}	1.10	1.36	2.459	174.1°

Table 39: *Selected bond lengths (Å), bond angles (°) and torsion angles of compound **XXXIV**. Symmetry code: (i) 2-x, -y, 2-z*

bond length (Å)		bond angles (°)		torsion angles (°)	
P1—S1	1.967(5)	O1—P1—S1	111.3(1)	O2—P1—O1—C1	-177.0(1)
P1—O1	1.606(3)	O2—P1—S1	119.2(1)	O3—P1—O1—C1	-62.0(4)
P1—O2	1.483(4)	O3—P1—S1	104.4(3)	O3A—P1—O1—C1	-57.2(3)
P1—O3	1.585(9)	O3A—P1—S1	106.4(3)	S1—P1—O1—C1	53.3(2)
P1—O3A	1.638(1)	O1—P1—O3	110.2(2)	P1—O1—C1—C2	179.0(1)
O1—C1	1.443(6)	O1—P1—O3A	96.6(2)	C6—N1—C5—C8i	-173.1(2)
C1—C2	1.498(2)	O2—P1—O1	103.9(1)	C7—N1—C5—C8i	68.0(2)
C3—C4	1.493(5)	O2—P1—O3	107.6(3)	C8—N1—C5—C8i	-55.4(2)
C3A—C4A	1.497(5)	O2—P1—O3A	116.9(3)	C6—N1—C8—C5i	173.0(1)
C3—O3	1.436(1)	O1—C1—C2	108.2(2)	C7—N1—C8—C5i	-68.2(2)
C3A—O3A	1.477(2)	O3—C3—C4	112.0(4)	C5—N1—C8—C5i	55.4(2)
C5—C8	1.508(8)	O3A—C3A—C4A	111.3(4)	C4—C3—O3—P1	88.1(4)
N1—C5	1.507(6)	C1—O1—P1	121.3(1)	O2—P1—O3—C3	36.8(4)
N1—C6	1.502(6)	C3—O3—P1	119.8(6)	O1—P1—O3—C3	-76.0(4)
N1—C7	1.503(6)	C3A—O3A—P1	120.9(7)	S1—P1—O3—C3	164.4(3)
N1—C8	1.507(6)	C6—N1—C7	108.0(1)	C4A—C3A—O3A—P1	-88.2(5)
		C6—N1—C8	108.5(1)	O2—P1—O3A—C3A	49.9(5)
		C6—N1—C5	108.5(1)	O1—P1—O3A—C3A	-59.5(5)
		C7—N1—C8	111.6(1)	S1—P1—O3A—C3A	-174.0(4)
		C7—N1—C5	111.7(1)		
		C8—N1—C5	108.5(2)		
		N1—C5—C8	112.3(1)		
		N1—C8—C5	112.2(1)		

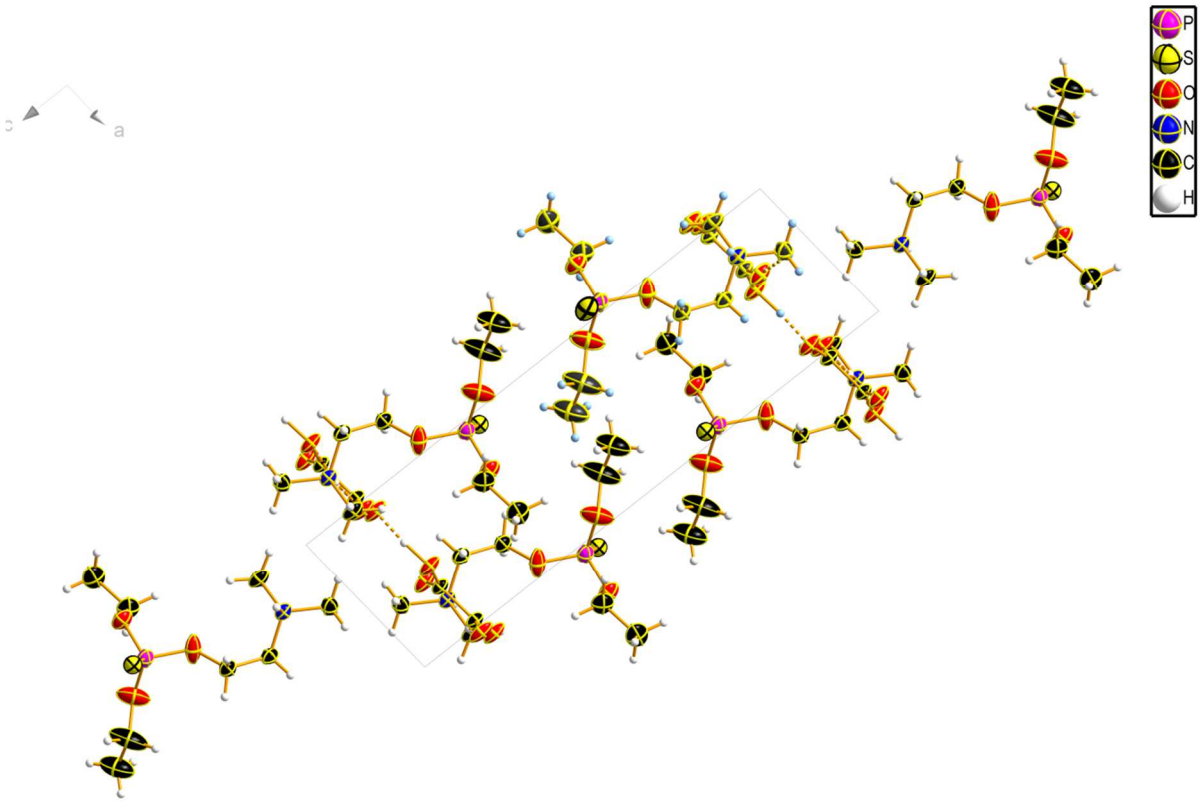

Figure 70: *Molecular structure of* ***XXXIII*** *in the crystal (unit cell with hydrogen bonds and grown fragments), DIAMOND [275] representation; thermal ellipsoids are drawn at 50 % probability level. View along b-axis. The broken bonds indicate hydrogen bonds.*

4.5.3.4 2-[(Diethoxyphosphorothioyl)oxy]-*N*-isopropyl-*N*-methylethanaminium iodide (XXXVI)

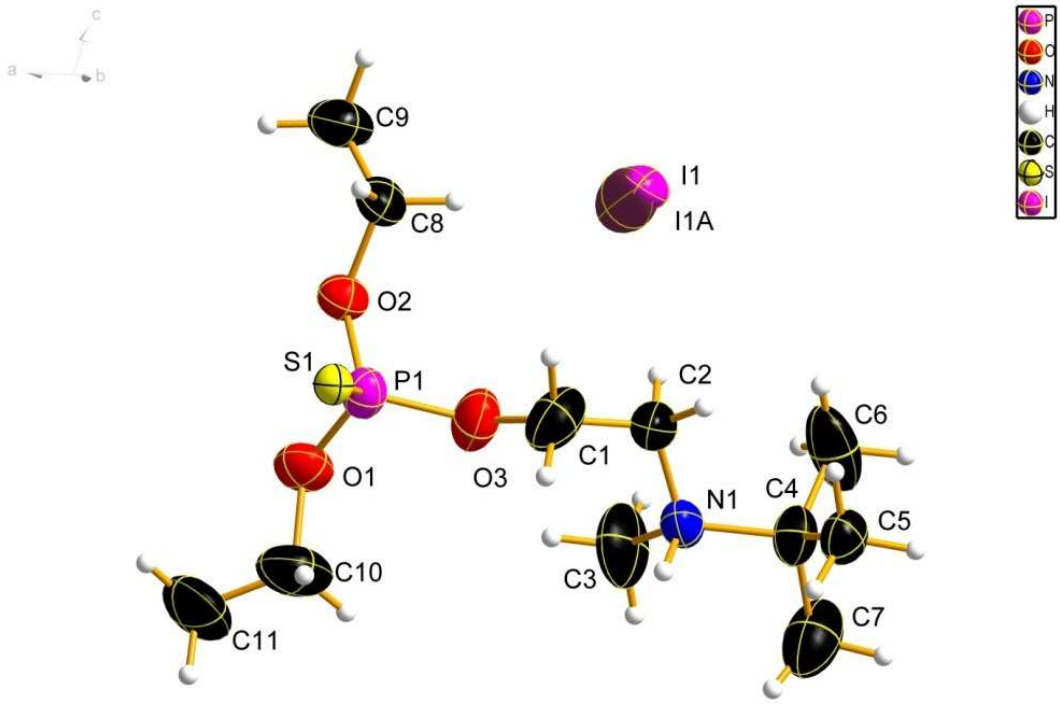

Figure 71: *Molecular structure of the compound* ***XXXVI*** *in the crystal (asymmetric unit), DIAMOND [275] representation; thermal ellipsoids are drawn at 50 % probability level.*

The N-methylation product of compound **XX** crystallizes in the monoclinic space group $P2_1/c$ and has a total of four molecules in the unit cell (not shown). Each compound **XX** molecule is positively charged due to the N-methylation. The anionic part of the salt is formed by a negatively charged iodine atom which is disordered over two positions. The asymmetric unit is shown in Figure 71 and the crystal structure, with viewing direction along the *b*-axis, is shown in Figure 72. Obviously, the ethoxy moieties are not disordered in this case, as compared to previously described crystal structures, but especially C10 and C11 show larger displacement parameters than the other atom positions of the molecule. Selected bond lengths, bond angles and torsion angles are given in Table 40. In the crystal no hydrogen bonds could be found. O – P – O bond angles are about 10 degrees smaller than those of the O – P – S system. Again, the P1 - S1 bond length is longer than the respective phosphorus – oxygen bonds.

Table 40: *Selected bond lengths (Å), bond angles (°) and torsion angles of compound* ***XXXVI****.*

bond length (Å)		bond angles (°)		torsion angles (°)	
P1—O1	1.540(5)	O1—P1—O2	97.7(2)	O1—P1—O2—C8	176.6(5)
P1—O2	1.560(4)	O1—P1—O3	104.2(3)	O3—P1—O2—C8	-76.4(5)
P1—O3	1.571(5)	O2—P1—O3	104.8(3)	S1—P1—O2—C8	50.7(5)
P1—S1	1.925(3)	O1—P1—S1	117.5(2)	O2—P1—O1—C10	-176.3(6)
O2—C8	1.458(7)	O2—P1—S1	116.2(2)	O3—P1—O1—C10	76.2(6)
O1—C10	1.458(9)	O3—P1—S1	114.2(2)	S1—P1—O1—C10	-51.3(6)
N1—C3	1.481(9)	C8—O2—P1	119.7(4)	P1—O2—C8—C9	-172.7(5)
N1—C2	1.483(9)	C10—O1—P1	119.9(5)	C3—N1—C2—C1	69.9(9)
N1—C4	1.537(8)	C3—N1—C2	110.3(6)	C4—N1—C2—C1	-160.8(6)
C9—C8	1.464(1)	C3—N1—C4	114.5(6)	C3—N1—C4—C5	-166.2(7)
C5—C4	1.512(9)	C2—N1—C4	113.1(5)	C2—N1—C4—C5	66.5(7)
C2—C1	1.461(2)	O2—C8—C9	108.9(5)	C3—N1—C4—C6	74.2(8)
C11—C10	1.437(8)	C1—C2—N1	116.4(6)	C2—N1—C4—C6	-53.1(8)
C6—C4	1.524(2)	C5—C4—C6	110.0(6)	C3—N1—C4—C7	-50.0(9)
C4—C7	1.540(2)	C5—C4—N1	108.6(5)	C2—N1—C4—C7	-177.2(7)
O3—C1	1.482(9)	C6—C4—N1	108.6(6)	P1—O1—C10—C11	144.6(7)
		C5—C4—C7	107.8(6)	O1—P1—O3—C1	-141.1(6)
		C6—C4—C7	114.4(7)	O2—P1—O3—C1	116.7(6)
		N1—C4—C7	107.2(6)	S1—P1—O3—C1	-11.6(6)
		C11—C10—O1	109.7(7)	N1—C2—C1—O3	-73.0(9)
		C1—O3—P1	123.4(5)	P1—O3—C1—C2	-167.6(5)
		C2—C1—O3	111.3(7)		

The *tert*-butyl group located at the nitrogen atom is almost ideally forming a tetrahedral configuration with the C4-atom sitting in the center. The respective bond angels are ranging from 107.2(6)° to 110.0(6)°.The crystal structure of compound **XXXVI**, as shown in Figure 72, is formed from the unit cell by applying two symmetry operations. First, the unit cell content has to be mirrored along the axes of the crystal lattice and second, needs to be twisted by 180°. This means that every second set of anion-cation pairs has the same orientation along any of the three lattice axes.

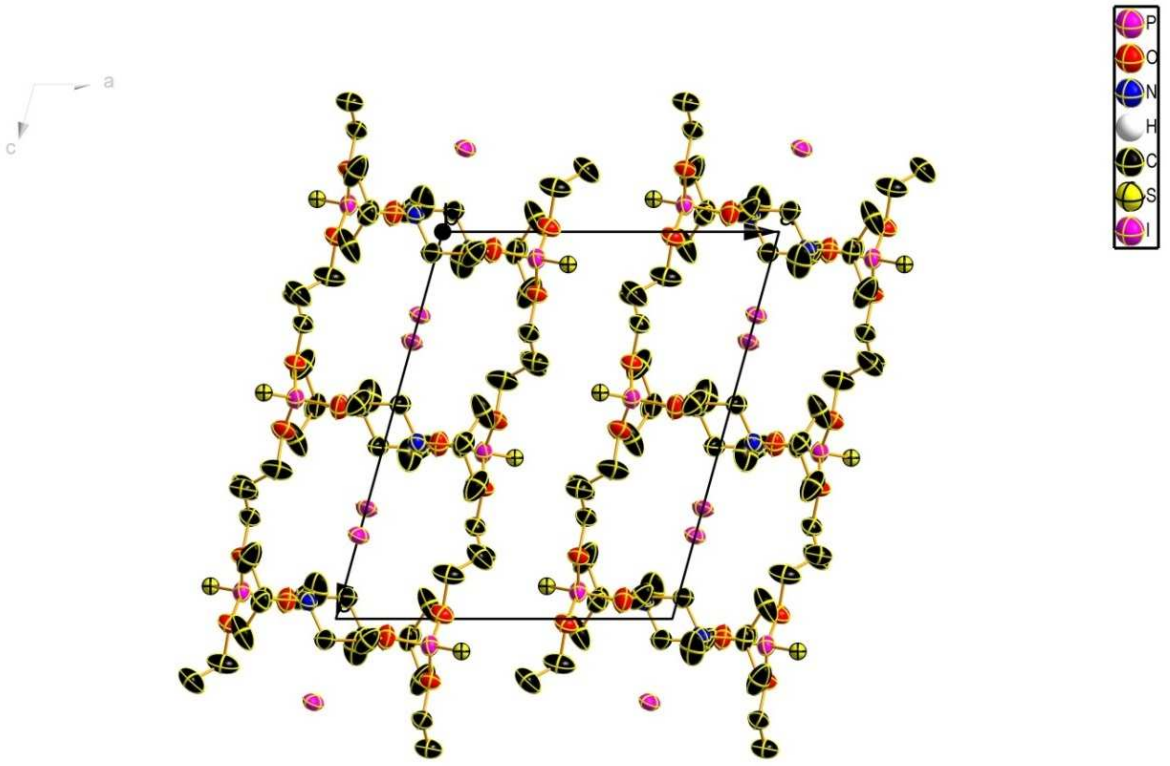

Figure 72: *Crystal structure of compound **XXXVI**, DIAMOND [275] representation along b-axis of the crystal lattice; thermal ellipsoids are drawn at 50 % probability level. Hydrogen atoms and split positions are omitted for better clarity.*

4.5.3.5 1-{2-[(Diethoxyphosphorothioyl)oxy]ethyl}-1-methylpiperidinium iodide (XXXVIII)

The N-methylation product of compound **XXV** crystallizes in the monoclinic space group $P2_1/c$ and has a total of four molecules in the unit cell. This is not surprisingly the same for as was the case for compound **XXXVII**. Each compound **XXV** molecule is positively charged by the additional methyl group attached to the nitrogen atom. The anionic part of the salt is again formed by a negatively charged iodine atom. The asymmetric unit is shown in Figure 71 and the unit cell with viewing direction along the *b*-axis is shown in Figure 74. Selected bond lengths, bond angles and torsion angles are given in Table 41. In the crystal no hydrogen bonds could be found. This time, no disordered split positions are present in the crystal structure. However, most ellipsoids show a prominent displacement, especially those of the oxygen atoms. The unit cell structure is slightly different from the one of compound

XXXIX. The cations are not twisted by 180° from one position to the other and thus not forming alternating chains with head-to tail orientation. Moreover, they are packed that way that all nitrogen moieties with the six-membered ring allow to view through the ring-system along the c-axis (*cf*. Figure 74).

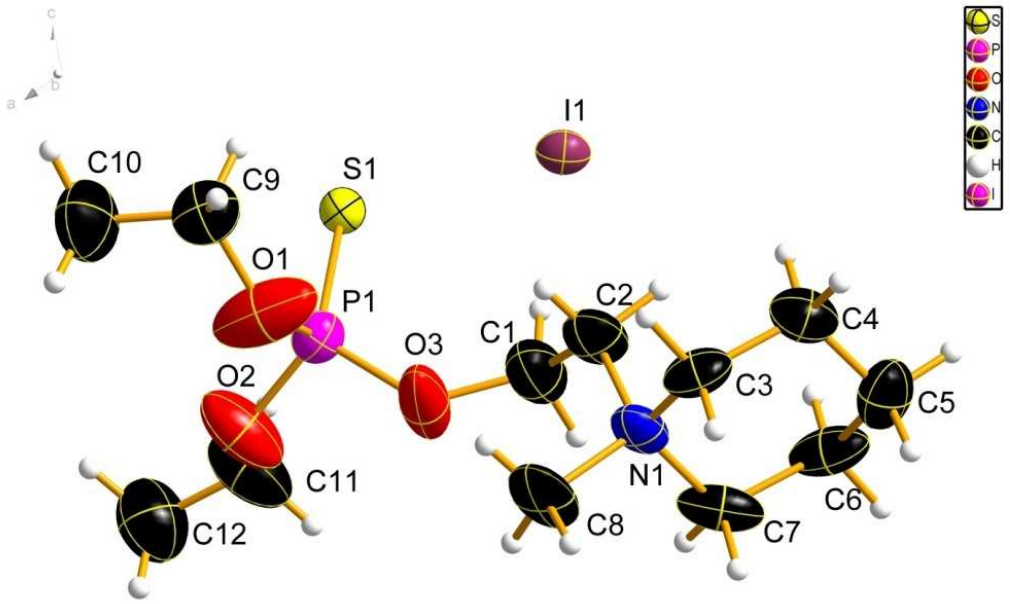

Figure 73: *Crystal structure of compound* ***XXXVIII****, DIAMOND [275] representation; thermal ellipsoids are drawn at 50 % probability level.*

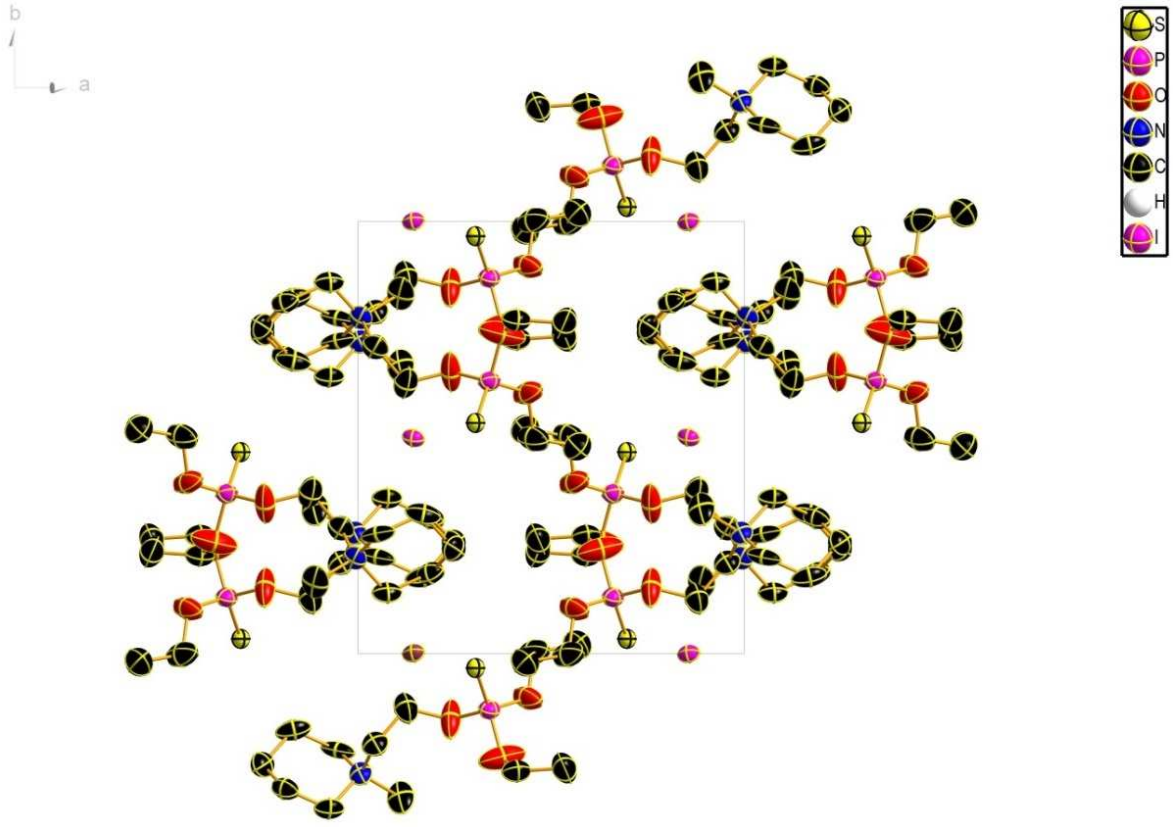

Figure 74: *Crystal structure of compound* ***XXXVIII****, DIAMOND [275] representation along the c-axis of the crystal lattice; thermal ellipsoids are drawn at 50 % probability level. Hydrogen atoms and split positions are omitted for better clarity.*

In this case all P-O bond length are of comparable values and are shorter than the P-S bond. Additionally, the O-P-O angles are quite similar as well as the O-P-S angles are; only the latter ones are about 15° larger. Besides the C7-N1-C2 angle of 115.3(9)° all other angles involving the nitrogen atom are smaller but close to the typical tetrahedral angel of 109.5°.

Table 41: *Selected bond lengths (Å), bond angles (°) and torsion angles of compound* ***XXXVI****.*

bond length (Å)		bond angles (°)		torsion angles (°)	
S1—P1	1.914(4)	O2—P1—O3	102.5(6)	O2—P1—O1—C9	-110.8(2)
P1—O2	1.519(8)	O2—P1—O1	101.2(6)	O3—P1—O1—C9	143.9(2)
P1—O3	1.541(8)	O3—P1—O1	101.1(6)	S1—P1—O1—C9	18.0(2)
P1—O1	1.544(9)	O2—P1—S1	117.5(4)	O3—P1—O2—C11	-84.4(2)
O1—C9	1.440(2)	O3—P1—S1	115.4(4)	O1—P1—O2—C11	171.4(2)
O2—C11	1.474(2)	O1—P1—S1	116.6(4)	S1—P1—O2—C11	43.2(2)
O3—C1	1.389(2)	C9—O1—P1	126.4(8)	O2—P1—O3—C1	141.0(2)
N1—C7	1.491(2)	C11—O2—P1	121.2(8)	O1—P1—O3—C1	-114.7(2)
N1—C8	1.497(2)	C1—O3—P1	129.2(8)	S1—P1—O3—C1	12.0(2)
N1—C3	1.515(2)	C7—N1—C8	108.3(9)	P1—O3—C1—C2	105.9(2)
N1—C2	1.520(2)	C7—N1—C3	108.4(8)	O3—C1—C2—N1	81.2(2)
C1—C2	1.442(2)	C8—N1—C3	107.8(1)	C7—N1—C2—C1	59.3(2)
C6—C7	1.520(2)	C7—N1—C2	115.3(9)	C8—N1—C2—C1	-63.1(2)
C9—C10	1.446(2)	C8—N1—C2	109.5(9)	C3—N1—C2—C1	-179.8(2)
		C3—N1—C2	107.3(8)	C7—N1—C3—C4	55.7(1)
		O3—C1—C2	117.0(2)	C8—N1—C3—C4	172.8(9)
		C1—C2—N1	116.8(1)	C2—N1—C3—C4	-69.4(1)
		C4—C3—N1	112.3(9)	N1—C3—C4—C5	-57.1(2)
		C3—C4—C5	112.2(9)	C3—C4—C5—C6	54.8(2)
		C6—C5—C4	109.6(1)	C4—C5—C6—C7	-53.9(2)
		C5—C6—C7	112.0(9)	C8—N1—C7—C6	-171.8(9)
		N1—C7—C6	112.7(8)	C3—N1—C7—C6	-55.1(2)
		O1—C9—C10	112.1(2)	C2—N1—C7—C6	65.1(2)
		C12—C11—O2	111.3(2)	C5—C6—C7—N1	56.3(2)
				P1—O1—C9—C10	89.4(2)
				P1—O2—C11—C12	-157.5(2)

4.5.3.6 1-{2-[(Diethoxyphosphorothioyl)oxy]ethyl}piperidinium oxalate (XXXIX)

Compound **XXXIX** crystallizes in the monoclinic space group $P2_1/c$ and has four formula units in the unit cell. One of the ethoxy groups is disordered over two positions (*cf.* Figure

75). Furthermore, the crystal shows some hydrogen bonds which are depicted in Figure 76. The respective values are reported in Table 43. Again, hydrogen bonds between O4 and H7 coordinate the negatively charged oxalic acid parts with each other to form chains along the *c*-axis of the crystal lattice. At the same time the protonated nitrogen is donating its proton towards the oxalic acid molecules. Here a weaker hydrogen bond can be found.

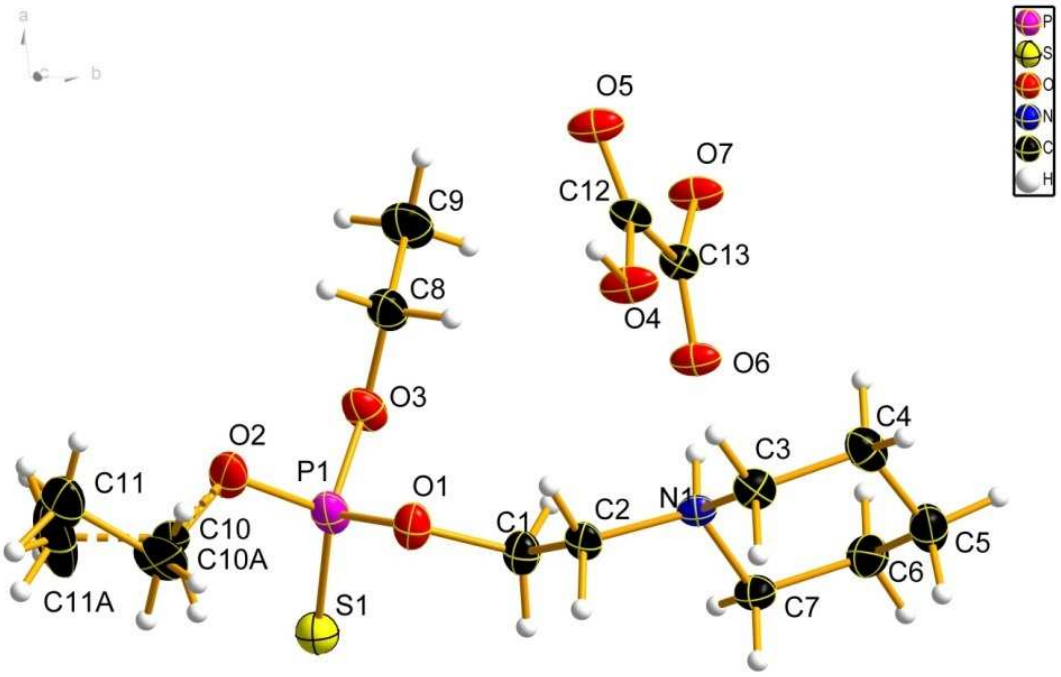

Figure 75: *Molecular structure of compound* ***XXXIX****, DIAMOND [275] representation; thermal ellipsoids are drawn at 50 % probability level. The broken bonds indicate a split position of the respective atoms.*

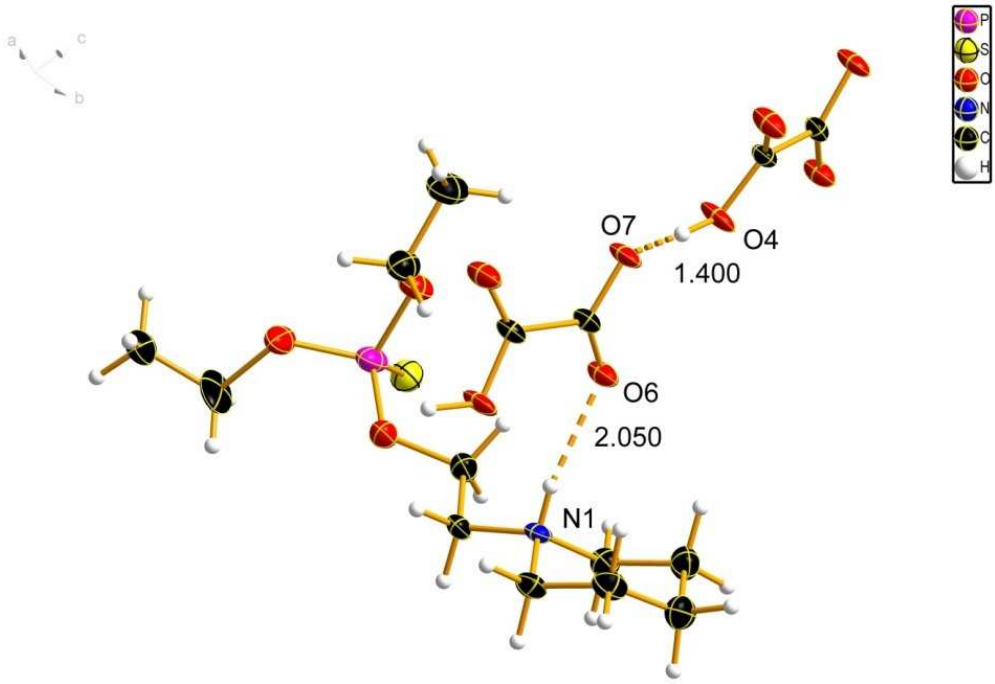

Figure 76: *Hydrogen bonding situation in compound* ***XXXIX****, DIAMOND [275] representation; thermal ellipsoids are drawn at 50 % probability level. The broken bonds indicate hydrogen bonds with given bond lengths in Å. The split positions are omitted for better clarity.*

Table 42: *Selected bond lengths (Å), bond angles (°) and torsion angles of compound* ***XXXIX****.*

bond length (Å)		bond angles (°)		torsion angles (°)	
P1—O2	1.568(2)	O2—P1—O3	102.8(1)	O2—P1—O1—C1	-175.2(2)
P1—O3	1.569(2)	O2—P1—O1	100.5(1)	O3—P1—O1—C1	-68.3(2)
P1—O1	1.591(2)	O3—P1—O1	106.5(1)	S1—P1—O1—C1	56.4(2)
P1—S1	1.918(1)	O2—P1—S1	118.2(1)	O2—P1—O3—C8	57.2(2)
O7—C13	1.268(2)	O3—P1—S1	111.6(1)	O1—P1—O3—C8	-48.0(2)
O4—C12	1.304(2)	O1—P1—S1	115.7(1)	S1—P1—O3—C8	-175.2(2)
O6—C13	1.240(2)	C1—O1—P1	118.5(1)	C7—N1—C2—C1	-61.2(2)
O1—C1	1.446(2)	C8—O3—P1	121.5(1)	C3—N1—C2—C1	174.5(2)
O5—C12	1.213(2)	C2—N1—C7	112.6(2)	O3—P1—O2—C10A	-176.8(1)
O3—C8	1.464(2)	C2—N1—C3	110.8(2)	O1—P1—O2—C10A	-67.1(1)
N1—C2	1.494(2)	C7—N1—C3	110.5(2)	S1—P1—O2—C10A	59.8(1)
N1—C7	1.501(2)	N1—C2—C1	111.1(2)	O3—P1—O2—C10	171.0(7)
N1—C3	1.507(2)	C10A—O2—P1	124.7(6)	O1—P1—O2—C10	-79.3(7)
C2—C1	1.521(3)	C10—O2—P1	118.9(5)	S1—P1—O2—C10	47.6(7)
O2—C10A	1.39(2)	O6—C13—O7	126.8(2)	O6—C13—C12—O5	-167.1(2)
O2—C10	1.52(2)	O6—C13—C12	118.8(2)	O7—C13—C12—O5	11.6(3)
C13—C12	1.547(2)	O7—C13—C12	114.4(2)	O6—C13—C12—O4	10.7(3)
C3—C4	1.512(3)	O5—C12—O4	125.6(2)	O7—C13—C12—O4	-170.5(2)
C7—C6	1.512(3)	O5—C12—C13	121.8(2)	C2—N1—C3—C4	-175.3(2)
C5—C6	1.518(3)	O4—C12—C13	112.6(2)	C7—N1—C3—C4	59.2(2)
C5—C4	1.521(3)	N1—C3—C4	110.0(2)	C2—N1—C7—C6	177.0(2)
C8—C9	1.498(3)	N1—C7—C6	110.8(2)	C3—N1—C7—C6	-58.8(2)
C11—C10	1.45(2)	C6—C5—C4	110.8(2)	N1—C7—C6—C5	55.4(2)
C11A—C10A	1.47(3)	C7—C6—C5	111.9(2)	C4—C5—C6—C7	-52.5(2)
		O3—C8—C9	107.8(2)	P1—O3—C8—C9	-174.5(2)
		O1—C1—C2	106.2(2)	P1—O1—C1—C2	170.4(2)
		C3—C4—C5	111.8(2)	N1—C2—C1—O1	-150.6(2)
		C11—C10—O2	104.7(1)	N1—C3—C4—C5	-57.0(2)
				C6—C5—C4—C3	53.6(2)
				P1—O2—C10—C11	-167.0(7)

The structural motif of the oxalic acid molecules in the crystal lattice can be seen in Figure 77 and is very comparable to the one found for compound **XXX**. Quite different appearances have the positive counterions in the crystal. They seem to form a wave-like band structure along the *b*-axis of the lattice and are aligned with each other head-to-tail in the viewing direction along the *c*-axis (*cf.* Figure 77). Selected bond length, bond angles

and torsion angles are given in Table 42. Obviously the O-P-S angles are larger compared to the O-P-O angles. This is true for all obtained crystal structures of the Amiton derivatives.

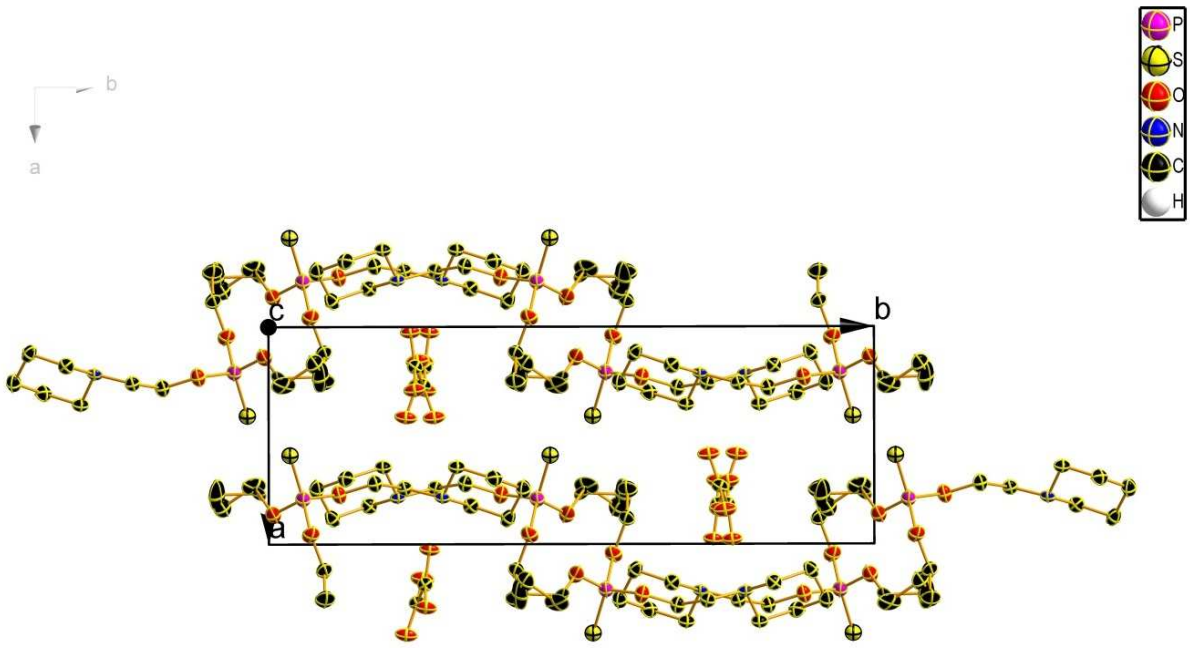

Figure 77: *Crystal structure of compound* ***XXXIX****, view of the unit cell along the c-axis, DIAMOND [275] representation; thermal ellipsoids are drawn at 50 % probability level. Hydrogen atoms and split positions are omitted for better clarity.*

Table 43: *Parameters of the hydrogen bonds of compound* ***XXXIX****. Symmetry codes: (i) +x, 1/2-y, -1/2+z, (ii) +x, 1/2-y, 1/2+z.*

D---H...A	D--H [Å]	H--A [Å]	D--A [Å]	D--H-----A
N1---H1...O6	0.84	2.05	2.842	157.3°
O4---H4...O7^{ii}	1.07	1.40	2.465	171.8°
O4^{i}---H4^{i}...O7	1.07	1.40	2.465	171.8°

4.5.3.7 1-{2-[(Diethoxyphosphorothioyl)oxy]ethyl}-1-methylpyrrolidinium iodide (XL)

Compound **XL** crystallizes in the monoclinic space group $P2_1/c$ and has four formula units in the unit cell. Each of the four formula units consits of one negatively charged iodine atom and a positively charged compound **XXVI** molecule which is methylated at its nitrogen cation. The molecule is strongly disordered over two positions. The disordering affects both ethoxy moieties and the oxygen atom of the nitrogen containing sidechain. The disorder of the nitrogen containing sidechain has not been observed amongst any other compound studied within this thesis. A representation of the asymmetric unit is given in Figure 78. The unit cell is depicted in Figure 79. In the crystal no hydrogen bonds could be identified. Bond lengths, bond angles and torsion angles are of expected values and are given in Table 44. Again, O-P-S angles are larger compared to the O-P-O angles as well as the respective bond lengths are.

Table 44: *Selected bond lengths (Å), bond angles (°) and torsion angles of compound* ***XL****.*

bond length (Å)		bond angles (°)		torsion angles (°)	
S1—P1	1.927(1)	O1A—P1—O3A	105.4(5)	C7—N1—C3—C4	-160.1(2)
P1—O1A	1.514(4)	O2—P1—O3	103.6(2)	C6—N1—C3—C4	-40.8(2)
P1—O2	1.517(2)	O2—P1—O1	103.2(3)	C2—N1—C3—C4	77.7(2)
P1—O3A	1.550(4)	O3—P1—O1	99.7(4)	C7—N1—C6—C5	161.0(2)
P1—O3	1.593(2)	O1A—P1—O2A	100.0(6)	C3—N1—C6—C5	41.5(2)
P1—O1	1.593(4)	O3A—P1—O2A	99.5(4)	C2—N1—C6—C5	-72.9(2)
P1—O2A	1.648(5)	O1A—P1—S1	117.3(2)	C7—N1—C2—C1A	56.8(9)
N1—C7	1.490(2)	O2—P1—S1	118.1(2)	C6—N1—C2—C1A	-69.6(9)
N1—C6	1.508(2)	O3A—P1—S1	117.1(2)	C3—N1—C2—C1A	179.5(9)
N1—C3	1.511(2)	O3—P1—S1	115.5(1)	C7—N1—C2—C1)	61.4(3
N1—C2	1.517(2)	O1—P1—S1	114.3(2)	C6—N1—C2—C1	-64.9(3)
C3—C4	1.525(3)	O2A—P1—S1	114.6(2)	C3—N1—C2—C1	-175.8(3)
C6—C5	1.514(3)	C7—N1—C6	111.6(2)	N1—C3—C4—C5	25.1(2)
C2—C1A	1.383(2)	C7—N1—C3	112.1(2)	N1—C6—C5—C4	-26.2(2)
C2—C1	1.522(6)	P1—O1A—C1A	121.3(7)	C3—C4—C5—C6	0.6(2)
C4—C5	1.534(3)	C2—C1A—O1A	105.9(1)	O3—P1—O2—C8	177.3(5)
O2—C8	1.488(6)	C1—O1—P1	124.0(4)	O1—P1—O2—C8	73.7(6)
C8—C9	1.492(7)	O1—C1—C2	118.0(6)	S1—P1—O2—C8	-53.5(6)
O2A—C8A	1.492(2)	C6—N1—C3	101.4(2)	P1—O2—C8—C9	157.0(4)
C8A—C9A	1.27(2)	C7—N1—C2	111.0(2)	S1—P1—O1A—C1A	31.3(2)
O3—C10	1.486(2)	C6—N1—C2	113.0(2)	N1—C2—C1A—O1A	-91.3(1)
C10—C11	1.61(3)	C3—N1—C2	107.2(2)	O1A—P1—O2A—C8A	179.4(2)
O3A—C10A	1.42(2)	N1—C3—C4	104.5(2)	O3A—P1—O2A—C8A	-72.9(2)
C10A—C11A	1.27(4)	N1—C6—C5	104.9(2)	S1—P1—O2A—C8A	53.0(2)
O1—C1	1.406(8)	C1A—C2—N1	116.5(7)	P1—O2A—C8A—C9A	-170.0(2)
O1A—C1A	1.517(2)	N1—C2—C1	116.2(3)	O2—P1—O3—C10	94.6(1)
		C3—C4—C5	105.3(2)	O1—P1—O3—C10	-159.2(1)
		C6—C5—C4	105.3(2)	S1—P1—O3—C10	-36.1(1)
		C8—O2—P1	118.1(3)	P1—O3—C10—C11	-80(2)
		O2—C8—C9	105.6(5)	S1—P1—O3A—C10A	40.7(2)
		C8A—O2A—P1	118.1(8)	O2—P1—O1—C1	-152.1(8)
		C9A—C8A—O2A	113.7(2)	O3—P1—O1—C1	101.3(9)
		C10—O3—P1	124.5(7)	S1—P1—O1—C1	-22.6(1)
		O3—C10—C11	121.2(2)	P1—O1—C1—C2	-100.8(9)
		C10A—O3A—P1	119.1(2)	N1—C2—C1—O1	-80.3(5)

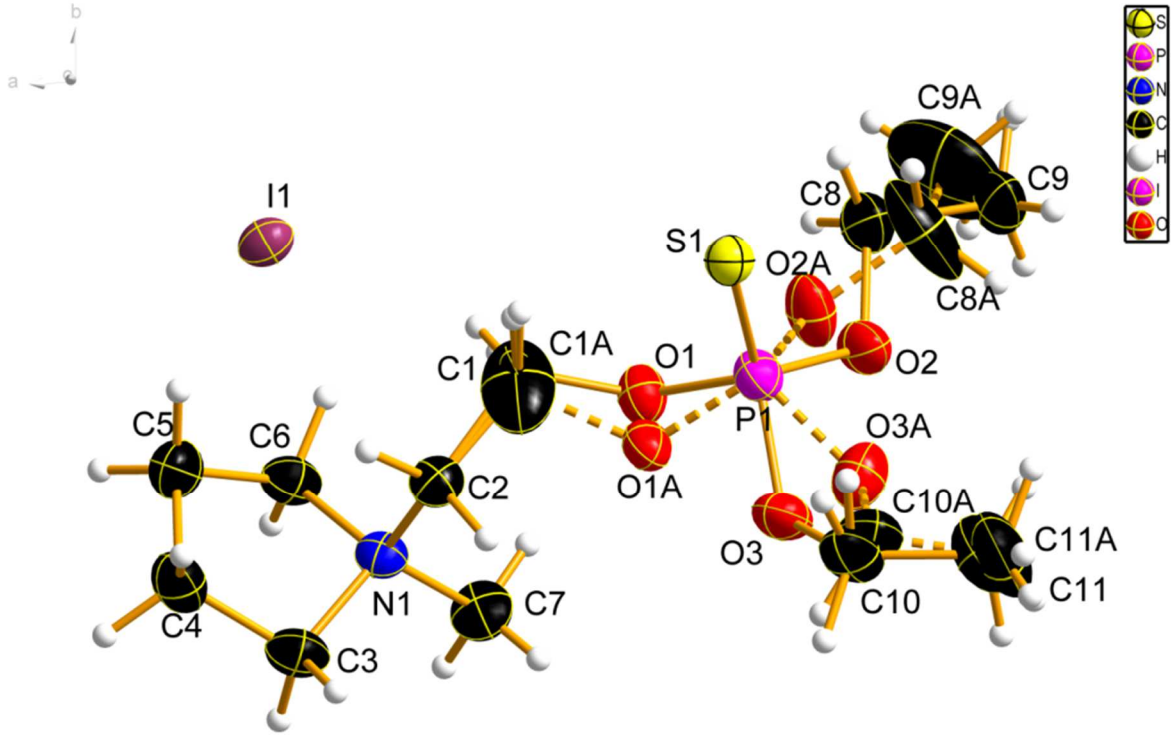

Figure 78:*Molecular structure of compound* ***XL****, DIAMOND* ***[275]*** *representation; thermal ellipsoids are drawn at 50 % probability level. The broken bonds indicate a split position of the respective atoms.*

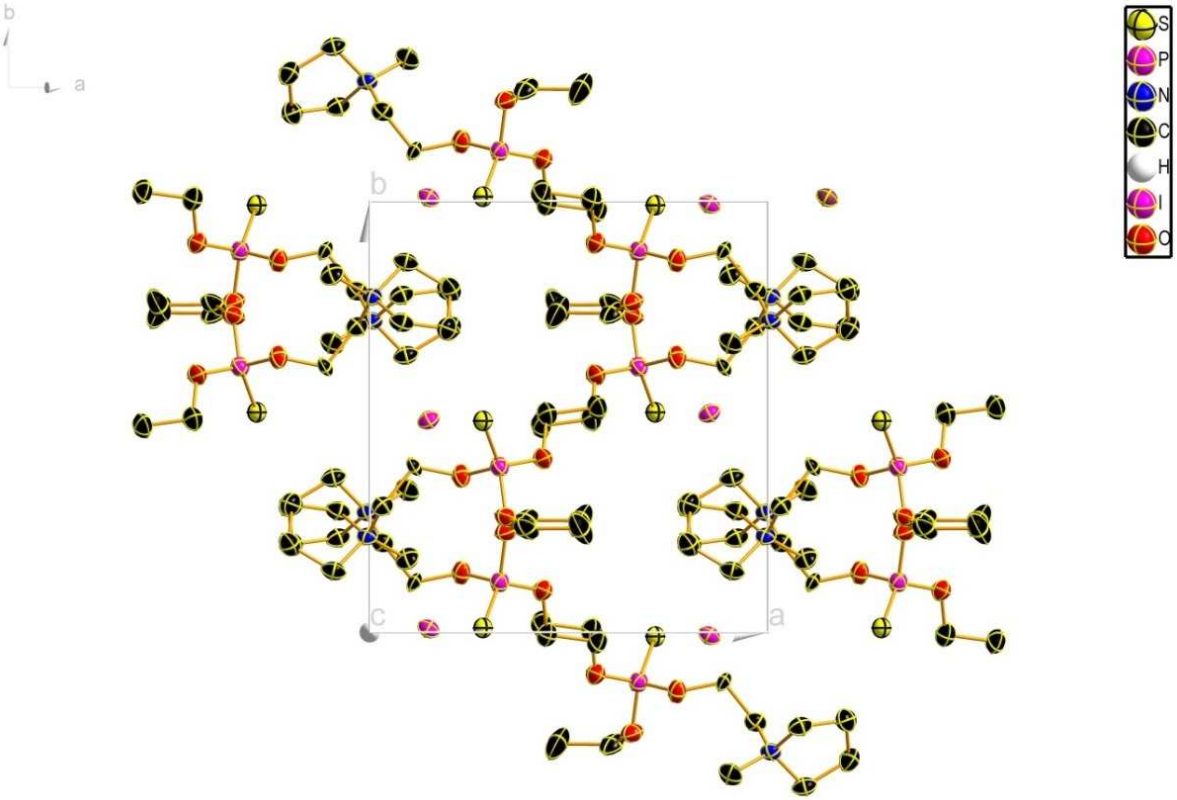

Figure 79: *Crystal structure of compound* ***XL****, view of the unit cell along the c-axis, DIAMOND [275] representation; thermal ellipsoids are drawn at 50 % probability level. Hydrogen atoms are omitted for better clarity.*

Although some of the thermal ellipsoids have large displacement parameters no better refinement solution could be obtained. The arrangement of the crystal structure in the unit cell is very similar to the one described for compound **XXXVIII** (*cf.* Figure 74). Particularly, the nitrogen containing five-membered ring is packed that way along the *c*-axis that the rings are superimposable every second cation. Along the *a*-axis, the compounds are running head-to-tail.

4.5.3.8 1-{2-[(Diethoxyphosphorothioyl)oxy]ethyl}pyrrolidinium oxalate (XLI)

Compound **XLI** crystallizes in the triclinic space group *P*-1 with two formula units in the unit cell. The asymmetric unit is shown in Figure 80. The oxalic acid molecules are deprotonated and thus represent the anionic part of the crystal. The cationic part is formed by a protonated **XXVI** molecule. In Figure 81 a different representation of the crystal structure is given to better understand the hydrogen bonding situation of the crystal. The respective data values are presented in Table 46. The oxalic acid molecules are 'connected' to each other *via* hydrogen bonds between H4 and O7. This connection results in chains of oxalic acid molecules along the *a*-axis of the crystal (*cf.* Figure 82) as could be observed for compound **XXXIX**. Furthermore, the oxalic acid molecules are coordinated *via* a second set of hydrogen bridges between the hydrogen atom bond to the nitrogen of the cation and O4 and O6 of the anion.

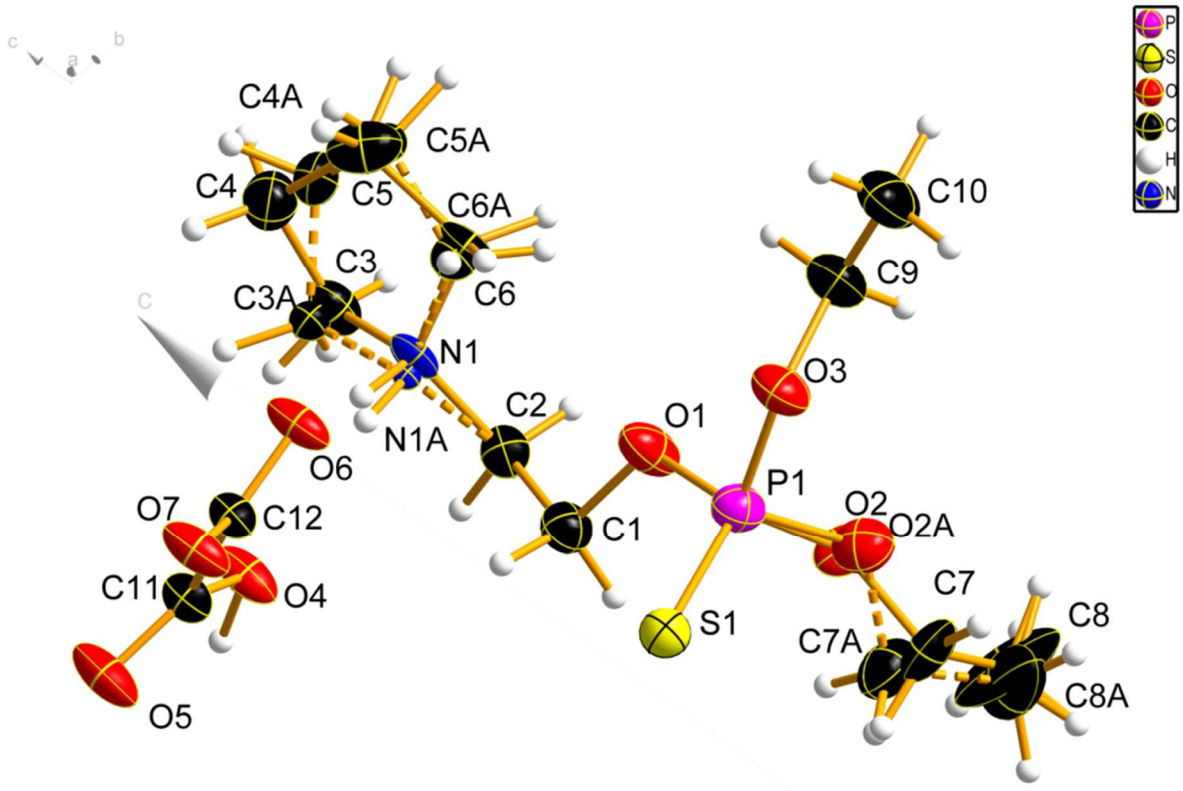

Figure 80: *Molecular structure of compound* ***XLI*** *in the crystal (asymmetric unit), DIAMOND [275] representation; thermal ellipsoids are drawn at 50 % probability level. The broken bonds indicate a split position of the respective atoms.*

Table 45: *Selected bond lengths (Å), bond angles (°) and torsion angles of compound* ***XLI****.*

bond length (Å)		bond angles (°)		torsion angles (°)	
P1—O2A	1.544(2)	O2A—P1—O3	100.0(6)	O2—C7—C8	103.6(2)
P1—O3	1.562(2)	O2A—P1—O1	109.8(5)	C7A—O2A—P1	124.0(2)
P1—O1	1.574(2)	O3—P1—O1	101.8(2)	C8A—C7A—O2A	113.6(2)
P1—O2	1.62(2)	O3—P1—O2	110.7(8)	C3—C4—C5	105.1(5)
P1—S1	1.912(1)	O1—P1—O2	94.9(6)	N1—C3—C4	102.1(6)
O4—C11	1.298(3)	O2A—P1—S1	114.6(6)	C4—C5—C6	107.6(6)
O5—C11	1.213(3)	O3—P1—S1	113.1(1)	N1—C6—C5	102.3(8)
O7—C12	1.261(3)	O1—P1—S1	115.7(8)	C3—N1—C2	110.8(7)
O3—C9	1.468(3)	O2—P1—S1	118.2(8)	C3—N1—C6	106.4(7)
O1—C1	1.447(3)	C9—O3—P1	122.5(2)	C2—N1—C6	116.9(8)
C11—C12	1.539(4)	C1—O1—P1	120.6(2)	C5A—C4A—C3A	110.1(2)
C2—N1A	1.44(3)	O5—C11—O4	125.2(3)	C4A—C3A—N1A	109.5(3)
C2—C1	1.500(4)	O5—C11—C12	122.1(2)	C4A—C5A—C6A	106.6(3)
C2—N1	1.503(9)	O4—C11—C12	112.7(2)	N1A—C6A—C5A	115.3(4)
C9—C10	1.496(4)	N1A—C2—C1	110.5(2)	C2—N1A—C6A	113.2(3)
O2—C7	1.47(2)	C1—C2—N1	114.2(4)	C2—N1A—C3A	117.8(2)
C8—C7	1.47(3)	O1—C1—C2	109.7(2)	C6A—N1A—C3A	99.7(3)
O2A—C7A	1.462(2)	O3—C9—C10	107.1(3)	O6—C12—O7	126.3(2)
C8A—C7A	1.456(2)	C7—O2—P1	117.4(2)	O6—C12—C11	118.8(2)
C4—C3	1.496(1)	O7—C12—C11	115.0(2)	C1—C2—N1A—C6A	92.8(4)
C4—C5	1.512(1)	O2—C7—C8	103.(2)	C1—C2—N1A—C3A	-164.4(2)
C3—N1	1.482(2)	C7A—O2A—P1	124.0(2)	N1—C2—C1—O1	-67.2(6)
C5—C6	1.525(2)	C8A—C7A—O2A	113.6(2)	P1—O3—C9—C10	-168.8(2)
C6—N1	1.504(2)	C3—C4—C5	105.1(5)	O3—P1—O2—C7	98.3(2)
C4A—C5A	1.35(4)	N1—C3—C4	102.1(6)	C3—C4—C5—C6	-15.4(1)
C4A—C3A	1.53(4)	C4—C5—C6	107.6(6)	C4—C5—C6—N1	8.8(2)
C3A—N1A	1.56(5)	N1—C6—C5	102.3(8)	C4—C3—N1—C2	-172.0(9)
C5A—C6A	1.50(5)	C3—N1—C2	110.8(7)	C3—C4—C5—C6	-15.4(1)
C6A—N1A	1.48(5)	C3—N1—C6	106.4(7)	C4—C5—C6—N1	-8.8(2)
O6—C12	1.239(3)	C2—N1—C6	116.9(8)	C4—C3—N1—C2	-172.0(9)
		C5A—C4A—C3A	110.1(2)	C4—C3—N1—C6	-40.9(2)
		C4A—C3A—N1A	109.3(3)	C5A—C6A—N1A—C2	126.5(5)
		C4A—C5A—C6A	106.4(3)	C4A—C3A—N1A—C2	-119.7(4)
		C2—N1A—C6A	113.2(3)	O5—C11—C12—O6	-166.4(2)
		C2—N1A—C3A	117.7(2)	O4—C11—C12—O6	13.8(4)

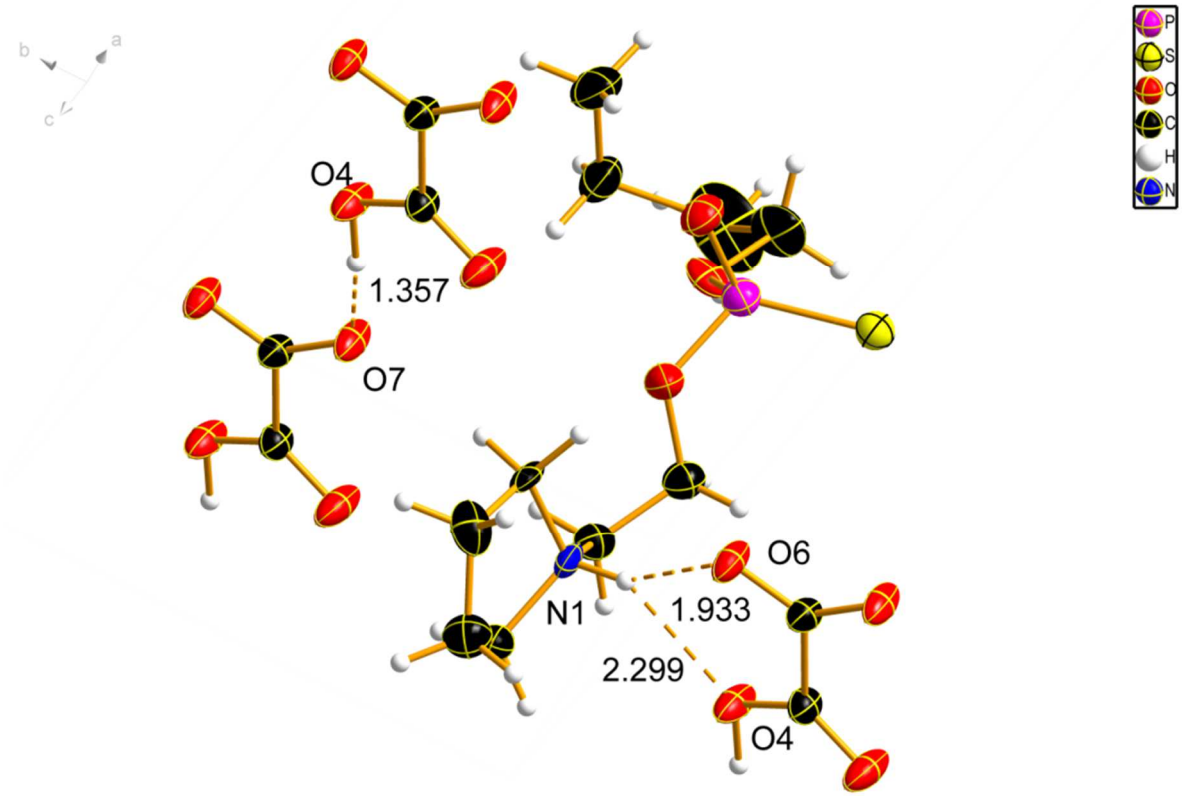

Figure 81: *Molecular structure of compound* ***XLI*** *in the crystal (asymmetric unit), DIAMOND [275] representation; thermal ellipsoids are drawn at 50 % probability level. The dotted bonds indicate hydrogen bonds with given bond lengths in Å. The split positions are omitted for better clarity.*

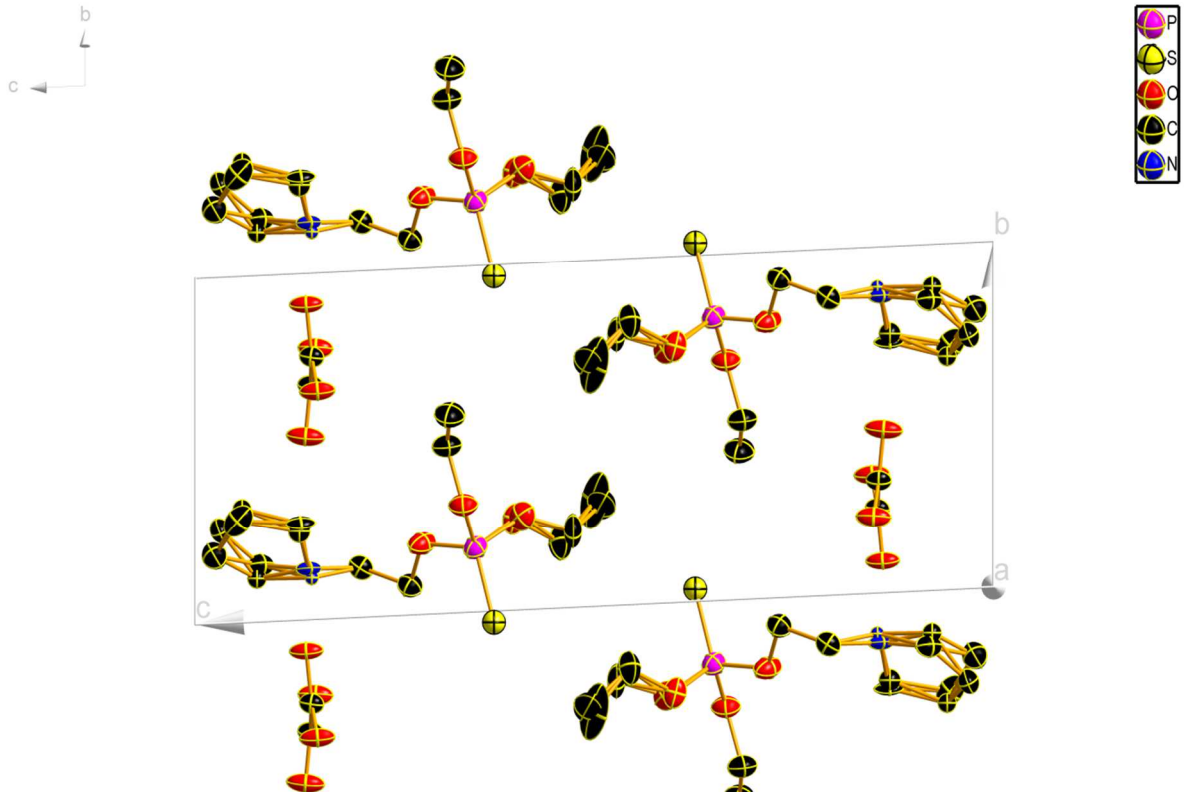

Figure 82: *Crystal structure of compound* ***XLI*** *view along the a-axis, DIAMOND [275] representation; thermal ellipsoids are drawn at 50 % probability level. Hydrogen atoms are omitted for better clarity.*

Additionally, it has to be noted that the five-membered ring is also disordered over two positions as well as is one of the ethoxy moieties. Bond length, bond angles and torsion angles for compound **XLI** are given in Table 45.

Table 46: *Parameters of the hydrogen bonds of compound **XLI**. Symmetry codes: (i) -1+x, +y, +z; (ii) 1+x, +y, +z*

D---H...A	D--H [Å]	H--A [Å]	D--A [Å]	D--H-----A
O4---H4...O7^{ii}	1.11	1.36	2.463	173.2°
O4^{i}---H4^{i}...O7	1.11	1.36	2.463	173.2°
N1---H1…O6	0.93	1.93	2.780	152,2°
N1---H1…O4	0.93	2.30	2.983	129.9°

4.5.4 Conclusion

In total fourteen quaternary ammonium salts could be successfully obtained by several reaction pathways. Either the alkylation with methyl iodide or the reaction of the respective Amiton derivative with an organic acid, e.g. oxalic acid, resulted in a salt. For nine of the Amiton derivatives it was possible to find crystals suitable single crystal X-ray diffraction. A major problem in the preparation process of the single crystals is the strong hygroscopicity of the ammonium salts, because most of them 'melt' at ambient conditions. So far none of the single crystal X-ray structures has been reported in literature before.

Most of the crystals crystalize in a monoclinic space group ($P2_1/n$ or $P2_1/c$), but also one orthorhombic as well as two triclinic structures could be found. Mainly, the oxalic acid anions are coordinated by hydrogen bridges to the positively charged nitrogen moiety. Furthermore, the oxalic acid molecules coordinate themselves by hydrogen bridges to form chain-like structures throughout the crystal. That might be one reason for the plate-like appearance of the prepared crystals. No general trend for the arrangement of the cations in the crystal could be identified.

However, it could be observed, that mostly one of the two ethoxy moieties were disordered over two positions. In one case (compound **XLI**) a very strong disorder was observed which involved the nitrogen moiety and one of the ethoxy groups.

Generally, it can be said that all bond lengths and bond angles were of expected values. The P-S bonds and the O-P-S angles are always larger than the respective P-O bond and O-P-O angles. The nitrogen atom bearing the positive charge of the cation was in most cases the center of an ideal tetrahedron showing bond angles with the next-neighboring atoms close to 104.5°.

The most impressive crystal structure showed compound **XXXIX** (*cf.* Figure 77*)*.

4.6 Vapor Pressure Determination

The majority of this data and discussion is the result of the collaboration with Martin Härtel of Professor Klapötke's group at the LMU. Both collaborators have an equal share on the described work. Furthermore, this chapter is a reproduction of the manuscript that has been submitted to the *Journal of Chromatography A* prior to writing of this thesis. It has been accepted and published in the meantime. For this reason, the layout, nomenclature of the compounds (Figure 83) and numbering of equations in this chapter differs from those in the other chapters of this work.

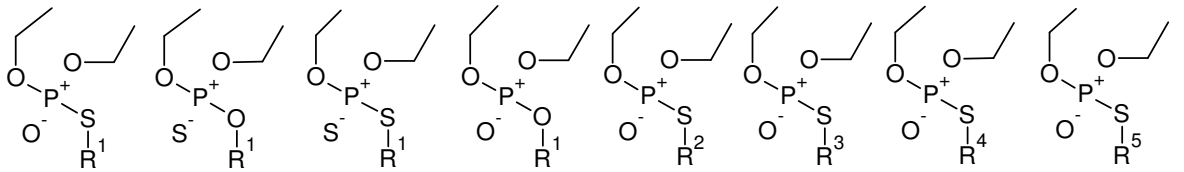

***Figure 83**: Chemical Structures of Amiton I and its derivatives II to VIII. They differ from each other by either i) the variation of the configuration of the phosphorus surrounding, ii) the variation in the amino sidechain by alternating the spacing between the oxygen and the nitrogen atom and iii) the variation of the alkyl substituent of the nitrogen atom.*

To overcome the lack of information on vapor pressure data and other physico-chemical values for Amiton, we synthesized a set of 8 different molecules (Figure 83), structurally closely related to each other, and determined: i) vapor pressure, p_{sat}, ii) and enthalpy of vaporization $\Delta_l^g H_m^\circ$ (298.15 K). Therefore, the vapor pressure in ambient temperature regimes of **I** (298 – 343 K), **II** (293 – 343 K), **III** (293 – 343 K), **IV** (298-343 K), **V** (293 -338 K), **VI** (279 – 318 K), **VII** (293 – 333 K) and **VIII** (283 – 323 K) was measured with the transpiration method, which is a well-established method for the determination of vapor pressures for medium to low volatility analytes.[168-170]

4.6.1 Determination of Vapor Pressure and Enthalpy of Vaporization

The vapor pressure of the analyte $p_{sat}(T_{exp})$ can be calculated using the Ideal Gas Law and Dalton's Law of partial pressures under the assumption that the volume of the carrier gas stream is significantly higher than that of the gaseous analyte.[168, 170]

$$p_{sat}(T_{exp}) = \frac{m_a \mathrm{R} T_{amb}}{\mathrm{M} V_{amb}} \quad (1)$$

with: p_{sat}: vapor pressure of the analyte [Pa],

T_{exp}: temperature of the saturator [K],

m_a: mass of analyte [kg],

T_{amb}: ambient temperature [K],

V_{amb}: volume of carrier gas at ambient conditions [m³],

M: molecular weight of the analyte [kg/mol],

R: universal gas constant: 8.31446 [J/(K mol)].

The p_{sat}-T_{exp} values obtained for each analyte are analyzed with a fitting function based on the Clarke-Glew Equation [278]:

$$\ln {}^{p_{\mathrm{sat}}}/_{p^{\mathrm{o}}} - \frac{\Delta_{\mathrm{l}}^{\mathrm{g}} C_{p,m}^{\circ}}{R} ln \frac{T}{T_0} = A - \frac{B}{T} \tag{2}$$

with: p^{o}: reference pressure being 1 [Pa],

$\Delta_{\mathrm{l}}^{\mathrm{g}} C_{p,m}^{\circ}$: molar heat capacity difference from liquid to gaseous state [J/(K mol)],

T: temperature [K],

T_0: reference temperature [K],

A, B: fitting coefficients (A: [ ], B: [K]).

The enthalpy of vaporization at temperature T can be calculated by:

$$\Delta_{\mathrm{l}}^{\mathrm{g}} H_{\mathrm{m}}^{\mathrm{o}}(T) = RB + \Delta_{\mathrm{l}}^{\mathrm{g}} C_{p,m}^{\mathrm{o}} T \tag{3}$$

with: $\Delta_{\mathrm{l}}^{\mathrm{g}} H_{\mathrm{m}}^{\mathrm{o}}(T)$: molar enthalpy of vaporization [J/mol]

The heat capacities $C_{p,m}^{\mathrm{o}}$ at 298.15 K of the analytes **I**-**VIII** in liquid state are calculated according to the empirical element-increment approach by *Hurst et al.*(*cf.* Table 48).[279] The corresponding heat capacity differences with the gaseous state are calculated according to the procedures by *Chickos et al.*[280], which were also used for the adjustment of the obtained enthalpies of vaporization to 298.15 K for the reason of comparability. The detailed error estimation and error calculation, which is valid for this work and its experiments was elucidated before [169] for a nearly identical experimental setup that was adapted in this work.

Table 47 is a compilation of the results obtained in this work in comparison with the few available literature values of Amiton (**I**) concerning the vaporization enthalpies investigated at the average temperature of the measurement and the reference temperature 298.15 K.[32, 164] Additionally, the vapor pressure at 298.15 K is stated. For all analytes the results obtained by the transpiration method for the absolute vapor pressures p_{sat} and thermodynamic properties of vaporization are available in Table B2 to Table B9 of the

appendix. A condensation of the data can be achieved by plotting a Clausius-Clapeyron plot (Figure 84) for each analyte, which allows a visual comparison of the results with literature data. Actually, authors not always derived vaporization enthalpies from the determined vapor pressures or applied different methodologies. The literature vapor pressures were thus treated using Eqs. (3) and (4) and calculated enthalpies of vaporization adjusted [280] to 298.15 K for the sake of comparison with our results (Table 47).

In terms of vapor pressure the following observations can be made for Amiton **I** (P=O, P-S), **II** (P=S, P-O), **III** (P=S, P-S), **IV** (P=O, P-O), which have different chalcogen coordination at the phosphorus atom but the same carbon backbone. **I** and **II** only differ in the position of the sulfur atom, which is located in the P-S single bond in one and in the formal P=S double bond in **II**.

Table 47: *Compilation of obtained data on enthalpies of vaporization, $\Delta_l^g H_m^\circ$, and saturation vapor pressures, p_{sat}[d], for compounds I - VIII.*

Compound[a]	Method[b]	T-Range	T_{avg}	$\Delta_l^g H_m^\circ(T_{avg})$	$\Delta_l^g H_m^\circ$(298.15 K)[c]	p_{sat}[d]	M
		K	K	kJ mol^{-1}	kJ mol^{-1}	Pa	g mol^{-1}
I	T	298.2 – 342.9	318.6	80.9 ± 0.2	83.6 ± 0.3	0.070	269.34
I [281]	n.a.	293.2 – 323.2	304.3	77.0 ± 0.5	78.4 ± 0.6	0.073	269.34
I [164]	n.a., O	358.0 – 407.0	382.3	94.5	106.0	0.005	269.34
II	T	293.3 – 343.0	314.2	76.2 ± 0.4	78.5 ± 0.5	0.278	269.34
III	T	293.2 – 342.9	315.7	83.8 ± 0.2	86.3 ± 0.3	0.045	285.40
IV	T	298.2 – 342.9	318.4	76.5 ± 0.2	79.0 ± 0.3	0.258	253.28
V	T	293.3 – 338.1	318.0	78.9 ± 0.2	81.4 ± 0.3	0.100	283.37
VI	T	278.5 – 318.1	297.7	72.7 ± 0.2	72.7 ± 0.3	0.988	241.29
VII	T	293.3 – 333.1	310.9	75.2 ± 0.2	76.9 ± 0.3	0.035	255.31
VIII	T	283.4 – 323.1	302.5	70.9 ± 0.2	71.5 ± 0.3	0.636	255.31

[a] Citation given for literature values, [b] Methods: T: Transpiration, O: Equation Only [c] Enthalpies of sublimation were adjusted according to Chickos et al. [280] with $\Delta_l^g C_{p,m}^\circ$ and $C_{p,m}^\circ$(liq) according to Table 2. [d] Vapor pressure at 298.15 K, calculated according to equation (3) n.a.: not available

With respect to the octet rule the formal P=S and P=O double bonds should be regarded as more polar P^+-S^- and P^+-O^- single bonds. **II** (p_{sat}(298.15 K): 0.278 Pa, $\Delta_l^g H_m^\circ$(298.15K): 78.5 ± 0.5 kJ mol^{-1}) is more volatile than **I** (p_{sat}(298.15 K): 0.070 Pa, $\Delta_l^g H_m^\circ$(298.15K): 83.6 ± 0.3 kJ mol^{-1}). This can be justified by the increased polarity of the P^+-0^- bond in **I** compared to the P^+-S^- bond in **II**. Increased bond polarity generally results in stronger intermolecular dipole-dipole interactions. Interestingly, compound **IV** (p_{sat}(298.15 K): 0.258 Pa, $\Delta_l^g H_m^\circ$(298.15K): 79.0 ± 0.3 kJ mol^{-1}) has a very similar vaporization behavior in comparison to the more toxic compound **II** [282]. Therefore, **IV** might be used as a precise simulant for compound **II** in terms of gas phase detectability. Compound **III** (p_{sat}(298.15 K):

0.045 Pa, $\Delta_l^g H_m^\circ$(298.15K): 86.3 ± 0.3 kJ mol^{-1}) has the highest molecular weight and is therefore the least volatile compound compared amongst Amiton and its derivatives **I**-**IV**.

Compounds **V**–**VIII** are derivatives of compound **II** with identical chalcogen coordination of the phosphorus atom (P=S, P-O). In compound **V** (p_{sat}(298.15 K): 0.100 Pa, $\Delta_l^g H_m^\circ$(298.15K): 81.4 ± 0.3 kJ mol^{-1}) the alkyl bridge between thiophosphate unit and amine functionality is extended by a CH_2-unit which results in a lower vapor pressure and a higher (+ 2.9 ± 0.6 kJ mol^{-1}) enthalpy of vaporization. In compound **VI** (p_{sat}(298.15 K): 0.988 Pa, $\Delta_l^g H_m^\circ$(298.15K): 72.7 ± 0.3 kJ mol^{-1}) the terminal *N*-ethyl chains are substituted with *N*-methyl substituents which results in a higher vapor pressure and lower (-5.8 ± 0.6 kJ mol^{-1}) enthalpy of vaporization.

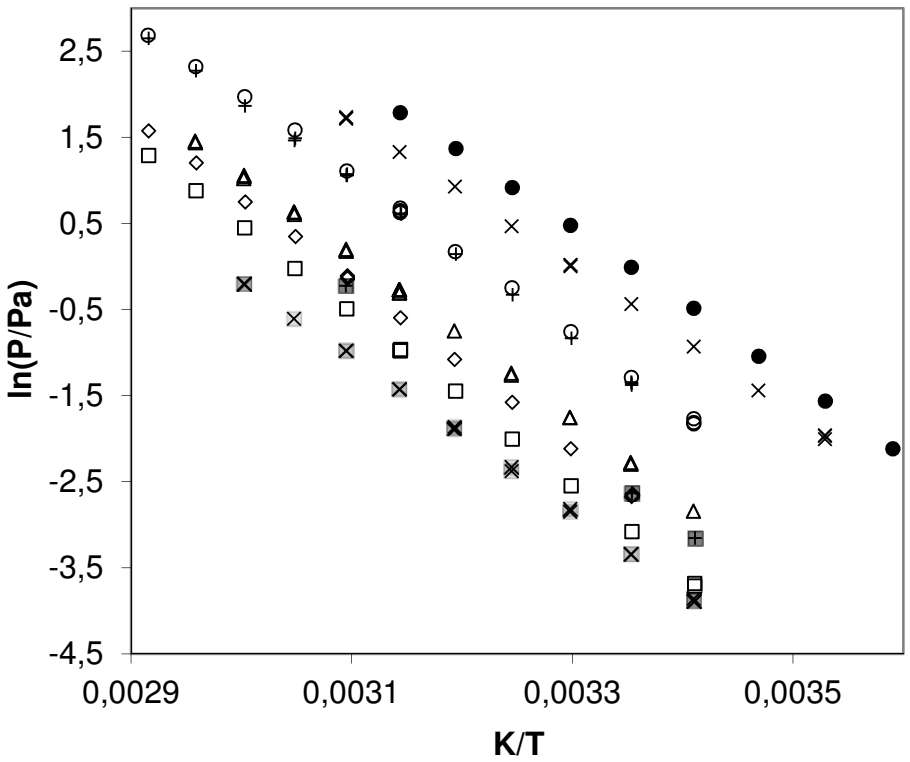

Figure 84: *Clausius Clapeyron plot of p-T-data of compounds I – VIII. * Literature data provided by Baldit[281]. ◊ I + I* ○ II □ III + IV Δ V ● VI × VII × VIII.*

The difference of compound **VII** (p_{sat}(298.15 K): 0.035, $\Delta_l^g H_m^\circ$(298.15K): 76.9 ± 0.3 kJ mol^{-1}) and compound **VI** is the length of the alkyl chain between thiophosphate and amine functionality. In compound **VII** it is extended by a CH_2 unit. With respect to this the vapor pressure and enthalpy of vaporization of **VII** are increased (+4.2 ± 0.4 kJ mol^{-1}) in comparison to **VI**. Compound **VIII** (p_{sat}(298.15 K): 0.636 Pa, $\Delta_l^g H_m^\circ$(298.15K): 71.5 ± 0.3 kJ mol^{-1}) is a branched constitutional isomer of compound **VII**. With respect to the reduced contact surface for *van der Waals interactions* of the alkyl functionalities the vapor

pressure of **VIII** is increased and the enthalpy of vaporization is decreased (-5.4 ± 0.4 kJ mol^{-1}) in comparison to **VII**.

For Amiton **I** one p-T-dataset (20, 25 and 50 °C) published by *Baldit* [281] and one p-T-equation published by *Stephenson et al.* [164] (358 – 407 K) are available. In both publications the purity of the sample and the method of measurement are not stated. The data derived from the p-T-data published by *Baldit* [281] (p_{sat}(298.15 K): 0.072 Pa, $\Delta_l^g H_m^\circ$(298.15K): 78.4 ± 0.6 kJ mol^{-1}) is in fair agreement with the values obtained in this work. Especially the literature value reported by *Baldit* [281] at 298.2 K (0.072 Pa) is in good agreement with the two values obtained in this work (0.071 ± 0.007 Pa, 0.069 ± 0.007 Pa, *cf.* Table B2). The vapor pressure of compound **I** at 323.2 K (0.800 Pa) reported by *Baldit* [281] does not match with the three values obtained in this work at 323.0 K (0.90 ± 0.03 Pa, 0.90 ± 0.03 Pa, 0.87 ± 0.03 Pa, *cf.* Table B2). Therefore, the value reported by *Baldit* [281] at 323.2 K is considered to be imperfect which explains the discrepancy regarding the enthalpies of vaporization. The data derived from the p-T equation published by *Stephenson et al.* [164] (p_{sat}(298.15 K): 0.005 Pa, $\Delta_l^g H_m^\circ$(298.15K): 106.0 kJ mol^{-1}) do not agree with the data obtained in this work and those published by *Baldit* [281].

4.6.2 Calculation of Concentration c_{dif} under Diffusion Conditions of Amiton in Air

Vapor pressures are measured under ideal saturation conditions. In a real case scenario the saturation equilibrium of the analyte will not be reached and diffusion processes will dictate the air concentration of the analyte. *Dravnicks et al.* [283] have stated a mathematical model for the estimation of the non-equilibrium air concentration of an explosive, which is applied to compounds **I** – **VIII** in the following using the equations and values provided by *Bird et al.* [284].

Fick's Law of Diffusion provides a suitable approximation for the rate of molecular vapor emission J:

$$J = A \times D_{AB} \times \frac{n_c - n_a}{d} \tag{4}$$

with: J: emission flux [molecules s^{-1}],
A: area of analyte exposed to air [cm^2],
D_{AB}: diffusivity of analyte vapor in air [cm^2 s^{-1}],
n_c: concentration of analyte under saturation conditions [molecules cm^{-3}],
n_a: concentration of the analyte in air [molecules cm^{-3}],
d: thickness of non-turbulent layer air [cm]

The concentration of the analyte in the air is considered to be negligibly small ($n_c - n_a \sim n_c$) and the thickness of the non-turbulent layer of air surrounding the analyte is considered to be 0.2 cm [283].

The diffusivity D_{AB} can be calculated by the following formula:

$$D_{AB} = 0.0018583 \sqrt{T^3 (\frac{1}{M_A} + \frac{1}{M_B})} \frac{1}{p\sigma_{AB}^2 \Omega_{D,AB}} \quad (5)$$

with: T: temperature [K] (298.15 K),
M_A: molecular mass of analyte [g mol^{-1}],
M_B: molecular mass of air [g mol^{-1}] (28.97 g mol^{-1}),
p: total pressure [atm] (1 atm),
σ_{AB}: combined collision diameter [Å],
$\Omega_{D,AB}$: collision integral for diffusion.

$$\sigma_{AB} = 1/2(\sigma_A + \sigma_B) \quad (6)$$

with: σ_A: collision diameter of analyte [Å],
σ_B: collision diameter of air [Å] (3.617 Å) [284]

$$\varepsilon_{AB} = \sqrt{\varepsilon_A \varepsilon_B} \quad (7)$$

with: ε_A: characteristic energy of analyte [J],
ε_B: characteristic energy of air [J]

While the collision diameter σ_B (3.617 Å) [284] and the characteristic energy ε_B (ε_B/κ = 97.0 K) [284] of air is known, the collision diameter of the analyte σ_A and its characteristic energy ε_A have to be estimated. These values may be estimated from the liquid at the boiling point (b):

$$\varepsilon/\kappa = 1.15 T_b; \qquad \sigma = 1.166 \sqrt[3]{V_b} \quad (8)$$

with: T_b: boiling point [K],
V_b: molar volume of the liquid at the boiling point [cm^3 mol^{-1}],
κ: Boltzmann's constant (1.38065 × 10^{-23} J K^{-1})

With ε_{AB} the collision integral for diffusion $\Omega_{D,AB}$ can be calculated according to:

$$\Omega_{D,AB} = \frac{1.16145}{T^{*0.15610}} + \frac{0.19300}{\exp(0.47635T^*)} + \frac{1.03587}{\exp(1.52996T^*)} + \frac{1.76474}{\exp(3.89411T^*)} \quad (9)$$

$$T^* = \kappa T/\varepsilon_{AB} \quad (10)$$

In case of compounds **I**-**VIII** the diffusion coefficient can be calculated from their boiling point, which is calculated by extrapolation of the p-T-data obtained in this work with equation (3) to the atmospheric pressure (101325 Pa). The molar volume V_b at the boiling point can be approximated from the density at 20 °C using an equation that was derived from the thermal expansion of the model compound triethylphosphate [285] by linear regression of the temperature-dependent density data provided:

$$\rho_b = \rho_{20°C} - 0.0009943(T_b - 293.15) \quad (11)$$

with: ρ_b: density at boiling point [g cm^{-3}],
$\rho_{20°C}$: density at 20 °C

The molar volume at the boiling point can be calculated by:

$$V_b = M/\rho_b \quad (12)$$

With equations 5 to 12 the diffusion coefficient of a liquid analyte in air can be approximated when solely its melting point and density are known; equation (5) can be used to calculate the mass flux of material from the analyte to the air. With A = 1 cm², n_a ~ 0 and d = 0.2 cm it can be written:

$$J = \frac{D_{AB}}{0.2} \times n_c \quad (13)$$

If the concentration n_c is converted to partial pressure (n_c = 3.3×10^{16}p, p: vapor pressure [Torr]) and the emission flux is converted into a mass flux (unit conversion factor: M/N_A) the mass flux can be calculated:

$$Q = \frac{D_{AB}}{0.2} \times 3.3\times10^{16} p \times (M/N_A) \quad (14)$$

with: Q: emission flux of analyte [g s^{-1} cm^{-2}],
N_A: Avogadro constant (6.022 × 10^{23} mol^{-1}).

An example of this calculation for Amiton (**I**) can be found in Table B1 in the appendix. With the emission flux Q in hands the concentration of the analyte in air can be calculated:

$$c_{dif} = S \times Q \times r \quad (15)$$

with: c_{dif}: concentration of analyte in air [g L^{-1}],
S: surface of analyte exposed to air [cm^2],
r: attenuation factor (10^{-4}) [s^{-1}]

The attenuation factor r has been established in the study by *Dravnicks et al.*[283]

For a surface area of 1 m^2 the following values for c_{dif} stated in Table 49 were obtained. These values can serve as a kind of standardized surface density if 1 m^2 is used as a reference area for the analyte under investigation. However, this value must be regarded as the maximum concentrations of analyte that can be present for detection in air in an open-exposure scenario under the given environmental conditions, e.g. temperature.

Table 48: *Calculation of molar heat capacity differences c_{dif} at T = 298.15 K.*

Compound	$C_{p,m}^o$(l)[a]	$\Delta_l^g C_{p,m}^o$[b]	Purity[c]	T_{boil}[d]	ρ[e]
	[J mol^{-1} K^{-1}]	[J mol^{-1} K^{-1}]	[%]	[°C]	[g cm^{-3}]
I	488.03	137.47	97.38	364	1.044
II	488.03	137.47	98.54	338	1.010
III	504.08	141.64	97.42	363	1.035
IV	471.98	133.29	95.07	326	1.061 [286]
V	519.51	145.65	99.07	405	1.015
VI	425.07	121.10	97.88	301	1.059
VII	456.55	129.28	99.71	312*	1.021
VIII	456.55	129.28	96.28	387	1.034

*[a] calculated with elemental increments by Hurst et al. [279], [b] calculated by $\Delta_l^g C_{p,m}^o = 10.58 + C_{p,m}^o(l) \times 0.26$ [280], [c] purity according to GC-FID analysis, [d] boiling point at 101325 Pa = 1 atm, [e] density at 298.15 K (gravimetric determination with calibrated Eppendorf pipette (100 µL)). * linear estimation with $\Delta_l^g C_{p,m}^o$ = 0 due to non-convergence of iteration process.*

From the calculated values for the concentration under diffusion conditions it is possible to estimate the sampling volume necessary to meet the analytical requirements of the instrument used. Moreover, it is possible to predict under which environmental conditions, e.g. operating temperature, it is possible to detect the analyte in the gas phase or not. Knowing this is crucial for first responders who are threatened by evaporating toxic gases. On the other hand if the detection device is not giving an alert one could easily be lulled into a false sense of security since the molecules investigated in this study still pose a threat to human live by being also active as a contact poison.

4.6.3 Conclusion

As a main finding of this work, the vapor pressure of Amiton (**I**) and seven derivatives (**II** – **VIII**) was determined by making use of the transpiration method approach. Furthermore, this approach proved viable for both, thermolabile and highly toxic compounds. Additionally, the concentration c_{dif} of freshly synthesized compounds **I** – **VIII,** of which compound **VII** has not yet been reported in the literature, was calculated based on a diffusion model stated by *Dravnicks et al*. [283]. With equations and values published by *Bird et al*. [284] it was possible to determine values for the concentrations c_{sat} and c_{dif}. They range from 3605 (**VII**) to 96166 ng L^{-1} (**VI**) for c_{sat} and from 0.7 (**VII**) to 20.9 ng L^{-1} (**VI**) for c_{dif}, respectively. The ratio of c_{sat}/c_{dif} is in the range of 4603 to 5738. A condensed summary of the values obtained is given in in Table 49.

Table 49: *Condensed summary of the calculated saturation concentration* $\boldsymbol{c_{sat}}$ *and concentration under diffusion conditions* $\boldsymbol{c_{dif}}$ *for the molecules of this study.*

Compound[a]	**I**	**II**	**III**	**IV**	**V**	**VI**	**VII**	**VIII**
$\boldsymbol{M}$ **[g mol^{-1}]**[b]	269.34	269.34	285.40	253.28	283.37	241.29	255.31	255.31
$\boldsymbol{\rho}$ **[g cm^{-3}]**[c]	1.044	1.011	1.035	1.061	1.015	1.059	1.021	1.034
$\boldsymbol{p_{sat}}$ **[Pa]**[d]	0.070	0.278	0.045	0.258	0.100	0.988	0.035	0.636
$\boldsymbol{c_{sat}}$ **[ng L^{-1}]**[e]	7606	30205	5181	26360	11431	96166	3605	65503
$\boldsymbol{c_{dif}}$ **[ng L^{-1}]**[f]	1.5	5.8	1.0	5.5	2.0	20.9	0.7	12.4
$\boldsymbol{c_{sat}/c_{dif}}$	5240	5215	5431	4835	5738	4603	4905	5262

[a] Compound according to Figure 83. [b] Molar weight. [c] density at 20 °C [d] vapor pressure at 25 °C [e] saturation concentration at 25 °C calculated according to equation 1. [f] concentration under diffusion conditions at 25 °C calculated according to equation 17 for an exposed surface of 1 m².

For a quick conservative estimation of c_{dif} for Amiton derivatives it is recommended to divide c_{sat} by 5000.

However, the concentration c_{dif} is a useful parameter for the choice of suitable gas phase detection equipment for Amiton and its derivatives since it can be directly compared with the limit of detection LOD [ng L^{-1}] of the device used.

The results allow now to easily estimate the necessary sampling volume, in case of analyte enrichment from the gas phase, by dividing the limit of detection by the concentration under diffusion conditions.

4.7 Analytical Studies *via* Solid-phase Micro Extraction

The findings of this chapter are published as a full paper in the *Talanta* journal as well as in a virtual special issue within the *Talanta* journal following a presentation of the results at the 2016 ExTech & ISSS conference in Torun, Poland, and thus mainly represent a reproduction of the manuscript.[287]

For the recovery and analytics of toxic substances from the environment SPME can be used since it combines both sampling and sample preparation techniques in one step. Here it should be proved that SPME is capable of detection of Amiton and Amiton-like compounds not only from headspace (HS) but also by a direct immersion (DI) process.

Table 50: *Summary of the main extraction parameters for the SPME experiments.*

Fiber type	65 µm PDMS/DVB, length:1 cm, (blue hub plain, 24 gauge)
Extraction time	3.0 min - 10.0 min (DI) / 30.0 min (HS)
Extraction temperature	20°C / 40°C / 60°C / 80°C
Sample matrices	sea sand, grass, foliage, tap water, phosphate buffer solutions
Phosphate buffer pH	4.00, 6.88, 9.22

The chosen sampling matrices were at first tap water, which was altered by different phosphate buffer solutions with varying pH values of 4.00, 6.88 and 9.22 to verify the influence of the pH value on the extraction efficiency. Additionally, salt was employed to facilitate the extraction of the analytes from the aqueous phase. Finally, since no method yet has been reported on a DI-method for the extraction of CWA from complex matrices, grass and foliage samples were investigated.

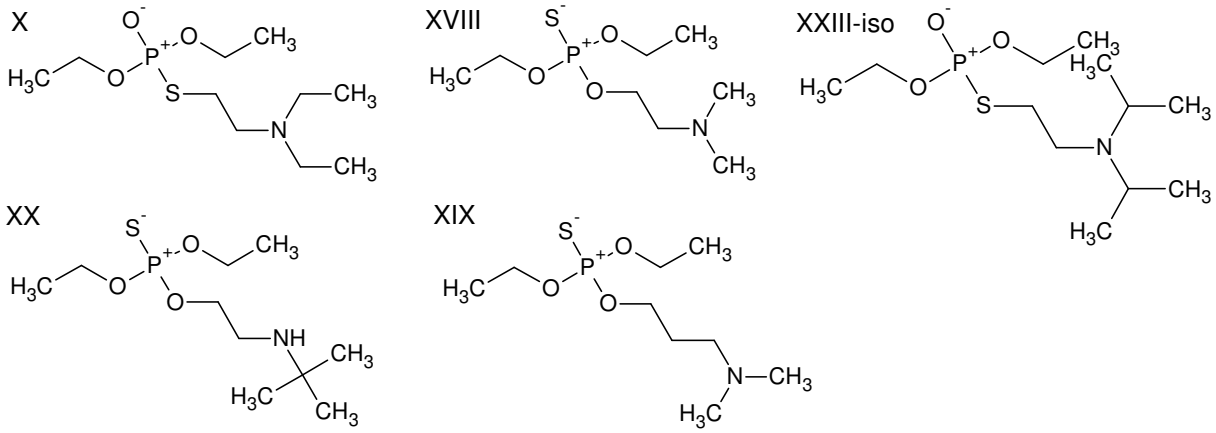

Figure 85: *Depiction of the molecules used to perform the SPME experiments as a proof of principle.*

Moreover, the new Bundeswehr CRN-reconnaissance vehicle MUNGO is equipped with a mass spectrometer which is able to handle SPME fibers, as well as the Hapsite ER can do,

and the also new sampling equipment comes along with several SPME fibers. Thus, the need of efficient and robust SPME methods is clearly identified and needs to be addressed.

In total, five different OTP's (Figure 85) have been investigated with the SPME technique as a proof of principle towards the applicability of the direct immersion technique for CWA's. However, it has to be mentioned that no optimization regarding the type of fiber was done, since a lot of literature dealing with the extraction of organophosphate pesticides from the environment is available in which the chosen 65µm PDMS/DVB fiber is performing best.[220, 232]

4.7.1 Calibration Curve Data and Determination of LOD and LOQ

First, calibration curves were recorded (Figure 86) in the regime of 0.05 to 25 µg ml^{-1} to later correlate the peak area to the amount of analyte extracted by the SPME fiber and to obtain LOD and LOQ values. The result is very precise and yields the nanogram extracted during the SPME experiment. Additionally, by knowing the distribution constant of the fiber it is possible to recalculate the exact concentration of the sample. The determination of LOD and LOQ was done by applying the following two equations:[288]

$$X_{LOD} = s_{x_0} \cdot t_{f,a} \cdot \sqrt{\frac{1}{m} + \frac{1}{n} + \frac{\bar{x}^2}{Q_x}} \quad \textbf{(4.3)}$$

$$X_{LOQ} = k \cdot s_{x_0} \cdot t_{f,a} \cdot \sqrt{\frac{1}{m} + \frac{1}{n} + \frac{\left(x_{LOQ} - \bar{x}\right)^2}{Q_x}} \approx k \cdot X_{LOD} \quad \textbf{(4.4)}$$

with:
- k = 3,
- s_{x_0} = standard deviation,
- $t_{f,a}$ = t-value,
- m = number of repetitions,
- n = number of calibration points,
- $\bar{x}$ = median concentration of the calibration standards,
- Q_x = total sum of squares

The results of this measurements and calculations are summarized in Table 51. As can be seen the coefficients of determination are very close to the value 1 which validates the use of this data as calibration curves for the following evaluation of the SPME experiments. Only for compound **II** a comparably large deviation is observed, resulting in a higher LOD and LOQ therefore.

Table 51: *Compilation of the calibration curve data for the different analytes and the determined LOD and LOQ thereof.*

Analyte	Coefficient of determination from calibration curve data	LOD [µg ml-1]	LOQ [µg ml-1]
X	0.9953	1.27	4.25
XVIII	0.9961	1.14	3.82
XIX	0.9987	0.66	2.25
XX	0.9985	0.71	2.70
XXIII-iso	0.9804	1.43	4.84

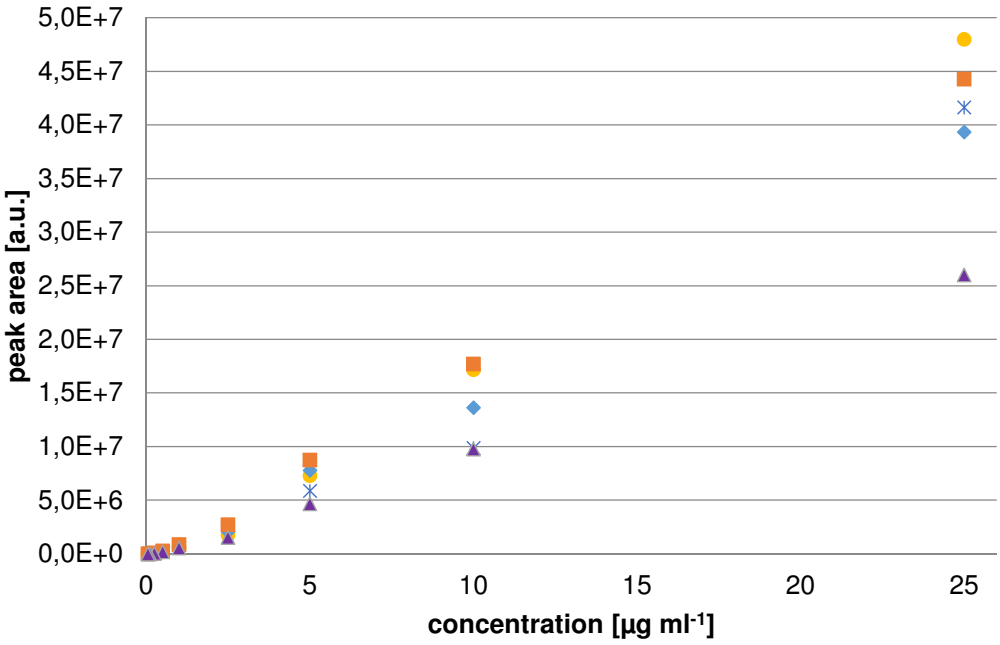

Figure 86*: Calibration curves for the analytes used in the SPME study.* ● = ***X***, ✳ = ***XXIII-iso***, ◆ = ***XVIII***, ■ = ***XIX*** *and* ▲ = ***XX***.

Second, extraction time profiles were recorded to determine the time regime in which the experiments could be performed (Figure 87). It was found that up to 45 minutes no equilibrium extraction had occurred for any analyte during the headspace extraction. For this reason, an extraction time of 30 minutes was selected for headspace extraction, thus being executed at pre-equilibrium conditions. For direct immersion extraction the extraction time was set to 10 minutes as at this point equilibrium was reached for the analytes. For 80°C extraction temperature also smaller extraction times could be used. The three-times longer extraction time for headspace extraction compared to direct immersion extraction is also necessary to overcome the low volatility of the analytes. This was especially true for compounds **X**, **XX** and **XXIII-iso**. Furthermore, in the headspace regime an additional equilibrium reaction (solid-phase – headspace) has to take place which requires more time for the system to reach equilibrium conditions. The reduced extraction time of the direct

immersion method is one clear advantage over well-established headspace extraction techniques and emphasizes the need of an optimized direct immersion extraction method.

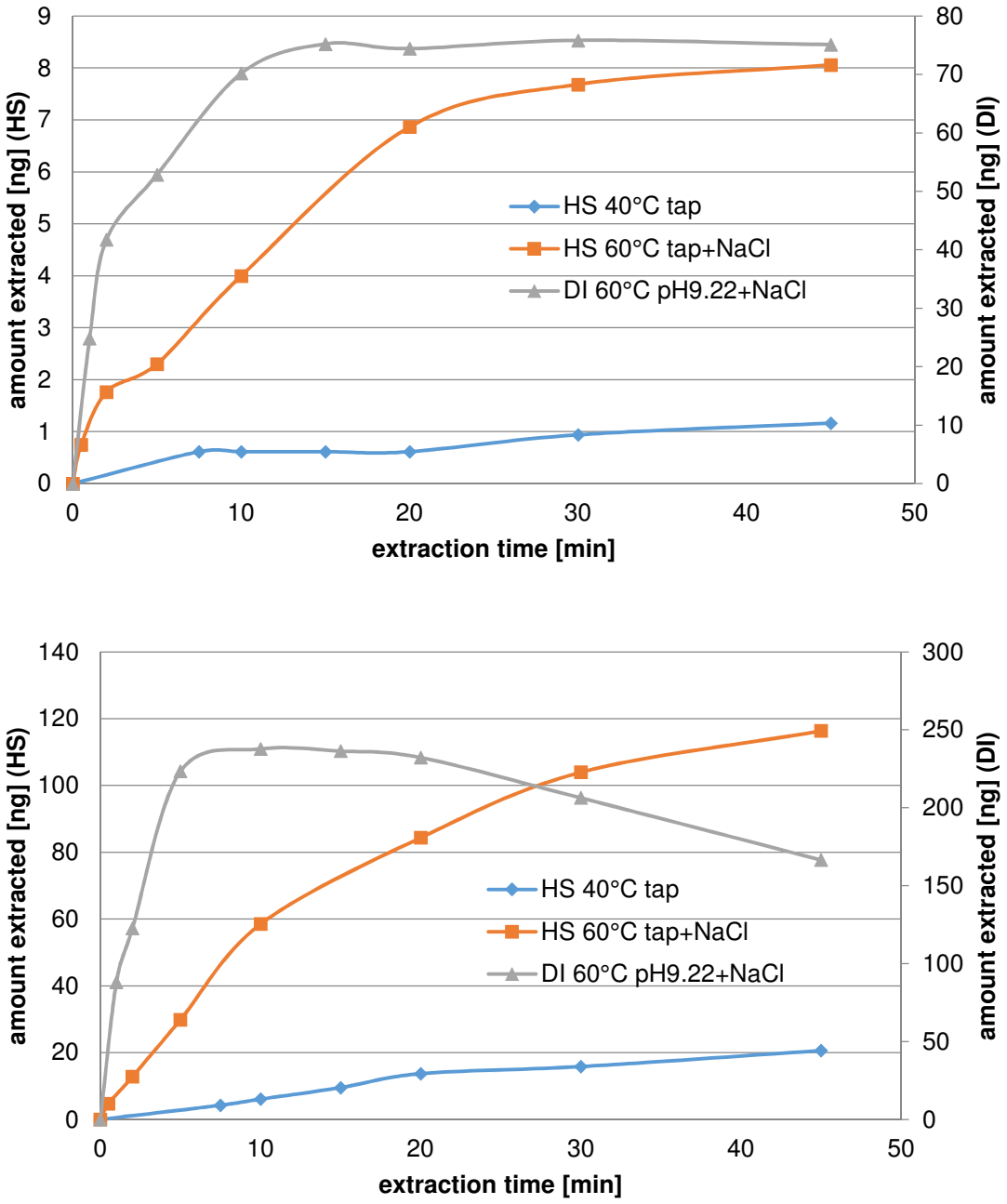

Figure 87: *Comparison of the extraction time profiles plotted as amount extracted in nanogram versus extraction time in minutes for Amiton, upper plot, and **XX**, lower plot, for headspace and direct immersion extraction methods.*

From Figure 87 it can be seen very obviously that the extraction efficiency for Amiton (**X**), which is a persistent compound and has little to no tendency to evaporate, an almost ten-fold higher amount could be extracted by direct immersion. Additionally, it has to be noted that the equilibrium is reached at about ten minutes extraction time compared to extraction times for headspace being > 45 minutes. However, also for compound **XX** (lower plot of

Figure 87), which is the most volatile of the compounds of this study, the extraction efficiency is still two-fold higher for direct immersion as for headspace extraction. Moreover, the increase in extraction temperature from 40 to 60 °C for the headspace extraction results into in seven-fold increase of the amount extracted for compound **X** and a five-fold increase for compound **XX**, respectively.

Generally it can be seen, that with increasing extraction time the amount of analytes adsorbed onto the fiber increases. However, for all of the analytes investigated at room temperature (20°C) no equilibrium extraction could be achieved within the given time frame. This finding is of minor importance since the longer the extraction process is, the more pronounced the competition of the individual analytes for the available adsorption sites on the fiber becomes. This means that it is best to choose extraction times in the linear regime of the initial slopes where the desorption process from the fiber back into the head space or sampling matrix can be neglected. With respect to the military task, to quickly obtain reliable results, it is also favorable not to 'waste" time for unnecessary tasks. Hence, it is crucial to keep the exact timing for the extraction time, which is easy to perform with an autosampler but harder to achieve in the field under stress by manual operation of the SPME equipment. Obviously, in the pre-equilibrium regime little alterations of the extraction time lead to larger errors in peak area or more precisely nanograms extracted. If one is only interested in qualitative identification of the target analyte, this issue can be neglected; but it is easily possible to calibrate the SPME experiment and to achieve exact values for the quantification task.

4.7.2 Evaluation of Headspace Extraction SPME Data

Figure 88 displays the experimental results of the headspace extractions. The most obvious fact is that in the acidic regime, i.e. at a pH value of 4.00, almost no analyte could be extracted by the SPME fiber, regardless of the salinity of the solution and the extraction temperature. The extreme low extraction efficiency can be attributed to the general basic nature of the molecules which are protonated at the present conditions. The ionized form is very soluble in water and has little to no tendency to evaporate into the headspace.[32] In case of pH 6.88 extraction temperatures of 60 to 80 °C are required to extract material in the low nanogram range. Hence, we were not employing distilled water in the present study, since the pH value of the water of 5.50 is still slightly acidic and little to no extraction was expected to be observed. The addition of salt at these temperatures really helps to extract more material in the same time frame. With increasing pH value and increasing temperature the extraction efficiency is also increasing. Headspace extraction at low salinity (no addition of salt) seems to be most effective at temperatures above 60 °C and alkaline conditions. At a pH value of 6.88 the addition of salt supports the phase transfer of the analyte between

the aqueous phase to the headspace, leading to about 10-fold higher amounts of extracted material as compared to the extraction experiment without the addition of salt.

However, in comparison with the results obtained from the studies in tap water, which has only a slightly higher pH value (7.40), the difference is less pronounced. This can be accounted to the fact that the local tap water itself contains certain amounts of 'salt' in the form of different inorganic species, like sulfate, carbonate or sodium and calcium ions.[289] Moreover, this property of the tap water finally adds on to the effect of salt addition under otherwise comparable conditions and results in the highest amounts extracted for the analytes during the headspace experiments at 80 °C.Compared to this, at a pH value of 9.22 the addition of salt of course is helpful for the analysis, but the effect at 60 °C extraction temperature is small compared to pH 6.88. Here the increased temperature from 60 to 80 °C is promoting the analyte into the headspace volume more than the addition of salt does have an effect.

In case of the solid matrix sea sand, the effect of increasing temperature becomes effective above 60 °C and is resulting in an about 10-fold higher amount extracted compared to 20 °C. For grass and foliage the extraction efficiencies at 60 °C are comparable to that of sea sand at 20 to 60 °C. Moreover, the pH dependence of the extraction efficiency from liquid matrices coincides with the pH dependence of direct immersion extraction from solid matrices: In this case only the solutions of pH 9.22 were suitable to 'wash off' the analyte from the matrix and to dissolve it into the buffer and thus make it also available in the headspace of the sample. This was done at 60 and 80 °C with the result, that the amount extracted was almost the same for both measurement series. The amount extracted increased by a factor of two to five compared to the measurement without the buffer solution. Again, the addition of salt, only performed for the 80 °C extraction, allowed to effectively increase the extraction efficiency by a factor of 10. In comparison this method worked better for grass than for foliage.

In general, it can be said, that the described findings hold true for all the analytes of this study. However, some of the analytes, e.g. compounds **XIX** and **XX**, have a more pronounced tendency to be present in the headspace than others, which can be correlated to the different vapor pressures and thus the ability to undergo a phase transition from liquid to vapor state.

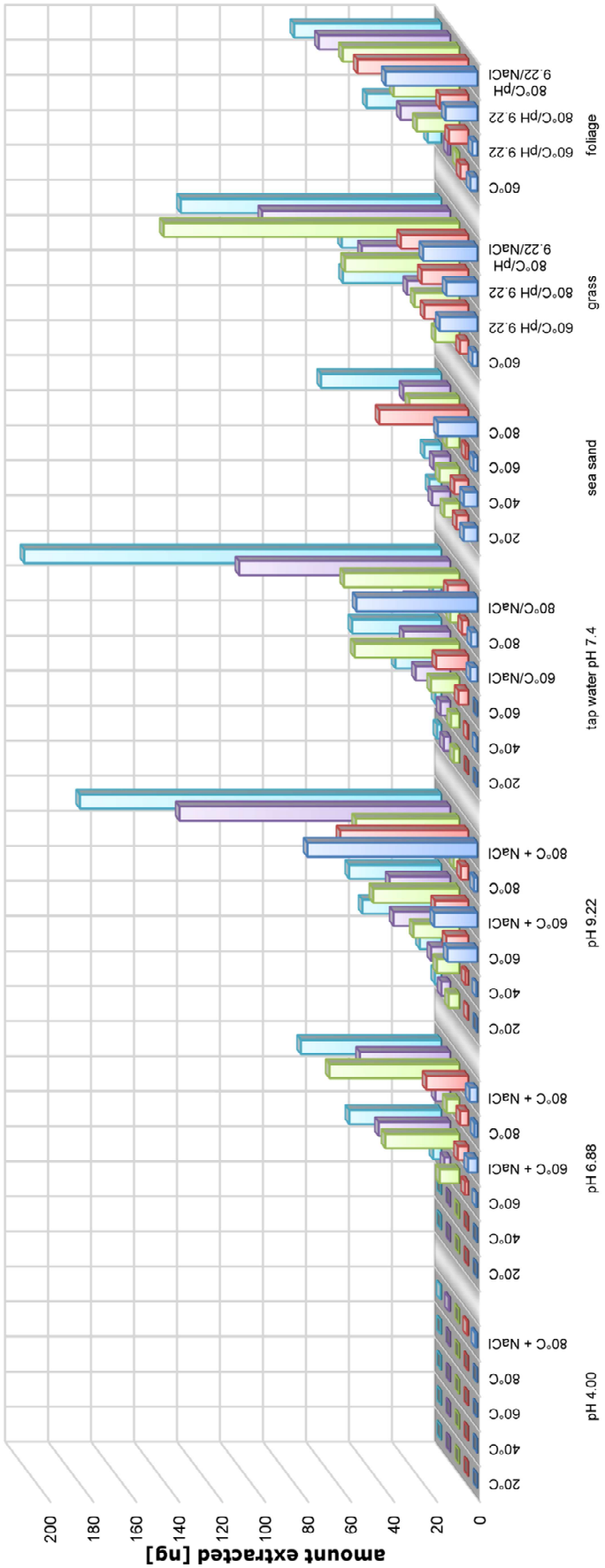

Figure 88: *Results of the headspace SPME experiments for different matrices, temperatures and salt addition for 30 minutes extraction time.* ■ *=* ***X****,* ■ *=* ***XXIII-iso****,* ■ *=* ***XVIII****,* ■ *=* ***XIX****,* ■ *=* ***XX****.*

4.7.3 Evaluation of Direct Immersion SPME Data

In analogy to the headspace SPME data the results of the direct immersion SPME experiments are summarized in Figure 89. For compounds investigated in pH 4.00 buffer solution almost no extraction could be observed. In two cases signals for two compounds could be detected which are significantly above the LOD, but somehow seem not be of any significance and can be denoted as outliers. Again, this results can be explained by the formation of quaternary ammonium salts, which are incompatible with the SPME experiment conditions as those molecules are 'solids' dissolved in water and have no tendency to interact with the polymeric matric of the SPME fiber. Also the addition of salt and applying heat does not significantly increase the extraction efficiency at all for this acidic extraction regime.

For the remaining three liquid phases a general trend can be observed. This is that with increasing temperature the amount extracted is also increasing as expected. The addition of salt at 60 or 80 °C does not play a very prominent role although the amounts extracted are increasing by this step. In case of pH 9.22, increasing the temperature from 60 to 80 °C is more efficient than adding salt to the 60 °C solution. That means that increasing the temperature is more effective than the salt addition for direct immersion.

Generally, the chosen extraction conditions prove to be best for the pH 9.22 buffer solutions. However, the effect of temperature change from 20 to 80 °C generates a two to three-fold increase of the amount extracted. This taken into account means that a prolonged extraction time at a lower sample temperature most likely results in the same amount extracted as it takes waiting for the sample to homogeneously reach the higher extraction temperature of 60 or 80 °C. This relationship can easily be derived from the extraction time profiles (Figure 87) taken as a prerequisite step at the beginning of the experiments, which show that extractions from 10 to 30 minutes are in the linear equilibrium regime.

By having obtained the results from the buffered samples in different pH values we directly used higher temperatures and a pH value of 9.22 for the complex matrices since the studies indicated that this would be the best extraction conditions. In that sense the water (buffered) samples were measured in advance as kind of method optimization steps for the complex matrices. Getting a closer look at the 'solid' samples grass and foliage, which were dispersed in buffer solutions of pH 9.22 and thoroughly vortexed, it can be seen that the extraction efficiency for the analytes from foliage or grass is very comparable. However, it is the case that a higher extraction temperature also results in higher amounts extracted. Also the addition of salt results in the depletion of the analyte in the aqueous phase and to accumulate on the PDMS/DVB fiber. Especially at 60 °C this effect is very useful whereas at 80 °C the effect is less obvious.

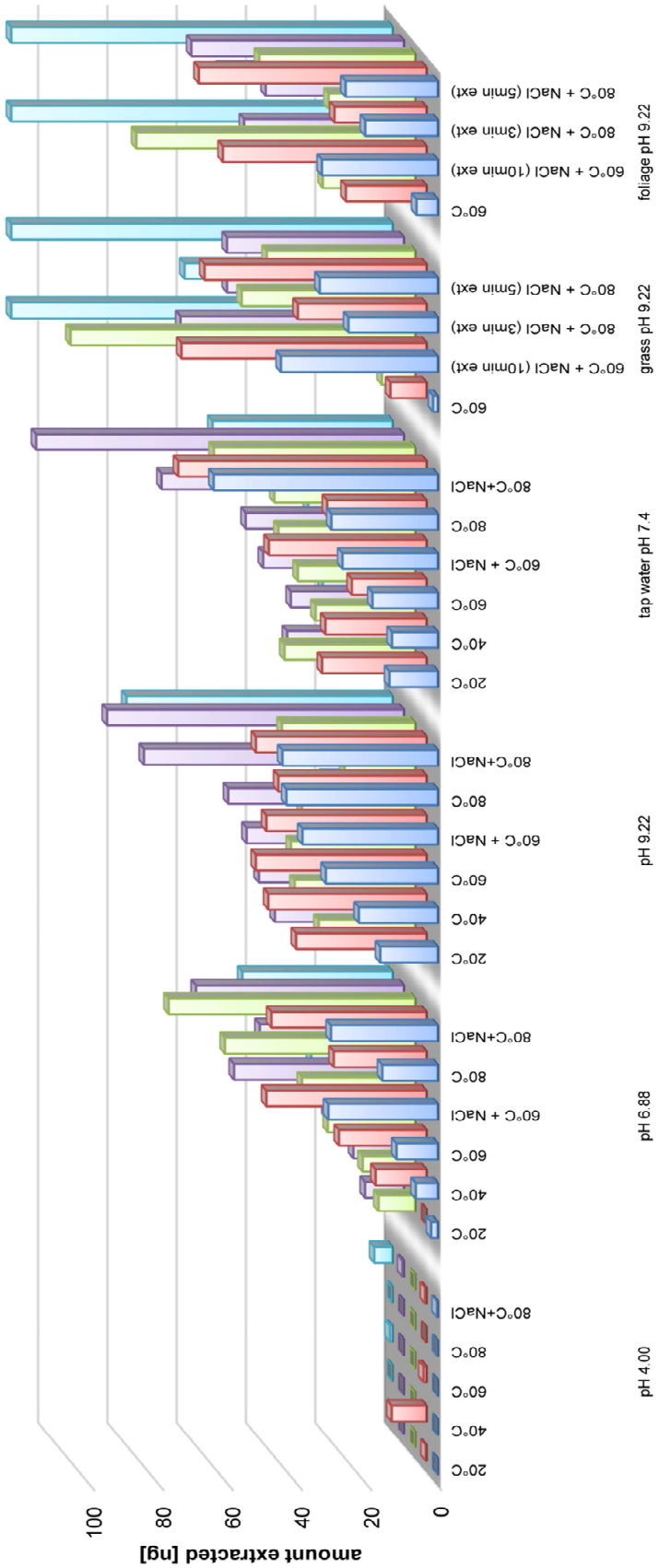

Figure 89: *Results of the direct immersion SPME experiments for different matrices, temperatures and salt addition for ten minutes extraction time for the aqueous samples and three to ten minutes for the complex matrices.* ■ = ***X***, ■ = ***XXIII-iso***, ■ = ***XVIII***, ■ = ***XIX***, ■ = ***XX***.

Moreover, the extraction times were varied for the extraction of the analytes from grass and foliage which very nicely shows that the chosen method also performs under pre-equilibrium conditions. The obtained results show that an extraction time of five minutes at 80 °C compared to the initially chosen ten minutes and 60 °C almost results in the same amount of analytes extracted. Additionally, also extraction times of three minutes and 80 °C under the addition of salt result in amounts extracted which are about twenty-fold higher than the calculated limit of detection and at least five-fold higher than the calculated limit of quantification of this method.

4.7.4 Comparison of HS and DI SPME

First, it has to be noted that the extraction times for headspace and direct immersion do differ by a factor of three. It turned out that especially for the lower temperature regime of 20 and 40° C ten minutes extraction time were not sufficient to extract enough material from the sample by the headspace method. Furthermore, the obtained results would have been below the LOQ and thus data evaluation would not have been very meaningful. However, for the direct immersion experiments a ten minute time period seemed to be convenient since the equilibrium conditions were met at this point. A comparable 30 minutes extraction time would have also worked with respect to the capacity of the fiber. On the other hand 30 minutes seemed to be too long in the sense of having the task to process a larger number of samples under routine laboratory conditions. It has to be accounted that additionally to the incubation time the extraction time and the run time of the analytical instrument has to be added to calculate the overall experimental time for processing one sample.

In comparison of the obtained results for headspace and direct immersion SPME for the investigated matrices water and buffer solutions it can be concluded that in both cases all analytes could be successfully detected, with the exemption that an acidic extraction regime of, e.g. pH 4.22,is not suitable for the compound class under investigation. Moreover, in both cases we observed that increasing pH and increasing temperature leads to an increase of the amounts extracted. The addition of salt is generally spoken, also helpful, especially in case of the headspace extraction where the analytes are forced out of solution into the headspace. The effect of salt addition is less pronounced in case of the direct immersion experiments since analytes leaving the liquid phase into the headspace cannot be adsorbed onto the SPME fiber that is exposed to the liquid phase. However, increasing the temperature by 20 °C is more effective than adding salt to the same sample. Moreover, the salinity of the tap water does also play a minor role for the direct immersion experiments than it does for the headspace experiments. The obtained results for the extracted amounts of analytes are in the same range for headspace and direct immersion under neutral to basic pH values and the addition of salt in a temperature regime of 60 to 80 °C. However,

the comparably short extraction time for direct immersion proves this method to be superior for aqueous samples.

Regarding the complex matrices grass, foliage and sand the above said is also true. In a direct comparison of the extraction efficiency, the direct immersion extraction is also more effective than the headspace extraction. However, sea sand was not investigated by direct immersion since this would have only tested the extraction efficiency of the applied 'solvent' instead of the SPME experiment itself. On the other hand the influence of swirling sand could have possibly damaged the SPME fiber during the extraction experiment.

Even at pre-equilibrium conditions of three and five minutes for the direct immersion extraction compared to headspace the efficiency of the method is very high. This shows that the matrix does not affect the extraction performance at all. Furthermore, direct immersion is obtaining the same amounts extracted at 1/10 of the extraction time showing a clear advantage again.

4.7.5 Conclusion

For the first time, it could be successfully shown that direct immersion SPME is a suitable technique for the fast and reliable detection and analysis of different organophosphates closely related to the CWC with the aid of an automated GC-MS system from complex matrices. The proper adjustment of the sampling parameters like time, pH and salt concentration has a pronounced influence on the efficiency of the method and LOD and LOQ levels in the low one-figure ppm range can be achieved. Furthermore, the obtained results lead to the conclusion that this method can most likely be applied for other chemical warfare agents, like VX or Sarin as well.

By comparing the absolute numbers of the amounts extracted for headspace and direct immersion SPME it can be stated that by matching the applied different extraction times, the direct immersion method in all cases is more sensitive compared to the headspace extraction and can dramatically shorten the necessary experimental time down to 1/10 with respect to the extraction time.

Additionally, the developed direct immersion technique can be performed either under pre-equilibrium or equilibrium conditions within three to ten minutes and still results in amounts extracted at least five-fold above the LOQ and about twenty-fold above LOD.

4.8 Toxicological Studies

As mentioned in the introduction, the knowledge about the toxicity is crucial information since it will specify safety measures including the personal protective gear. Furthermore, it can be assumed, whether a substance could be of relevance for being employed as a harmful substance and thus methods for the detection could have to be developed. However, if only a low toxicity value is determined the molecule is not of less importance since little to no information on other chemical and physical properties and spectra are available and therefore further investigation has to be done.

4.8.1 Determination of K_M and v_{max}

The careful processing and proper evaluation of all experimental data is of great importance. Thus, additional remarks are necessary to present which did not fit in the experimental section of this work. Furthermore, the calculated results are necessary for the evaluation for the kinetic constants of the inhibition reaction in the following.

Before the actual kinetic investigation could be done the auto hydrolysis of the substrate has to be determined. The hydrolysis data have been extrapolated and were used to correct the individual raw data readings. Only by applying this procedure it is possible to obtain true reaction kinetic data. Thus, for different concentrations of the substrates the auto hydrolysis rates were determined. Acethylthiocholine iodide (AcTChI) and Butyrylthiocholine iodide (BuTChI) were selected as substrates for the respective enzyme. The finally chosen substrate concentration was 0.9 mM since the auto hydrolysis was very slow. Furthermore, the substrate concentration was still high enough to saturate the enzyme during the desired observation time of up to 30 min.

From the obtained kinetic readings at 412 nm wavelength for the reaction of pure enzyme without the influence of an inhibitor molecule the Michalis-Menten constant K_M and the maximum enzyme velocity v_{max} were determined. Therefore, the enzyme was challenged with different substrate concentrations. By plotting the initial slope of the individual readings versus the corresponding substrate concentration a graph for the reaction kinetics could be obtained which can be nicely fitted by a logarithmic function (Figure 90). From the asymptotic value of this graph, v_{max} can be derived. Since the asymptotic behavior of the classical Michaelis-Menten plot is rarely reached in a suitable time frame it is most convenient to apply linearization methods. Generally two different methods are available for this task: i) the Lineweaver-Burk (Figure 91) or ii) the Eadie-Hofstee (Figure 92) linearization method. In the Lineweaver-Burk plot the slope represents K_M / v_{max}, the y-intercept is equal to the reciprocal value of v_{max} and the x-intercept is the negative reciprocal value of the

Michaelis-Menten constant. In case of the Eadie-Hofstee linearization method the value for v_{max} can be obtained from the y-intercept and K_M equals the slope multiplied by -1. In Figure 90 the two obtained data series for the AChE and BuChE molecule are plotted.

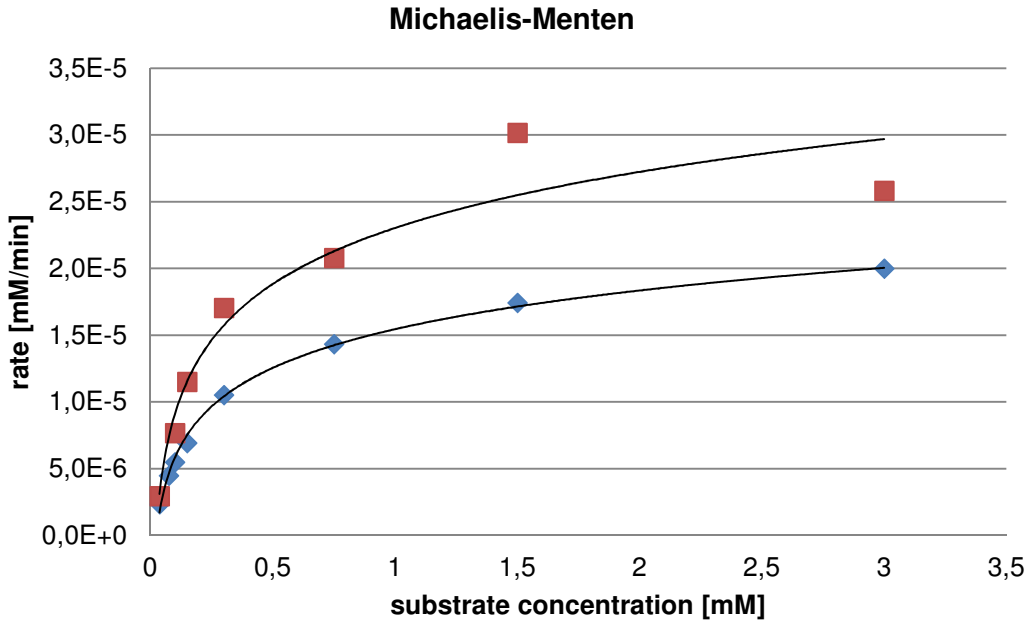

Figure 90: *Michaelis-Menten plot for the BuChE molecule measured according to Ellman.[144]. Red symbols (squares) represent values for AChE and blue ones(rhombs) represent BuChE values, respectively.*

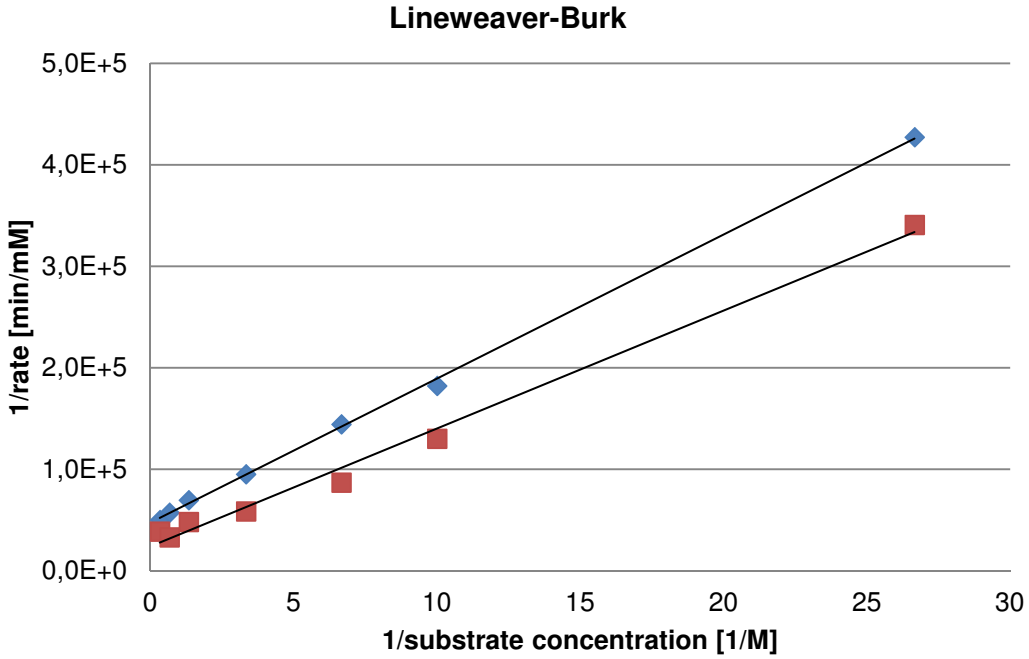

Figure 91: *Lineweaver-Burk plot for AChE and BuChE molecule. Red symbols(squares) represent values for AChE and blue ones(rhombs) represent BuChE values, respectively.*

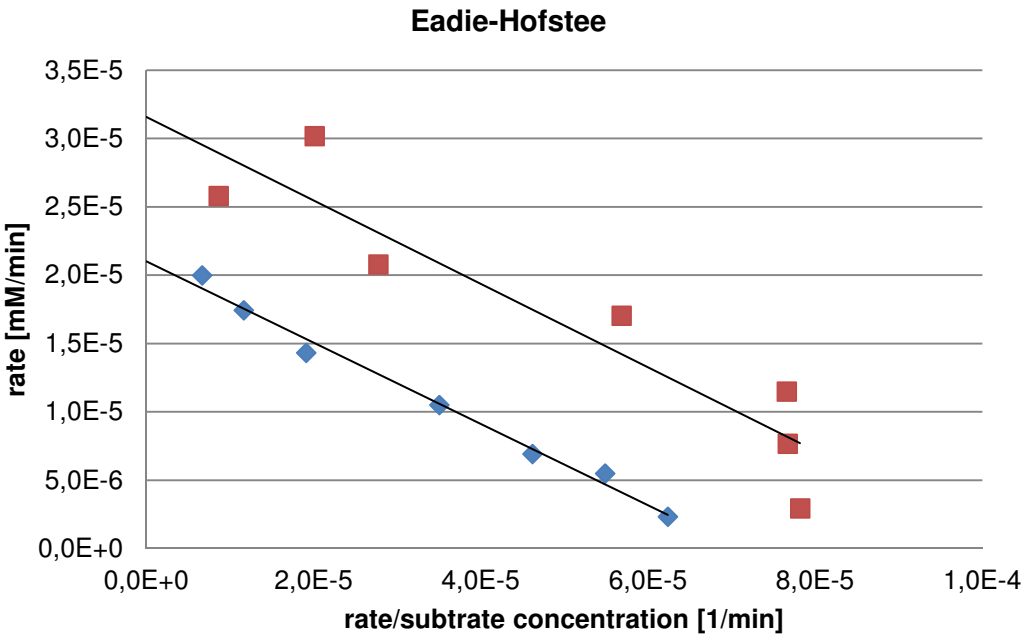

Figure 92: *Eadie-Hofstee plot for AChE and BuChE molecule. Red symbols (squares)represent values for AChE and blue ones (rhombs) represent BuChE values, respectively.*

It can be seen that the values of 1.5 and 3 mM substrate concentration for the AChE do hardly fit to the regression curve. In the following Lineweaver-Burk linearization these deviations are of less influence, whereas in the Eadie-Hofstee diagram minor deviations play a major role. Figure 92 shows this fact very impressively and the R^2-values are clearly worse compared to those for the Lineweaver-Burk plot. This can also be seen from the calculated results for K_M and v_{max} in Table 52. For this reason the Lineweaver-Burk method is most often preferred in the experimental analysis of kinetic data.[290] However, in case of the BuChE molecule both methods lead to very precise results and very good R^2 values.

Table 52: *Comparison of the results for the kinetic constants for AChE and BuChE obtained from Figure 91 and Figure 92.*

Method	Enzyme	K_M [mM]	v_{max} [mM/min]	R^2
Lineweaver-Burk	BuChE	0.301	2.11E-05	0.9993
	AChE	0.485	4.17E-05	0.9921
Eadie Hofstee	BuChE	0.297	2.10E-05	0.9894
	AChE	0.305	3.16E-05	0.8707

4.8.2 AChE and BuChE Activity Assay

The bimolecular rate constants of the inhibition reactions were determined by applying the double reciprocal method of *Hart and O'Brian* which was also used by *Barak et al.*[122, 123] Additionally, this method allows the determination of the dissociation constant for the enzyme-inhibitor complex and the phosphorylation constant. This can be achieved by

establishing pseudo-first-order conditions, meaning to challenge the enzyme with an excess of substrate and inhibitor at the same time for varying inhibitor concentrations.

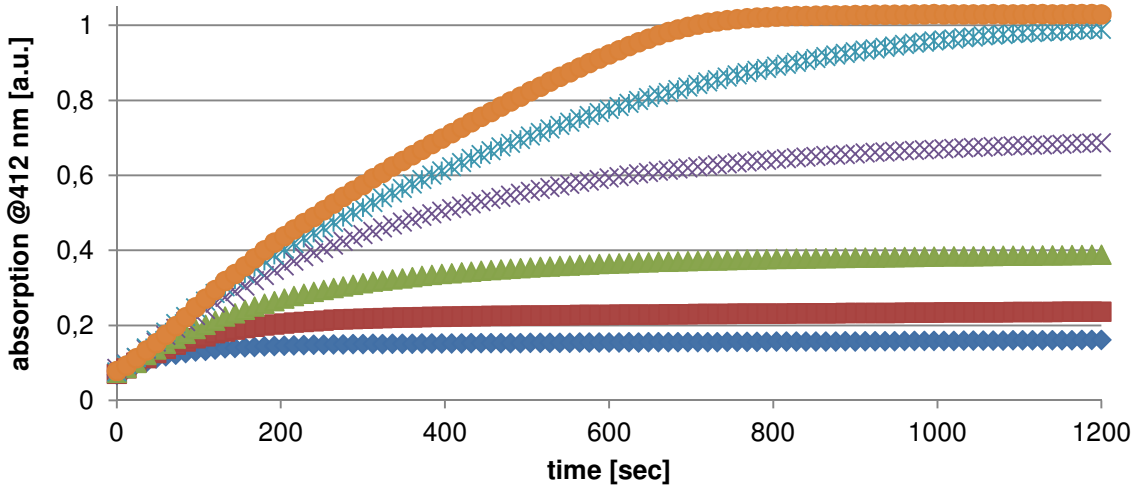

Figure 93: *Experimental results of the kinetic study for BuChE challenged with varying concentrations of compound **X** and constant substrate concentration. The mismatch in not meeting the origin (0,0) is due to the delay from adding the enzyme until the start of the first measurement. Concentration levels: ◆ = 0.24 mM, ■ = 0.12 mM, ▲ = 60 nM, ✕ = 30 nM, ✳ = 15 nM, ● = 7.5 nM*

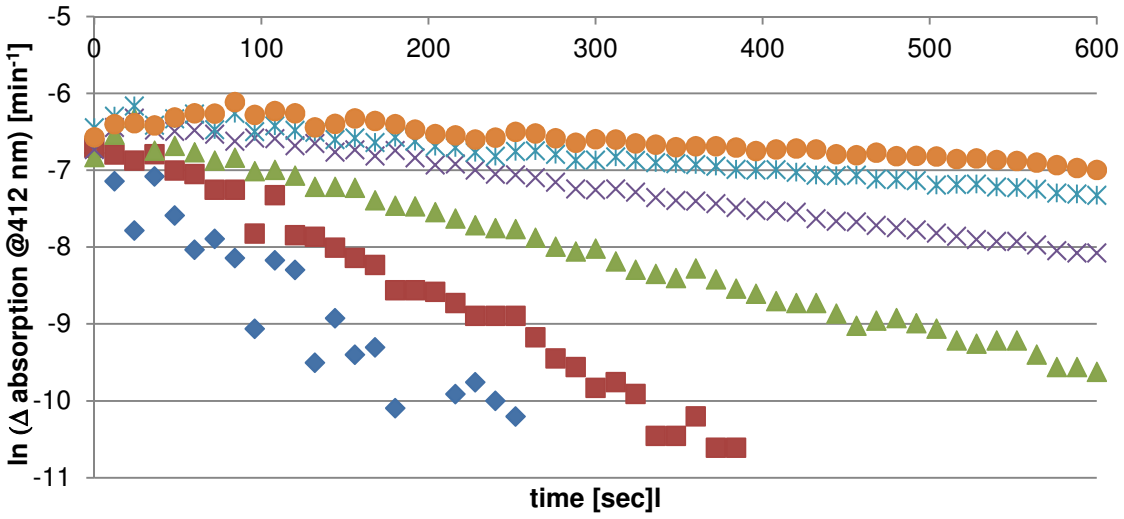

Figure 94: *Linear time dependence of the initial slopes (ln values) of the progressive inhibition curves shown in Figure 93. Concentration levels: ◆ = 0.24 mM, ■ = 0.12 mM, ▲ = 60 nM, ✕ = 30 nM, ✳ = 15 nM, ● = 7.5 nM.*

First, the obtained spectral data are plotted against time (Figure 93). Second, the initial slopes of the curves are determined in each data point by calculating the tangents in each data point. The obtained tangents are then plotted in semi logarithmic fashion to yield a linear correlation for the different inhibitor concentrations applied (Figure 94).[122, 291] The slopes k_{obs} of the latter plot could then be calculated by linear regression which finally were plotted against $1/([PX](1-\alpha))$ with $\alpha = [S]/(K_M+[S])$ (*cf.* Figure 95 and *cf.* Chapter 1.1). This final plot allows the calculation of K_D/k_2 as the slope and $1/k_2$ as the ordinate intercept.

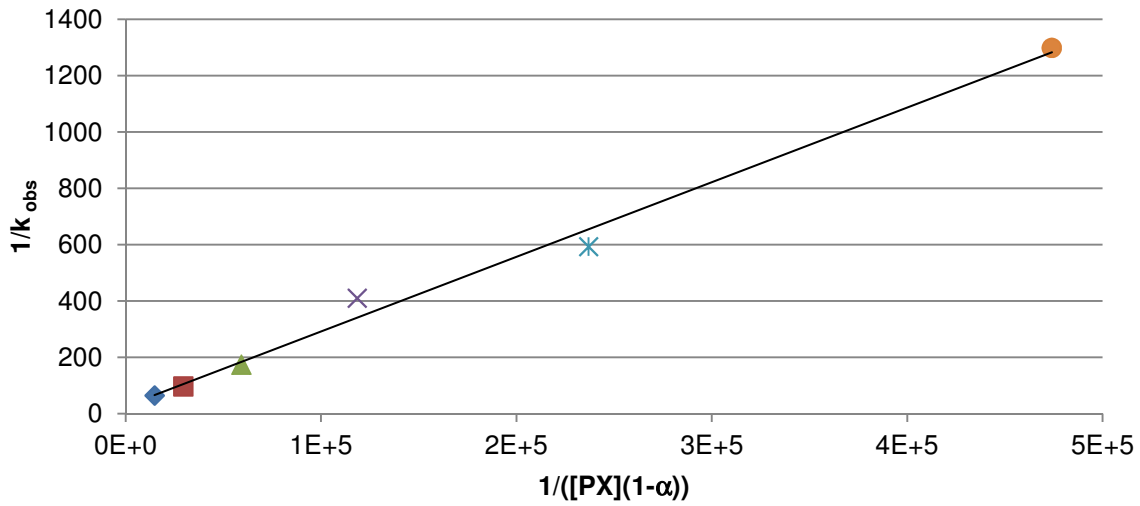

Figure 95: *Double reciprocal plot of k_{obs} vs inhibitor concentration corrected for the presence of substrate (1 - α; where α = [S]/K_M+ [S]) with data from Figure 93 and Figure 94. The plot allows deriving the rations K_D/k_2 and $1/k_i$ from the slope and the intercept, respectively. Concentration levels: ◆ = 0.24 mM, ■ = 0.12 mM, ▲ = 60 nM, × = 30 nM, ✳ = 15 nM, ● = 7.5 nM.*

Finally, the inhibition rate constant k_i can be obtained from the inverse of the slope from Figure 95, which is nothing else as the division of k_2 by K_D which was first described by *Main*.[126] Although the inhibitory potency is more properly expressed by the inhibition rate constant, for practical reasons it is most often expressed by the IC_{50} value which is referred to as the half maximal inhibitory concentration, by taking advantage of the following expression:[125]

$$IC_{50} = \frac{0.695}{k_i} \qquad \textbf{(4.5)}$$

with: k_i = inhibition rate constant [$M^{-1}s^{-1}$]

IC_{50} = half maximal inhibitory concentration [M]

This now represents the molar concentration of the inhibitor needed to cause 50% inhibition of the enzyme activity at a fixed time of incubation. However, it is also quite common to present this value in the logarithmic form as pIC_{50} value.[134]

Additionally, for a better comparison towards other molecules the obtained data can be transformed *via* the Cheng-Prusoff equation into values for the binding affinity of the inhibitor towards the enzyme for a given substrate concentration *via*:[292, 293]

$$K_i = \frac{IC_{50}}{1 + \frac{[S]}{K_M}} \qquad \textbf{(4.6)}$$

with: K_i = absolute inhibition constant [M]

IC_{50} = half maximal inhibitory concentration [M]

K_M = Michaelis-Menten constant [M]

[S] = substrate concentration [M]

This procedure of data evaluation is done for all the molecules investigated. The obtained results are summarized separately for AChE and BuChE and discussed in the following two sections.

4.8.2.1 Inhibition of Acetylcholinesterase

The results of the inhibition kinetic studies of the AChE molecule with different OP's can be found in Table 53. Here the inhibition rate constant k_i, the dissociation constant K_D and the unimolecular phosphorylating constant k_2 are reported. The experimentally found values clearly indicate that only Amiton itself does have a significant inhibitory potential which is more than 1000 times larger than that of any other molecule investigated in this study. This can be very impressively seen in Figure 96 where the compounds are ordered by their increasing inhibition rate constant.

Although some of the k_2, and K_D–values have relatively large standard deviations the resulting k_i values of the different molecules and the relative order reflect the general known structural effects on toxicity. For example the distance between the P-O(S)-----N-R_2 moiety in the molecule has a significant effect on the toxicity with shorter spacing leading to higher toxicity values. Moreover, it is found that the bulkier residues at the nitrogen atom result in less toxic compounds. The only exemption to this rule is the isopropyl-group which seems to add an important amount for the toxicity of a compound. In comparison with the VX-molecule, which bears the same functional group at the nitrogen atom as compound **XXIII** does, that fact seems also to be true.

Additionally, it can be said that a 'bridge-length' of 5 CH_2-groups (**XVII**) between the chalcogen atom and nitrogen atom is no more toxic for the AChE molecule, whereas for a molecule of three CH_2-groups (**XV**) as a spacer the toxicity drops by one tenth.

Additionally, the results for the inhibitory constant are plotted in ascending order in Figure 96 and thus allow a direct optical comparison of the values. It can be seen very nicely that by proper selection of the molecule structure a desired inhibitory constant can be achieved. However, this finding is a rough estimate but can serve as a kind of library for toxicity increment studies and target design.

Unfortunately, only some literature results for Amiton could be found to be compared with the results of this study. The one reported by *Varo et al*. is in very good agreement with the determined value (*cf.* Figure 96).[294] From this it can be concluded that the other values are also of good quality.

Table 53: *Means and standard error of the calculated kinetic parameters based on 2-3 repetitions of the kinetic parameters of the AChE-inhibition studies for the different compounds. Data treatment is described in the previous chapter. * No inhibition observed. # Samples could not be investigated because the thioalcohol educt, which itself reacts with the DTNB reagent, could not be removed from the final sample.*

compound	k_2 [s^{-1}]	K_D [M]	k_i [$M^{-1}s^{-1}$]	IC_{50}[M]
IX	7.51 ± 0.3E-3	4.69 ± 2.2E-5	160 ± 68	4.3 ± 1.3E-3
X	2.80 ± 0.4E-2	4.40 ± 1.9E-8	6.37 ± 2E5	1.1 ± 0.3E-6
XI	5.53 ± 1.3E-3	2.23 ± 0.8E-5	25 ± 2	2.8 ± 0.2E-2
XII	1.56 ± 0.1E-3	2.28 ± 0.2E-2	0.07 ± 0.01	9.9 ± 1.2
XIII	1.51 ± 0.1E-2	3.11 ± 0.2E-4	48 ± 2	1.4 ± 0.1E-2
XIV	#	#	#	#
XV	4.33 ± 4.7E-4	4.30 ± 2.1E-5	10 ± 6	6.9 ± 2.6E-2
XVII	*	*	*	*
XVIII	8.49 ± 0.2E-5	3.3 ± 0.3E-5	29 ± 15	2.4 ± 0.8E-2
XIX	5.92 ±1.2E-4	5.65 ± 0.7E-6	104 ± 35	6.6 ± 1.7E-3
XX	1.37 ± 0.1E-3	1.48 ± 0.9E-4	9 ± 5	7.7 ± 2.7E-2
XXI	1.67 ± 0.1E-2	1.72 ± 0.4E-4	97 ± 12	7.1 ± 0.8E-3
XXII	7.49 ± 0.8E-3	2.22 ± 0.5E-5	337 ± 38	2.0 ± 0.2E-3
XXIII	1.07 ± 0.4E-2	1.86 ± 0.9E-5	658 ± 157	1.2 ± 0.2E-3
XXIV	7.14 ± 0.4E-3	4.22 ± 0.2E-4	17 ± 0.4	4.1 ± 0.1E-2
XXV	2.32 ± 0.1E-3	7.77 ± 0.6E-5	29 ± 3	2.4 ± 0.2E-2
XXVI	2.01 ± 0.1E-4	4.82 ± 0.7E-5	4.2 ± 0.1	1.6 ± 0.1E-1
XXVII	3.35 ± 0.5E-4	2.55 ± 1.2E-5	13 ± 4	5.3 ± 1.2E-2
XXIX	5.25 ± 0.6E-3	5.17 ± 2.6E-3	1 ± 0.4	6.9 ± 2.0E-1
XXVIII	2.01 ± 0.2E-2	1.13 ± 0.5E-4	178 ± 57	3.9 ± 0.9E-3
XXXIII	9.20 ± 1.7E-3	5.15 ± 1.3E-3	1.8 ± 0.1	3.8 ± 0.2E-1
XXXIII_iso	3.57 ± 0.1E-2	4.26 ± 0.7E-5	838 ± 102	8.2 ± 0.9E-4
Paraoxon ethyl	2.73 ± 0.1E-2	2.33 ± 0.5E-5	1175 ± 219	5.9 ± 0.9E-4
Paraoxon methyl	9.65 ± 0.6E-3	2.27 ± 0.6E-5	426 ± 86	1.6 ± 0.3E-3

The value reported by *Main* was measured at 5 °C and is expectedly lower than the observed ones in this study.[295] Additionally, one has to know that the trivial name Tetram is another synonym or trade name for Amiton. However, the most often available information from literature is on molecules being able to inhibit the enzyme AChE but no direct inhibitory investigation with any AChE was reported.[136]

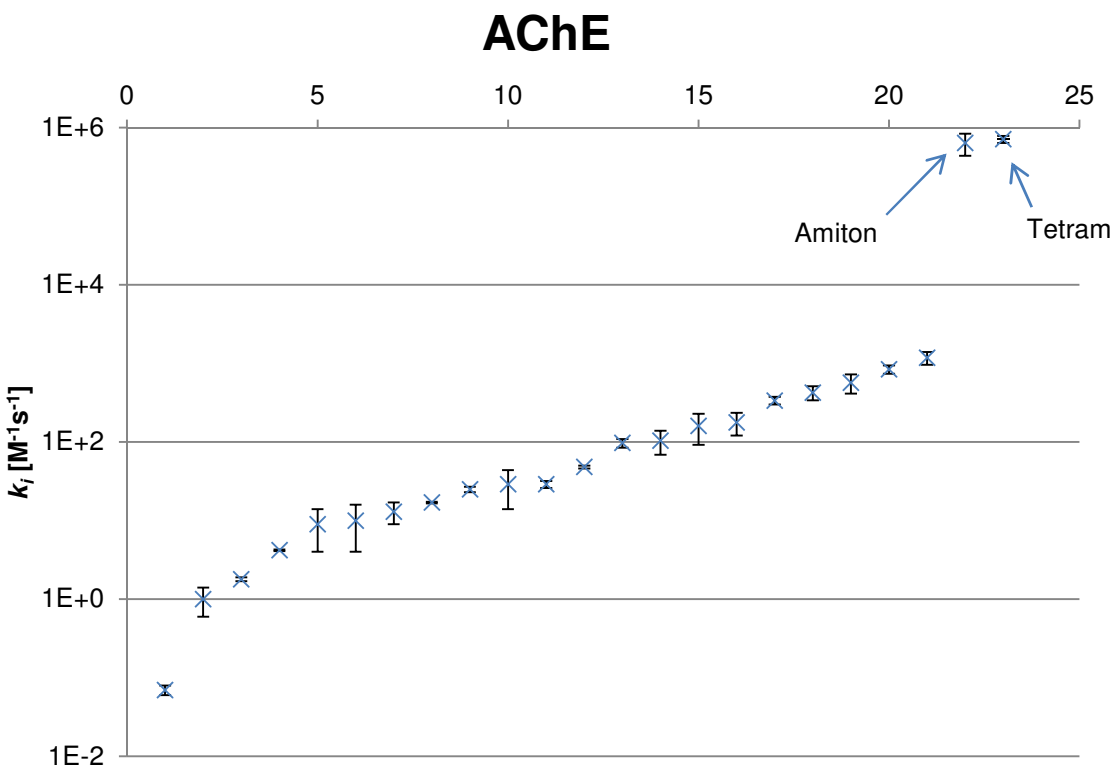

Figure 96: *Semi-logarithmic plot to compare results of inhibition rate constant k_i for AChE challenged with OP's according to Table 53. Compounds are sorted in ascending order. Caption names in the graph, besides Amiton, relate to additional literature data from Main.[294]*

4.8.2.2 Inhibition of Butyrylcholinesterase

The results of the inhibition kinetic studies of the BuChE molecule with different OP's can be found in Table 54. Here the inhibition rate constant k_i, the dissociation constant K_D and the unimolecular phosphorylating constant k_2 are reported. In comparison with the results of the inhibition rate constants for AChE the difference in the k_i–value of Amiton to the other compounds is not so significant and they are very close together. The closest value could be found for compound **XIII**. Additionally, for the BuChE inhibition values from the literature are available for DFP, Paraoxon, Sarin, VX and Soman for comparison and are also reported in Figure 97 as numbers 10, 18 and 26 to 28, respectively. To prove the chosen methodology and results right, the calculated value for Paraoxon is in very good agreement with the found literature value within the determined error bars.[146] Thus, it is safe to assume that the other values are also of good quality. Unfortunately no standard deviation of the literature values was given. As is true for AChE the toxicity of the compound can be precisely tuned by the alteration of the nitrogen moiety. The huge difference in the toxicity compared to the CWA's GB and VX for example can be explained by the coordination of the phosphorus being a phosphate or thiophosphate for the compounds of this study and being a phosphonate for the mentioned CWA's. In general it can be concluded that the most compounds are more toxic towards BuChE than to AChE.

Table 54: *Means and standard error of the calculated kinetic parameters based on 2-3 repetitions of the kinetic parameters of the BuChE-inhibition studies for the different compounds. Data treatment is described in the previous chapter. * No inhibition observed .# Samples could not be investigated because the thioalcohol educt, which itself reacts with the DTNB reagent, could not be totally removed from the final sample.*

compound	k_2 [s^{-1}]	K_D [M]	k_i [$M^{-1}s^{-1}$]	IC_{50}[M]
IX	2.40 ±0.1E-2	4.44 ±2.8E-5	541 ± 190	1.3 ± 0.3E-3
X	1.99 ± 0.2E-4	5.22 ± 1.0E-7	3.8 ± 0.4E4	1.8 ± 0.2E-5
XI	4.20 ± 0.8E-3	1.45 ± 0.1E-4	29 ± 2	2.4 ± 0.1E-2
XII	5.23 ± 0.7E-3	9.18 ± 2.4E-5	57 ± 7	1.2 ± 0.1E-2
XIII	1.48 ± 0.4E-3	1.35 ± 0.8E-6	1.1 ± 0.3E4	6.3 ± 1.4E-5
XIV	#	#	#	#
XV	*	*	*	*
XVII	8.12 ± 0.8E-4	1.10 ± 0.1E-4	7 ± 1	9.9 ± 1.2E-2
XVIII	1.07 ± 0.1E-2	2.98 ± 0.3E-5	357 ± 31	1.9 ± 0.1E-3
XIX	9.86 ± 0.2E-4	1.45 ± 0.1E-5	67 ± 20	1.0 ± 0.2E-2
XX	2.59 ± 0.1E-2	2.41 ± 1.3E-4	107 ± 42	6.4 ± 1.8E-3
XXI	3.02 ± 0.5E-2	1.17 ± 0.5E-5	2580 ± 663	2.7 ± 5.5E-4
XXII	4.75 ± 0.9E-2	2.09 ± 0.9E-4	227 ± 60	3.0 ± 0.6E-3
XXIII	4.67 ± 0.4E-2	1.84 ±0.6E-5	2530 ± 605	2.7 ± 0.6E-4
XXIV	6.15 ± 0.7E-4	4.32 ± 0.3E-3	0.14 ± 0.01	6.9 ± 0.1E-1
XXV	1.17 ± 0.1E-2	2.46 ± 0.2E-5	478 ± 31	1.4 ± 0.9E-3
XXVI	1.21 ± 0.1E-3	2.75 ± 0.2E-6	439 ± 50	1.6 ± 0.2E-3
XXVII	3.89 ± 0.7E-3	1.43 ± 0.1E-5	272 ± 30	2.5 ± 0.3E-3
XXIX	4.44 ± 1.5E-3	6.95 ± 0.5E-5	63 ± 16	1.1 ± 0.2E-2
XXVIII	3.08 ± 0.2E-2	4.02 ±2.8E-5	766 ± 497	9.0 ± 3.5E-4
XXXIII	2.67 ± 0.7E-3	1.55 ± 0.9E-5	17 ± 4	4.1 ± 0.8E-2
XXXVI	1.09 ± 0.2E-4	4.09 ± 0.4E-4	3 ± 0.3	2.3 ± 0.2E-1
XXIII-iso	4.35 ± 0.4E-2	9.56 ± 0.3E-6	4557 ± 1110	1.5 ± 0.3E-4
Paraoxon ethyl	1.56 ± 0.1E-2	5.28 ± 1.6E-6	2949 ± 653	2.3 ± 0.4E-4
Paraoxon methyl	1.18 ± 0.1E-1	4.81 ± 0.8E-5	2460 ± 400	2.8 ± 0.4E-4

Besides this, it can be stated that also compound **XIII** which has two thio-ethoxy moieties bond to the phosphorus instead of ethoxy groups, exhibits a very comparable toxicity value as Amiton (**X**). Regarding the fact that molecules can be assigned to a certain type of cholinesterase inhibitor by their property to inhibit AChE and BuChE differently or in the same way a classification can be done according to *Otoguro et al* and *Kapkova*.[296, 297]

- Type A: compounds predominantly inhibiting AChE
- Type B: compounds inhibition AChE and BuChE to the same extent
- Type C: compounds of higher activity towards BuChE
- Type D: compound predominantly inhibiting BuChE

According to this classification the following can be stated:

- Type A compounds: **X**, **XXIV**
- Type B compounds: **XI**, **XIX**, **XXII**
- Type C compounds: **XII**, **XIV**, **XVI**, **XVII**, **XVIII**, **XX**, **XXIII**, **XXIII-iso**, **XXV**, **XXVII, XXVIII**
- Type D compounds: **XIII**, **XV**, **XXI**, **XXVI, XXIX**

In other words, this means that compounds **X** and **XXIV** are most likely to cause body damage as do CWAs. Type B compounds could be scavenged by treatment with BuChE since they have more or less the same binding affinity towards AChE as they have to BuChE.

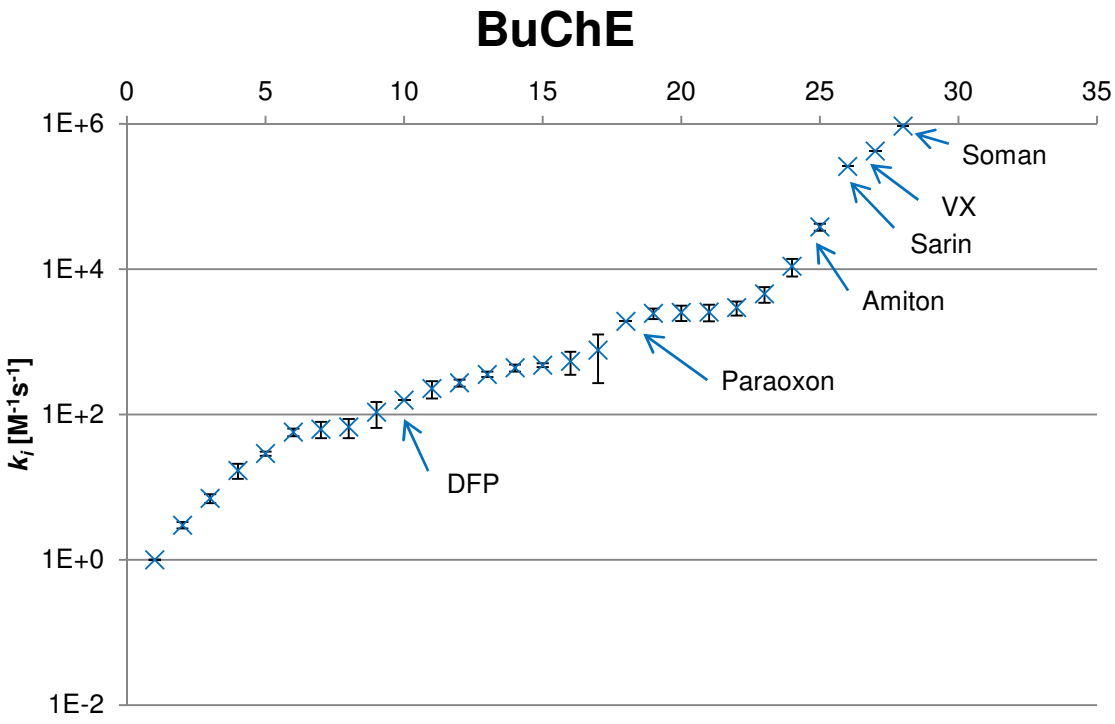

Figure 97: *Semi-logarithmic plot to compare results of inhibition rate constant k_i for BuChE challenged with OP's according Table 54. Compounds are sorted in ascending order. Caption names in the graph, besides Amiton, relate to additional literature data from Forsberg and Puu.[146]*

In some other investigation on the influence of the alkyl amine side chain on the toxicity of some chlorochalcone molecules by *Gao et al*. it was also found that the diethyl substituents results in a higher IC_{50} value compared to a dimethyl configuration.[141] Furthermore, a six-

membered ring compared to a five-membered ring with the nitrogen embedded has always given an increased IC_{50} value.

4.8.3 Conclusion

Generally it can be said that the main result of the toxicological studies is the full description of the AChE and BuChE inhibitory capacity of a whole set of structural isomers, which has not been reported before in such a condensed manner. Noteworthy, the toxicity value can be very precisely tuned by proper choosing the structural features of the amino functionalized side chain of the molecule.

Especially, the di-isopropyl moiety at the nitrogen atom can be identified to have a big impact on the toxicity compared to the di-methyl of di-ethyl substituent. However, the toxicity towards BuChE is for almost all compounds higher than for AChE. Although the inhibitory constant k_i of **X**, Amiton, is almost double the number for AChE compared to BuChE clearly giving proof for the compound being correctly listed in schedule 2 of the CWC. Noteworthy, the structural isomer bearing two thio-ethoxy groups at the phosphorus central atom (**XIII**) has a comparably high k_i-value which is almost a quarter the value for Amiton bearing two ethoxy groups.

Additionally, these findings lead to the conclusion that the newly synthesized molecules may be suitable as ideal candidates for the training of hazard defense personnel, since they have low AChE activity but high BuChE activity. The latter one is the active part of the Dräger test tubes for organophosphates und therefore a positive test result will be expected. This will be proved in Chapter 4.10 Detection with Military Equipment and Hand-held Analytical Instruments.

Finally, the found values could be compared with available literature data and the chosen measurement and data processing methods could be proved correct.

4.9 Mass Spectrometric Fragmentation Pathways

For a clear identification of a molecule in the mass spectrometer different parameters have to be verified. This can be for example the isotopic pattern of the fragments or the fragmentation itself. Also the relative intensity of the fragments can play an important role as could be shown in the ESI-MS studies, where the P=O isomers show a different fragmentation behavior than the P=S isomers; regarding the most prominent fragment (Figure 48). It can also be helpful to know fragmentation patterns of precursor molecules which are part of the original molecule under investigation, which makes it easier to explain the formation of certain fragments. Such a study on the fragmentation of amino alcohols was done by *Reddy et al.* in 2003.[298] The major finding was, that most likely a bond in proximity of the nitrogen atom with a spacing of one CH_2-group is broken (*cf.* Figure 98) and, thus, a stable carbon-nitrogen double bond can form with the nitrogen atom remaining positively charged. The other fragment then keeps the radical. Having their findings in mind, the interpretation of the obtained data of this section becomes easier.

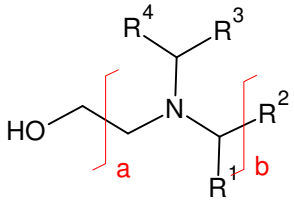

Figure 98: *Proposed fragmentation sites of dialkyl amino alcohols according to Reddy et al.[298]*

The Auto-SRM-study tool from Thermo Fisher, which was originally designed for the development of MS/MS methods, was used to elucidate the fragmentation pathways. In the first step a regular mass spectrum is measured and in the second step an optimization of the experimental condition with respect to the applied energy in the collision cell (quadrupole 2 segment) is performed to detect the observed fragments in the third quadrupole of the instrument.

In the following the results of the Auto-SRM studies are presented for each studied molecule. A complete fragmentation pathway without the explanation of the underlying individual fragmentation reaction is drawn separately for each compound. Of course, important fragmentation reactions of prominent fragments are explained. The location of the radical cation in the parent molecule is in all cases drawn on the nitrogen atom for convenience. Additionally, the description of all tautomeric forms of the fragments would go beyond the scope of this study which is why only the most important isomers are depicted in this manuscript. Generally, it is a rule that the larger number of existing tautomeric forms correlates with the stability of the respective fragment. As a general rule it is most likely that fragments of high m/z values result from breakdown of the molecule instead of

fragmentation of daughter fragments. Additionally, it is also most likely that the most prominent fragments result from a single fragmentation of the respective molecule. In all studies only signals above 5% of signal intensity of the highest signal were subjected to the Auto-SRM procedure. Furthermore it is assumed that fragments not formed by a daughter fragment must originate from the molecule itself by primary fragmentation. However, fragments of low m/z ratios especially below 50 are not significant for the compounds of this thesis but are only reported for completeness.

It has to be noted that in this chapter a double bond between phosphorus and sulfur/oxygen was drawn although there is no true double bond in the molecule. This is in accordance with the recommendations given by *Timperley* and makes it easier to elucidate the radical-cationic species of the respective fragments.[76]

4.9.1 Fragmentation of Amiton and its Thiono-Isomer

In Figure 99 the EI mass spectra of compound **IX**. As can be seen, the most prominent fragments are m/z = 86 and m/z = 99. These two fragments of highest abundance in the respective EI-MS spectra can originate by the fragmentation pathway depicted in Figure 102. Additionally, from the fragmentation studies it could also be proved that those fragments are themselves parent ions to further fragments of the spectrum.

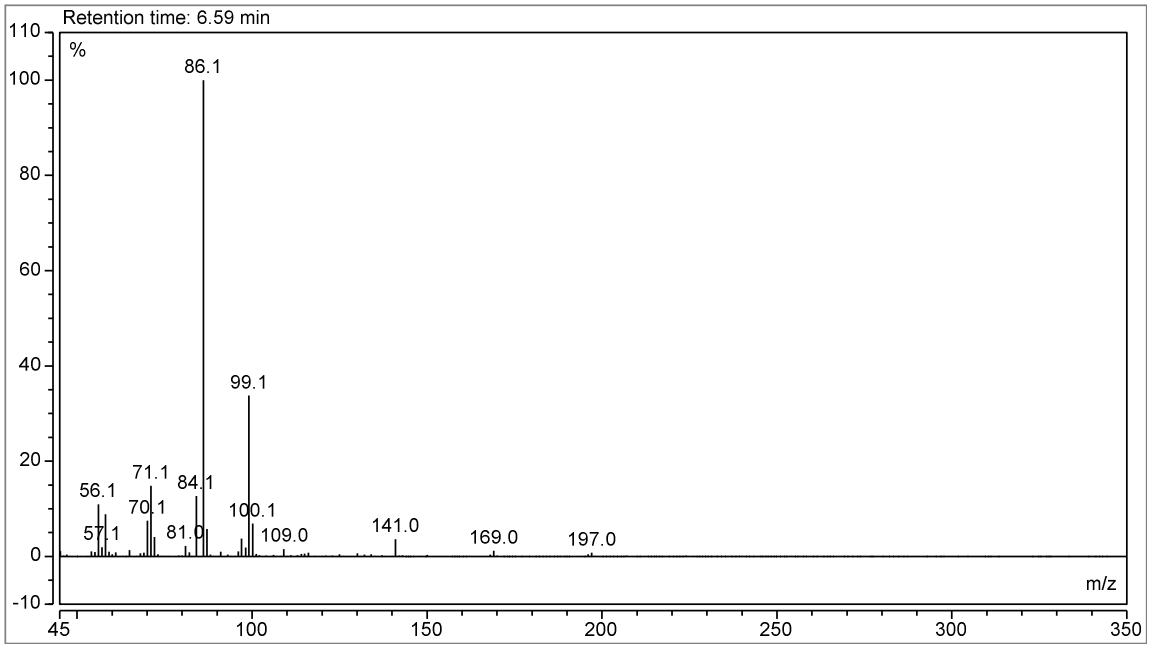

Figure 99: *Representation of the EI mass spectrum of compound **IX**.*

The results of the fragmentation study of Amiton (**X**) are given in Table 56. The proposed fragmentation pattern is illustrated in Figure 105. The respective data of compound **IX** are given in Table 55 and Figure 106. As is true for all Amiton-like compounds the molecule fragments in two generally different patterns: one for the alkyl amino sidechain residue and

one pathway basing on the phosphorus moiety. Both pathways lead to the formation of different fragments without having a single fragment in common. Obviously, the fragment of m/z = 84 offers a lot of possible decay reactions and, thus, is most likely the reason for the appearance of a large number of smaller peaks in the spectrum. Compared to this the m/z = 86 fragment is very stable since it can only fragment into four secondary daughter ions which are also accessible *via* m/z = 84 and m/z = 58 fragments.

The m/z = 86 fragment which is in both cases the most prominent one emerges from an α-cleavage between the two CH_2-groups of the N-alkyl sidechain (*cf.* Figure 100). This reaction is followed twice by a so called onium reaction which is typical to follow an α-cleavage reaction. The onium fragmentation is initiated by the positive charge on the nitrogen atom and cleaves an adjacent bond to the nitrogen under rearrangement of a hydrogen atom of the leaving group to the remaining part of the molecule, resulting in the fragments of m/z = 58 and m/z = 30, respectively.

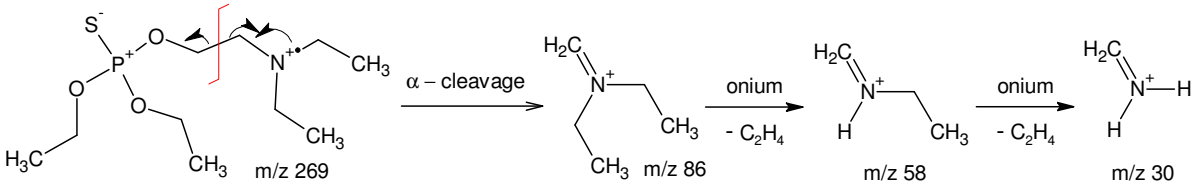

Figure 100: *Elucidation of the possible fragmentation reactions to form the most prominent fragment m/z = 86 and corresponding daughter ions in the EI mass spectra of compounds bearing a R-N-(Et)$_2$ substituent, e.g. compound* ***IX****.*

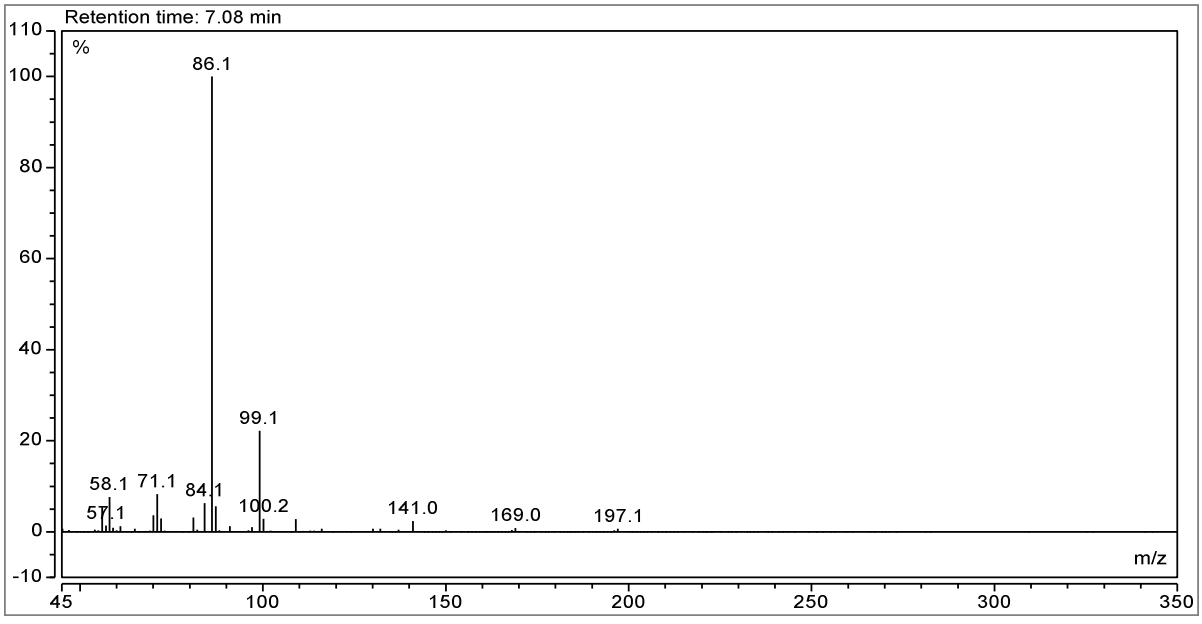

Figure 101: *Representation of the EI-mass spectrum of compound* ***X****.*

The onium reaction is driven by the formation of an ethylene molecule, which is a very good leaving group. The latter one is not observed in the regular EI-MS spectrum since the lower

limit of the detector (in regular operational mode) is m/z = 46, but could be found during the fragmentation studies where the lower detection limit is set to m/z ratios of 15.

Compared to the mass spectrum of compound **X** no significant difference can be identified at first glance. However, the relative intensity of the fragment ions varies and especially masses below m/z = 86 are higher populated in the spectra of compound **IX**. Moreover, the ratio of the peak intensities for m/z = 58 and m/z =56 is inversed. Additionally, the m/z = 100 fragment in the spectrum of compound **IX** is not only resulting from ^{13}C carbon atoms representing the isotopic peak signal but is belonging to a true fragment and is double the population as for compound **X**.

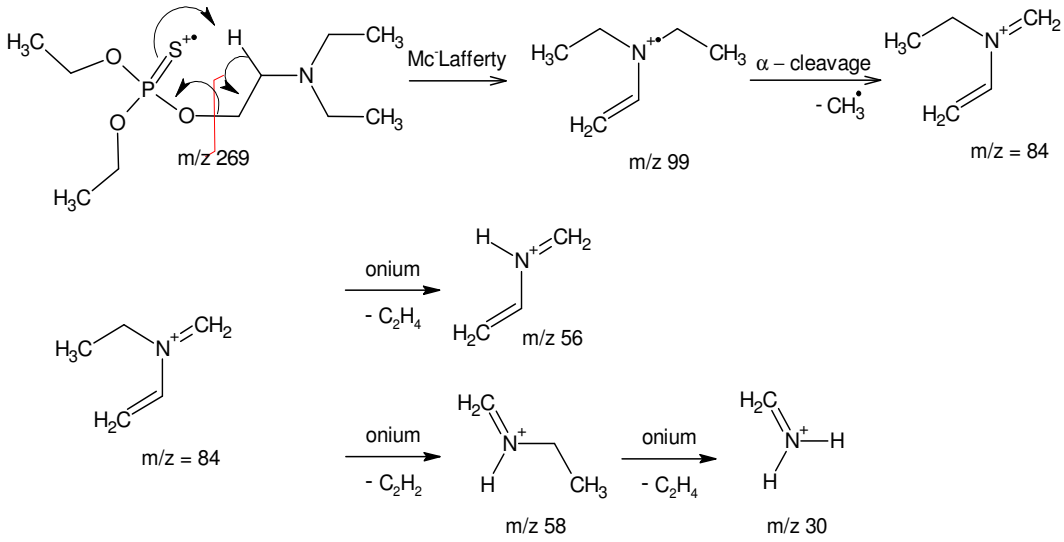

Figure 102: *Elucidation of the possible fragmentation reactions to form the second most prominent fragment m/z = 99 and corresponding daughter fragments in the EI mass spectra of compounds bearing a R-N-(Et)$_2$ substituent, e.g. compound **IX**.*

In Figure 102 the formation of the second most abundant fragment m/z = 99 is explained. The formation is achieved by a very common Mc Lafferty rearrangement *via* the typical six-membered ring structure. This rearrangement is followed by an α-cleavage to set free a methyl group. Consecutively, the newly formed fragment m/z = 84 is further fragmented following the onium reaction. In this particular case two reaction pathways exist and, thus, two more signals can be explained (bottom part of Figure 102). The m/z = 58 fragment is also able to form the m/z = 56 fragment by the thermal dissociation of a hydrogen atom and the formation of a new double bond. The same reaction can be applied to the m/z = 86 and m/z = 84 fragments.

Another important fragment is m/z =141. This fragment is formed by the decay of fragments m/z = 197 and m/z = 169. The mechanism of the formation is illustrated in Figure 103. Herein two consecutive Mc Lafferty rearrangements take place leading again to the formation of an ethylene molecule each. The initial formation of the m/z = 197 fragment can be explained by a charge induced cleavage of the nitrogen-carbon bond.

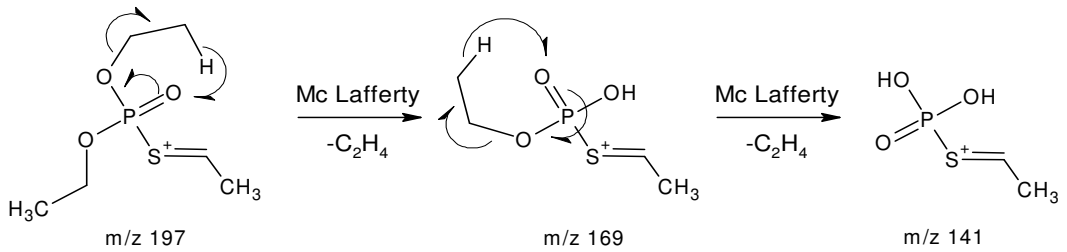

Figure 103: *Elucidation of the possible fragmentation reactions to form the second most prominent fragment m/z = 99 and corresponding daughter fragments in the EI mass spectra of compounds bearing a R-N-(Et)$_2$ substituent, e.g. compound **IX**.*

Both described pathways could be found in the respective fragmentation study of the m/z = 84 fragment as the parent ion. The identified fragments and pathways are in very good agreement with a study on the structurally similar VX-molecule published by the ECBC in 2008.[208]

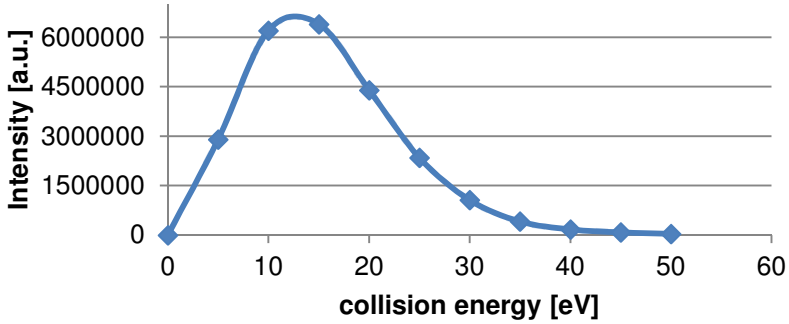

Figure 104: *Result of the energy optimization step of the autoSRM method for the fragmentation transition of m/z = 254 to m/z = 141 of compound **IX**.*

Table 55: *Overview of the secondary fragmentation study results of compound **IX**.*

Parent ion m/z	Daughter ion m/z(optimum collision energy [eV])
254	226(10), 197(10), 169(10), 141(10), 84(10)
197	169(5), 141(10), 45(25)
169	141(5), 61(25), 45(20)
141	123(10), 97(15), 81(25), 61(15), 45(10)
99	84(5), 71(5), 70(10), 56(10)
86	58(5), 30(10), 29(15), 27(30)
84	69(15), 68(20), 57(10), 56(5), 44(15), 43(10), 42(10), 41(15), 39(25)
71	56(5)
70	55(15) ,42(10), 29(10), 28(15)
58	30(5), 29(10), 27(20)
56	55(5), 41(20), 40(30), 30(10), 29(10), 28(5), 27(20)

Besides the fragmentation results the Auto-SRM Software in the last step offers to optimize the collision energy for the chosen transitions to finally increase sensitivity towards a low

detection limit. For instance, Figure 104 shows the dependence of the signal intensity on the collision energy for the transition of m/z = 254 to m/z = 141 of compound **IX**.

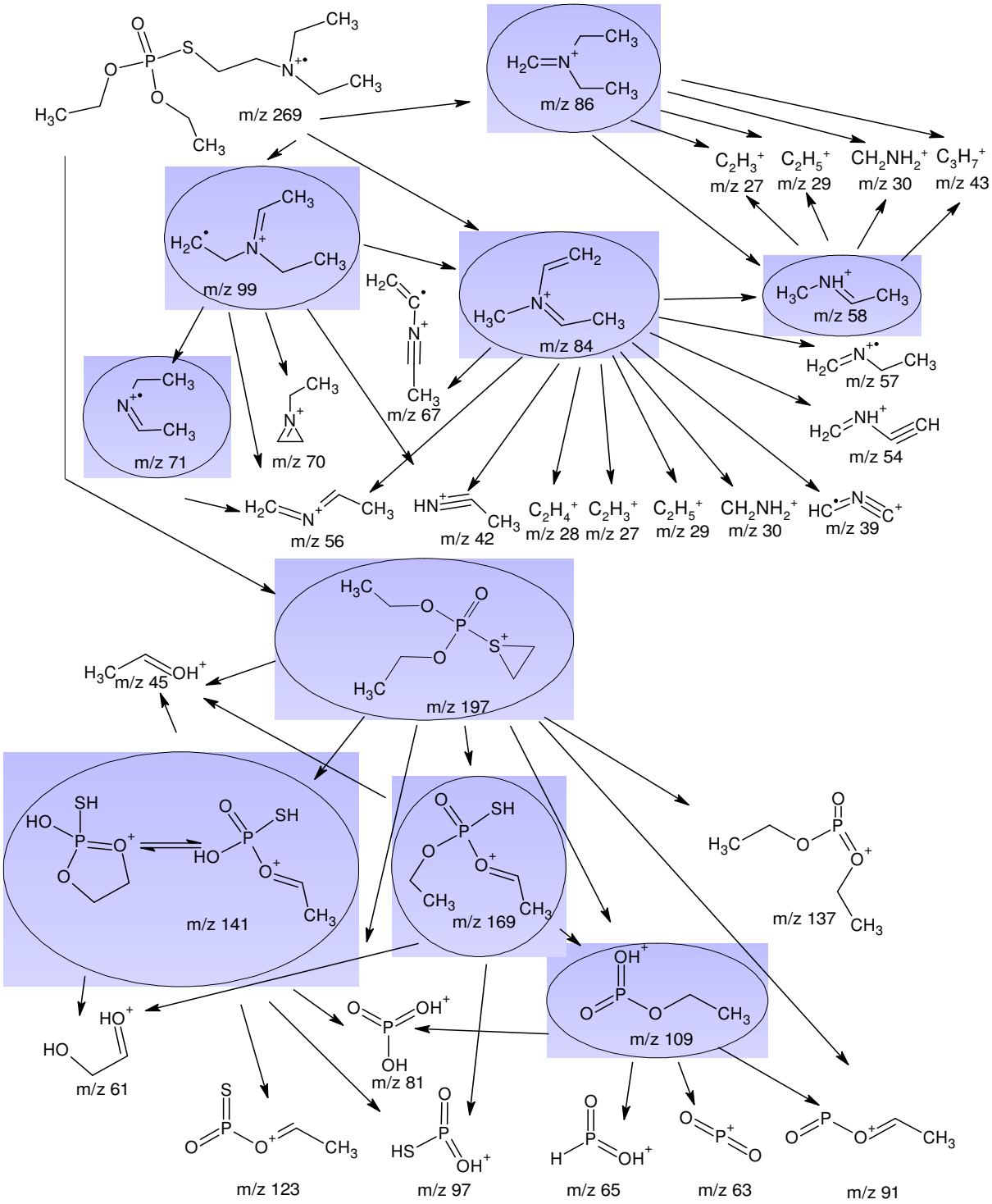

Figure 105: *Proposed mass spectral fragmentation pathways for compound **X**. Color-coded fragments indicate those of the initial mass spectrum used for further MS-MS investigation.*

It unambigiously identifies an applied current in the collision cell of 10-15 eV as optimum collision energy. Noteworthy, the isomeric structure of the fragment with m/z = 141 found in this study deviates from the one observed in the ESI-MS/MS study of Amiton by Ellis-

Steinborner et al.[206] They proposed a structure in which the ring is formed by sulfur and oxygen bridging two CH_2-groups. However, the fragment of m/z = 61 of the EI-MS/MS study cannot form *via* this isomeric structure but has to be comprised of two oxygen atoms and two CH_2-groups instead.

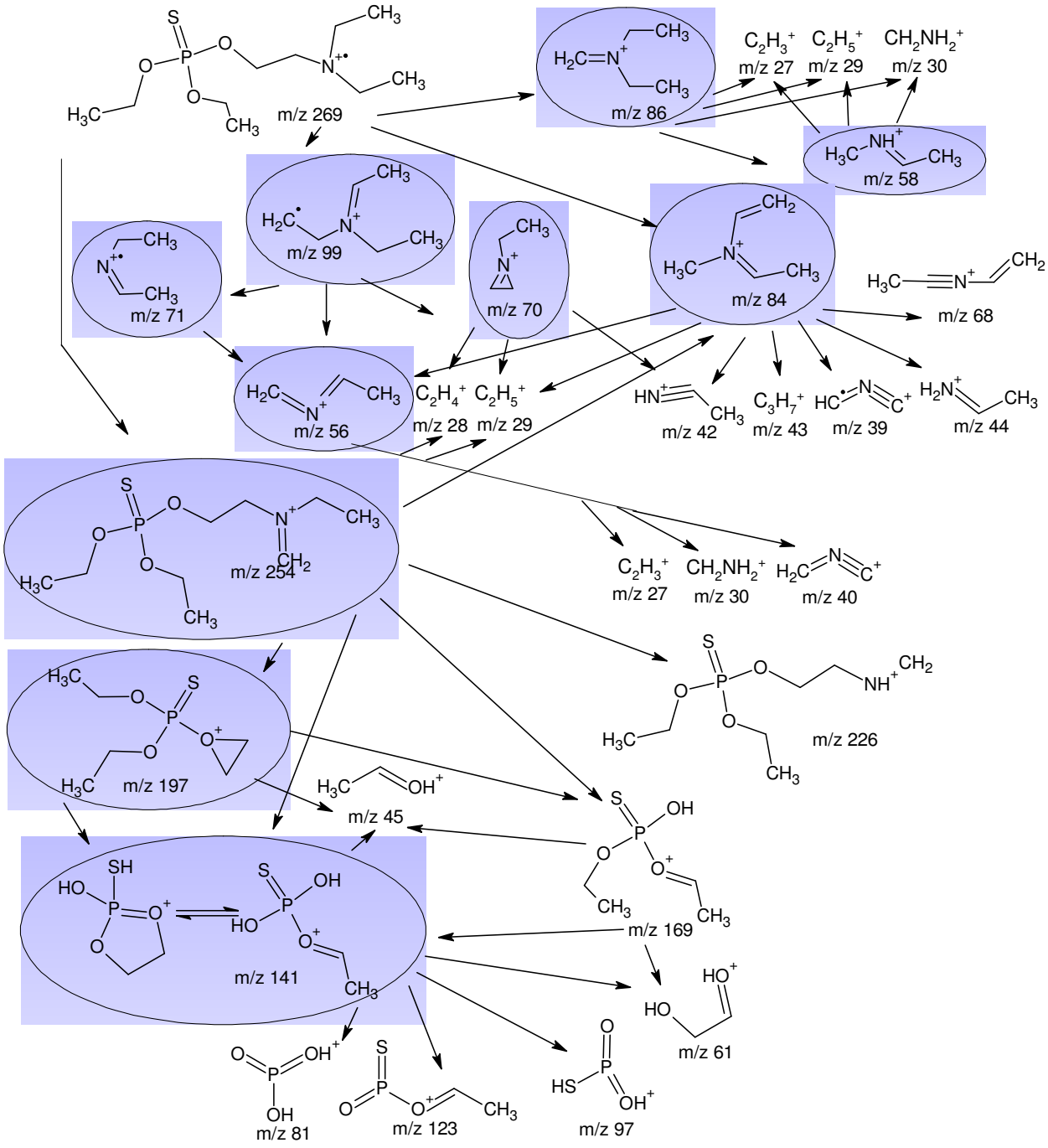

Figure 106: *Proposed mass spectral fragmentation pathways for compound* ***IX****. Color-coded fragments indicate those of the initial mass spectrum used for further MS-MS investigation.*

Otherwise the formation of the m/z = 45 fragment cannot be explained. The same holds true for the m/z = 169 fragment without which it would not be possible to derive fragment m/z =

97. Moreover, from their proposed fragment m/z = 99 to be a protonated phosphonothioic acid the observed fragments m/z = 84, 71, 10, 56 and 42 cannot be explained in this study.

Hence, the m/z = 99 fragment must be different for ESI-MS and EI-MS, which is reasonable since two different ionization techniques are employed. Furthermore, this assumption is supported by the presence of the isotopic peak of the m/z = 100 fragment in the MS spectrum which is about 15% of the height of the m/z = 99 signal which perfectly matches with the theoretically expected value. The same holds true for the m/z = 87 fragment which has not been identified yet and is the isotopic signal of m/z = 86 fragment. Due to the chosen cut-off of 3% signal intensity for fragments in the mass spectrum to be investigated by the AutoSRM studies the obtained fragmentation pathways do differ by the total number of fragments depicted. However, it can be assumed, that all fragmentations of compound **IX** can also be observed for compound **X** if the cut off is lowered even more, since they structurally very closely related to each other.

Table 56: *Overview of the secondary fragmentation study results of compound* ***IX.***

Parent ion m/z	Daughter ions m/z (optimum collision energy [eV])
197	169(10), 141(10), 137(10), 109(10), 91(20), 81(20), 45(20)
169	141(10), 97(10), 61(20), 45(20)
141	123(10), 97(10), 81(20), 61(20), 45(10)
109	91(10), 81(10), 65(10), 63(30)
99	84(10), 71(10), 70(10), 56(10), 42(10)
86	58(10), 30(10), 29(20), 27(30)
84	67(10), 58(10), 57(10), 56(10), 54(20), 42(10), 41(10), 39(20), 30(10), 29(20), 28(10), 27(30)
71	56(10)
58	43(10), 30(10), 29(10), 27(20)

Towards the formation of the smaller fragments of m/z-ratios around and below m/z = 30 no detailed formation reactions are given, since those compounds are not significant for the proper identification of the molecule itself. Most likely these fragments are formed by charge induced reactions or simply by splitting of (several) hydrogen atoms or complex rearrangement reactions of the parent fragment.

4.9.2 Fragmentation of Compounds also Bearing a R-N-$(Et)_2$ Substituent

In this part the remaining six structurally very closely related Amiton-like compounds are investigated. Those are compounds are **XI**, **XII**, **XIII**, **XIV**, **XV** and **XVII**. They either differ in the configuration of the phosphorus atom, or have a different length of the alkyl amine side

chain (compounds **XV** and **XVII**). Unsurprisingly, the most prominent fragments are again m/z = 86 and m/z = 99 since they all have its origin in the alkyl amino side chain and can be explained by the same reaction pathways as given in the previous chapter. The only exemption to this is compound **XII** which has an additional prominent fragment, i.e. m/z = 100.

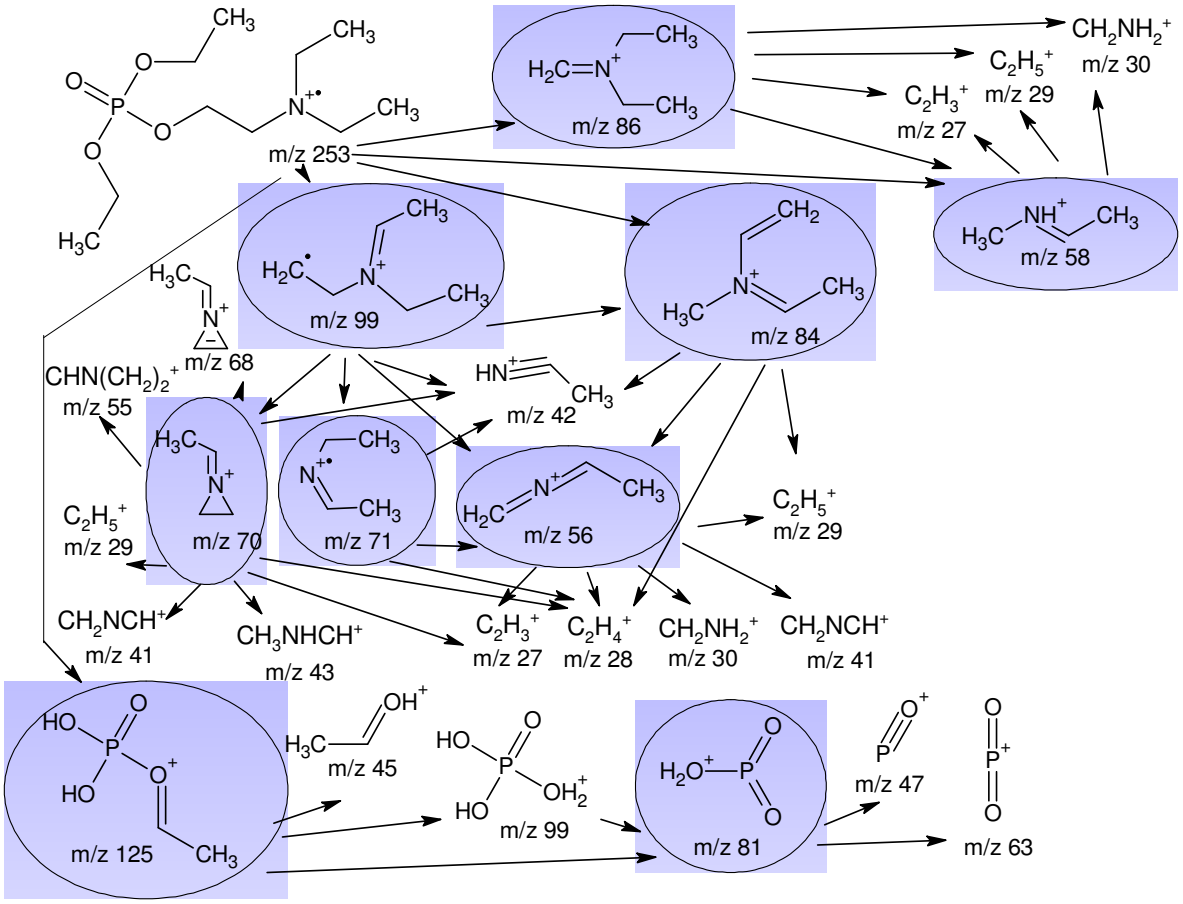

Figure 107: *Proposed mass spectral fragmentation pathways for compound **XI**. Color-coded fragments indicate those of the initial mass spectrum used for further MS-MS investigation.*

The results are presented in tabular form to report the individual fragments and the corresponding collision energy to obtain the optimum fragmentation yield. Additionally, the results are presented in fragmentation pathway figures for each compound. The corresponding mass spectra are reported in the annex (Chapter A.4).

Starting with the discussion of compound **XI** which is comprised of four oxygen atoms bonded to the central phosphorus atom a fragmentation pathway very similar to the one of compound **IX** is expected for the fragmentation of the nitrogen containing side chain. That this is the case can be seen from either the graphical illustration in Figure 107 or Table 57. For the phosphorus containing moiety fragmentation pathway also similar fragments could be found but most of them have m/z ratios 16 amu smaller than those of compounds **IX** and **X** because of the oxygen sulfur exchange. Again, they have the m/z = 81 fragment in

common. Furthermore, the m/z = 99 fragment has to be present in two different chemical configurations since from the phosphorus containing m/z = 99 fragment none of the nitrogen containing daughter ion fragments can be explained and vice versa.

Table 57: *Overview of the secondary fragmentation study results of compound* ***XI****.*

Parent ion m/z	Daughter ions m/z (optimum collision energy [eV])
125	99(10), 81(10), 45(10)
99	84(10), 81(10), 71(10), 70(10), 56(10), 42(10)
86	58(10), 30(10), 29(20), 27(30)
84	56(10), 42(10), 29(20), 28(10), 27(30)
81	63(20), 47(30)
71	56(10), 42(10), 28(10)
70	68,(10),55(20), 43(10), 42(10), 41(10), 29(20), 28(10), 27(20)
58	30(10), 29(10), 27(20)
56	41(30), 40(30), 30(10), 29(10), 28(10), 27(20)

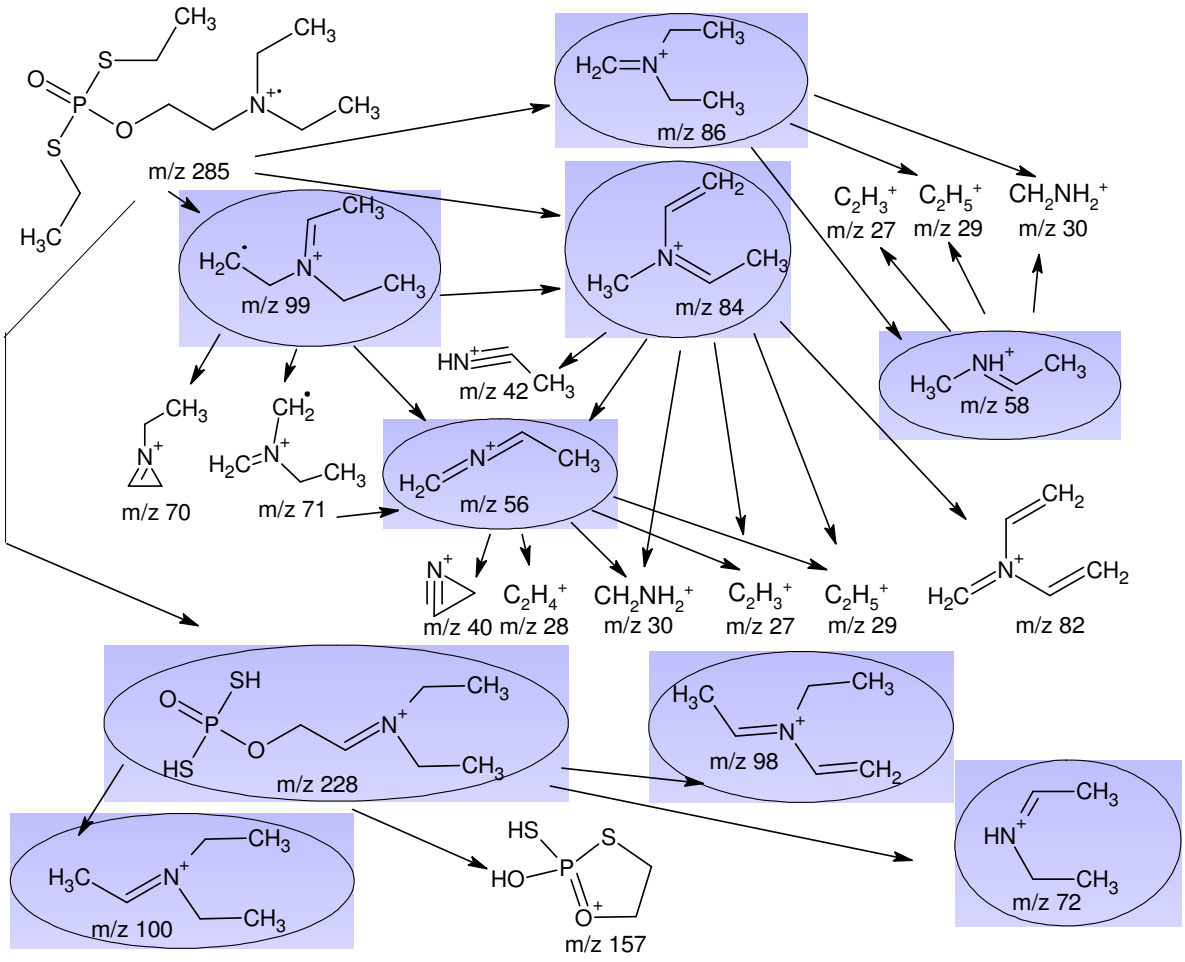

Figure 108*: Proposed mass spectral fragmentation pathways for compound* ***XII****. Color-coded fragments indicate those of the initial mass spectrum used for further MS-MS investigation.*

Next, the fragmentation pathway of compound **XII** is investigated. The results are presented in Figure 108 and Table 58. Interestingly, only one fragment with m/z = 228 offers access to a protonated phosphorus species. From the fragmentation pattern it can be concluded that the two sulfur atoms in the thio-ethoxy side chains must have a comparably lower tendency than the oxygen atoms to stabilize the positive charge. Moreover, the m/z = 157 fragment is not present in the standard EI mass spectra and was only detectable by applying MS/MS techniques. This finding is interesting since the corresponding fragment with m/z = 141 of the other compounds is relatively prominent in the MS spectra. Here also the mass difference of 16 amu is due to the oxygen sulfur exchange. The rest of the fragments can be identified to belong to the nitrogen moiety of the compound.

Table 58: *Overview of the secondary fragmentation study results of compound* ***XII****.*

Parent ion m/z	Daughter ions m/z (optimum collision energy [eV])
228	157(5), 100(10), 98(5), 72(5)
100	72(10), 44(15), 29(20)
99	84(10), 71(5), 70(10), 56(10)
98	83(10), 70(10), 56(10), 43(15), 29(20), 28(15)
86	58(5), 30(10), 29(15)
84	82(5), 56(5), 42(10), 29(15), 28(10), 27(30)
72	70(10), 57(5), 44(5), 42(20), 29(15), 27(25)
58	43(10), 30(5), 29(10), 27(20)
56	40(25), 30(10), 29(10), 28(5), 27(15)

Table 59: *Overview of the secondary fragmentation study results of compound* ***XIII****.*

Parent ion m/z	Daughter ions m/z (optimum collision energy [eV])
169	141(5), 113(10), 95(25)
141	113(5), 95(15), 29(15)
113	98(5), 95(10)
99	84(10), 71(5), 70(10), 56(10)
86	58(10), 30(15), 29(15), 27(30)
84	56(5), 42(10), 29(15), 28(10), 27(30)
71	56(5)
58	30(5), 29(10), 27(20)
56	40(30), 29(10), 28(5), 27(20)

Interestingly, compound **XIII** which has three sulfur atoms bonded to the central phosphorus atom shows the least number of fragments in the EI mass spectrum. Here, the two major fragmentation routes are present, too. Also the prominent fragments of m/z = 99 and m/z = 84 representing the nitrogen moiety are very prominent in the mass spectrum (Figure

240) as well as signals for the m/z = 169 and m/z = 141 fragments originating from the phosphorus containing part of the molecule. Noteworthy, especially these two fragments will lead to false conclusions regarding the composition of the molecule. Thus, it is of great importance to have a close look at the isotopic peak pattern in the analysis of the mass spectra. The sulfur atoms contribute very significant to the isotopic peak at m/z = 143 and m/z = 171, respectively. The relative intensity of these peaks is 8.8% of that of the non-isotopic signal which is in perfect agreement with the theoretically expected value, since ^{34}S has a naturally abundance of 4.2% (*cf.*Table 3). On the other hand, the isotopic signal of the carbon does not play an important role in this case since the overall signal intensity of the respective non-isotopic peak is too low to be observable.

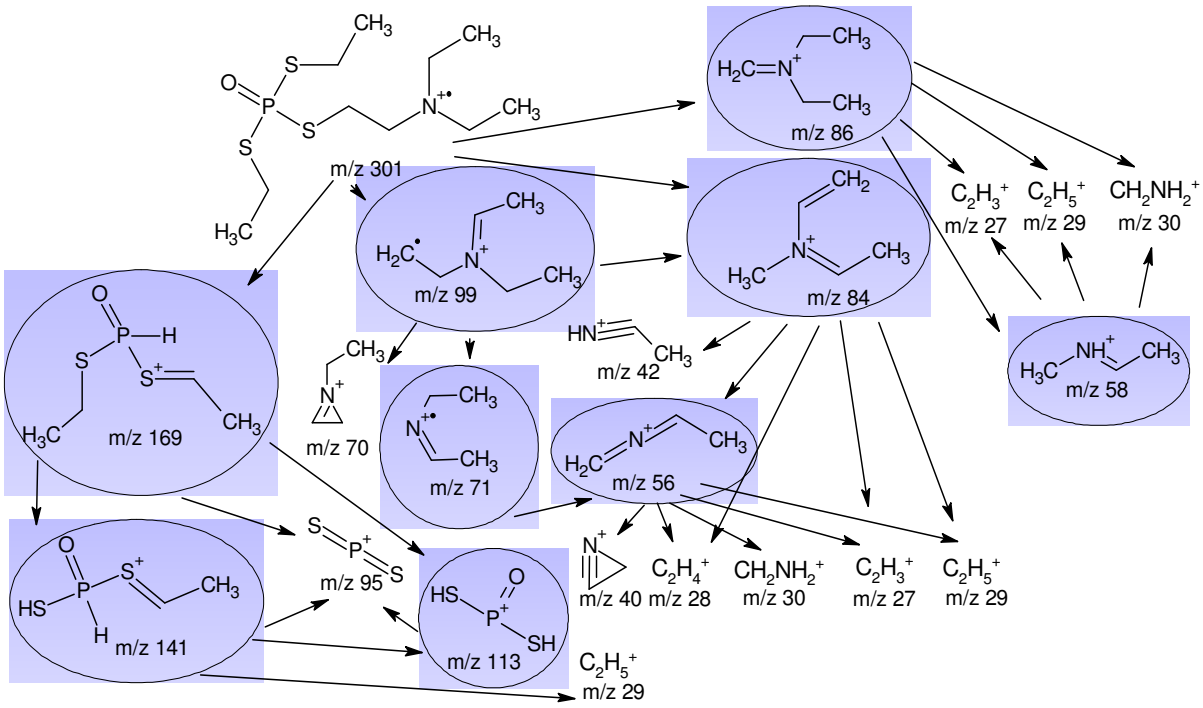

Figure 109: *Proposed mass spectral fragmentation pathways for compound **XIII**. Color-coded fragments indicate those of the initial mass spectrum used for further MS-MS investigation.*

The difference of the fragmentation pattern compared to compound **XIV** is found in the phosphorus fragmentation pathway as well since the amino alcohol side chain is still identically structured. The most prominent fragments are very well comparable with each other amongst the different compounds. The phosphorus containing fragments alter once more by 16 amu but still have the same chemical structures due to the presence of only two instead of three sulfur atoms in the molecule.

Additionally, the isotopic pattern of the peaks is of great importance for a clear assignment. This is extremely challenging when the non-isotopic peak intensity is very low. It is impossible to resolve the pattern for non-isotopic peak signal intensities below three

percent. The corresponding proposed fragmentation pathway for compound **XIV** is shown in Figure 110 with the respective tabular overview being presented in Table 60.

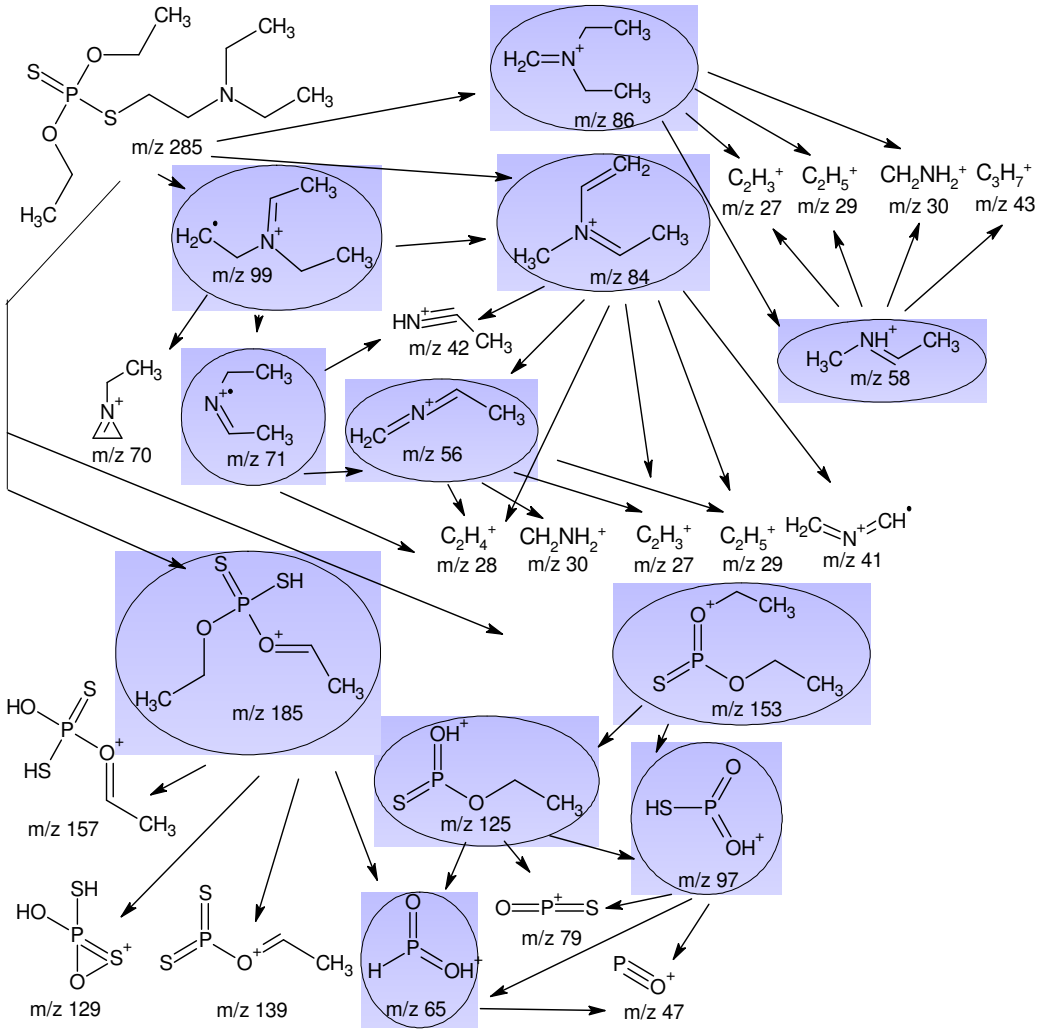

Figure 110: *Proposed mass spectral fragmentation pathways for compound **XIV**. Color-coded fragments indicate those of the initial mass spectrum used for further MS-MS investigation.*

In Figure 111 the proposed fragmentation pathway for compound **XV** is given. As for the other compounds, two separate fragmentation pathways can be identified. The first one (top of Figure 111) is based on fragments formed from the alkyl amine side chain. Actually, the same fragmentation pathways as for compounds **IX** and **X** (*cf.* Figure 100, Figure 102 and Figure 103) apply for this compound besides the fact that due to the prolonged alkyl chain the m/z ratios are 14 amu higher than for compounds **IX** or **X**. The fragmentation sites are still the same.

Moreover, the second pathway starting from fragment m/z = 268 is driven by the phosphorus moiety. Furthermore, the number of detectable fragments of the nitrogen moiety definitely outnumbers those found for the phosphorus moiety. Additionally, both described pathways have two fragments in common which are m/z = 41 and m/z = 39.

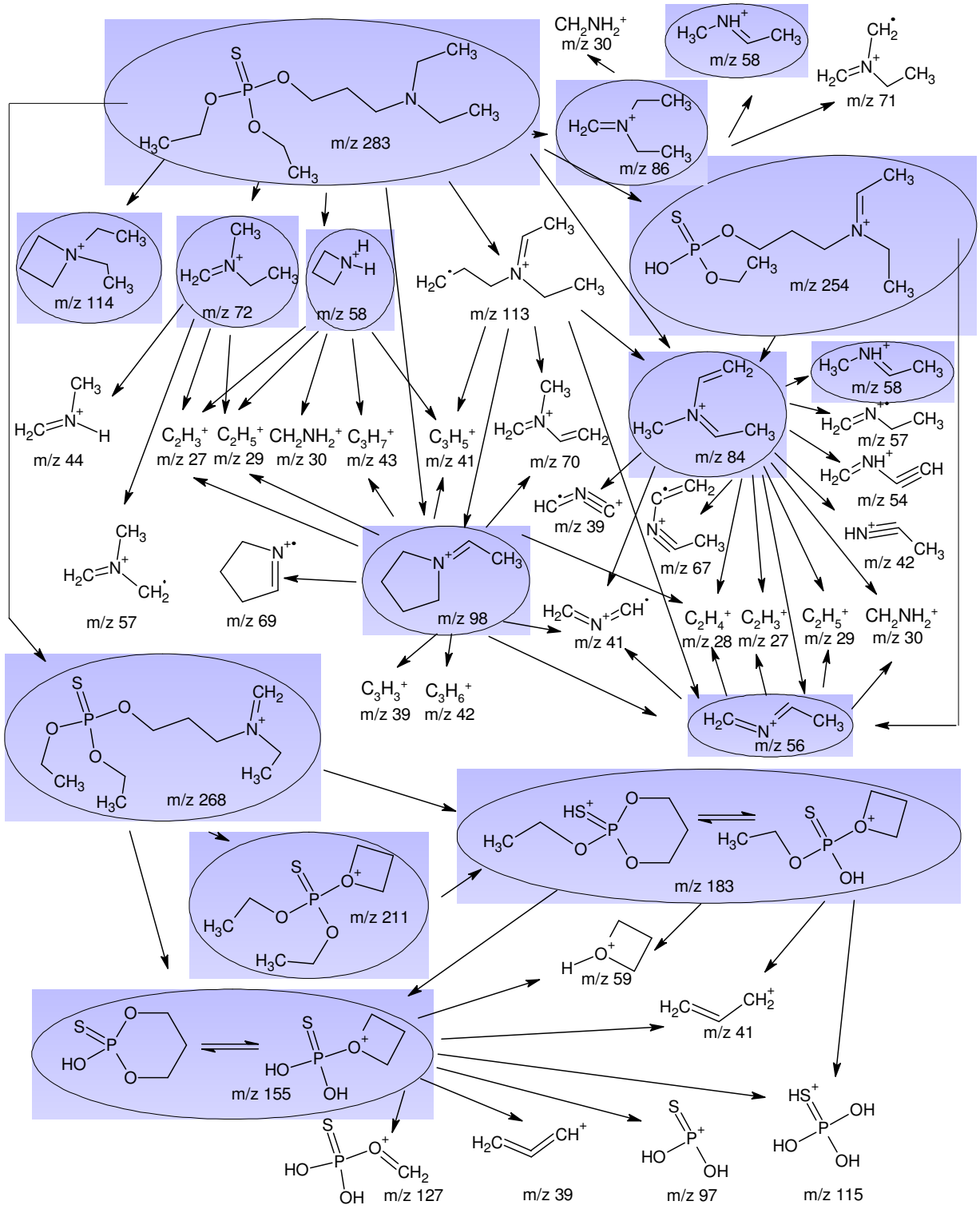

Figure 111: *Proposed mass spectral fragmentation pathways for compound* ***XV****. Color-coded fragments indicate those of the initial mass spectrum used for further MS-MS investigation.*

However, it could be possible that they are of different chemical structure. This open question could be addressed by subjecting labeled molecules to mass spectrometry which allows to analyze the structural identity. For this purpose either the carbon-containing substituents of the nitrogen would need to be labeled by exchanging the ^{12}C by ^{13}C-atoms or those carbon atoms of the O-N-bridge.

Table 60: *Overview of the secondary fragmentation study results of compounds* ***XIV****.*

Parent ion m/z	Daughter ions m/z (optimum collision energy [eV])
185	157(10), 139(10), 129(10), 65(30)
153	125(10), 97(10)
125	97(10), 79(20), 65(20)
99	84(10), 71(10), 70(10), 56(10)
97	79(10), 65(20), 47(30)
86	58(10), 30(10), 29(20), 27(30)
84	56(10), 42(10), 41(10), 29(20), 28(10), 27(30)
71	56(10), 42(10), 28(10)
65	47(10)
58	43(10), 30(10), 29(10), 27(20)
56	41(30), 30(10), 29(10), 28(10), 27(20)

Table 61*: Overview of the secondary fragmentation study results of compounds* ***XV****.*

Parent ion m/z	Daughter ions m/z (optimum collision energy [eV])
283	254(10), 114(10), 98(10), 86(10), 84(10), 72(10), 58(30)
268	211(20), 183(10), 155(20), 72(10), 59(20)
254	86(30), 84(10)
211	183(10),155(10)
183	155(10), 115(10), 59(10), 41(20),
155	127(10), 115(10), 97(20), 59(10), 41(10), 39(30)
114	98(10), 84(10), 70(10), 56(10), 41(10)
98	70(10), 69(10), 56(10), 43(10), 42(10), 41(10),39(30), 29(10), 28(10), 27(30)
86	71(10), 58(10), 30(10)
84	67(10), 58(10), 57(10), 56(10), 54(20), 42(10), 41(10), 39(20), 30(10), 29(20), 28(10), 27(30)
72	54(10), 44(10), 29(20), 27(30)
58	43(10), 41(10), 30(10), 29(10), 27(20)
56	41(20), 30(10), 29(10), 28(10), 27(20)

The last molecule to be discussed in this section is compound **XVII** which is at the same time the one with the most fragments formed and thus the most complex one to describe. The comparable large alkyl amino side chain offers a lot more fragmentations than it was the case for the other compounds. Basically, most of the fragments of the nitrogen moiety of the smaller compounds of this thesis are also present in this case.

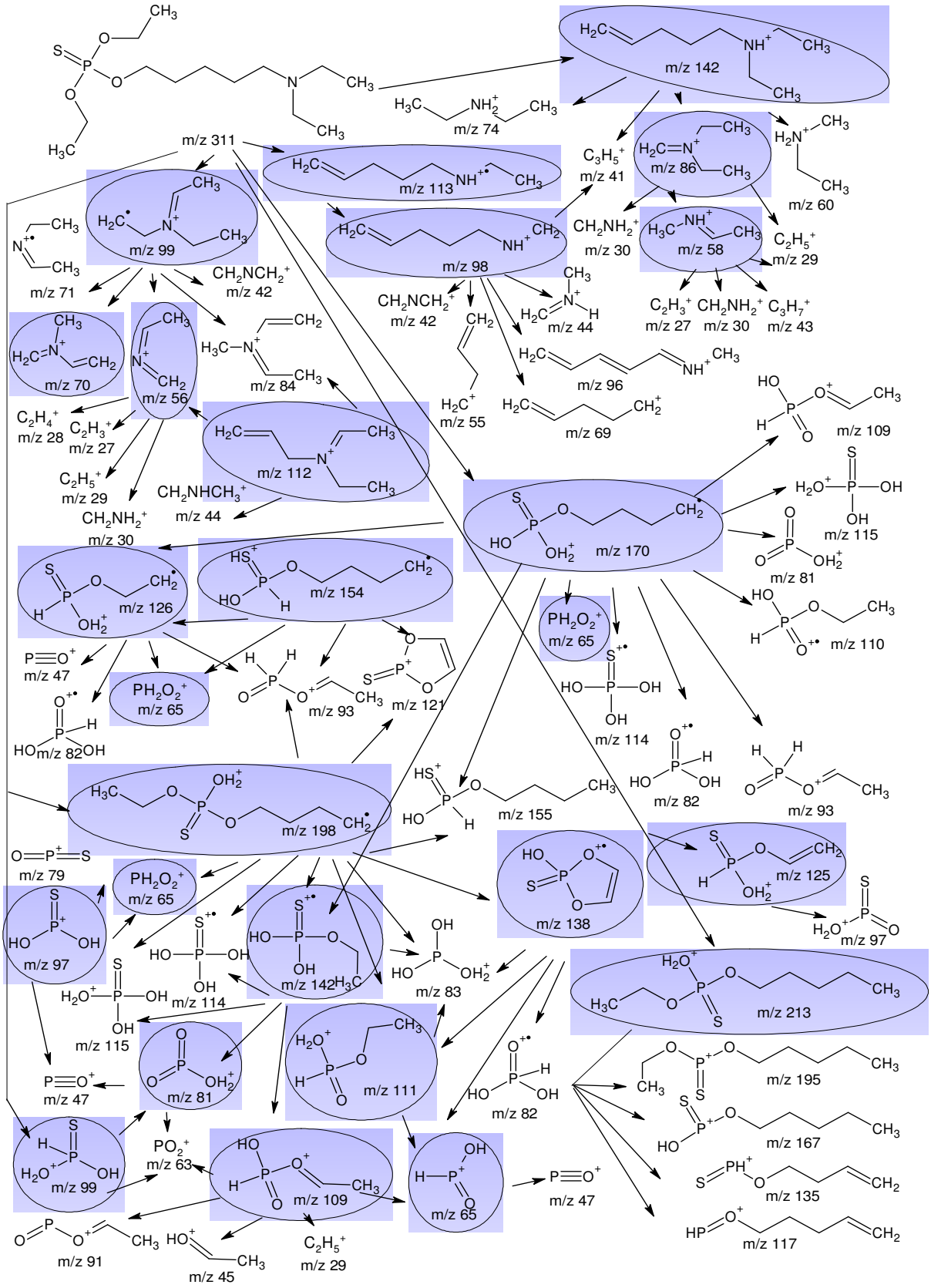

Figure 112: *Proposed mass spectral fragmentation pathways for compound* ***XVII****. Color-coded fragments indicate those of the initial mass spectrum used for further MS-MS investigation.*

The m/z =86 fragment is again the most prominent one. Additionally, a large number of fragments arise from the longer alkyl chain of the O-N-bridge, which can very well stabilize the positive charge at the nitrogen atom. Interestingly, only two fragments larger than m/z = 55 could be found which did not contain a hetero atom. Although, some fragments containing phosphorus and a large number of carbon atoms are identified, these do never result in fragments without a hetero atom.

Table 62: *Overview of the secondary fragmentation study results of compounds* ***XVII****.*

Parent ion m/z	Daughter ions m/z (optimum collision energy [eV])
213	195(10), 167(15), 135(20), 117(35)
198	155(15), 142(5), 138(10), 126(10), 121(10), 115(20), 114(10), 111(10), 97(35), 93(15), 83(20), 82(25), 65(25)
170	155(10), 142(5), 126(5), 115(15), 114(10), 110(10), 109(10), 98(10), 93(10), 83(10), 82(10), 81(25), 65(25)
154	126(5), 121(5), 93(5), 65(15)
142	115(10), 114(5), 109(5), 86(10), 83(5), 81(20), 74(15), 61(10), 60(15), 41(20)
138	111(5), 83(10), 82(15), 66(10), 65(25)
126	98(5), 93(5), 82(10), 72(10), 65(10), 62(10), 47(30)
125	97(5)
113	98(5)
112	84(10), 83(10), 69(5), 56(15), 41(15)
111	83(5), 65(20)
109	91(5), 81(10), 65(15), 63(30), 45(5), 29(10)
99	84(10), 81(15), 71(5), 10(10), 63(30), 56(10), 42(15)
98	96(5), 70(5), 69(10), 55(10), 44(10), 42(15), 41(10), 42(15), 41(20)
97	79(10), 65(15), 47(25)
86	58(5), 30(10), 29(15)
81	63(15), 47(35)
70	42(10)
65	47(10)
58	43(10), 30(5), 29(10), 27(20)
56	30(10), 29(10), 28(5), 27(15)

Furthermore, the number of fragments containing phosphorus is also increasing. These do still have very small signal intensity but are detectable and help to clarify the proper identification of the molecule. Moreover, they act as intermediates for the population of the lower m/z-signals in the mass spectrum. Noteworthy, fragment m/z = 99 appears in two different chemical configurations which was also the case for compound **XI** (*cf.* Figure 107). It can arise either from the nitrogen- or the phosphorus-containing part of the molecule. That

this is true can be proved by having a closer look at the daughter ions of the m/z = 99 fragment. Since fragments of m/z = 81 and m/z = 63 cannot be formed by purely containing carbon and nitrogen and hydrogen atoms. The same is true for fragment m/z = 142. This phenomenon can most likely be observed amongst larger molecules, since statistically the possible number of different atom configurations leading to the same fragment masses increases drastically with increasing molecular weight.

4.9.3 Fragmentation of Compounds Bearing a R-N-(Me)$_2$ substituent

Two molecules, compounds **XVIII** and **XIX**, prepared during this thesis apply to this section. They differ only by the length of their nitrogen containing sidechain. The respective mass spectra are shown in Figure 113. They have at least four common fragments which are in descending order of their relative abundance: m/z = 58, 70, 97 and 115. However, the signal of m/z = 207 is an artefact of the septum and does not belong to the compounds spectra. Only in the spectrum of compound **XIX** a very small molecule peak is observable at m/z = 255. Furthermore, the second largest peak in the spectrum of compound **XIX** is m/z = 85 whereas it is m/z = 71 for compound **XVIII**.

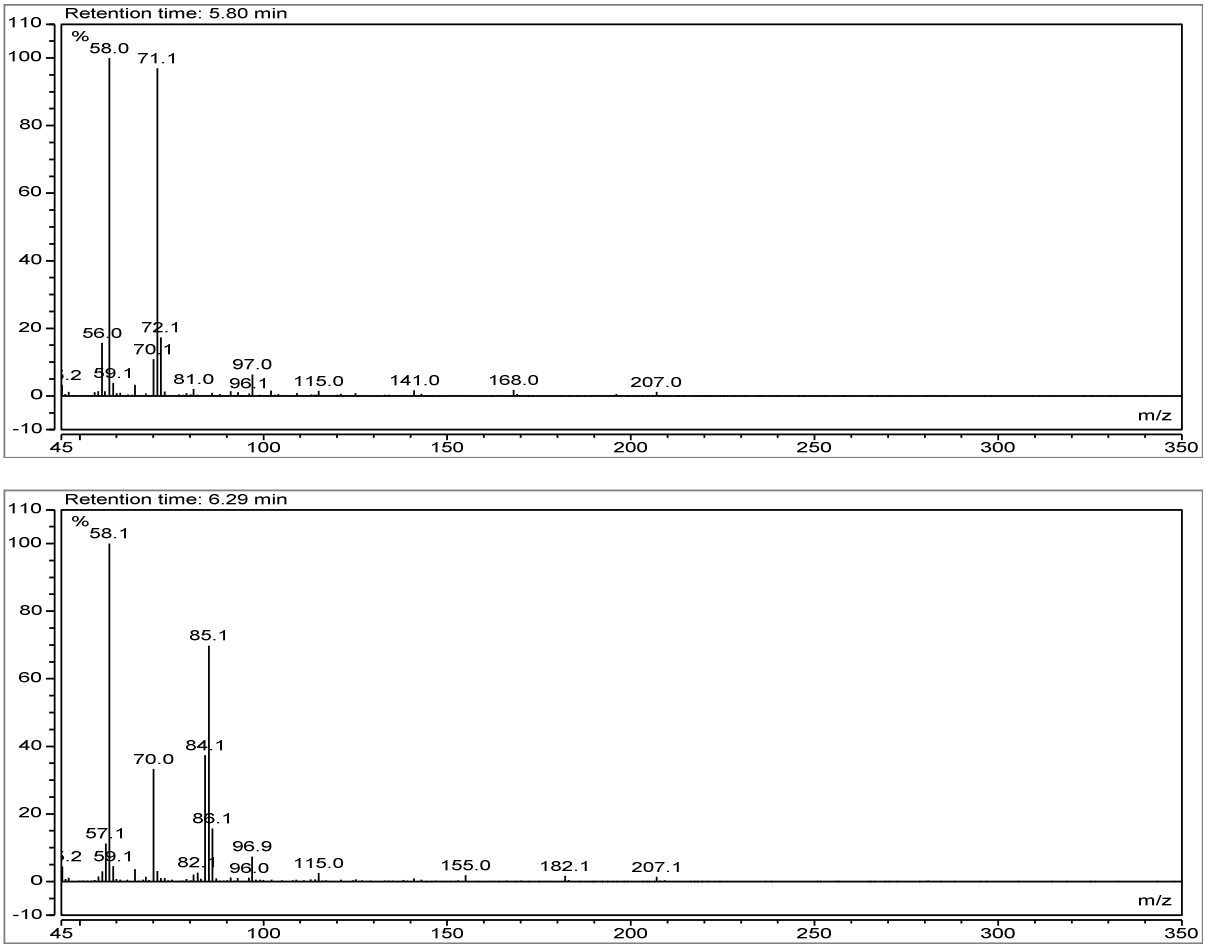

Figure 113: *EI-MS spectra of compound **XVIII** (top) and compound **XIX** (bottom).*

The two possible fragments are of the same structure as the ones observed for compounds with $N(Et)_2$-moiety besides the fact that the ethyl substituents are exchanged by methyl groups and thus the m/z values differ by 28 amu for compound **XVIII** and 14 amu for compound **XIX**. This finding and the findings in the previous chapter lead to the assumption that the most prominent fragmentation site in the Amiton-like compounds is the chalcogen-CH_2-bond in the amino alkyl side chain of the compounds. By knowing this it is very easy to determine the chemical composition of this moiety, but not the actual structure.

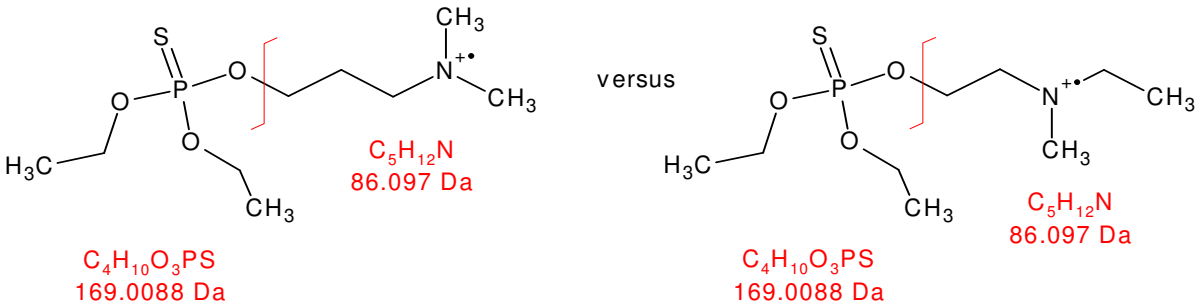

Figure 114: *Comparison of the assumed most prominent fragments of compound **XIX** (left) and a structural isomer resulting in the same fragments.*

The actual structure can only be determined by investigation of the secondary daughter ions to see whether the nitrogen is symmetrically substituted or not since different configurations could still lead to the same primary daughter ions. This is illustrated in Figure 114 and would need to be proved in praxis. Beyond this, this is also true for all compounds having more than two CH_2-groups as spacer between the respective chalcogen and nitrogen atom, e.g. compound **XVII**, or different alkyl groups as substituents of the nitrogen atom.

Table 63: *Overview of the secondary fragmentation study results of compounds **XVIII**.*

Parent ion m/z	Daughter ions m/z (optimum collision energy [eV])
141	123(10), 97(20), 81(20), 61(20), 45(10)
125	97(10), 79(20), 65(20), 61(10), 45(10)
115	97(10), 81(20), 79(20), 65(30), 63(30)
109	91(10), 81(10), 65(10), 63(30), 45(10), 29(10)
97	79(10), 65(10), 47(30),
91	65(10), 47(20), 43(10), 27(20)
81	63(20), 47(30)
71	56(10), 43(10)
65	47(10)
58	56(10), 43(10), 42 (20), 30(10), 29(10)
56	41(20), 40(30), 30(10), 29(10), 28(10), 27(10)

However, in this particular case the m/z ratio of the respective fragments is below the regular detection range of a standard mass spectrometric run operated at a lower m/z value limit of 45 amu. One additional fact to notice from Figure 115 and Figure 116 is that the phosphorus containing part of the molecule allows a relatively high number of possible reaction pathways. On the other hand, especially for compound **XVIII**, very few decay routes are observed for the nitrogen moiety. Compared to this the additional side CH_2-group in compound **XIX** again offers more transition decay routes for the total breakdown of the molecule.

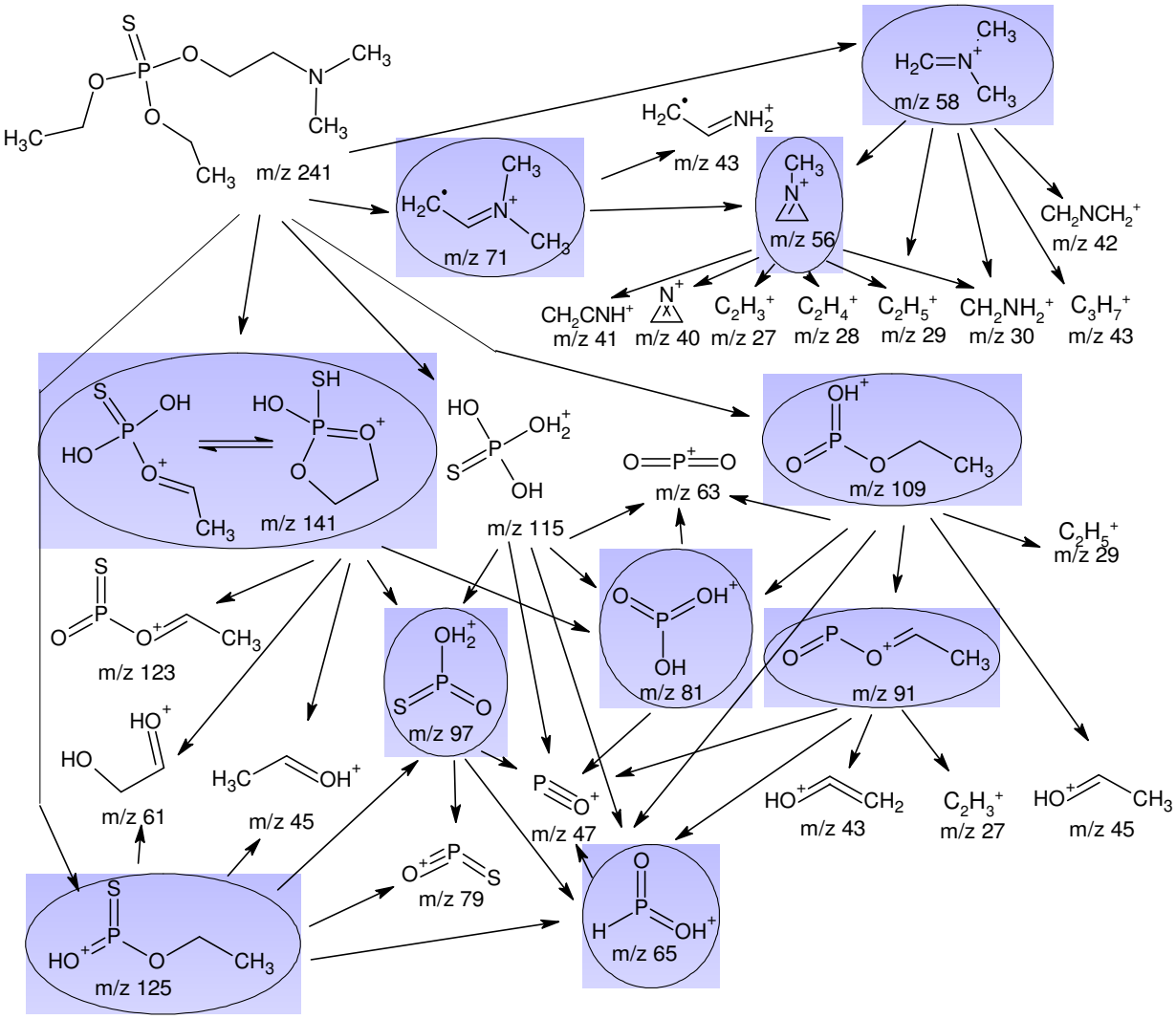

Figure 115: *Proposed mass spectral fragmentation pathways for compound **XVIII**. Color-coded fragments indicate those of the initial mass spectrum used for further MS-MS investigation.*

Interestingly, there are also fragments observed, e.g. m/z = 84, which have the same m/z ratios as they are observed for Amiton (**X**) and do also result from the nitrogen containing moiety. Furthermore, two important fragments (m/z = 182 and m/z = 155) are detected which also offer the two general fragmentation pathways for the nitrogen and phosphorus containing part of the compound.

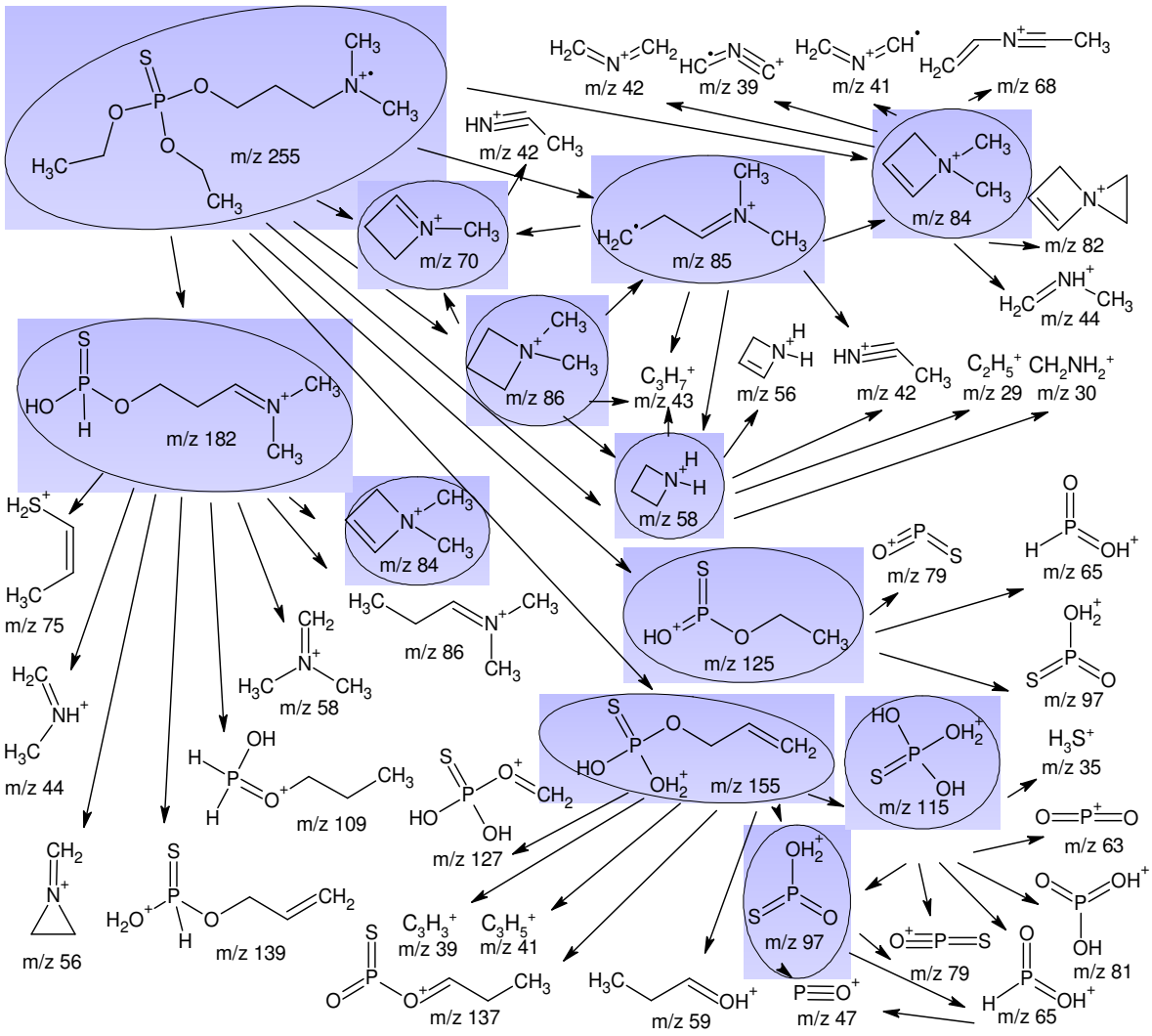

***Figure 116**: Proposed mass spectral fragmentation pathways for compound **XIX**. Color-coded fragments indicate those of the initial mass spectrum used for further MS-MS investigation.*

***Table 64:** Overview of the secondary fragmentation study results of compounds **XIX**.*

Parent ion m/z	Daughter ions m/z (optimum collision energy [eV])
255	86(10), 85(10), 84(20), 70(20), 58(20)
182	139(10), 109(20), 86(10), 84(10), 75(10), 58(20), 56(30), 44(20)
155	137(10), 127(10), 115(10), 97(20), 59(10), 41(10), 39(30)
125	97(10), 79(20), 65(20)
115	97(10), 81(20), 79(20), 65(30), 63(30), 35(10)
97	79(10), 65(10), 47(30),
86	85(10), 71(10), 70(10), 58(10), 56(20), 43(20)
85	84(10), 70(10), 58(10), 43(10), 42(10)
84	82(10), 68(20), 44(20), 42(10), 41(20), 39(20)
70	42(10)
58	56(10), 43(10), 42 (20), 30(10), 29(10)

Furthermore, the fragment of m/z = 141, which is not described for compound **XIX** but is also observed in the respective mass spectra, was not investigated since the fragmentation pathway was expected to be the same as for the ten previously described compounds. Additionally, the signal intensity of the m/z = 141 fragment of compound **XIX** was very low.

4.9.4 Fragmentation of Compounds Bearing a R-N-(*i*Pr)$_2$ Substituent

In this chapter compounds **XXII** and **XXIII** are compared with each other, the major difference is the chalcogen coordination at the phosphorus atom. Compound **XXII** has four oxygen atoms attached to the phosphorus whereas compound **XXIII** is the thiono derivative thereof. Here also two main fragmentation pathways can be observed. Unsurprisingly, the fragmentation of the alkyl amino sidechain is nearly identical for both compounds. The respective full scan mass spectra are given in Figure 117.

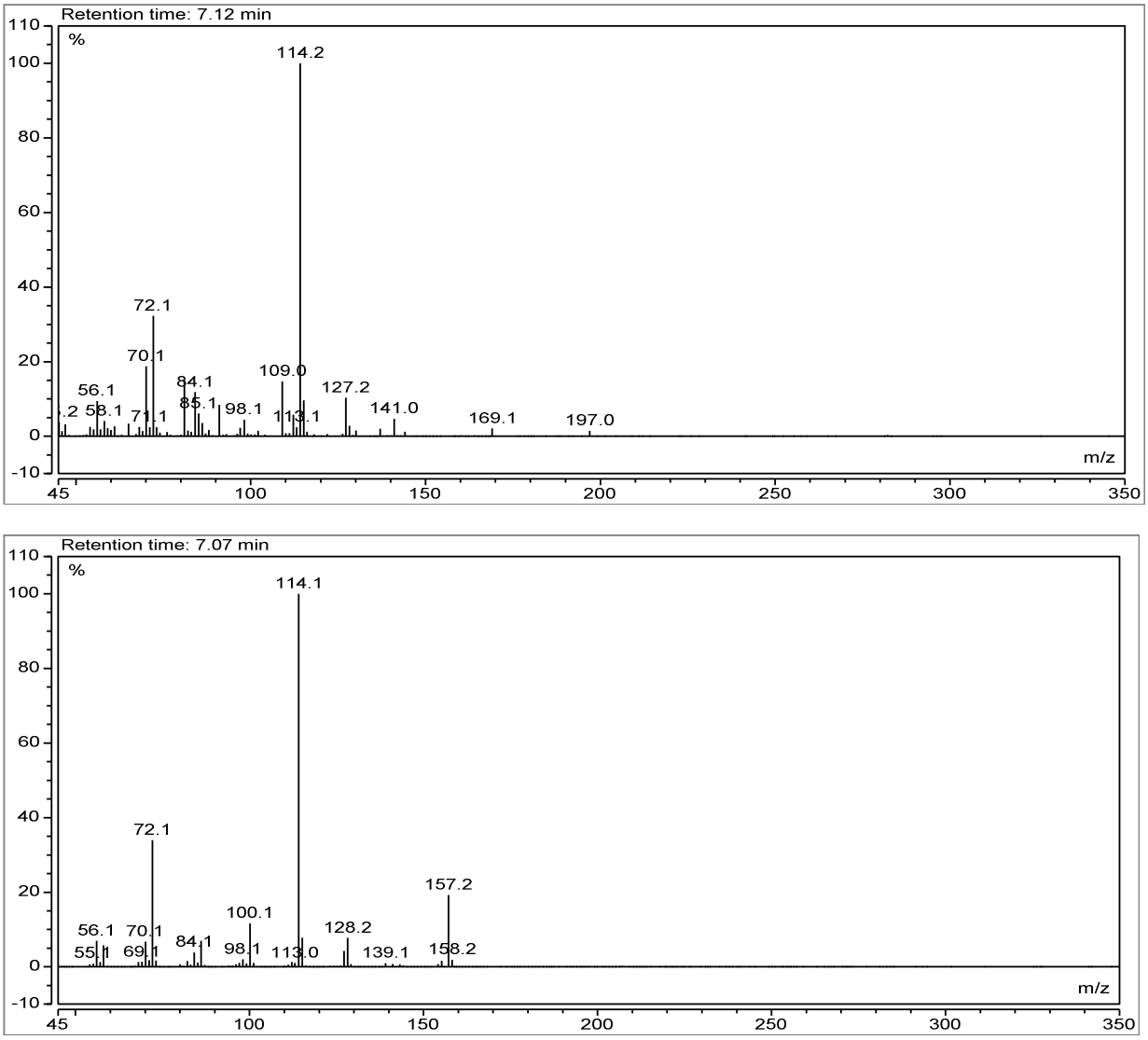

Figure 117: *Full Scan EI mass spectra of compounds **XXII** (bottom) and **XXIII** (top).*

The most obvious difference is the absence of the fragments m/z = 141, 169 and 197 in the spectrum of compound **XXIII** and the additional presence of a fragment with m/z = 157. Also, in the low mass region two major differences can be observed. First, the signal for fragment of m/z = 72 is very prominent in both spectra but is only accompanied by the m/z = 70 fragment for compound **XXIII**. Second, they also differ in the presence/absence of the m/z = 100 and m/z = 109 fragments.

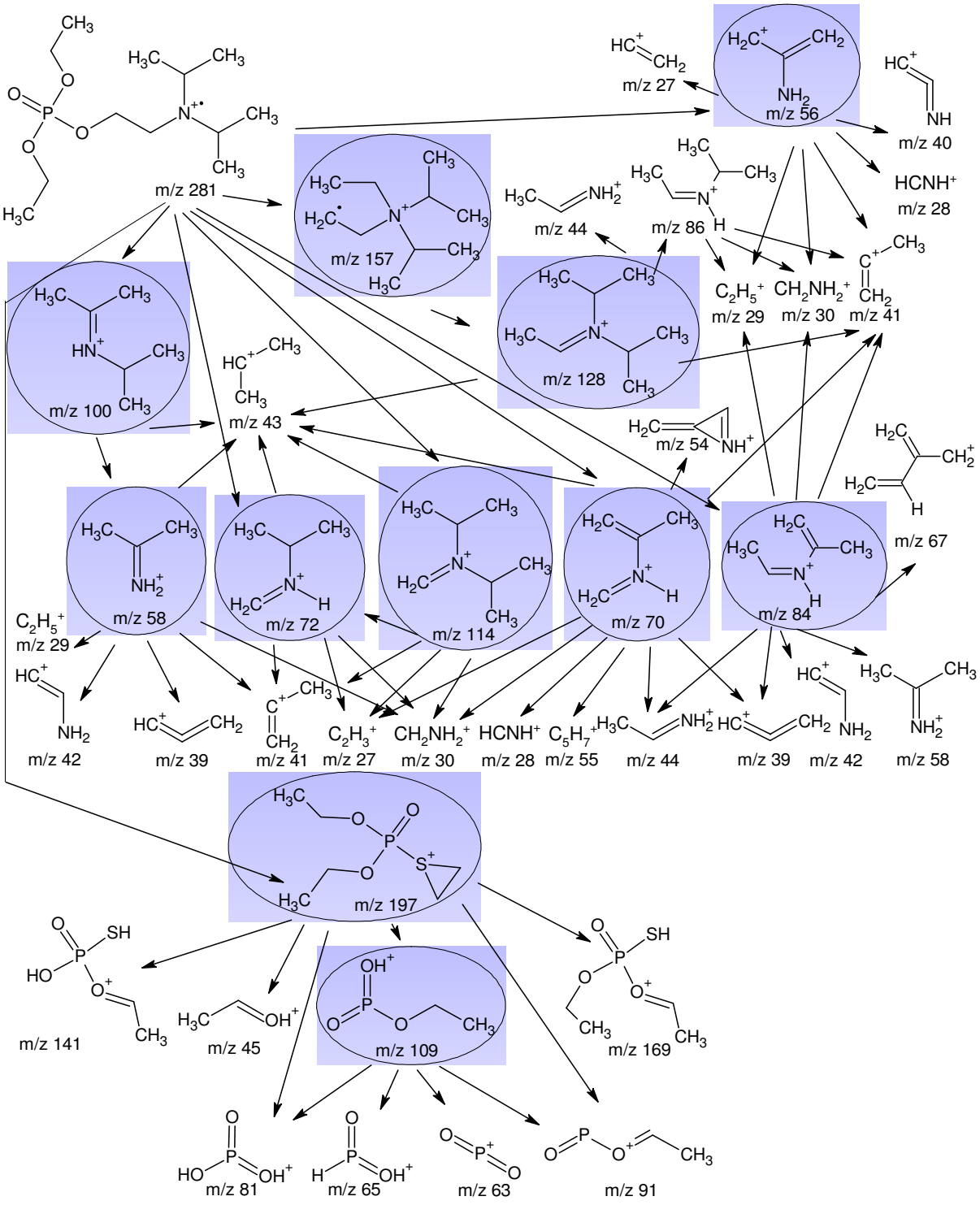

Figure 118: *Proposed mass spectral fragmentation pathways for compound **XXII**. Color-coded fragments indicate those of the initial mass spectrum used for further MS-MS investigation.*

Table 65: *Overview of the secondary fragmentation study results of compound* ***XXII****.*

Parent ion m/z	Daughter ions m/z (optimum collision energy [eV])
197	169(5), 141(5), 109(10), 91(20), 81(20), 45(20)
157	128(10), 114(10), 100(10), 86(10), 72(20), 58(10)
128	86(10), 44(10), 43(20), 41(30)
114	72(5), 43(20), 41(20), 30(10), 27(30)
109	91(5), 81(10), 65(15), 63(30)
100	58(10), 43(20)
86	41(20), 30(10), 29(20)
84	67(10), 58(20), 44(20), 42(10), 41(20), 39(20), 30(10), 29(20)
72	43(10), 41(20), 30(10), 27(20)
70	55(10), 54(20), 44(20), 43(10), 42(10), 41(10), 39(20), 30(10), 28(10), 27(20)
58	43(20), 42(20), 41(10), 39(20), 30(10), 29(10)
56	41(20), 40(30), 30(10), 29(10), 28(10), 27(20)

The very prominent fragment of m/z = 157 in the spectrum of compound **XXII** caused the most difficulties to be solved. From the formed daughter fragments it is quite obvious that each fragment differs by a value of 14 amu which most likely results from the loss of a CH_2-group which is typical for aliphatic structures. However, the high value of the m/z = 157 fragment would mean to be comprised of ten or eleven carbon atoms in a row. This is obviously not possible by simply breaking down the structure of the molecule. The longest continued side chain contains only a total of eight carbon atoms and one nitrogen atom. Thus, a major rearrangement of the molecule must occur to form the respective m/z-fragment. Also a second alternate fragment can be thought of which would have a m/z-ratio of 157 but not all of the six secondary fragmentation ions can be formed from this one (Figure 119).

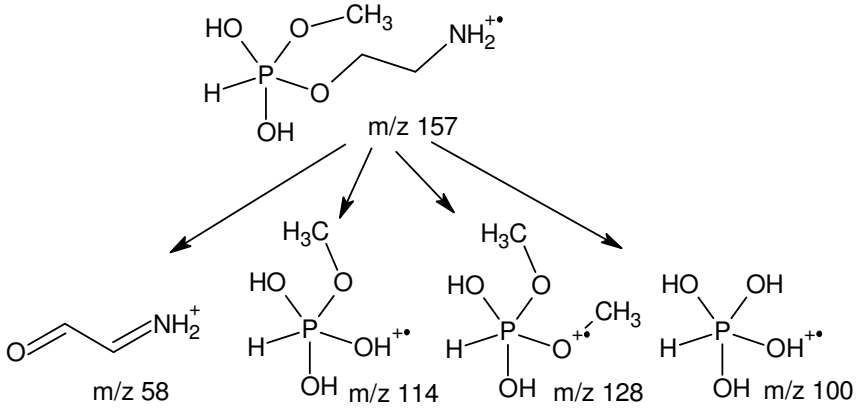

Figure 119: *Structure of the alternate m/z = 157 fragment and four of the needed six daughter fragments.*

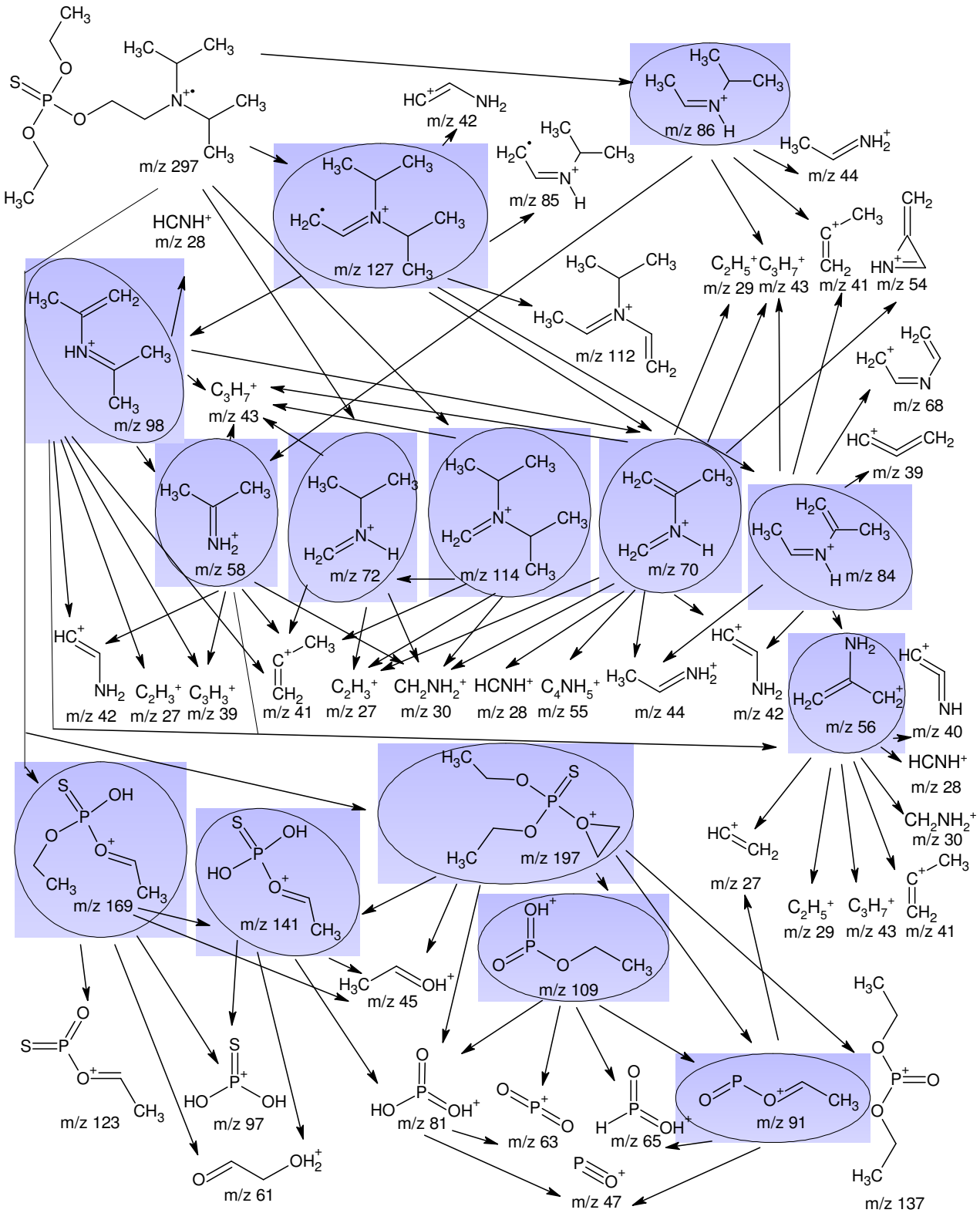

Figure 120: *Proposed mass spectral fragmentation pathways for compound* ***XXIII****. Color-coded fragments indicate those of the initial mass spectrum used for further MS-MS investigation.*

However, although the rearrangement to form the m/z = 157 fragment is quite unlikely, the expected associated isotopic peaks do not match with the alternate postulated fragment and its possible daughter ions depicted in Figure 119. The second big fragmentation route is the one of the breakdown of the phosphorus containing part of the molecule. Here, the

fragment with m/z = 197 is of particular importance. This fragment could also be identified in compounds bearing a $N(Et)_2$-moiety. In both compounds it gives rise to a large number of fragments of which all but one, m/z = 45, still contain phosphorus.

Table 66: *Overview of the secondary fragmentation study results of compounds* ***XXIII****.*

Parent ion m/z	Daughter ions m/z (optimum collision energy [eV])
197	141(5), 137(5), 109(10), 81(20), 45(20)
169	141(5),123(15), 97(20), 61(20), 45(15)
141	97(20), 81(30), 61(20), 45(10)
127	112(5), 98(5), 85(5), 84(10), 70(10), 42(25)
114	72(5), 43(20), 41(20), 30(10), 27(30)
109	91(5), 81(10), 65(15), 63 (30)
98	83(15), 70(10), 58(15), 56(5), 43(15), 42(20), 41(25), 39(40), 28(15),27(40)
91	65(10), 47(15), 27(15)
86	71(5), 58(5), 44(5), 43(10)
84	69(15), 68(20), 56(10), 44(15), 43(10), 42(10), 41(15), 39(20)
72	43(10), 41(15), 30(5), 27(20)
70	55(15), 44(15), 43(5), 42(10), 41(10), 30(10), 29(10), 28(10, 27(25)
58	57(5), 56(5), 43(15), 42(20), 41(10), 39(15), 30(5)
56	41(15), 40(25), 30(10), 29(10), 28(5), 27(15)

Although the relative intensity is very small it is of great importance for the recognition of the organophosphorus nature of the molecule. The same is true for the m/z = 169 fragment of compound **XXIII** which is not present in the mass spectrum of compound **XXII** and the relative intensity of m/z = 197 fragment lies below one percent making it challenging for the correct detection and identification of the molecule.

4.9.5 Fragmentation of Compounds with N-Atom in a Cyclic Structure

The two compounds with the nitrogen atom incorporated in a ring structure are expected to show a different fragmentation pattern. The reason for this is, that ring systems are most likely to form stable fragments due to good delocalization of radical functions or positive charges. The respective EI full scan mass spectra are depicted in Figure 121 for compound **XXV** and in Figure 123 for compound **XXVI**, respectively. Surprisingly, the spectrum of compound **XXV** shows only very few signals. None of the observed fragments contains a phosphorus atom at all. However numerous fragments for the amino alcohol functionalized side chain could be identified (Figure 122 and Table 67). At first glance one could assume that these signals would only represent the pure amino alcohol educt.

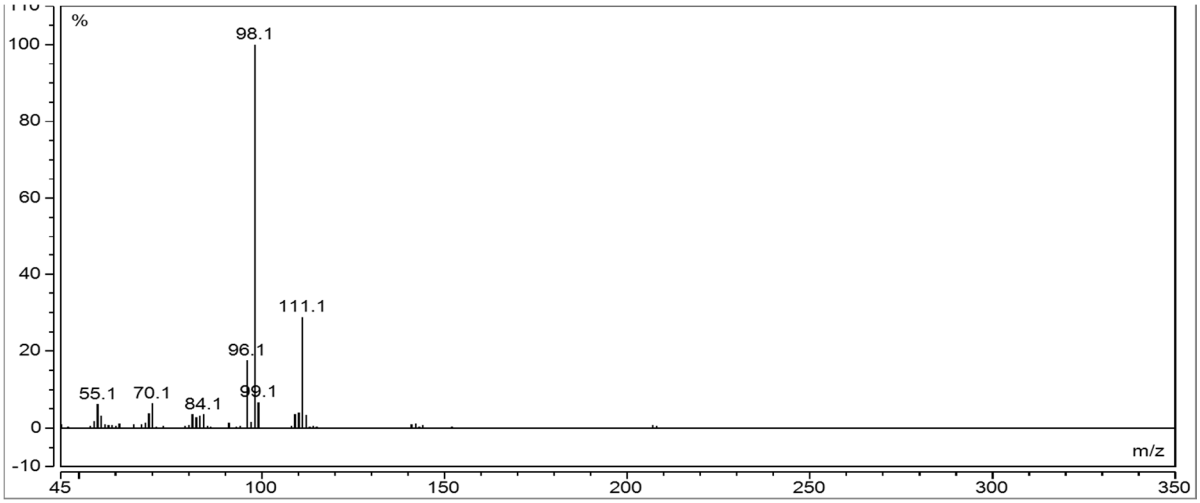

***Figure 121**: Full Scan EI mass spectrum of compound **XXV**.*

This postulation could easily be disproved by analyzing the amino alcohol itself and performing chemical ionization experiments which revealed the correct molecular mass of the compound. Quite obviously, fragment with m/z = 98 offers a lot of pathways for further mass spectrometric breakdown of the compound and can be identified to be a key fragment for the identification of this particular molecule. Especially *via* its daughter fragment m/z = 96 a lot of fragments preserving the ring structure by simply losing a H_2 molecule can be identified. A second pathway for the formation of fragment with m/z = 96 is starting from the largest fragment with m/z 111. Furthermore, for the fragments of m/z = 98, 96 and 94 also isomeric structures of seven membered rings can be drawn, as for example is done for the fragment with m/z = 98 in Figure 122. This feature is well-known for six-membered aromatic rings by forming the so-called Tropylium cation of m/z =91.[299]

***Table 67:** Overview of the secondary fragmentation study results of compounds **XXV**.*

Parent ion m/z	Daughter ions m/z (optimum collision energy [eV])
111	96(10), 82(15), 69(15), 57(15)
98	96(10), 70(10), 69(10), 55(10), 44(20), 42(15), 41(20), 39(20), 29(25)
96	94(10), 81(10), 80(10), 79, 77, 70, 68(10), 67, 54(15), 41(20), 28(25), 27(20)
86	58(15), 30(15)
55	39(20), 29(25), 28(25), 27(20)

Additionally, the suppression of the fragmentation of the phosphorus containing part of the molecule can be explained by the fact that the ring structure can very well distribute the positive charge amongst the ring members. Furthermore, in no case the positive charge is thus necessary to be stabilized amongst the relatively electronegative atoms, e.g. oxygen and sulfur. Hence, no signal for radical containing compound can be observed in the mass spectrum.

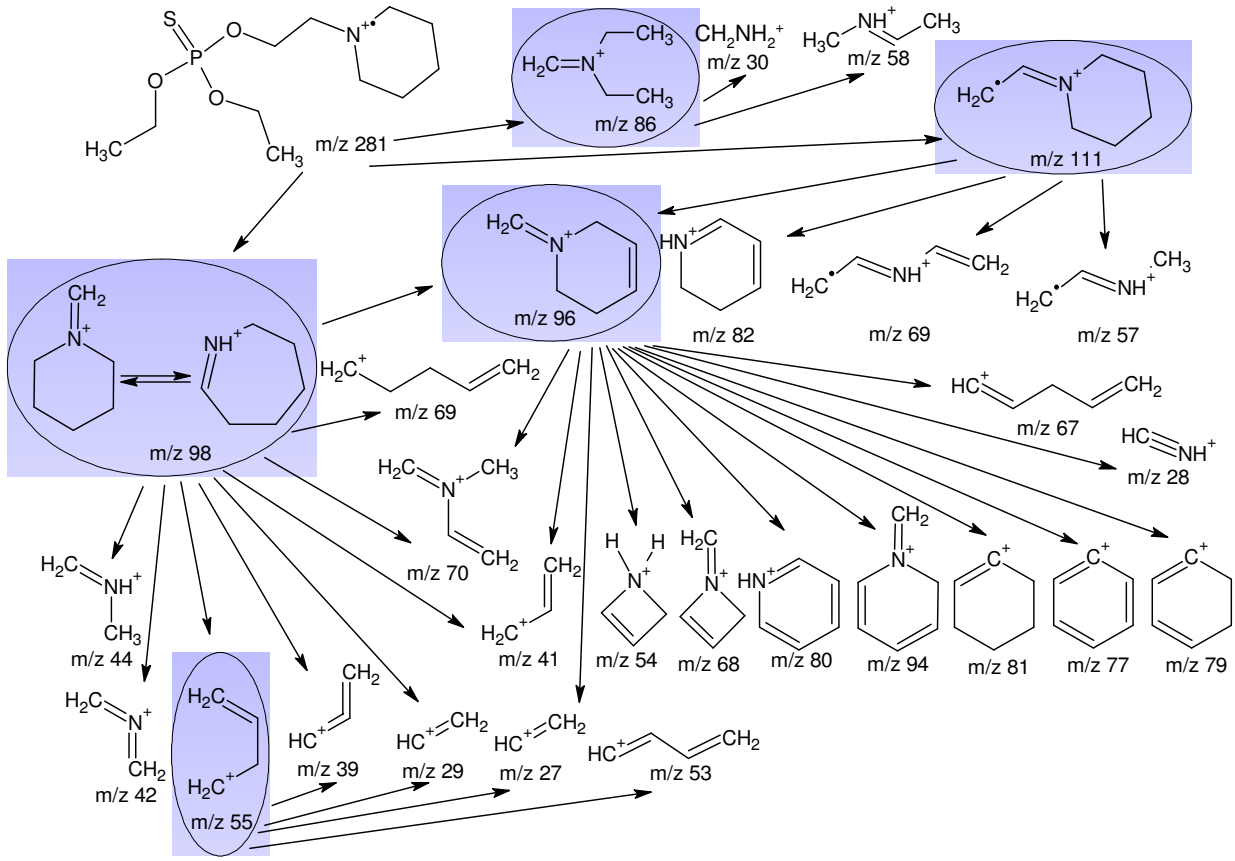

Figure 122: *Proposed mass spectral fragmentation pathways for compound **XXV**. Color-coded fragments indicate those of the initial mass spectrum used for further MS-MS investigation.*

For compound **XXVI** which has the nitrogen embedded in a five membered ring the situation is different again. The most prominent fragment is the one with m/z = 86 and second most prominent fragment is the one with m/z = 98. Furthermore a comparably large number of larger m/z ratio fragments are observed which make it quite easy to determine the chemical structure of the compound.

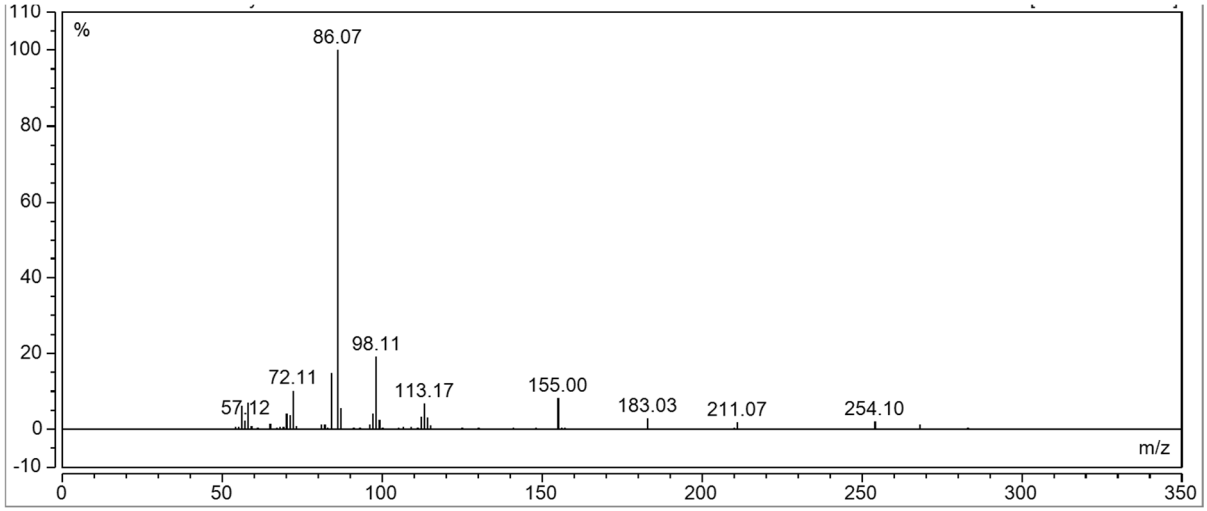

Figure 123: *Full Scan EI mass spectrum of compound **XXVI** taken during the first step of the Auto SRM procedure.*

Table 68: *Overview of the secondary fragmentation study results of compounds* ***XXVI****.*

Parent ion m/z	Daughter ions m/z (optimum collision energy [eV])
254	211(5), 155(15), 116(15), 84(10), 56(30)
211	183(5), 155(10), 59(20)
183	155(5), 115(20), 59(15)
155	137(5), 127(5), 115(10), 97(20), 59(10)
113	98(5), 84(10), 70(10), 56(10)
98	70(10), 44(10), 29(15), 27(25)
86	58(15), 30(15)
72	44(10), 29(15), 27(25)

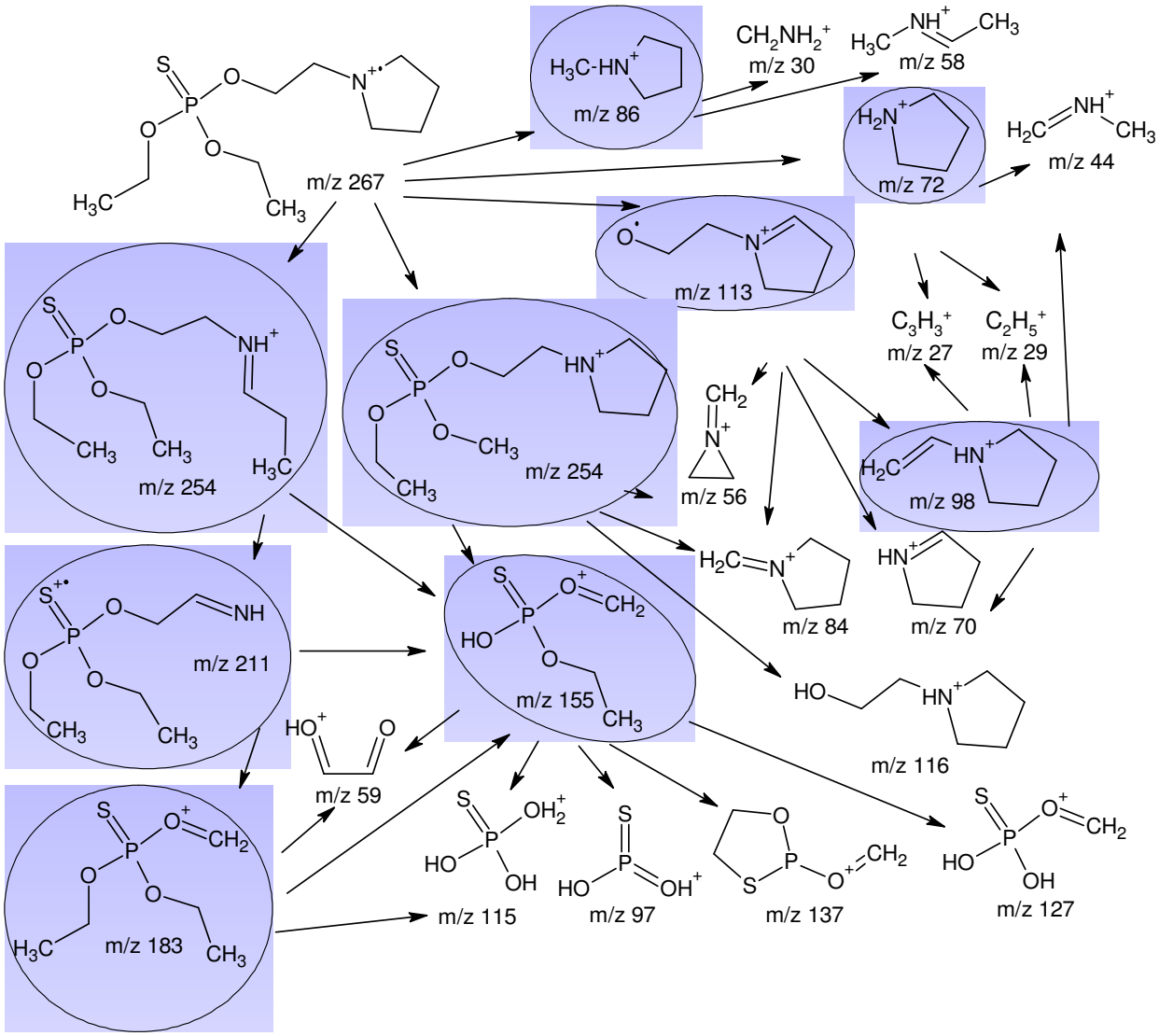

Figure 124: *Proposed mass spectral fragmentation pathways for compound* ***XXVI****. Color-coded fragments indicate those of the initial mass spectrum used for further MS-MS investigation.*

Compared to compound **XXV** the m/z = 86 fragment must have a different creation process which must be very similar to that illustrated for the m/z = 72 fragment in Figure 125. Quite obviously both fragments cannot be formed by a simple bond cleavage but must be accompanied by two hydrogen rearrangements.

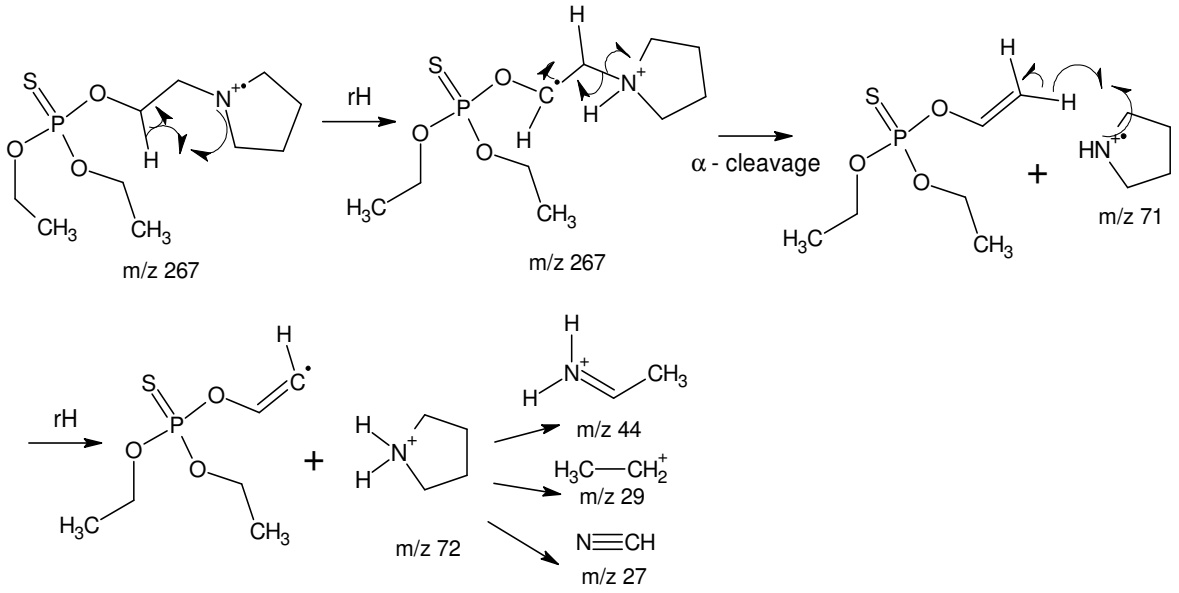

Figure 125: *Elucidation of the possible fragmentation reactions to form the m/z =72 fragment of compound* ***XXVI****.*

Furthermore, the m/z = 254 fragment must exist in two different modifications, since fragments are formed containing either nitrogen or phosphorus. The preservation of the nitrogen containing ring is especially important for the explanation of the fragment with m/z = 116 but on the other hand cannot be used to explain the formation of the fragment with m/z = 183. This leads to the conclusion that two different species for the fragment with m/z = 254 must exist. Also for the m/z = 211 fragment a structure preserving the nitrogen ring moiety can be found but again from this the m/z = 183 fragment cannot be explained. Hence, these findings need to be clarified in future examinations by techniques like high resolution MS/MS experiments or by the preparation of labeled compounds.

4.9.6 Fragmentation of Compounds Bearing Various Alkyl Amino Side Chains

In this chapter the remaining compounds not fitting into the above chapters are discussed regarding their mass spectrometric fragmentation pathways. The first compound described is compound **XXIV**. Results are reported in Table 69 and Figure 126. This compound is characterized by an additional methyl group in the alkyl amino sidechain compared to compound **XVIII**. Again two major fragmentation pathways can be observed. Surprisingly for the phosphorus moiety one additional fragment is observed (m/z = 75) which could not be explained by other means than containing a phosphorus. Additionally, the branching methyl

group also gives rise to at least one new fragment (m/z = 68) in the second major fragmentation route. This is accessible since now a four membered ring can be formed by the three adjacent carbon atoms without rearrangement of the whole molecule.

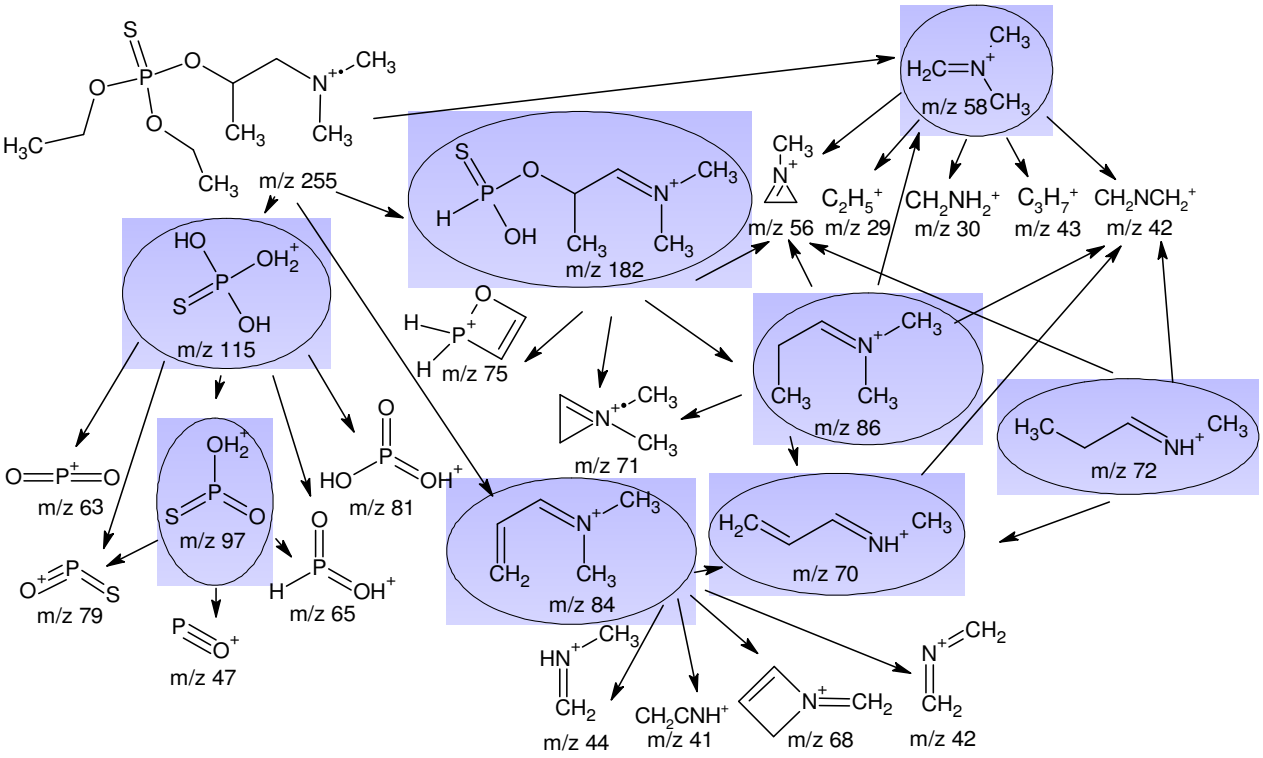

Figure 126: *Proposed mass spectral fragmentation pathways for compound **XXIV**. Color-coded fragments indicate those of the initial mass spectrum used for further MS-MS investigation.*

Table 69: *Overview of the secondary fragmentation study results of compounds **XXIV**.*

Parent ion m/z	Daughter ions m/z (optimum collision energy [eV])
182	86(10), 75(10), 71(10), 56(30)
115	97(10), 81(20), 79(30), 65(30), 63(20)
97	79(10), 65(20), 47(30)
86	71(10), 70(10), 58(10), 56(20), 42(20)
84	70(10), 68(20), 44(20), 42(10), 41(20), 39(20)
72	70(10), 57(10), 56(20), 44(10), 42(10)
70	42(10)
58	56(20), 43(10), 42(10), 30(10), 29(10)

The next two compounds, compound **XX** and compound **XXI** are again quite similar to each other, by having both a *tert*-butyl group substituted at the nitrogen atom. Furthermore, in compound **XXI** the nitrogen atom is bearing a methyl group instead of a hydrogen atom. Both compounds show a slightly different fragmentation pattern compared to the other compounds since quite a few fragments of large m/z-ratios can be observed.

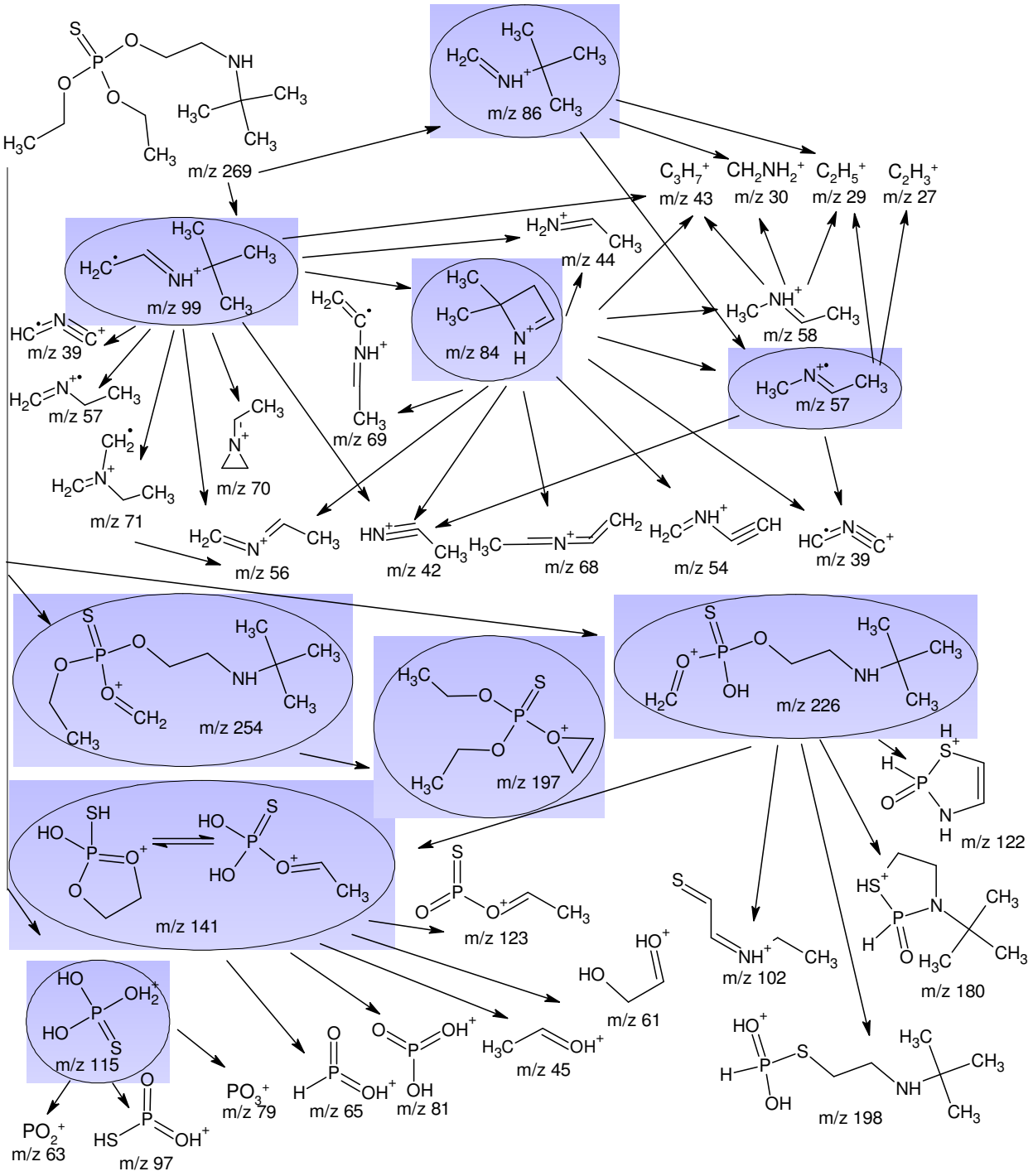

Figure 127: *Proposed mass spectral fragmentation pathways for compound **XX**. Color-coded fragments indicate those of the initial mass spectrum used for further MS-MS investigation.*

This fact facilitates the identification of the compounds. The reason for the presence of the heavier fragments can be explained by the presence of the very stable *tert*-butyl group, which slightly destabilizes the positive charge at the nitrogen atom since the central carbon atom of the *tert*-butyl group itself has a strong positive character by nature. Nonetheless, these heavy fragments mostly result in phosphorus containing daughter fragments. Only for compound **XXI** there is a cross-connectivity observable for both major fragmentation routes *via* the m/z = 98 fragment. Moreover, this experiment indicates that fragmentation of the

nitrogen containing part of the molecules is not resulting in the numerous fragments of m/z ratios around and below m/z = 40.

Table 70: *Overview of the secondary fragmentation study results of compound* ***XX****.*

Parent ion m/z	Daughter ions m/z (optimum collision energy [eV])
254	197(10), 169(10)
226	198(10), 180(10), 141(10), 122(10), 102(10), 84(10)
197	141(10), 45(20)
141	123(10), 97(20), 81(30), 61(20), 45(10)
115	97(10), 81(20), 79(20), 65(30), 63(30)
99	84(10), 57(10), 56(10), 44(10), 43(10), 42(20)
86	57(10), 30(10), 29(20)
84	69(10), 68(20), 58(10), 57(10), 56(10), 44(10), 43(10), 42(10), 39(20)
57	42(10), 39(20), 29(20), 27(10)

Table 71: *Overview of the secondary fragmentation study results of compound* ***XXI****.*

Parent ion m/z	Daughter ions m/z (optimum collision energy [eV])
268	197(5), 169(10), 141(15), 137(10), 109(15), 98(5), 91(30), 81(35)
197	169(5), 141(5), 137(5), 109(10), 91(20), 81(20), 45(20)
169	141(5), 97(20), 45(20)
141	123(10), 97(15), 81(25), 61(15), 45(10)
137	109(5), 91(10), 81(10), 63(35), 29(25)
113	98(5), 70(10), 57(10), 56(20), 42(15)
109	91(5), 81(10), 65(15), 42(15)
98	68(20), 56(10), 42(10)
86	30(10), 30(10), 29(15)
81	63(15), 47(35)
70	42(10), 30(10)
58	56(5), 43(10), 42(15), 30(5), 28(20)
57	29(10), 28(15), 27(15)
56	28(5), 15(20)

Compared to the other compounds, e.g. compound **IX**, the m/z = 84 fragment must be of a different structure since the central carbon atom of the *tert*-butyl group cannot offer a hydrogen atom to undergo hydrogen rearrangement. The possibility to join a double bond with the nitrogen atom, as can do the other adjacent CH_2 groups like in compound **IX**, is not given here. Thus, one of the methyl groups must be cleaved off. The proposed reaction

pathway is depicted in Figure 129. Furthermore, the determined optimum collision gas energy of 10 eV perfectly matches with the ones found in the NIST web book of about 9.8 eV for the formation of the methyl radical.[300]

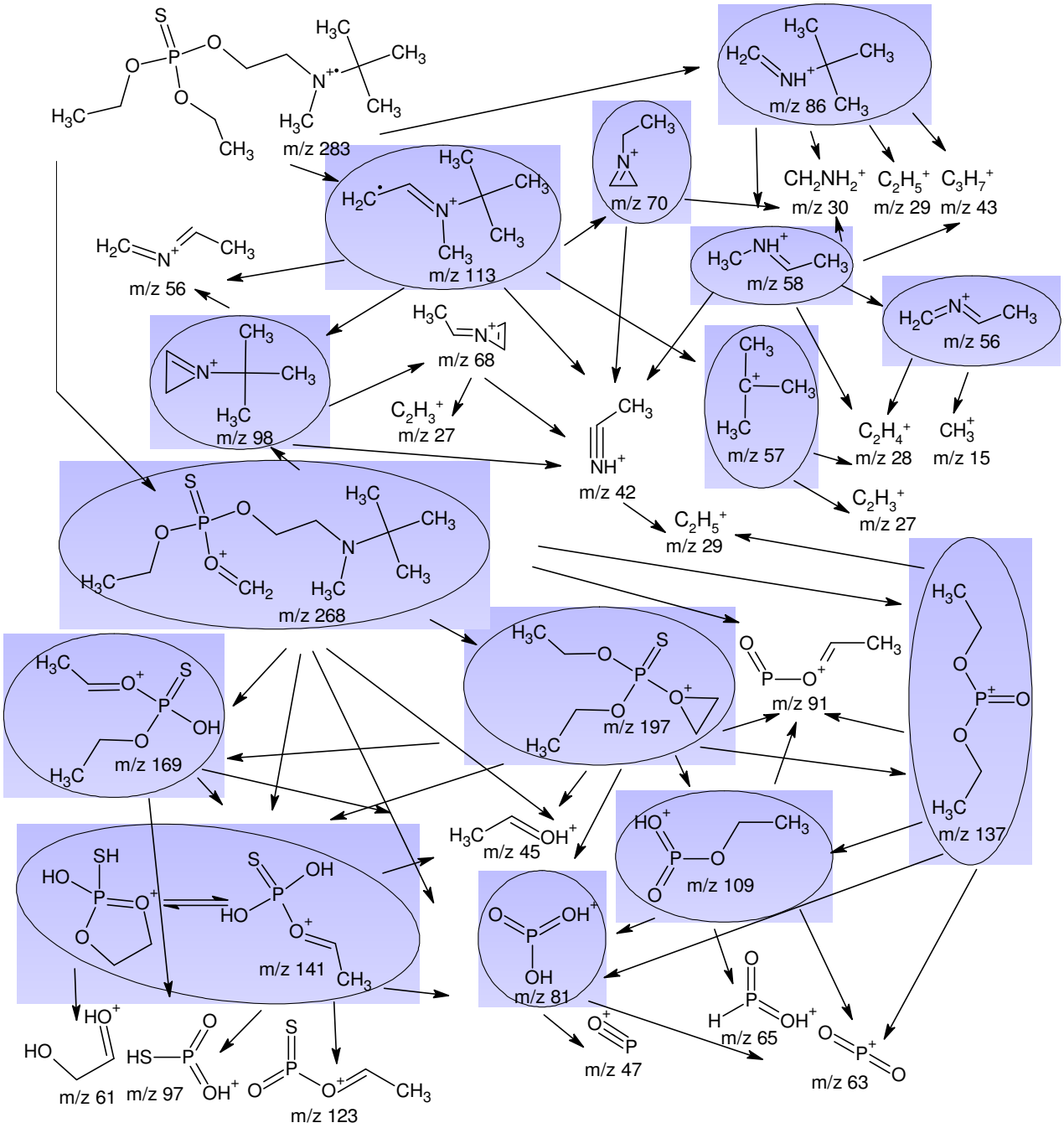

Figure 128: *Proposed mass spectral fragmentation pathways for compound* ***XXI****. Color-coded fragments indicate those of the initial mass spectrum used for further MS-MS investigation.*

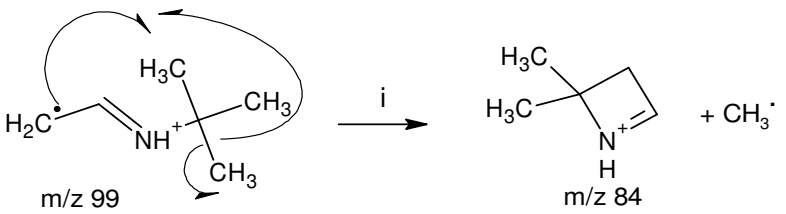

Figure 129: *Proposed mechanism of the radical induced fragmentation of the m/z = 99 fragment of compound* ***XXI*** *to form the m/z = 84 daughter fragment and a methyl radical.*

4.9.7 Conclusion

In this chapter almost all OP's and OTP's of this study were subjected to a full mass spectrometric fragmentation study to reveal the individual fragmentation pathways. Moreover, this study can be used to lower the limit of detection by choosing the proper transitions conditions in two or more dimensional mass spectrometry. Furthermore, these studies help to clearly differentiate the structurally closely related compounds of this thesis. Now it is possible to not only recognize them by their retention time or Kovats index, but also by mass spectrometry.

Generally it can be said that the differences in the obtained mass spectra are significant enough to determine the exact molecular configuration. However, in one case (compound **XXV**) in which no fragments for the phosphorus moiety could be found in the mass spectra it is not possible to identify the compound by EI mass spectrometry alone. Furthermore, the structurally similarity of the molecules makes it almost impossible to clearly identify any of the molecules by the standard mass spectrometric libraries. The non-experienced user would just account the next best hit as the true molecule and would assume the missing or additional peaks to the background since the differences are very small and report a false compound. This is especially true for the compounds having all the same amino alcohol sidechain which causes most of the prominent fragments of the compound. However, by paying attention to the weak signals of 1-3% of absolute signal intensity in the mid to high mass region it is possible to clearly identify the molecule correctly.

Some important fragments could be found which are common amongst most of the compounds and give clear hints to the presence of a phosphate compound. Those are: (i) m/z = 81 for a molecules based on phosphate and (ii) m/z = 97 for thiophosphate containing molecules.

To totally resolve the fragmentation pathway further studies have to be performed to clarify for example from which part of the molecule the CH_2-groups in fragment with m/z = 141 of compound **XX** is originated. Additionally, it has to be proved by several neutral loss scans

that ethylene or water are lost by the corresponding parent ion fragment if the mass difference is 28 or 18, respectively.

Finally, this study represents the first comprehensive study of the mass spectrometric fragmentation pathways of several Amiton-like compounds whereas only single compound studies of Amiton itself are available in the literature to date.

4.10 Detection with Military Equipment and Hand-held Analytical Instruments

4.10.1 Chemical Agent Detector Paper

The color reaction of the two tested papers is based on the ability of the target substances to dissolve one or more of the immobilized dyes. Thus a color appearance indicates the presence of either a nerve (V or G-type) or a blister agent. According to their chemical structure all target molecules within this study are accounted to the V-type agents and a dark green color should occur upon contact with the detector paper.

However, the results listed in Table 72 and Table 73 do not match with the true nature of the analyte molecules. Especially for compounds **XIV**, **XVI** and **XXVII** a reddish color appeared which is indicating a blister agent instead of a V-type nerve agent. Thus, a reliable result was not obtained. On the one hand one could say that for the everyday soldier or first responder it is crucial which agent is present, since it is known that any agent is present and precautions have to be taken. On the other hand it is also possible that a regular chemical substance which is not a CWA or a like substance can cause a color reaction indicating a false positive result. Here, it is of great importance to know that this can happen and although false negative results are possible as it is for example in case of compounds **XV**, **XXIII** and **XXVI** in the present study. This is even more of concern as the effective inhibiting capacity of AChE and BuChE for compound **XXVIII** were the highest observed for a thiono-isomer of this study.

Table 72: *Breakdown of the different OP's and OTP's tested against the chemical agent detector paper with NSN 6665-12-858-8494 and the chemical agent simulant detector paper as depicted in Table 73.*

	column 1	column 2	column 3	column 4
row 1	**IX**	**XXIII**	**XVIII**	**XXV**
row 2	**XXVI**	**XX**	**XIX**	**XVII**
row 3	**XV**	**XIV**	**X**	**XI**
row 4	**XXII**	**XXVII**	**XXIV**	**XVI**
row 5	**XII**	**XIII**	empty	empty

As can be seen from Image 19 the simulant test paper shows no color reaction at all. The darker impression results from the wetting of the paper by the test substance. This finding is not surprising since the red dye would be set free by citric acid from the chemical agent simulant or any other acidic compound, whereas the test substances are of basic character and therefore no color reaction is expected.

Table 73: *Test results for the chemical agent detector paper with NSN 6665-12-858-8494 for the different OP's and OTP's as given in Table 72.*

	column 1	column 2	column 3	column 4
row 1	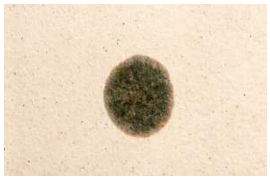	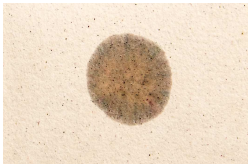		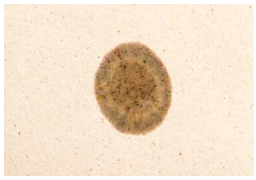
row 2				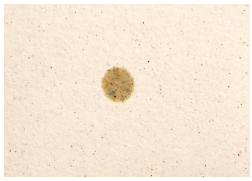
row 3	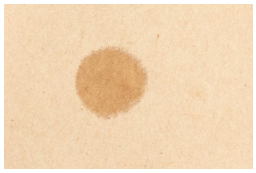			
row 4		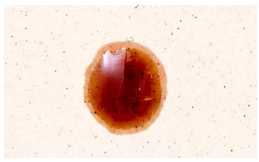	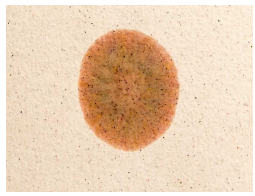	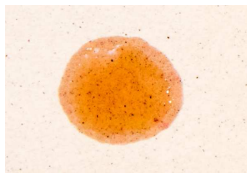
row 5	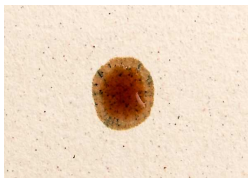	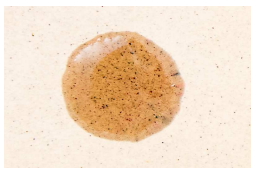	empty	empty

However, the colorful results are a clear indication for the limitations of such a detection device. Compared to the results from classical chemical warfare agents it has to be pointed out that the 3-way-chemical detector paper is very sensitive towards the detection of CWA's but has strong limitations because of the dyes being able to also be dissolved by other organic compounds and thus leads to false positive and false negative results unless the user of the detection paper is well trained and knows the originally intended color indication.

Table 74: *Breakdown of the precursors tested against the chemical agent detector paper with NSN 6665-12-858-8494 as depicted in Table 75.*

	column 1	column 2	column 3	column 4
row 1	**I**	**II**	**III**	**V**
row 2	**VI**	**VII**	**VIII**	empty

This is also very important as the 3-way-detector paper is used amongst all the soldiers and not only by CBRN personnel. Noteworthy, some the synthesized precursors show a color reaction with the detection paper Table 74 and Table 75, which does make things even worse, because this would be a true false result, which could lead to the very wrong conclusions and measures taken at the respective scenario. Interestingly, compound **VIII**, which is an acidic compound, generates the same color reaction as it would be expected for sulfur mustard.

Table 75: *Test results for the chemical agent detector paper with NSN 6665-12-858-8494 for the precursors as given in Table 74.*

	column 1	**column 2**	**column 3**	**column 4**
row 1			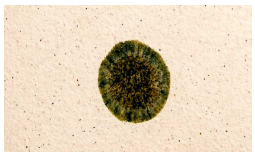	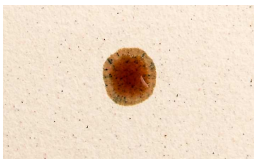
row 2	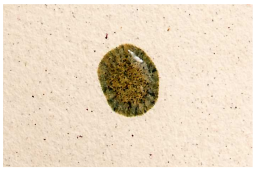		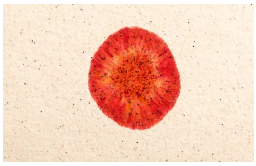	empty

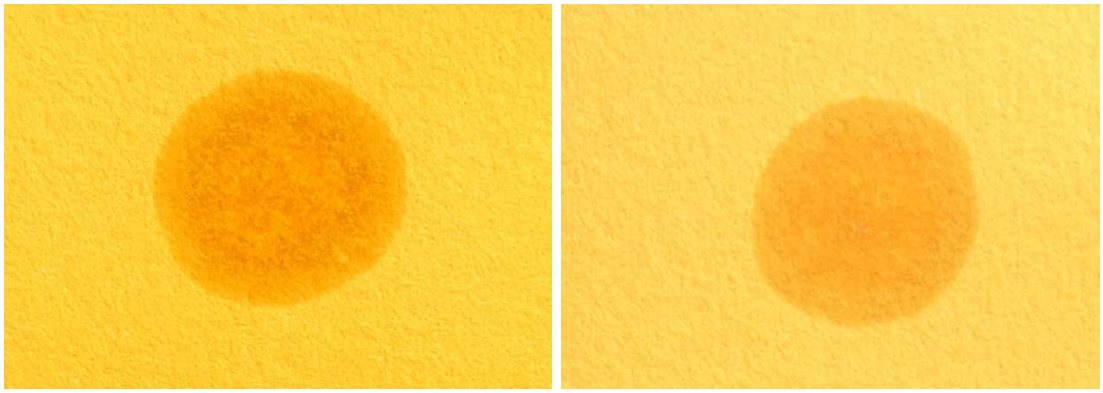

Image 19: *Test results for the chemical agent simulant detector paper with NSN 6665-12-329-6688 for two of the OTP's (compounds **XI** and **XXIV**) to show the color impression which was almost the same for all the other molecules.*

4.10.2 Dräger Test Tubes

The setup for the experiment was chosen that way that the concentration in the HDPE bag did not change during the suction process of the accuro pump. This could easily be established since the HDPE bag inflated during the suction process and therefore each stroke withdrew an equal comprised aliquot of 100ml.

Table 76: *Results of the Dräger Test Tube test after challenging them with the respective Amiton derivative at a level of 0.4 ppm, which is well above the limit of detection.*

compound	resulting test tube	test result
blank		-
IX		+
X		+
XI		+
XII		+
XIII		+-
XIV	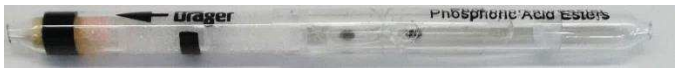	+-
XV		+
XVI		+
XVII		-
XVIII		+
XIX		+
XX		-
XXII		+
XXIII		+
XXIV		+
XXV		+
XXVI		+
XXVII		+-

The results shown in Table 76 show that all substances clearly react with the Dräger test tubes. At least this is the case, if the concentration is well above the limit of detection, which was ensured by applying a concentration of about 0.4 ppm to the test tubes. All results are in good agreement with the results of the in-vitro enzyme kinetic studies.

The test tubes only show a negative result for compounds **XVII** and **XX** which are the substances which also had low toxicity values in the in-vitro enzyme kinetic study and therefore may not actually pose a direct threat towards vertebrates. Surprisingly, also other compounds having the comparable IC50 values for BuChE do give a positive result. Only with respect to the large error in accuracy of 30% these results can be explained.

Table 77: *Results of the Dräger Test Tube test after challenging them with the respective Amiton derivative at a level of 0.05 ppm, which is at the limit of detection.*

compound	resulting test tube	test result
blank		-
IX		+
X		+
XI		-
XII	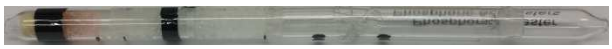	+
XIII		-
XIV		-
XV		+
XVI		-
XVII	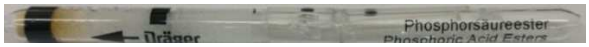	-
XVIII		-
XIX		+
XX		-
XXII		-
XXIII		+
XXIV		+
XXV		-
XXVI		+
XXVII		-

In case the concentration level meets the detection limit of the test tubes the results are slightly different (*cf.*Table 77). This can be partly accounted to the large standard deviation of the test tube and mainly to the fact that the compounds do not inhibit the BuChE enzyme strong enough at this concentration level and thus do prevent the second reaction step

(*cf.* Chapter 3.7.2.2) in the test tube. However, also nine compounds result in a positive test result. Furthermore no false positive result compared to the measurements at high concentration was observed.

4.10.3 Ion Mobility Spectrometry

IMS-spectra could be recorded for all synthesized molecules. Additionally, the precursor molecules were tested. The signals were only recorded in the positive mode since no signals could be observed in the negative mode. This finding is not surprising due to the fact that the molecules do inherit a nitrogen moiety which can be easily charged by a positive ion cluster. Nearly all of the molecules resulted in a false positive alert by the LCD 3.3 instrument. A basic overview of the results for the LCD 3.3 and Raid-M 100 are summarized in Table 78 and Table 81, respectively.

The LCD 3.3 measurements resolved at least one peak in the IMS chromatogram and some gave two peaks. Those spectra can be analyzed by the Trim Scan Software which allows a deeper analytical evaluation of the chromatogram. Additionally, using this software the corresponding K_0-values can be determined. For most of the tested compounds the LCD 3.3 alerted for different CWA's, which do not have any structural similarities with the analyzed compound, as can be seen from Table 78. Furthermore, in comparison with the Raid-M 100 the calculated K_0-values differ from each other to some extent and in most cases the Raid-M 100 could resolve sometimes more than two different cluster ions reaching the detector. On the contrary, the LCD 3.3 resulted only in a maximum of two different peaks. The difference in the K_0-values can be accounted to the different ionization techniques of the two instruments and therefore the different clusters formed during the ionization process. Since the LCD 3.3 uses ammonia as a dopant molecule the expected clusters are heavier and therefore should have larger drift times resulting in smaller K_0-values.

According to the manufacturer, the underlying algorithm for the calculation of the amu units by the Raid-M 100 is optimized for phosphor organic compounds. This algorithm has to be changed for other molecules or substance classes in order to exclude misinterpretations. To be absolutely sure about the correctness of the calculated values it would be best to connect the instruments drift tube to a MS-instrument, which is not possible for the user, but which was done during the development of the instrument.[301]

The general theory of the formation of dimer and monomer clusters is correct for the amino alcohol precursor molecules (compounds **I** and **II**) which cannot form fragments easily. The larger K_0-value belongs to the monomer cluster which must be formed by collision with a protonated water ion resulting in an amu value of 150 (= 19 + 131 amu) for compound **I** and

164 (= 19 + 145 amu) for compound **II**. Hence, the correlation of the K_0-values with amu values seems to be sufficient. If this holds true and the fact that up to 67keV of ionization energy used in the Raid-M 100 would be sufficient to fragment the analyte molecules, some of the other amu values can possibly be explained.

Table 78: *Results of the IMS measurements of the Amiton derivatives using the LCD 3.3 after challenging the instrument for two to three seconds with the respective compound. Given are the indicated alerts on the instruments display as well as the bar levels. Moreover, the K_0-values for the resulting peaks in the IMS chromatograms are listed.*

compound	alert	bar levels	K_0	K_0
IX	GD	4	1.81	1.37
X	VX	6	1.85	1.34
XI	GD	3	1.78	1.24
XII	VXR	8		
XIII	GD	1		
XIV	VXR	4	1.62	1.30
XV	VXR	5	1.64	1.30
XVI	HD	6		
XVII	VXR	3	1.30	-
XVIII	**-**	**-**	1.92	1.41
	VXR	3	1.29	-
XIX	GD	4	1.39	-
XX	VXR	3	1.82	-
XXI	VXR	8		
	GD	1		
XXII	GB	6	1.69	1.19
XXIII	VXR	4	1.65	1.27
XXIV	GD	3		
XXV	VXR	4	1.31	-
XXVI	VXR	4	1.29	-
XXVII	GD	1		

Moreover, for compounds **XVII**, **XVIII** and **XIX** also the monomer cluster ions with K_0-values of 1.37, 1.27 and 1.17, respectively, could be identified as the $M+H^+$-ions. The observation of fragment ions by IMS is sometimes possible under certain circumstances, which can be: temperatures in the drift tube between 60 and 150°C – accelerating isomerization processes - [302], presence of heavy metals, like mercury [303] or high energy levels due to the use of a strong radiation source [304].

A somehow similar reaction pattern can be observed for the results of the LCD 3.3 where small K_0-values correlate with the monomeric cluster, e.g.1.29 for compound **XIX**, 1.31 for compound **XXV** and 1.27 for compound **XXIII**, respectively. The higher K_0-values in this measurement series must than also be accounted to the presence of fragment ion clusters which form less frequent compared to the measurement series of the Raid-M 100. This findings are reasonable as one takes into account that the drift tube of the LCD 3.3 works only at ambient temperatures and the analytes, OTP's and OP's, do not tend to isomerize readily at this temperature.

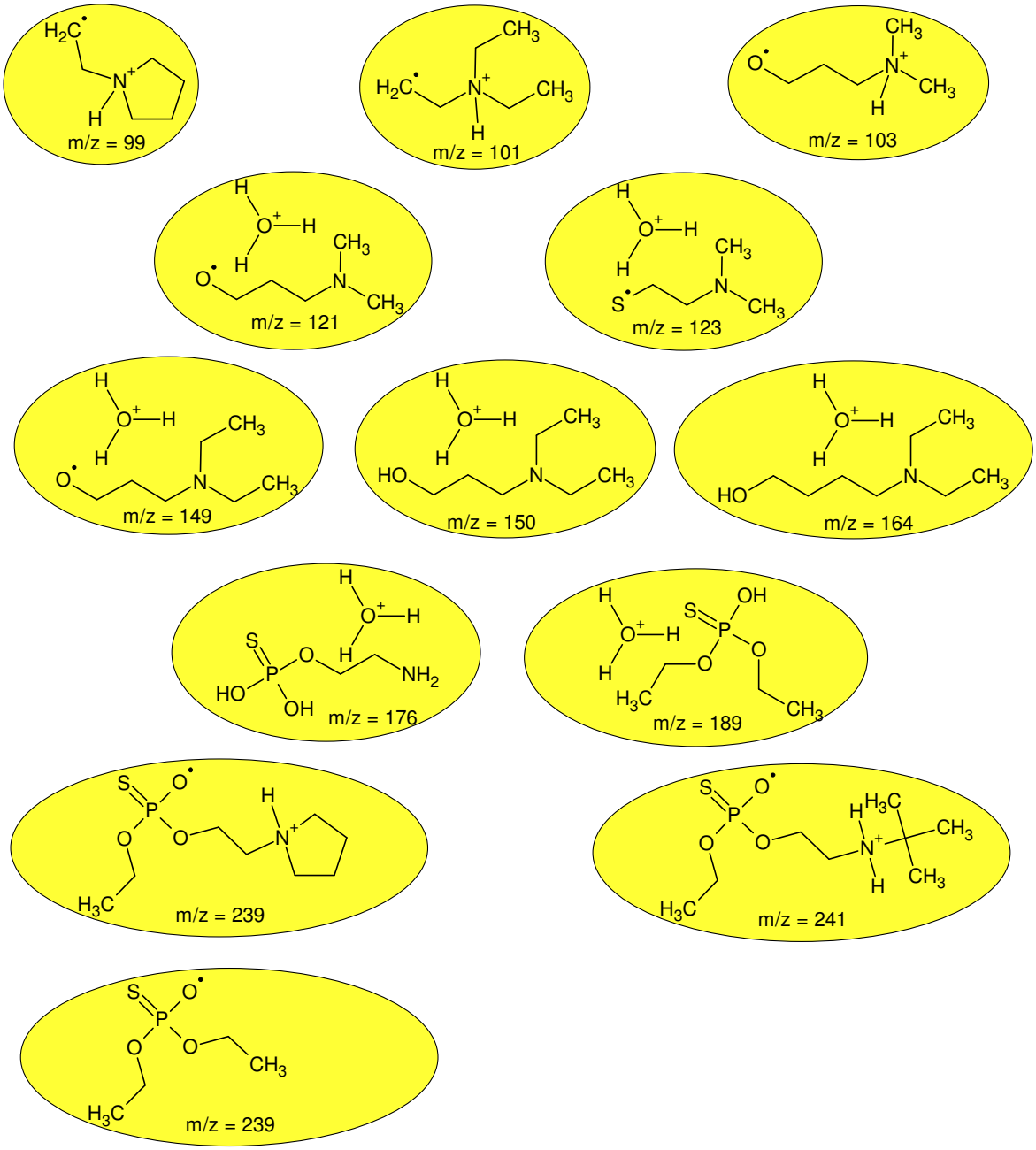

Figure 130: *Summary of the possibly identified fragment ion clusters during the IMS investigations of the analytes with the Raid-M 100 instrument.*

Table 79: *Results of the IMS measurements of the precursor molecules by the LCD 3.3 after challenging the instrument for two to three seconds with the respective compound. Given are the indicated alerts on the instruments display as well as the bar levels. Moreover, the K_0-values for the resulting peaks in the IMS chromatograms are listed.*

compound	alert	bar levels	K_0	K_0
I	VXR	5	1.77	-
II	VXR	3	1.69	1.19
III	VX	4		
IV	-			
V	-			
VI	VXR	3		
VII	-			
VIII	-			

Whether the reported signals belong to those proposed clusters cannot be told by only using an IMS instrument. It would be necessary to couple these instruments with another detection device like a MS instrument, which is unfortunately not possible. The results of the Raid-M 100 give a strong hint that the target molecules undergo a fragmentation reaction upon passing the radioactive ionization source because the measured amu values are low compared to the molecular mass of the analytes. If this would be the case, the results could easily be compared to the soft ionization mass spectra. Furthermore, also the observed difference of the IMS spectra for compounds **IX** and **X**, its thiol-isomer, can be explained in the same way as the individual mass spectra are also different, not in the observed peaks, but in the observed peak intensity as it is especially the case for ESI-MS spectra.

Table 80: *Results of the IMS measurements of the precursor molecules with the Raid-M 100 after challenging the instrument for two to three seconds with the respective compound. Entries in bold represent the relationship between the alert and the corresponding entry in the table. Furthermore, the table shows the indicated alerts on the instrument's display as well as the K_0-values for the resulting peaks in the IMS chromatograms and the corresponding amu levels for the respective peak.*

compound	alert	K_0	amu	K_0	amu	K_0	amu
I	-	1.73	150	1.26	276	-	-
II	-	1.67	164	1.26	276	-	-
III	-						
IV	-						
V	-						
VI	**-**						
VII	-						
VIII	GD/GB						

A good example for the fragmentation hypothesis is the finding that compound **I**, which is the precursor for compound **XV**, gives the same K_0-value. Furthermore, the compounds were checked for any educt molecules by means of HPLC-MS measurements which were in all cases negative. Thus, the presence of educt amino alcohol can be excluded.

Table 81: *Results of the IMS measurements of the Amiton derivatives with the Raid-M 100 after challenging the instrument for two to three seconds with the respective compound. Entries in bold represent the relationship between the alert and the corresponding entry in the table. Furthermore, the table shows the indicated alerts on the instrument's display as well as the K_0-values for the resulting peaks in the IMS chromatograms and the corresponding amu levels for the respective peak.*

Compound	Alert	K_0	amu	K_0	amu	K_0	amu
IX	-	2.04	101	1.70	156	-	-
X	-	1.95	114	1.52	198	-	-
XI	**GB**	1.73	151	1.45	218	**1.19** **1.03**	315 376
XII	-						
XIII	-						
XIV	-	1.89	123	1.73	151	1.59	182
XV	-	1.74	149	1.67	164	1.60	180
XVI	-						
XVII	GB/**GD**	**1.36**	241	1.17	312	0.99	390
XVIII	**-**	1.67	164	1.37	242	-	-
XIX		2.02	103	1.89	121	1.64	170
	-	1.52	198	1.36	245	1.27	273
XX	-	1.84	131	1.66	166	1.37	241
XXI	-						
XXII	DPM/**GB**	1.66	166	**1.56**	189	**1.16**	315
XXIII	-	1.60	176	1.36	245	-	-
XXIV	-						
XXV	-	1.65	167	1.36	245	-	-
XXVI	-	2.05	99	1.65	167	1.38	239
XXVII	-						

Finally, it has to be stated that the LCD 3.3 is not designed to be capable of the detection of chemical compounds others than those in the library and that the underlying scenario during the cold war was not an asymmetric threat potential but rather it was quite clear what was the challenge. For this task the instrument works very well. Moreover, it is quite understandable that also for the amino alcohols sometimes RVX is reported as a detection result, since the RVX similar to VX molecule itself bears the same amino alcohol moiety

which is responsible for the specific entry in the instruments database. However, this fact would than cause a military commander to draw the wrong conclusions from just this measurement if an amino alcohol precursor would be present instead of the real chemical warfare agent.

4.10.4 Flame Spectrophotometry

To compare some of the main detection technologies a test of almost all substances with the Proengin AP4C[11] was performed to see whether there are differences in the reported results compared to the devices running on IMS technology (chapter 4.10.3) or not. The obtained results show that the AP4C is somewhat superior to the IMS technology but also has some restrictions as for instance no library is included and thus an identification of any molecule is not possible.

Table 82: *Detection levels as given by the manufacturer for the different channels of the AP4C instrument.[188]*

Bar Levels	"G,V" mg/m³ of P	"HN,AC" mg/m³ of HNO	"CH" mg/m³	"L,SA" mg/m³ of AS	"HD,HL" mg/m³ of S
Overpassing	5	1000	6000	100	6
Blinking	3	500	1200	30	5
5	0,625	200		10	2,5
4	0,125	80		4	1,0
3	0,025	30		2	0,400
2	0,005	10		1	0,150
1	0,002	4		0,5	0,100

The results are summarized in Table 83 for the Amiton derivatives and Table 84 for the synthesized precursors, respectively. A very simple test setup was chosen since the instrument was made available by the Proengin company for just one day. Thus, the compounds were measured directly from their storage containers by allowing the instrument to suck in the vapor phase above the samples. This improvised set-up in the end turned out to be successful and at the same time is much more comparable to a regular measurement in the field than any other way of doing this examination. If no response of the instrument was observed from the gas phase measurements, the substance was evaporated by use of the liquid agent device.

The first thing to notice is that although most of the Amiton derivatives are comprised of phosphorus and sulfur only phosphorus was detected. The only exemptions to this rule are compounds **XIV** and **XIII**; those have more than one sulfur atom in their structure.

[11] http://www.proengin.com/chemical-detection/

Noteworthy is that compound **XII** has also two sulfur atoms but does not show a signal on the sulfur channel and compound **XVI** compared to compound **XVII** shows a signal on the HNO channel although it has a CH_2 group less than compound **XVII**.

Table 83: *Results of the measurements for different Amiton derivatives with the AP4C after challenging the instrument with the respective liquid compound for the given period of time until a reading on the display was achieved or a maximum of 20 seconds without any reading elapsed. The second part of the table reports the results from the samples not detected directly from the liquid state but measured with the liquid agent device. CH stands for the additional immediate blinking of the CH diode.*

Compound	Time [s]	P	liquid HNO	S	Time [s]	P	vaporized HNO	S
IX	4	3	-	-				
X	12	1	-	-				
XI	CH	3	-	-				
XII	4	4	-	-				
XIII	20	-	-	3				
XIV	1	2	-	1				
XV	3	2	-	-				
XVI	CH	5	2	-				
XVII	3	2	-	-				
XVIII	3	3	-	-				
XIX	2	2	-	-				
XX	CH	5	-	-				
XXI	*not available at test date*							
XXII	7	2	-	-				
XXIII	5	2	-	-				
XXIV	1	4						
XXV	10	2	-	-				
XXVI	5	2	-					
XXVII	>20	-	-	-	2	3	-	-

By having a look at the detection levels for the different channels these findings become clearer and are understandable in the way that for example the phosphorus channel is 50-fold more sensitive than the sulfur channel. The reason for the different levels are the fact that the values are orientated at the hazard threshold values for unprotected people and the instrument poses a warning if the lowest level is detected and a warning above level one.[188] Accordingly, the time until a reading on the instrument occurred can be used to compare the volatility of the different substances very roughly.

None surprisingly the amino alcohols do not show any signal for phosphorus and sulfur whereas compound **VIII** shows only a signal for phosphorus. Additionally, three of the amino alcohols are of low volatility and had to be measured with aid of the liquid agent device (Image 11) to evaporate them by forced heating giving the expected result on the HNO channel immediately after the heating button of the device was pressed.

Table 84: *Results of the measurements for different precursors of this thesis with the AP4C after challenging the instrument with the respective liquid compound for the given period of time until a reading on the display was achieved or a maximum of 20 seconds without any reading elapsed. The second part of the table reports the results from the samples not directly detected from the liquid state but measured with the liquid agent device. CH stands for the additional immediate blinking of the CH diode.*

Compound	Time [s]	P	liquid HNO	S	Time [s]	P	vaporized HNO	S
I	5	-	2	-				
II	10	-	1	-				
III	>20	-	-	-	1	-	3	-
IV	CH	-	5	-				
V	>20	-	-	-	1	-	3	-
VI	4	-	2	-				
VII	>20	-	-	-	1	-	3	-
VIII	CH	3	-	-				

In comparison to the results of the LCD 3.3, which mostly resulted in an alert for RVX and even for GD in case of the Amiton derivatives, the AP4C gave no false positive results. Moreover, the reported potential V or G series agent meaning the detection of an airborne molecule comprised of a certain amount of phosphorus was always a correct reading. Additionally, the false positive results of the LCD 3.3 for the amino alcohols were not observed. This first very rough investigation with the AP4C leads to the conclusion that this instrument can add value to the analytics of unknown chemical compounds in the field of hazard defense since it is a simple instrument towards detecting pure presence of phosphorus, sulfur, arsenic and molecules having HNO and C_xH_y groups.

4.10.5 Benchtop NMR Spectroscopy

As described in the introduction of this thesis (*cf.* Chapter 3.7.3.4) a new kind of portable instrument being able to perform NMR experiments is on the rise. These so called Benchtop NMR spectrometers operate on comparably very low frequencies leading to poorer resolutions and strong limitations regarding experimental results. In the framework of this thesis an initial test of these instruments towards the applicability in the hazard defense sector was done in close cooperation with Magritech company in Aachen, Germany.

4.10.5.1 General Remarks

Those instruments offer some quite unique features worth being mentioned in the results section since important conclusions can be drawn from their knowledge. This is vital towards the implementation of these instruments in the battlefield.

First thing to mention is that the operator does not necessarily need to be an experienced NMR specialist. The operation of the instrument is straight forward and the machine is ruggedized in that sense that a permanent magnet is in place which does not need to be shimmed by the user. Moreover, the instrument does not need a solvent for referencing as is usually the case for the big laboratory instruments. Additionally, the sample does not necessarily be diluted by the operator meaning that the sample preparation is very easily done by adding a proper amount of sample into a standard NMR tube. With the aid of an additional tool the NMR tube is positioned in the tube holder and can be directly introduced into the instrument for measurement. Furthermore, in case of a broken NMR tube during the insertion process, which did not occur during the test session in Aachen, the broken glass and analyte can be simply washed out of the instrument by rinsing the insertion port with an adequate organic solvent which can afterwards be evaporated by simply blowing air through the machine, since it has an opening at the bottom of the sample introduction port. Last but not least the size and weight of the machine are that impressively small and low, respectively. That it will easily fit into a standard Zarges-Box and can be transported to the place needed for operation. However, so far the only limitation seems to be that it is operated at 230 V.

Regarding the possible measurements the machine is available having magnetic fields being optimized to a dominant nucleus like ^{31}P or ^{13}C. Additionally, to this base nucleus it is always possible to detect a second NMR active nucleus like ^{1}H alongside the base nucleus, making also 2D NMR experiments available on the instrument. In other words, this means that a measurement of carbon and phosphorus at the same time requires two different instruments. Until today no machine is capable of having tunable magnets to changing the base nucleus.

4.10.5.2 Discussion of Experimental Results

As an example of the instruments performance the spectra of Amiton (**X**) and of its structural isomer (**IX**) of the benchtop instrument are compared to those measured on the standard NMR instrument used for the general characterization of the compounds.

In first comparing the ^{31}P coupled with ^{1}H NMR spectra (Figure 131) of compound **IX** the most obvious difference is the number of clearly identifiable lines of the multiplet. The benchtop spectrum only gives five discrete lines und two additional smaller ones indicated at the outside of the multiplet, whereas the standard instrument nicely resolves the

expected septet. The chemical shift value is 69.04 ppm for the standard instrument and 69.71 ppm for the benchtop NMR and the respective coupling constants are 9.6 Hz and 9.5 Hz, respectively. These numbers are in very good agreement with each other. Noteworthy, the benchtop spectrum was recorded within less than 4 minutes by accumulating only 256 scans of the sample. Obviously the signal to noise ratio is better for the standard instrument. The respective decoupled spectra are not presented as they would not give rise to any more information. However, the ^{31}P signal is clearly noticeable after 16 scans (> 1 minute instrument time) with the benchtop NMR instrument.

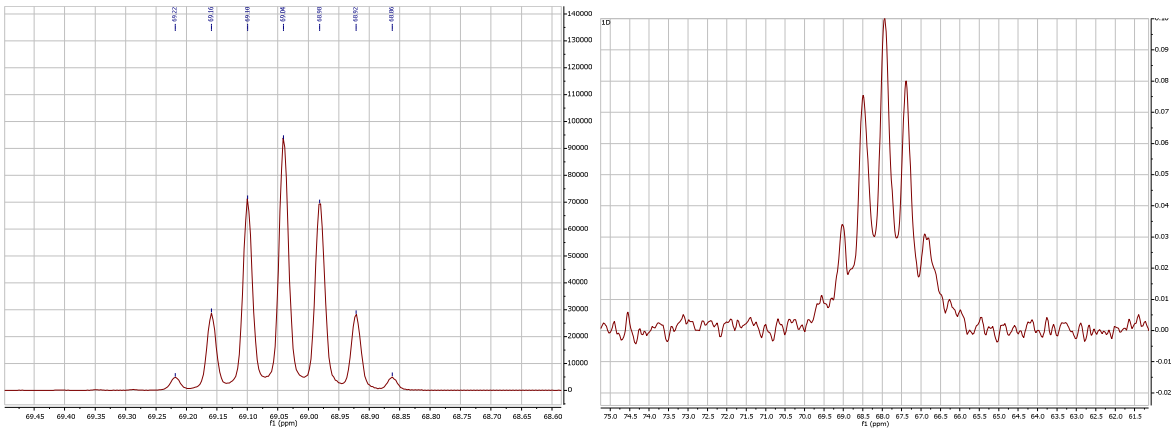

Figure 131: *Comparison of ^{31}P NMR coupled to ^{1}H NMR spectra for the standard instrument (left) and the benchtop NMR instrument (right) for compound* ***IX****.*

This means that this is a very fast and reliable method to prove whether the sample contains phosphorus or not. Additionally, by knowing the chemical shift value of the most important analytes it would be possible to also tell the chemical coordination of the phosphorus (*cf.* Chapter 4.3.2.3). In the respective decoupled carbon NMR experiment the differences are smaller since the difference in field strength of the instruments is not as big as it was for the protons; 101 MHz vs 43 MHz for carbon atoms and 400 MHz vs 60 MHz for protons, respectively. Furthermore, both spectra in Figure 132 show the same features with respect to relative signal intensity, splitting pattern and chemical shift values at an acquisition time of only ten minutes. Additionally, those carbon atoms in proximity of the phosphorus can be clearly identified by the presence of the characteristic doublet structure in the respective carbon signals.

In case of the proton spectra the differences are more pronounced as can be seen from Figure 133. The benchtop spectrum was taken after an accumulation of only 4 scans and the main features are detectable. Already the two triplets of the two different methyl groups (δ = 0.97 ppm and δ = 1.29 ppm) are clearly distinguishable by one another.

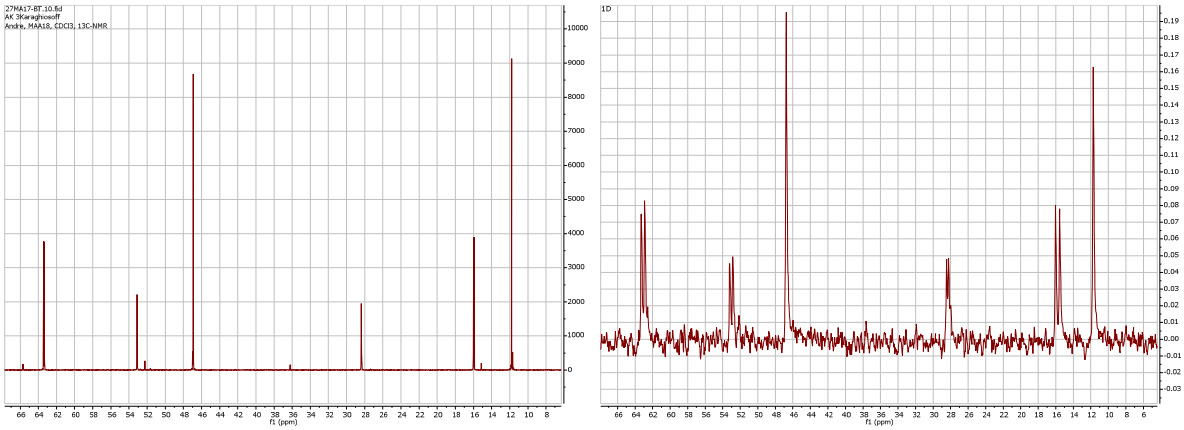

Figure 132: *Comparison of ^{13}C-NMR spectra for the standard instrument (left) and the benchtop NMR instrument (right) for compound* ***X****.*

However, the doublet coupling with the phosphorus of the triplet at δ=1.29 ppm is not resolved. Furthermore, all other spectral parameters are present but due to strong intramolecular coupling no further details can be obtained after this short measurement time. However, also the multiplet analysis of the one at δ= 4.4 -3.6 ppm was also not trivial for the spectrum obtained by the standard instrument.

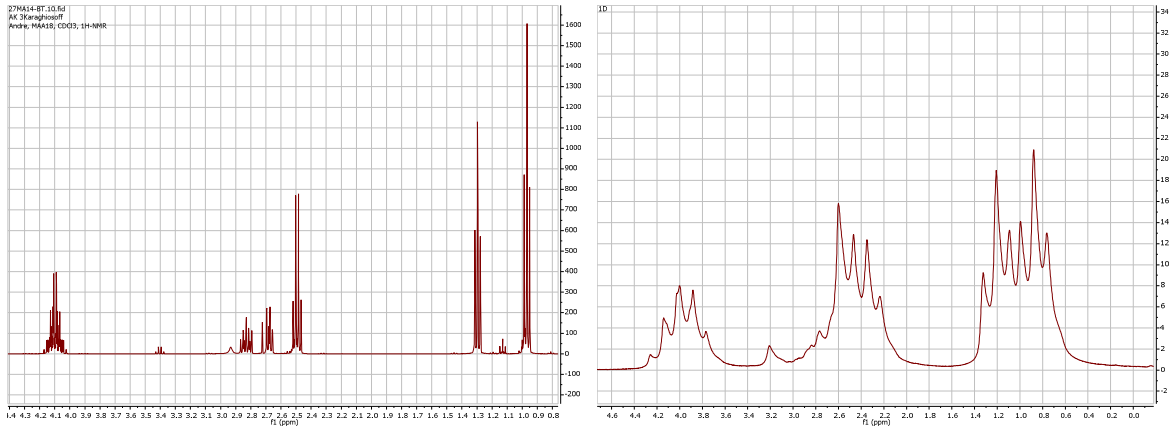

Figure 133: *Comparison of ^{1}H-NMR spectra for the standard instrument (left) and the benchtop NMR instrument (right) for compound* ***IX****.*

In Addition to the one dimensional experiments it is possible to perform two dimensional experiments, like HSQC (Figure 134) or COSY (Figure 135) to further elucidate the structure of the molecule. These experiments of course require longer measurement times, but thus allow an easier interpretation of the molecules. Furthermore, in combination with other two dimensional experiments it would be possible to also analyze mixtures of compounds.

The experiment shown in Figure 134 took 35 minutes to be available in the quality presented. However, the long experimental time is worth to spend since now it is quite easy to identify the number of protons hiding in the preliminary unresolved proton NMR spectrum. It has to be noted that the chemical shift values of the carbon atoms are not matching with

those reported in Figure 133 because the measurement was performed on a benchtop instrument of different field strength. Additionally, the two dimensional experiments also allows to partially better resolve the multiplet splitting patterns.

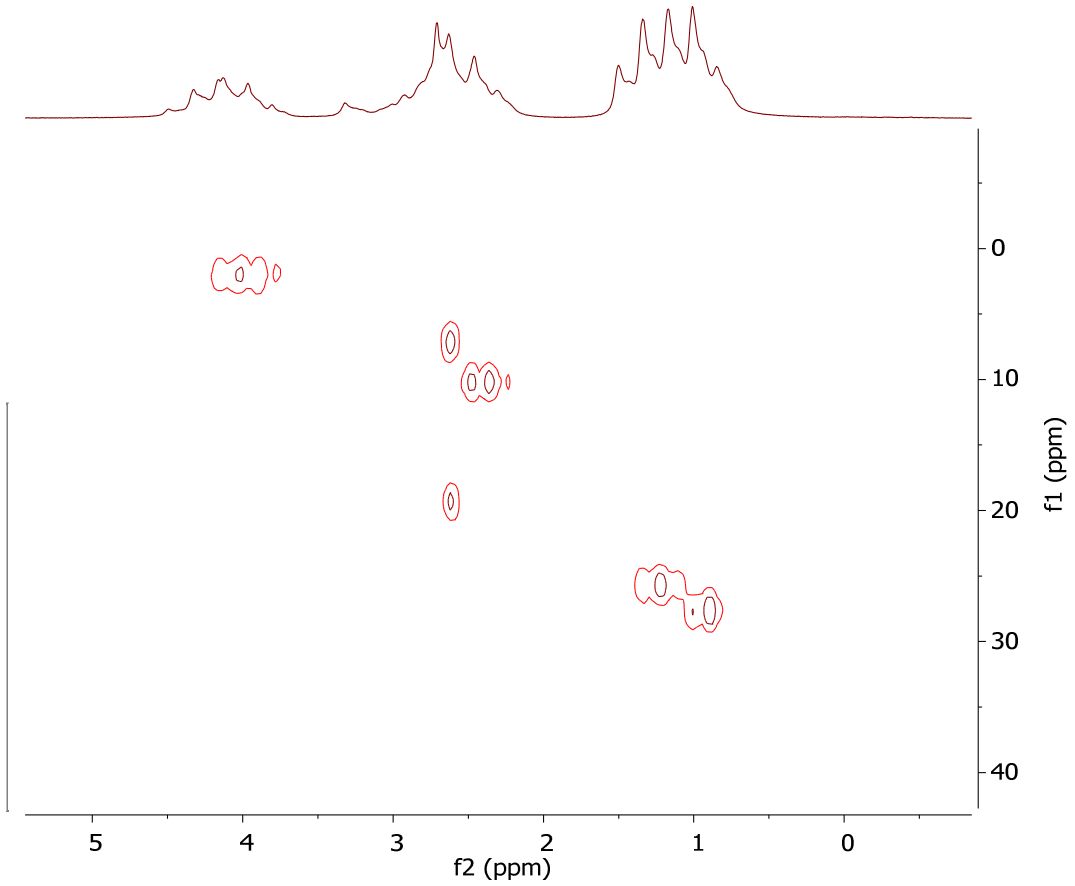

Figure 134: *^{1}H, ^{13}C HSQC NMR spectrum of the benchtop NMR spectrometer of compound* ***X****.*

Other two dimensional techniques like the COSY experiment are performed even within ten minutes and results in a very accurate spectra as can be seen in Figure 135. Here, not only the cross peaks are very well noticeable and even give a better resolution of the one dimensional proton spectra but also the coupling pattern of the protons can be resolved very easily. Furthermore, the number of protons can also be identified as it was the case for the HSQC experiment (Figure 134).

Finally, by a total instrument time of about one hour all necessary spectra are recorded and can be evaluated. Compared to GC-MS or HPLC this seems to be quite a long time, but the main advantage of the NMR experiment is, that especially for pure substances and non-volatiles it offers a very robust technique.

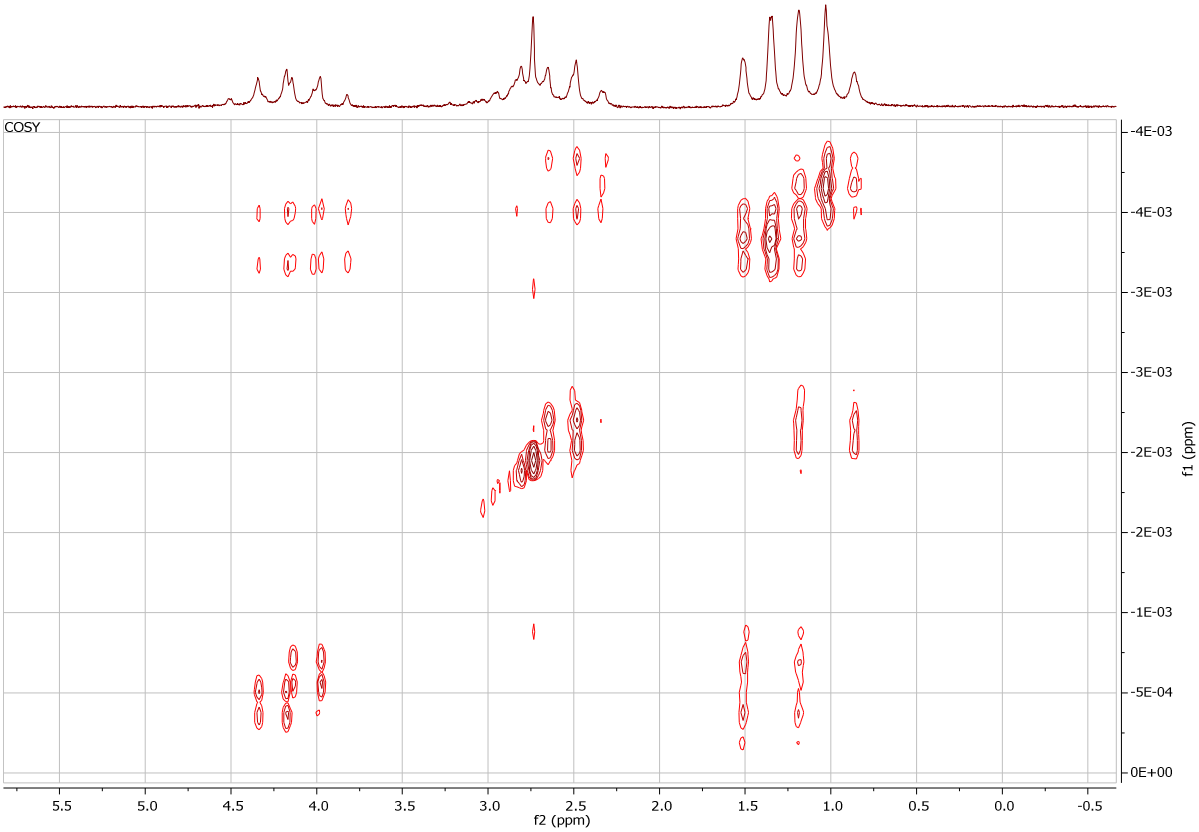

Figure 135: *^{1}H, ^{1}H COSY NMR spectrum of compound **X** obtained by benchtop NMR instrument.*

Furthermore, no derivatization methods have to be applied and by proper choosing the order of the NMR experiments results are obtained very well below one hour, which is imminent in a stressful situation where correct and reliable decisions have to be made by military commanders. Thus, by simply running a one minute ^{31}P NMR experiment all phosphor organic nerve agents can be directly dismissed from the list of potential candidates. Knowing this makes it even easier for the medical personnel to take the proper countermeasures, which in the case of OP poisoning would be needed immediately to be applied to the patients.

Having in mind the potential of the deconvolution algorithm of Prof. Kalthoff, described in chapter 4.3.2.3, the comparatively low resolution of, especially, the proton NMR signals could be enhanced drastically and thus lead to an absolute competitive analytical method for a multitude of applications.

4.10.6 IR and Raman Spectroscopy

The hand-held IR and Raman spectrometer of the Bundeswehr CBRN forces were also used to be challenged with the respective molecules of this study. The results of the Raman spectroscopy measurements with the First Defender are discussed in the individual chapters of the respective compound class. Regarding the obtained IR spectra of the Hazmat ID instrument it has to be noticed that the detector range is the same as of the

laboratory instrument used. This is due to the fact that both instruments are ATR instruments and have an upper limit of detection of 600 cm^{-1}. Furthermore, the spectral resolution of the Hazmat ID is lower compared to a standard laboratory instrument.

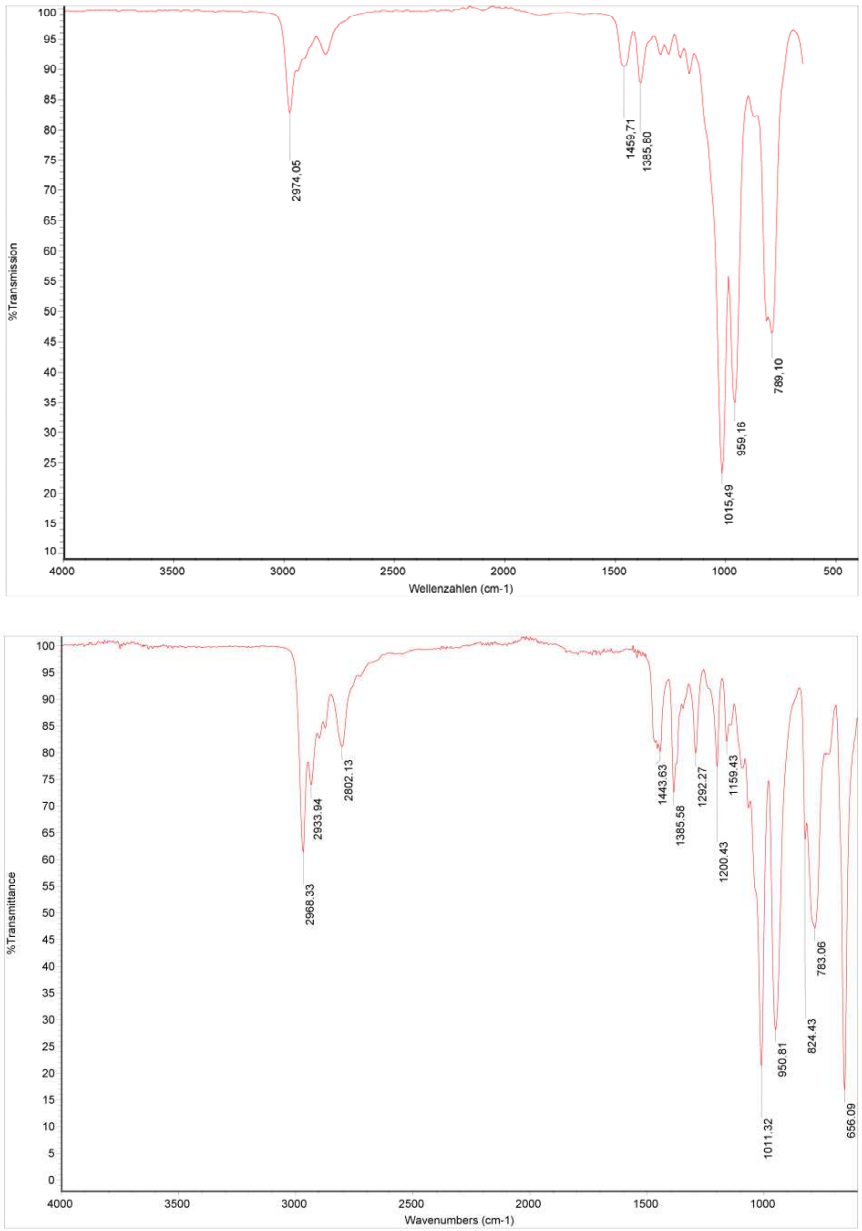

Figure 136: *Comparison of the IR spectra of compound **XIV** obtained by the hand-held Hazmat ID (top) and the standard lab instrument (bottom).*

However, the spectra are expected to look very similar, which can be very nicely seen as an example for compound **XIV** in Figure 136. However, the basic features of the spectra can be identified also with the Hazmat ID and prove the instrument capable of the requested task. The fingerprint region obviously has fewer lines but the main vibrational band at about 790 cm-1 also splits up into the typical doublet structure of the P=S moiety. A further discussion of the instruments performance is dispensable since no additional information

from the Hazmat ID spectra could be obtained. As is true for the laboratory instrument it is most important to have reasonable databases on hands to clearly identify the target molecules and in addition to that well trained users, who are able to interpret the obtained spectra.

4.10.7 Conclusion

The established hand-held devices were not designed to detect the target molecules of this study. Nonetheless, the devices are capable of detecting some of those, due to the underlying general chemical or physical reaction principle which is valid for some target molecules discussed in this study, too. Although the detection devices were designed to specifically detect the molecules included in their library, other compounds with similar behavior in the instrument are monitored as well. Detection in this case does of course not mean identification.

Since the chemical agent test papers react very differently with the tested substances and therefore no trustworthy results are obtained, this method has to be discarded for the general detection of organophosphates. The Dräger test-tubes have a better detection behavior and seem to be a good indicator for the presence of organophosphates, since most of them do have a BuChE inhibiting capacity.

Regarding the IMS-technology the hand-held instruments are useless in the field because their libraries are limited in the number of detectable substances. The cross sensitivity therefore is quite low and false positive results are reduced, whereas on the other hand false negatives are omitted and potentially harmful compounds are detected but not reported on the display of the instrument. This allegedly disadvantage can be overcome by the use of the additional software of the instrument. Thereby it is possible to use the instrument as a lab instrument and the IMS-chromatograms could be used to identify the compounds. Since this is not trivial and identification can only be done by comparing the drift times and not by clearly identifying the resulting peaks, this method is inappropriate for the regular service man in the field. Even in the laboratory the detection needs to be confirmed by measuring the according reference standard, which is most often not available.

Depending on the scenario in the field it is most suitable to take samples of the air and transfer them to an analytical (field)-laboratory. The methods and instruments available there are capable of dealing with the task to clearly identify the (airborne) compounds. Consequently, a necessary prerequisite is that the sampling team did a proper sampling and in the best case used the available hand-held instruments and reported the results of their instruments readings properly.

Furthermore, a more modern device based on flame spectrometry technology, like the Proengine's AP4C[12] should be used, since it is not limited to the detection of substances listed in its database but rather displays whether the compound is comprised of phosphorus, sulfur, arsenic or emits an H-NO molecule when burned in an hydrogen flame. Additionally, this instrument is not limited to vapor phase investigations, but can also examine liquids, dust and solids. Otherwise the established quick indication or detection devices are not able to do a proper detection and new ways and methods for a quick and reliable detection need to be thought of.

Regarding the IR and Raman Spectroscopy technique, both available instruments do record good spectra, which can be compared to a database which still needs to be completed by the addition of non-standard compounds. The most important fact is that the measurement is only as good as the databases are and therefore, since the substances under investigation were not available in the databases, the instruments failed to provide a matching entry and could not identify the analytes. This again shows that it is of great importance to have good databases available for the identification process. However, IR and Raman spectroscopy both offer first information about the analyzed molecule or substance. Both techniques show the characteristic group frequencies and therefore do also make it possible for the user to interpret the spectrum and do a manually identification. This is at least possible for the compound class, if the user knows how to interpret the spectroscopic results and is trained for this purpose. This actually is very rarely the case since most of the operators have only very basic knowledge of chemistry and especially of analytical chemistry itself. So far neither an instruction course for the interpretation for IR or Raman spectra nor a common database of obtained spectra during operations is available within the Bundeswehr. This is the most important issue to be addressed in the future with respect to vibrational spectroscopy techniques.

The first impressions of the possibilities and performance of the benchtop NMR-instruments to me clearly indicates that those machines must be taken into account for future field deployable laboratories as well as for regular analytical labs as the investment costs and the costs for maintenance are dramatically lower compared to high field NMR-instruments. Maybe it is also possible to integrate them into existing recce vehicles like the FOX, which would dramatically increase the analytical capabilities towards the identification of non-volatile liquid substances. Furthermore, the fast exclusion of organophosphates by ^{31}P benchtop NMR experiment within one minute experimental time is even faster than the Dräger Test tube experiment and manifold more trustworthy, that it is of absolute necessity to employ those instruments where possible and reasonable.

[12] http://www.proengin.com/chemical-detection/

5 Outlook and Future Perspective

First of all, the long existing class of Amiton-like molecules is not that well described in the literature compared to other organophosphates and, thus, knowledge is rather not up to date, if not outdated. The recent political developments in the Middle East show that people do not care about existing laws or the rights and well-being of other people. The latest reports show that numerous toxic chemicals and also chemical warfare agents are employed by governments and terrorists alike, making it even more important to be prepared for the worst.

Second, it could be proved that Amiton-like compounds are relatively easy synthesized in good yields and high purities on a lab scale. The scale up from a terrorist's perspective can be assumed to be achieved without great difficulty, since those pesticides were also produced on a large scale. However, the determined inhibitory constants for the investigated compounds show that only Amiton itself has a great inhibitory potential towards AChE. All other compounds showed at least a hundred times lower inhibitory capacity. On the other hand most of the compounds investigated show comparable efficiencies towards the inhibition of BuChE. This fact and the findings of the investigations with hand-held military equipment allow the reasonable conclusion that:

i) the Dräger test tubes based on BuChE inhibition will result in false positive alerts in the sense of being used to detect organophosphorus nerve agents
ii) some of the substances could be used as model substances for training purposes under non-lethal conditions.

Furthermore, the results of the vapor pressure study indicate that by proper choosing of the chemical configuration of the molecules, for example compound **XI** exactly mimics the gas phase behavior of compound **IX**, new simulants could be identified. A clever combination of the observed effects would allow obtaining an ideal test-substance for analytical instruments based on gas-phase detection techniques which is at the same time several orders of magnitude less toxic than the actual nerve agents but still prevails most of the chemical and physical properties of the original poison. Today's test substances are far a way of simulating the actual gas phase behavior, since they are smaller compounds not having the same chemical structures or functional groups and thus are behaving different during the detection and analysis process.

For the first time a whole set of instrumental analytical data for this compound class is reported within this thesis. The investigations with IR and Raman spectroscopy show that these techniques are very suitable for the identification of the phosphorus or thiophosphorus

moiety of the molecule but fail in distinguishing the individual derivatives, because of their close chemical relationship. Moreover, for the majority of the compounds no Raman spectrum can be obtained due to high fluorescence levels of the samples.

A clear identification of the compounds is also hard but not impossible to achieve by means of GC-MS and HPLC-MS. In this particular investigation it was clearly seen that the most prominent fragments in the respective mass spectra result from fragmentations of the nitrogen containing part of the molecule. However, the identification is more complicated if the compound is capable of isomerization *via* thiono-thiol rearrangement, resulting in two more or less independent signals in the gas-chromatogram. Additionally, a comprehensive investigation of the fragmentation was done for almost all OP and OTP compounds allowing clear identification of the compounds in combination with chemical ionization experiments and knowledge of the Kovats indexes.

Additionally, most of the available detection instruments of the Bundeswehr could be challenged with the prepared compounds and a lot of insight into their capabilities was obtained. In general words, to not disclose any classified information, those instruments and devices perform very well and are of great value for the scenarios and tasks they were developed for.

In the meantime, there are also other techniques available on the market which showed also a very excellent performance regarding the detection of Amiton and its derivatives. For example the AP4C based on flame photometry never ran into a false positive or false negative result and was able to detect all of the substances and their precursors alike. Likewise, the miniaturized benchtop NMR instruments are especially useful for a fast and reliable detection and identification of not only the compounds of this study. Furthermore, these benchtop NMR instruments are in some cases superior to classical GC-MS instruments since the NMR experiment very easily allows determining the absolute chemical configuration of the phosphorus atom within minutes. If additionally also fluorine atom would be detected at the same time a very strong hint is given towards the presence of a Schedule 1 compound of the Chemical Weapons Convention. Furthermore, in a first test series parallel to this thesis also several home-made explosives were successfully detected and identified with ease.

The successfully development of this solid-phase microextraction method gives access to a complete new field of sample matrices from the environment for the first time. By the direct immersion mode the limit of detection could be lowered drastically. The described method now needs future evaluation with other chemical warfare agents and over longer periods of time, making it potentially possible to identify the use of forbidden substances by their plant metabolites.

Studies on the thiono-thiol rearrangement resulted in the recognition of two different rate laws for the decay of the thiono isomer and the formation of the thiol isomer for the first time. Additionally, the rate of formation is in all cases of second or pseudo zero order and has the same rate constants for a large number of compounds. Furthermore, the results obtained in this preliminary study should be extended to different catalysts, e.g. $FeCl_3$. The available literature studies are very few and most often report semi-quantitative results.

As further future projects could be identified:

i) Scientifically important tasks
   a. Development of a work-up routine for tertiary amino alcohol synthesis.
   b. Further investigation of the thiono-thiol rearrangement since still no general rule or mechanism could be identified for different compound classes.
   c. Implementation of benchtop NMR instruments in daily lab routines.
   d. Examination of plant metabolites of CWA's in vegetation by means of SPME.
   e. Investigation of the complexation behavior of OP's nerve agents by Lanthanoides.

ii) Military important tasks
   a. Implementation of benchtop NMR in the detection and identification routines of CWA's and HME's by key signals.
   b. Development of NMR spectrometric data bases for CWA's and HME's
   c. Transfer of the developed SPME methodology to the field.
   d. Intensified training of personnel in the units with analytical instruments towards the differentiation of closely related compounds.
   e. Further investigations to prove the identified simulant substances feasible for the application in training scenarios and the evaluation of instruments.

6 Materials and Experimental Procedures

6.1 General Procedures and Analytics

6.1.1 Safety Aspects

Firstly, it has to be mentioned that organophosphorus compounds in general can be extremely toxic to vertebrates and pose a crucial threat to life. As a precaution in the handling of those substances, unless the toxicity values are known or determined, wearing of proper personal safety equipment is mandatory. During the preparation of the organophosphate target molecules butyl-gloves Butoject® 898, which were purchased from Carl Roth, were used. Moreover, all substances were strictly handled in the fume hood unless they were diluted at least by a factor of 1000.

6.1.2 Analytical Methods and Instrumentation

NMR Spectroscopy:

In the analytical department of the LMU different NMR spectrometers were available, of which the following ones were used:

JEOL:

Eclipse 270+ (B = 6.34545 T; 270 MHz),
Eclipse 400+ (B = 9.38977 T; 400 MHz),
ECX 400 (B = 9.39916 T; 400 MHz),

Bruker:

AV400 (B = 9.4 T; 400 MHz),
AV400TR (B = 9.4 T; 400 MHz)

Nucleus	**Standard**	**Frequency [MHz]**				
	(δ = 0.00 ppm)	J270	J400	J400e	AV400	AV400TR
^{1}H	Me_4Si	270.17	399.78	400.18	400.18	400.13
^{13}C	Me_4Si	67.94	100.53	100.63	100.64	100.62
^{31}P	H_3PO_4 (85 %)	109.37	161.83	161.99	162.00	161.98

Unless otherwise noted, spectra were recorded at room temperature. Standards for the measurements were applied externally. Data processing and evaluation of the obtained spectra was done by MestreNova 10.0 Software.

IR Spectroscopy:

The IR Spectra were recorded on a spectrum one FT-IR spectrometer from Perkin Elmer, equipped with a Golden Gate ATR™ unit from Specac. The spectra were recorded from 600 to 4000cm^{-1}. As a rule, before and after each measurement a blank was taken and 4 spectra were accumulated to give a good average. To process the data, the OMNIC 8 Software from Thermo Scientific™ was used.

Raman Spectroscopy:

The Raman spectra were recorded on a First Defender RMX instrument from Analyticon. Generally, a blank was taken before and after each measurement. For data processing, the OMNIC 8 Software from Thermo Scientific™ was used.

GC-MS/MS:

A Thermo Scientific™ Trace GC 1310 with PTV injector and an Agilent J&W GC-column (CP-Sil 8 CB Low Bleed/MS, 30m 0.25µm), Triplus RSH™ auto sampler and TSQ Duo triple quadrupole mass spectrometer was used. Chromeleon™ 7.2 Chromatography Management Software was used for system control and data processing. For fragmentation studies the AutoSRM Software from Thermo Scientific™ was used.

Measurement conditions are: oven temperature of 70°C held for one minute, ramped with 30°C/min to 280°C and held again for one minute. Total run time: 9 minutes. Split ratio 1/50, injection volume 1µl and concentration injected: 10 ppm.

GC-MS:

For regular GC-MS measurements either the GC-MS/MS system described above was used in single quadropole mode or a Varian CP 38 gas chromatograph with Saturn 2000 MS ion trap instrument, capable of electronic and chemical ionization, was used. All instruments were equipped with an Agilent J&W GC-column (CP-Sil 8 CB Low Bleed/MS, 30m 0.25µm). Chromeleon™ 7.2 Chromatography Management Software was used for system control and data processing in case of the quadrupole instrument or Varian MS Workstation Version 6.42 respectively for the Varian instrument.

Measurement conditions are: oven temperature of 70°C held for one minute, ramped with 30°C/min to 280°C and held again for one minute. Total run time: 9 minutes. Split ratio 1/50, injection volume 1µl and concentration injected: 10 ppm.

GC-FID:

A Thermo Scientific™ Trace GC 1310 with PTV Injector; FID module and Triplus RSH™ auto sampler was used. The instrument was equipped with an Agilent J&W GC-column (CP-Sil 8 CB Low Bleed/MS, 30m 0.25µm). Chromeleon™ 7.2 Chromatography Management Software was used for system control and data processing. Measurement conditions are: oven temperature of 70°C held for one minute, ramped with 30°C/min to 280°C and held again for one minute. Total run time: 9 minutes. Split ratio 1/50, injection volume 1µl and concentration injected: 10 ppm.

HPLC-DAD-ESI-MS:

Separations were performed on a modular DIONEX UltiMate™ 3000HPLC System (Thermo Scientific*TM) equipped with a SRD-3400 (4-channel degasser) Solvent Racks, HPG-3400SD gradient pump, WPS-3000TSL (Analytical) auto sampler, TCC-3000SD column oven, DAD-3000 Photometer , MSQ-Plus mass detector. An Accucore RP-MS column (3.0 x 150.0 mm, particle size 2.6 µm Thermo Scientific™ Part.No.17626-153030) was used for separation. Chromeleon™ 7.2 Chromatography Management Software was used for system control and data processing. The employed gradient is shown in Figure 137. Unless otherwise noted the following conditions were applied on the instrument:

Mobile Phase:	Eluent A: 95/5 water/Methanol + 0.1Vol% formic acid
	Eluent B: 5/95 Water/Methanol + 0.1Vol%formic acid
Flow:	0.3ml/min
Run Time:	20 min
Injection Volume:	5µl
Sample Temp:	20°C
Column Temp:	30°C
MS-Detector:	Mass Range: 50-350m/z
	Time Range: 1.00-20.00min
	Peak Format: Centroid
	Scan Time: 0.3s
	Polarity: +ve
	Cone Voltage: FS 1: 80V, FS 2 50V, FS 3: 30V

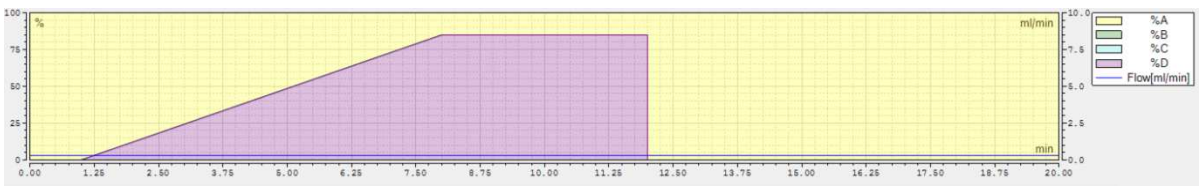

Figure 137: *Standard gradient as employed during the HPLC measurements. Eluent A=95/5 Water/Methanol + 0.1 Vol% formic acid, Eluent B: 5/95 Water/Methanol + 0.1 Vol% formic acid.*

X-Ray Single Crystal Structure Analysis:

For X-Ray single crystal structure measurements an Oxford Xcalibur 3 diffractometer equipped with a Spellman generator (voltage: 50 kV, current: 40 mA) and a Kappa CCD detector from Oxford Diffraction was used. The X-ray wavelength was the one of Mo-K_α with λ = 0.71073 Å. The crystals were prepared on an object slide in a drop of perfluorinated oil (KEL-F®). With the help of a polarization microscope a suitable single crystal was carefully chosen and directly mounted on top of a thin glass wire which was attached to the goniometer head of the diffractometer while the sample cooling was running.

Data acquisition was done by CrysAlis CCD software [305] and data reduction was achieved by CrysAlis RED software.[306] Absorption correction using the SCALE3 ABSPACK multiscan method was applied [307]. Structures were solved with SHELXS-97 software [308], refined by SHELXL-97 [309] and SHELXL [310] in the last step and finally checked finally by PLATON software.[311-313] Heavy atoms were refined anisotropically and hydrogen atoms were placed on ideal positions and isotropically refined. Necessary absorption corrections were achieved by using SCALE3 ABSPACK multiscan method. Finally, the obtained cif-files were checked by the online available checkCIF-Service of the International Union of Crystallography.[13] The Mercury program version 3.9 [314] and Ortep for windows [313] were used to prepare the drawings of the crystal structure. All programs were embedded in the WINGX software.[313]

Elemental Analysis:

Samples to determine the elemental composition regarding carbon, hydrogen, oxygen, sulfur and nitrogen were handed over to the central analytical department of the chemistry department of the LMU. The available instruments there were a: vario el and a vario micro from elementar.

Refractive Index Measurements:

Refractive Index measurements were executed on an Abbe-refractometer equipped with a tempered water bath. Unless otherwise noted, all measurements were executed at 20°C and are uncorrected.

Melting Point Measurements:

Melting Points were recorded either on a Büchi B-545 melting point apparatus and are uncorrected or on a Linseis PT-10 instrument at a heating rate of 5°C/min.

[13] http://checkcif.iucr.org/

6.2 Materials

Unless otherwise noted, all chemicals, reagents, and materials were obtained from commercially available suppliers and were used without further purification. All organic extracts were dried over anhydrous sodium sulfate and filtrated through a POR 2 filter; remaining solvents were evaporated with a Büchi rotary evaporator at the corresponding reduced pressure. Yields are reported with respect to the limiting reagent of the respective reaction.

6.3 Synthesis and Characterization of Amino Alcohol-Precursors

General Procedure for Derivatization GC/MS with MBTFA

In a 1ml micro reaction vessel 200µl of dichloromethane and 200µl of MBTFA were added. To this mixture 2µl of the respective amino alcohol was added. A slight formation of smoke upon the addition of the amino alcohol was observed. The reaction mixture was incubated at 50°C for 30 minutes and afterwards diluted to the proper concentration to be processed by the GC/MS system.

***N,N*-Diethylpropanolamine (I)**

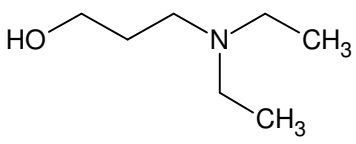

Lithium hydride (0.59 g, 0.075 mol) was weighed into a 100ml three-neck round-bottom flask under nitrogen atmosphere. 50 ml of anhydrous Tetrahydrofuran were added and the reaction vessel was equipped with a condenser. 3-Amino-1-propanol (2.81 g, 0.037 moles) was slowly added while the mixture was stirred. The solution changed its color from grey to bright yellow to almost transparent, which coincides with the end of hydrogen formation, with self-heating of the mixture. Iodoethane (11.67 g, 0.075 mol) was added dropwise and the mixture was stirred for another hour during which the color changed from orange to reddish-brown. The reaction was quenched with methanol (3 ml) and sodium hydroxide (1N, 25 ml) and afterwards extracted three times with diethylether (5 ml each), dried over anhydrous sodium sulfate and the solvent was removed by rotary evaporation, resulting in a yellowish liquid.

Yield: 2.22 g, 0.017 mol (45.9%)

EA: calc.: C(64.07%), H(13.06%), N(10,67%)
found: C(60.82%), H(12.39%), N(9.78%)

NMR: *cf.* Table 6

***N,N*-Diethylbutanolamine (II)**

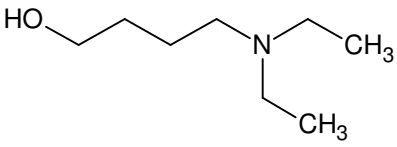

Lithium hydride (0.79 g, 0.100 mol) was weighed into a 100ml three-neck round-bottom flask under nitrogen atmosphere. 50 ml of anhydrous Tetrahydrofuran were added and the reaction vessel was equipped with a condenser. 4-Amino-1-butanol (3.59 g, 0.039 mol) was slowly added while the mixture was stirred. The solution changed color from grey to bright yellow to almost transparent, which coincides with the end of hydrogen formation, with self-heating of the mixture. Iodoethane (15.08 g, 0.095 mol) was added dropwise and the mixture was stirred for another hour during which the color changed from orange to reddish-brown. The reaction was quenched with methanol (3 ml) and sodium hydroxide (1N, 25 ml) and afterwards extracted three times with diethylether (5 ml each), dried over anhydrous sodium sulfate and the solvent was removed by rotary evaporation, resulting in a yellowish liquid.

Yield: 2.61 g, 0.018 mol (45.0%)

EA: calc.: C(66.16%), H(13.19%), N(9.64%)

found: C(31.29%), H(11,82%); N(5,36%)

NMR: *cf.* Table 6

***N,N*-Diethylpentanolamine (III)**

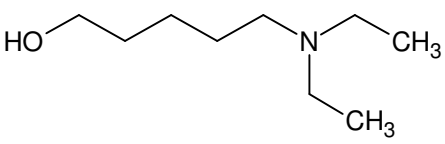

Lithium hydride (0.46 g, 0.058 mol) was weighed into a 100ml three-neck round-bottom flask under nitrogen atmosphere. 25 ml of anhydrous Tetrahydrofuran were added and the reaction vessel was equipped with a condenser. 5-Amino-1-pentanol (2.91 g, 0.028 mol) was slowly added while the mixture was stirred. The solution changed color from grey to bright yellow to almost transparent, which coincides with the end of hydrogen formation, with self-heating of the mixture. Iodoethane (9.30 g, 0.060 mol) was added dropwise and the mixture was stirred for another hour during which the color changed from orange to reddish-brown. The reaction was quenched with methanol (3 ml) and sodium hydroxide (1N, 25 ml) and afterwards extracted three times with diethylether (5 ml each), dried over anhydrous sodium sulfate and the solvent was removed by rotary evaporation, resulting in a yellowish liquid.

Yield: 3.37 g, 0.021 mol (74.9%)

b.p.: 107-112°C at 0.2 mbar

EA: calc.: C(67.87%), H(13.29%), N(8.79%)

found: C(64.77%), H(13.05%), N(12.06%)

NMR: *cf.* Table 6

***N,N*-Diisopropylpropanolamine (IV)**

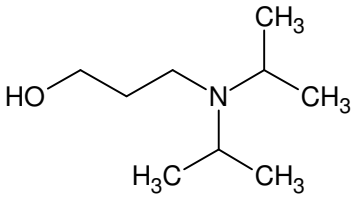

Lithium hydride (0.46 g, 0.058 mol) was weighed into a 100 ml three-neck round-bottom flask under nitrogen atmosphere. 25 ml of anhydrous Tetrahydrofuran were added and the reaction vessel was equipped with a condenser. 3-Amino-1-propanol (2.19 g, 0.029 mol) was slowly added while the mixture was stirred. The solution changed color from grey to bright yellow to almost transparent, which coincides with the end of hydrogen formation, with self-heating of the mixture. 2-Iodopropane (10.24 g, 0.060 mol) was added dropwise and the mixture was stirred for another hour during which the color changed from orange to reddish-brown. The reaction was quenched with methanol (3 ml) and sodium hydroxide (1N, 25 ml) and afterwards extracted three times with diethylether (5 ml each), dried over anhydrous sodium sulfate and the solvent was removed by rotary evaporation, resulting in a yellowish liquid.

Yield: 1.95 g, 0.012 mol (42.31%)

EA: calc.: C(67.87%), H(13.29%), N(8.79%)

found: C(34.30%), H(7.33%), N (34,30%)

NMR: not obtained

***N,N*-Diisopropylbutanolamine (V)**

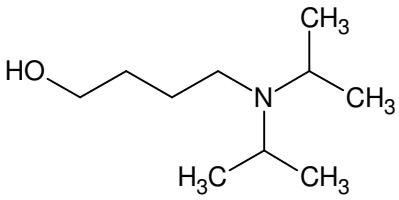

Lithium hydride (0.55 g, 0.069 mol) was weighed into a 100 ml three-neck round-bottom flask under nitrogen atmosphere. 25 ml of anhydrous tetrahydrofuran were added and the reaction vessel was equipped with a condenser. 4-amino-1-butanol (3.33 g, 0.037 mol) was slowly added while the mixture was stirred. The solution changed color from grey to bright yellow to almost transparent, which coincides with the end of hydrogen formation, with self-heating of the mixture. 2-Iodopropane (12.43 g, 0.073 mol) was added dropwise and the mixture was stirred for another hour during which the color changed from orange to reddish-brown. The reaction was quenched with methanol (3 ml) and sodium hydroxide (1N, 25 ml) and afterwards extracted three times with diethylether (5 ml each), dried over anhydrous sodium sulfate and the solvent was removed by rotary evaporation, resulting in a yellowish liquid

Yield: 1.95 g, 0.012 mol (42.31%)

EA: calc.: C(67.87%), H(13.29%), N(8.79%)

found: C(8.69%), H(10.97%), N(8.69%)

NMR: not obtained

***N,N*-Dimethylpentanolamine (VI)**

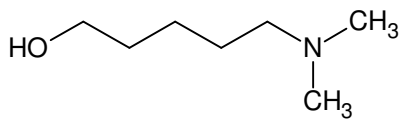

Lithium hydride (0.42 g, 0.053 mol) was weighed into a 100 ml three-neck round-bottom flask under nitrogen atmosphere. 50 ml of anhydrous Tetrahydrofuran were added and the reaction vessel was equipped with a condenser. 5-Amino-1-pentanol (3.13 g, 0.030 mol) was slowly added while the mixture was stirred. The solution changed its color from grey to bright yellow to almost transparent, which coincides with the end of hydrogen formation, with self-heating of the mixture. Iodomethane (4.66 g, 0.033 mol) was added dropwise and the mixture was stirred for another hour during which the color changed from orange to reddish-brown. The reaction was quenched with methanol (3 ml) and sodium hydroxide (1N, 25 ml) and afterwards extracted three times with diethylether (5 ml each), dried over anhydrous sodium sulfate and the solvent was removed by rotary evaporation, resulting in a yellowish liquid.

Yield: 1.968 g, 0.015 mol (49.5%)

EA: calc.: C(64.07%), H(13.06%), N(10.67%)

found: C(51.08%), H(11.94%), N(10.61%)

NMR: *cf.* Table **7**

***N,N*-Diphenylethanolamine (VII)**

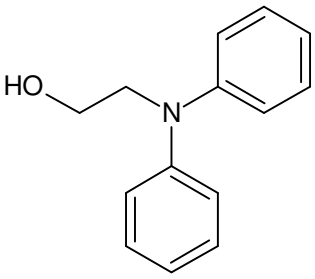

Preparation of Copper(I) chloride as catalyst: Copper(II) chloride dihydrate (6.80 g, 0.040 mol) and Ascorbic acid (10.10 g, 0.057 mol) were dissolved in distilled water (50 ml each) combined and refluxed for one hour. The resulting fine white powder was filtered off under nitrogen atmosphere to prevent oxidation, washed with diethylether to remove water, and dried under reduced pressure. Yield: 3.40 g, 0.034 mol (85.86%).

To the freshly prepared Copper(I) chloride (0.10 g, 0.001 mol) Potassium hydroxide (2,50 g, 0.046 mol) and Iodobenzene (4.19 g, 0.20 mol) were given and the mixture was secured under nitrogen atmosphere. By carefully adding Ethanolamine (1.82 g, 0.030 mols) the temperature of the reaction mixture increased from ambient temperature to 50°C due to the exothermic nature of the reaction. During this the color turned from a light dark green to a dark brown, almost black color. The mixture was quenched and diluted with distilled water (15 ml) and extracted three times with ethyl Acetoacetate (5 ml each), dried over anhydrous Sodium sulfate and the solvent was removed by rotary evaporation, resulting in a dark liquid.

Yield: 3.34 g, 0.016 mol (76.20%)

GC: KI = 962.64

EA: calc.: C(78.84%), H(7.09%),N(6.57%)

found: C(64.69%), H(7.26%),N(9.62%)

NMR: *cf.* Table **7**

6.4 Synthesis and Characterization of Dialkylchloro(thio)phosphate Precursors

***S,S*-Diethyl phosphorochloridodithioate (VIII)**

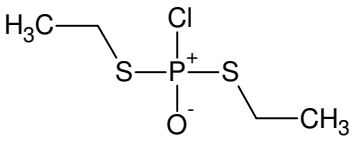

Option A: Dried pyridin (87 ml, 0.97 mol) and mercapto ethanol (78 ml, 1.1 mol, dissolved in 100 ml of dried benzene were added dropwise to a solution of phosphoric trichloride (50 ml, 0.54 mol) in 200 ml of dried benzene in a two-neek round-bottom flask under a nitrogen blanket. The reaction mixture was kept below 20°C and stirred for three hours. The formed pyridine hydrochloride was filtered of and washed twice with fresh dry benzene. Benzene and remaining phosphoric trichloride were rotary evaporated yielding in a bright yellowish solution which turned into a dark reddish violet upon storage at 2°C overnight. Pyridine, mercapto ethanole and the resulting products were separated by vacuum distillation. Fraction I was pyridine boiling at 30-32°C at 25 mbar, fraction II was found to be mercapto ethanole boiling at 74-76°C at 2 mbar, fraction III was the mono thiolated isomer boiling at 90-94°C at 0.7 mbar and fraction IV was verified as the product boiling at 107-112°C at 0.2 mbar

Yield: 6.69 g, 0.033 mol (6.1%)
b.p.: 107-112°C at 0.2 mbar

Option B: Aluminium chloride (13.19 g, 0.099 mol) was dispensed in Phosphorus trichloride (14,26 g, 0.104 mol) which was chilled with an ice bath to 0°C. After the dropwise addition of Diethyl disulfide (12.20 g, 0.100 mol) was finished the mixture was stirred at ambient temperature for 7 hours. The reaction product was poured onto crushed ice (100 g) and concentrated Hydrochloric acid (25 ml) was added carefully. The resulting suspension was extracted three-times with Dichloromethane (20ml each) and the resulting Dichloromethane extract was extracted three-times with 5% Hydrochloric acid (5 ml each) and was immediately dried over anhydrous Sodium sulfate. The solvent was removed by rotary evaporation and the crude product purified by vacuum distillation yielding a colorless clear liquid.

Yield: 12.56 g, 0.061 mol (62.0%)
EA: calc.: C(23.47%), H(4.92%), S(31.33)
found: C(24.92%), H(5.32%), S(33.24)
NMR: *cf.* Table 9

6.5 Synthesis and Characterization of Organophosphorus Compounds

***O*,*O*-Diethyl *O*-[2-(diethylamino)ethyl] phosphorothioate (IX)**

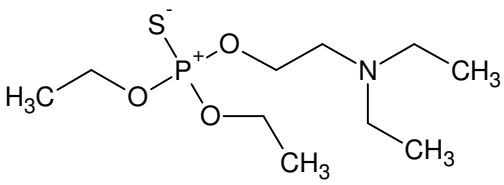

Sodium hydride(1.44 g, 0.060 mol) was weighed into a 100 ml three-neck round-bottom flask under nitrogen atmosphere. 40ml of anhydrous benzene were added and the solution was stirred and refluxed. Carefully 2-(diethylamino) ethanol (6.89 g, 0.059 mol) was added dropwise to the solution. Upon the formation of 2-(diethylamino) ethanolate anion the solution turned almost transparent. The reaction mixture was cooled on an ice bath and O,O'-diethyl chlorothiophosphate (10.82 g, 0.057 mol) was added dropwise. The reaction mixture was allowed to warm to room temperature till the next day and was carefully extracted three-times with distilled water of pH 2. Then ammonia solution (8% v/v) was added to this fraction until a pH value of >10 was reached. This solution was washed three-times with 5 ml of Diethyl ether, dried over anhydrous Sodium sulfate and the solvent was removed by rotary evaporation, resulting in a slightly yellowish liquid.

Yield: 14.35 g, 0.053 mol (90.3%)

EA: calc.: C(44.59%), H(8.98%), N(5.20%), S(11.90%)

found: C(44.62%), H(9.01%), N(5.23%), S(11.94%)

NMR: *cf.* Table 12 and Table 14

***O*,*O*-Diethyl *S*-[2-(diethylamino)ethyl] phosphorothioate (Amiton, VG) (X)**

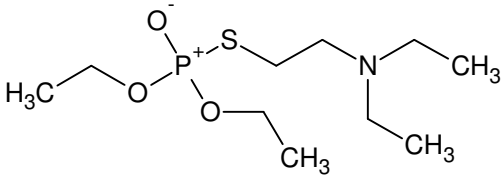

2-(Diethylamino) ethanethiol hydrochloride (9.42 g, 0.056 mol) was added to ammonia-solution (20 ml, 8% v/v) to yield the free base. The mixture was extracted three times with diethylether (5 ml), dried over anhydrous sodium sulfate and rotary evaporated. Sodium hydride (1.04 g, 0.043 mol) was weighed into a 100 ml three-neck round-bottom flask under nitrogen atmosphere. 40ml of anhydrous benzene were added and the solution was stirred and refluxed. Carefully 2-(diethylamino) ethanethiol (5.73 g, 0.043 mol) was added dropwise to the solution. Upon the formation of 2-(diethylamino) ethanethiolate anion the solution turned transparent. The reaction mixture was cooled on an ice bath and O,O'-diethyl chlorophosphate (7.85 g, 0.042 mol) was added dropwise. The reaction mixture was allowed to warm to room temperature till the next day and was carefully extracted with distilled water of pH 2. Then ammonia solution (8% v/v) was added

to this fraction until a pH value of 10 was reached. This solution was washed three-times with 5 ml of diethyl ether, dried over anhydrous sodium sulfate and the solvent was removed by rotary evaporation. The resulting slightly yellowish liquid was further purified by vacuum distillation.

Yield: 7.16 g, 0.027 mol (61.79%)
b.p.: 91.5°C at 0.007 hPa
RI: nD20 = 1.4668
EA: calc.: C(44.59%), H(8.98%),N(5.20%), S(11.90%)
found: C(44.51%), H(8.97%),N(5.39%), S(12.08%)
NMR: *cf.* Table 12 and Table 14

***O,O*-Diethyl O-[2-(diethylamino)ethyl] phosphate (XI)**

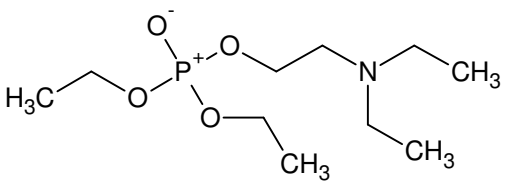

Sodium hydride (1.13 g, 0.047 mol) was weighed into a 100 ml three-neck round-bottom flask under nitrogen atmosphere. 40 ml of anhydrous benzene were added and the solution was stirred and refluxed. Carefully 2-(diethylamino) ethanol (5.61 g, 0.048 mol) was added dropwise to the solution. Upon the formation of 2-(diethylamino) ethanolate anion the solution turned transparent. The reaction mixture was cooled on an ice bath and O,O'-diethyl chlorophosphate (8.10 g, 0.047 mol) was added dropwise. The reaction mixture was allowed to warm to room temperature till the next day and was carefully extracted with distilled water of pH 2. Then ammonia solution (8% v/v) was added to this fraction until a pH value of 10 was reached. This solution was washed three times with 5 ml of diethyl ether, dried over anhydrous sodium sulfate and the solvent was removed by rotary evaporation, resulting in a slightly yellowish liquid.

Yield: 5.04 g, 0.025 mol (52.8%)
EA: calc.: C(46.48%), H(9.55%), N(5.53%)
found: C(45.86%), H(9.54%), N(5.71%)
NMR: *cf.* Table 12 and Table 15

***O*-[2-(Diethylamino)ethyl] *S,S*-diethyl phosphorodithioate (XII)**

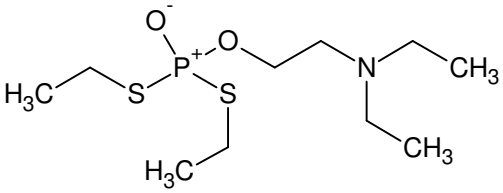

Sodium hydride (0.69 g, 0.029 mol) was weighed into a 100 ml three-neck round-bottom flask under nitrogen atmosphere. 40 ml of anhydrous benzene were added and the solution was stirred and

refluxed. Carefully 2-(diethylamino) ethanol (3.54g, 0.030 mol) was added dropwise to the solution. Upon the formation of 2-(diethylamino) ethanolate anion the solution turned transparent. The reaction mixture was cooled on an ice bath and *S,S'*-diethyl phosphorochloridodithioate (2.86 g, 0.014 mol) was added dropwise. The reaction mixture was allowed to warm to room temperature till the next day and was carefully extracted with distilled water of pH 2. Then ammonia solution (8% v/v) was added to this fraction until a pH value of 10 was reached. This solution was washed three times with 5 ml of diethyl ether, dried over anhydrous sodium sulfate and the solvent was removed by rotary evaporation, resulting in a slightly yellowish liquid.

Yield: 1.6843 g, 0.059 mol (42.3%)
EA: calc.: C(42.08%), H(8.48%), N(4.91%), S(22.47%)
found: C(49.07%), H(8.48%), N(8.15%), S(10.19%)
NMR: *cf.* Table 12 and Table 16

_S_-[2-(diethylamino)ethyl] _S,_S-diethylphosphorotrithioate (XIII)

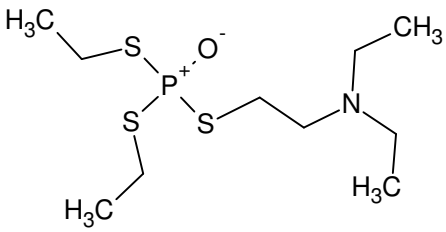

Sodium hydride (0.91 g, 0.038 mol) was weighed into a 100 ml three-neck round-bottom flask under nitrogen atmosphere. 40 ml of anhydrous benzene were added and the solution was stirred and refluxed. Carefully 2-(diethylamino) mercaptoethanol (3.02 g, 0.023 mol) was added dropwise to the solution. Upon the formation of 2-(diethylamino) mercaptoethanolate anion the solution turned transparent. The reaction mixture was cooled on an ice bath and *S,S*-ddiethyl phosphorochloridodithioate (4.68 g, 0.023 mol) was added dropwise. The reaction mixture was allowed to warm to room temperature till the next day and was carefully extracted with distilled water of pH 2. Then ammonia solution (8% v/v) was added to this fraction until a pH value of 10 was reached. This solution was washed three times with 5 ml of diethyl ether, dried over anhydrous sodium sulfate and the solvent was removed by rotary evaporation, resulting in a slightly yellowish liquid.

Yield: 3.8892 g, 0.013 mol (56.83%)
EA: calc.: C(39.84%), H(8.02%), N(4.65%), S(31.91%)
found: C(41.29%), H(8.39%), N(5.24%), S(30.77%)
NMR: *cf.* Table 12 and Table 16

O,O-Diethyl *S*-[2-(diethylamino)ethyl] phosphorodithioate (XIV)

2-(Diethylamino) ethanethiol hydrochloride (6.02 g, 0.028 mol) was added to ammonia-solution (20 ml, 8% v/v) to yield the free base. The mixture was extracted three times with diethylether (5 ml each), dried over anhydrous sodium sulfate and rotary evaporated. The yield was 3,82 g or 0.023 mol (82.4%).

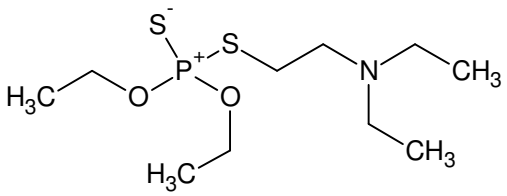

Sodium hydride (0.81 g, 0.034 mol) was weighed into a 100 ml three-neck round-bottom flask under nitrogen atmosphere. 40ml of anhydrous benzene were added and the solution was stirred and refluxed. Carefully the freshly prepared 2-(diethylamino) ethanethiol (3.81 g, 0.029 mol) was added dropwise to the solution. Upon the formation of 2-(diethylamino) ethanethiolate anion the solution turned transparent. The reaction mixture was cooled on an ice bath and O,O'-diethyl chlorothiophosphate (6.03 g, 0.031 mol) was added dropwise. The reaction mixture was allowed to warm to room temperature till the next day and was carefully extracted with distilled water of pH 2. Then ammonia solution (8% v/v) was added to this fraction until a pH value of 10 was reached. This solution was washed three-times with 5 ml of diethyl ether, dried over anhydrous sodium sulfate and the solvent was removed by rotary evaporation. The resulting slightly yellowish liquid was further purified by distillation.

Yield: 4.50 g, 0.016 mol (54.87%)

EA: calc.: C(42.08%), H(8.48%), N(4.91%), S(22.47%)
found: C(44.76%), H(9.20%), N(6.15%), S(22.51%)

NMR: *cf.* Table 12 and Table 15

O,O-Diethyl *O*-[2-(diethylamino)propyl] phosphorothioate (XV)

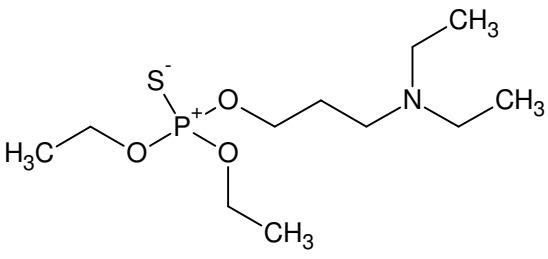

Sodium hydride (0.23 g, 0.009 mol) was weighed into a 100 ml three-neck round-bottom flask under nitrogen atmosphere. 20 ml of anhydrous benzene were added and the solution was stirred and refluxed. Carefully 3-diethylamino-1-propanol (1.19 g, 0.009 mol) was added dropwise to the solution. Upon the formation of 3-diethylamino-1-propanolate anion the solution turned almost transparent. The reaction mixture was cooled on an ice bath and O,O'-diethyl chlorothiophosphate (1.77 g, 0.009 mol) was added dropwise. The reaction mixture was allowed to warm to room temperature till the next day and was carefully extracted three-times with distilled water of pH 2. Then ammonia solution (8% v/v) was added to this fraction until a pH value of >10 was reached. This solution was washed

three-times with 5 ml of diethyl ether, dried over anhydrous sodium sulfate and the solvent was removed by rotary evaporation, resulting in a slightly yellowish liquid.

Yield: 1.62 g, 0.006 mol (63.1%)

EA: calc.: C(46.62%), H(9.25%), N(4.94%), S(11.32%)

found: C(47.21%), H(9.67%), N(5.06%), S(11.10%)

NMR: *cf.* Table 12 and Table 17

_O_,_O_-Diethyl _O_-[2-(diethylamino)butyl] phosphorothioate (XVI)

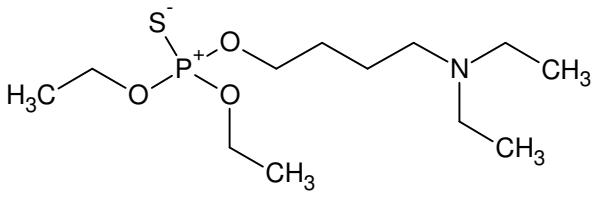

Sodium hydride (0.37 g, 0.015 mol) was weighed into a 100 ml three-neck round-bottom flask under nitrogen atmosphere. 40 ml of anhydrous benzene were added and the solution was stirred and refluxed. Carefully 4-dietylamino-1-butanol (1.49 g, 0.010 mol) was added dropwise to the solution. Upon the formation of 4-(diethylamino) butanolate anion the solution turned almost transparent. The reaction mixture was cooled on an ice bath and O,O'-Diethyl chlorothiophosphate (2.50 g, 0.013 mol) was added dropwise. The reaction mixture was allowed to warm to room temperature till the next day and was carefully extracted three-times with distilled water of pH 2. Then ammonia solution (8% v/v) was added to this fraction until a pH value of >10 was reached. This solution was washed three-times with 5 ml of diethyl ether, dried over anhydrous sodium sulfate and the solvent was removed by rotary evaporation, resulting in a slightly yellowish liquid.

Yield: 0.23 g, 0.001 mol (10.0%)

EA: calc.: C(48.46%), H(9.47%), N(4.71%), S(10.78%)

found: C(50.45%), H(10.04%), N(4.63%), S(10.13%)

NMR: not obtained

_O_,_O_-Diethyl _O_-[2-(diethylamino)pentyl] phosphorothioate (XVII)

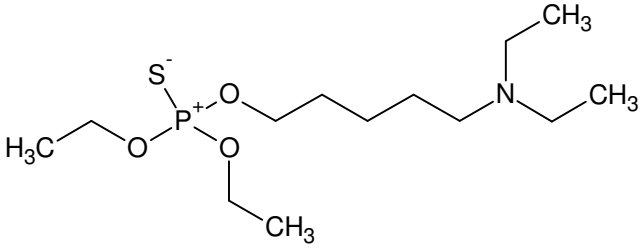

Sodium hydride (0.01 g, 4.27 mmol) was weighed into a 100 ml three-neck round-bottom flask under nitrogen atmosphere. 40 ml of anhydrous benzene were added and the solution was stirred and refluxed. Carefully 5-Dietylamino-1-pentanol (0.46 g, 2.87 mmol) was added dropwise to the solution. Upon the formation of 5-diethylamino-1-

pentanolate anion the solution turned almost transparent. The reaction mixture was cooled on an ice bath and O,O'-diethyl chlorothiophosphate (0.56 g, 2.97 mmol) was added dropwise. The reaction mixture was allowed to warm to room temperature and was carefully extracted three-times with distilled water of pH 2. Then ammonia solution (8% v/v) was added until a pH value of >10 was reached. This solution was washed three-times with 5 ml of diethyl ether, dried over anhydrous sodium sulfate and the solvent was removed by rotary evaporation, resulting in a yellowish liquid.

Yield: 1.30 g, 1.30 mmol (45.3%)

EA: calc.: C(50.14%), H(9.71%), N(4.50%), S(10.30%)

found: C(50.45%), H(10.04%), N(4.63%), S(10.13%)

NMR: *cf.* Table 12 and Table 17

***O,O*-Diethyl *O*-[2-(dimethylamino)ethyl] phosphorothioate (XVIII)**

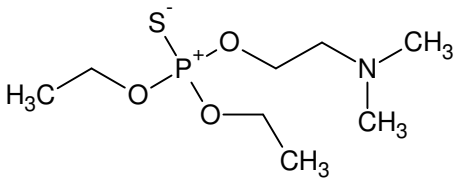

Sodium hydride (0.85 g, 0.035 mol) was weighed into a 100 ml three-neck round-bottom flask under nitrogen atmosphere. 40 ml of anhydrous benzene were added and the solution was stirred and refluxed. Carefully 2-(dimetylamino) ethanol (3.14 g, 0.035 mol) was added dropwise to the solution. Upon the formation of 2-(dimethylamino) ethanolate anion the solution turned almost transparent. The reaction mixture was cooled on an ice bath and O,O'-diethyl chlorothiophosphate (6.85 g, 0.035 mol) was added dropwise. The reaction mixture was allowed to warm to room temperature till the next day and was carefully extracted three-times with distilled water of pH 2. Then ammonia solution (8% v/v) was added to this fraction until a pH value of >10 was reached. This solution was washed three-times with 5 ml of Diethyl ether, dried over anhydrous sodium sulfate and the solvent was removed by rotary evaporation, resulting in a slightly yellowish liquid.

Yield: 6.60 g, 0.027 mol (77.1%)

EA: calc.: C(39.82%), H(8.35%), N(5.80%), S(13.29%)

found: C(39.79%), H(8.32%), N(5.82%), S(13.24%)

NMR: *cf.* Table 12 and Table 18

***O,O*-Diethyl *O*-[3-(dimethylamino)propyl] phosphorothioate (XIX)**

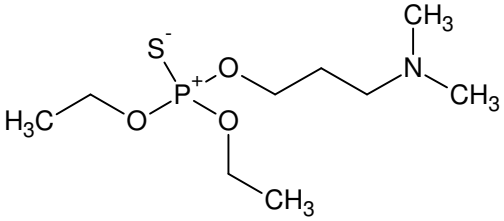

Sodium hydride (0.92 g, 0.038 mol) was weighed into a 100 ml three-neck round-bottom flask under nitrogen atmosphere. 40 ml of anhydrous benzene were added and the solution was stirred and

refluxed. Carefully 3-dimetylamino-1-propanol (4.17 g, 0.038 mol) was added dropwise to the solution. Upon the formation of 3-dimethylamino-1-propanolate anion the solution turned almost transparent. The reaction mixture was cooled on an ice bath and O,O'-diethyl chlorothiophosphate (7.42 g, 0.038 mol) was added dropwise. The reaction mixture was allowed to warm to room temperature till the next day and was carefully extracted three-times with distilled water of pH 2. Then ammonia solution (8% v/v) was added to this fraction until a pH value of >10 was reached. This solution was washed three-times with 5 ml of diethyl ether, dried over anhydrous sodium sulfate and the solvent was removed by rotary evaporation, resulting in a slightly yellowish liquid.

Yield: 8.71g, 0.034mol (88.31%)

EA: calc.: C(42.34%), H(8.69%), N(5.49%), S(12.56%)

found: C(43.96%), H(8.57%), N(5.52%), S(12.08%)

NMR: *cf.* Table 12 and Table 18

_O_,_O_-Diethyl _O_-[2-(_tert_-butylamino)ethyl] phosphorothioate (XX)

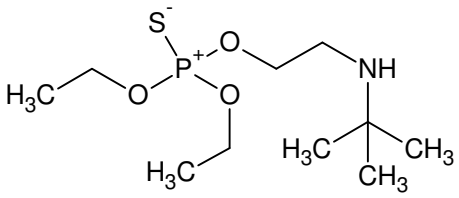

Sodium hydride (0.80 g, 0.033 mol) was weighed into a 100 ml three-neck round-bottom flask under nitrogen atmosphere. 40 ml of anhydrous benzene were added and the solution was stirred and refluxed. Carefully 2-(*tert*-Butylamino) ethanol (3.81 g, 0.032 mol) was added dropwise to the solution. Upon the formation of 2-(*tert*-Butylamino) ethanolate anion the solution turned almost transparent. The reaction mixture was cooled on an ice bath and O,O'-diethyl chlorothiophosphate (5.63 g, 0.030 mol) was added dropwise. The reaction mixture was allowed to warm to room temperature till the next day and was carefully extracted three-times with distilled water of pH 2. Then ammonia solution (8% v/v) was added to this fraction until a pH value of >10 was reached. This solution was washed three-times with 5 ml of diethyl ether, dried over anhydrous sodium sulfate and the solvent was removed by rotary evaporation, resulting in a slightly yellowish liquid.

Yield: 5.98 g, 0.022 mol (74.4%)

EA: calc.: C(44.59%), H(8.98%), N(5.20%), S(11.90%)

found: C(44.69%), H(9.39%), N(5.11%), S(11.70%)

NMR: *cf.* Table 12 and Table 19

_O_,_O_-Diethyl O-[2-(_tert_-butyl(methyl)amino)ethyl] phosphorothioate (XXI)

O,*O*-Diethyl O-[2-(*tert*-butylamino)ethyl] phosphorothioate (**XX**) (0.41 g, 1.5 mmol) and iodomethan (1.04 g, 7.3 mmol) were each dissolved in the double amount of dry

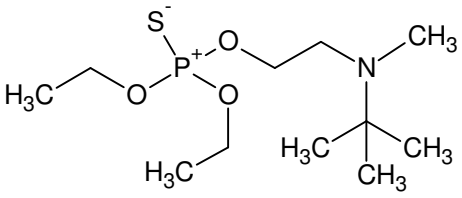

nitromethane. The combined solutions were slightly heated on a water bath (~50°). After a reaction time of one hour the remaining solvent was evaporated in vacuum and dry diethyl ether (10 ml) added which was again removed. The so prepared protonated title product was transferred into deionized water (5 ml) and mixed with ammonia solution (1 ml, 8% v/v) to liberate the free base. After vigorous shaking the title product was extracted three-times with diethylether (5 ml), dried over anhydrous sodium sulfate and the solvent was removed by rotary evaporation, resulting in a slightly yellowish liquid.

Yield: 0.13g, 0.5 mmol (30.0%)

EA: calc.: C(46.62%), H(9.25%), N(4.94%), S(11.32%)

found: C(46.30%), H(9.19%), N(4.93%), S(11.62%)

NMR: not obtained

***O*,*O*-Diethyl *O*-[2-(diisopropylamino)ethyl] phosphate (XXII)**

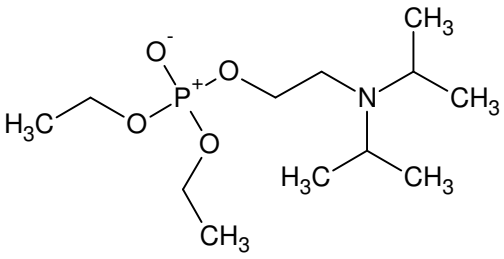

Sodium hydride (1.01 g, 0.042 mol) was weighed into a 100 ml three-neck round-bottom flask under nitrogen atmosphere. 40 ml of anhydrous benzene were added and the solution was stirred and refluxed. Carefully 2-(diisopropylamino) ethanol (5.79 g, 0.040 mol) was added dropwise to the solution. Upon the formation of 2-(diisopropylamino) ethanolate anion the solution turned almost transparent. The reaction mixture was cooled on an ice bath and O,O'-diethyl chlorophosphate (7.07 g, 0.041 mol) was added dropwise. The reaction mixture was allowed to warm to room temperature till the next day and was carefully extracted three-times with distilled water of pH 2. Then ammonia solution (8% v/v) was added to this fraction until a pH value of >10 was reached. This solution was washed three-times with 5 ml of diethyl ether, dried over anhydrous sodium sulfate and the solvent was removed by rotary evaporation, resulting in a slightly yellowish liquid.

Yield: 7.98 g, 0.028 mol (70.9%)

EA: calc.: C(51.23%), H(10.03%),N(4.98%)

found: C(52.19%), H(10.43%),N(5.39%)

NMR: *cf.* Table 12 and Table 20

_O_,_O_-Diethyl _O_-[2-(diisopropylamino)ethyl] phosphorothioate (XXIII)

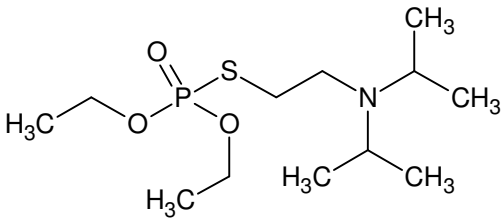

Sodium hydride (1.03 g, 0.043 mol) was weighed into a 100 ml three-neck round-bottom flask under nitrogen atmosphere. 40 ml of anhydrous benzene were added and the solution was stirred and refluxed. Carefully 2-(diisopropylamino) ethanol (5.88 g, 0.041 mol) was added dropwise to the solution. Upon the formation of 2-(diethylamino) ethanolate anion the solution turned almost transparent. The reaction mixture was cooled on an ice bath and O,O'-diethyl chlorothiophosphate (7.51 g, 0.040 mol) was added dropwise. The reaction mixture was allowed to warm to room temperature and was carefully extracted three-times with distilled water of pH 2. Then ammonia solution (8% v/v) was added until a pH value of >10 was reached. This solution was washed three-times with 5 ml of diethyl ether, dried over anhydrous sodium sulfate and the solvent was removed by rotary evaporation, resulting in a yellowish liquid.

Yield: 7.54 g, 0.025 mol (63.4%)

EA: calc.: C(48.46%), H(9.49%), N(4.71%), S(10.78%)

found: C(49.40%), H(9.59%), N(4.88%), S(10.60%)

NMR: *cf.* Table 12 and Table 20

_O_,_O_-Diethyl _S_-[1-(dimethylamino)propan-2-yl] phosphorodithioate (XXIV)

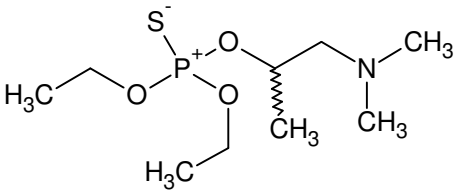

Sodium hydride (1.10 g, 0.046 mol) was weighed into a 100 ml three-neck round-bottom flask under nitrogen atmosphere. 40 ml of anhydrous benzene were added and the solution was stirred and refluxed. Carefully 1-dimethylamino-2-propanol (3.53 g, 0.047 mol) was added dropwise to the solution. Upon the formation of 1-(dimethylamino)-2-propanethiolate anion the solution turned transparent. The reaction mixture was cooled on an ice bath and O,O'-diethyl chlorothiophosphate (8.67 g, 0.046 mol) was added dropwise. The reaction mixture was allowed to warm to room temperature till the next day and was carefully extracted with distilled water of pH 2. Then ammonia solution (8% v/v) was added to this fraction until a pH value of 10 was reached. This solution was washed three-times with 5 ml of diethyl ether, dried over anhydrous sodium sulfate and the solvent was removed by rotary evaporation. The resulting slightly yellowish liquid was further purified by distillation.

Yield: 6.8459 g, 0.027 mol (58.51%)

EA: calc.: C(42.43%), H(8.69%), N(5.49%), S(12.56%)

found: C(42.57%), H(8.75%), N(5.47%), S(12.58%)

NMR: *cf.* Table 12 and Table 22

O,O-Diethyl *O*-[2-(piperidyl)ethyl] phosphorothioate (XXV)

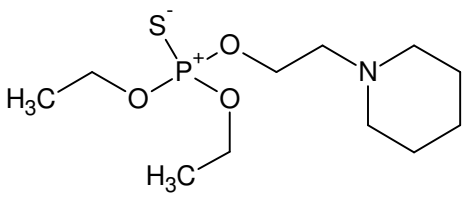

Sodium hydride (0.96 g, 0.040 mol) was weighed into a 100 ml three-neck round-bottom flask under nitrogen atmosphere. 40 ml of anhydrous benzene were added and the solution was stirred and refluxed. Carefully 1-(2-Hydroxyethyl) piperidine (4.96 g, 0.038 mol) was added dropwise to the solution. Upon the formation of the ethanolate anion the solution turned almost transparent. The reaction mixture was cooled on an ice bath and O,O'-diethyl chlorophosphate (7.07 g, 0.037 mol) was added dropwise. The reaction mixture was allowed to warm to room temperature till the next day and was carefully extracted three-times with distilled water of pH 2. Then ammonia solution (8% v/v) was added to this fraction until a pH value of >10 was reached. This solution was washed three-times with 5 ml of diethyl ether, dried over anhydrous sodium sulfate and the solvent was removed by rotary evaporation, resulting in a slightly yellowish liquid.

Yield: 8.16 g, 0.029 mol (78.4%)

EA: calc.: C(46.96%), H(8.60%), N(4.98%), S(11.40%)

found: C(47.07%), H(8.69%), N(4.94%), S(11.36%)

NMR: *cf.* Table 12 and Table 21

O,O-Diethyl *O*-[2-(pyrrolidyl)ethyl] phosphorothioate (XXVI)

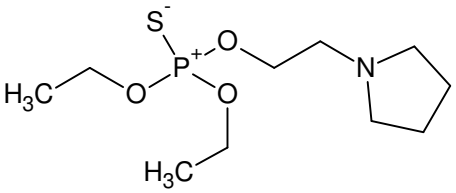

Sodium hydride (0.87 g, 0.036 mol) was weighed into a 100 ml three-neck round-bottom flask under nitrogen atmosphere. 40 ml of anhydrous benzene were added and the solution was stirred and refluxed. Carefully 1-(2-hydroxyethyl) pyrrolidine (4.17 g, 0.036 mol) was added dropwise to the solution. Upon the formation of the ethanolate anion the solution turned almost transparent. The reaction mixture was cooled on an ice bath and O,O'-diethyl chlorophosphate (6.83 g, 0.036 mol) was added dropwise. The reaction mixture was allowed to warm to room temperature till the next day and was carefully extracted three-times with distilled water of pH 2. Then ammonia solution (8% v/v) was added to this fraction until a pH value of >10 was reached. This solution was washed three-times with 5 ml of diethyl ether, dried over anhydrous Ssdium sulfate and the solvent was removed by rotary evaporation, resulting in a slightly yellowish liquid.

Yield: 7.29 g, 0.027 mol (75.0%)

EA: calc.: C(44.93%), H(8.30%), N(5.24%), S(11.99%)

found: C(44.89%), H(8.27%) ,N(5.20%), S(11.02%)

NMR: *cf.* Table 12 and Table 21

_O_,_O_-Diethyl O-[2-(diphenylamino)ethyl] phosphorothioate (XXVII)

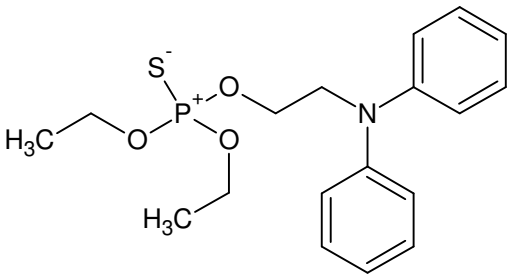

Sodium hydride (0.34 g, 14.1 mmol) was weighed into a 100 ml three-neck round-bottom flask under nitrogen atmosphere. 40 ml of anhydrous benzene were added and the solution was stirred and refluxed. Carefully N,N-diphenylethanolamine (2.48 g, 11.6 mmol) was added dropwise to the solution. The reaction mixture was refluxed for one hour and afterwards cooled on an ice bath and O,O'-diethyl chlorothiophosphate (2.56 g, 13.6 mmol) was added dropwise. The reaction mixture was allowed to warm to room temperature till the next day and was carefully extracted three-times with distilled water of pH 2. Then ammonia solution (8% v/v) was added to this fraction until a pH value of >10 was reached. This solution was washed three-times with 5 ml of diethyl ether, dried over anhydrous sodium sulfate and the solvent was removed by rotary evaporation, resulting in a yellowish liquid.

Yield: 1.30 g, 3.6 mmol (30.6%)

EA: calc.: C(50.14%), H(9.71%), N(4.50%), S(10.30%)

found: C(55.92%), H(10.80%), N(5.38%), S(6.95%)

NMR: *cf.* Table 12 and Table 22

6.6 Synthesis and Characterization of Quaternary Ammonium Salts

Chemical structures presented for oxalates and citrates only give the mono-coordinated structure. The exact coordination is unknown as long as no single crystal X-ray structure is available for the molecules. This can also be seen from the elemental analysis results.

2-[(Diethoxyphosphorothioyl)oxy]-*N,N*-diethylethanaminium citrate (XXVIII)

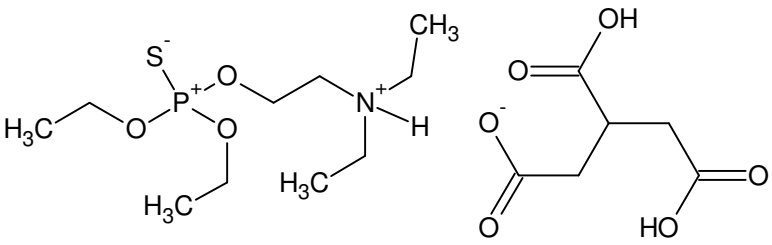

Citric acid (0.71 g, 0.004 mol) was dissolved in 1 ml of ethly acetate to which *O*,*O*-Diethyl *O*-[2-(diethylamino)ethyl] phosphorothioate (**IX**) (1.05 g, 0.004 mol) was added while heating the suspension to 75°C. Afterwards the solution was allowed to cool to room temperature upon which white needle-like crystals formed immediately. Recrystallization was done from acetone.

EA: calc.: C(43.14%), H(7.24%), N(3.14%), S(7.20%) mono-coordinated
calc.: C(43.69%), H(7.90%), N(3.92%), S(8.97) di-coordinated
calc.: C(43.93%), H(8.19%), N(4.27%), S(9.77%) tri-coordinated
found: C(42.30%), H(7.20%), N(3.07%), S(7.12%)

2-[(Diethoxyphosphorothioyl)oxy]-*N,N*-diethylethanaminium oxalate (XXIX)

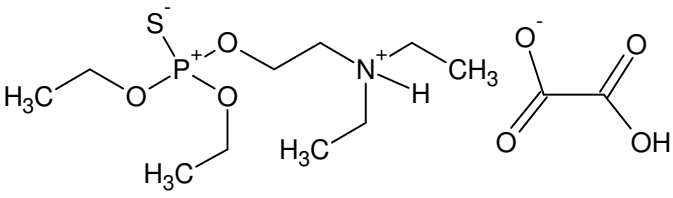

Oxalic acid (0.15 g, 0.002 mol) was dissolved in 1 ml of ethly acetate to which *O*,*O*-diethyl *O*-[2-(diethylamino)ethyl] phosphorothioate (**IX**) (1.05 g, 0.004 mol) was added while heating the suspension to 75°C. Afterwards the solution was allowed to cool to room temperature upon which white platelet-like crystals formed immediately. Recrystallization was done from acetone.

EA: calc.: C(40.11%), H(7.29%), N(3.90%), S(8.92%) mono-coordinated
calc: C(42.03%), H(8.02%), N(4.46%), S(10.20%) mono-coordinated
found: C(40.08%), H(7.26%), N(3.60%), S(8.65%)

2-[(Diethoxyphosphorothioyl)sulfanyl]-*N,N*-diethylethanaminium oxalate (XXX)

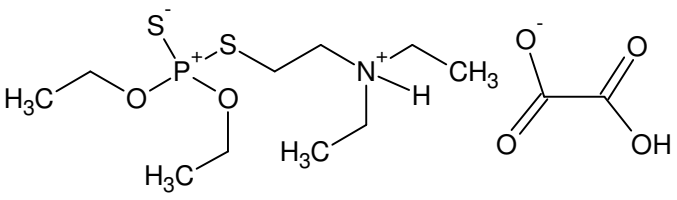

Oxalic acid · H_2O (0.04 g, 0.3 mmol) was dissolved in Acetone (2ml) to which O,O-Diethyl S-[2-(diethylamino)ethyl] phosphorodithioate (**XIV**) (0.20 g, 0.6 mmol) was added dropwise. Instantaneously a white crystalline fall out was observed. The crystals were recrystallized from Acetone and Ethanol.

EA: calc.: C(38.39%), H(6.98%), N(3.73%), S(17.08%) mono-coordinated
calc.: C(39.98%), H(7.63%), N(4.24%), S(19.41%) di-coordinated
found: C(39.11%), H(7.14%), N(4.11%), S(17.31%)

2-[(Diethoxyphosphorothioyl)oxy]-*N,N,N*-trimethylethanaminium iodide (XXXI)

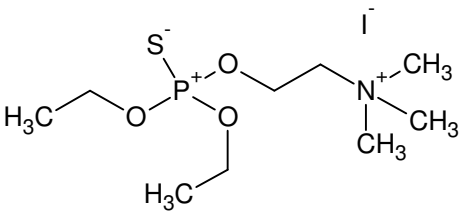

O,O-Diethyl O-[2-(dimethylamino)ethyl] phosphorothioate (**XVIII**) (1.02 g, 0.004 mol) was dissolved in 2 ml of dry nitromethane. To this solution methyl iodide (5.98 g, 0.042 mol) also dissolved in 10 ml of nitromethane was added. The solution was stirred at ambient temperature for 60 minutes and afterwards heated until boiling for 30 minutes. Upon cooling and evaporation of the solvent under reduced pressure crystals were forming. The crystals were recrystallized from ethyl acetate.

EA: calc.: C(28.21%), H(6.05%), N(3.65%), S(8.37%)
found: C(28.19%), H(6.06%), N(3.70%), S(8.37%)

2-[(Diethoxyphosphorothioyl)oxy]-*N,N*-dimethylethanaminium citrate (XXXII)

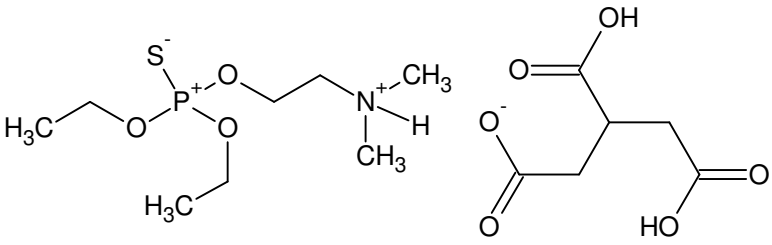

O,O-Diethyl O-[2-(dimethylamino)ethyl] phosphorothioate (**XVIII**) (1.02 g, 0.003 mol) was dissolved in 10 ml of dry acetone and citric acid added (0.80 g, 0.006 mol). Upon the evaporation of the solvent a white microcrystalline powder formed which was recrystallized from dry ethanol.

EA: calc.: C(40.28%), H(6.76%), N(3.36%), S(7.68%) mono-coordinated

calc.: C(40.11%), H(7.34%), N(4.25%), S(9.74%) di-coordinated
calc.: C(39.47%), H(7.18%), N(4.60%), S(10.54%) tri-coordinated
found: C(38.34%), H(6.62%), N(3.32%), S(7.65%)

2-[(Diethoxyphosphorothioyl)oxy]-*N,N*-dimethylethanaminium oxalate (XXXIII)

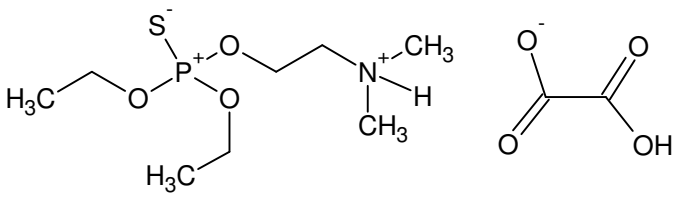

O,O-Diethyl O-[2-(dimethylamino) ethyl] phosphorothioate (**XVIII**) (6.75 g, 0.028 mol) were dissolved in 25 ml of dried methanol to which oxalic acid was added (1.26 g, 0.014 mol) and the solvent allowed to evaporate. The crude product was dissolved in 24 ml of acetone, heated and filtered hot. Upon cooling white, needle like crystals are forming, which were dried under vacuum. Recrystallization was done from ethanol.

EA: calc.: C(36.25%), H(6.69%), N(4.23%), S(9.68%) mono-coordinated
calc.: C(37.89%), H(7.07%), N(4.91%), S(11.24%) di-coordinated
found: C(32.80%), H(6.17%), N(3.24%), S(8.45%)

1,1,4,4 Tetramethylpiperazinium di-*O,O*-diethyl phosphorothioate (decomposition product of XVIII) (XXXIV)

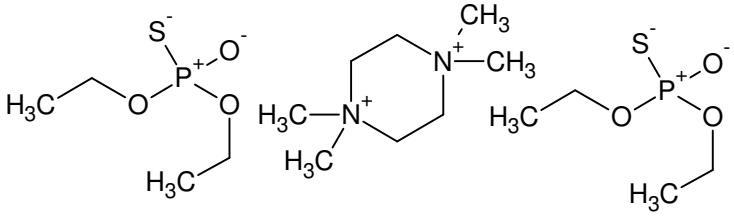

1,4,4 Tetramethylpiperazinium di-*O,O*-diethyl phosphorothioate as the decomposition product compound **XVIII** was found as a tiny single crystal in a stored NMR-tube which was kept at 4°C in the fridge for about one year. The NMR solvent was d_8 toluene.

Direct synthesis was successful by the following procedure: Step A (synthesis of the cation): anhydrous piperazine (0.67 g, 7.8 mmol) was dissolved in 15 ml dried acetonitrile. Iodmethane (4.65 g, 31.2 mmol) was dissolved in 10 ml of dried acetonitrile. Both solutions were carefully mixed upon which a white powder was forming under the production of excess heat. The intermediate A (1,1,4,4 tetramethylpierazinediium diiodite) was filtered and washed three times with dried acetonitrile. Step B (synthesis of the anion according to *Friedrich et al.*[216]): *O,O*-diethylthiophosphorylchloride (3.05 g, 16 mmol) was added to 40 ml of 1N sodiumhydroxid solution and the solution was allowed to react for 12 hours under stirring at room temperature. The solid intermediates were isolated by vacuum evaporation of the remaining water. The obtained white powder was dissolved in methanol to separate from insoluble sodium chloride by filtration. The methanol was vacuum evaporated and

intermediate B (sodium *O*,*O*-diethylthiophosphorate) obtained as white powder. Equal amounts of intermediate A and B were dissolved in distilled water and mixed together in a round bottom flask. The water was allowed to evaporate over time so that crystallization starts forming the title compound.

EA: calc.: C(39.82%), H(8.35%), N(5.80%), S(13.29%)
found: C(39.79%), H(8.32%), N(5.82%), S(13.24%).

2-[(Diethoxyphosphorothioyl)oxy]-*N*,*N*-dimethylpropanaminium oxalate (XXXV)

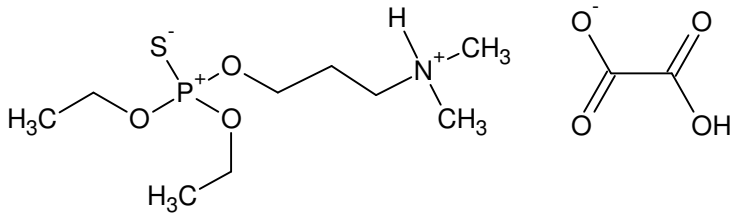

O,*O*-Diethyl O-[2-(dimethylamino) propyl] phosphorothioate (**XIX**) (0.5 g, 0.002 mol) were dissolved in 5 ml of dried ethanol to which oxalic acid was added (0.25 g, 0.001 mol) and the solvent allowed to evaporate. The crude product was dissolved in 5 ml of dry acetone, heated and filtered hot. Upon cooling white, needle like crystals are forming, which were dried under vacuum. Recrystallization was done from ethanol.

EA: calc: C(38.26%), H(7.00%), N(4.06%), S(9.28%) mono-coordinated
calc.: C(39.99%), H(7.72%), N(4.66%), S(10.68%) di-coordinated
found: C(37.38%), H(7.61%), N(3.95%), S(9.30%).

2-[(Diethoxyphosphorothioyl)oxy]-*N*-isopropyl-*N*-methylethanaminium iodide (XXXVI)

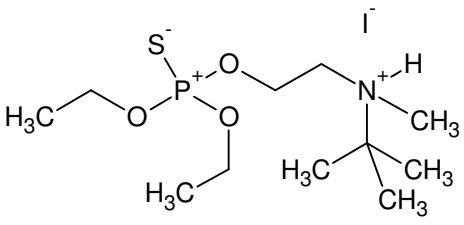

O,*O*-Diethyl O-[2-(*tert*-buthylamino)ethyl] phosphorothioate (**XX**) (0.41 g, 0.002 mol) was dissolved in 1 ml of dry nitromethane. To this solution methyl iodide (1.04 g, 0.007 mol) also dissolved in 2 ml of nitromethane was added. The solution was stirred at ambient temperature for 60 minutes and afterwards heated until boiling for 30 minutes. Upon cooling and evaporation of the solvent by addition of 10 ml dried ethanol under reduced pressure crystals were forming. The crystals were recrystallized from ethyl acetate.

EA: calc.: C(32.51%), H(6.62%), N(3.41%), S(7.80%)
found: C(32.25%), H(6.68%), N(3.45%), S(7.73%)

2-[(Diethoxyphosphorothioyl)oxy]-*N,N*-dimethylpropan-1-aminium oxalate (XXXVII)

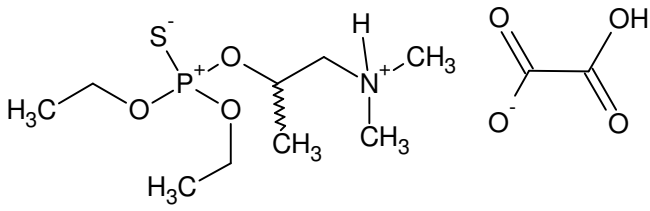

O,O-Diethyl *S*-[1-(dimethylamino)propan-2-yl] phosphorodithioate (0.5 g, 0.002 mole) was dissolved in 5ml of dried ethanol to which oxalic acid was added (0.25 g, 0.001 mol) and the solvent allowed to evaporate. The crude product was dissolved in 5 ml of dry acetone, heated and filtered hot. Upon cooling white, needle like crystals are forming, which were dried under vacuum. Recrystallization was done from ethanol.

EA: calc.: C(38.26%), H(7.00%), N(4.06%), S(9.28%)
found: C(38.15%), H(7.04%), N(3.82%), S(9.44%)

1-{2-[(diethoxyphosphorothioyl)oxy]ethyl}-1-methylpiperidinium iodide (XXXVIII)

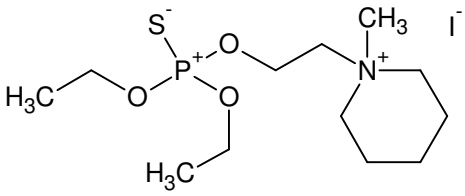

O,O-Diethyl O-[2-(piperidyl)ethyl] phosphorothioate (**XXV**) (0.95 g, 0.003 mol) was dissolved in 2 ml of dry nitromethane. To this solution methyl iodide (5.96 g, 0.042 mol) also dissolved in 10 ml of nitromethane was added. The solution was stirred at ambient temperature for 60 minutes and afterwards heated until boiling for 30 minutes. Upon cooling and evaporation of the solvent under reduced pressure crystals were forming. The crystals were recrystallized from ethyl acetate.

EA: calc.: C(34.05%), H(6.43%), N(3.31%), S(7.58%)
found: C(33.71%), H(6.44%), N(3.28%), S(7.22%)

1-{2-[(diethoxyphosphorothioyl)oxy]ethyl}piperidinium oxalate (XXXIX)

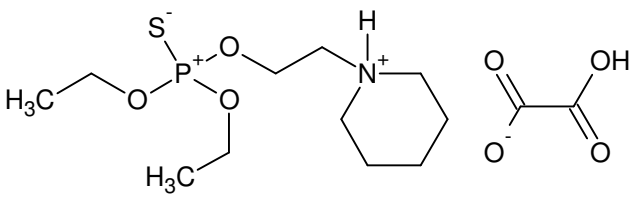

O,O-Diethyl *O*-[2-(piperidyl)ethyl] phosphorothioate (**XXV**) (1.04 g, 0.004 mol) was dissolved in 5 ml of acetone to which oxalic acid was added (0.35 g, 0.004 mol) and the solvent allowed to evaporate. The crude product was dissolved in 5 ml of dry acetone, heated and filtered hot. Upon cooling white, plate-like crystals are forming, which were dried under vacuum. Recrystallization was done from ethanol.

EA: calc.: C(42.04%), H(7.06%), N(3.77%), S(8.63%)
found: C(42.10%), H(7.08%), N(3.84%), S(8.79%)

1-{2-[(diethoxyphosphorothioyl)oxy]ethyl}-1-methylpyrrolidinium iodide (XL)

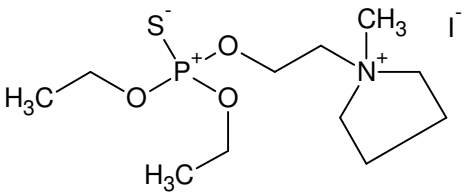

O,O-Diethyl O-[2-(pyrrolidin-1yl-)ethyl] phosphorothioate (**XXVI**) (1.04 g, 0.004 mol) was dissolved in 2 ml of dry nitromethane. To this solution methyl iodide (6.36 g, 0.045 mol) also dissolved in 10 ml of nitromethane was added. The solution was stirred at ambient temperature for 60 minutes and afterwards heated until boiling for 30 minutes. Upon cooling and evaporation of the solvent under reduced pressure crystals were forming. The crystals were recrystallized from ethyl acetate.

EA: calc.: C(32.28%), H(6.16%), N(3.42%), S(7.83%)
found: C(32.25%), H(6.34%), N(3.46%), S(8.09%)

1-{2-[(diethoxyphosphorothioyl)oxy]ethyl}pyrrolidinium oxalate (XLI)

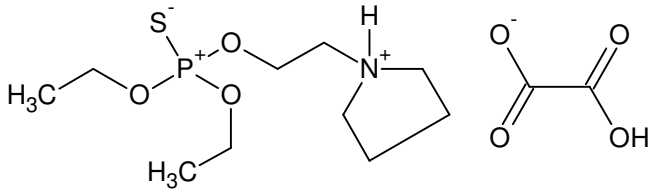

O,O-Diethyl O-[2-(pyrrolidin-1yl-)ethyl] phosphorothioate (**XXVI**) (7.49 g, 0.028 mol) was dissolved in 25 ml of dried methanol to which oxalic acid was added (1.26 g, 0.014 mol) and the solvent allowed to evaporate. The crude product was dissolved in 24 ml of acetone, heated and filtered hot. Upon cooling white, needle like crystals are forming, which were dried under vacuum.

EA: calc.: C(40.36%), H(6.77%), N(3.92%), S(8.97%)
found: C(40.11%), H(6.49%), N(3.89%), S(8.83%)

2-[(Diethoxyphosphorothioyl)oxy]-*N,N*-diphenylethanaminium oxalate (XLII)

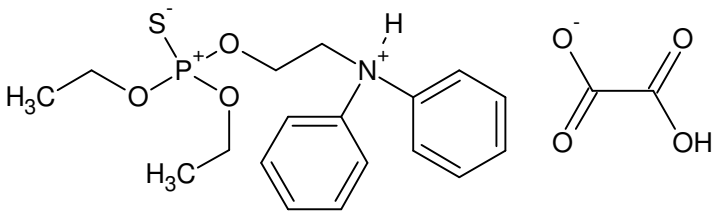

O-[2-(diphenylamino)ethyl]-*O,O*-diethyl phosphorothioate (0.5 g, 0.002 mol) was dissolved in 5 ml of dried ethanol to which oxalic acid was added (0.25 g, 0.001 mol) and the solvent allowed to evaporate. The crude product was dissolved in 5 ml of dry acetone, heated and filtered hot. Upon cooling white, needle like crystals are forming, which were dried under vacuum. Recrystallization was done from ethanol

EA: calc.: C(44.32%), H(5.85%), N(3.69%), S(8.45%) mono-phenyl derivative

calc.: C(52.74%), H(5.75%), N(3.08%), S(7.04%) di-phenyl derivative

found: C(44.73%), H(6.37%), N(3.34%), S(8.81%)

6.7 Thiono-Thiol Rearrangement Investigations

To investigate the thiono-thiol rearrangement the substances were dissolved and diluted in different solvents, e.g. acetonitrile, methanol and acetone. For investigations in water the substances had to be pre-dissolved in an organic solvent, preferably acetonitrile, and were then transferred into distilled water of given pH value so that the total amount of organic solvent was less than 1% in the mixture and could be neglected in the further studies. Due to limitations in the temperature range of the autosampler of the HPLC-system automated temperature profiles could only be taken up to a maximum of 45°C. Samples at higher temperatures were executed in a heating block and aliquots taken at given intervals of time which were processed by the same analytical method as those samples prepared *via* the autosampler. The same holds true for the investigation of the isomerization in stock solution without any diluent. The analytical conditions of the HPLC system did not differ from the standard parameters given in chapter 6.1.2.

6.8 Vapor Pressure Measurements

The basic concept of the transpiration method has already been established [168-170] and is realized in this work as follows (Figure 138): From a nitrogen tank **1** the carrier gas (Nitrogen 5.0) is conducted through a pressure reduction valve **2** and a phosphorus pentoxide (Sicapent®) drying tower. The flow-rate of the carrier gas is adjusted and kept constant by a mass flow controller **4** (Natec Sensors MC-100 CCM) before it reaches the saturator **5**, which is a cylindrical glass vessel (height 25 cm, diameter 10 cm) containing a U-shaped tube (length 50 cm, diameter 0.8 cm) filled with glass beads (diameter 1 mm). The glass beads are coated with the analyte of choice by mixing of the liquid and beads in a beaker. The saturator is thermostatted by a circulation thermostat (Huber Ministat 230) pumping a thermofluid (ethylene glycol (50% aq.)) through it. At the end of the saturator the carrier gas stream reaches its saturation equilibrium with the analyte and then passes a cooling trap with the temperature T_{CT} (-30 °C). The flowrate of the carrier gas stream is measured under ambient conditions (T_{amb}, p_{amb}) with a soap film flowmeter (HP #0101-0113). The experimental time to generate one data point ranges from 15 minutes to 24 hours. This time is needed to collect a sufficient amount of analyte (see Table B2 to Table B9) in the cooling trap to meet the requirements of the analytical instruments used for quantification. At the end of the experiment the condenser pipe is separated from the saturator and *tert*-butyl methyl ether solvent is added together with a solution of the internal standard (*n*-alkanes C-12, C-14 or C-16) of known concentration (≈1 mg/mL). The solution of analyte and standard is then used for internal standard quantification using either a Thermo Fisher Scientific GC/FID system equipped with a TriPlus RSH autosampler or a Shimadzu VO-GC/MS [315] system equipped with an AOC-20i autosampler.

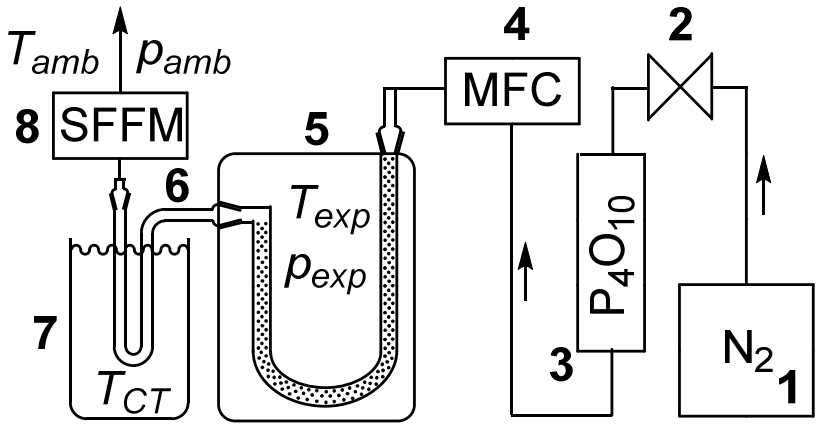

Figure 138: *The transpiration method experimental setup. 1: nitrogen reservoir, 2: pressure reduction valve, 3: P_4O_{10} drying tower, 4: mass flow controller, 5: saturator, 6: condenser pipe, 7: cooling trap, 8: soap film flowmeter.*

The exact chromatographic setup and operational modes can be found in the in Table 85 and Table 86, respectively.

Table 85: *Compilation of VO-GC/MS parameters*

GC/MS	Shimadzu QP2010SE® with LabSolution GCMSsolution v4.11
injector	Atas Optic 4 with Evolution Workstation v4.1
liner	10 mm V2A stainless steel tube, 5 mm wall thickness, equipped with silanized glass wool (2 mm injection needle penetration into wool)
restriction	0.025 mm capillary, 8.11 mm length (Restek #23097)
column connector	SGE Siltite µ-Union® (Restek #073562)
analytical column	Restek RTX-TNT 1® (6 m, 0.53 mm, 1.5 µm)
oven program	40 °C (hold 0.10 min) → 280 °C (rate 60 °C min-1)
injector head pressure	472 kPa
virtual column	100 m, 0.25 µm film thickness, 0.20 mm i.d. (entry for GCMSsolution)
column flow	2.33 mL min-1 (calculated according to [316])
split ratio	18.7 (entered in LabSolutions GCMSsolution)
purge flow	5 mL min-1
injection volume	1 µL
ion source	250 °C
MS interface	250 °C
MS	SCAN (for purity check): 30-500 amu event-time 300 ms SIM (for quantification): 1 quantification (strongest relative intensity) + 3 reference ion channels, event time 100 ms, time-dependent program for analyte and internal standard

For an initial validation of the experimental setup the following reference compounds were chosen: naphthalene, anthracene, *iso*-amyl acetate, *n*-hexanol and *n*-octanol and the obtained results were compared to a large number of literature values. Detailed information on the results of this study are available as supporting material of the article published by the author in reference [317]. The weight of the substance sample for the internal standard calibration was corrected by the purities stated in Table 48.

Table 86: *Compilation of GC-FID parameters*

GC/FID	Thermo Fisher Scientific Trace 1310 operated via Chromeleon Data Handling Software V. 7.2 SR 4
autosampler	TriPlus RSH with syringe tool, tray holder, and standard wash station
injector	PTV, temperature 200 °C
liner	4 mm V2A stainless steel tube
analytical column	Agilent J&W GC columns, CP-Sil 8, low bleed/MS (30m, 0,25mm, 0,25µm)
oven program	40 °C (hold 1 min) → 260 °C (rate 20 °C / min)
column flow	1 mL / min
split ratio	1/20
purge flow	5.0 mL / min
injection volume	1 µL
detector temperature	280 °C

6.9 Toxicological Studies

Determination of the enzyme inhibition kinetic was either performed at the Georgia Institute of Technology, School of Chemistry and Biochemistry, Atlanta, Georgia, USA on a Tecan Infinite M 200 Pro with Costos 96 well flat transparent plates, or at the pharmaceutics department of the LMU on a Molecular Devices Spectra Max M2E instrument with Falcon 96 well flat transparent plates. Data handling was performed with icontrol 1.1 or soft max pro 5.4 software respectively.

During a typical measurement eight wells were used at a time limited by the fact that an eight-channel multi pipette was used and the starting time therefore for all wells could exactly be determined by adding the enzyme at the same time to the individual wells under investigation. The reaction was monitored at a wavelength of 402nm at the shortest possible repetition time of the instrument. Because of the fast measurement of the instruments three individual readings were taken to generate an averaged signal for these three readings.

6.9.1 Preparation of Analytical Standards

All prepared solutions were kept in the dark and refrigerated. The samples were exposed to the reaction conditions just before use to avoid any advanced reactions and to prolong the shelf life of the samples.

0.1M phosphate buffer solution:

A 0.1M Na_2HPO_4-solution was titrated by a 0.1M NaH_2PO_4-solution until the pH reached a value of 7.4. Before use the buffer solution was filtrated through a 0.22µm syringe filter.

Ellmann's reagent:

A stock solution of 2.5mg 5,5'-dithiobis-(2-nitrobenzoic acid) in 5.0ml of 0.1 phosphate buffer was prepared which was diluted to a working solution of 0.3mM concentration freshly each day.

Solutions of inhibitors:

0.1mM stock solutions of the investigated OP's and OTP's were prepared in 2-propanol. The working solutions are prepared freshly before the measurements by first taking 5µl out of the stock solution and filling it up to 1ml to give a 0.5µM solution and second withdrawing 30µl of the latter dilution and again filling it up to 1ml to give a 15.0nM solution. Distilled

water was used as solvent in these steps to reduce the amount of organic solvent in the overall reaction mixture.

Acetylcholine esterase:

A stock solution of 1.0µg/ml acetylcholine esterase from electric eel equal to 126.2U/mg solid enzyme and working solutions thereof of 5.0µg/ml enzyme were prepared in distilled water and kept in the freezer.

S-butyrylcholine esterase:

A stock solution of 1.0µg/ml S-butyrylcholine esterase from equine serum equal to 422U/mg solid enzyme and working solutions thereof of 5.0µg/ml enzyme were prepared in distilled water and kept in the freezer.

Acetylthiocholine iodide and Butyrylthiocholine iodide:

Two individual working solutions of 9.0mM and 0.9mM were prepared in distilled water and kept in the dark to prevent aging.

6.9.2 Determination of K_M-Values

To determine K_M of AChE and BuChE the respective enzyme, DTNB, buffer and TChI had to be mixed together and measured at varying concentrations of TChI (Table 87). After the premixing *via* a multichannel pipette, the 96 well plate was immediately transferred into the instrument to be shaken, tempered to 37°C and measured for at least 30 minutes at the shortest possible interval. Corresponding to the scheme in Table 87, a blank without enzyme was measured to determine the rate of auto hydrolysis of the reaction mixture. This value was subsequently subtracted from further measurements.

Table 87: *Shown is the pipette scheme for the determination of KM for AChE and BuChE respectively. Enzyme, DTNB, buffer and the corresponding TChI were premixed by repeated pull up in the pipette.*

well no.	1	2	3	4	5	6	7	8
enzyme [µl]	2.0	2.0	2.0	2.0	2.0	2.0	2.0	2.0
DTNB [µl]	50.0	50.0	50.0	50.0	50.0	50.0	50.0	50.0
Buffer [µl]	50.0	75.0	87.5	50.0	75.0	83.3	87.5	93.8
TChI [9.0mM] [µl]	50.0	25.0	12.5					
TChI [0.9mM][µl]				50.0	25.0	16.7	12.5	6.2

6.9.3 Determination of Inhibition Constants

For the determination of the inhibition constants for each inhibitor a starting amount 50µl of the 0.5mM stock solution were added to the first slot of the 96 well plate and subsequently the amount was cut down by half for each of the other seven wells in the specific series under investigation. To yield the same amount of liquid and therefore the same optical path length in each well, the missing volume was replaced by adding an appropriate amount of buffer (Table 88).

If the inhibition was to strong and no reasonable inhibition could be measured due to the limited effective range of the absorption measurement, the amount of inhibitor was further reduced. In the opposite case a higher concentrated stock solution was prepared.

Table 88: *Shown is the general pipette scheme for the determination of the inhibition constants for AChE and BuChE respectively. Enzyme, DTNB and buffer were premixed by repeated pull up in the pipette.*

well no.	1	2	3	4	5	6	7	8
enzyme [µl]	2.0	2.0	2.0	2.0	2.0	2.0	2.0	2.0
DTNB [µl]	50.0	50.0	50.0	50.0	50.0	50.0	50.0	50.0
Buffer [µl]	0.0	25.0	37.5	43.7	46.8	48.4	49.2	49.6
Inhibitor [µl]	50.0	25.0	12.5	6.3	3.2	1.6	0.8	0.4
Substrate 9mM [µl]	50	50	50	50	50	50	50	50

6.10 SPME-Methods

SPME-investigations were performed on a Thermo Scientific™ Trace 1310 GC with PTV injector and an Agilent J&W GC-column (CP-Sil 8 CB Low Bleed/MS, 30m 0.25µm), TSQ Duo triple quadrupole mass spectrometer and Triplus RSH™ auto sampler equipped with SPME tool, fiber conditioning station and temperature controlled drawer. Fiber types are given at the individual experiment. Chromeleon™ 7.2 Chromatography Management Software was used for system control and data processing.

6.10.1 Recovery of Organophosphates from the Environment

Analytical samples were prepared by first adding the sampling matrix into a 10 ml vial for direct immersion experiments and a 20 ml vial for head space experiments, respectively. Sample matrices were sea sand, grass and foliage which were taken from plants growing in front of the chemistry building, water from the tap and different phosphate buffer solutions of pH 4.00, 6.88 and 9.22. In case of solid matrices one gram of each material has been used and in case of liquid matrices a sample volume of nine milliliters was chosen. Grass and foliage were vortex thoroughly to give homogeneous mixtures. Afterwards the samples were spiked with the analytes which were prepared in a stock solution of isopropanol, to reach a final concentration of 30 ppm per analyte in the sample. Necessary dilutions of the stock solution were prepared in the desired matrix or distilled water in case of the solid matrices in that way that the final sample contained less than one percent of organic solvent.

After incubation time of one hour the samples were placed on the liquid cooled tray of the TriPlus RSH autosampler and processed for the analysis by SPME with a 65 µm PDDMS/DVB fiber subsequently. Chosen extraction times were ten minutes for direct immersion and 30 minutes for head space extraction, respectively. Extraction temperatures were 20, 40, 60, and 80°C. A summary of the extraction parameters is given in Table 89. All experiments were executed at least two times for determination of the repeatability with a freshly prepared sample for each experiment. In a second measurement cycle one gram of salt, sodium chloride, was added to the liquid type samples. The extraction was then processed the same way as described before.

Table 89: *Summary of the extraction parameters for the SPME experiment.*

Fiber type	65 µm PDMS/DVB, length:1 cm, (blue hub plain, 24 gauge)
Extraction time	10 min (DI) / 30 min (HS)
Extraction temperature	20°C / 40°C / 60°C / 80°C
Sample matrices	sea sand, grass, foliage, tap water, phosphate buffer solution
Phosphate buffer pH	4.00, 6.88, 9.22

Parameters of the gas chromatograph and mass spectrometer used are given in Table 90. The obtained peak areas from the SPME experiment were correlated to a seven point calibration curve of a liquid injection, ranging from 0.1 to 25 µg/ml of the respective analyte, to obtain absolute values of nanogram extracted by the SPME experiment.

Table 90: *Summary of the gas chromatography parameters.*

Gas Chromatograph	Thermo Fisher Scientific Trace 1310 with PTV Injector
Data System	Chromeleon 7.2
Autosampler	Thermo Fisher Scientific Triplus RSH with: automatic tool change station, fiber conditioning station, SPME tool, liquid syringe tool, agitator and liquid cooled tray.
Analytical column	Agilent J&W GC-column (CP-Sil 8 CB Low Bleed/MS, 30m 0.25µm)
Oven conditions:	
Temperature program	70(1) -290°C at 30°C min^{-1}, Post temperature 290°C (1)
Carrier gas	Helium BIP®[14]
Injection conditions:	
Injector temperature	250°C
Injection type	a) liquid injection: Splitless, Injection volume 1µl b) SPME: Splitless 5 min, afterwards split 1/60
Purge flow	1.20 ml/min
Liner type	130 mm x 1.0 mm ID glass liner
Injection depth	65 mm
Mass spectrometer	Thermo Fisher Scientific TSQ Duo, Triple Quadrupole Scan time: 0.2 sec, Full scan start mass 50 amu, end mass 350 amu
Transfer line temperature	280°C
Ion source temperature	280°C
Ionization mode	EI

The obtained data points were fitted by a standard linear regression curve ($y = m \cdot x + b$). Furthermore, the data points of the calibration curve are used to determine LOD and LOQ in accordance with the method described in DIN 32645. [318] All calculations were done with the help of a Microsoft Office Excel worksheet.

[14] http://www.tig.de/produkte/bip-gasreinigungs-technologie.html

6.11 Procedures for Military Hand-held Detection Equipment

6.11.1 Chemical Detector Paper

The different chemical detector papers were supplied *via* the Bundeswehr supply chain and were as follows:

- Papier, Spür, chemische Agenzien, NSN: 6665-21-858-8494
- Papier, Spür, chemische Agenzien, NSN: 6665-12-329-6688

Each sheet was equally cut into four pieces prior to use. For each measurement a 2µl drop was placed in the middle of the sheet with an Eppendorf pipette. To visualize the actually resulting color change a picture was taken after 2 minutes of reaction time. To keep the actual color impression pictures were taken with the aid of a gray filter card.

6.11.2 Dräger Test Tubes

The Dräger test tube for phosphoric acid ester 0.05/a was used for testing the applicability of the test tube for the target substance. To perform the measurement two different concentration levels were established: i)10µl of the respective substance were transferred with an Eppendorf pipette into a 3L HDPE freezer bag which was flushed by gaseous nitrogen of quality 5.0 beforehand.

Image 20: *Setup for the gas phase analysis of spiked nitrogen flushed HDPE freezer bag. The tube on the right delivers the nitrogen for flushing the bag prior to the addition of the respective substance under investigation. The tube on the left connects the inside atmosphere with the test tube. Both tubes can be squeezed so that the bag is sealed from the outside air via a hose clamp.*

This allows reaching a maximum concentration of about 0.4 ppm within the bag, ensuring that the detection limit of the test tube lies well below the applied concentration; ii) in a similar manner to i) 1.2µl of the respective substance were transferred into the freezer bag to achieve a concentration of 0.05 ppm which matches the detection limit of the test tube. After allowing the substance to saturate the gas phase at 20°C for 5 minutes the atmosphere was analyzed by a phosphoric acid ester test tube according to the procedure of the manufacturer.[175] Therefore the Dräger-Tube pump accuro was connected with the HDPE bag by a flexible tube. The results were recorded by taking a picture of the test tube.

6.11.3 Ion-Mobility Spectrometry

Two instruments were used to measure the ion mobility spectra: the lightweight chemical detector LCD 3.3 from Smiths Detection and the Raid-M100 from Bruker Corporation. Data evaluation was performed with Smiths Detection's TrimScan 2.0 Version 0.3 and Bruker's XIMS NT 3.0 Version 3.04 software respectively. For testing the substances the respective vial was opened in the fume hood, flushed with nitrogen and the evaporating gas phase was measured for two to five seconds each. Recorded was a series of measurements including two to three blanks as background spectra and to confirm the complete recovery of the dopant peak after the detection of the respective analyte.

6.11.4 Flame Spectrophotometry with AP4C

An analyte was exposed to the instrument directly from its storage flask, which was opened at room temperature and allowed to evaporate in front of the instruments nozzle. If there was no detection from the vapor phase then the liquid handling device was employed to help the analyte under investigation to get into the vapor state.

6.11.5 IR Spectroscopy

The IR spectra were measured by the ATR technology on the Smith Detections Hazmat ID by adding a few µl or µg, in case of a solid, of the substance onto the ATR unit. For data processing the OMNIC 8.0 software from Thermo Fisher Scientifc was used.

6.11.6 Raman Spectroscopy

For the execution of the Raman spectra the Inficon First Defender RMX was used. As a rule the general setting was medium laser intensity. The measurements were either performed through the glass of the storage vial or directly through the round bottom flask after having evaporated the solvent directly after the work up of the synthesis. For data processing the OMNIC 8.0 software from Thermo Fisher Scientifc was used.

Supplement

A Additional Analytical Data

A.1 IR Spectra

i. Amino Alcohol Spectra

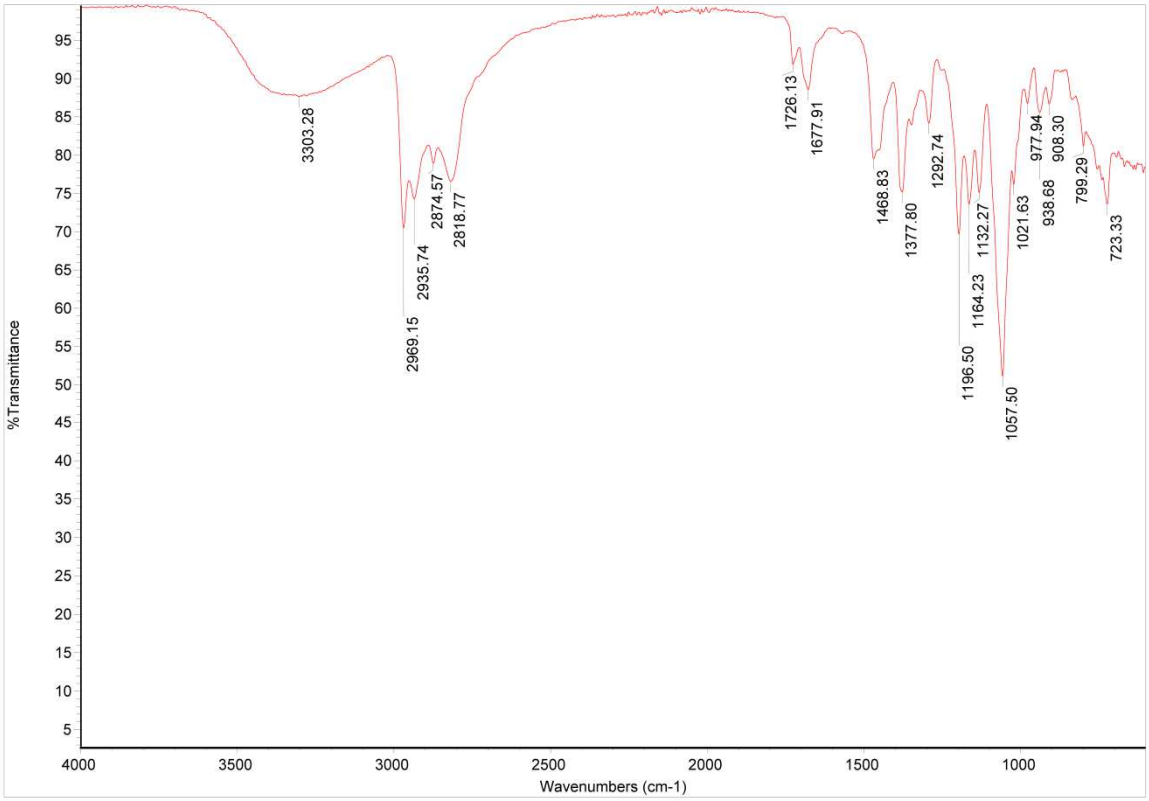

Figure 139: *IR Spectrum of* ***I****.*

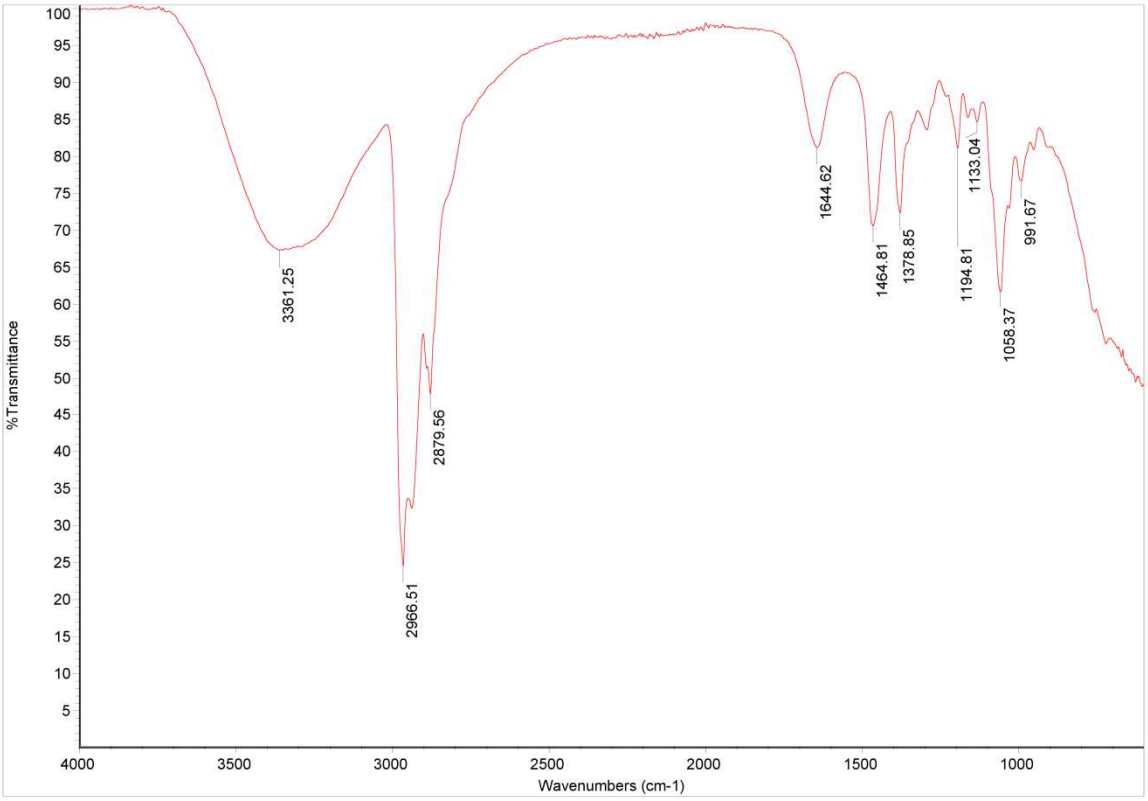

Figure 140: *IR Spectrum of* ***II.***

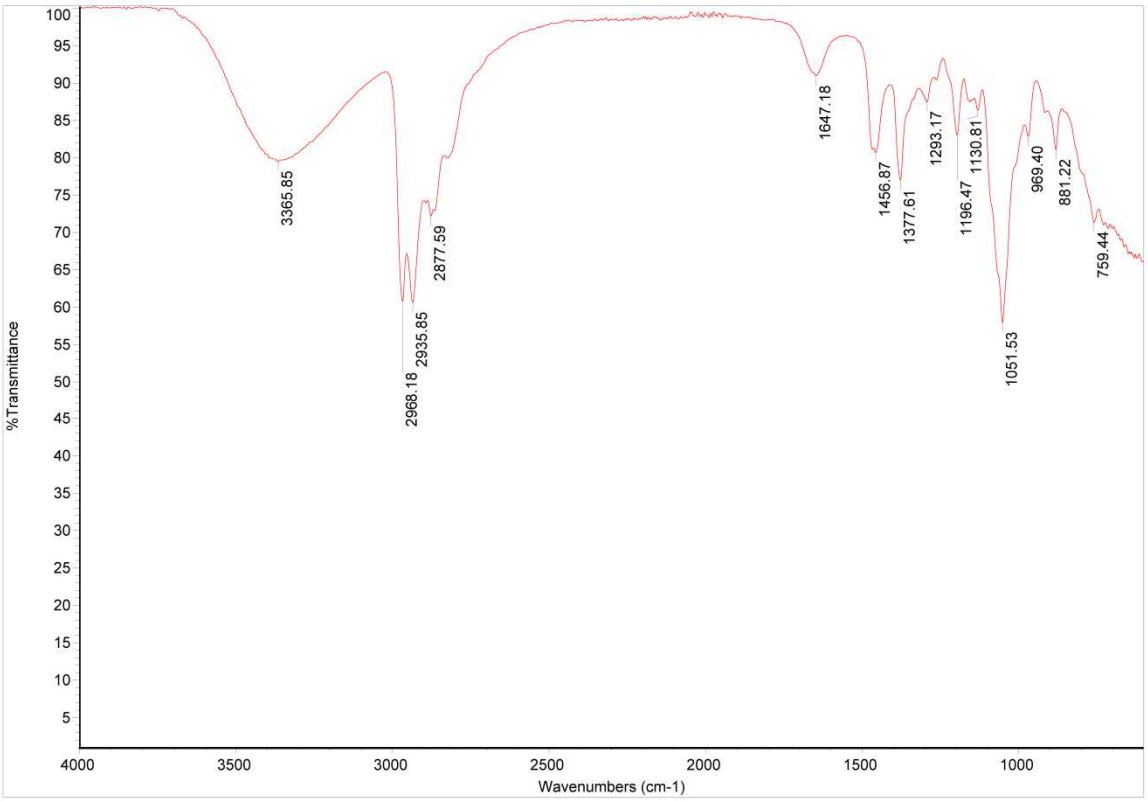

Figure 141: *IR Spectrum of* ***III****.*

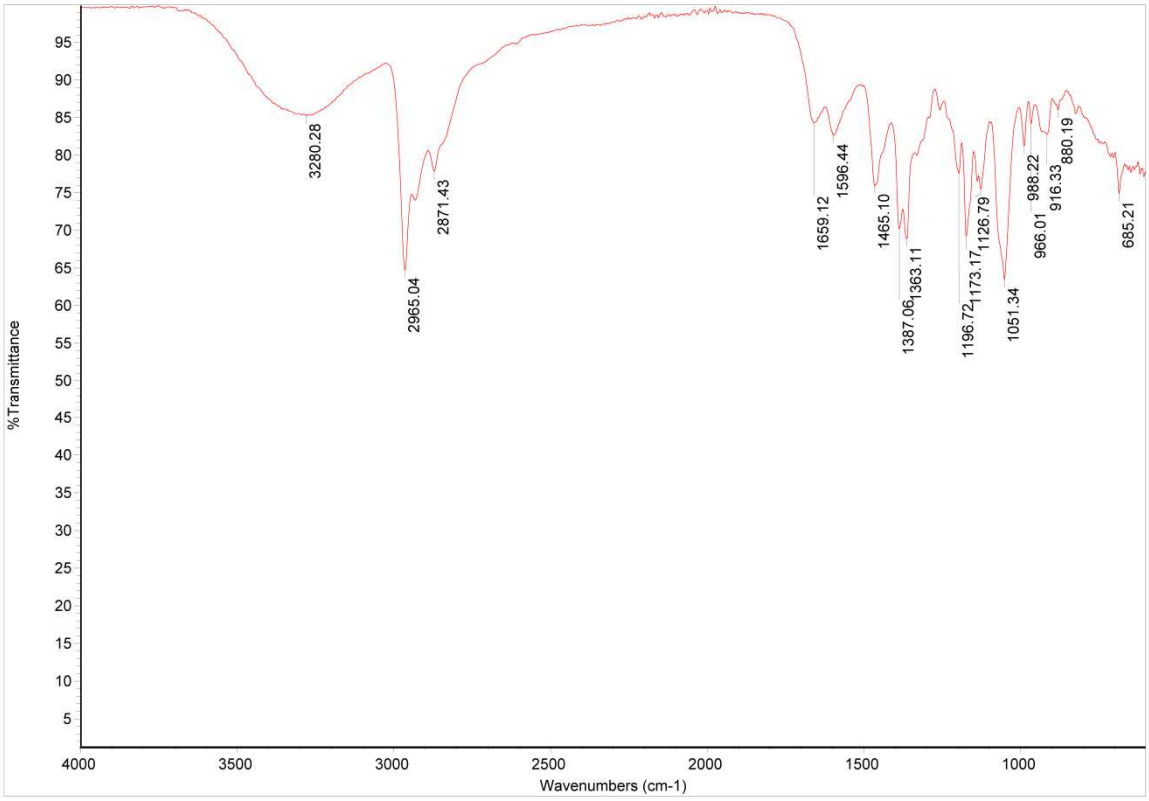

Figure 142: *IR Spectrum of* ***IV****.*

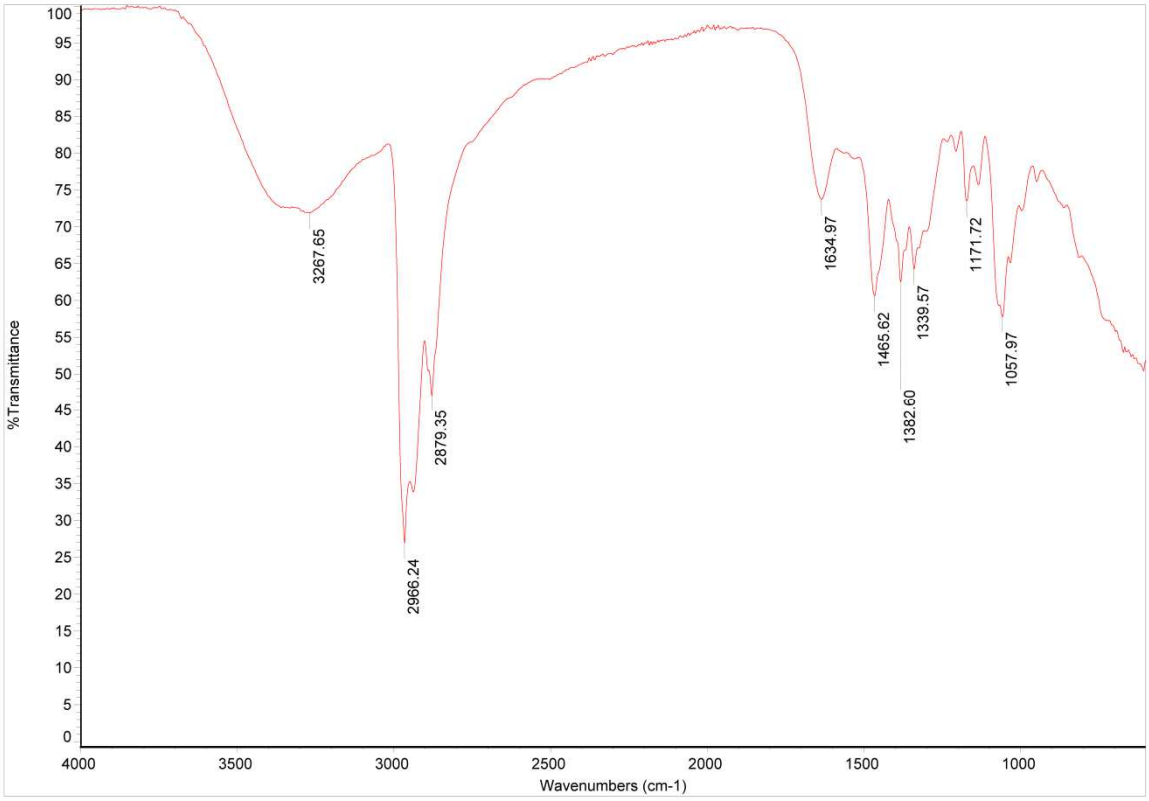

Figure 143: *IR Spectrum of* ***V****.*

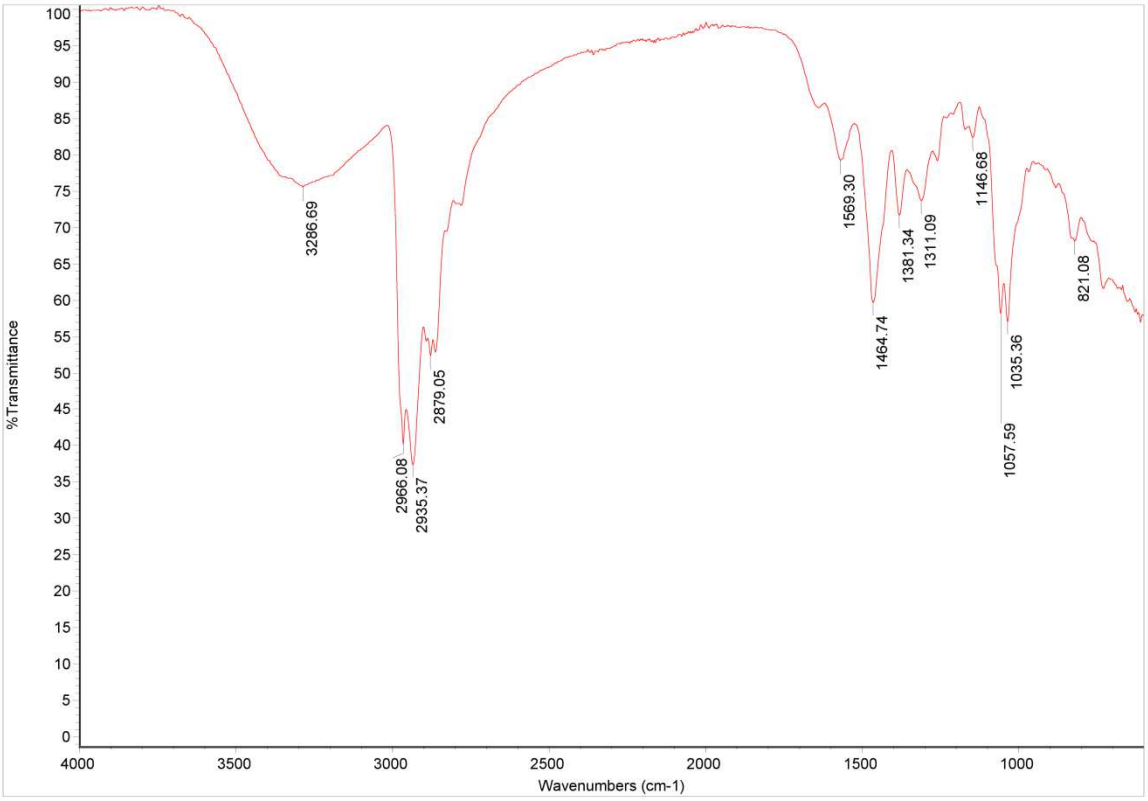

Figure 144: *IR spectrum of* ***VI****.*

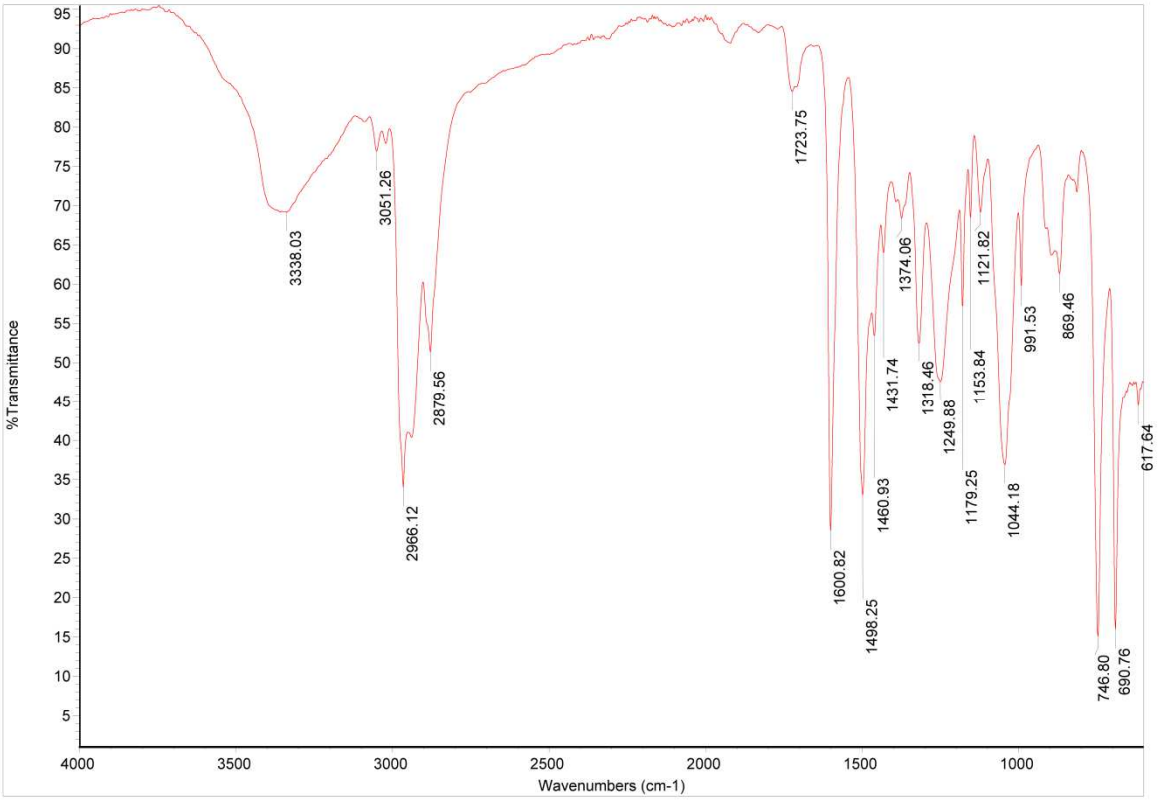

Figure 145: *IR Spectrum of* ***VII****.*

ii. O,O'-Diethyl(thio)phosphorylchloride Spectra

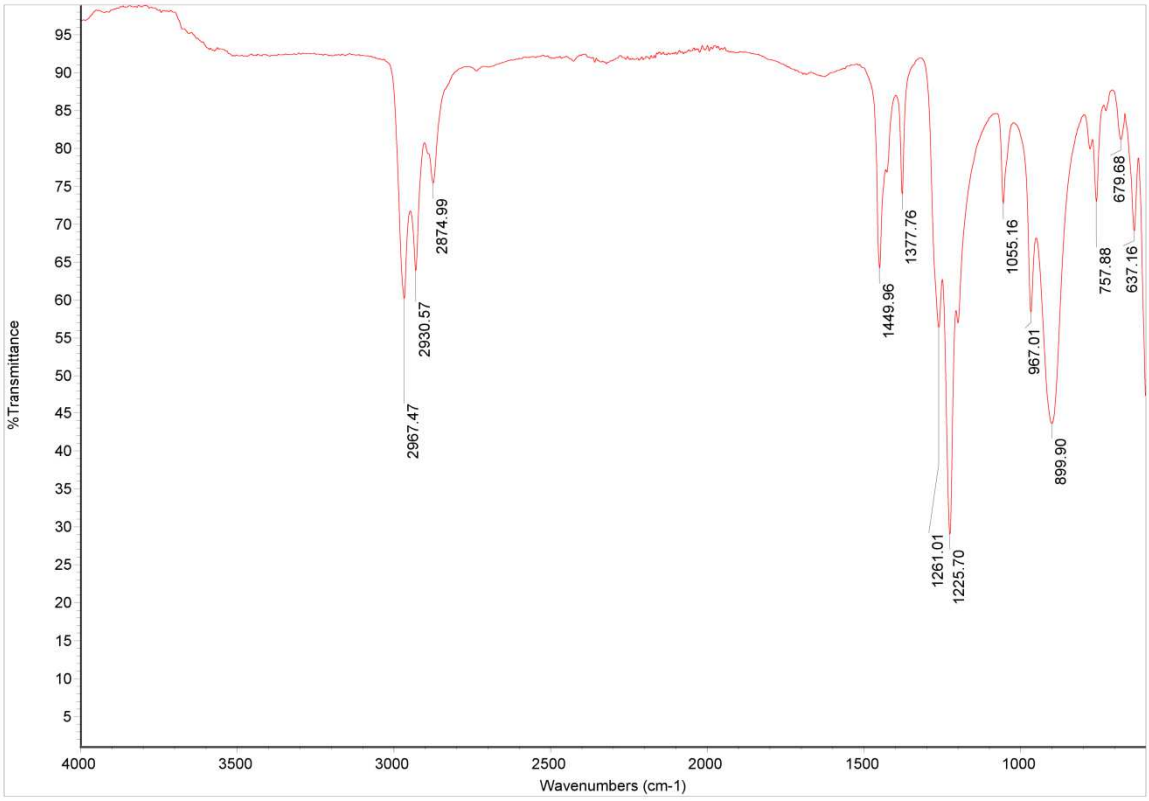

Figure 146: *IR Spectrum of* ***VIII****.*

iii. O,O'-Diethyl(thio)phosphates

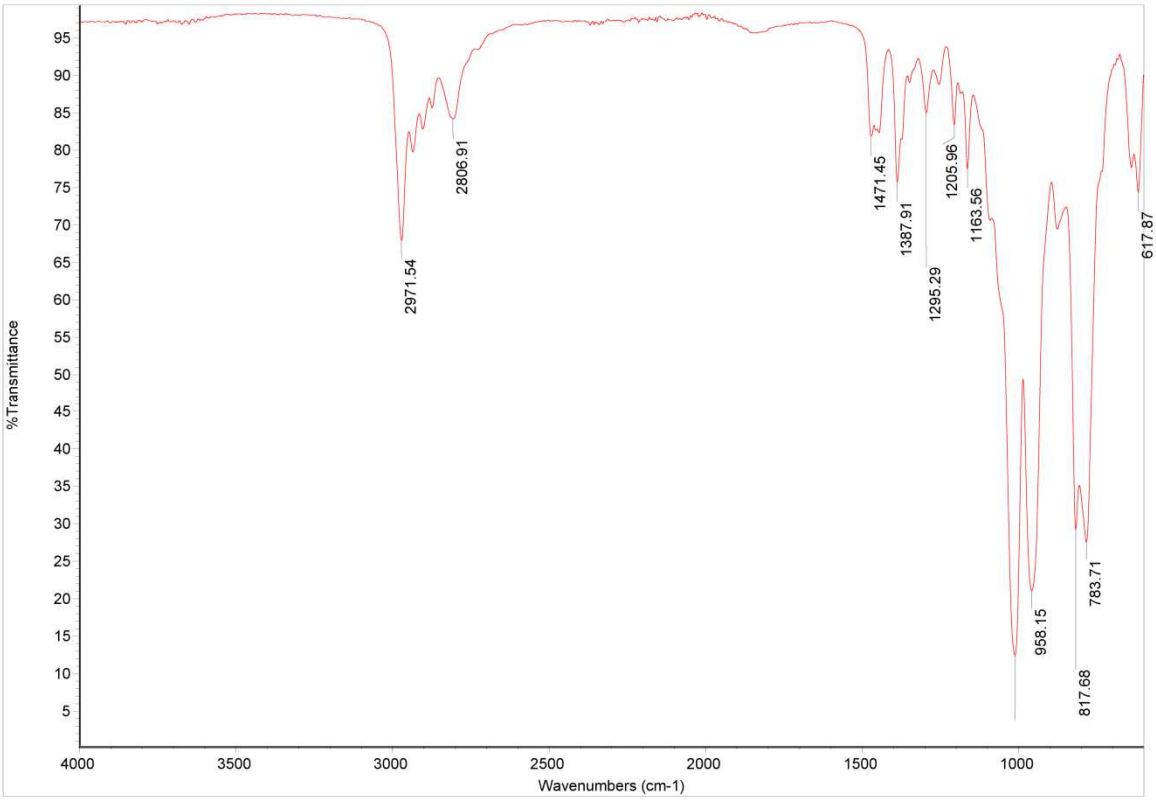

Figure 147: *IR Spectrum of* ***IX****.*

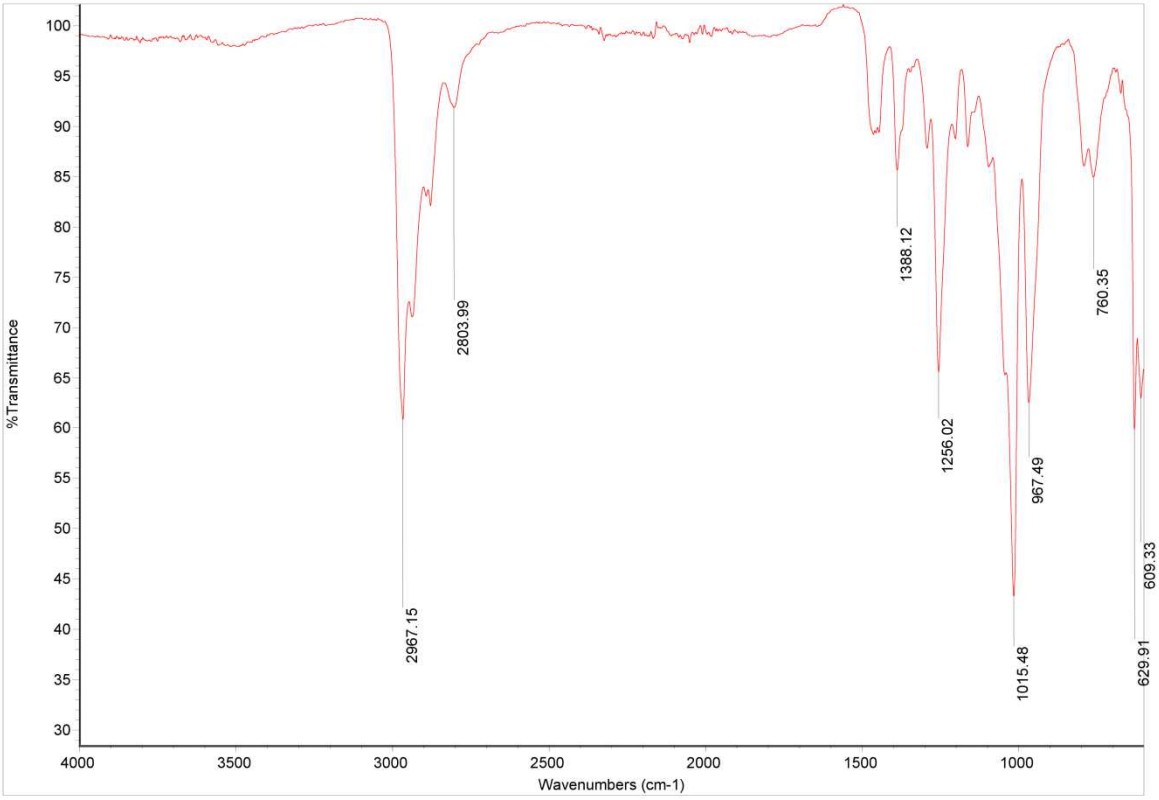

Figure 148: *IR Spectrum of* ***X****.*

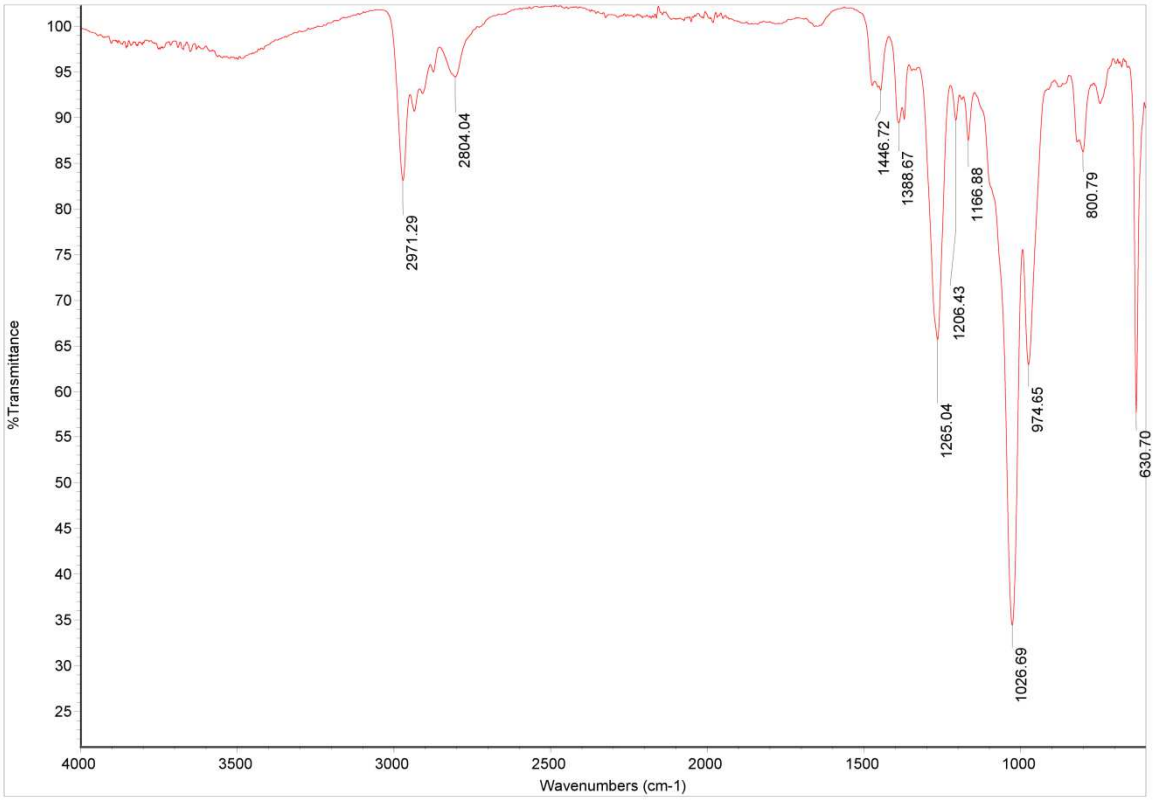

Figure 149: *IR Spectrum of* ***XI****.*

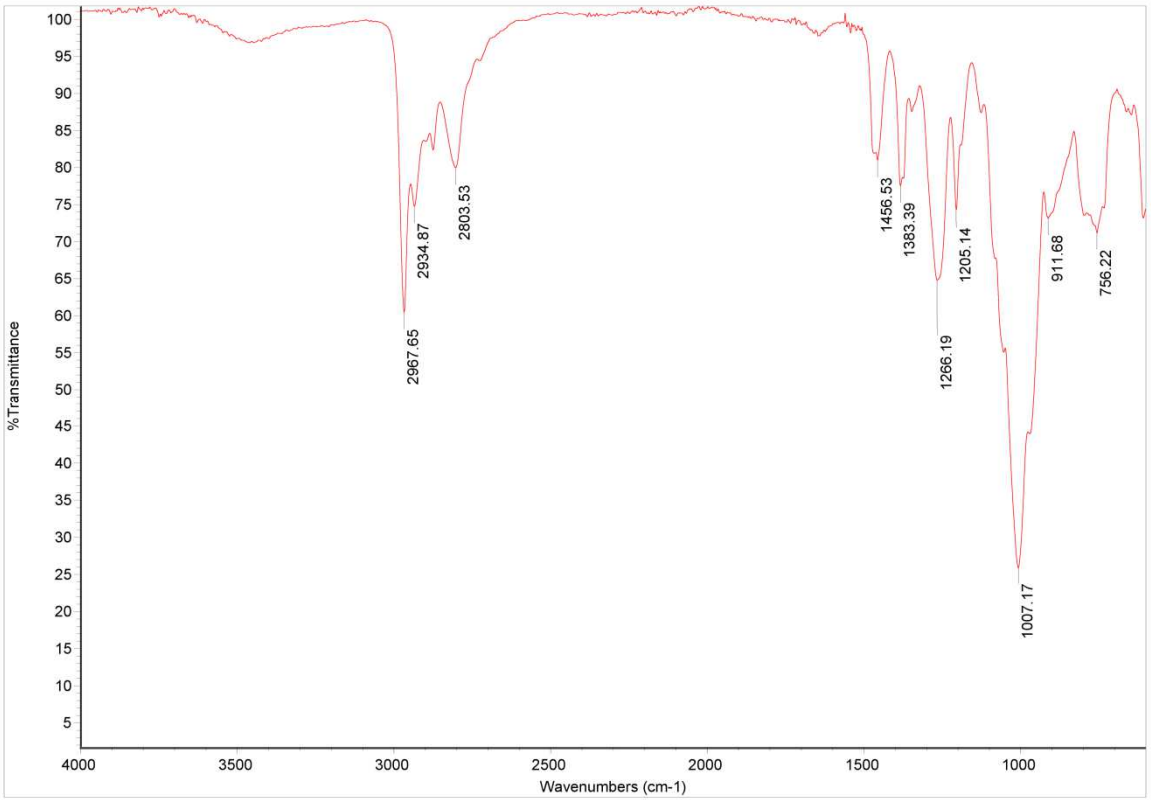

Figure 150: *IR spectrum of* ***XII****.*

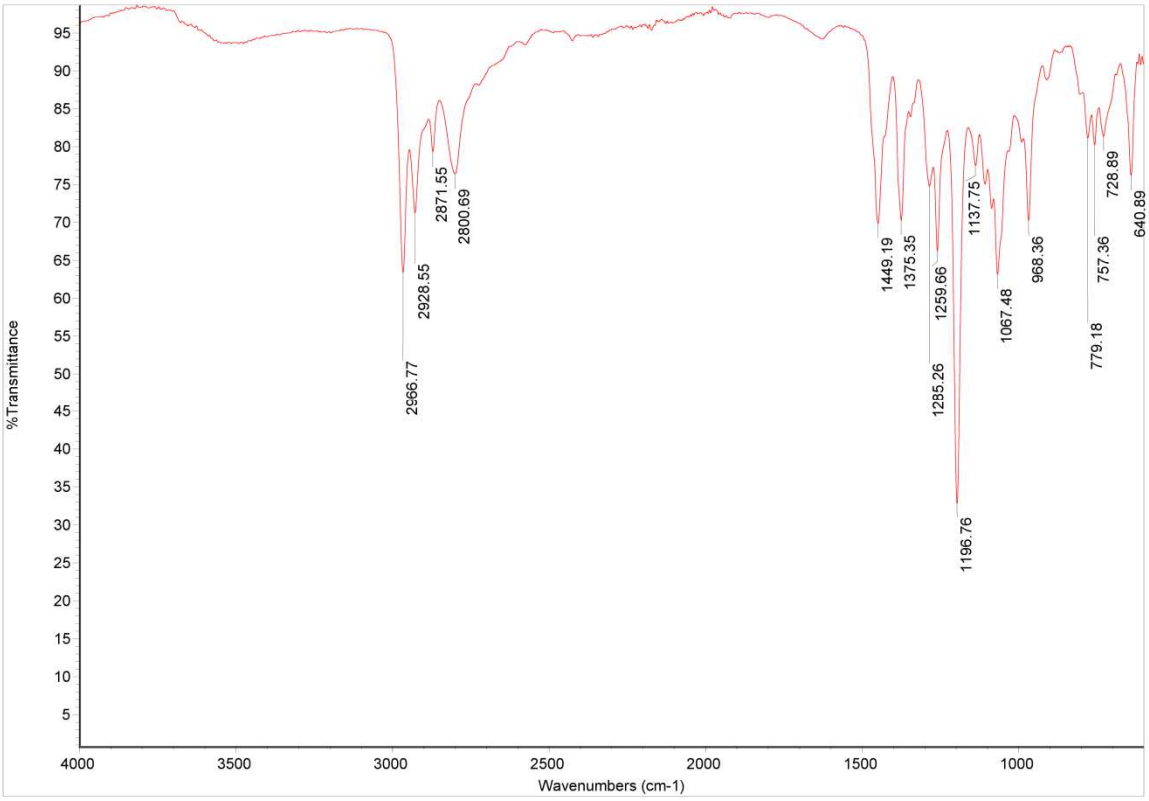

Figure 151: *IR spectrum of* ***XIII****.*

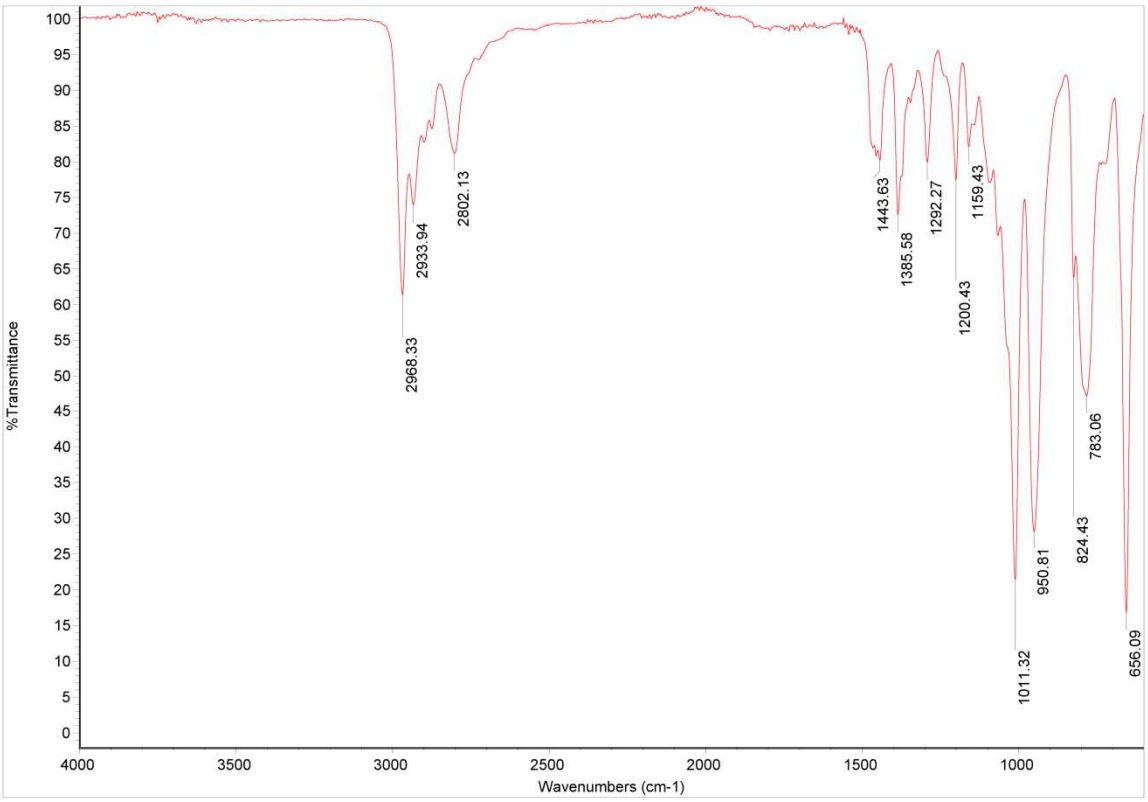

Figure 152*: IR spectrum of* ***XIV****.*

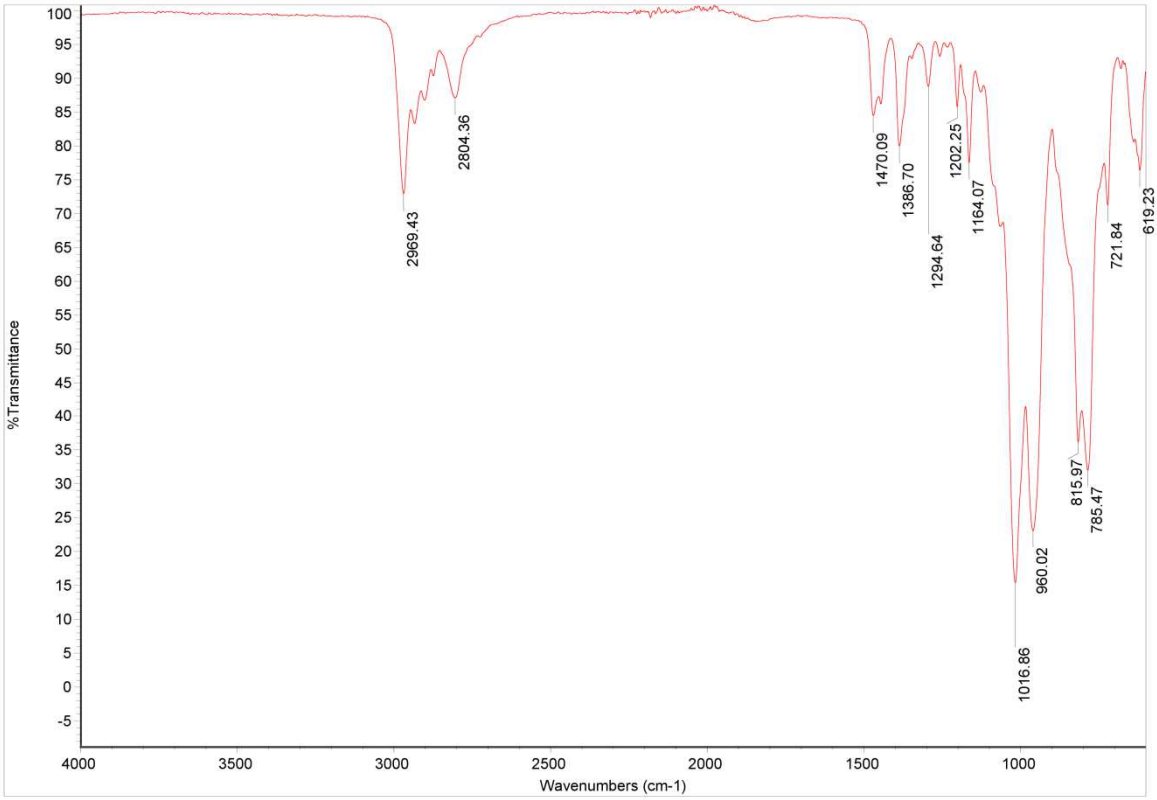

Figure 153: *IR Spectrum of* ***XV****.*

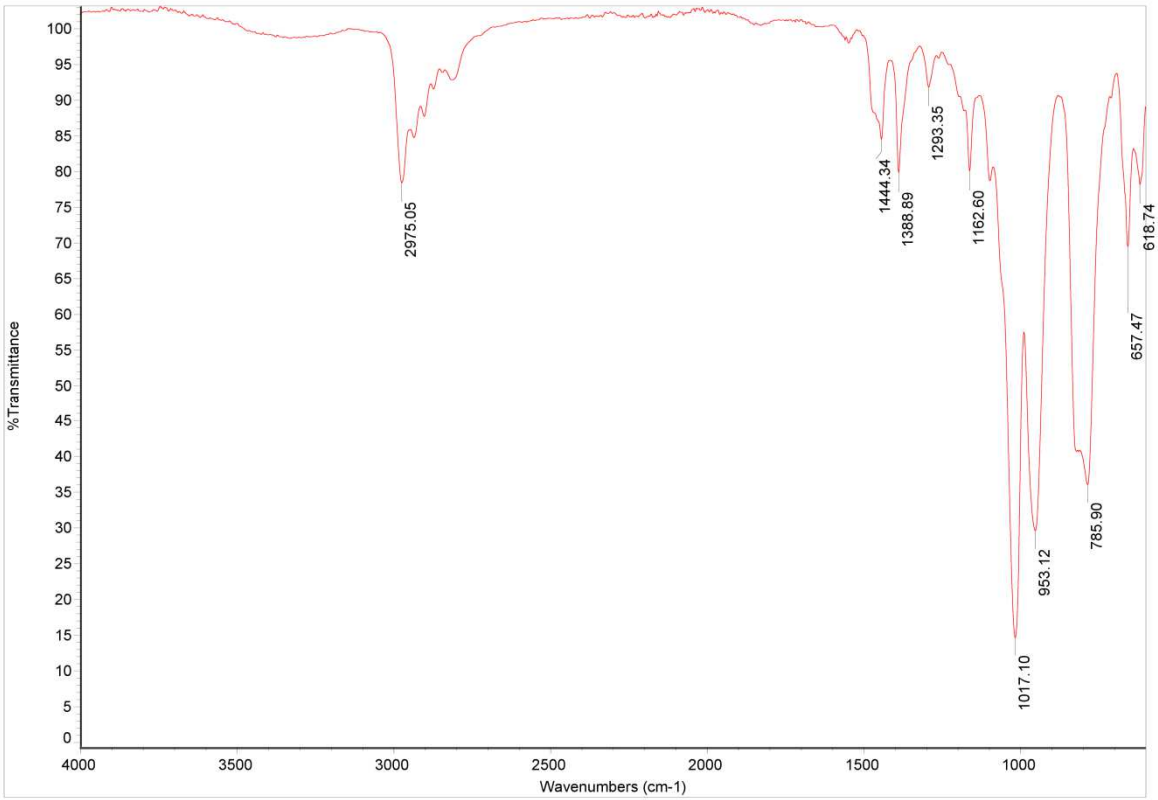

Figure 154: *IR spectrum of* ***XVI****.*

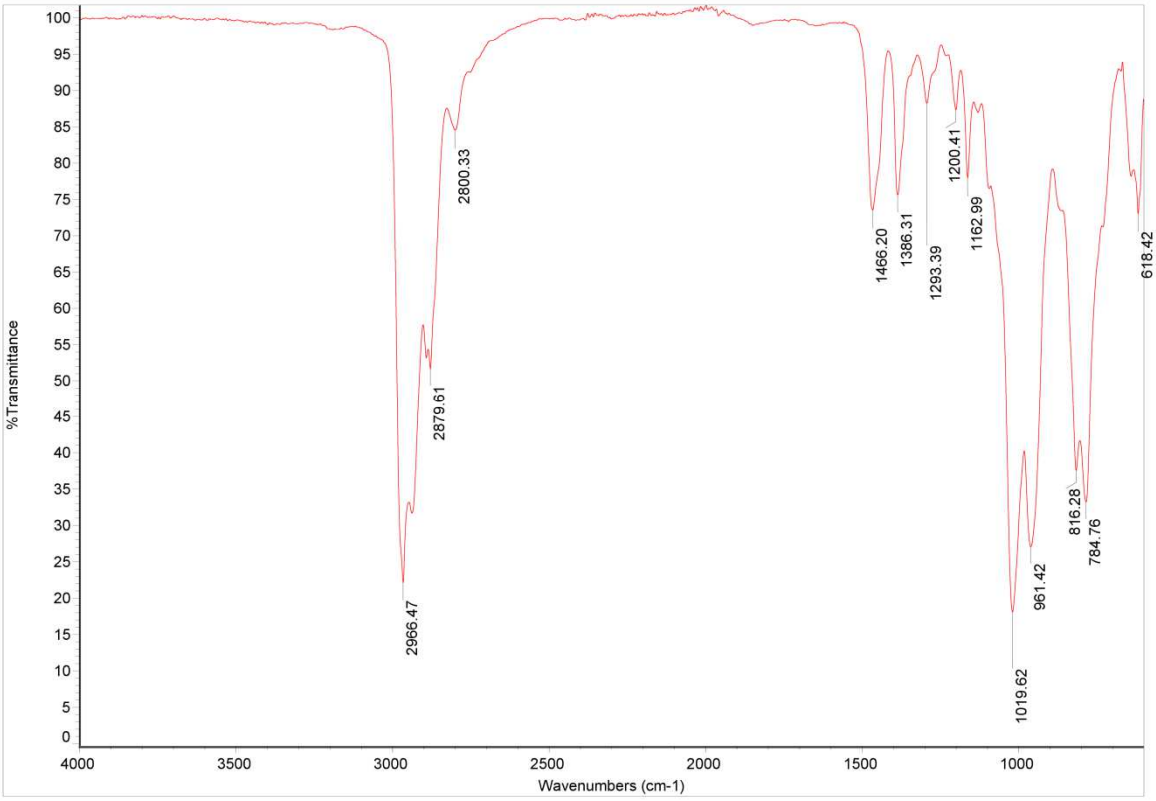

Figure 155: *IR Spectrum of* ***XVII****.*

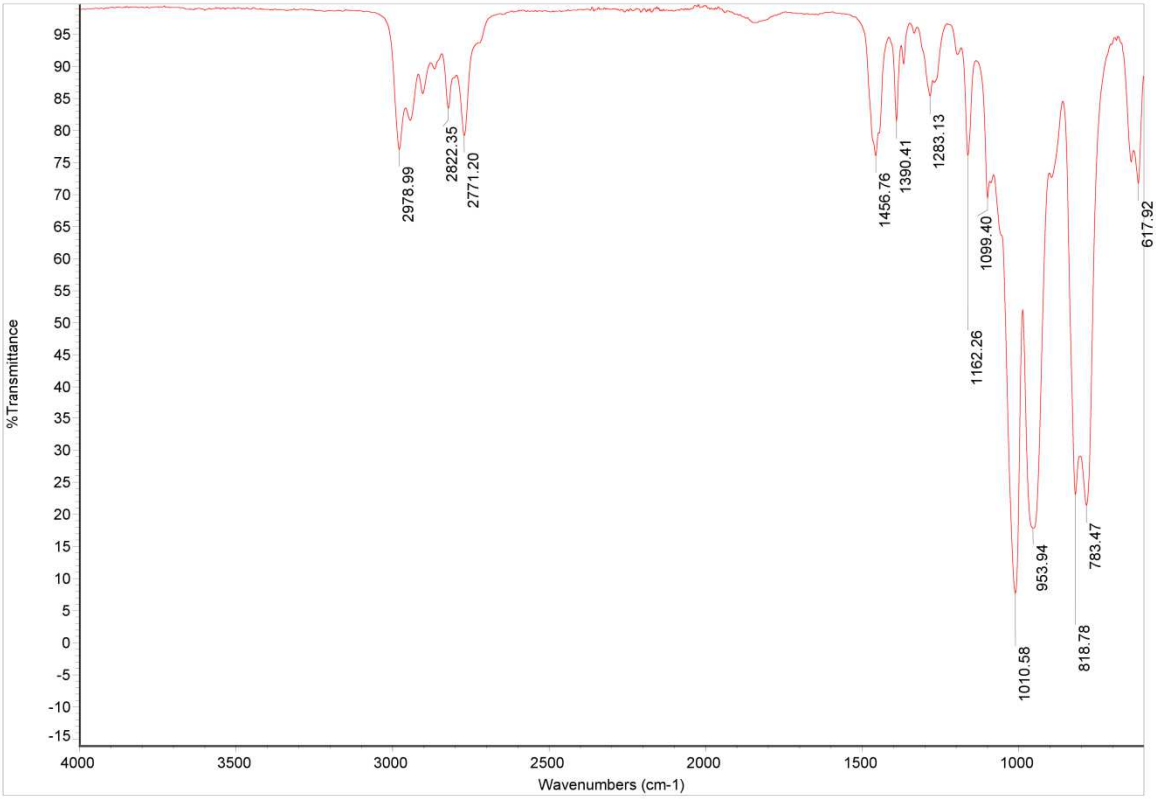

Figure 156: *IR Spectrum of* ***XVIII****.*

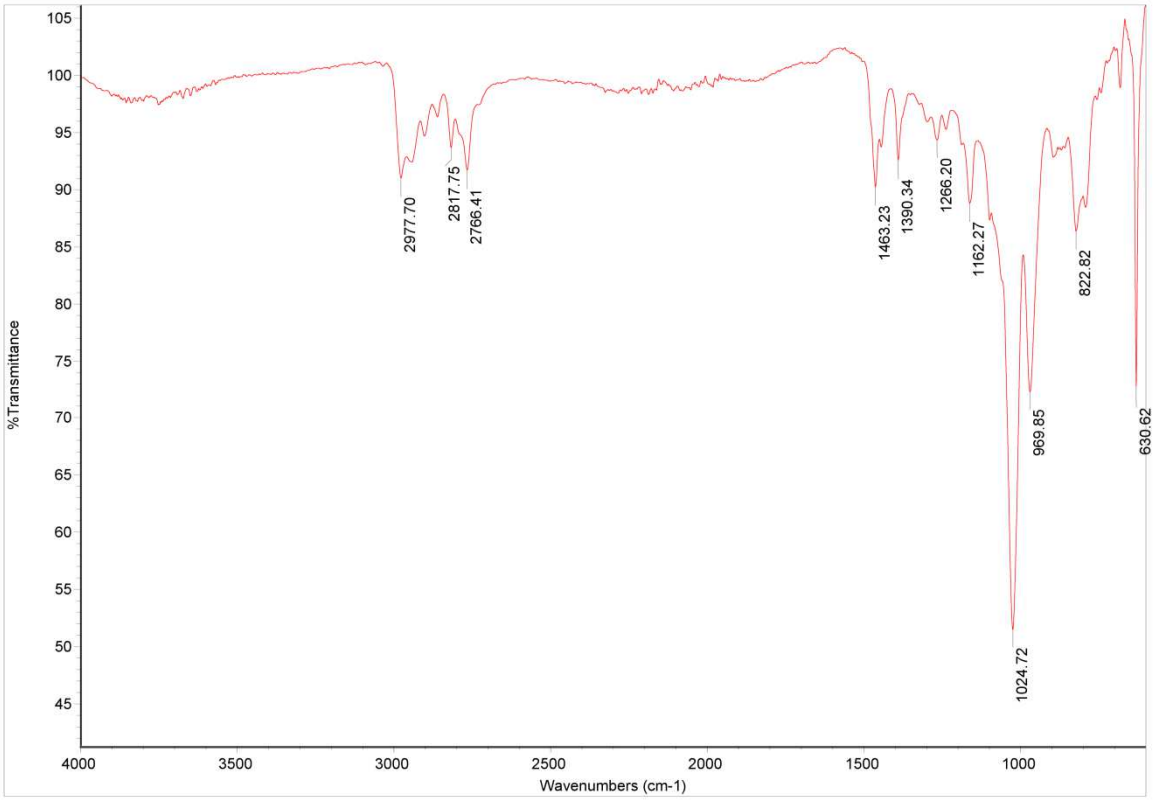

Figure 157: *IR Spectrum of* ***XIX****.*

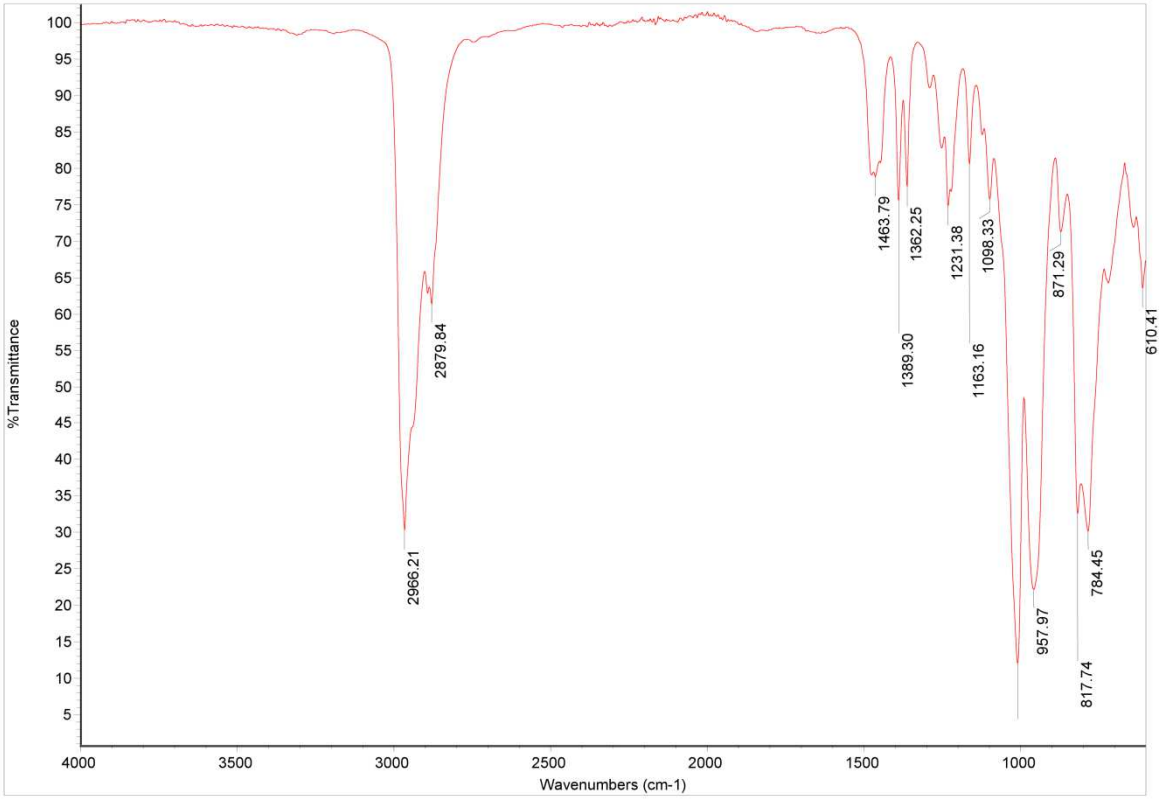

Figure 158: *IR Spectrum of* ***XX****.*

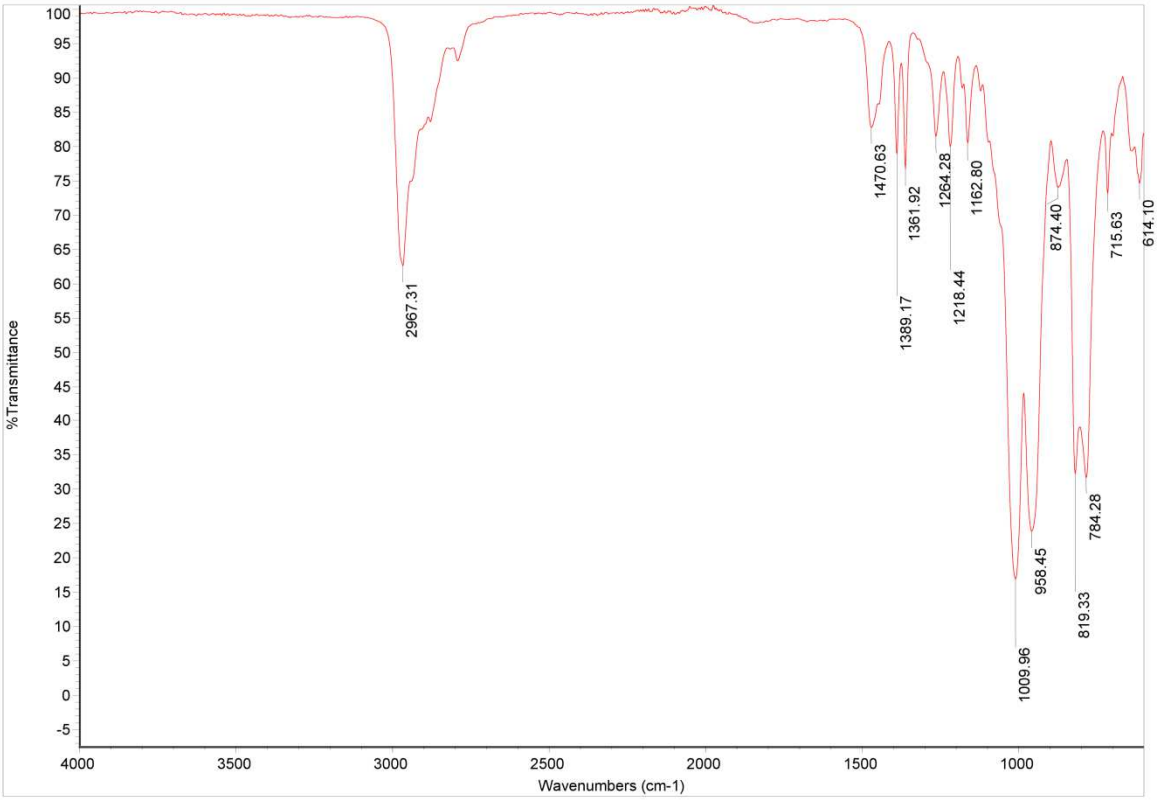

Figure 159: *IR Spectrum of* ***XXI****.*

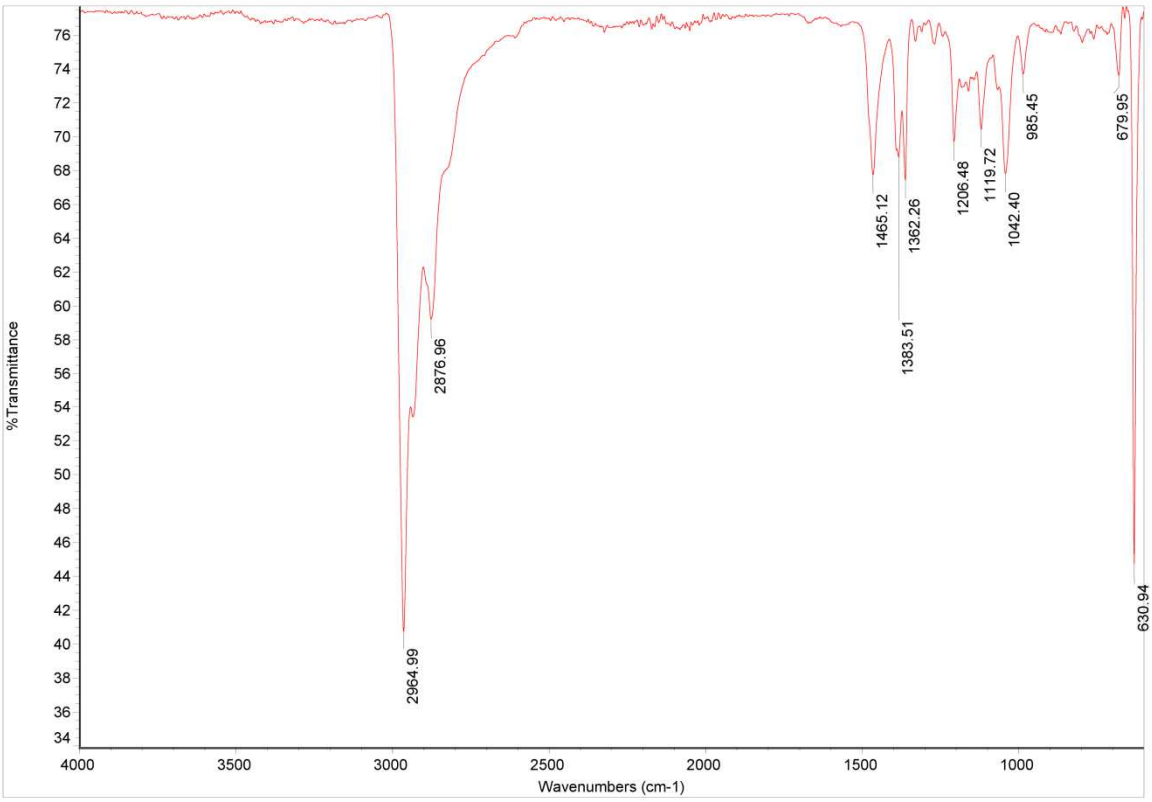

Figure 160: *IR Spectrum of* ***XXII****.*

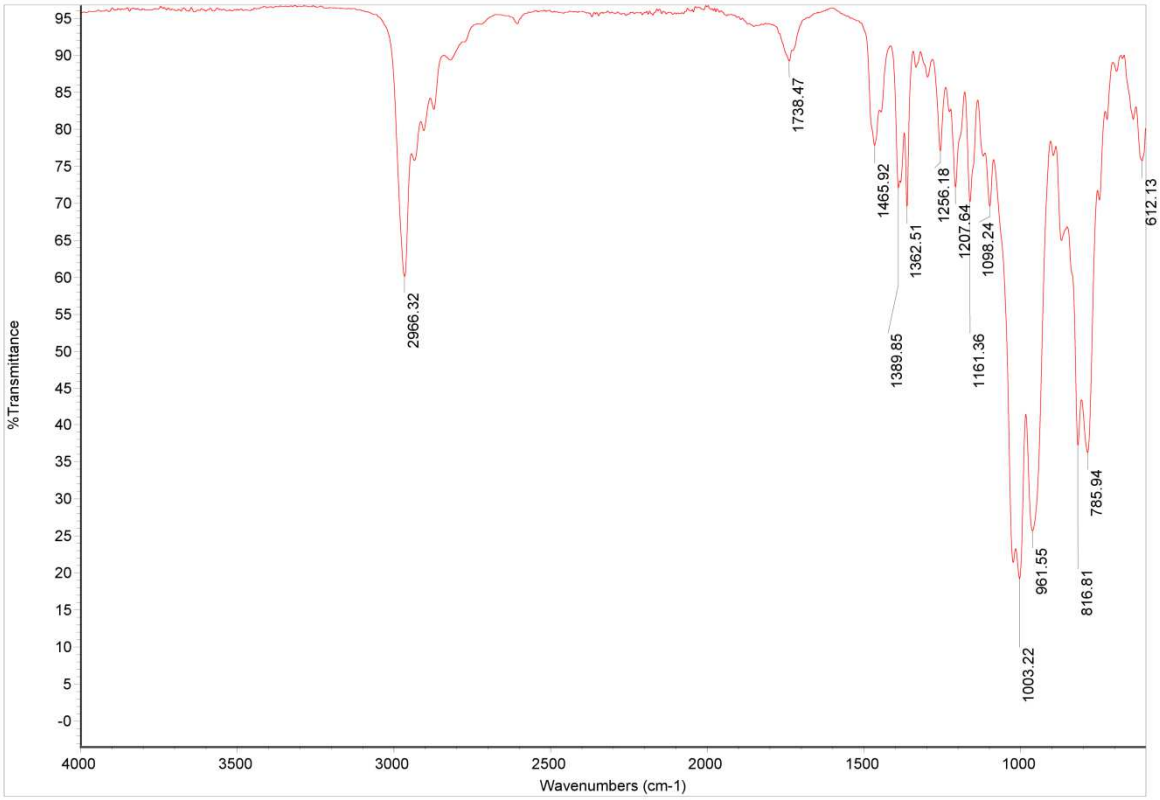

Figure 161: *IR Spectrum of* ***XXIII****.*

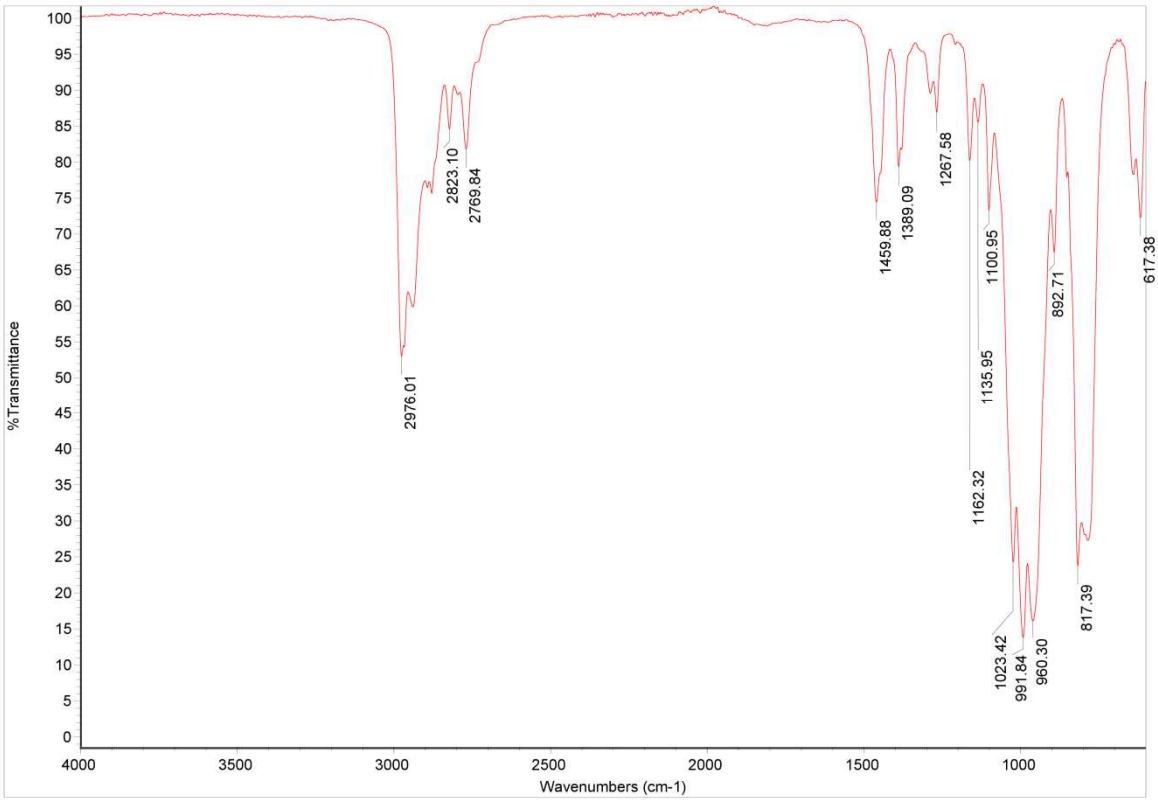

Figure 162: *IR spectrum of* ***XXIV****.*

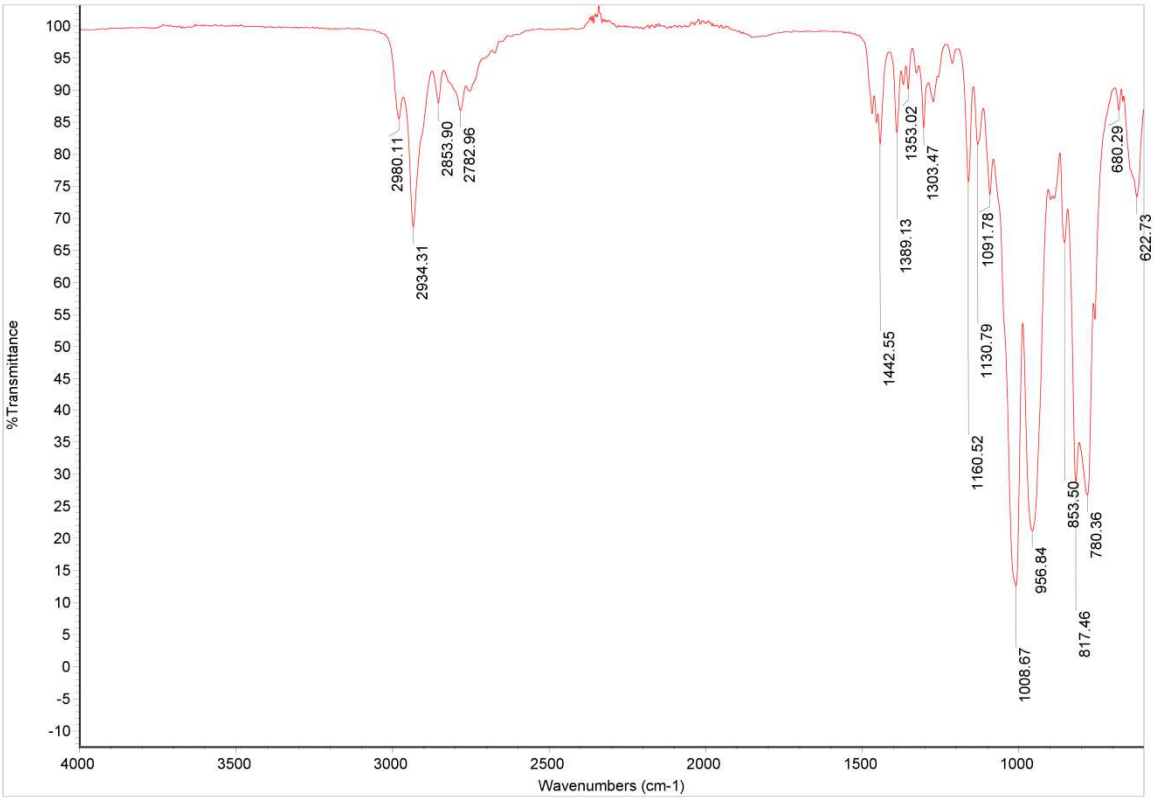

Figure 163: *IR Spectrum of* ***XXV****.*

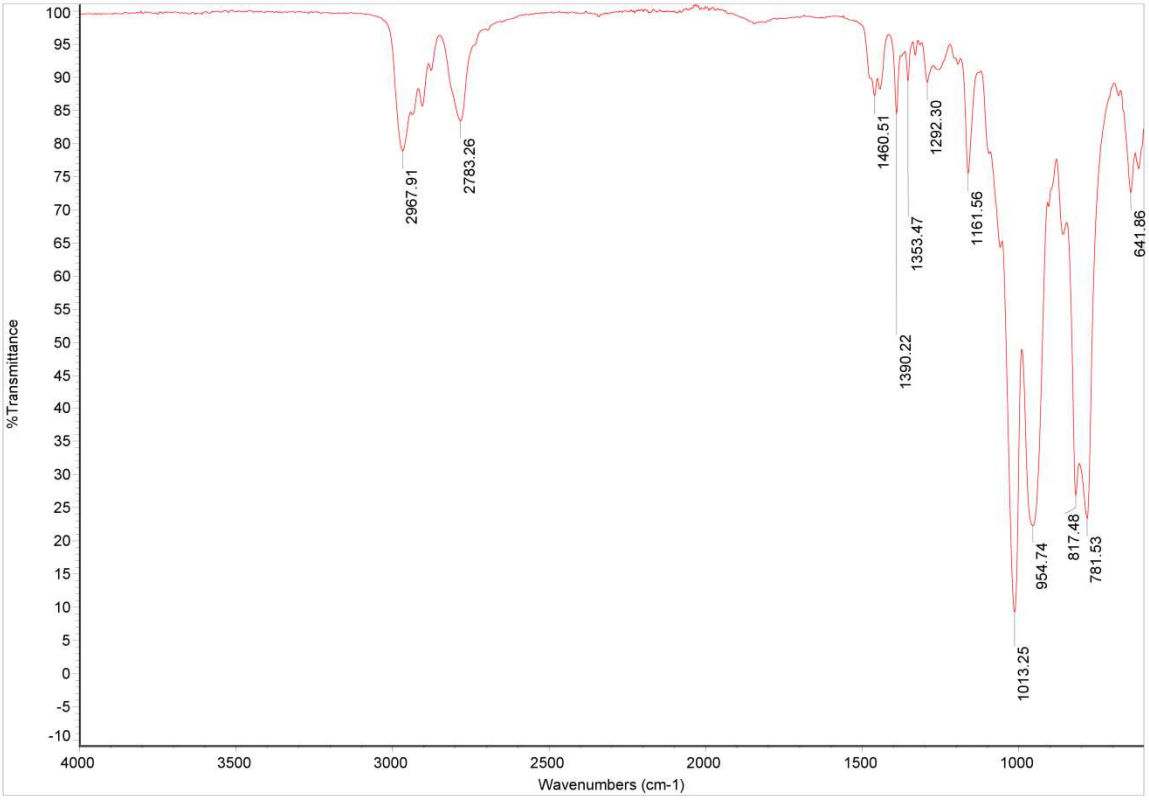

Figure 164: *IR Spectrum of* ***XXVI****.*

iv. Organothiophosphate Salts

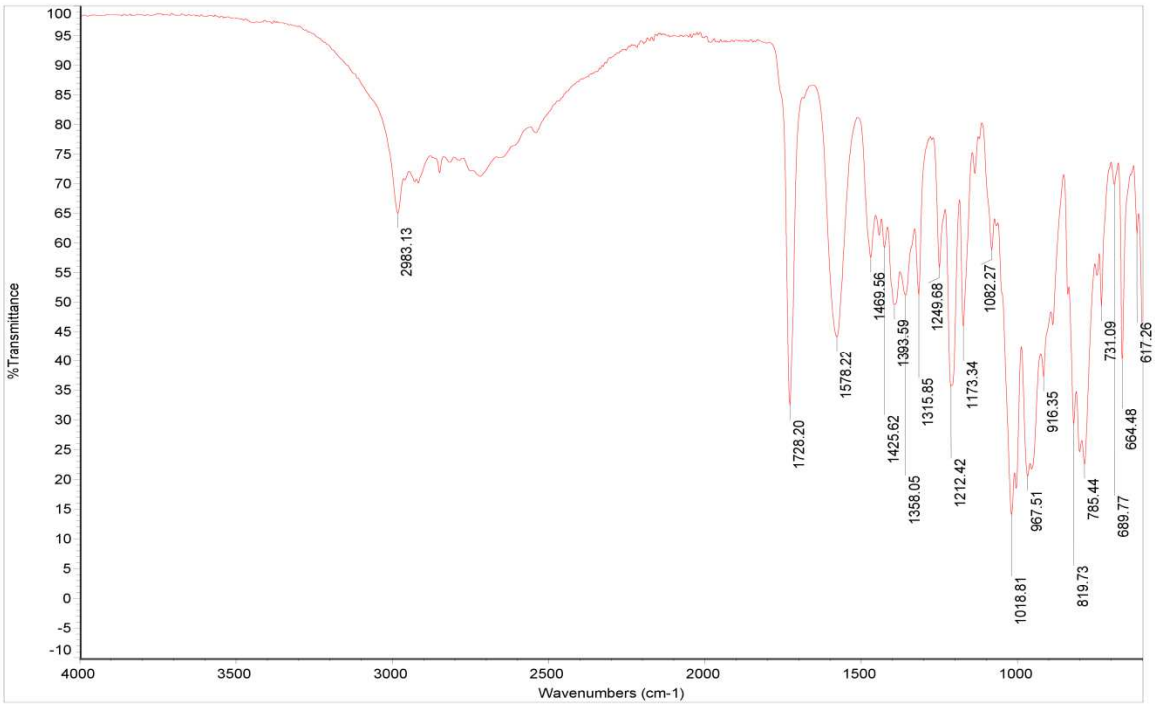

***Figure 165**: IR Spectrum of **XXVIII**.*

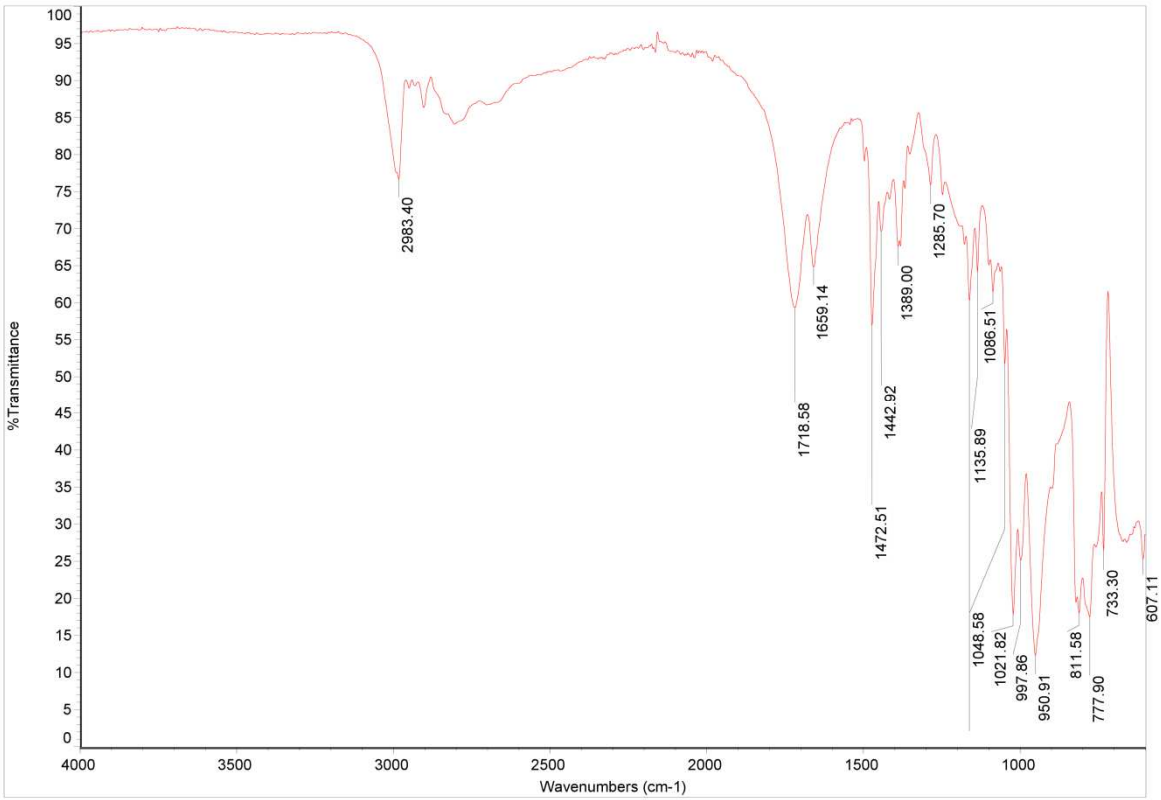

***Figure 166:** IR Spectrum of **XXIX**.*

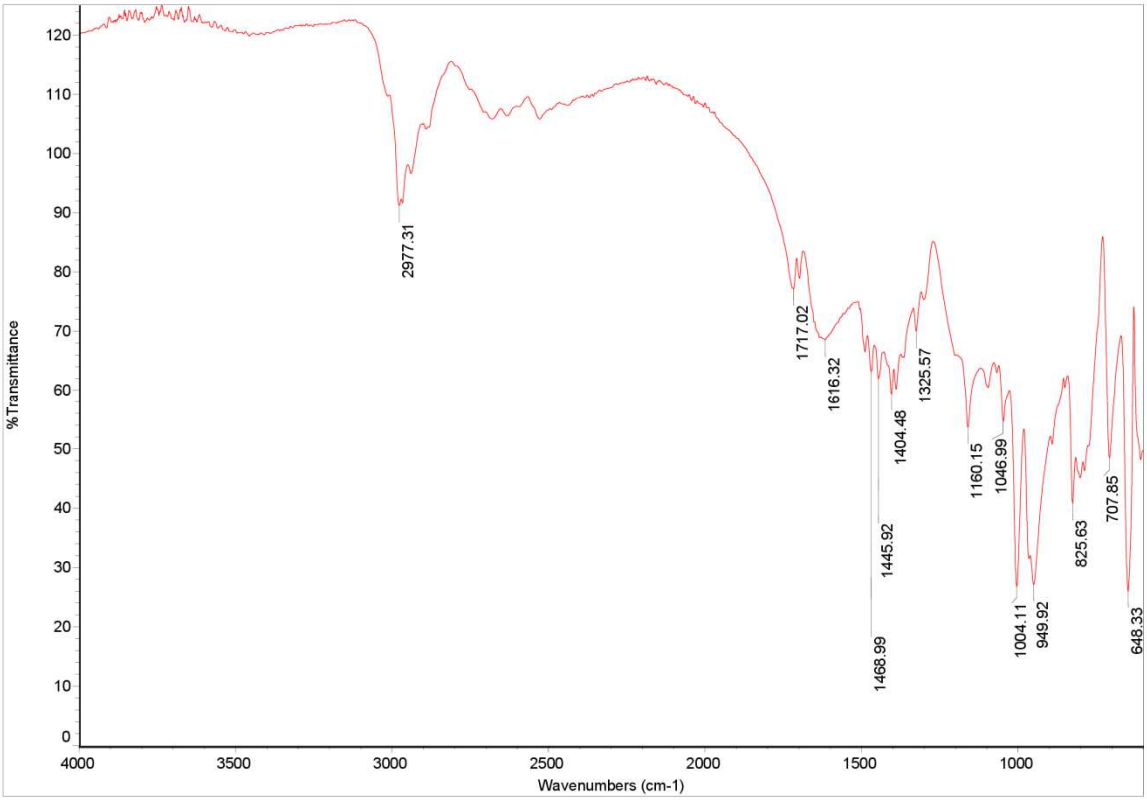

Figure 167: *IR Spectrum of* ***XXX****.*

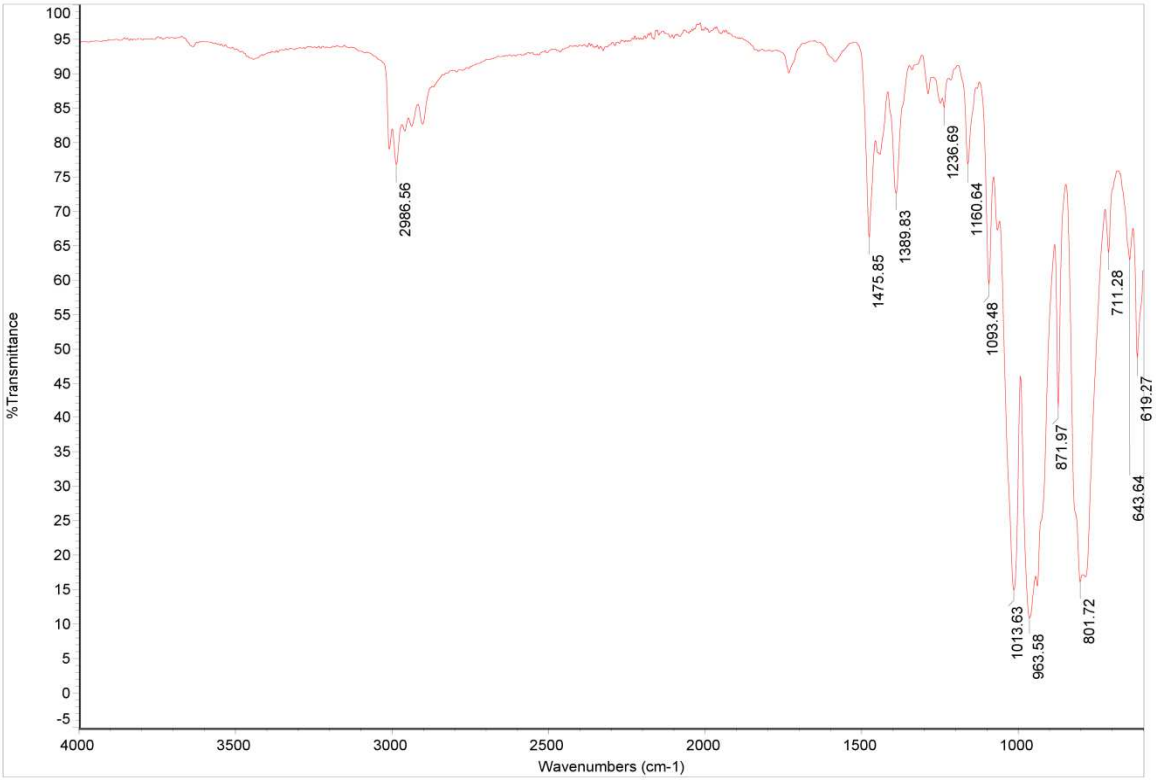

Figure 168: *IR Spectrum of* ***XXXI****.*

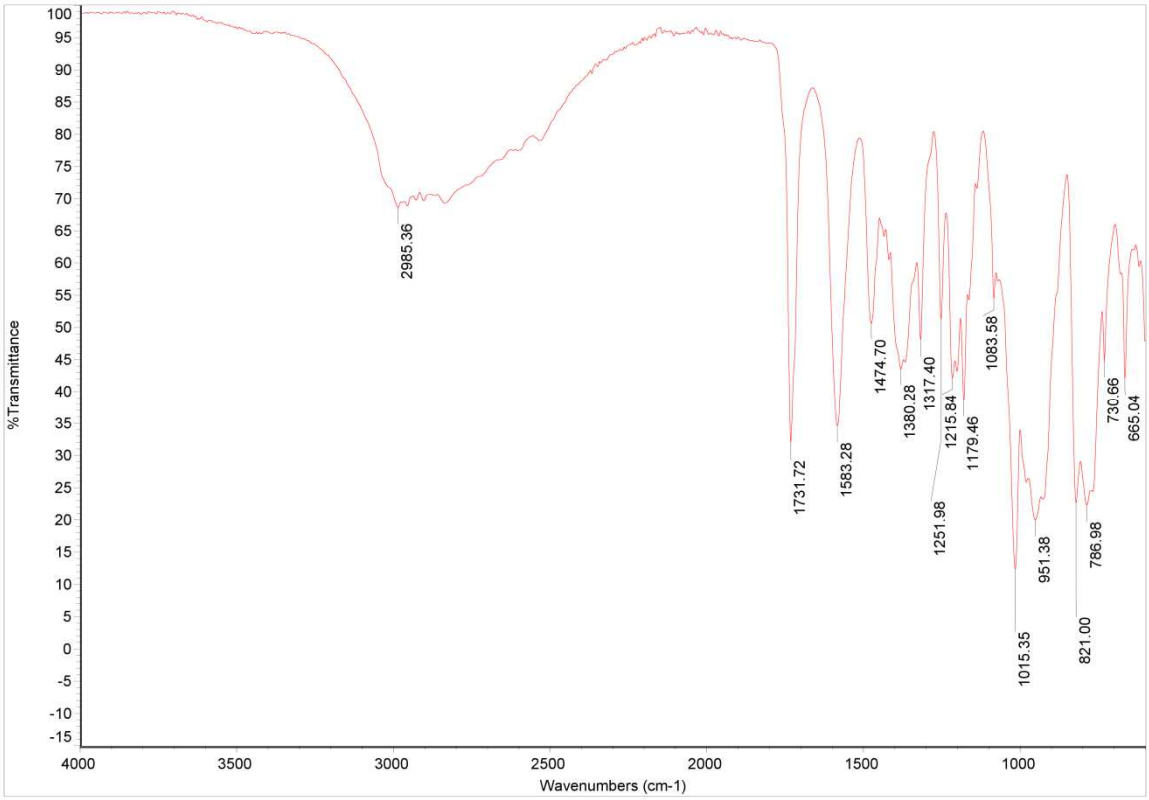

Figure 169: *IR Spectrum of* ***XXXII****.*

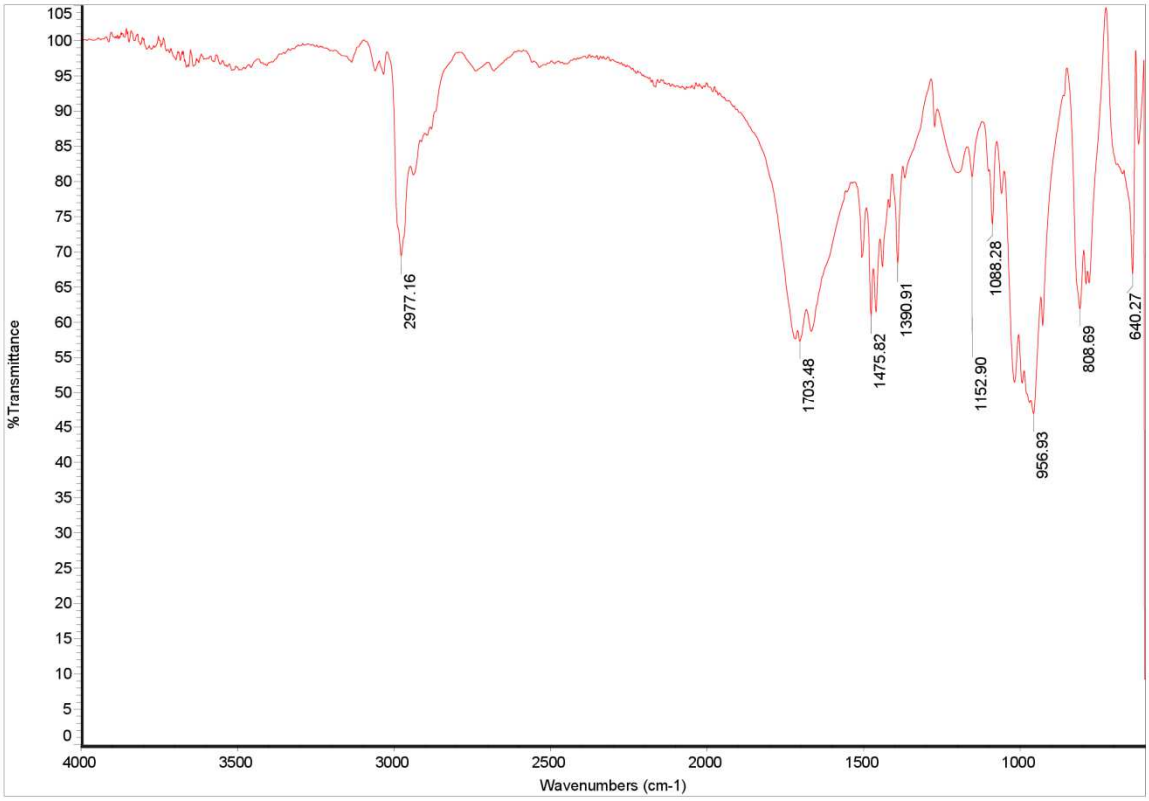

Figure 170: *IR Spectrum of* ***XXXIII****.*

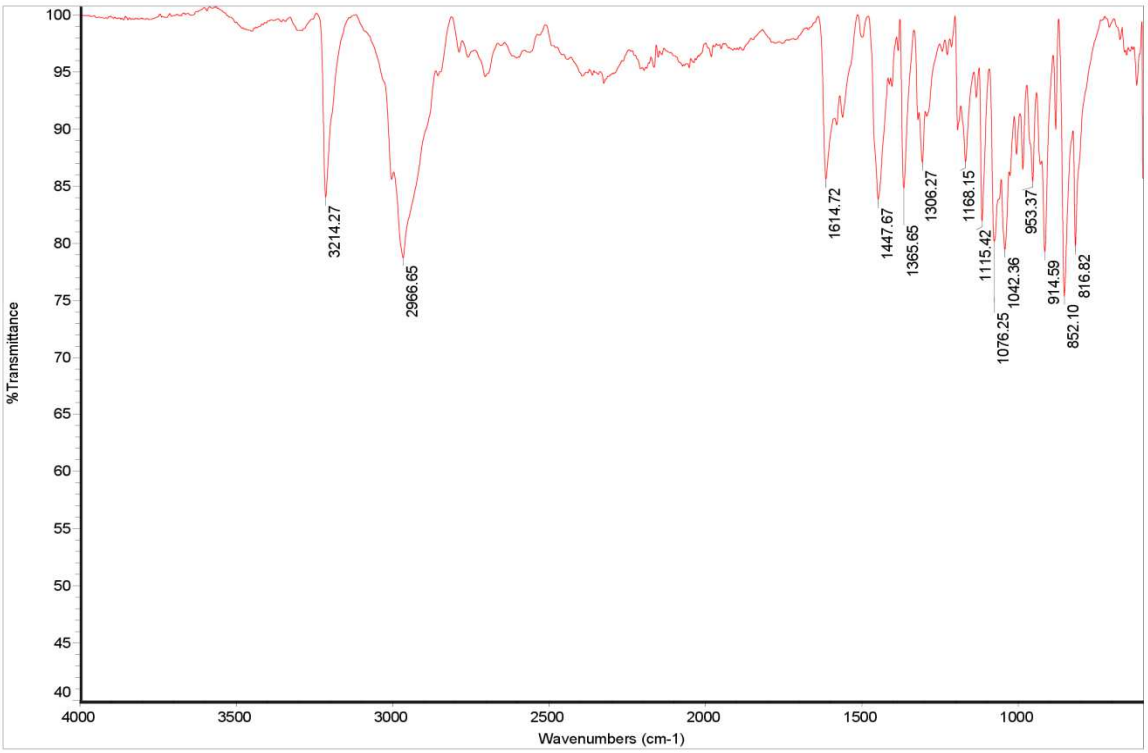

Figure 171: *IR Spectrum of the decomposition product of* ***XVIII = XXXIV****.*

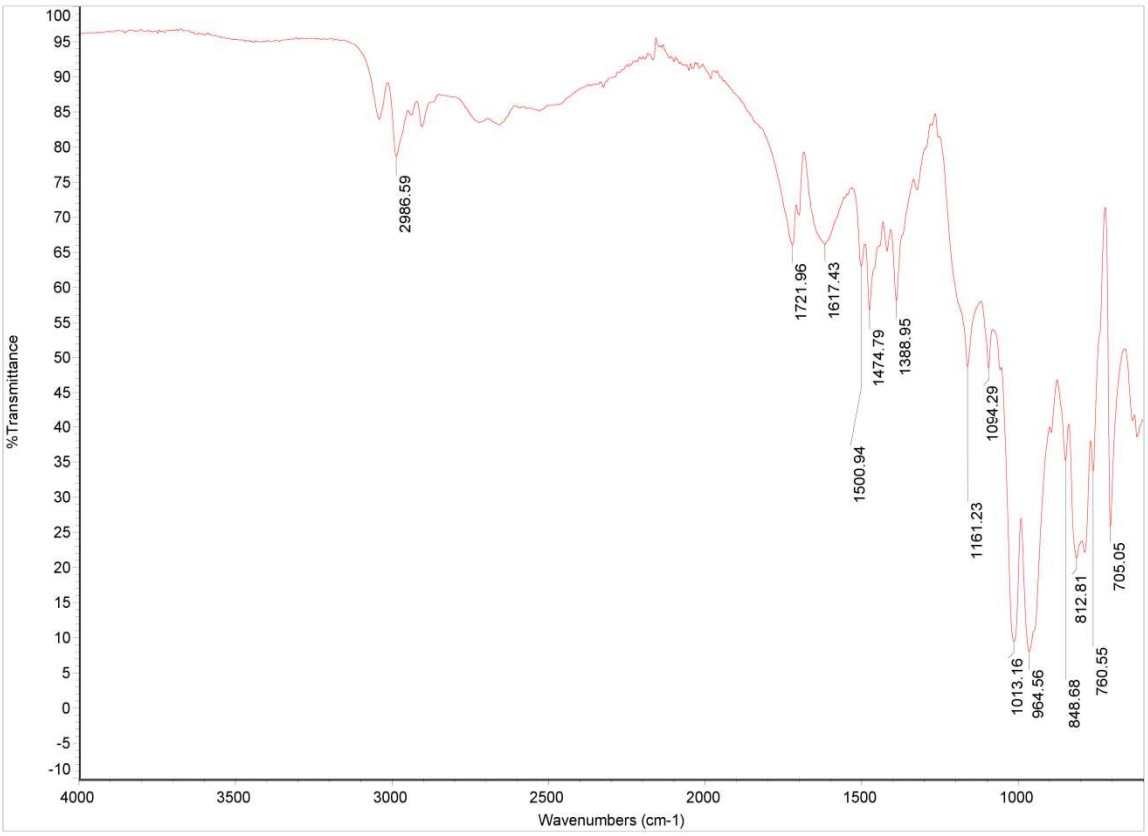

Figure 172: *IR Spectrum of* ***XXXV****.*

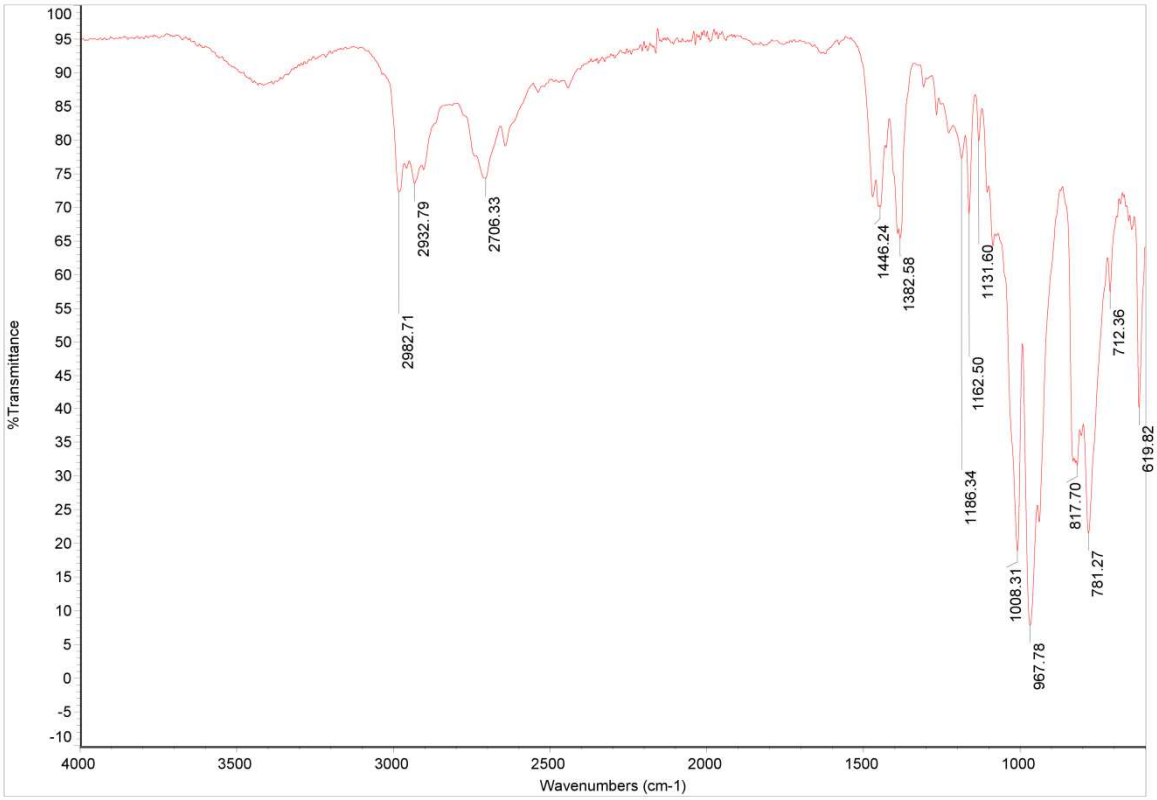

Figure 173: *IR Spectrum of* ***XXXVI****.*

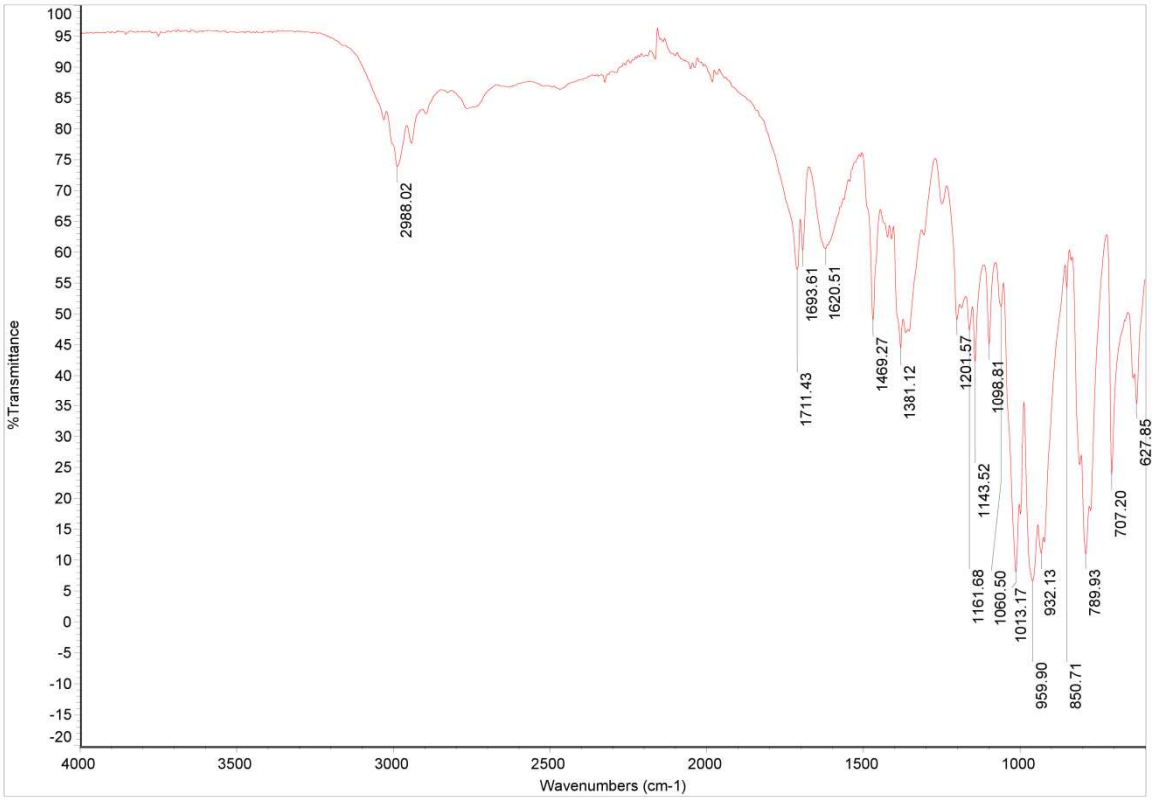

Figure 174: *IR Spectrum of* ***XXXVII****.*

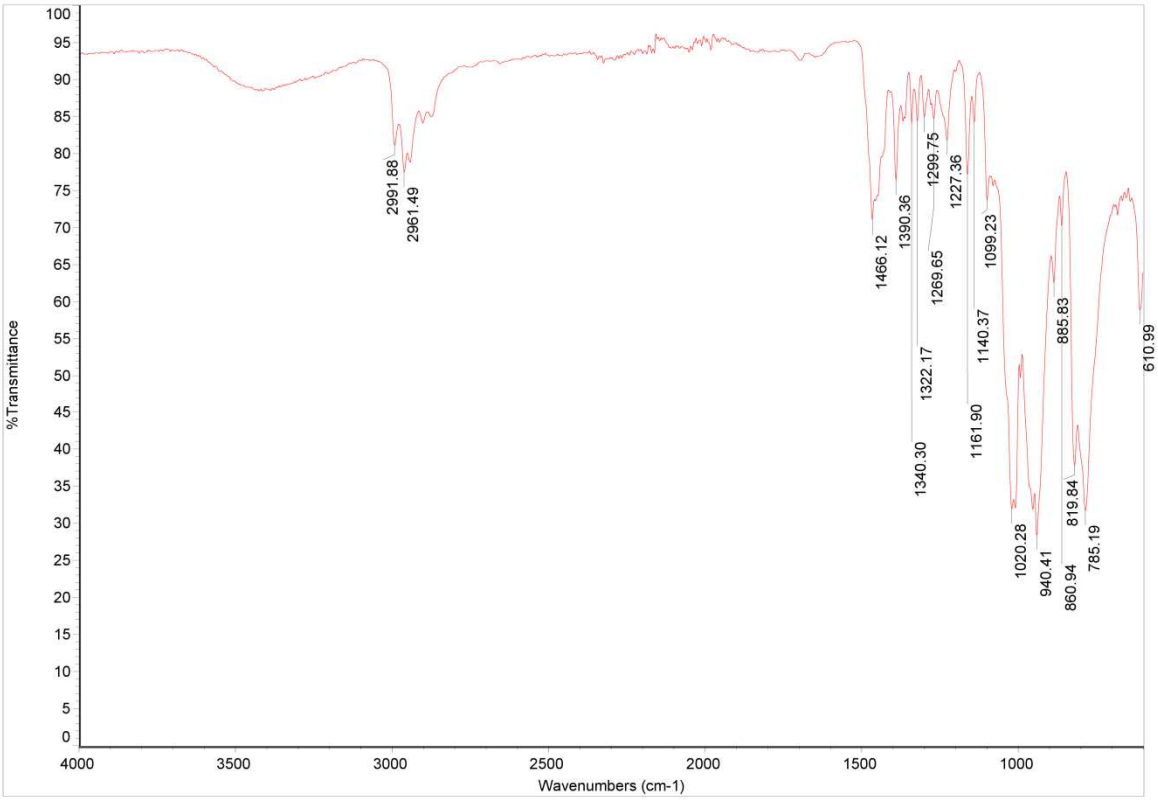

Figure 175: *IR Spectrum of* ***XXXVIII.***

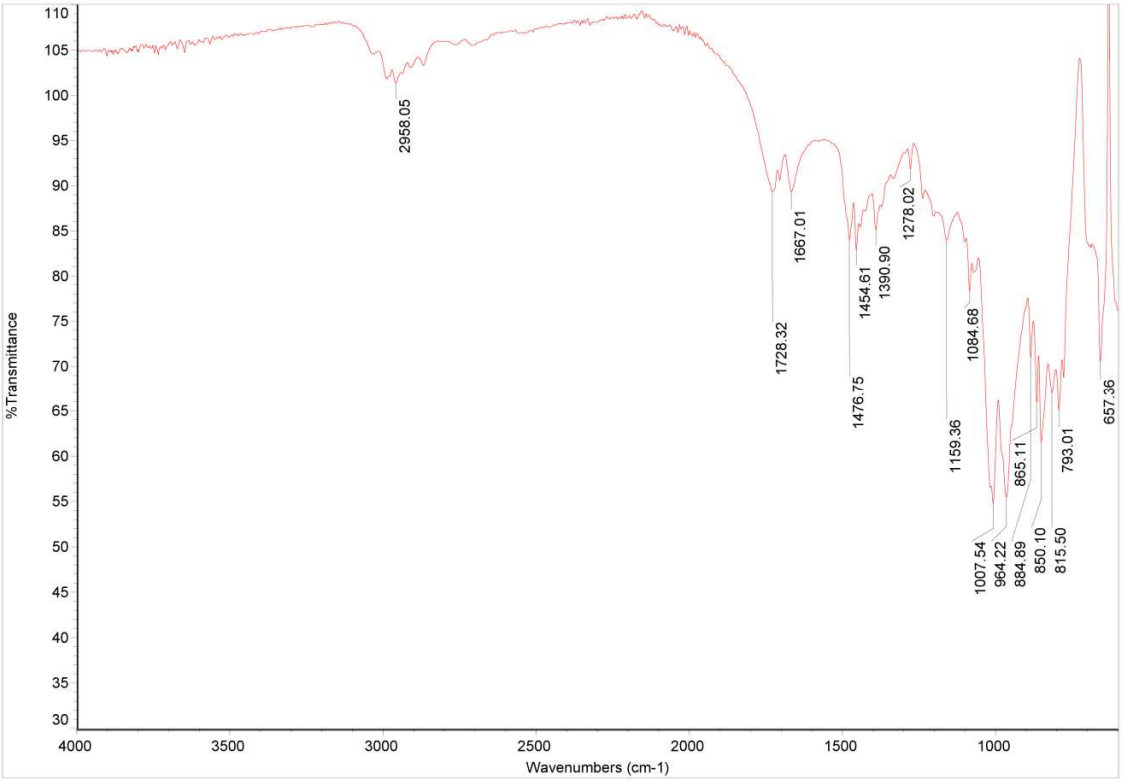

Figure 176: *IR Spectrum of* ***XXXIX.***

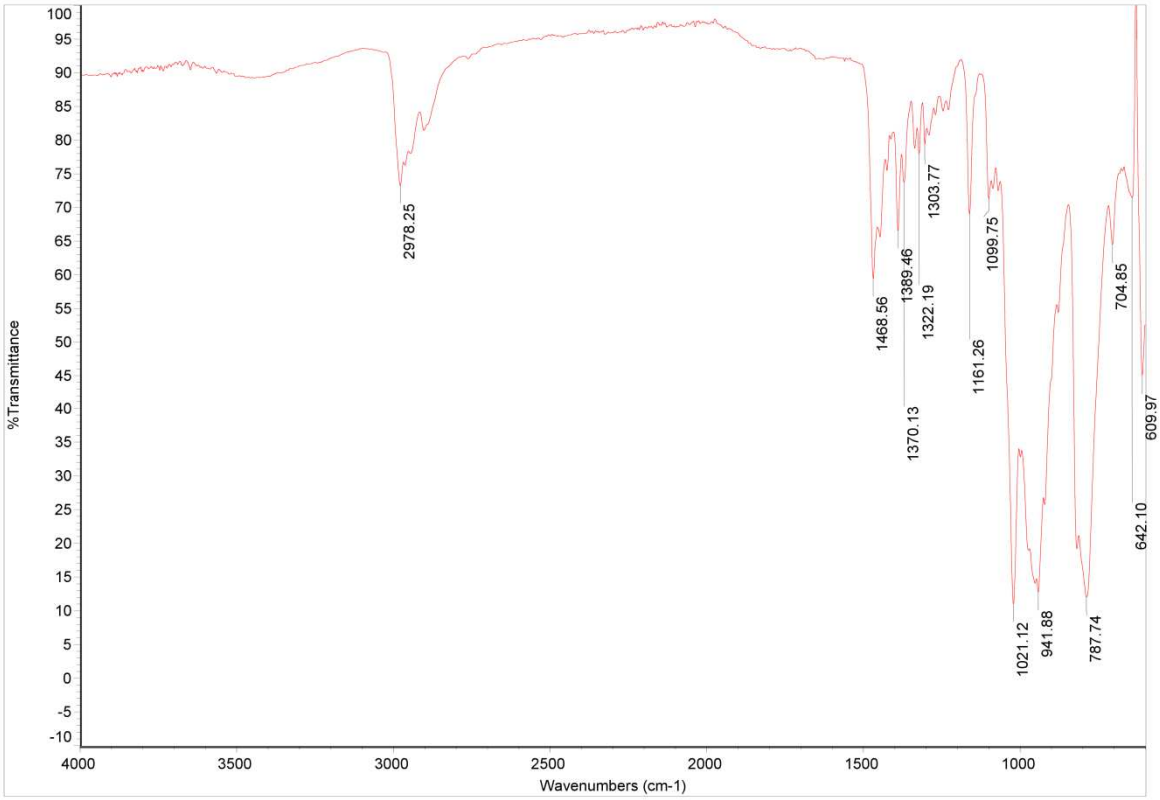

Figure 177: *IR Spectrum of* ***XL.***

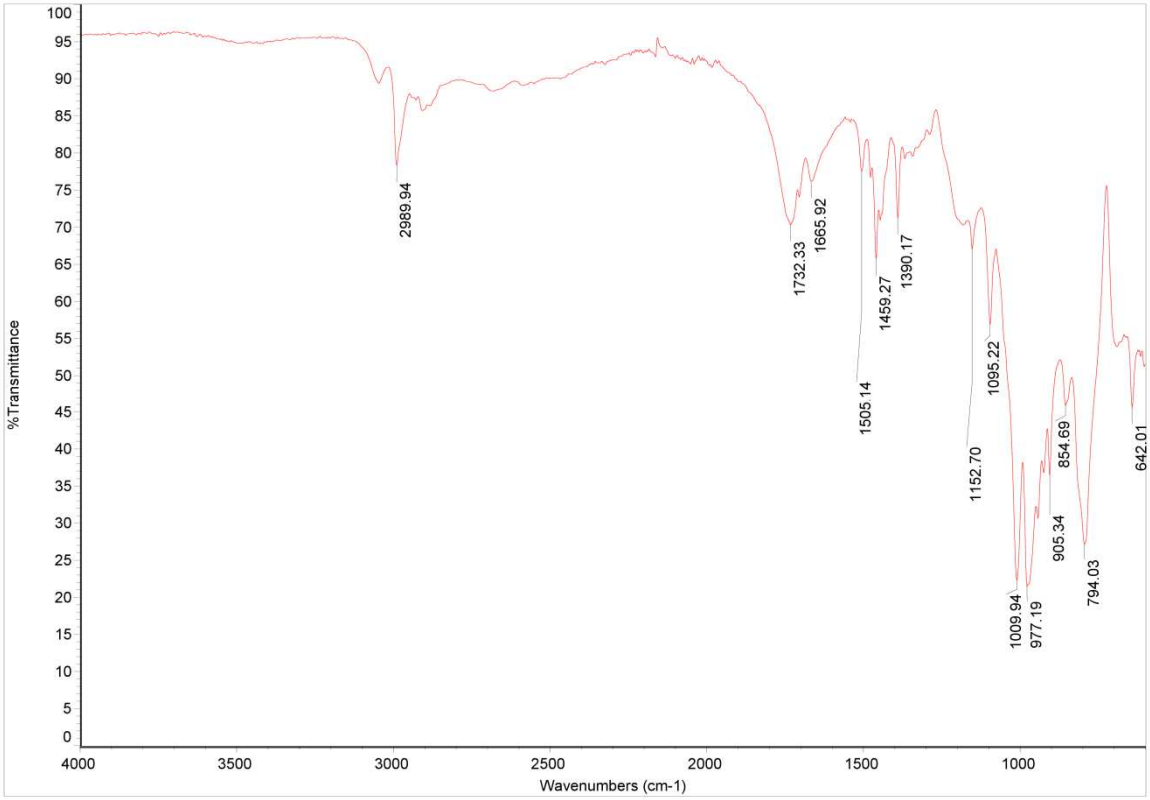

Figure 178: *IR Spectrum of* ***XLI****.*

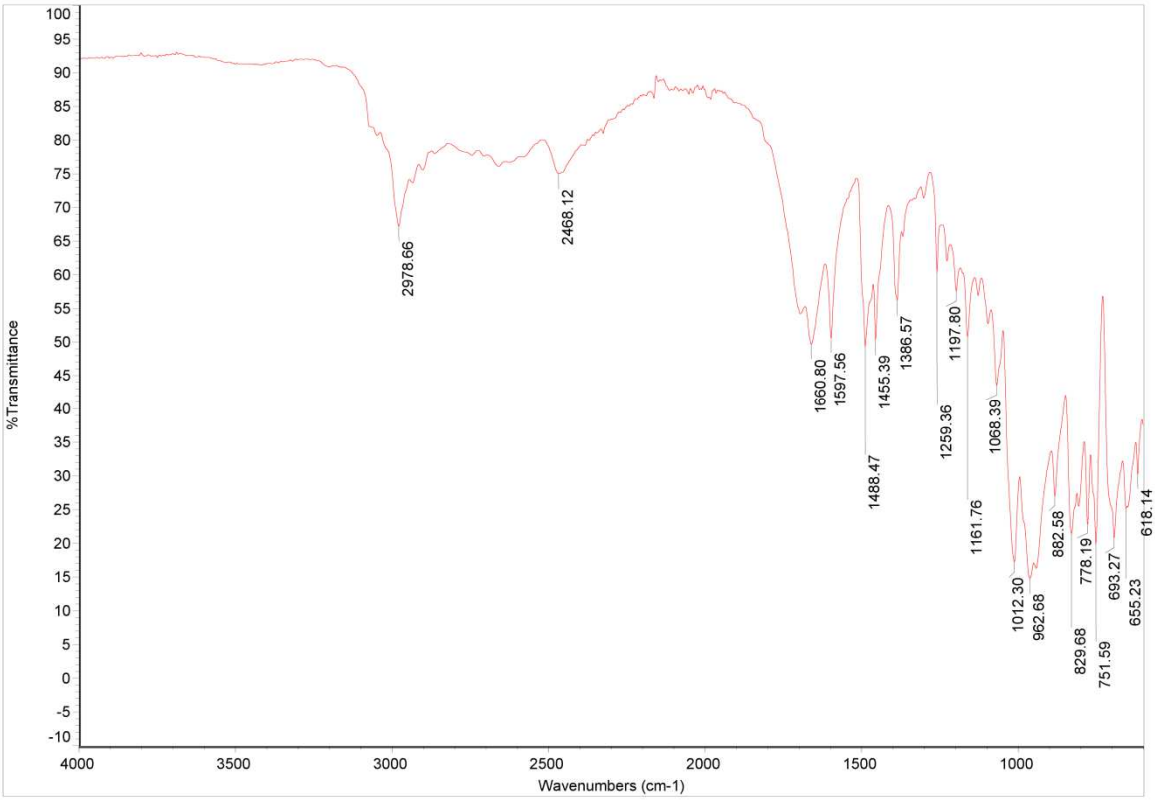

Figure 179: *IR Spectrum of* ***XLII****.*

.

A.2 Raman Spectra

i. Amino Alcohol Spectra

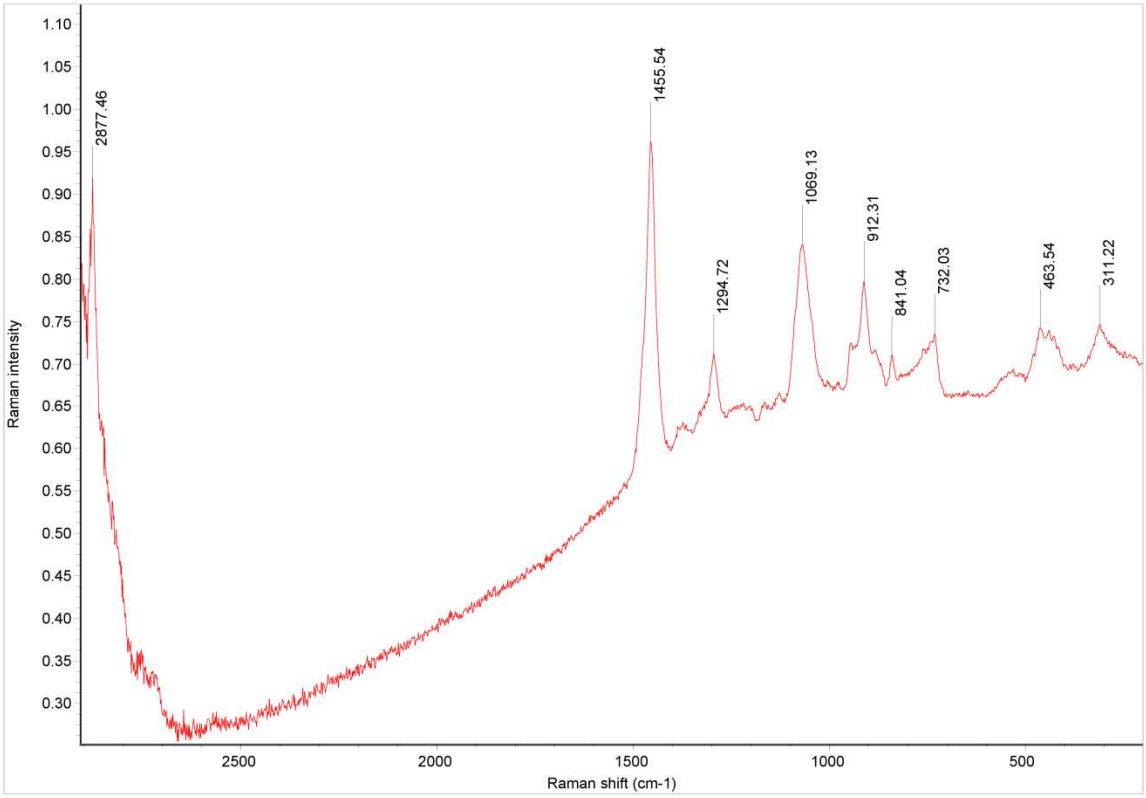

Figure 180: *Raman Spectrum of* ***I****.*

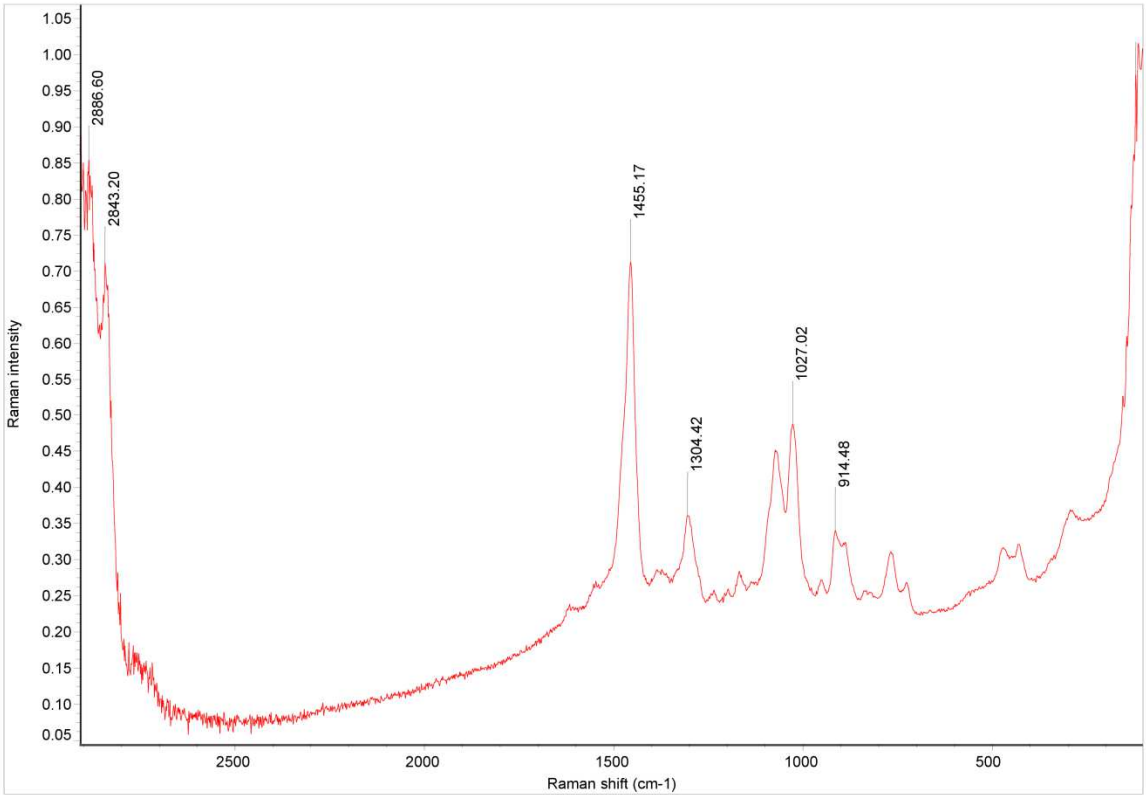

Figure 181: *Raman Spectrum of* ***II****.*

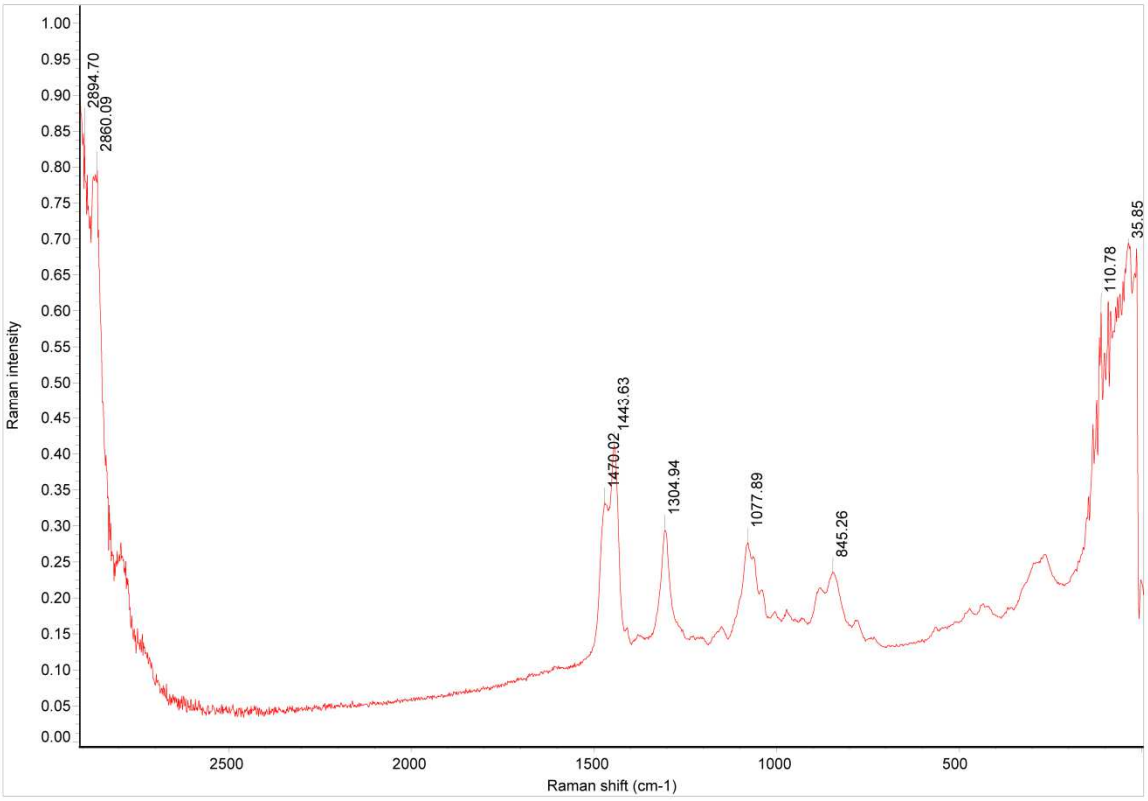

Figure 182: *Raman spectrum of* ***VI****.*

ii. O,O'-Diethyl(thio)phosphorylchloride Spectra

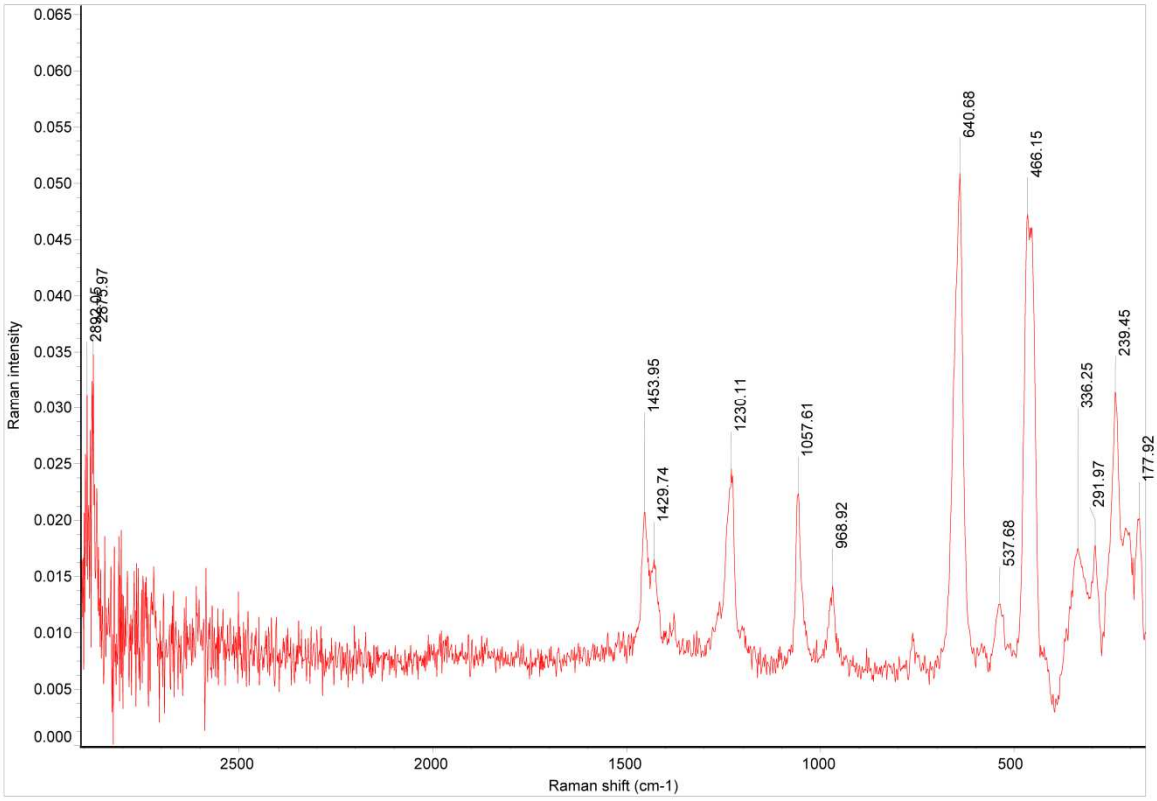

Figure 183: *Raman spectrum of* ***VIII****.*

iii. Organo(thio)phosphates

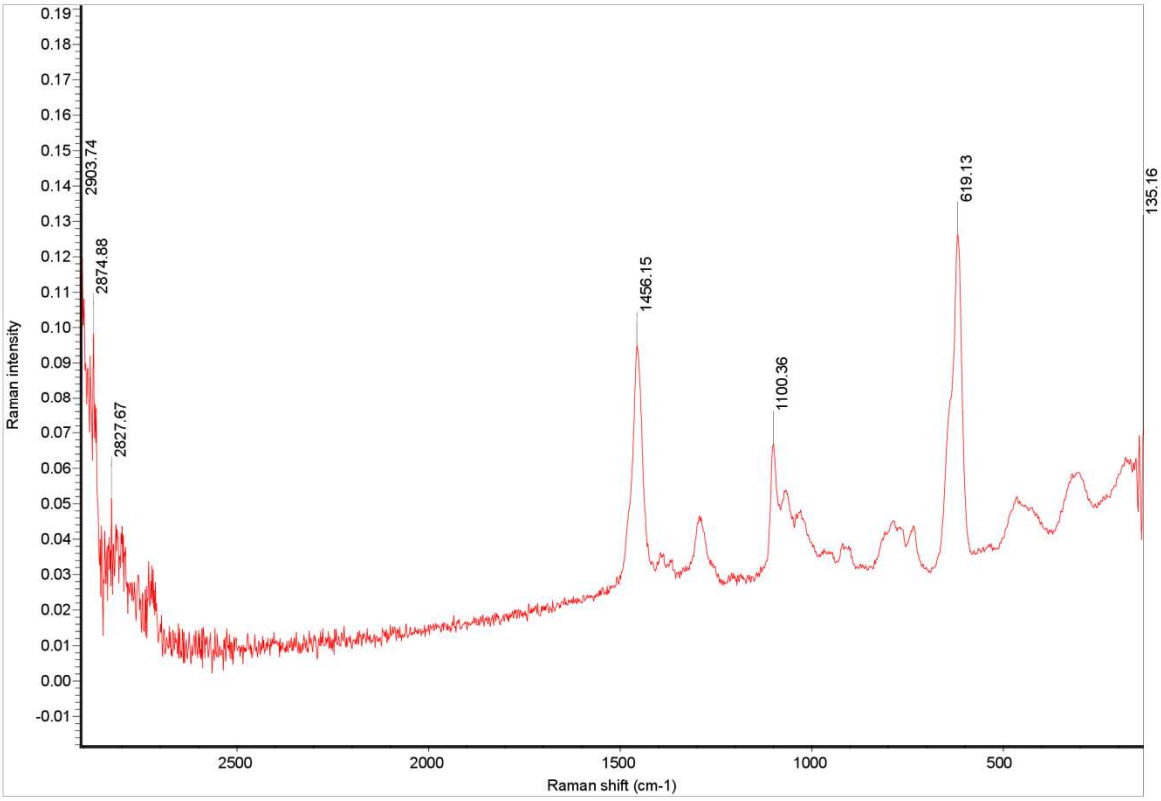

Figure 184: *Raman Spectrum of* ***IX****.*

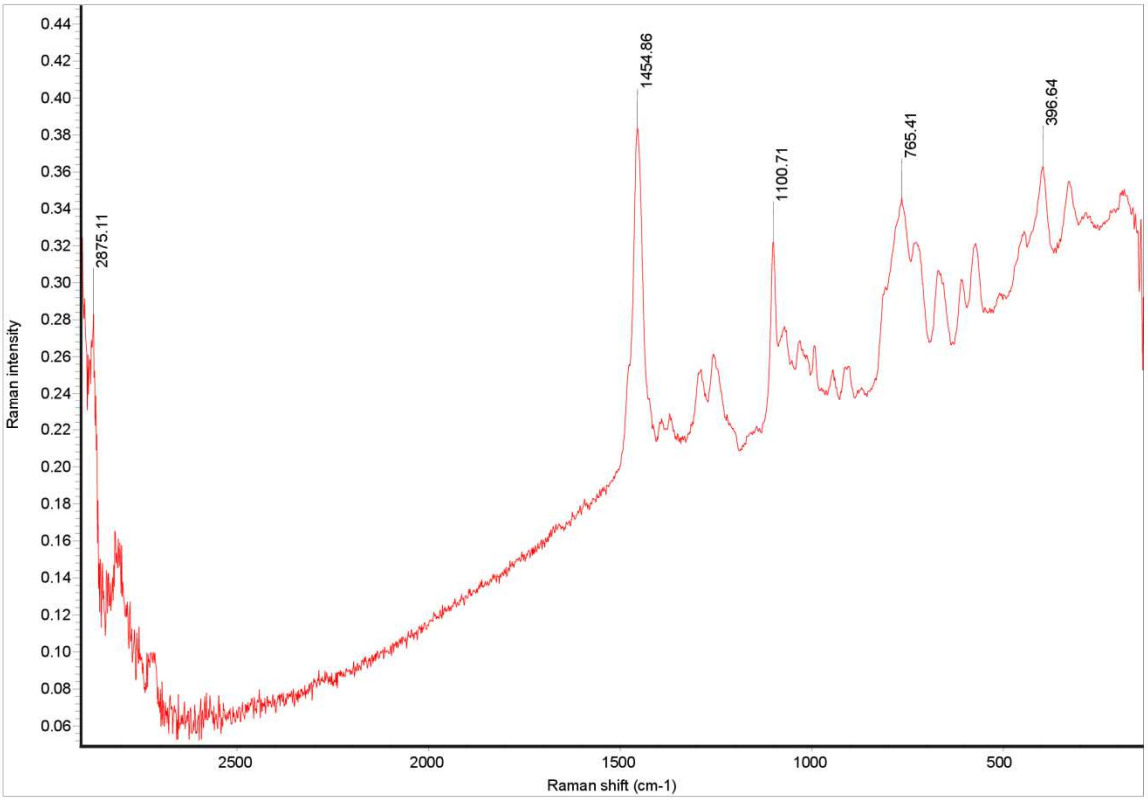

Figure 185: *Raman Spectrum of* ***X****.*

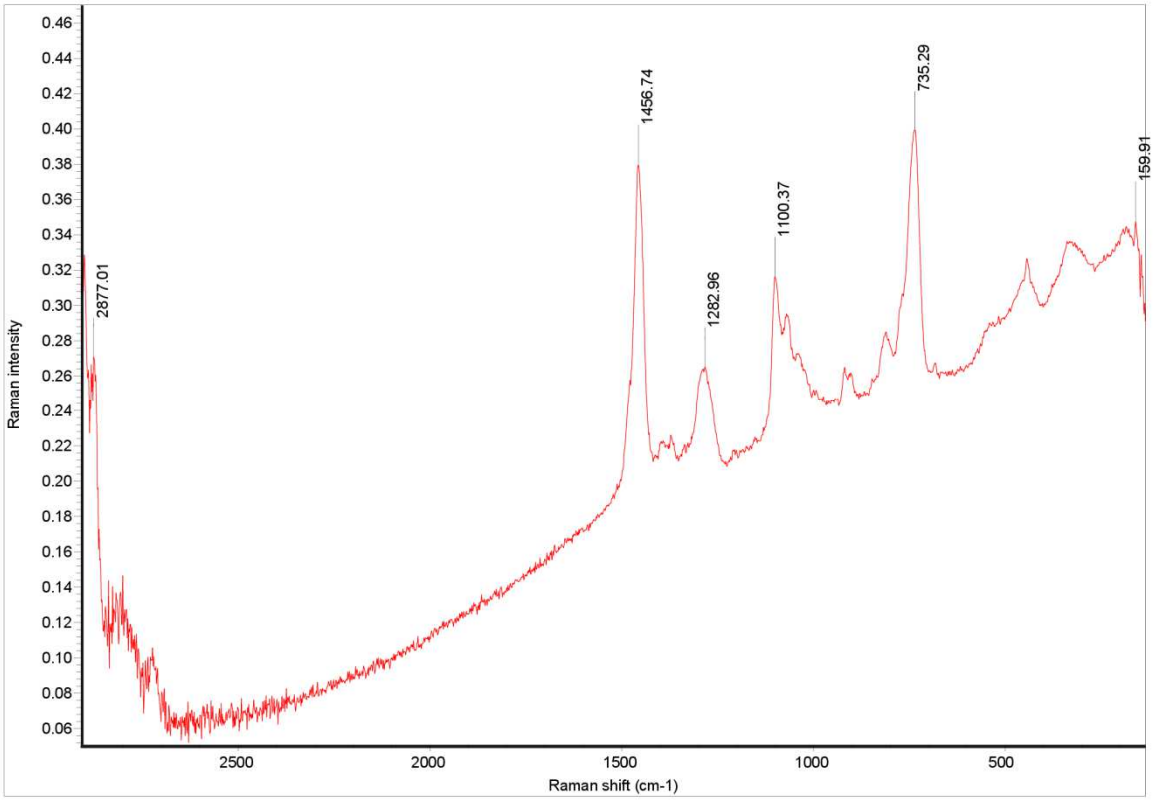

Figure 186: *Raman Spectrum of* ***XI****.*

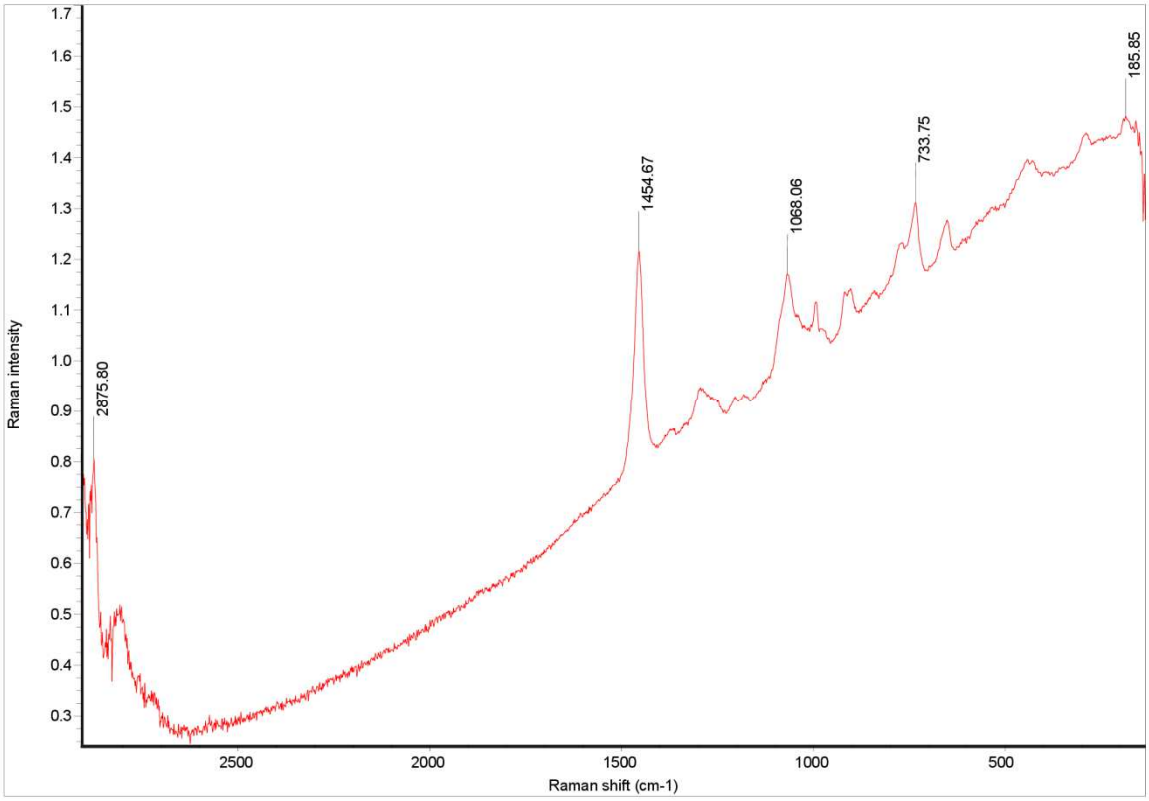

Figure 187: *Raman Spectrum of* ***XII****.*

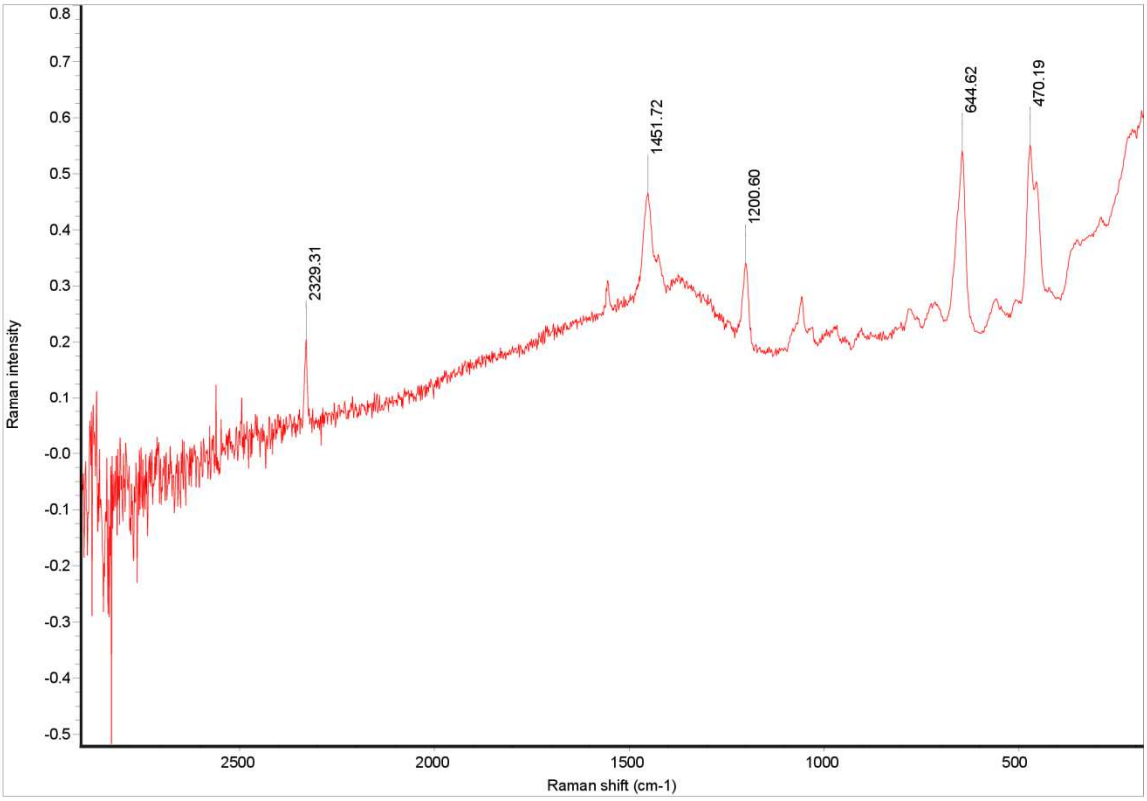

Figure 188: *Raman Spectrum of* ***XIII****.*

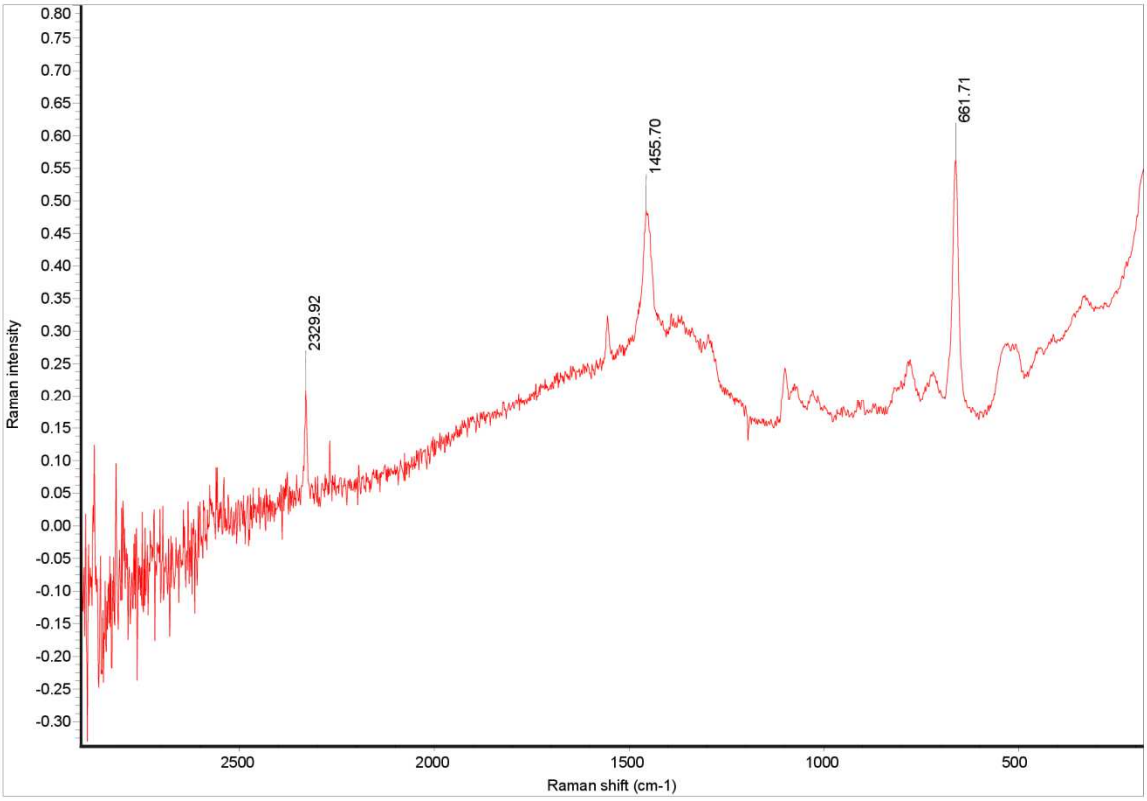

Figure 189: *Raman Spectrum of* ***XIV****.*

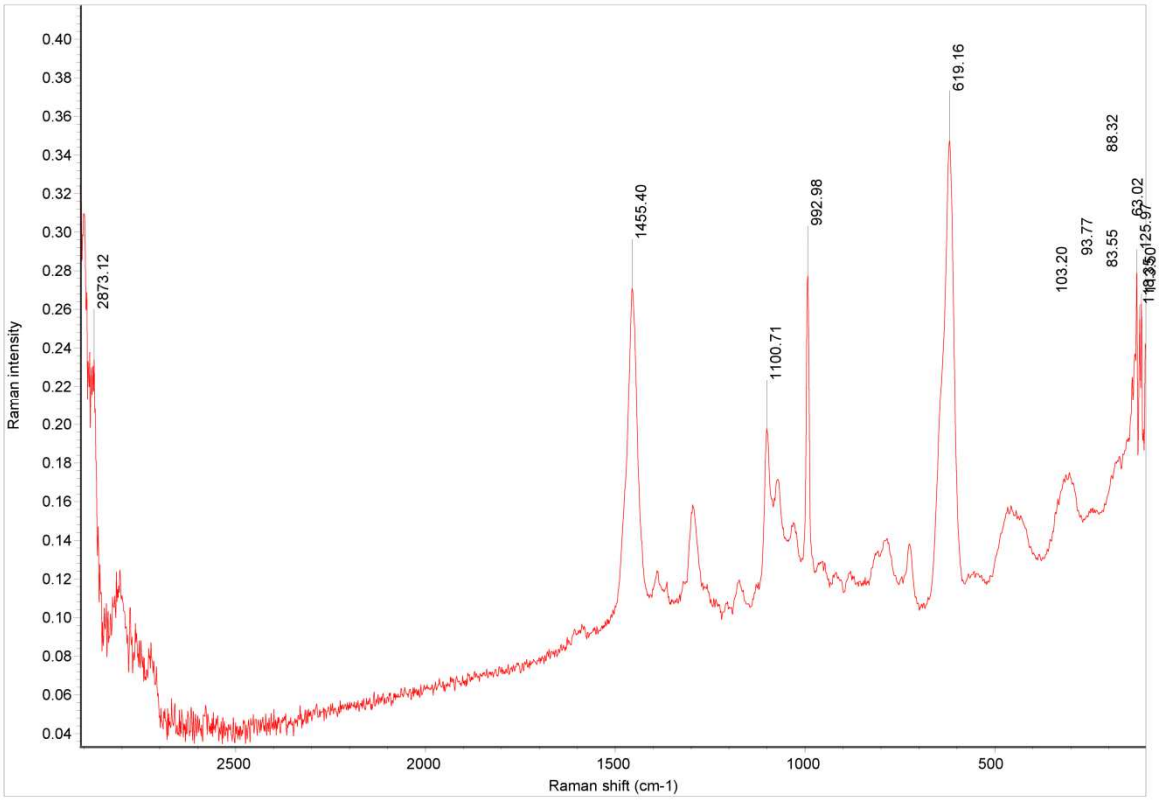

Figure 190: *Raman Spectrum of* ***XV****.*

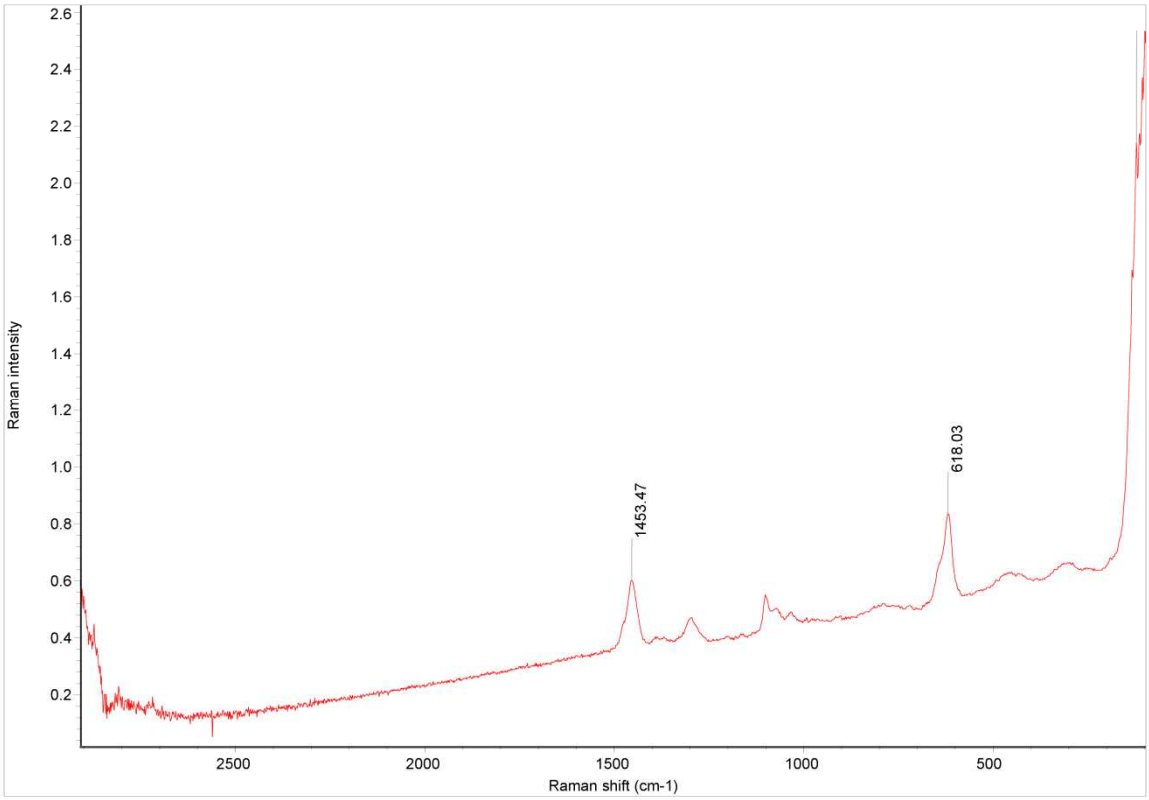

Figure 191: *Raman Spectrum of* ***XVII****.*

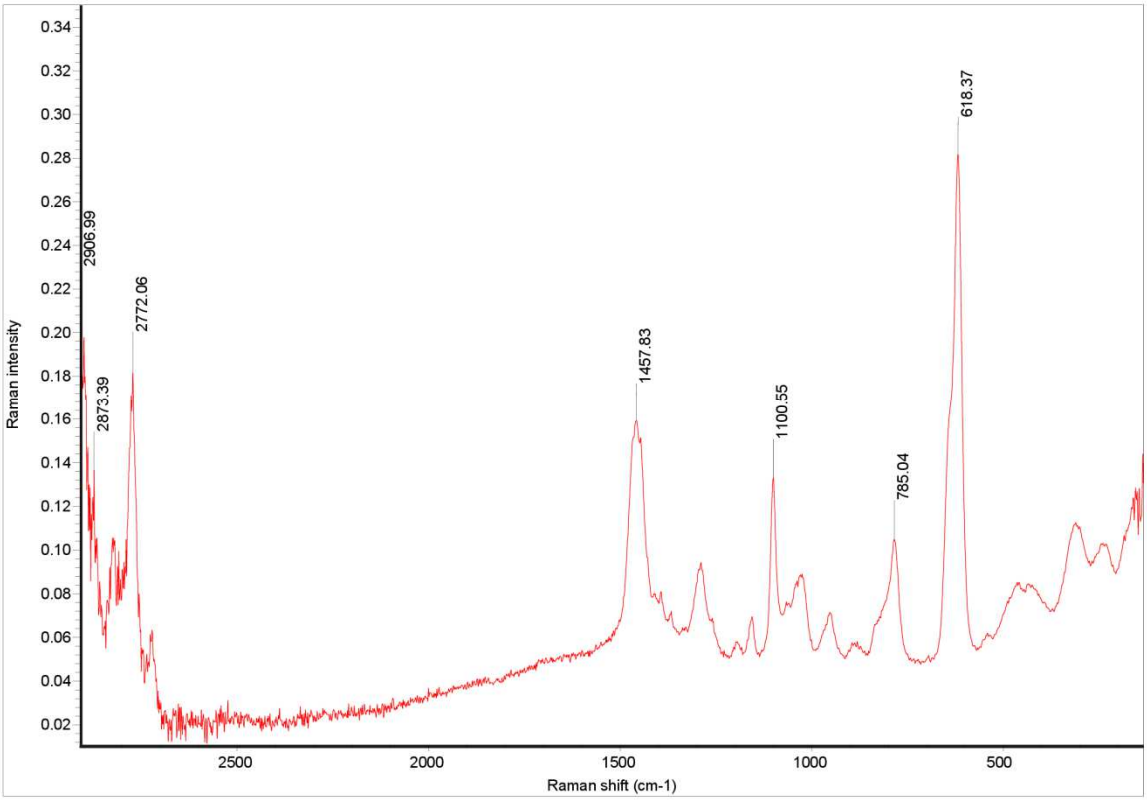

Figure 192: *Raman Spectrum of* ***XVIII****.*

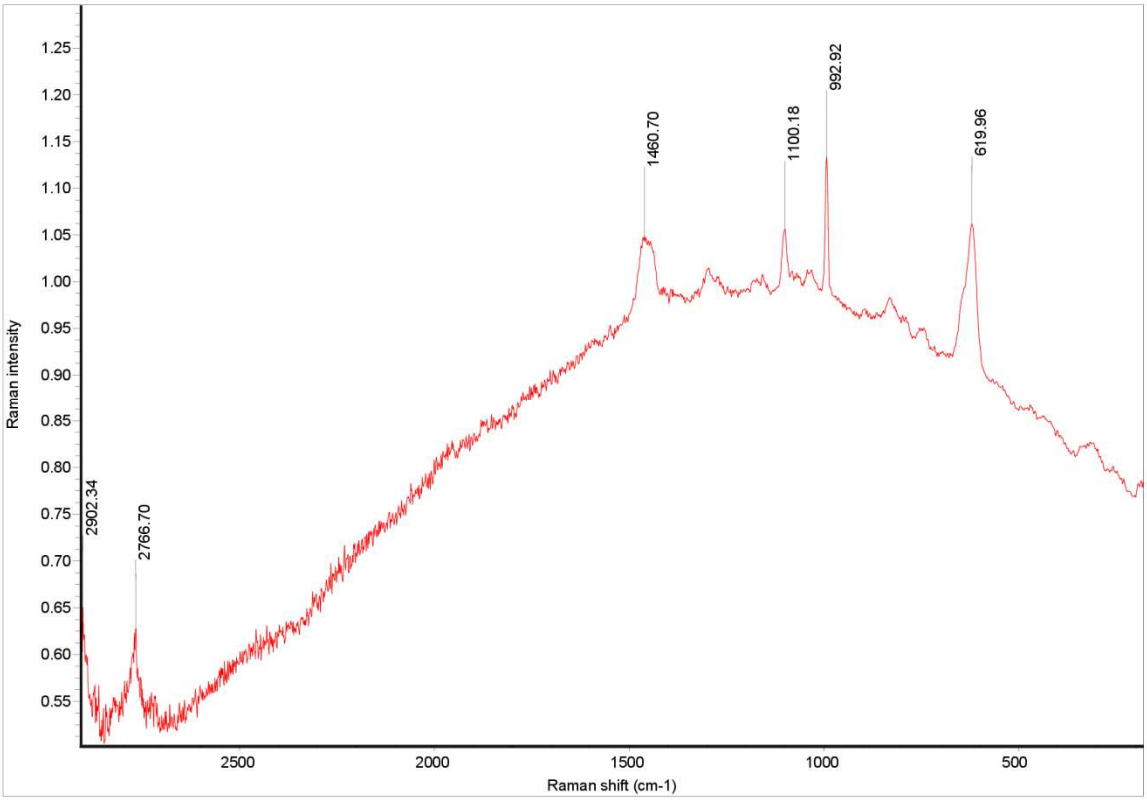

Figure 193: *Raman Spectrum of* ***XIX****.*

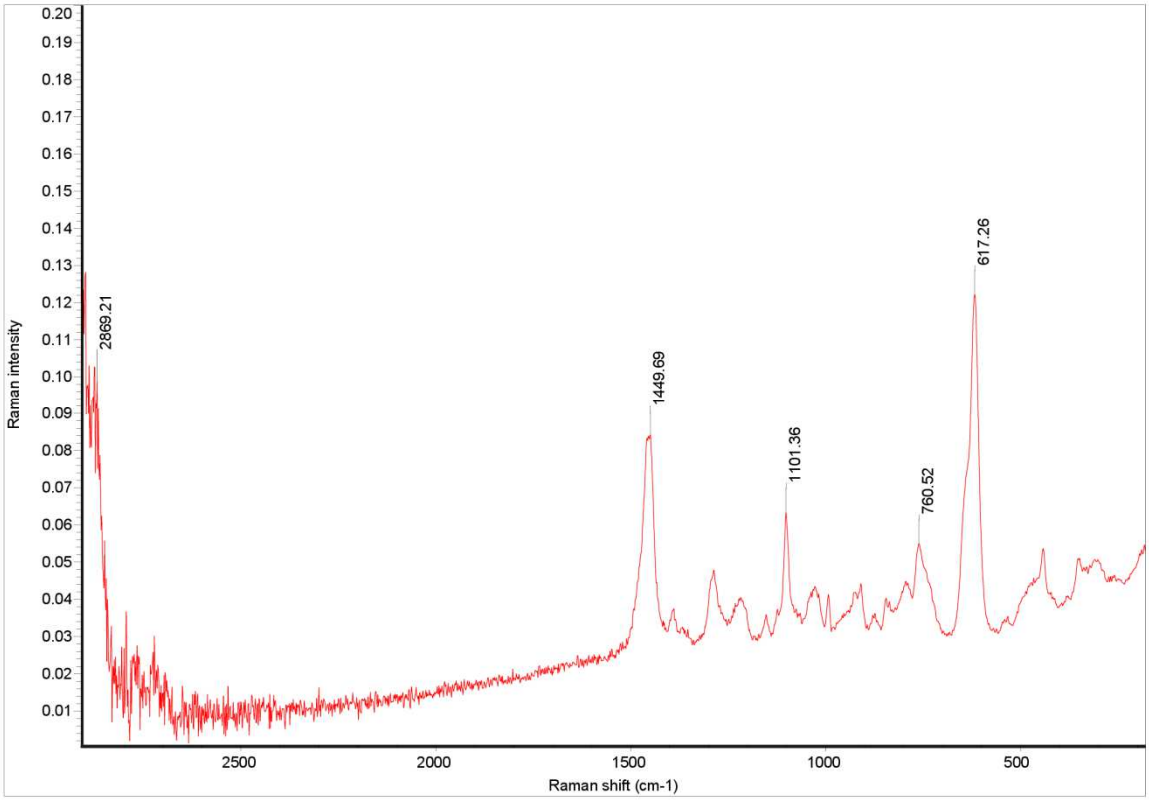

Figure 194: *Raman Spectrum of* ***XX****.*

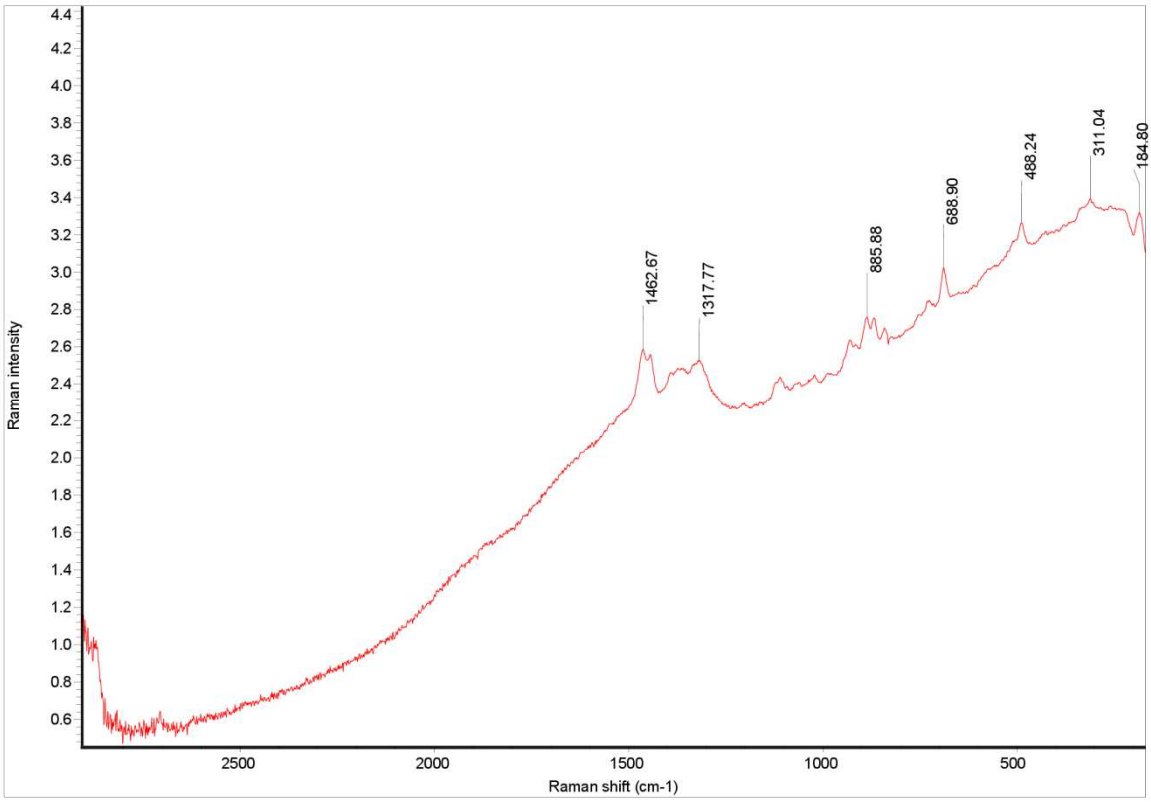

Figure 195: *Raman Spectrum of* ***XXII****.*

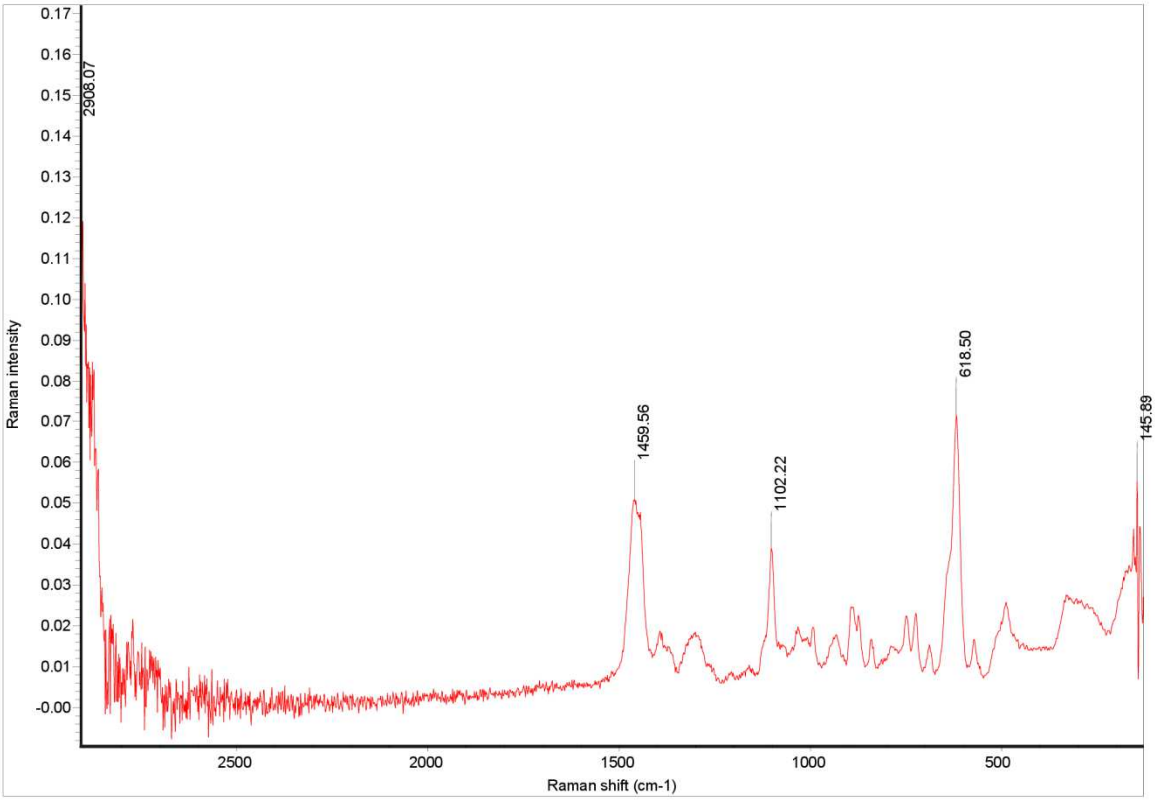

Figure 196: *Raman Spectrum of* ***XXIII****.*

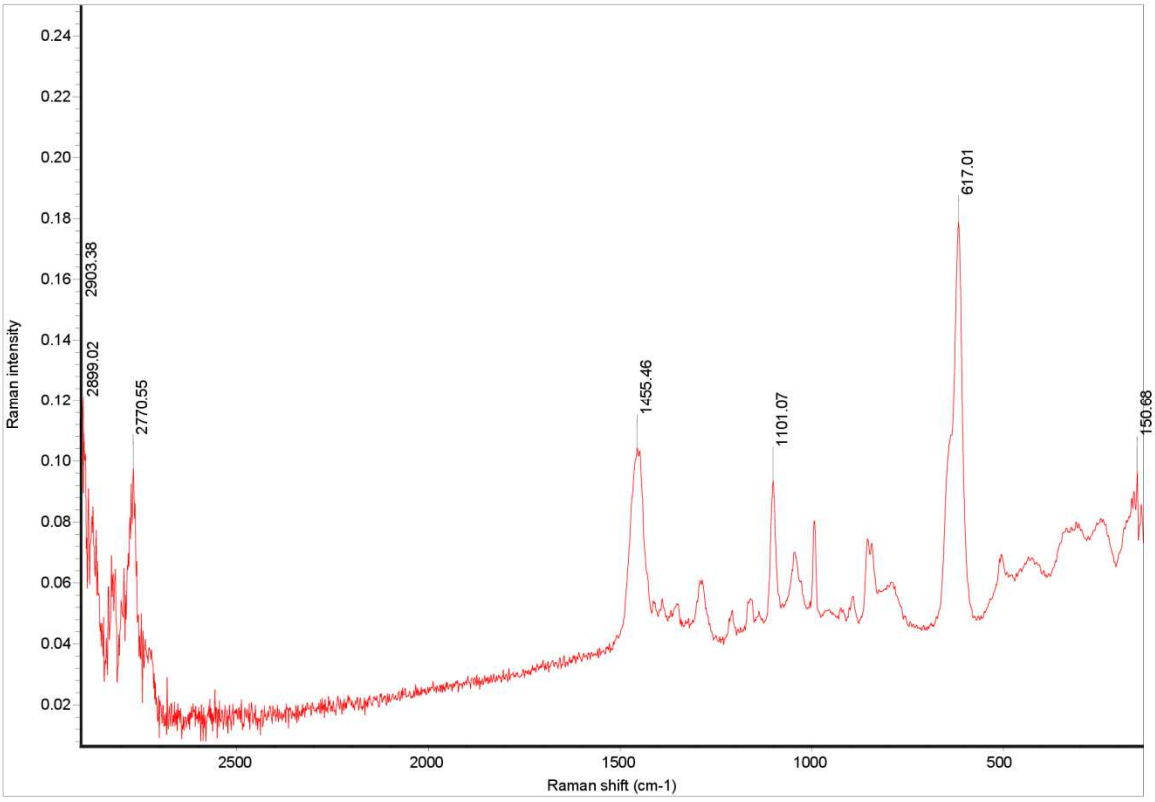

Figure 197: *Raman Spectrum of* ***XIV****.*

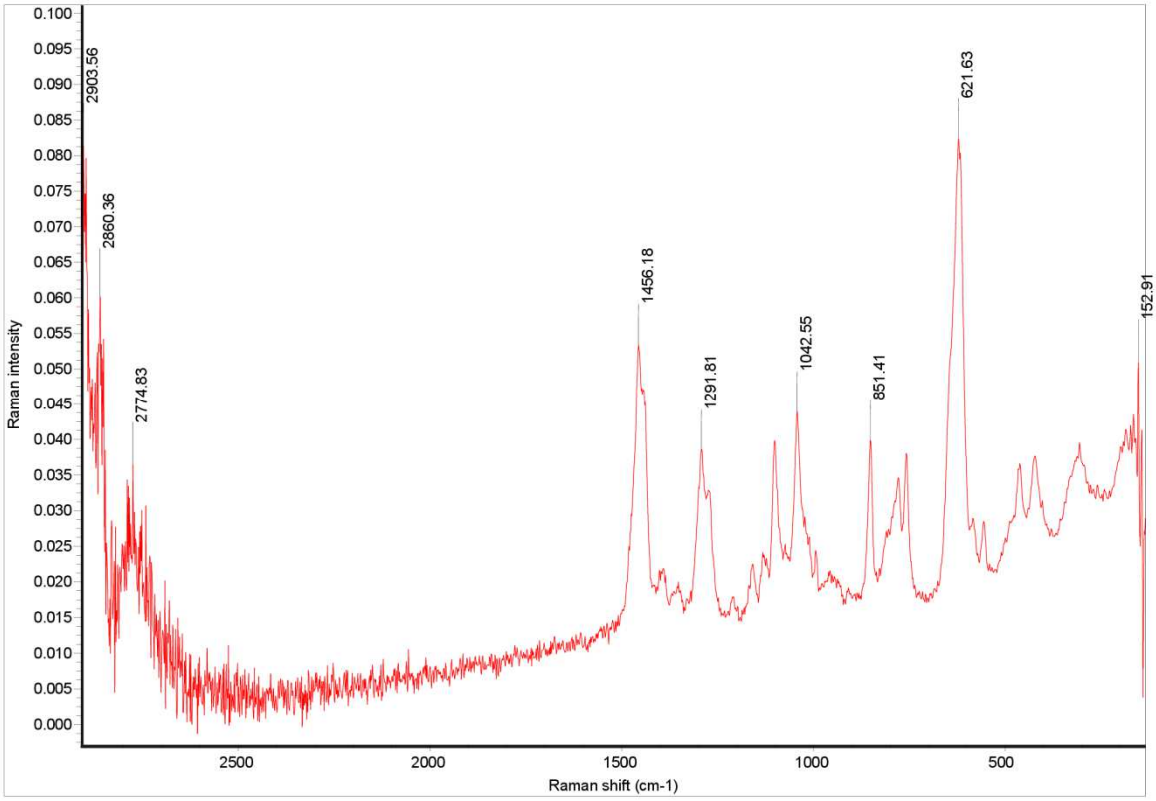

Figure 198: *Raman Spectrum of* ***XXV****.*

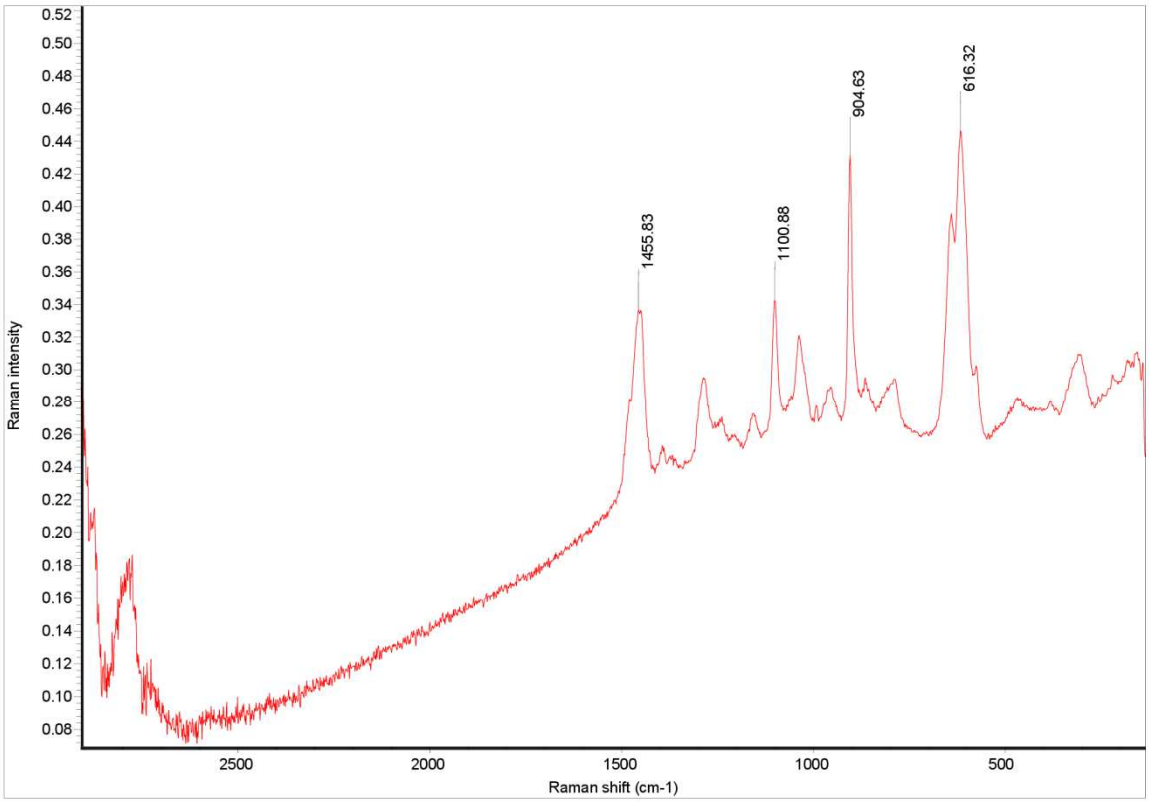

Figure 199: *Raman Spectrum of* ***XXVI****.*

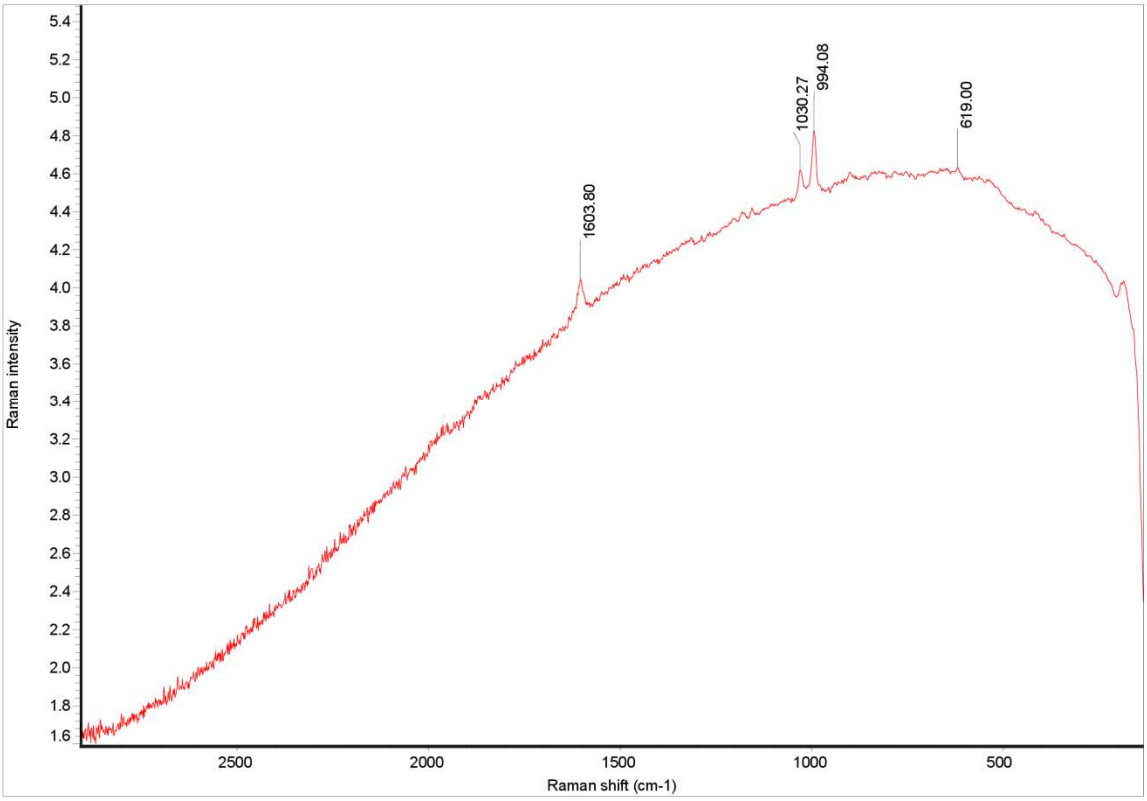

Figure 200: *Raman Spectrum of* ***XXVII****.*

iv. Organo(thio)phosphate Salts

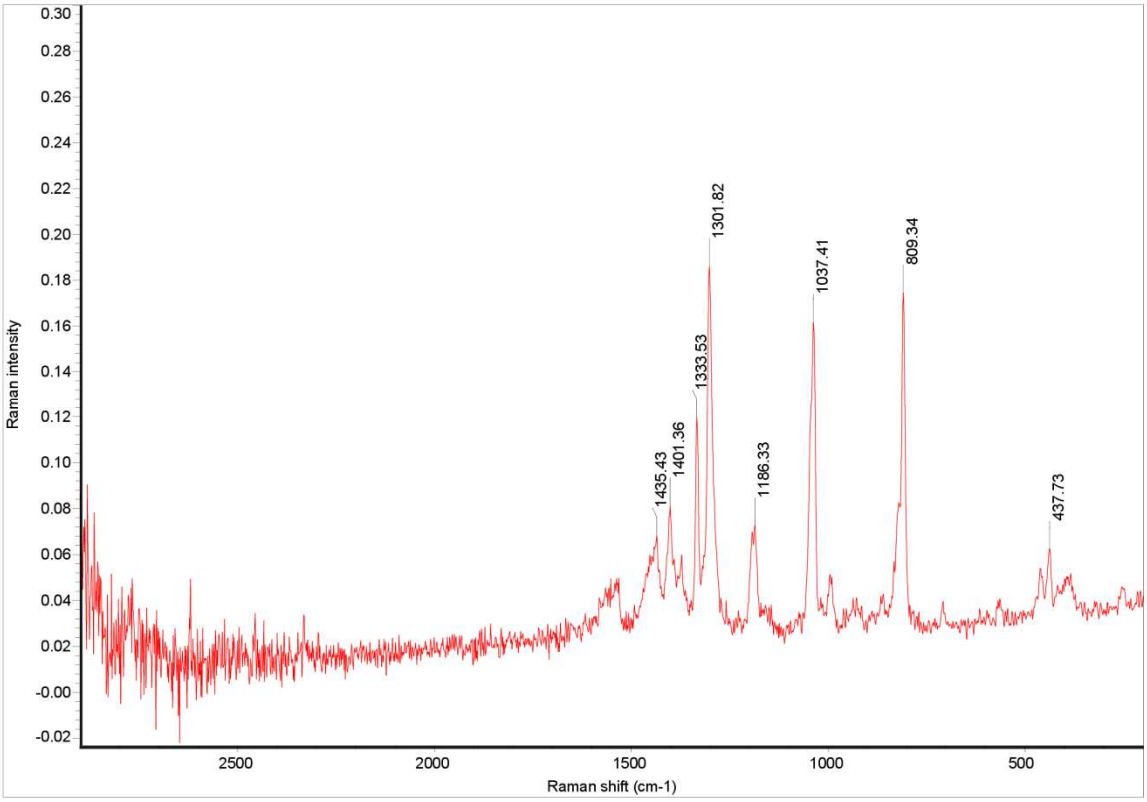

Figure 201: *Raman Spectrum of the decomposition product of* ***XVIII*** *=* ***XXXIV****.*

A.3 HPLC-ESI/MS-Spectra

i. Amino Alcohol Spectrum

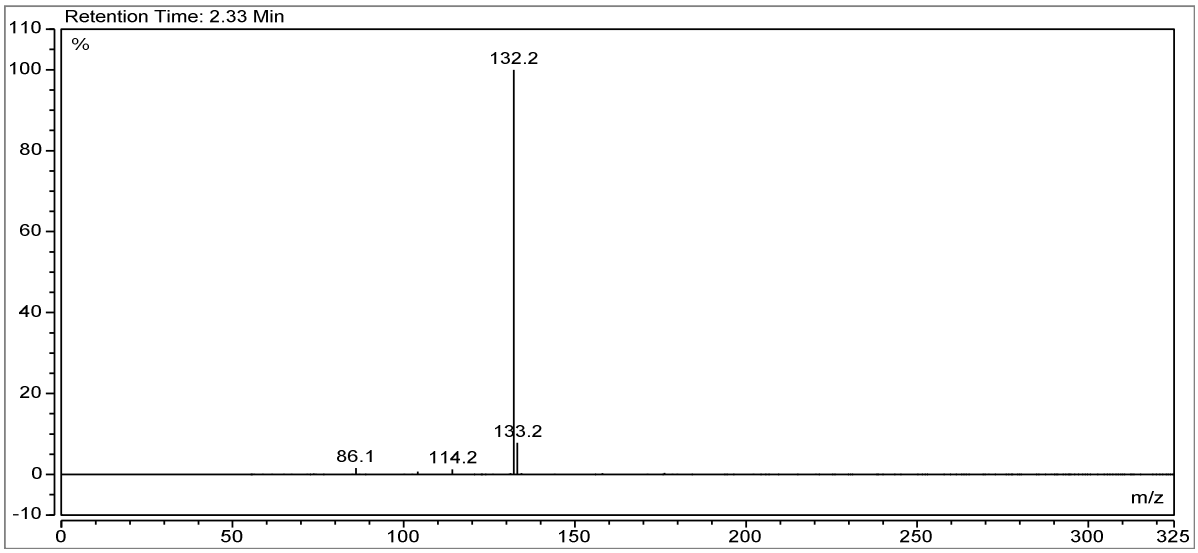

Figure 202: *ESI-MS Spectrum of* ***I****.*

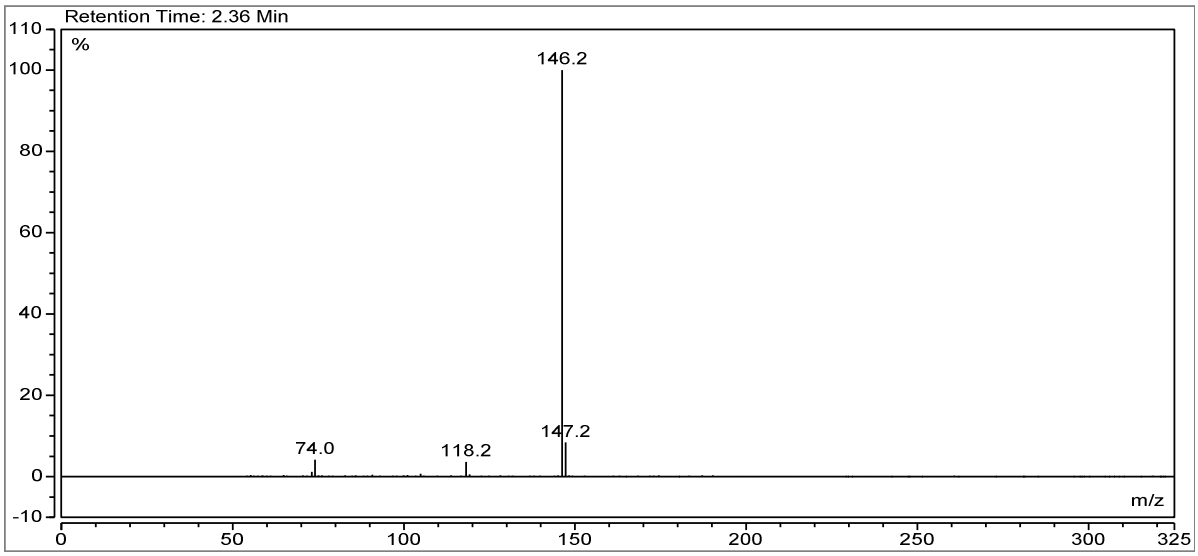

Figure 203: *ESI-MS Spectrum of* ***II****.*

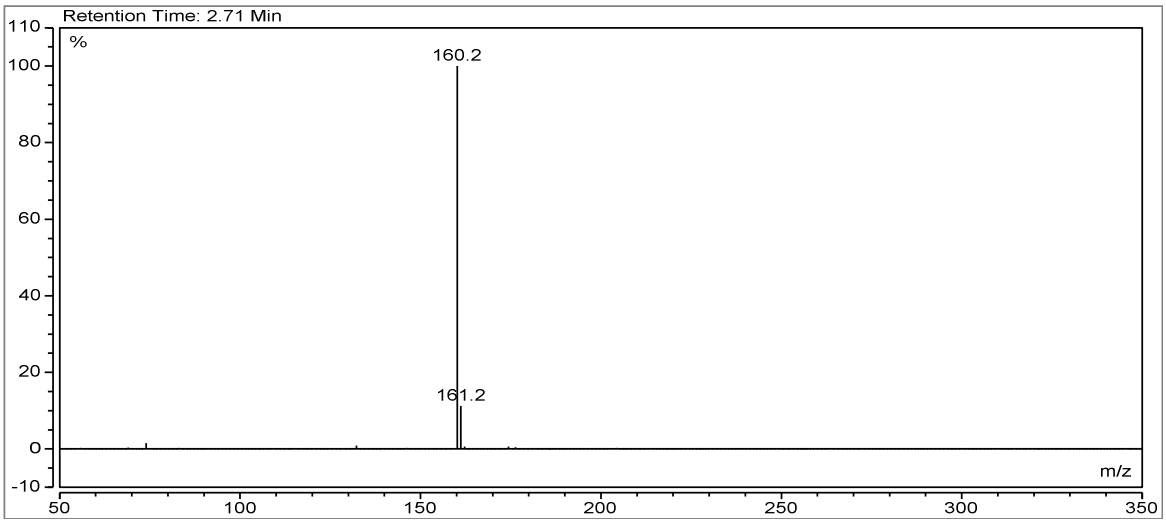

Figure 204: *ESI-MS Spectrum of* ***III****.*

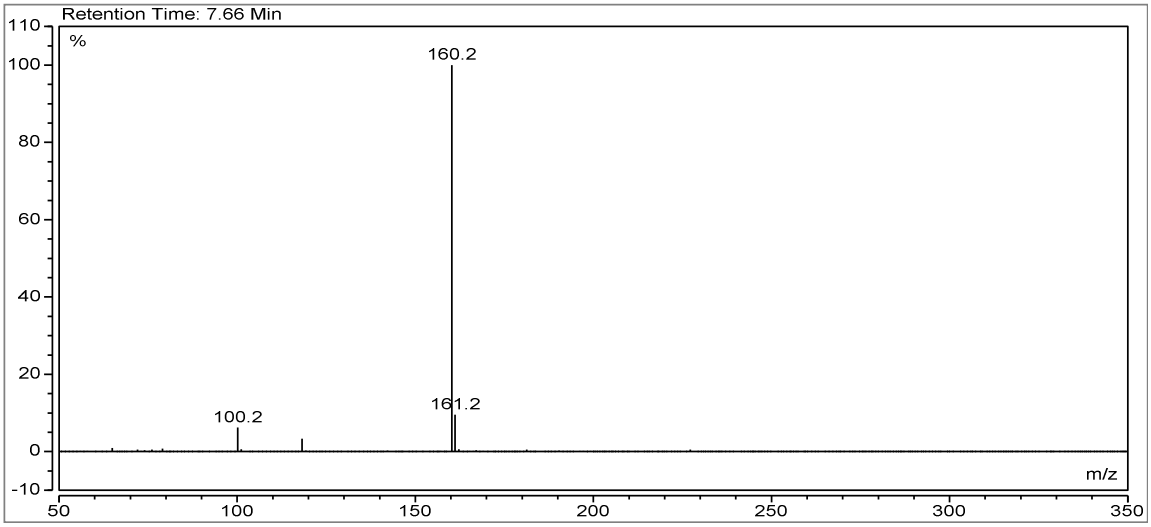

Figure 205: *ESI-MS Spectrum of* ***IV****.*

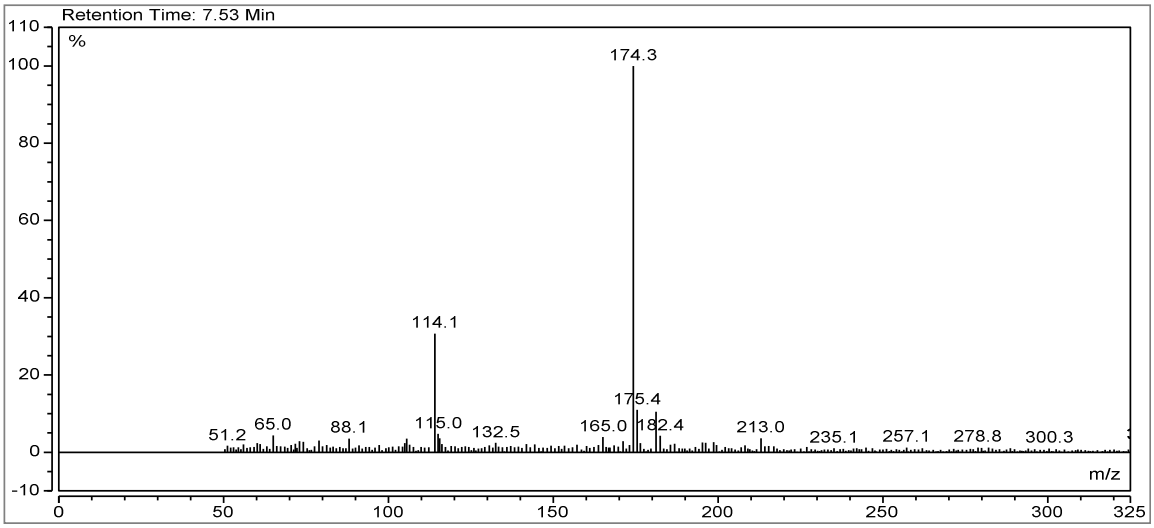

Figure 206: *ESI-MS Spectrum of* ***V****.*

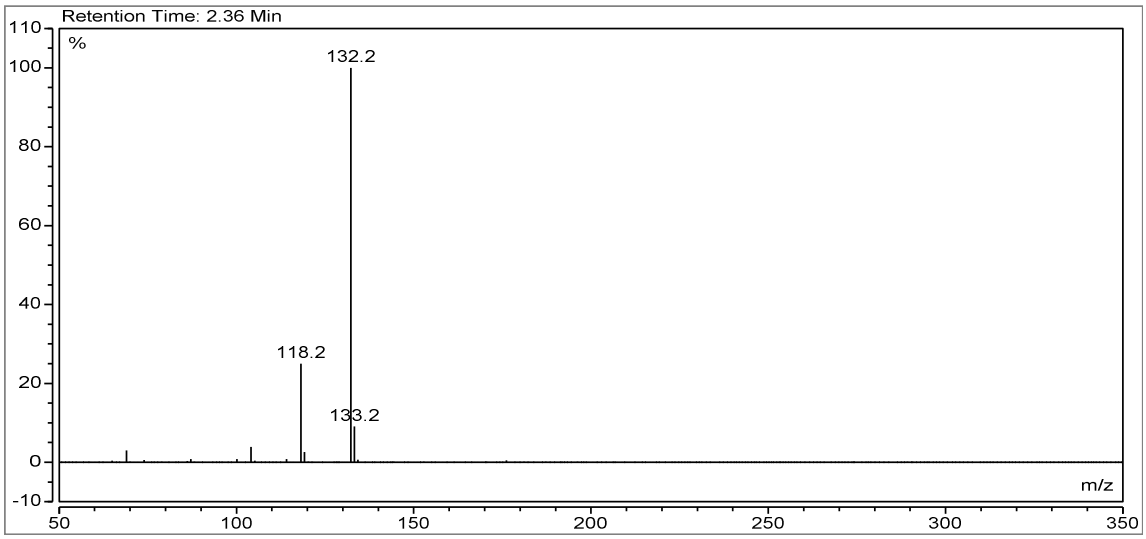

Figure 207: *ESI-MS Spectrum of* ***VI****.*

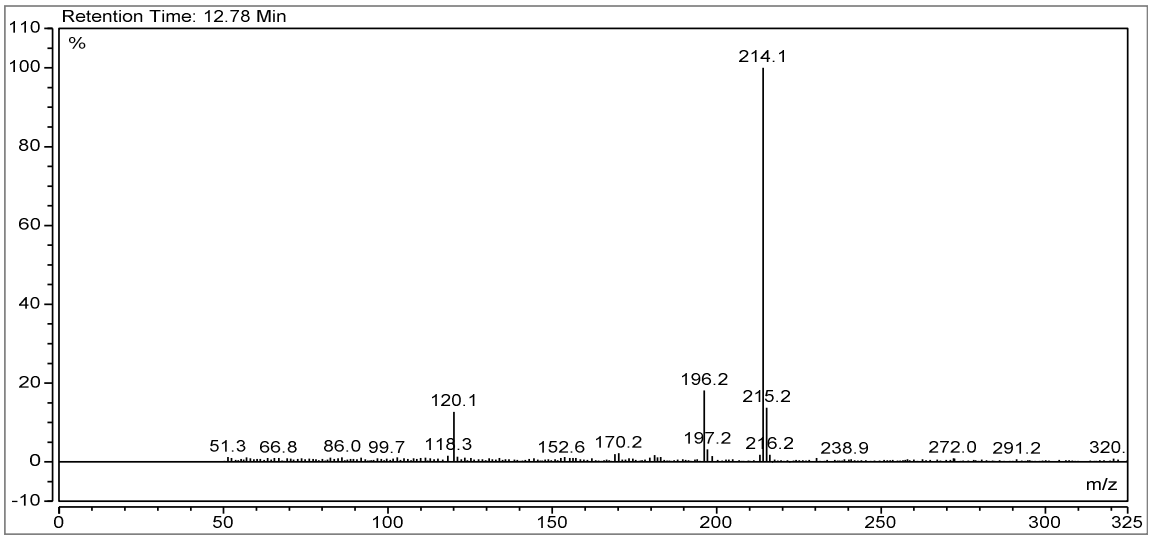

Figure 208: *ESI-MS spectrum of* ***VII****.*

ii. Organo(thio)phosphates

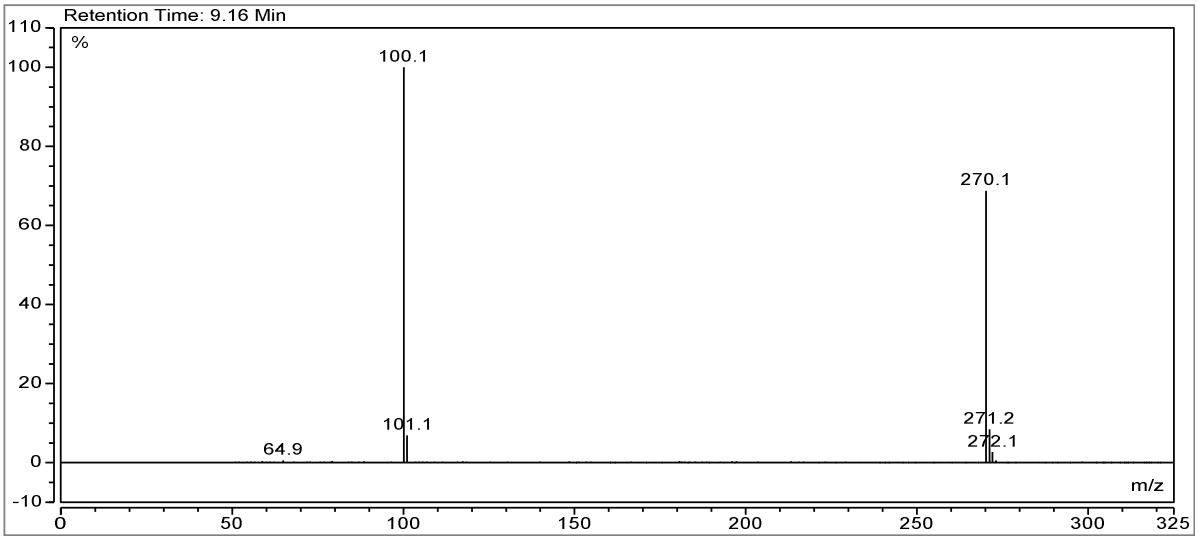

Figure 209: *ESI-MS Spectrum of* ***IX****.*

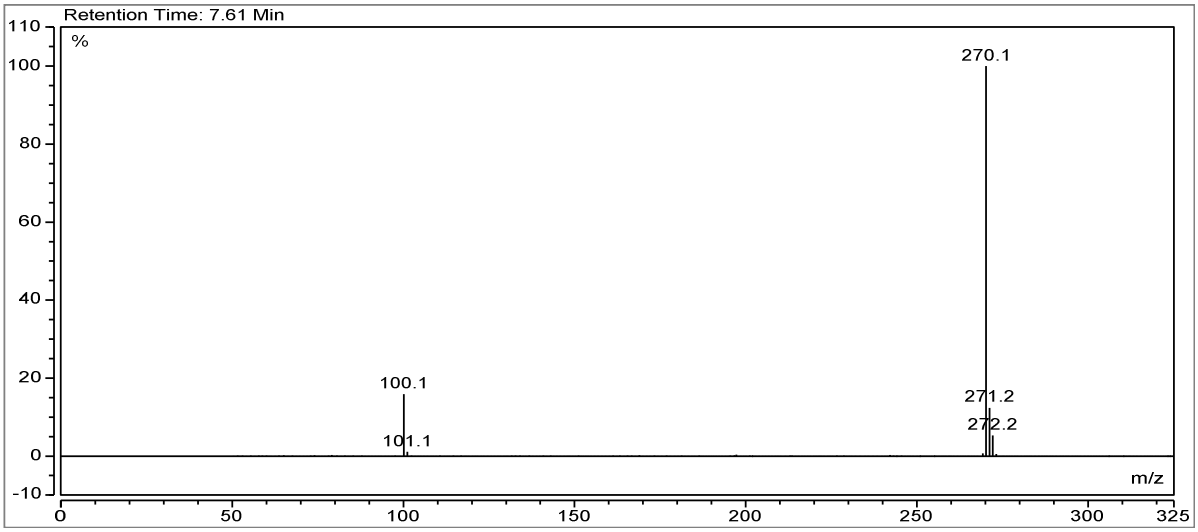

Figure 210: *ESI-MS Spectrum of* ***X****.*

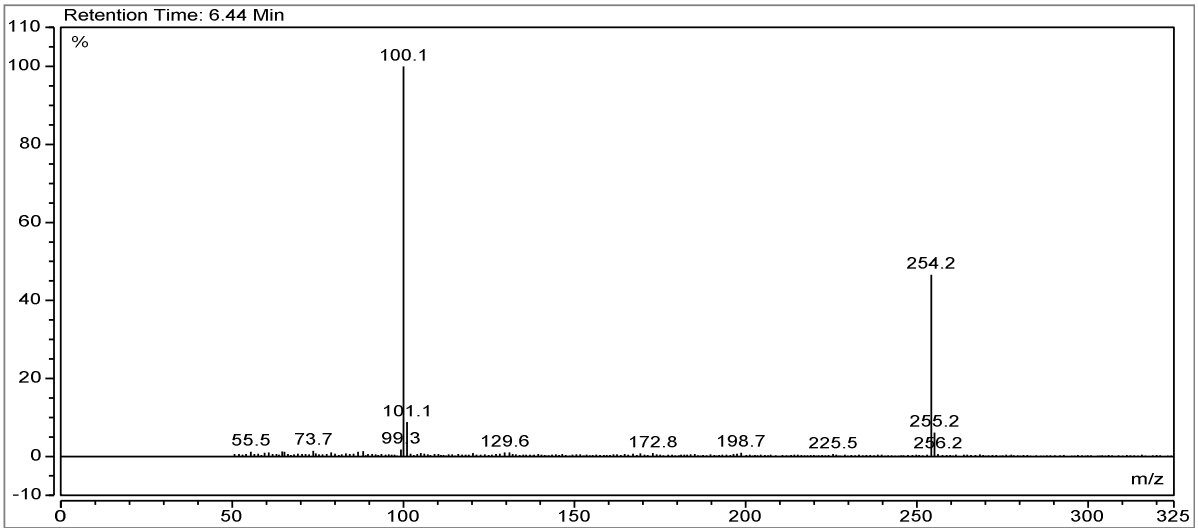

Figure 211: *ESI-MS Spectrum of* ***XI****.*

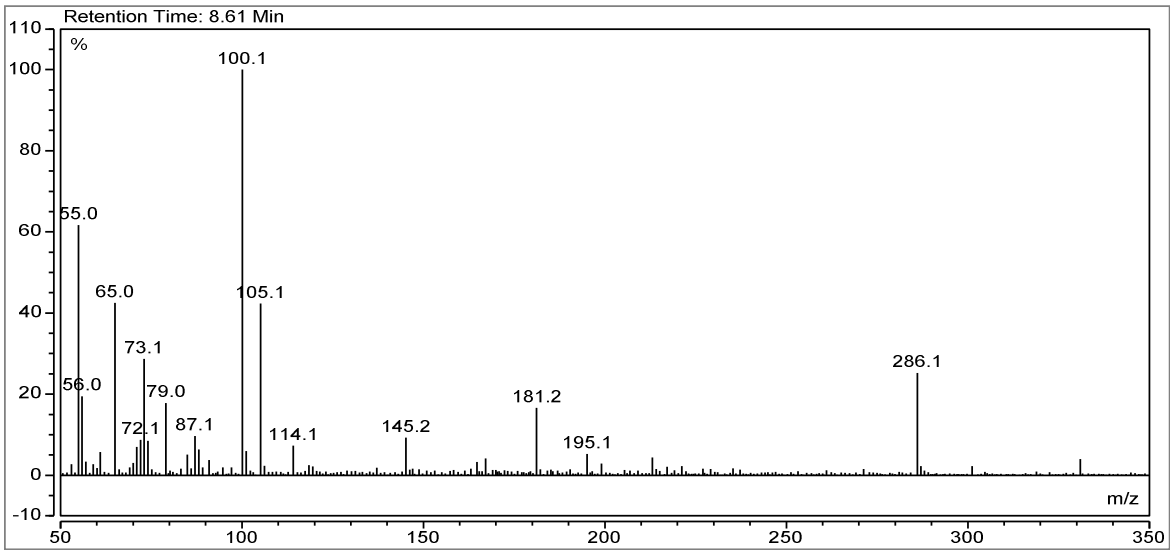

Figure 212: *ESI-MS Spectrum of* ***XII****.*

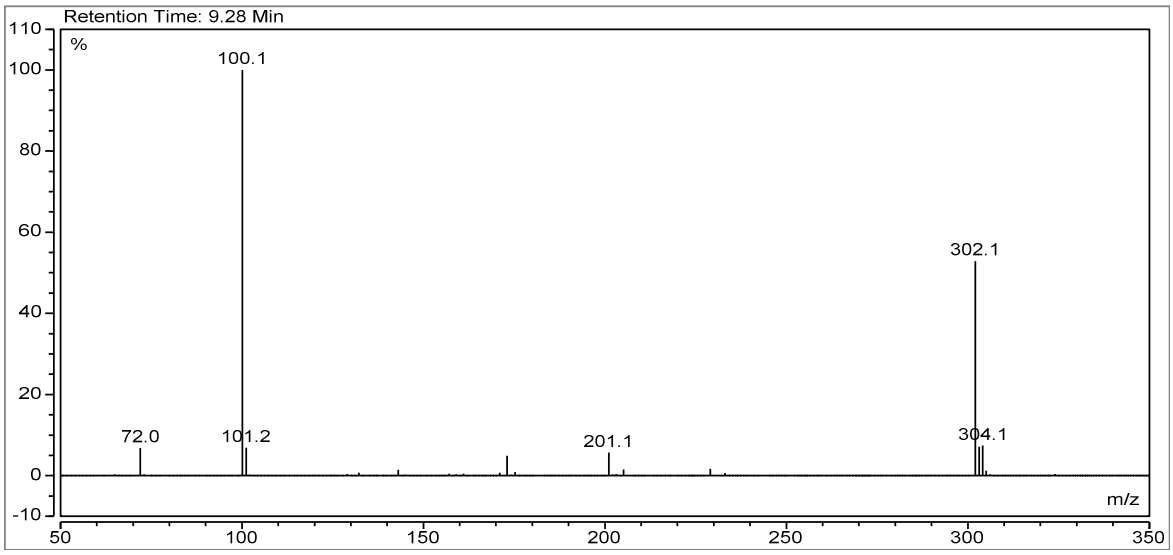

Figure 213: *ESI-MS Spectrum of* ***XIII****.*

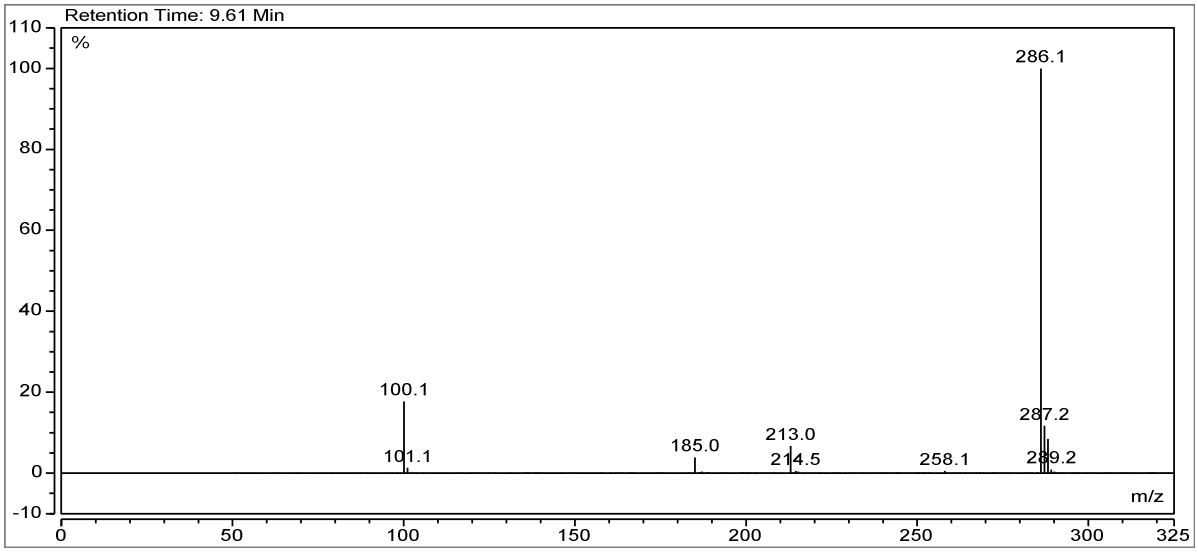

Figure 214: *ESI-MS Spectrum of* ***XIV****.*

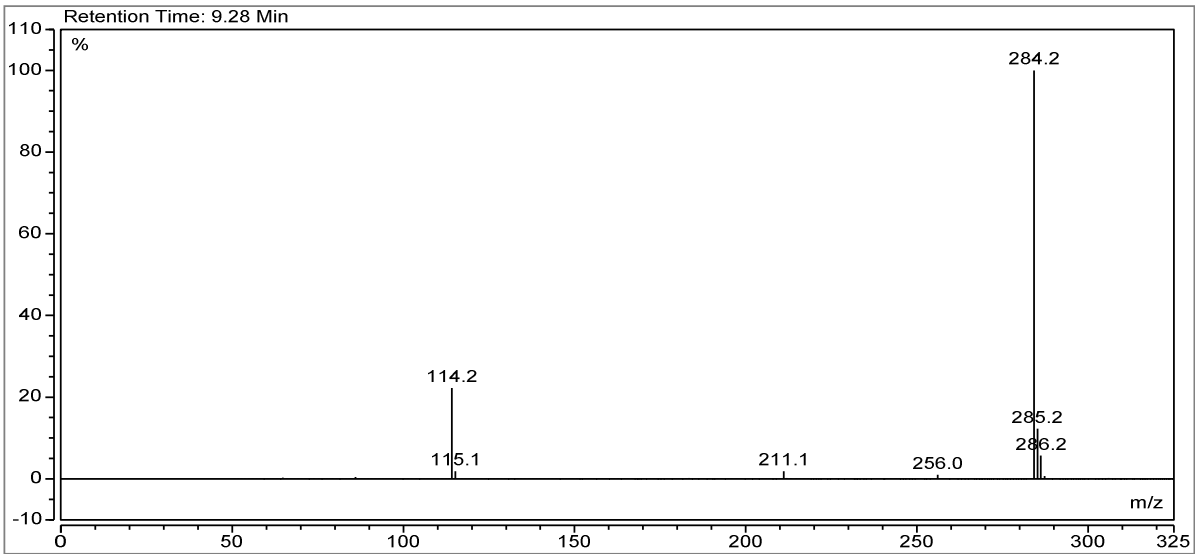

Figure 215: *ESI-MS Spectrum of* ***XV****.*

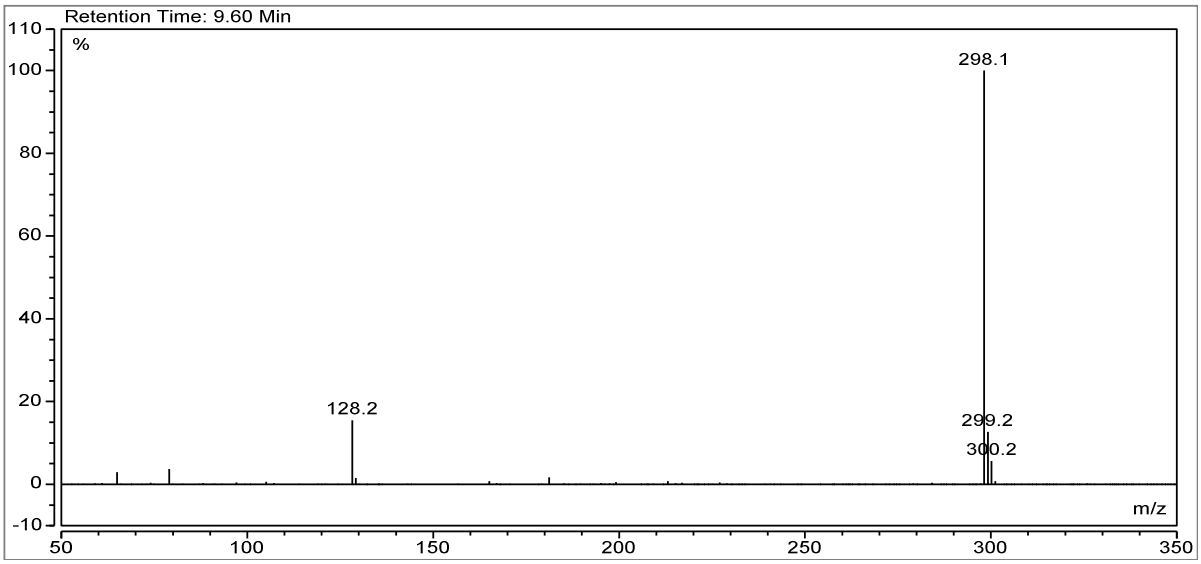

Figure 216: *ESI-MS Spectrum of* ***XVI****.*

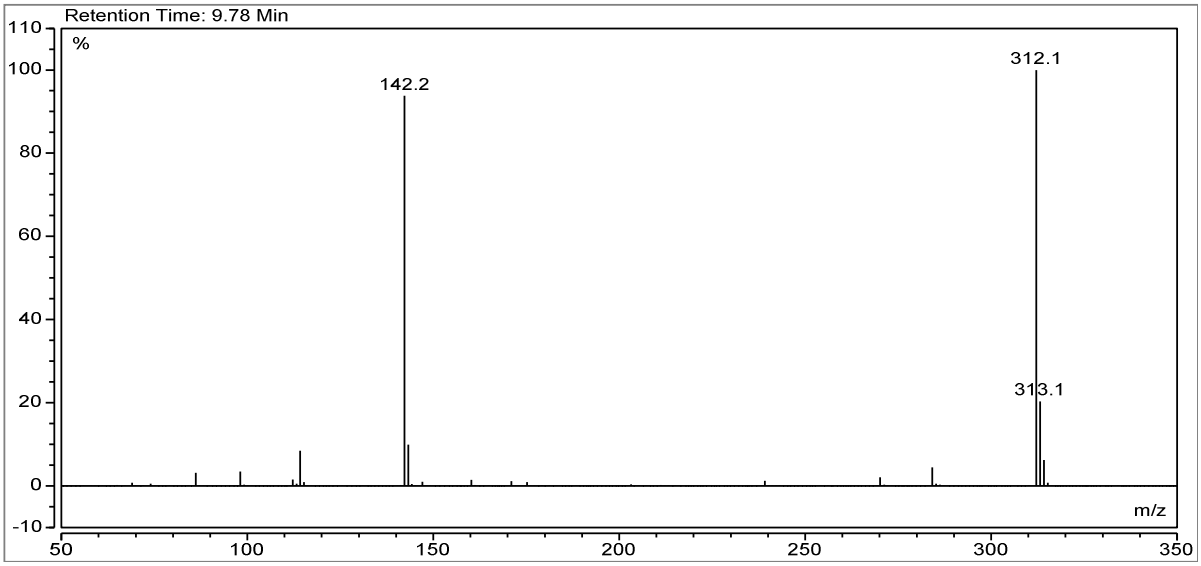

Figure 217: *ESI-MS Spectrum of* ***XVII****.*

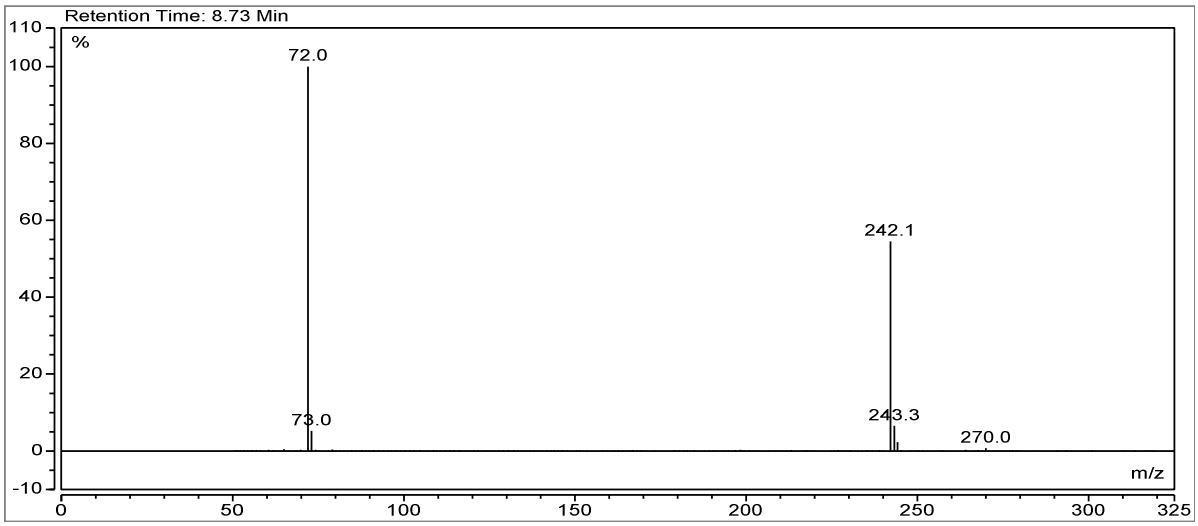

Figure 218: *ESI-MS Spectrum of* ***XVIII****.*

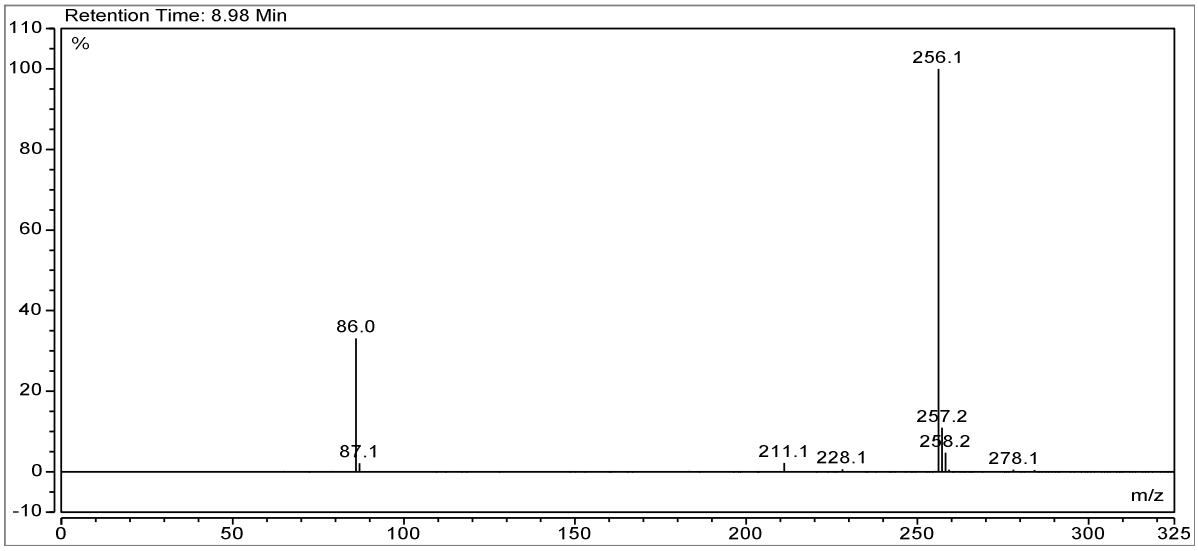

Figure 219: *ESI-MS Spectrum of* ***XIX****.*

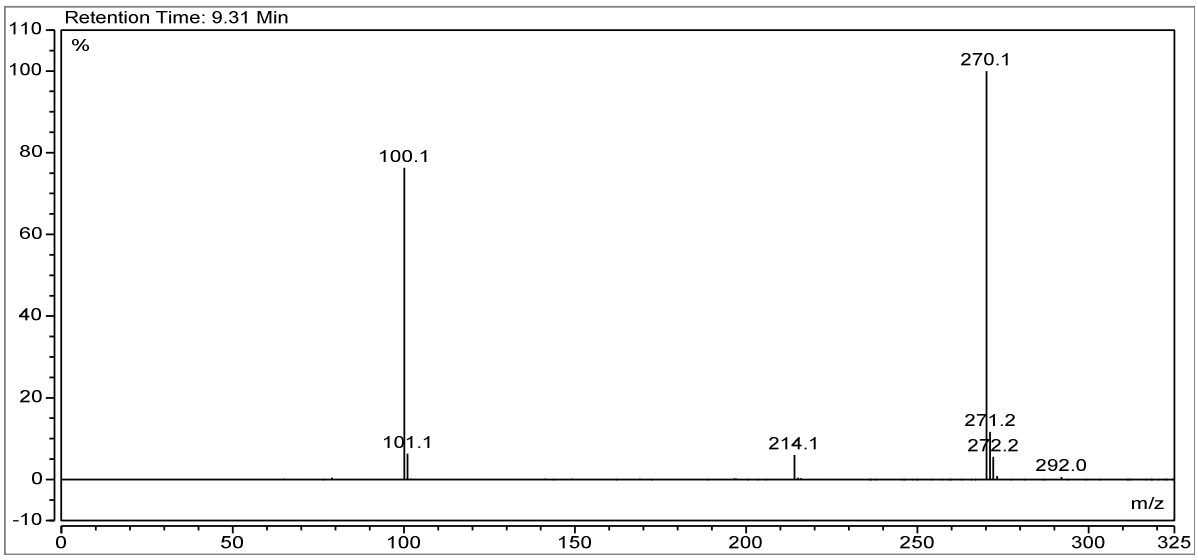

Figure 220: *ESI-MS Spectrum of* ***XX****.*

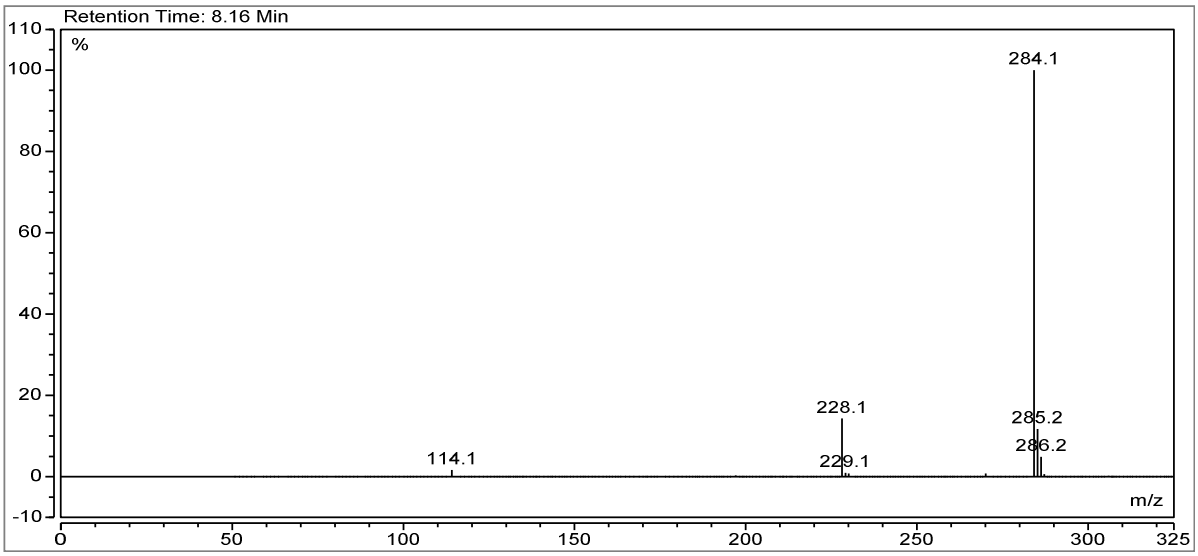

Figure 221: *ESI-MS Spectrum of* ***XXI****.*

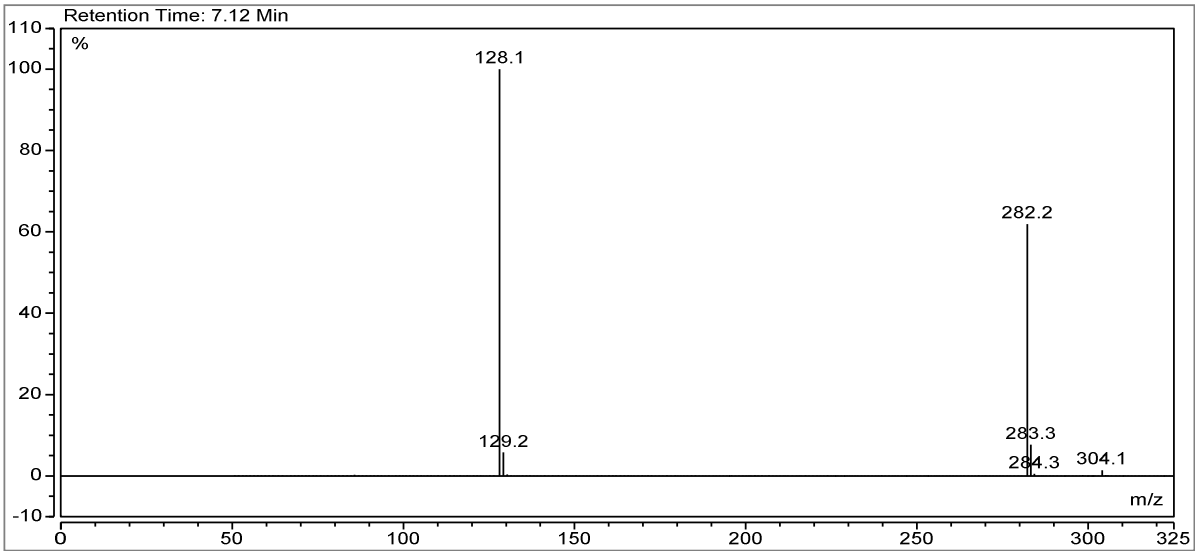

Figure 222: *ESI-MS Spectrum of* ***XXII***

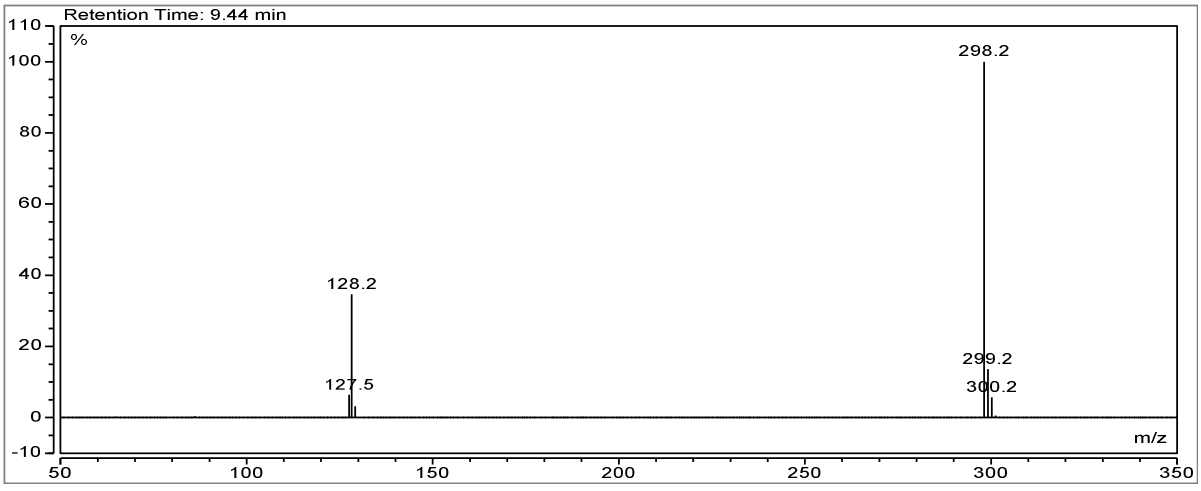

Figure 223: *ESI-MS Spectrum of* ***XXIII****.*

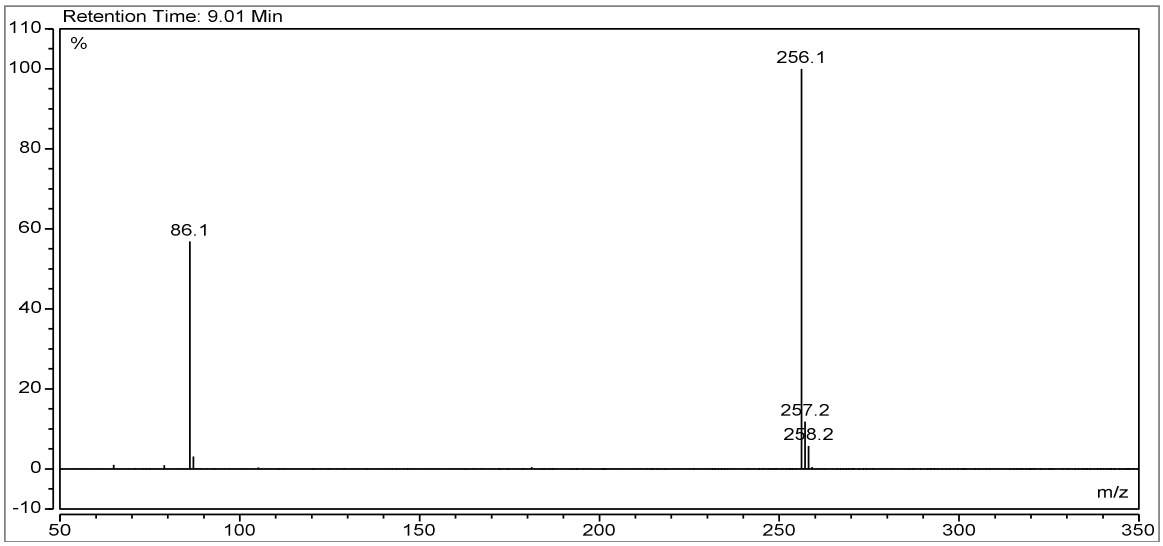

Figure 224: *ESI-MS Spectrum of* ***XXIV****.*

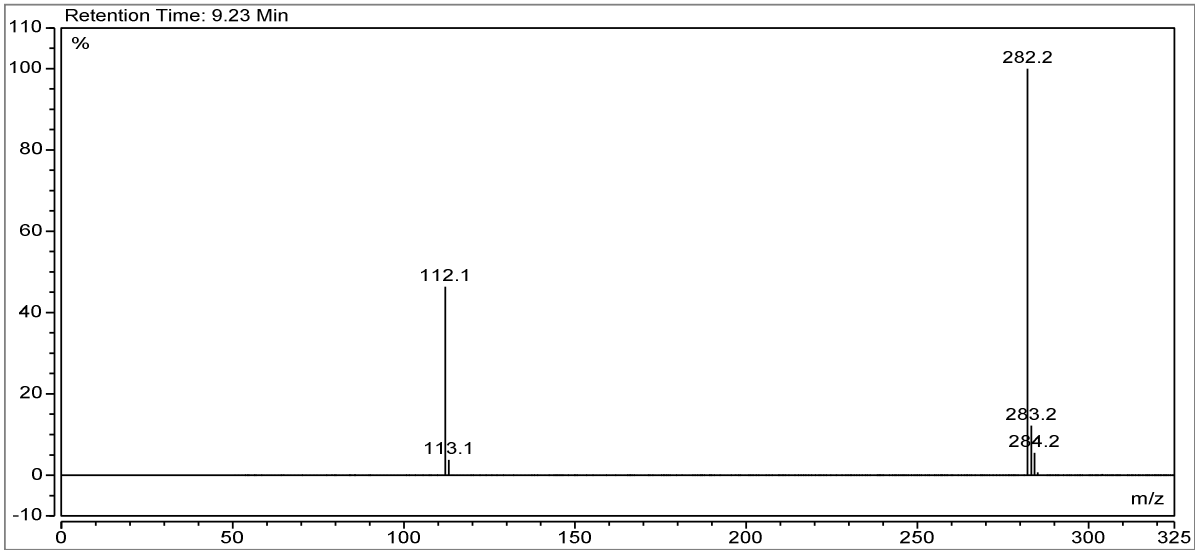

Figure 225: *ESI-MS Spectrum of* ***XXV****.*

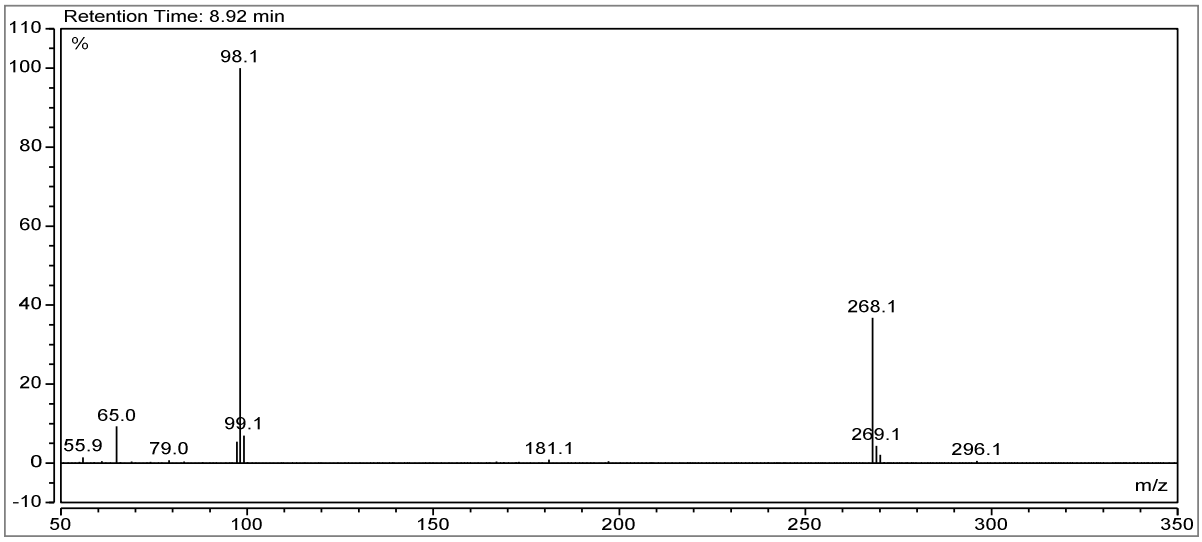

Figure 226: *ESI-MS Spectrum of* ***XXVI****.*

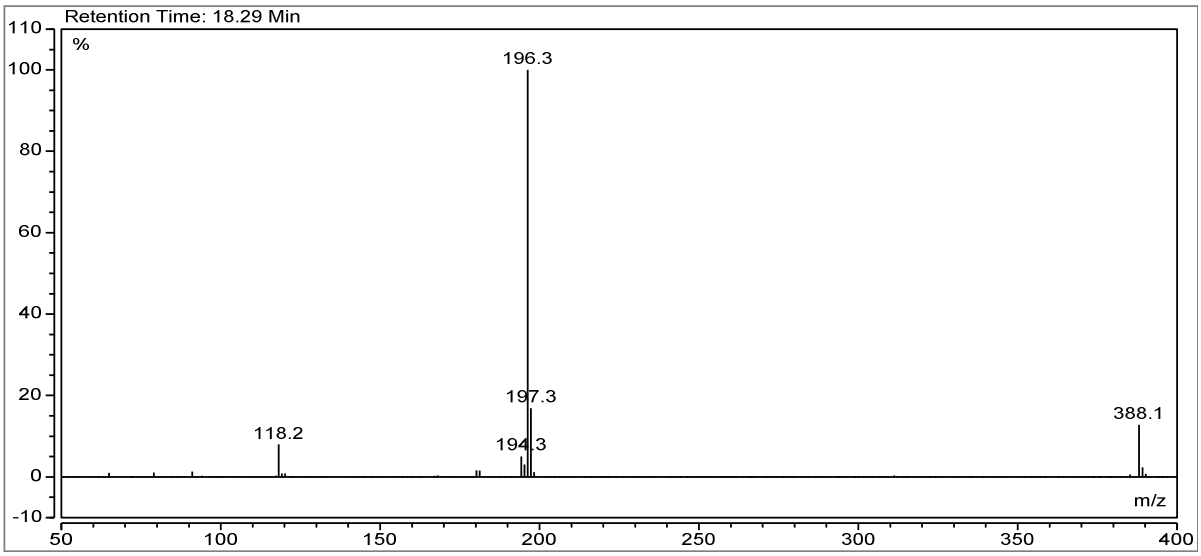

Figure 227: *ESI-MS Spectrum of* ***XXVII****.*

A.4 GC/MS(EI) Spectra

i. Amino Alcohol Spectra

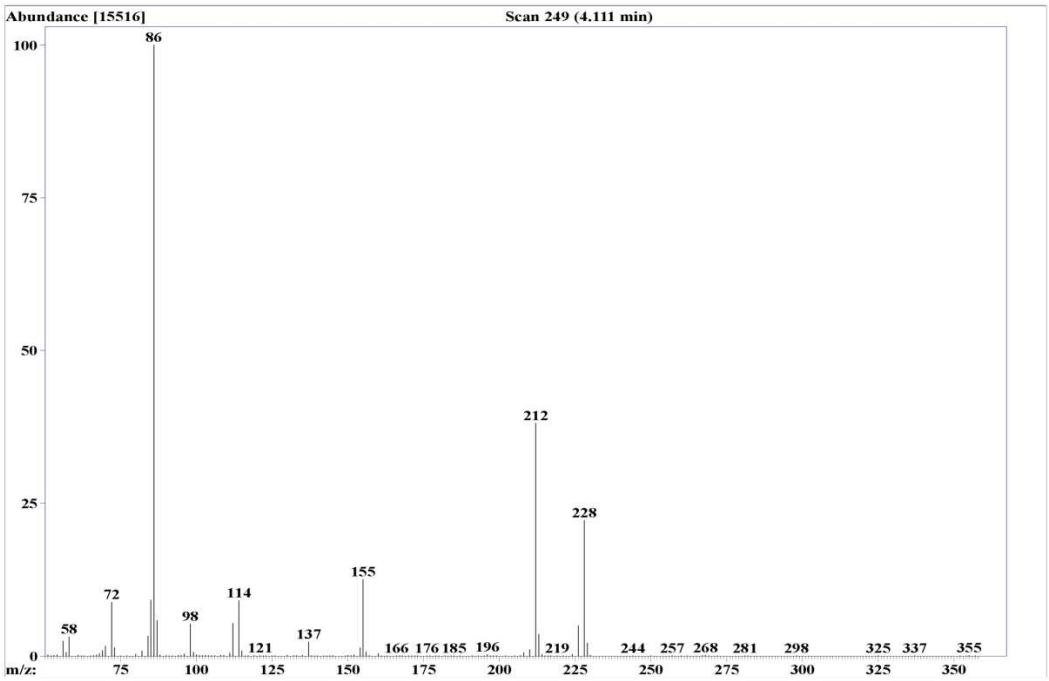

Figure 228: *GC-MS spectrum of derivatized* ***I****.*

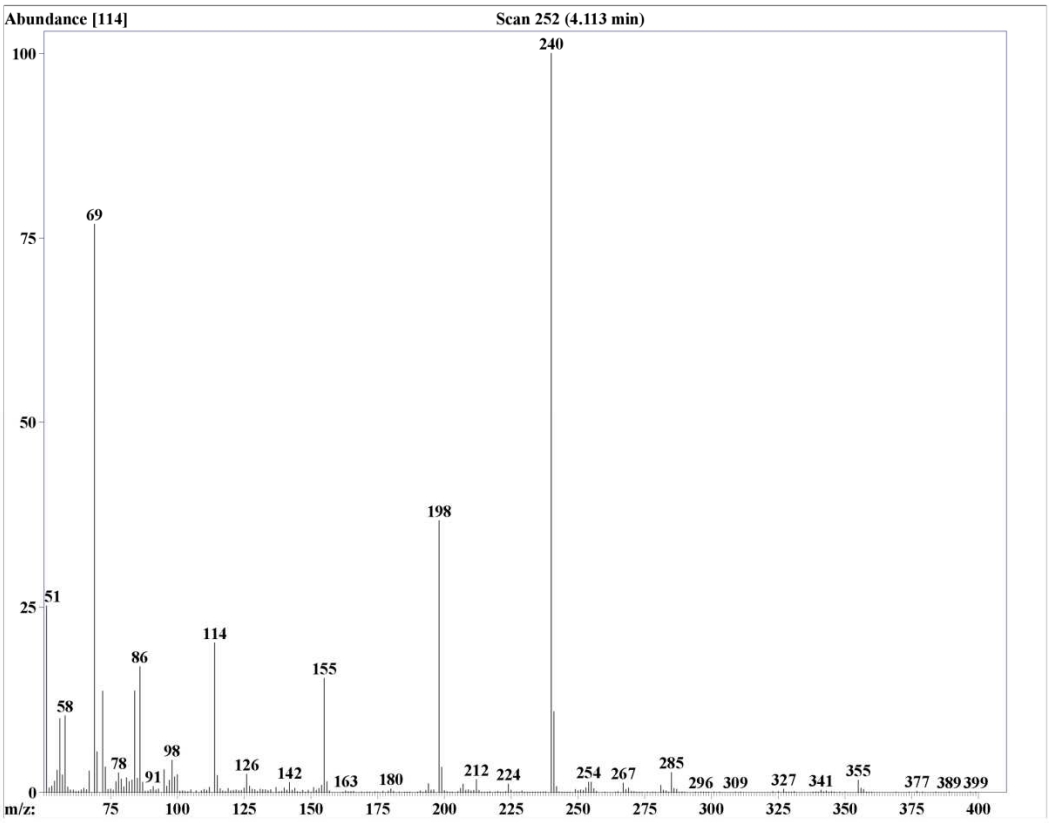

Figure 229: *GC-MS spectrum of derivatized* ***II****.*

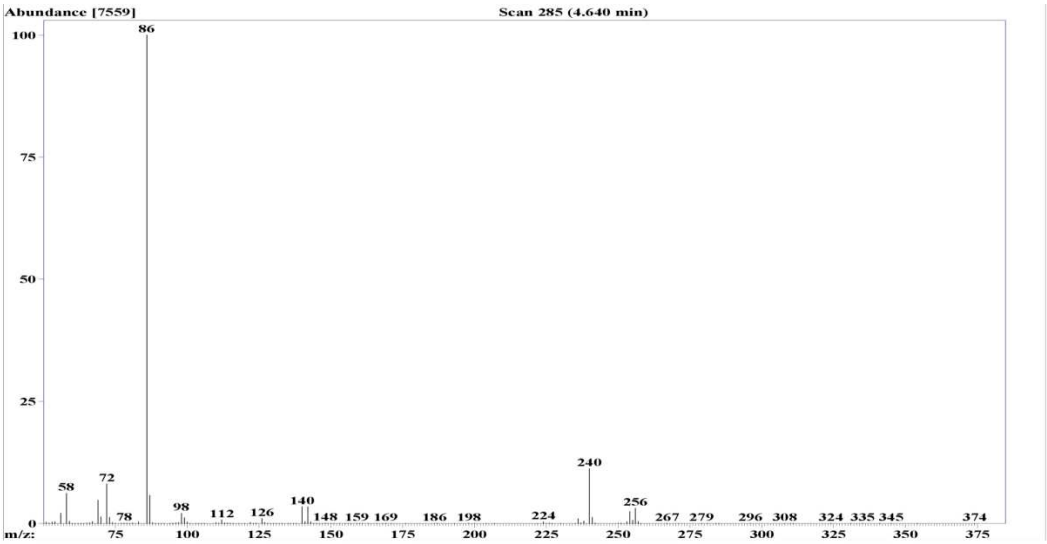

Figure 230: *GC-MS spectrum of derivatized* ***III****.*

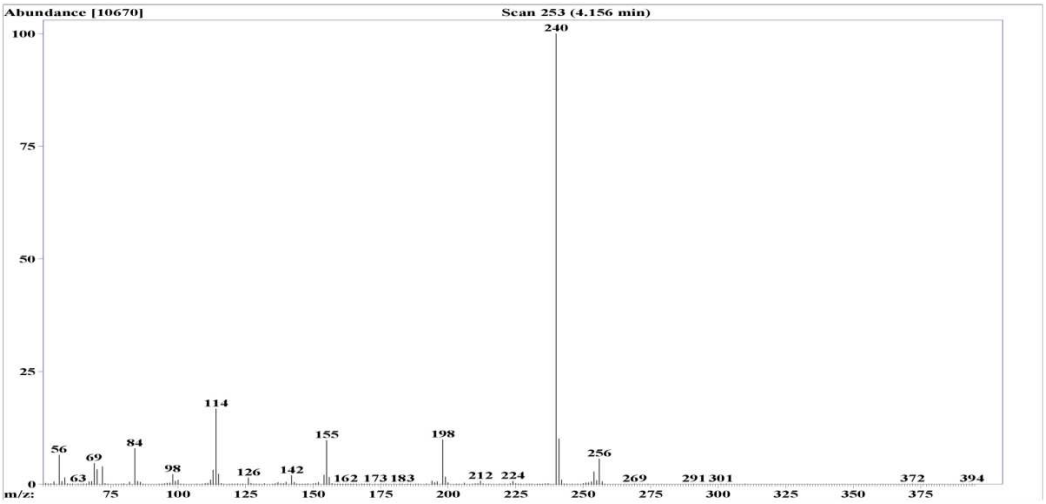

Figure 231: *GC-MS spectrum of derivatized* ***IV****.*

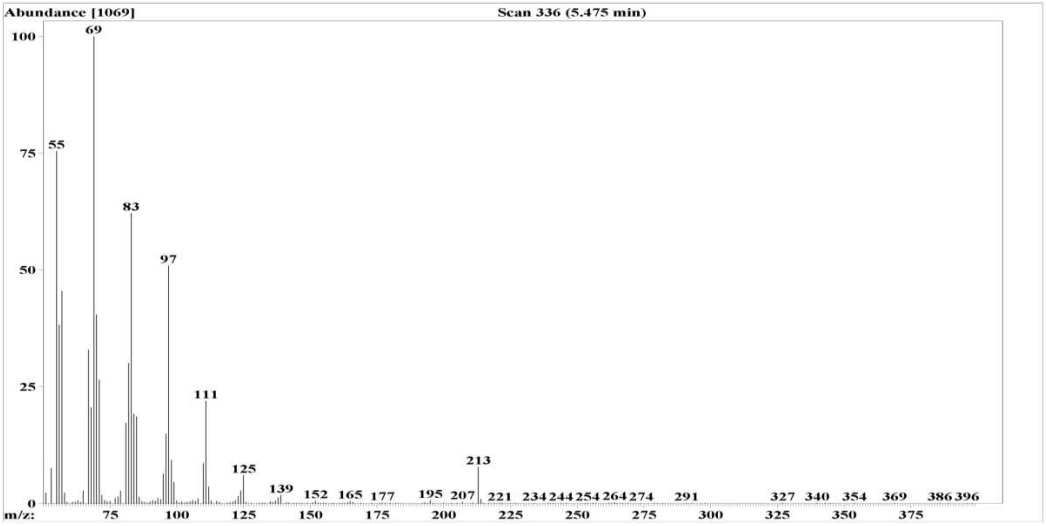

Figure 232: *GC-MS spectrum of derivatized* ***V****.*

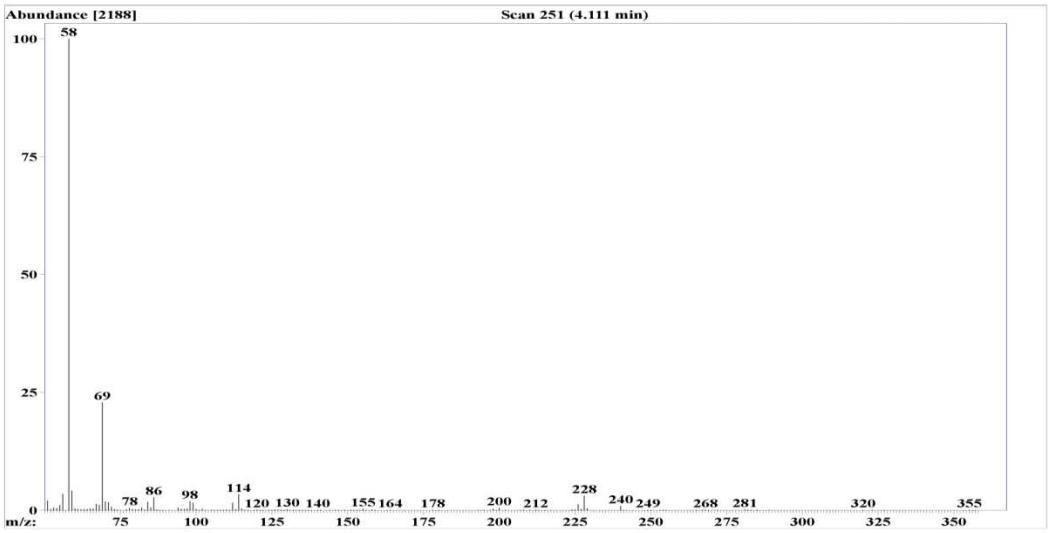

Figure 233: *GC-MS spectrum of derivatized* ***VI****.*

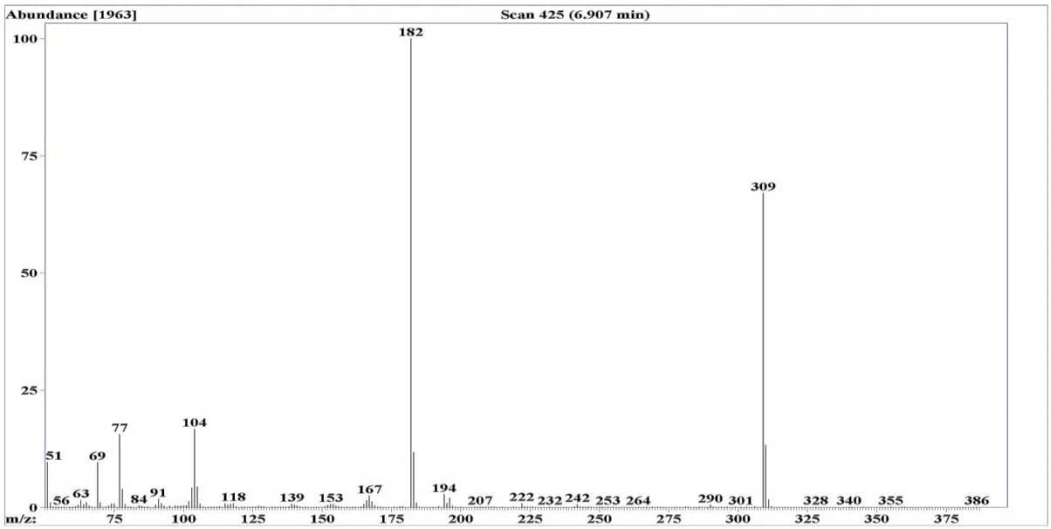

Figure 234: *GC-MS spectrum of derivatized* ***VII.***

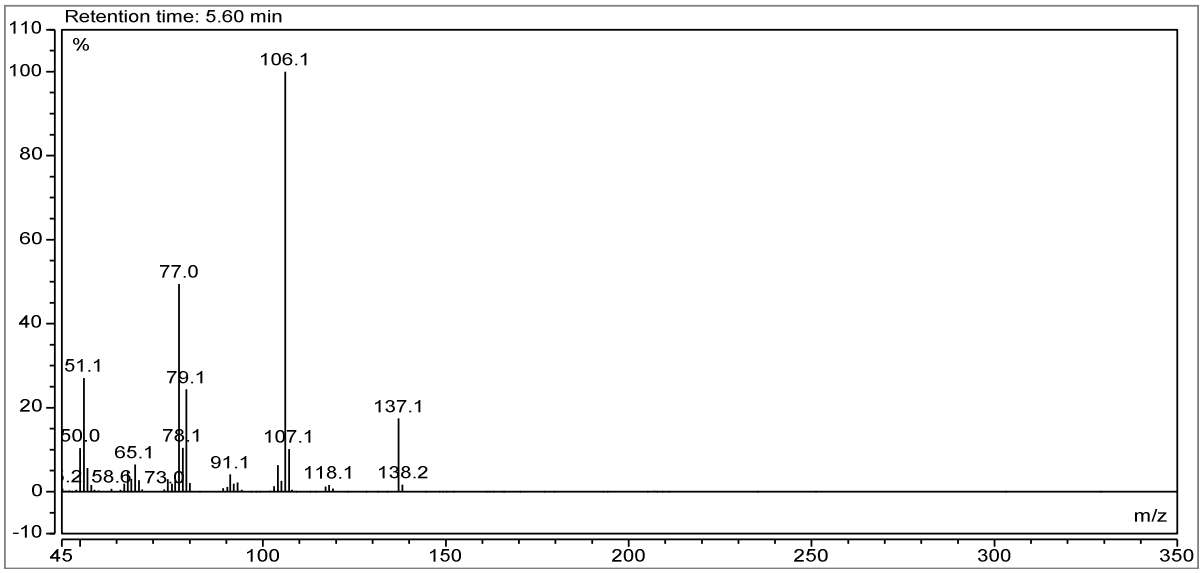

Figure 235: *GC-MS spectrum of non-derivatized* ***VII****.*

ii. Organo(thio)phosphate Spectra

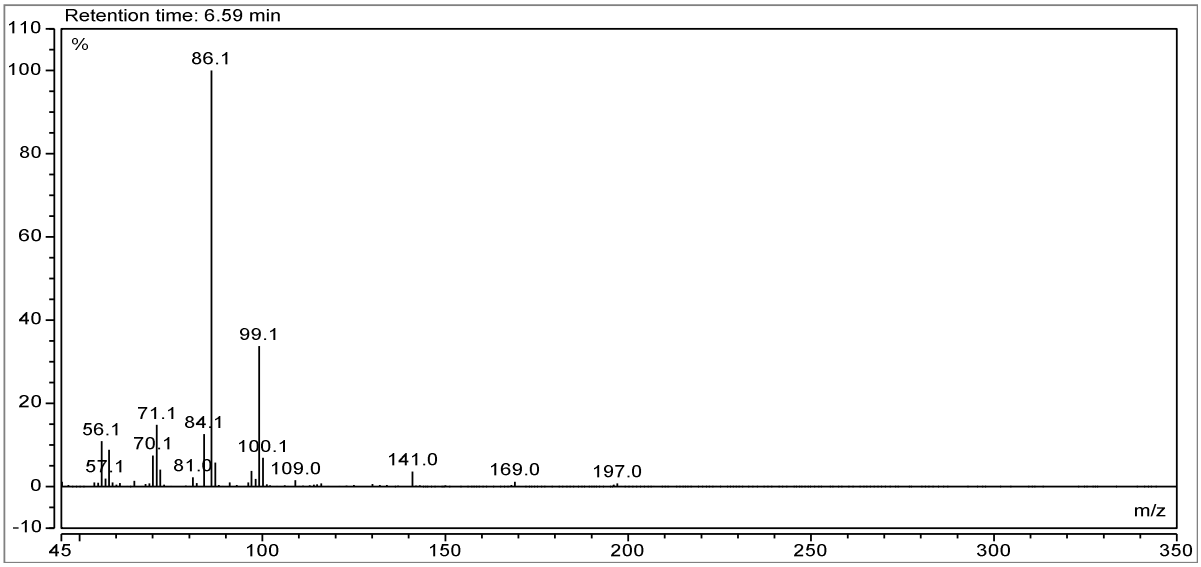

Figure 236: *GC-MS spectrum of compound* ***IX****.*

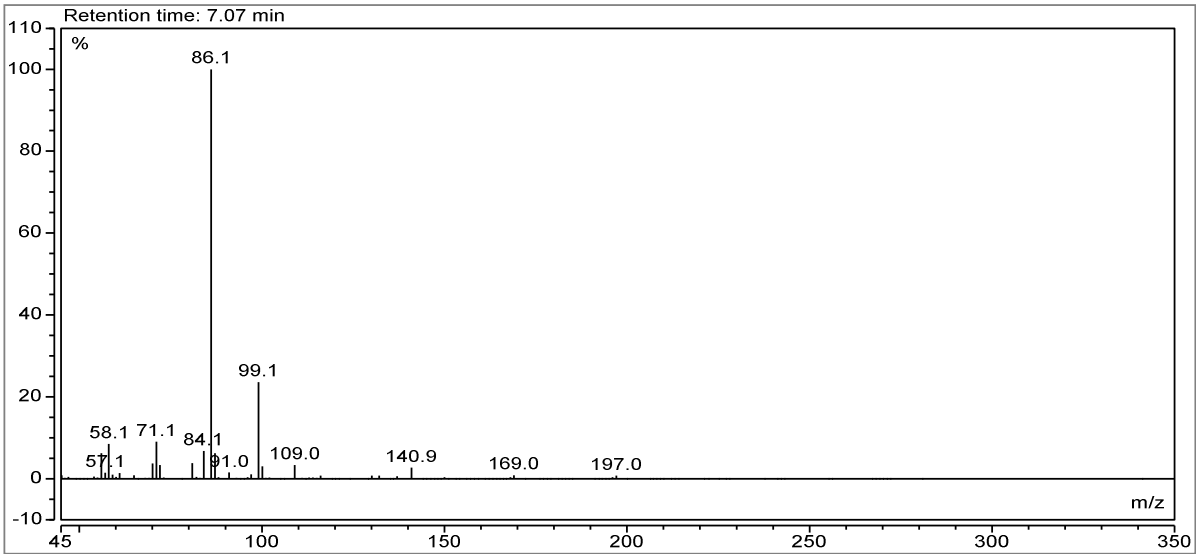

Figure 237: *GC-MS spectrum of compound* ***X****.*

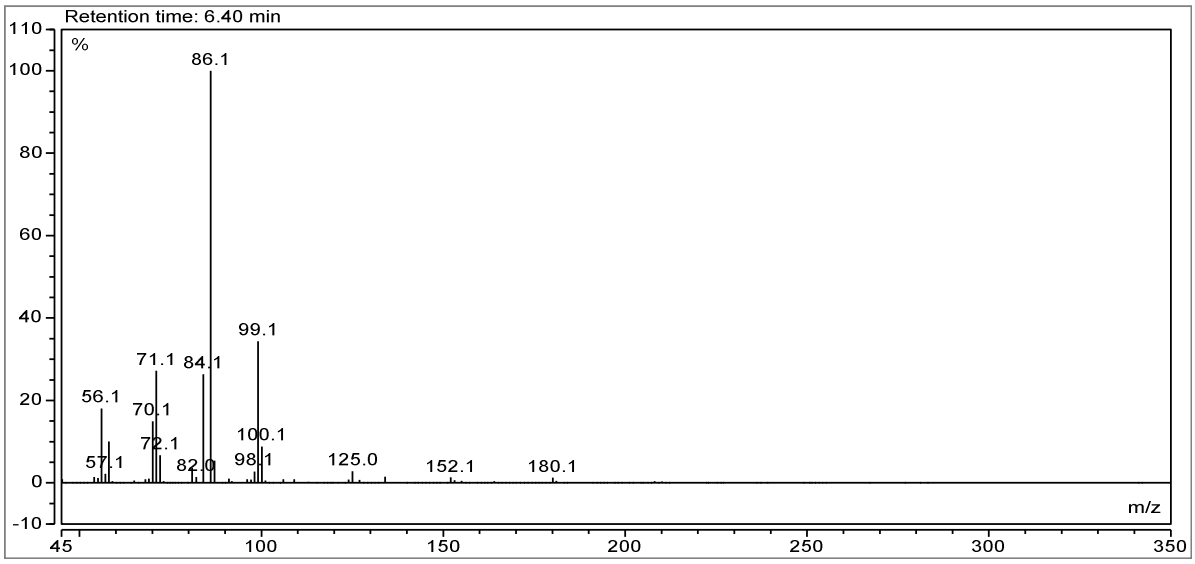

Figure 238: *GC-MS spectrum of compound* ***XI****.*

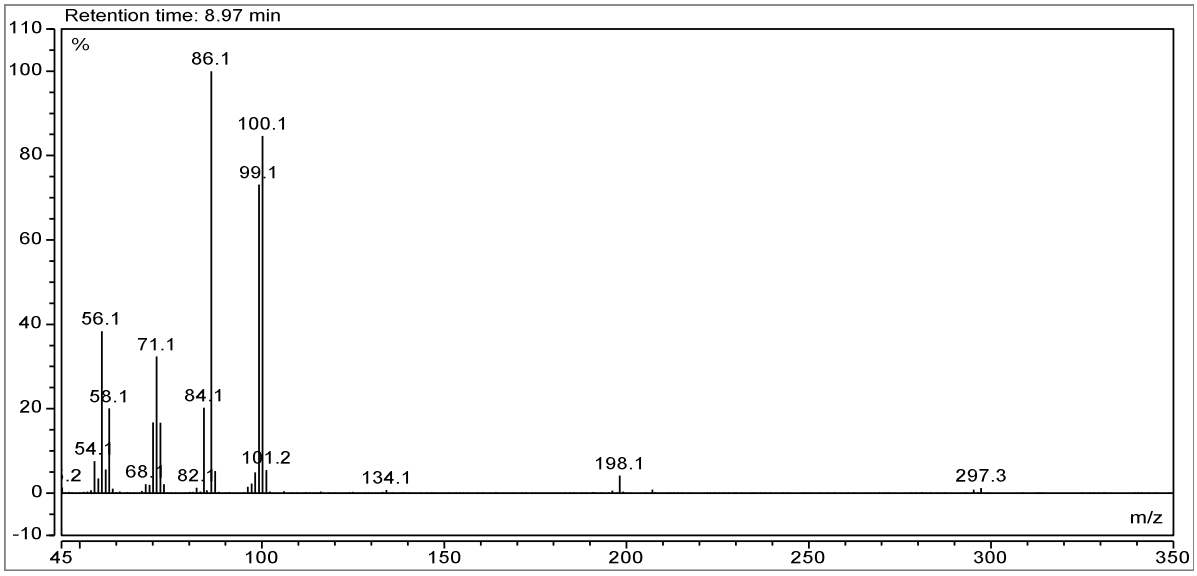

Figure 239: *GC-MS spectrum of compound* ***XII****.*

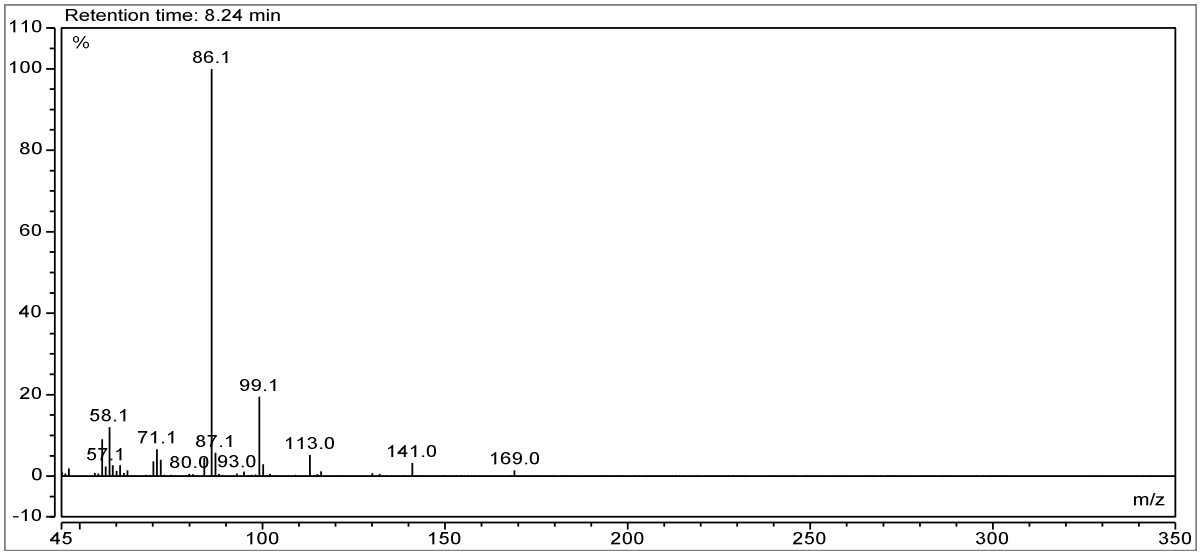

Figure 240: *GC-MS spectrum of compound* ***XIII****.*

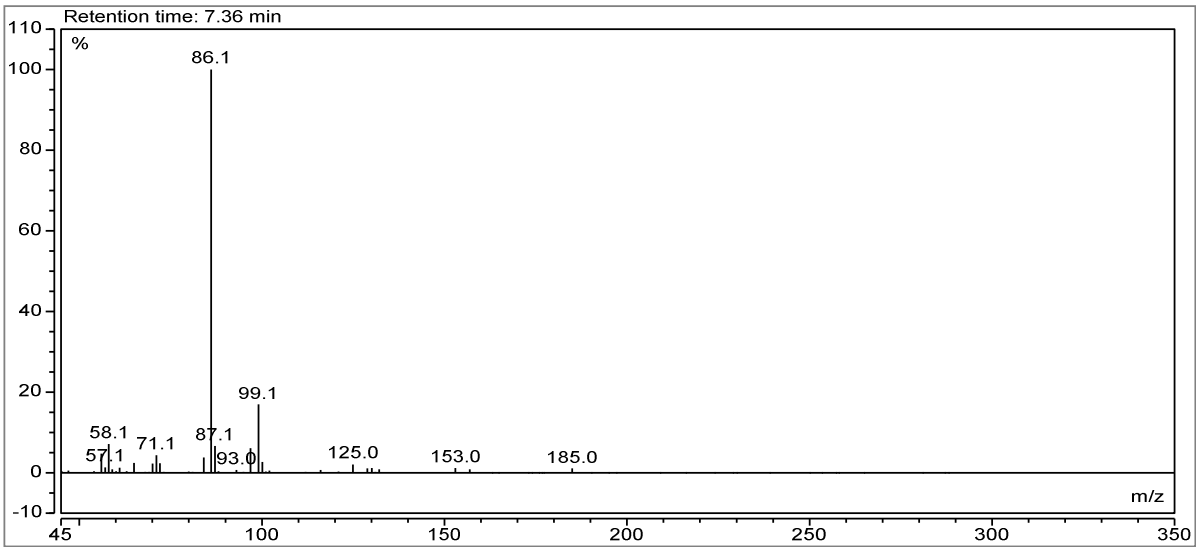

Figure 241: *GC-MS spectrum of compound* ***XIV****.*

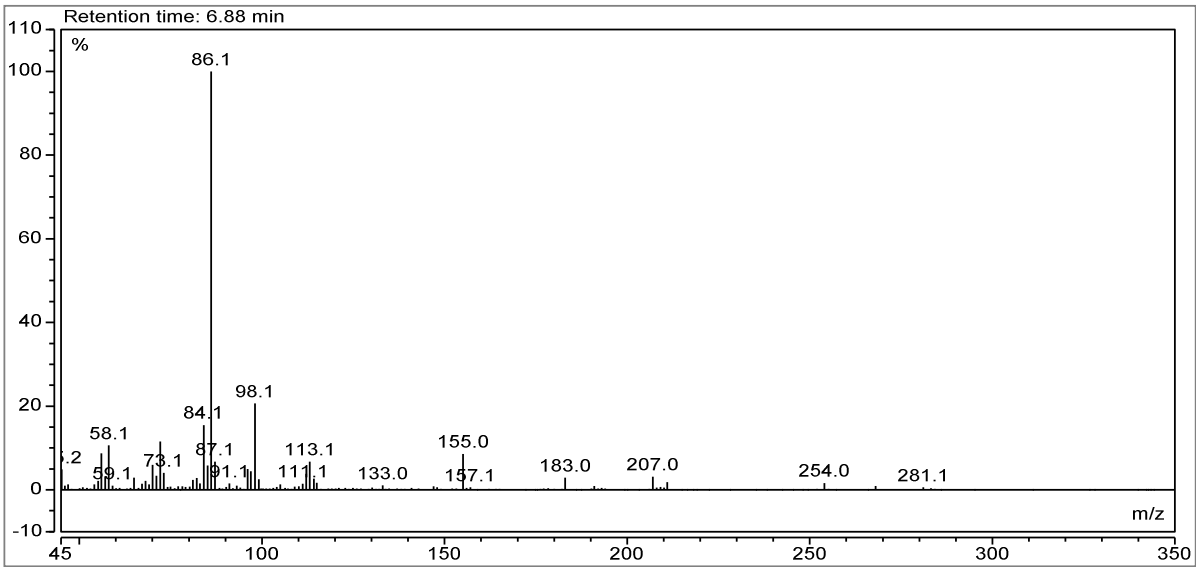

Figure 242: *GC-MS spectrum of compound* ***XV****.*

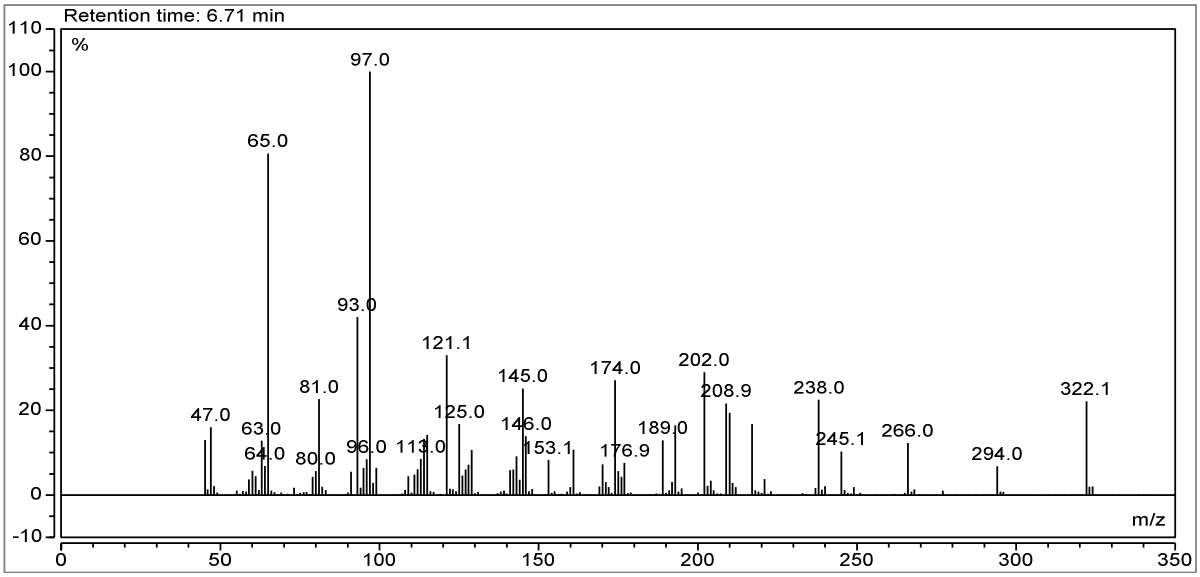

Figure 243: *GC-MS spectrum of compound* ***XVI****.*

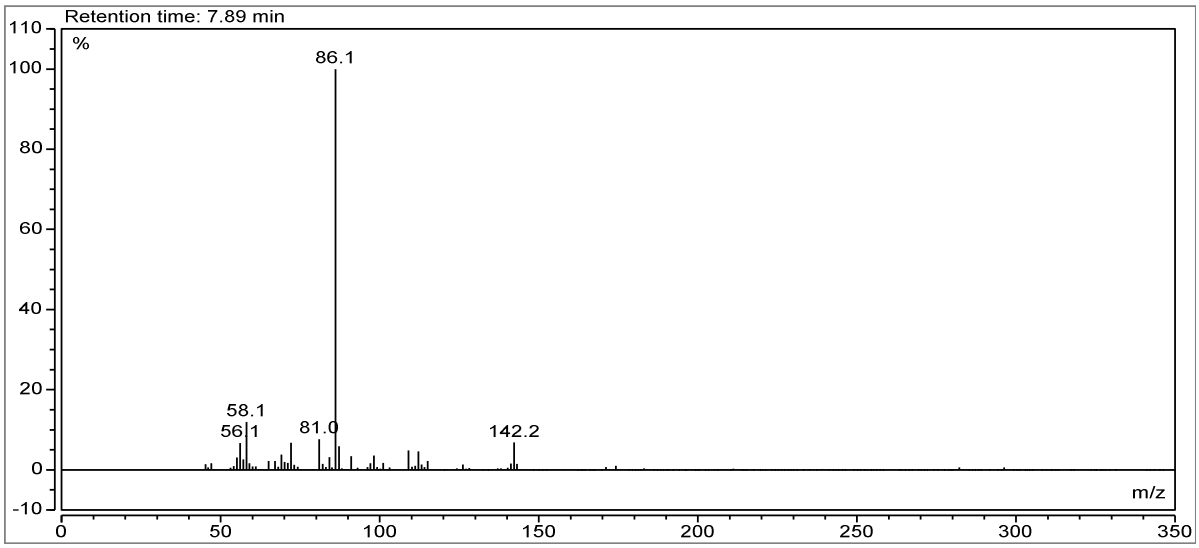

Figure 244: *GC-MS spectrum of compound* ***XVII****.*

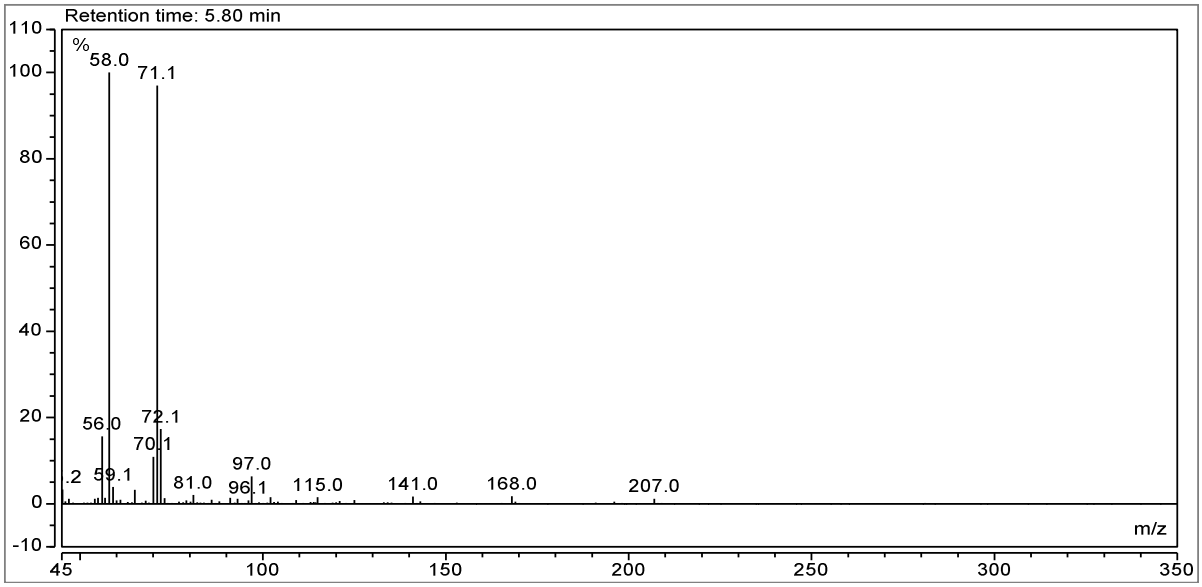

Figure 245: *GC-MS spectrum of compound* ***XVIII****.*

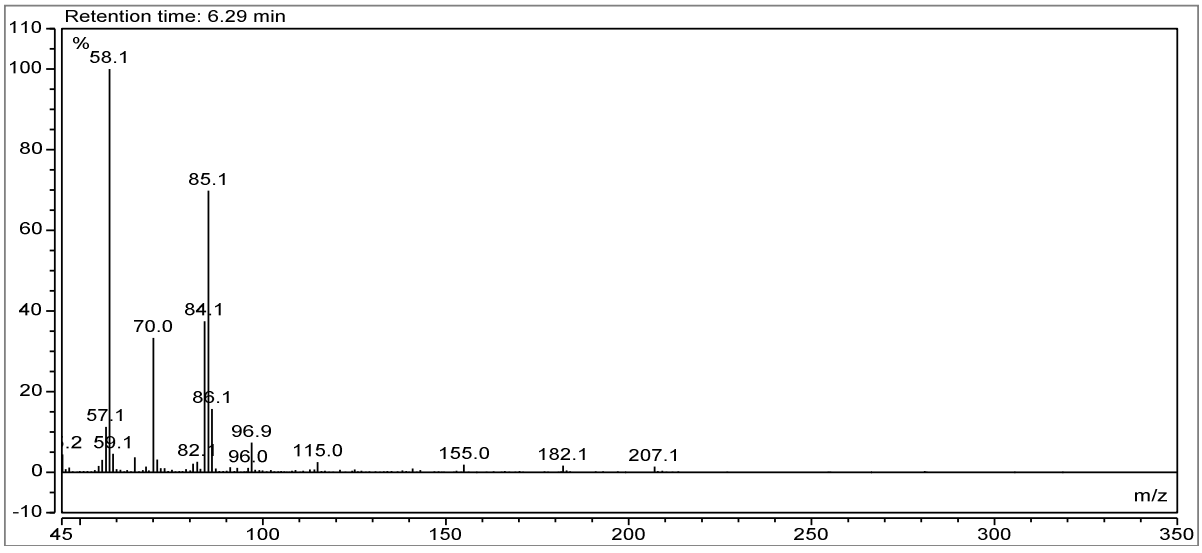

Figure 246: *GC-MS spectrum of compound* ***XIX****.*

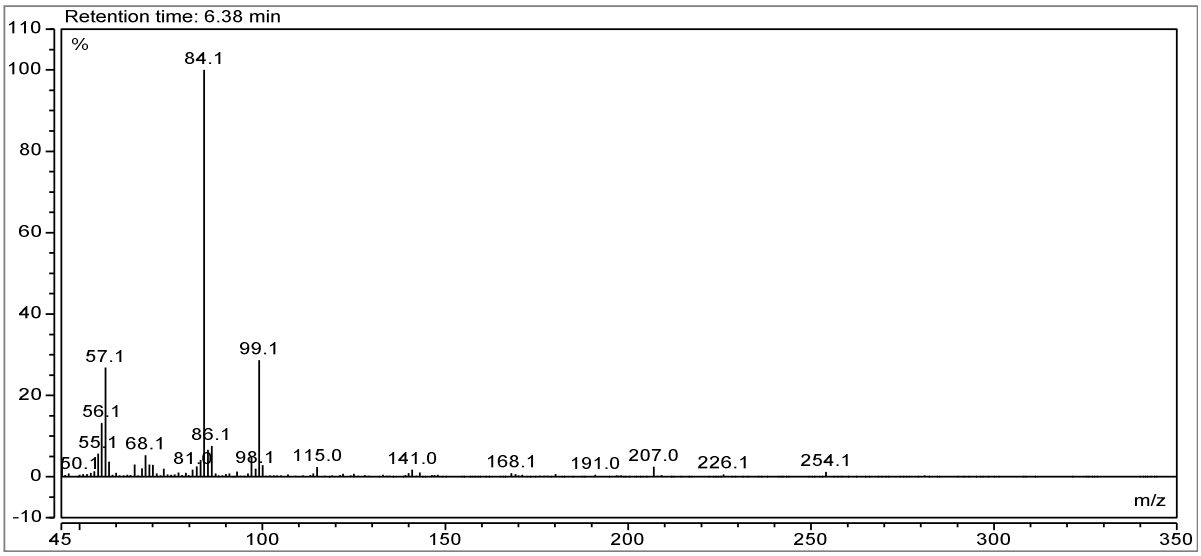

Figure 247: *GC-MS spectrum of compound* ***XX****.*

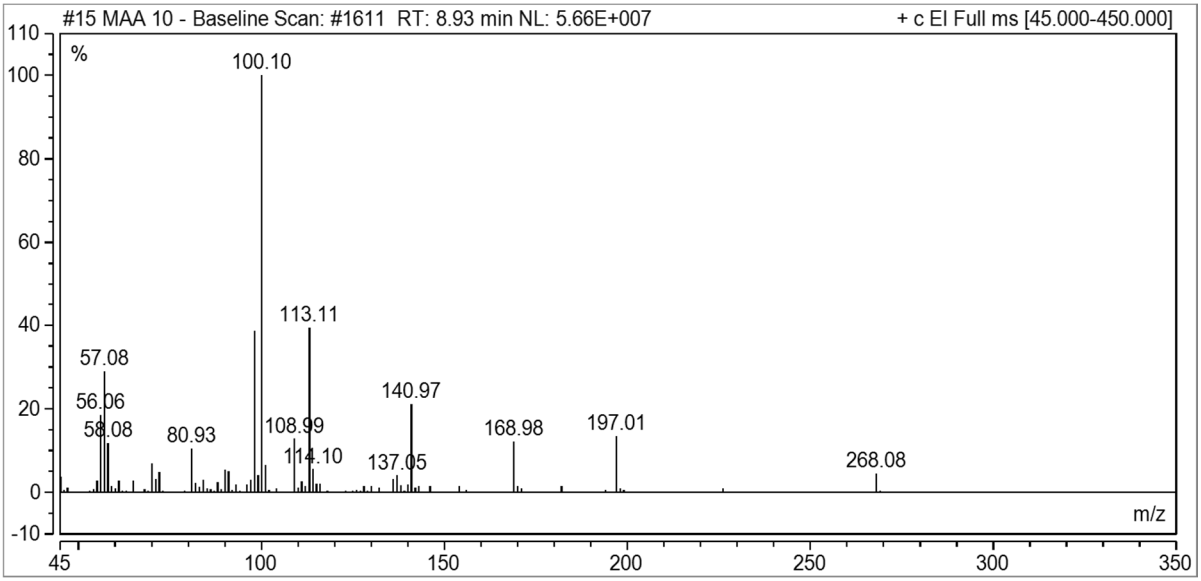

Figure 248: *GC-MS spectrum of compound* ***XXI****.*

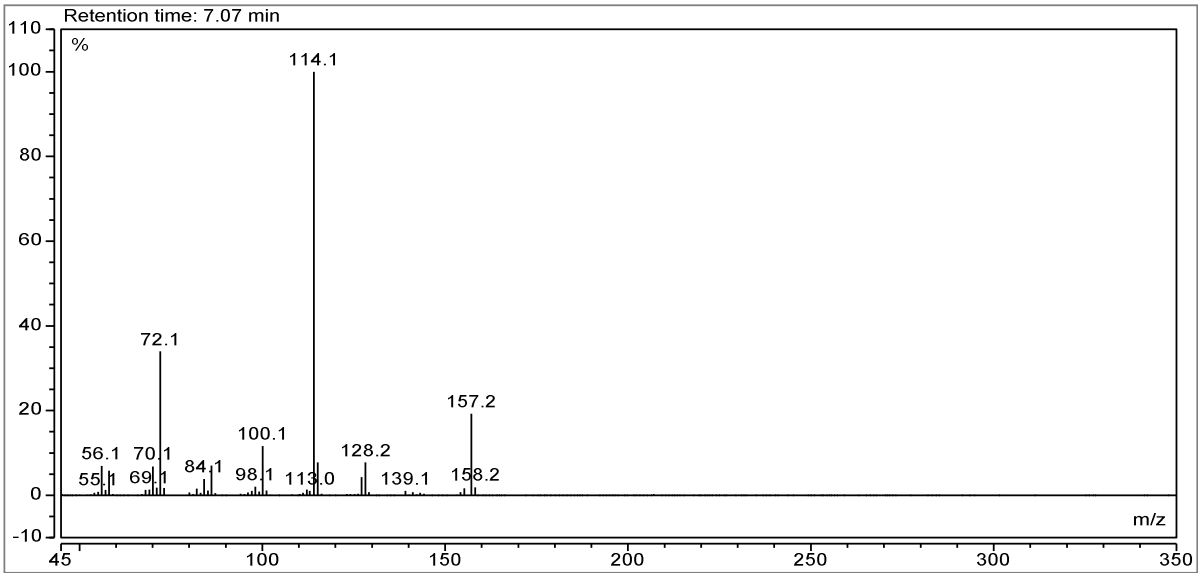

Figure 249: *GC-MS spectrum of compound* ***XXII****.*

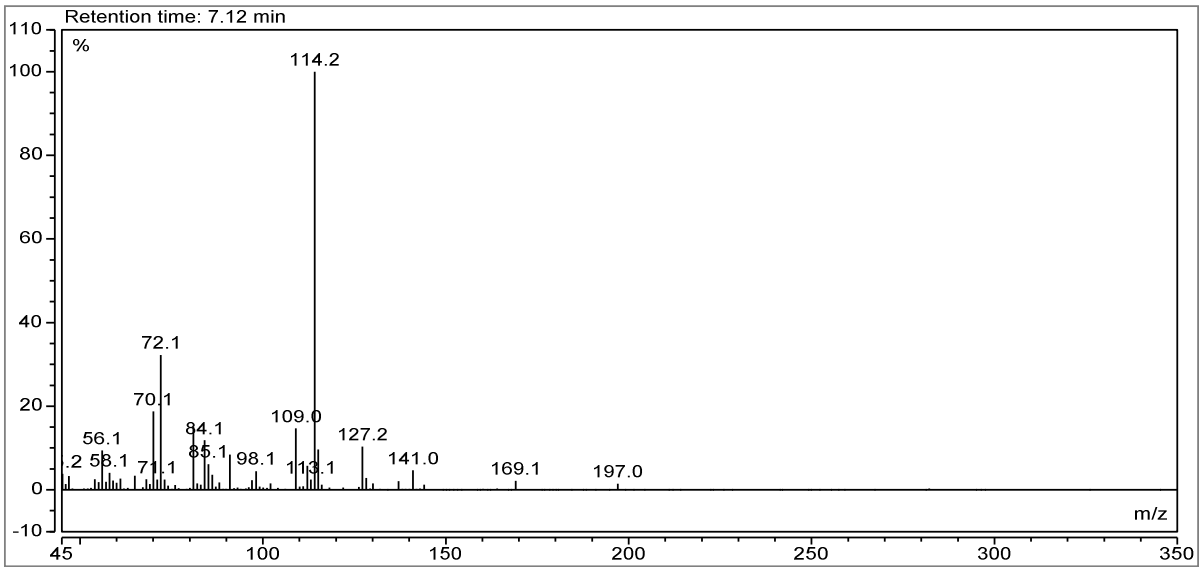

Figure 250: *GC-MS spectrum of compound* ***XXIII****.*

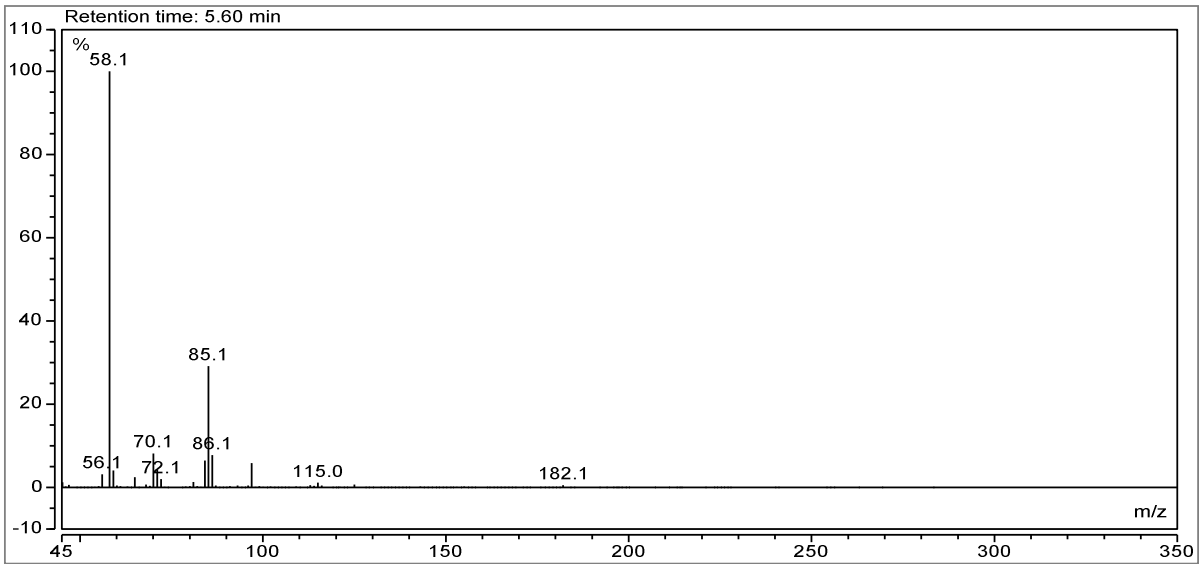

Figure 251: *GC-MS spectrum of compound* ***XIV****.*

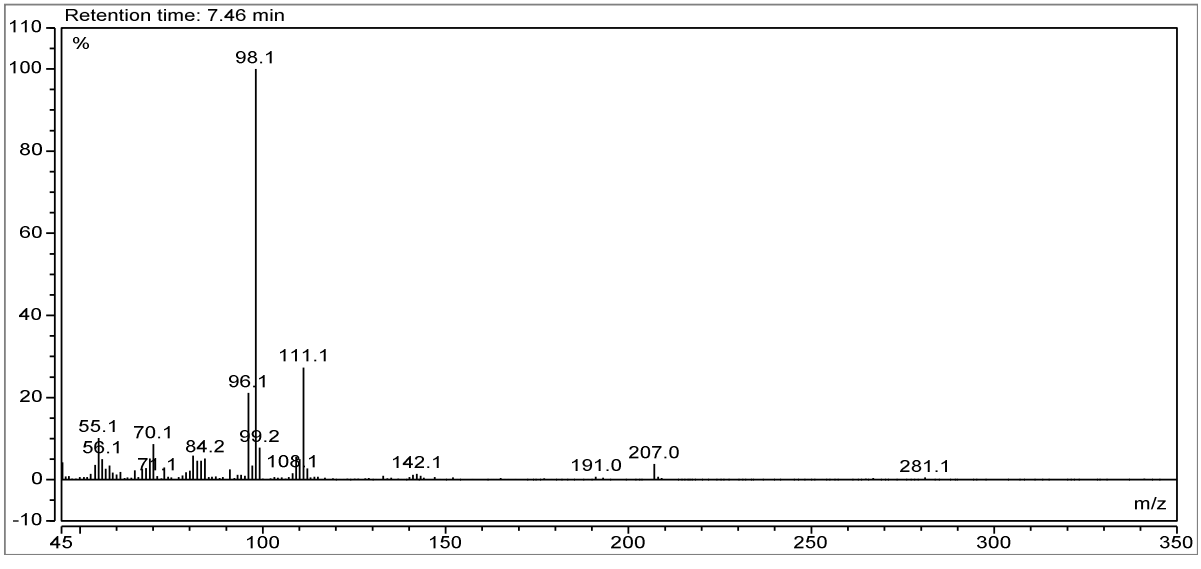

Figure 252: *GC-MS spectrum of compound* ***XV****.*

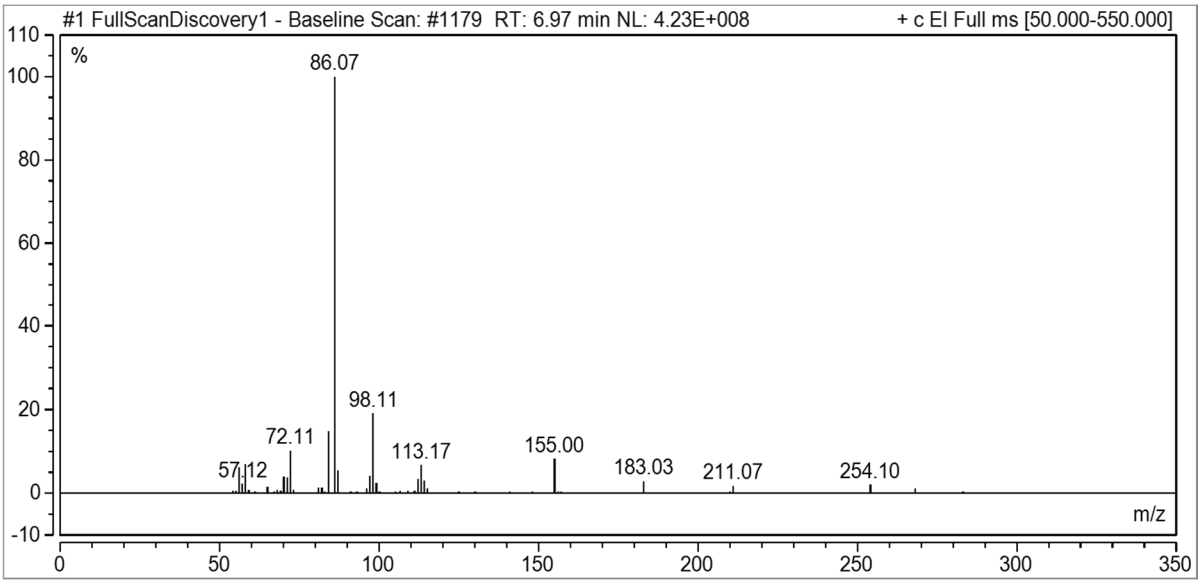

Figure 253: *GC-MS spectrum of compound* ***XXVI****.*

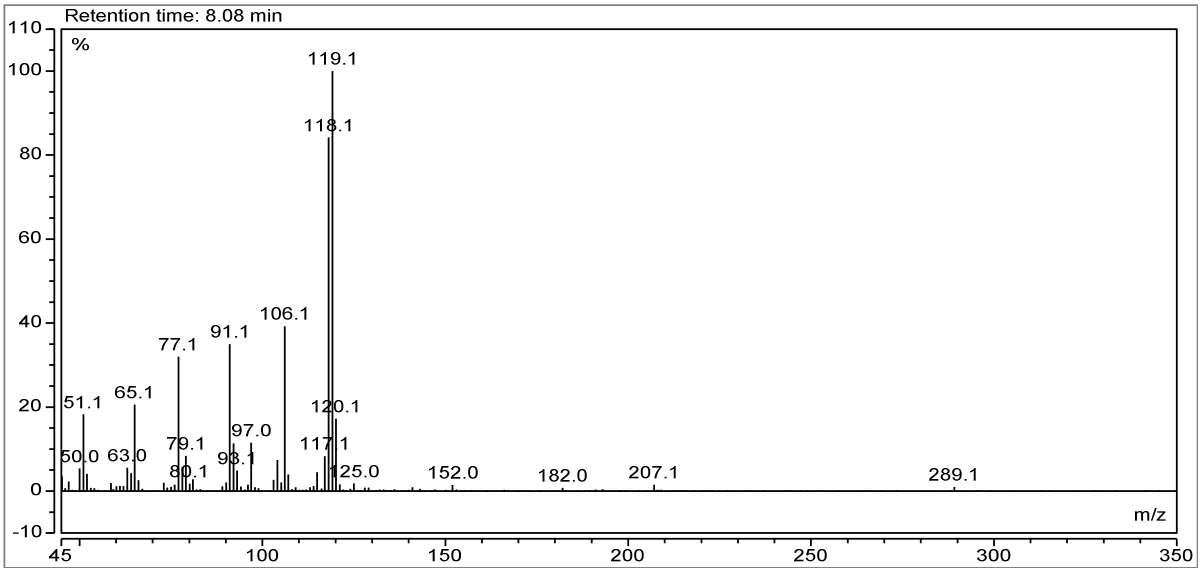

Figure 254: *GC-MS spectrum of compound* ***XXVII****.*

A.5 X-Ray Crystal Structure Parameters

Table A1: *Details for X-ray data collection and structure refinement for compounds* ***XXIX****,* ***XXX*** *and* ***XXXIII****.*

	XXIX	**XXX**	**XXXIII**
Empirical formula	$C_{12}H_{26}NO_7PS$	$C_{12}H_{26}NO_6PS_2$	$C_{10}H_{22}NO_7PS$
Formula mass	359.37	375.43	331.31
T[K]	100(2)	173(2)	173(2)
Crystal size [mm]	0.32 × 0.29 × 0.07	0.30 × 0.22 × 0.13	0.35 × 0.10 × 0.05
Crystal description	platelet	block	colorless rod
Crystal system	monoclinic	orthorhombic	triclinic
Space group	P 21/n #14	*Pbca*	*P*-1
a [Å]	7.8370(3)	11.2230(3)	5.5611(4)
b [Å]	21.6900(8)	15.2380(4)	8.4383(5)
c [Å]	11.0070(4)	21.4760(6)	18.3071(16)
α [°]	90.00	90.00	98.090(6)
β [°]	105.364(4)	90.00	93.525(7)
γ [°]	90.00	90.00	105.213(5)
V [Å^3]	1804.15(12)	3672.74(17)	816.36(11)
Z	4	8	2
$\rho_{calcd.}$ [g cm^{-3}]	1.323	1.358	1.348
μ [mm^{-1}]	0.298	0.401	0.323
F(000)	768	1600	352
Θ range [°]	4.15– 26.73	4.21– 25.35	4.12 – 25.24
Index ranges	-9 ≤ *h* ≤ 9	-13 ≤ *h* ≤ 13	-6 ≤ *h* ≤ 6
	-20 ≤ *k* ≤ 27	-18 ≤ *k* ≤ 18	-10 ≤ *k* ≤ 10
	-13 ≤ *l* ≤ 13	-25 ≤ *l* ≤ 25	-22 ≤ *l* ≤ 22
Reflns. collected	14962	23932	11935
Reflns. obsd.	3037	2684	2412
Reflns. unique	3804 (R_{int} = 0.0486)	3341 (R_{int} = 0.0486)	3304 (R_{int} = 0.0519)
R_1, wR_2 (2σ data)	0.0404, 0.0929	0.0518, 0.1274	0.0467, 0.1102
R_1, wR_2 (all data)	0.0563, 0.1024	0.0663, 0.1381	0.0707, 0.1253
GOOF on F^2	1.030	1.026	1.043
Peak/hole [e Å^{-3}]	0.673 /-0.385	0.993 /-0.395	0.609 / -0.447

Table A2: *Details for X-ray data collection and structure refinement for compounds* ***XXXIV****,* ***XXXVI*** *and* ***XXXVIII****.*

	XXXIV	**XXXVI**	**XXXVIII**
Empirical formula	$C_8H_{20}NO_3PS$	$C_{11}H_{27}INO_3PS$	$C_{12}H_{27}INO_3PS$
Formula mass	241.28	411.27	423.28
T[K]	173(2)	173(2)	143(2)
Crystal size [mm]	0.46 × 0.34 × 0.26	0.25 × 0.22 × 0.04	0.22 × 0.14 × 0.03
Crystal description	colorless block	colorless platelet	colorless platelet
Crystal system	monclinic	monoclinic	monoclinic
Space group	P 21/n	P 21/c	P 21/c
a [Å]	7.4660(2)	11.5100(6)	12.7800(16)
b [Å]	13.5370(4)	11.8850(8)	12.8950(8)
c [Å]	11.8560(4)	13.7420(7)	12.1000(13)
α [°]	90.00	90.00	90.00
β [°]	92.861(3)	105.405(6)	115.452(15)
γ [°]	90.00	90.00	90.00
V [Å^3]	1196.76(6)	1812.32(18)	1800.5(3)
Z	4	4	4
$\rho_{calcd.}$ [g cm^{-3}]	1.339	1.507	1.561
μ [mm^{-1}]	0.389	1.971	1.987
F(000)	520	832	856
Θ range [°]	4.36 – 25.24	4.33– 25.35	4.19 – 25.35
Index ranges	-9 ≤ h ≤ 9	-13 ≤ *h* ≤ 13	-13 ≤ *h* ≤ 15
	-18 ≤ k ≤ 18	-14 ≤ *k* ≤ 13	-15 ≤ *k* ≤ 14
	-15 ≤ l ≤ 15	-16 ≤ *l* ≤ 16	-14 ≤ *l* ≤ 14
Reflns. collected	10777	11568	11400
Reflns. obsd.	2517	2564	2171
Reflns. unique	2943 (R_{int} = 0.046)	3283 (R_{int} = 0.0417)	3280 (R_{int} = 0.0591)
R_1, wR_2 (2σ data)	0.0293, 0.0727	0.0535, 0.1332	0.0667, 0.1634
R_1, wR_2 (all data)	0.0374, 0.0779	0.0719, 0.1453	0.0991, 0.1823
GOOF on F^2	1.041	1.063	1.046
Peak/hole [e Å^{-3}]	0.303 / -0.259	0.895 /-0.500	2.776 / -0.829

Table A3: *Details for X-ray data collection and structure refinement for compounds* ***XXXIX****, XL and* ***XLI****.*

	XXXIX	**XL**	**XLI**
Empirical formula	$C_{13}H_{26}NO_7PS$	$C_{11}H_{25}INO_3PS$	$C_{12}H_{24}NO_3PS$
Formula mass	371.38	409.25	357.35
T[K]	143(2)	173(2)	173(2)
Crystal size [mm]	0.15 × 0.10 × 0.05	0.35 × 0.28 × 0.07	0.25 × 0.12 × 0.02
Crystal description	colorless block	colorless plate	colorless platelet
Crystal system	monclinic	monoclinic	triclinic
Space group	P 21/c	P 21/c	P-1
a [Å]	8.0260(5)	12.7330(3)	5.5720(4)
b [Å]	21.3620(15)	12.5380(2)	8.4390(6)
c [Å]	11.1240(7)	11.7650(2)	19.6070(14)
α [°]	90.00	90.00	91.369(6)
β [°]	107.152(7)	114.307(2)	94.051(6)
γ [°]	90.00	90.00	105.848(6)
V [Å^3]	1822.4(2)	1711.74(6)	883.81(11)
Z	4	4	2
$\rho_{calcd.}$ [g cm^{-3}]	1.354	1.588	1.343
μ [mm^{-1}]	0.297	2.087	0.304
F(000)	792	824	380
Θ range [°]	4.17 – 26.73	4.33 – 25.35	0.995 – 26.37
Index ranges	-10 ≤ h ≤ 10	-16 ≤ *h* ≤ 16	-6 ≤ *h* ≤ 6
	-27 ≤ k ≤ 26	-16 ≤ *k* ≤ 16	-10 ≤ *k* ≤ 10
	-13 ≤ l ≤ 14	-15 ≤ *l* ≤ 15	-24 ≤ *l* ≤ 24
Reflns. collected	14891	29344	11075
Reflns. obsd.	2892	3730	2276
Reflns. unique	3839 (R_{int} = 0.0544)	4225 (R_{int} = 0.0252)	3572 (R_{int} = 0.0604)
R_1, wR_2 (2σ data)	0.0415, 0.0953	0.0210, 0.0521	0.0508, 0.0987
R_1, wR_2 (all data)	0.0615, 0.1076	0.0252, 0.0546	0.0946, 0.1175
GOOF on F^2	1.046	1.039	1.004
Peak/hole [e Å^{-3}]	0.436/ -0.315	0.725 /-0.422	0.296 / -0.291

A.6 NMR-Spectra

The full set of NMR spectra (raw data) can be requested from the author and are not presented here for the reason of not totally overloading this manuscript. Furthermore, in interactive view of the files is best to interpret the given data. The provided files can either be opened with the MestreNova software or any other NMR software capable of processing fid data.

Available spectra types are:

- ^{1}H,
- ^{13}C,
- $^{13}C\{^{1}H\}$,
- ^{31}P,
- $^{31}P\{^{1}H\}$,
- $^{1}H,^{1}H$ COSY,
- $^{1}H,^{13}C$ HMQC,
- $^{1}H,^{13}C$ HMBC

B Data Sets of Vapor Pressure Determinations

Table B1: *Example of calculation for the emission flux of Amiton I at STP conditions (298.2 K, 1 atm).*

	Amiton I	Unit
T_b	636.98[a]	K
ρ_{20}	1.044[a]	g cm^{-3}
ρ_m	0.702	g cm^{-3}
M	222.237	g mol^{-1}
V_m	383.444	cm^3 mol^{-1}
σ_A	8.470	Å
ε_B	732.527	K
σ_{AB}	6.044	Å
ε_{AB}	266.561	J
$\kappa T/\varepsilon_{AB}$	1.118	[]
$\Omega_{D,AB}$	1.365	[]
D_{AB}	0.038	cm^2 s^{-1}
p_{sat}	0.070	Pa
Q	1.452	ng/cm^2 s

[a] value obtained in this work

For all following tables a common footnote has to be applied:

[a] Saturation temperature ($u(T)$ = 0.1 K). [b] Mass of transferred sample condensed at T = 243 K [c] Volume of nitrogen ($u(V)$ = 0.005 dm^3) used to transfer m ($u(m)$ = 0.0001 g) of the sample. [d] T_a is the temperature of the soap bubble meter used for measurement of the gas flow. [e] Vapor pressure at temperature T, calculated from the m and the residual vapor pressure at the condensation temperature calculated by an iteration procedure; p°=1 Pa. [f] Standard uncertainty in p was calculated with $u(p/\text{Pa}) = 0.025+0.025(p/\text{Pa})$ for p > 5 to 3000 Pa and $u(p/\text{Pa}) = 0.005+0.025(p/\text{Pa})$ for p < 5 Pa.

Table B2 *Compound I: absolute vapor pressures* $\boldsymbol{p_{sat}}$ *and thermodynamic properties of vaporization obtained by the transpiration method in this work.*

Compound I: $\Delta_l^g H_m^\circ$ (298.15 K) = 83.6 ± 0.3 kJ mol^{-1}

$$\ln p_{sat}/p^\circ = \frac{395.8}{R} - \frac{124623.0}{RT} + \frac{137.5}{R} ln \frac{T}{298.15\text{K}}$$

T_{exp} [a]	m [b]	V_{N2} [c]	T_{amb} [d]	Gasflow	p_{sat} [e]	$u(p_{sat})$ [f]	$\Delta_l^g H_m^\circ$	$\Delta_l^g S_m^\circ$
[K]	[mg]	[dm³]	[K]	[dm³ h^{-1}]	[Pa]	[Pa]	[kJ mol^{-1}]	[J mol^{-1} K^{-1}]
298.2	0.33	43.4	300.3	2.98	0.071	0.007	83.64	162.8
298.2	0.28	37.0	300.1	2.65	0.069	0.007	83.63	162.6
303.1	0.19	14.4	300.9	4.81	0.12	0.01	82.95	160.3
308.1	0.26	11.9	301.5	4.84	0.21	0.01	82.27	158.2
313.2	0.19	5.18	301.1	5.18	0.34	0.01	81.57	155.8
318.0	0.17	2.84	299.9	4.87	0.55	0.02	80.90	153.7
323.0	0.17	1.78	299.9	4.86	0.90	0.03	80.22	151.7
323.0	0.29	3.01	300.6	4.02	0.90	0.03	80.22	151.7
323.0	0.25	2.67	300.7	4.01	0.87	0.03	80.22	151.5
328.0	0.17	1.13	299.8	4.86	1.42	0.04	79.54	149.7
332.9	0.18	0.786	300.3	3.14	2.11	0.06	78.85	147.3
337.9	0.41	1.15	301.7	3.14	3.33	0.09	78.17	145.6
342.9	0.46	0.889	302.3	3.14	4.83	0.13	77.48	143.3

Table B3: *Compound II: absolute vapor pressures* $\boldsymbol{p_{sat}}$ *and thermodynamic properties of vaporization obtained by the transpiration method in this work.*

Compound II: $\Delta_l^g H_m^\circ$ (298.15 K) = 78.5 ± 0.5 kJ mol^{-1}

$$\ln p_{sat}/p^\circ = \frac{390.0}{R} - \frac{119442.7}{RT} + \frac{137.5}{R} ln \frac{T}{298.15\text{K}}$$

T_{exp}[a]	m[b]	V_{N2}[c]	T_{amb}[d]	Gasflow	p_{sat}[e]	$u(p_{sat})$[f]	$\Delta_l^g H_m^\circ$	$\Delta_l^g S_m^\circ$
[K]	[mg]	[dm³]	[K]	[dm³ h^{-1}]	[Pa]	[Pa]	[kJ mol^{-1}]	[J mol^{-1} K^{-1}]
293.3	0.15	8.20	296.1	2.86	0.171	0.009	79.13	159.4
293.3	0.12	6.78	296.2	3.60	0.164	0.009	79.13	159.0
293.3	0.15	8.38	295.9	2.86	0.161	0.009	79.13	158.9
298.2	0.14	4.71	296.1	2.88	0.276	0.012	78.45	156.6
303.2	0.15	2.87	296.5	2.87	0.470	0.017	77.77	154.5
308.1	0.29	3.35	297.0	2.88	0.780	0.025	77.08	152.4
313.1	0.25	1.92	297.4	2.88	1.19	0.03	76.40	149.7
318.1	0.25	1.15	297.0	2.86	1.97	0.05	75.72	148.0
318.1	0.24	1.15	297.1	2.87	1.92	0.05	75.72	147.7
318.1	0.23	1.15	296.9	2.86	1.88	0.05	75.72	147.6
318.1	0.24	1.20	297.1	2.87	1.87	0.05	75.72	147.5
323.1	0.35	1.05	296.5	2.86	3.03	0.08	75.03	145.8
328.0	0.63	1.18	296.4	2.83	4.88	0.13	74.35	144.1
333.0	1.23	1.56	296.5	2.84	7.19	0.20	73.66	141.9
338.0	1.06	0.950	296.6	2.85	10.2	0.3	72.98	139.5
343.0	1.14	0.711	296.7	2.84	14.7	0.4	72.29	137.4

Table B4: *Compound III: absolute vapor pressures* $\boldsymbol{p_{sat}}$ *and thermodynamic properties of vaporization obtained by the transpiration method in this work.*

Compound III: $\Delta_l^g H_m^\circ$ (298.15 K) = 86.3 ± 0.3 kJ mol^{-1}

$$\ln p_{sat}/p^\circ = \frac{405.1}{R} - \frac{128482.1}{RT} + \frac{141.6}{R} ln \frac{T}{298.15\text{K}}$$

T_{exp} [a]	m [b]	V_{N2} [c]	T_{amb} [d]	Gasflow	p_{sat} [e]	$u(p_{sat})$ [f]	$\Delta_l^g H_m^\circ$	$\Delta_l^g S_m^\circ$
[K]	[mg]	[dm³]	[K]	[dm³ h^{-1}]	[Pa]	[Pa]	[kJ mol^{-1}]	[J mol^{-1} K^{-1}]
293.2	0.023	7.75	296.9	3.87	0.025	0.006	86.96	170.3
293.2	0.024	8.59	296.6	3.12	0.024	0.006	86.96	170.0
298.1	0.025	4.65	296.5	3.10	0.046	0.006	86.25	168.0
303.1	0.048	5.29	297.2	3.11	0.078	0.007	85.55	165.3
308.1	0.024	1.56	297.3	3.12	0.13	0.01	84.84	163.0
313.1	0.28	10.4	295.9	3.10	0.24	0.01	84.14	161.0
318.1	0.23	5.23	297.1	3.11	0.38	0.01	83.43	158.6
318.1	0.051	1.16	297.7	3.88	0.38	0.01	83.43	158.5
318.1	0.051	1.17	297.6	3.89	0.38	0.01	83.43	158.5
318.1	0.050	1.16	297.6	3.87	0.38	0.01	83.43	158.5
323.0	0.26	3.64	297.5	3.12	0.61	0.02	82.73	156.3
328.0	0.23	2.08	297.5	3.12	0.98	0.03	82.02	154.1
333.0	0.35	1.91	296.6	3.10	1.57	0.04	81.32	152.2
338.0	0.33	1.19	297.0	3.10	2.41	0.07	80.61	150.1
342.9	0.48	1.14	295.9	3.10	3.62	0.10	79.91	148.0

Table B5: *Compound IV: absolute vapor pressures* $\boldsymbol{p_{sat}}$ *and thermodynamic properties of vaporization obtained by the transpiration method in this work.*

IV: $\Delta_l^g H_m^\circ$ (298.15 K) = 79.0 ± 0.3 kJ mol^{-1}

$$\ln p_{sat}/p^\circ = \frac{387.0}{R} - \frac{118746.4}{RT} + \frac{133.3}{R} ln \frac{T}{298.15\text{K}}$$

T_{exp}[a]	m[b]	V_{N2}[c]	T_{amb}[d]	Gasflow	p_{sat}[e]	$u(p_{sat})$[f]	$\Delta_l^g H_m^\circ$	$\Delta_l^g S_m^\circ$
[K]	[mg]	[dm³]	[K]	[dm³ h^{-1}]	[Pa]	[Pa]	[kJ mol^{-1}]	[J mol^{-1} K^{-1}]
298.2	1.30	49.1	296.4	3.00	0.26	0.01	79.00	158.0
298.2	1.17	45.2	297.4	2.98	0.25	0.01	79.00	157.8
298.2	0.52	19.3	297.4	3.95	0.26	0.01	79.00	158.0
303.1	0.23	5.16	297.2	3.01	0.43	0.02	78.34	155.8
308.1	0.38	5.19	296.5	2.99	0.72	0.02	77.68	153.7
313.0	0.24	2.00	296.8	3.01	1.15	0.03	77.02	151.5
318.0	0.49	2.61	298.0	3.02	1.84	0.05	76.36	149.5
318.1	0.53	2.79	298.4	5.08	1.85	0.05	76.35	149.5
323.0	0.58	1.95	298.9	5.08	2.92	0.08	75.69	147.5
323.0	0.47	1.61	298.9	4.02	2.89	0.08	75.69	147.4
323.0	0.47	1.61	298.9	4.02	2.89	0.08	75.69	147.4
323.1	0.50	1.68	298.4	4.02	2.89	0.08	75.69	147.4
323.1	0.57	1.93	298.3	3.04	2.88	0.08	75.69	147.4
328.0	1.14	2.54	299.5	5.07	4.43	0.12	75.03	145.4
328.1	1.01	2.28	298.4	3.04	4.32	0.11	75.02	145.1
333.0	1.17	1.79	299.8	3.06	6.45	0.19	74.36	143.1
338.0	1.16	1.17	299.8	3.05	9.73	0.27	73.70	141.2
342.9	1.09	0.755	298.8	3.02	14.12	0.38	73.04	139.3

Table B6: *Compound V: absolute vapor pressures* $\boldsymbol{p_{sat}}$ *and thermodynamic properties of vaporization obtained by the transpiration method in this work.*

V: $\Delta_l^g H_m^\circ$ (298.15 K) = 81.4 ± 0.3 kJ mol^{-1}

$$\ln p_{sat}/p^\circ = \frac{399.6}{R} - \frac{124860.5}{RT} + \frac{145.7}{R} ln \frac{T}{298.15\mathrm{K}}$$

T_{exp}[a]	m[b]	V_{N2}[c]	T_{amb}[d]	Gasflow	p_{sat}[e]	$u(p_{sat})$[f]	$\Delta_l^g H_m^\circ$	$\Delta_l^g S_m^\circ$
[K]	[mg]	[dm³]	[K]	[dm³ h^{-1}]	[Pa]	[Pa]	[kJ mol^{-1}]	[J mol^{-1} K^{-1}]
293.3	0.041	6.23	299.8	3.06	0.058	0.006	82.15	160.7
298.2	0.040	3.43	299.2	2.39	0.10	0.01	81.42	158.4
298.2	0.043	3.75	298.0	3.63	0.10	0.01	81.42	158.3
298.2	0.041	3.57	299.5	3.06	0.10	0.01	81.42	158.2
303.2	0.041	2.10	300.4	3.07	0.17	0.01	80.70	155.8
303.2	0.041	2.10	300.1	3.07	0.17	0.01	80.70	155.8
308.2	0.042	1.28	300.2	3.08	0.29	0.01	79.97	153.5
308.2	0.041	1.28	300.3	3.08	0.28	0.01	79.97	153.3
313.2	0.041	0.770	300.5	3.08	0.47	0.02	79.25	151.1
318.1	0.11	1.20	296.3	3.00	0.76	0.02	78.53	148.9
318.2	0.14	1.62	298.4	3.04	0.76	0.02	78.52	148.8
318.2	0.067	0.771	300.7	3.08	0.76	0.02	78.52	148.8
318.2	0.067	0.772	300.5	3.09	0.76	0.02	78.52	148.8
318.1	0.064	0.763	298.3	3.05	0.74	0.02	78.52	148.6
318.2	0.064	0.772	300.4	3.09	0.73	0.02	78.52	148.5
323.1	0.11	0.801	297.0	3.00	1.22	0.04	77.80	146.7
323.1	0.14	1.016	299.1	3.05	1.21	0.04	77.80	146.6
323.1	0.10	0.764	299.1	3.06	1.19	0.03	77.80	146.5
328.1	0.16	0.762	299.6	3.05	1.89	0.05	77.07	144.4
328.1	0.17	0.800	296.7	3.00	1.87	0.05	77.07	144.4
328.1	0.16	0.768	299.5	3.07	1.83	0.05	77.07	144.2
333.1	0.25	0.750	296.9	3.00	2.88	0.08	76.35	142.3
333.1	0.25	0.765	300.1	3.06	2.85	0.08	76.35	142.2
333.1	0.24	0.770	300.3	3.08	2.78	0.07	76.35	142.0
338.1	0.37	0.771	300.2	3.08	4.28	0.11	75.62	140.1
338.1	0.37	0.775	300.8	3.10	4.24	0.11	75.62	140.0
338.1	0.37	0.770	300.4	3.08	4.20	0.11	75.62	139.9

Table B7: *Compound VI: absolute vapor pressures* $\boldsymbol{p_{sat}}$ *and thermodynamic properties of vaporization obtained by the transpiration method in this work.*

Compound VI: $\Delta_l^g H_m^\circ$ (298.15 K) = 72.7 ± 0.3 kJ mol^{-1}

$$\ln p_{sat}/p^\circ = \frac{364.7}{R} - \frac{108756.3}{RT} + \frac{121.1}{R} ln \frac{T}{298.15\text{K}}$$

T_{exp}[a]	m[b]	V_{N2}[c]	T_{amb}[d]	Gasflow	p_{sat}[e]	$u(p_{sat})$[f]	$\Delta_l^g H_m^\circ$	$\Delta_l^g S_m^\circ$
[K]	[mg]	[dm³]	[K]	[dm³ h^{-1}]	[Pa]	[Pa]	[kJ mol^{-1}]	[J mol^{-1} K^{-1}]
278.5	0.18	15.4	300.4	2.64	0.12	0.01	75.03	156.1
283.3	0.28	14.0	301.3	4.01	0.21	0.01	74.44	154.0
288.3	0.26	7.72	300.4	3.62	0.35	0.01	73.85	151.8
293.3	0.72	12.1	300.1	3.96	0.62	0.02	73.24	150.0
298.2	0.52	5.41	300.8	4.01	0.99	0.03	72.64	147.8
303.2	0.57	3.63	299.5	3.97	1.62	0.05	72.04	145.9
308.1	0.49	2.00	298.4	3.99	2.50	0.07	71.44	143.8
313.1	0.51	1.34	300.4	4.01	3.94	0.10	70.85	142.0
318.1	0.58	0.995	299.3	3.98	5.98	0.17	70.24	140.0

Table B8: *Compound VII: absolute vapor pressures* $\boldsymbol{p_{sat}}$ *and thermodynamic properties of vaporization obtained by the transpiration method in this work.*

VII: $\Delta_l^g H_m^\circ$ (298.15 K) = 76.9 ± 0.3 kJ mol^{-1}

$$\ln p_{sat}/p^\circ = \frac{359.5}{R} - \frac{115475.8}{RT} + \frac{129.3}{R} ln \frac{T}{298.15\text{K}}$$

T_{exp} [a]	m [b]	V_{N2} [c]	T_{amb} [d]	Gasflow	p_{sat} [e]	$u(p_{sat})$ [f]	$\Delta_l^g H_m^\circ$	$\Delta_l^g S_m^\circ$
[K]	[mg]	[dm³]	[K]	[dm³ h^{-1}]	[Pa]	[Pa]	[kJ mol^{-1}]	[J mol^{-1} K^{-1}]
293.3	0.0066	3.01	296.8	3.01	0.021	0.006	77.56	136.7
293.3	0.0064	3.00	297.0	3.60	0.021	0.006	77.56	136.5
293.3	0.0090	4.25	299.3	3.64	0.021	0.006	77.56	136.5
293.3	0.0066	3.12	297.0	4.16	0.021	0.006	77.56	136.5
298.2	0.011	3.03	299.3	3.64	0.035	0.006	76.92	134.4
298.2	0.0070	1.92	296.8	3.59	0.035	0.006	76.92	134.4
303.2	0.011	1.80	296.6	3.60	0.060	0.006	76.28	132.5
303.2	0.0072	1.20	297.0	3.59	0.058	0.006	76.28	132.2
308.2	0.012	1.20	298.0	3.60	0.10	0.01	75.64	130.4
308.2	0.0086	0.901	297.4	3.60	0.09	0.01	75.63	129.9
313.2	0.014	0.904	298.3	3.62	0.15	0.01	74.99	128.2
313.2	0.014	0.905	298.4	3.62	0.15	0.01	74.99	128.2
313.2	0.014	0.903	298.0	3.61	0.15	0.01	74.99	128.1
318.1	0.022	0.905	299.1	3.62	0.24	0.01	74.35	126.2
318.1	0.022	0.909	299.2	3.63	0.24	0.01	74.35	126.1
323.1	0.035	0.906	299.2	3.62	0.38	0.01	73.70	124.3
323.1	0.035	0.913	299.2	3.65	0.38	0.01	73.70	124.3
328.1	0.051	0.912	299.6	3.65	0.55	0.02	73.06	121.9
333.1	0.077	0.915	300.2	3.66	0.82	0.03	72.42	120.0
333.1	0.076	0.913	300.2	3.65	0.82	0.03	72.42	120.0
333.1	0.077	0.919	300.4	3.67	0.82	0.03	72.42	120.0

Table B9: *Compound VIII: absolute vapor pressures* $\boldsymbol{p_{sat}}$ *and thermodynamic properties of vaporization obtained by the transpiration method in this work.*

Compound VIII: $\Delta_l^g H_m^\circ$ (298.15 K) = 71.5 ± 0.3 kJ mol^{-1}

$$\ln p_{sat}/p^\circ = \frac{365.2}{R} - \frac{110006.2}{RT} + \frac{129.3}{R} ln \frac{T}{298.15\text{K}}$$

T_{exp}[a]	m[b]	V_{N2}[c]	T_{amb}[d]	Gasflow	p_{sat}[e]	$u(p_{sat})$[f]	$\Delta_l^g H_m^\circ$	$\Delta_l^g S_m^\circ$
[K]	[mg]	[dm³]	[K]	[dm³ h^{-1}]	[Pa]	[Pa]	[kJ mol^{-1}]	[J mol^{-1} K^{-1}]
283.4	0.020	1.40	295.0	2.81	0.13	0.01	73.37	146.6
283.4	0.022	1.50	295.4	3.34	0.14	0.01	73.37	146.9
283.4	0.020	1.36	295.6	2.20	0.14	0.01	73.37	146.8
288.3	0.022	0.885	295.5	2.80	0.24	0.01	72.73	144.6
293.3	0.029	0.698	295.6	2.79	0.39	0.01	72.09	142.4
298.2	0.047	0.699	295.5	2.79	0.65	0.02	71.45	140.3
303.2	0.074	0.698	295.6	2.79	1.02	0.03	70.81	138.0
303.2	0.074	0.699	295.6	2.80	1.02	0.03	70.81	138.0
303.2	0.073	0.698	295.6	2.79	1.00	0.03	70.81	137.9
308.2	0.11	0.694	295.8	2.78	1.60	0.04	70.17	135.8
313.1	0.18	0.692	295.7	2.77	2.53	0.07	69.52	134.0
318.1	0.27	0.691	295.9	2.76	3.79	0.10	68.88	131.9
323.1	0.40	0.687	295.7	2.75	5.61	0.17	68.23	129.8
323.1	0.40	0.687	295.8	2.75	5.68	0.17	68.23	129.9
323.1	0.40	0.689	295.9	2.76	5.56	0.16	68.23	129.7

C Bibliography

1. Than, K., *Organophosphates: A Common but Deadly Pesticide.* National Geographic, 2013.

2. Online, Z. *Glyphosat: Vom Wundermittel Zur Potenziellen Gefahr*. ZEIT ONLINE 2016 [cited 2016 12.07.2016]; Available from: http://www.zeit.de/thema/glyphosat.

3. Murakami, H. and U. Gräfe, *Untergrundkrieg: Der Anschlag Von Tokyo*. 2011: DUMONT Buchverlag.

4. Hamdard, F., *Afghan Girls' School Feared Hit by Poison Gas*, in *Reuters*. 2013, Reuters: Online.

5. Tomlinson, S., *Hundreds of Afghan Girls Poisoned by Toxic Gas at Two Schools*, in *Daily Mail*. 2015, Daily Mail: UK.

6. Mora, E. *Afghanistan: 106 Girls Poisoned by Mystery Gas in School*. 2016 2016-04-25 [cited 2016 2016-05-29]; Available from: http://www.breitbart.com/national-security/2016/04/25/afghanistan-106-girls-poisoned-school/.

7. Sellström, A., *Report of the United Nations Mission to Investigate Allegations of the Use of Chemical Weapons in the Syrian Arab Republic on the Alleged Use of Chemical Weapons in the Ghouta Area of Damascus on 21 August 2013*, U.N.S. Council, Editor. 2013: The Hague. p. 38.

8. Bickel, M., *In Syrien Terrorisiert Assad Weiterhin Sein Volk Mit Giftgas*, in *Frankfurter Allgemeine Zeitung*. 2014, Frankfurter Allgemeine Zeitung GmbH: Germany.

9. OVCW. *The Nobel Peace Prize 2013*. 2013 2016-29-15; Available from: http://www.nobelprize.org/nobel_prizes/peace/laureates/2013/.

10. Harper, J., *Mv Cape Ray Gears up to Destroy Syria's Chemical Weapons.* Stars & Stripes, 2014.

11. Manager, J.P., *Field Deployable Hydrolysis System (Fdhs) Fact Sheet*, J.P.M.-. Elimination, Editor. 2014, Joint Program Executive Office - Chemical and Biological Defense: USA. p. 1.

12. Amt, A. *Vernichtung Syrischer Chemiewaffen*. 2016; Available from: http://www.auswaertiges-amt.de/DE/Aussenpolitik/Friedenspolitik/Abruestung/BioChemie/Chemiewaffen-Syrien.html.

13. Stanton, J., *Isis Militants Are Firing Chemical Weapons in Syria and Iraq*, in *Daily Mail Online*. 2015, Daily Mail: UK.

14. Schirra, B., *Isis - Der Globale Dschihad: Wie Der "Islamische Staat" Den Terror Nach Europa Trägt*. 2015: Ullstein eBooks.

15. Ackerman, G. and J. Tamsett, *Jihadists and Weapons of Mass Destruction*. 2009: CRC Press.

16. Stehle, S. and R. Schulz, *Pflanzenschutzmittel in Der Umwelt | Git-Labor – Portal Für Anwender in Wissenschaft Und Industrie - Portal Für Anwender in Wissenschaft Und Industrie.* GIT Laborjournal, 2016. **6**(2015): p. 6.

17. Unknown, *Scorched Earth, Poisoned Air*, in *SUDANESE GOVERNMENT FORCES RAVAGE JEBEL MARRA, DARFUR*. 2016, Amnesty International Ltd, Peter Benenson House, 1 Easton Street, London WC1X 0DW, UK: London. p. 1-109.

18. Bermudez, J.S., *North Korea's Chemical Warfare Capabilities*. 2013: http://38north.org/2013/10/jbermudez101013/.

19. Hoenig, S.L., *Compendium of Chemical Warfare Agents*. 2006: Springer New York.

20. Birstein, V.J., *The Perversion of Knowledge: The True Story of Soviet Science*. 2004: Westview.

21. Mirzayanov, V.S., *State Secrets: An Insider's Chronicle of the Russian Chemical Weapons Program*. 2008: Outskirts Press.

22. Heller, C.E., *Chemical Warfare in World War I: The American Experience, 1917-1918*. 1984, Combat Studies Institute, U.S. Army Command and General Staff College: Fort Leavenworth, Kansas, USA.

23. Bartelt-Hunt, S.L., D.R.U. Knappe, and M.A. Barlaz, *A Review of Chemical Warfare Agent Simulants for the Study of Environmental Behavior.* Crit. Rev. Environ. Sci. Technol., 2008. **38**(2): p. 112-136.

24. Paudyal, B.P., *Organophosphorus Poisoning.* Journal of Nepal Medical Association, 2008. **47**(4): p. 251-258.

25. Petroianu, G.A., *The Synthesis of Phosphor Ethers: Who Was Franz Anton Voegeli?* Die Pharmazie - An International Journal of Pharmaceutical Sciences, 2009. **64**(4): p. 269-275.

26. Lange, W. and G. v. Krueger, *Über Ester Der Monofluorphosphorsäure.* Berichte der deutschen chemischen Gesellschaft (A and B Series), 1932. **65**(9): p. 1598-1601.

27. Schrader, G., *Die Entwicklung Neuer Insektizider Phosphorsäure-Ester*. 1963: Verlag Chemie.

28. Rauterberg, E., *Schrader, G.: Die Entwicklung Neuer Insektizide Auf Grundlage Organischer Fluor-Und Phosphor-Verbindungen. Monographie Zu "Angewandte Chemie" Und "Chemie-Ingenieur-Technik". Verlag Chemie, G. M. B. H., Weinheim/Bergstraße, 1951, 62 Seiten. Dm 7.50.* Zeitschrift für Pflanzenernährung, Düngung, Bodenkunde, 1951. **54**(2): p. 178-178.

29. Unknown. *Alkylphosphate*. Lexikon der Neurowissenschaft [webpage] 2000 [cited 2016 227.05.2016]; Available from: http://www.spektrum.de/lexika/images/neuro/fff36.jpg.

30. Schrader, G., *Organische Phosphor-Verbindungen Als Neuartige Insektizide (Auszug).* Angewandte Chemie, 1950. **62**(20): p. 471-473.

31. Ghosh, R., *New Basic Esters of Phosphorus-Containing Acids*, T.P.O. London, Editor. 1952, Ghosh, Ranajit: GB738839 (A). p. 1-4.

32. Baldit, G.L., *Amiton - a New Acaricide and Scalicide.* Chemistry & Industry, 1958(4): p. 89-89.

33. Cadogan, J.I.G. and L.C. Thomas, *The Reactivity of Organophosphorus Compounds .3. The Decomposition of 2-Diethylaminoethyl Diethyl Phosphate and of S-2-Diethylaminoethyl Diethyl Phosphorothioate (Amiton).* Journal of the Chemical Society, 1960(MAY): p. 2248-2252.

34. Cadogan, J.I.G., *3. The Reactivity of Organophosphorus Compounds. Part Xi. High-Temperature Decomposition of S-2-Diethylaminoethyl Diethyl Phosphorothioate ("Amiton").* Journal of the Chemical Society (Resumed), 1962(0): p. 18-21.

35. Wegler, R., *Chemie Der Pflanzenschutz- Und Schädlingsbekämpfungsmittel*. 2012: Springer Berlin Heidelberg.

36. Tammelin, L.E., *Dialkoxy-Phosphorylthiocholines, Alkoxy-Methylphosphorylthiocholines and Analogous Choline Esters - Syntheses, Pka of Tertiary Homologues and Cholinesterase Inhibition.* Acta Chemica Scandinavica, 1957. **11**(8): p. 1340-1349.

37. Tucker, J.B., *War of Nerves: Chemical Warfare from World War I to Al-Qaeda*. 2006: Pantheon Books.

38. Harris, R. and J. Paxman, *A Higher Form of Killing: The Secret History of Chemical and Biological Warfare*. 2007: Random House Publishing Group. book.

39. Delfino, R.T., T.S. Ribeiro, and J.D. Figueroa-Villar, *Organophosphorus Compounds as Chemical Warfare Agents: A Review.* Journal of the Brazilian Chemical Society, 2009. **20**(3): p. 407-428.

40. Schrader, G., E. Schegk, and S. Hanshelmut, *Phosphonic Acid Esters*. 1961, Bayer AG: US3014943 (A).

41. Satoh, T. and R.C. Gupta, *Anticholinesterase Pesticides: Metabolism, Neurotoxicity, and Epidemiology*. 2011: Wiley.

42. Fest, C. and K.J. Schmidt, *The Chemistry of Organophosphorus Pesticides*. 2012: Springer Berlin Heidelberg.

43. Weil, S.V.L. and D. Edward, *A Review of Recent Progress in Phosphorus-Based Flame Retardants.* Journal of fire science, 2006. **24**: p. 345.

44. Wypych, G., *Handbook of Plasticizers*. 2004, Norwich, NY: ChemTec Publishing.

45. David, M.D. and J.N. Seiber, *Comparison of Extraction Techniques, Including Supercritical Fluid, High-Pressure Solvent, and Soxhlet, for Organophosphorus Hydraulic Fluids from Soil.* Analytical Chemistry, 1996. **68**(17): p. 3038-3044.

46. Engelhardt, F., et al., *Padding Auxiliaries and Processes for Dyeing Cellulose Fibers or Mixtures of Cellulose Fibers and Synthetic Fibers with Sulphur Dyestuffs, Sulphur Vat Dyestuffs, Vat Dyestuffs and Reactive Dyestuffs*. 1981: US 4300903.

47. Ghosh, A. and M. Bansal, *A Glossary of DNA Structures from a to Z.* Acta Crystallographica Section D, 2003. **59**(4): p. 620-626.

48. Dennison, G.H., M.R. Sambrook, and M.R. Johnston, *Vx and Vg Chemical Warfare Agents Bidentate Complexation with Lanthanide Ions.* Chem Commun (Camb), 2014. **50**(2): p. 195-197.

49. Sharma, R., et al., *Development and Structural Modifications of Cholinesterase Reactivators against Chemical Warfare Agents in Last Decade: A Review.* Mini-Reviews in Medicinal Chemistry, 2015. **15**(1): p. 58-72.

50. Sharma, S.P., et al., *Acetylcholinesterase Inhibition-Based Biosensor for Amperometric Detection of Sarin Using Single-Walled Carbon Nanotube-Modified Ferrule Graphite Electrode.* Sensors and Actuators B-Chemical, 2012. **166**: p. 616-623.

51. Wang, P.H., et al., *Synthesis and Evaluation of a New Phthalocyanine as Sensor Material for Sarin Detection.* Sensors and Actuators B-Chemical, 2013. **188**: p. 1306-1311.

52. Quagliano, J., Z. Witkiewicz, and S. Popiel. *Chemical Warfare Agents: Tlc Analysis*. 2010. CRC Press.

53. OPCW, *Convention on the Prohibition of the Development, Production, Stockpiling and Use of Chemical Weapons and on Their Destruction*. 1997: OPCW.

54. Sovalainen, K., *Regulatory Aspects of Anticholinesterase Pesticides*, in *Anticholinesterase Pesticides: Metabolism, Neurotoxicity, and Epidemiology*, T. Satoh and R.C. Gupta, Editors. 2010, John Wiley & Sons, Inc: Hoboken, New Jersey, USA. p. 569-580.

55. Metcalf, R.L. and R.B. March, *The Isomerization of Organic Thionophosphate Insecticides.* Journal of Economic Entomology, 1953. **46**(2): p. 288-294.

56. Emmett, W.G. and H.O. Jones, *Lxxviii.-Isomeric Monothiophosphates.* Journal of the Chemical Society, Transactions, 1911. **99**(0): p. 713-720.

57. Fukuto, T.R. and R.L. Metcalf, *Isomerization of Beta-Ethylmercaptoethyl Diethyl Thionophosphate (Systox).* Journal of the American Chemical Society, 1954. **76**(20): p. 5103-5106.

58. Fukuto, T.R. and E.M. Stafford, *The Isomerization of 0,0-Diethyl 0-2-Diethylaminoethyl Phosphorothionate.* Journal of the American Chemical Society, 1957. **79**(22): p. 6083-6085.

59. Tammelin, L.E., *Isomerisation of Omega-Dimethylaminoethyl-Diethyl-Thinophosphate.* Acta Chemica Scandinavica, 1957. **11**(10): p. 1738-1744.

60. Hilgetag, G. and G. Lehmann, *Beiträge Zur Chemie Der Thiophosphate. X. Über Den Mechanismus Der Isomerisierung Von Thionophosphaten.* Journal für Praktische Chemie, 1960. **12**(1-2): p. 6-10.

61. Yamada, Y., et al., *Palladium Catalyzed Thiono-Thiolo Allylic Rearrangement of O-Allyl Phosphorothionates and Phosphonothionates.* Tetrahedron Letters, 1979(52): p. 5015-5018.

62. Yamada, Y., et al., *Palladium(Ii) Catalyzed Thiono-Thiolo Rearrangement of Propargyl Thionophosphates.* Tetrahedron Letters, 1984. **25**(33): p. 3599-3602.

63. Stec, W.J., et al., *Protic Acid-Catalyzed Thiono-Thiolo Rearrangements of Phosphorus Esters.* Journal of Organic Chemistry, 1976. **41**(7): p. 1291-1293.

64. Kuntsivich, A.D., et al., *Thion-Thiol Izomerization Mechanism Investigation of Thion-Derivatives of Phosphoric Acids.* Doklady Akademii Nauk, 1996. **346**(3): p. 350-352.

65. Schaumann, E., *Sulfur-Mediated Rearrangements Ii*. 2007: Springer.

66. Schaumann, E. and S. Akai, *Sulfur-Mediated Rearrangements I*. 2007: Springer.

67. Reimschussel, W. and J. Adamus, *Mechanism of Thiono-Thiolo Isomerization of Thiophosphates - Kinetic Evidence for Hilgetag Hypothesis.* Phosphorus Sulfur and Silicon and the Related Elements, 1990. **49**(1-4): p. 77-80.

68. Bruzik, K. and W.J. Stec, *Thiono-Thiolo Rearrangement and Solvolysis of the Secondary Alkyl Phosphorothionates .3.* Journal of Organic Chemistry, 1981. **46**(8): p. 1618-1624.

69. Poulter, C.D. and D.S. Mautz, *Solvolysis of Allylic Isoprene Phosphorothioate Esters - a Mechanistic Study of the Thiono- Thiolo Rearrangement.* Journal of the American Chemical Society, 1991. **113**(13): p. 4895-4903.

70. Henglein, A., G. Schrader, and R. Muhlmann, *Quantitative Infrarotspektroskopische Bestimmung Des Isomerenverhaltnisses in Dem System-Insecticid Systox.* Fresenius Zeitschrift Fur Analytische Chemie, 1954. **141**(4): p. 276-281.

71. Henglein, A. and G. Schrader, *Zur Kenntnis Der Isomerie-Erscheinungen Bei Den System-Insektiziden Systox Und Metasystox.* Zeitschrift Fur Naturforschung Part B-Chemie Biochemie Biophysik Biologie Und Verwandten Gebiete, 1955. **10**(1): p. 12-19.

72. Muller, N. and J. Goldenson, *Rapid Analysis of Reaction Mixtures by Nuclear Magnetic Resonance Spectroscopy.* Journal of the American Chemical Society, 1956. **78**(20): p. 5182-5183.

73. Atkins, P.W. and J. De Paula, *Physikalische Chemie*. 2013: Wiley-VCH.

74. Connors, K.A., *Chemical Kinetics: The Study of Reaction Rates in Solution*. 1990: VCH.

75. Wedler, G. and H.J. Freund, *Lehrbuch Der Physikalischen Chemie*. 2014.

76. Timperley, C., *Best Synthetic Methods: Organophosphorus (V) Chemistry*. 2014: Elsevier Science.

77. Hartley, F.R., *The Chemistry of Organophosphorus Compounds, Ter- and Quinque-Valent Phosphorus Acids and Their Derivatives*. 1996: Wiley.

78. Edmundson, R., *Dictionary of Organophosphorus Compounds*. 1987: Taylor & Francis.

79. Patnaik, P., *Handbook of Inorganic Chemicals*. 2003: McGraw-Hill.

80. Gupalo, A.P., M.I. Khmilevskaya, and N.E. Tsepukh, *Thiophosphoric Acid Amino Esters .6. Reaction of Monoethanolamine with Thiophosphoric Acid-Chlorides.* Zhurnal Obshchei Khimii, 1979. **49**(1): p. 93-97.

81. Kashima, C., K. Harada, and Y. Omote, *The Influence of a Base on the Methylation of Aminoalcohols.* Canadian Journal of Chemistry-Revue Canadienne De Chimie, 1985. **63**(2): p. 288-290.

82. Ledgard, J.B., *The Laboratory History of Chemical Warfare Agents*. 2006: Paranoid Publications Group.

83. Ledgard, J., *The Preparatory Manual of Chemical Warfare Agents Third Edition*. 2012: Jared Ledgard.

84. Fester, U., D.B. Parker, and R. Bosworth, *Silent Death*. 1997: Festering Publications. book.

85. Stýskala, J., et al., *Synthesis of Some Deuterated Dialkylaminoethyls as Possible Standards for the Mass Spectrometric Monitoring of Chemical Warfare Agents.* Journal of Labelled Compounds and Radiopharmaceuticals, 2008. **51**(1): p. 19-22.

86. Andersen, K.E., et al., *Synthesis of Novel Gaba Uptake Inhibitors. 4. Bioisosteric Transformation and Successive Optimization of Known Gaba Uptake Inhibitors Leading to a Series of Potent Anticonvulsant Drug Candidates.* Journal of Medicinal Chemistry, 1999. **42**(21): p. 4281-4291.

87. Dupre, D.J., et al., *113. Analgesics. Part I. Esters and Ketones Derived from [Small Alpha]-Amino-[Small Omega]-Cyano-[Small Omega][Small Omega]Diarylalkanes.* Journal of the Chemical Society (Resumed), 1949(0): p. 500-510.

88. Melder, J.P., et al., *Preparation of a Pure Dialkylaminoethanol Stable against Discoloration*. 1997: US5663444.

89. Jakub Stýskala, P.C., Miroslav Soural, Petr Bednář, and Karel Lemr, *Preparation and Characterization of Some Unsymmetrical 2- Dialkylamino)Ethanethiols.* ARKIVOC, 2007. **2007**(15): p. 171-180.

90. Wang, Y.H., et al., *Reductive Hydroxyalkylation/Alkylation of Amines with Lactones/Esters.* Organic & Biomolecular Chemistry, 2012. **10**(32): p. 6504-6511.

91. Tokuyasu, J.K.C.L., et al., *Method for Manufacturing Aminoalcohol*. 2008: EP1074541B1.

92. Blackburn, D. and G. Burghard, *Synthesis of Diethylaminoethanol-1-14c.* Journal of Labelled Compounds, 1965. **1**(3): p. 226-228.

93. Yin, H., et al., *Solvent-Free Copper-Catalyzed N-Arylation of Amino Alcohols and Diamines with Aryl Halides.* Tetrahedron Letters, 2012. **53**(10): p. 1265-1270.

94. RYOJI, N., et al., *Method of Producing Tertiary Amine or Tertiary Amine Derivative*. 2015, NAGOYA UNIV: JP2013213167A.

95. Scriabine, M.I., *Procédé De Préparation De L'amino-5-Pentanol-1 Et De Ses Dérivés N. Substitués*. 1941, Societe des usines chimiques de Rhone-Poulenc: FR898936A. p. 2.

96. van der Waals, D., et al., *Ruthenium-Catalyzed Methylation of Amines with Paraformaldehyde in Water under Mild Conditions.* ChemSusChem, 2016. **9**(17): p. 2343-2347.

97. Limited, C., *Novel Basic Esters, Their Acid Salts and Quaternary Salts*. 1954, Cilag Limited: GB 781382A.

98. Martin, H. and E. Habicht, *Verfahren Zur Herstellung Von Spasmolytisch Wirksamen Basischen Estern, Ihren Saeureadditionssalzen Und Quartaeren Salzen*. 1959, Cilag AG: DE 1055546B.

99. H., D.W., *Verfahren Zur Herstellung Von N-Ethyl-Diisopropylamin*. 2015: WO20151244442A1.

100. Olin, J.F., *Manufacture of 5-Amino-1-Pentanol and Alkyl Derivatives Thereof*. 1950: US2516337A.

101. Carius, L., *5. Ueber Den Phosphorsäuren Sich Anschliessende Gruppen Neuer Organischer Körper.* Justus Liebigs Annalen der Chemie, 1861. **119**(3): p. 289-302.

102. Fletcher, J.H., et al., *The Synthesis of Parathion and Some Closely Related Compounds.* Journal of the American Chemical Society, 1950. **72**(6): p. 2461-2464.

103. Mastin, T.W., G.R. Norman, and E.A. Weilmuenster, *Chemistry of the Aliphatic Esters of Thiophosphoric Acids. I.* Journal of the American Chemical Society, 1945. **67**(10): p. 1662-1664.

104. Mastin, T., G. Norman, and E. Weilmuenster, *Chemistry of the Aliphatic Esters of Thiophosphoric Acids I. - Correction.* Journal of the American Chemical Society, 1953. **75**(24): p. 6357-6357.

105. Regel, E., *Dithiophosphorus Compounds*. 1966, Chemagro Corp. . US3294876A. p. 4 pp. Division of US 3193372.

106. Regel, E.K. and M.F. Botts, *S-(Carbethoxymethyl) S,S-Dialkyl Trithiophosphates as Soil Fungicides*. 1970, Chemagro Corp. . US35027771A. p. 3 pp.

107. Lippman, A.E., *O,S-Dialkyl Phosphorothioates.* The Journal of Organic Chemistry, 1965. **30**(9): p. 3217-3218.

108. Ghosh, R., *New Pesticidal Ester Salts of Phosphorothiolothionic Acid*, T.P.O. London, Editor. 1955: GB971588(A). p. 5.

109. Markowitz, M., *A Convenient Method for Preparation of Quaternary Ammonium Salts.* The Journal of Organic Chemistry, 1957. **22**(8): p. 983-984.

110. Hofmann, T., *Synthese Und Bakteriologische Untersuchung Einiger Quarternärer Ammoniumsalze*. 1951, ETH Zürich. p. 79.

111. Fitch, H.M., *Quaternary Ammonium Salts of Dialkylaminoalkyl Thiophosphate Esters*. 1959, Campbell Pharmaceuticals, Inc. . GB819735A.

112. Fitch, H.M., *Quaternary Salts of Dialkyl Thiophosphate Esters*. 1959, Campbell Pharmaceuticals, Inc. . US 2911430.

113. Sommer, H.Z. and L.L. Jackson, *Alkylation of Amines - a New Method for the Synthesis of Quaternary Ammonium Compounds from Primary and Secondary Amines*. 1969, DEPARTMENT OF THE ARMY EDGEWOOD ARSENAL: USA.

114. Gabelt, B.A.T., et al., *H-7 Effect on Outflow Facility after Trabecular Obstruction Following Long-Term Echothiophate Treatment in Monkeys.* Investigative Ophthalmology & Visual Science, 2004. **45**(8): p. 2732-2736.

115. Schwetlick, K., *Organikum*. 2015: Wiley VCH Verlag GmbH.

116. Vollhardt, K.P.C., H. Butenschön, and N.E. Schore, *Organische Chemie*. 2011: VCH [Imprint].

117. Ahluwalia, V.K., *Laboratory Techniques in Organic Chemistry*. 2010: I.K. International Publishing House Pvt. Limited.

118. Clayden, J., N. Greeves, and S. Warren, *Organic Chemistry*. 2012: OUP Oxford.

119. Bracha, P., *Interaction of an Amiton Analog with True Cholinesterase.* Israel Journal of Chemistry, 1967. **5**(3): p. 121-&.

120. Cohen, J.E., et al., *Genomic Implications of Anticholinesterase Sensitivities*, in *Anticholinesterase Pesticides: Metabolism, Neurotoxicity, and Epidemiology*, T. Satoh

and R.C. Gupta, Editors. 2010, John Wiley &Sons, Inc.: Hoboken, New Jersey, USA. p. 19-24.

121. Dale, H.H. and O. Loewi. *The Nobel Prize in Physiology or Medicine 1936*. 1936 [cited 2016 04/04/2016]; Available from: http://www.nobelprize.org/nobel_prizes/medicine/laureates/1936/.

122. Barak, D., et al., *Allosteric Modulation of Acetylcholinesterase Activity by Peripheral Ligands Involves a Conformational Transition of the Anionic Subsite.* Biochemistry, 1995. **34**(47): p. 15444-15452.

123. Hart, G.J. and R.D. Obrien, *Recording Spectrophotometric Method for Determination of Dissociation and Phosphorylation Constants for Inhibition of Acetylcholinesterase by Organophosphates in Presence of Substrate.* Biochemistry, 1973. **12**(15): p. 2940-2945.

124. Fukuto, T.R., *Mechanism of Action of Organophosphorus and Carbamate Insecticides.* Environmental Health Perspectives, 1990. **87**: p. 245-254.

125. Aldridge, W.N., *Some Properties of Specific Cholinesterase with Particular Reference to the Mechanism of Inhibition by Diethyl P-Nitrophenyl Thiophosphate (E 605) and Analogues.* Biochemical Journal, 1950. **46**(4): p. 451.

126. Main, A.R., *Affinity and Phosphorylation Constants for the Inhibition of Esterases by Organophosphates.* Science, 1964. **144**(3621): p. 992.

127. Chauhan, S., et al., *Chemical Warfare Agents.* Environmental Toxicology and Pharmacology, 2008. **26**(2): p. 113-122.

128. Doctor, B.P., et al., *Enzymes as Pretreatment Drugs for Organophosphate Toxicity*. Neuroscience & Biobehavioral Reviews, 1991. **15**(1): p. 123-128.

129. Romano, J.A., et al., *Chemical Warfare Agents: Chemistry, Pharmacology, Toxicology, and Therapeutics, Second Edition*. 2007: CRC Press.

130. Kropp, T.J. and R.J. Richardson, *Aging of Mipafox-Inhibited Human Acetylcholinesterase Proceeds by Displacement of Both Isopropylamine Groups to Yield a Phosphate Adduct.* Chemical Research in Toxicology, 2006. **19**(2): p. 334-339.

131. Quin, L.D., *A Guide to Organophosphorus Chemistry*. 2000: Wiley.

132. Toy, A.D.F., *Phosphorus Chemistry in Everyday Living*. 1976: American Chemical Society.

133. Kuzamyshev, V.M., et al., *Inhibition of Cholinesterases by S-[B-Aryl(Benzyl)Thio]Ethyl Esters of Thiophosphorous Acids.* Izv. Akad. Nauk SSSR, Ser. Khim., 1986(3): p. 648-652.

134. Etō, M., *Organophosphorus Pesticides: Organic and Biological Chemistry*. 1975: CRC Press.

135. Schrader, G., W. Lorenz, and R. Muhlmann, *Tetraalkyl-Monothiopyrophosphates - Their Preparation and Properites.* Angewandte Chemie-International Edition, 1958. **70**(22-3): p. 690-694.

136. Čolović, M.B., et al., *Acetylcholinesterase Inhibitors: Pharmacology and Toxicology*. Current Neuropharmacology, 2013. **11**(3): p. 315-335.

137. Chiriac, A., Z. Simon, and R. Vilceanu, *Structure-Biological Activity Correlations in Phosphororganic Compounds - Role of Electric Charge and Other Parameters for Acetylcholinesterase Inhibition.* Studia Biophysica, 1975. **51**(3): p. 183-192.

138. Bartling, A., et al., *Enzyme-Kinetic Investigation of Different Sarin Analogues Reacting with Human Acetylcholinesterase and Butyrylcholinesterase.* Toxicology, 2007. **233**(1-3): p. 166-172.

139. Nishizawa, Y., *New Low Toxic Organophosphorus Insecticides.* Bulletin of the Agricultural Chemical Society of Japan, 1960. **24**(7): p. 744-745.

140. Schrader, G., *Zur Kenntnis Neuer, Wenig Toxischer Insektizide Auf Der Basis Von Phosphorsaureestern.* Angewandte Chemie-International Edition, 1961. **73**(10): p. 331-&.

141. Gao, X.-h., et al., *Tertiary Amine Derivatives of Chlorochalcone as Acetylcholinesterase (Ache) and Buthylcholinesterase (Buche) Inhibitors: The Influence of Chlorine, Alkyl Amine Side Chain and A,B-Unsaturated Ketone Group.* Journal of Enzyme Inhibition and Medicinal Chemistry, 2016: p. 1-7.

142. Aharoni, A.H. and R.D. O'Brien, *Inhibition of Acetylcholinesterases by Anionic Organophosphorus Compounds.* Biochemistry, 1968. **7**(4): p. 1538-1545.

143. Schrader, G., *Chlorthion - Ein Neues, Wenig Giftiges Insektizid Aus Der Reihe Der Thiophosphorsaureester.* Angewandte Chemie, 1954. **66**(10): p. 265-267.

144. Ellman, G.L., et al., *A New and Rapid Colorimetric Determination of Acetylcholinesterase Activity.* Biochemical Pharmacology, 1961. **7**(2): p. 88-&.

145. Worek, F., P. Eyer, and H. Thiermann, *Determination of Acetylcholinesterase Activity by the Ellman Assay: A Versatile Tool for in Vitro Research on Medical Countermeasures against Organophosphate Poisoning.* Drug Testing and Analysis, 2012. **4**(3-4): p. 282-291.

146. Forsberg, A. and G. Puu, *Kinetics for the Inhibition of Acetylcholinesterase from the Electric-Eel by Some Organophosphates and Carbamates.* European Journal of Biochemistry, 1984. **140**(1): p. 153-156.

147. Gray, P.J. and R.M. Dawson, *Kinetic Constants for the Inhibition of Eel and Rabbit Brain Acetylcholinesterase by Some Organophosphates and Carbamates of Military Significance.* Toxicology and Applied Pharmacology, 1987. **91**(1): p. 140-144.

148. Worek, F., et al., *Recent Advances in Evaluation of Oxime Efficacy in Nerve Agent Poisoning by in Vitro Analysis.* Toxicology and Applied Pharmacology, 2007. **219**(2-3): p. 226-234.

149. Ozmen, M., et al., *In Vitro and in Vivo Acetylcholinesterase-Inhibiting Effect of New Classes of Organophosphorus Compounds.* Environmental Toxicology and Chemistry, 1999. **18**(2): p. 241-246.

150. O'Brien, R.D. and R.D. Hilton, *The Relation between Basicity and Selectivity in Organophosphates.* J. Agric. Food Chem., 1964. **12**(1): p. 53-55.

151. Komers, K., A. Cegan, and M. Link, *Kinetics and Mechanism of Hydrolysis of Acetylthiocholine by Butyrylcholine Esterase.* Zeitschrift Fur Naturforschung C-a Journal of Biosciences, 2002. **57**(11-12): p. 1072-1077.

152. Ma, T., et al., *A Quantitative Histochemistry Technique for Measuring Regional Distribution of Acetylcholinesterase in the Brain Using Digital Scanning Densitometry*. Analytical Biochemistry, 2001. **296**(1): p. 18-28.

153. Worek, F., et al., *Kinetic Analysis of Interactions between Human Acetylcholinesterase, Structurally Different Organophosphorus Compounds and Oximes.* Biochemical Pharmacology, 2004. **68**(11): p. 2237-2248.

154. Williams, A.M. and A. Alcaraz. *Sampling and Analysis Methods for the Forensic Determination of Chemical Warfare Agents and Their Associated Chemical Attribution Signatures in Food Matrices*. 2011. American Chemical Society.

155. Vu, A.K., H. Mulcahy, and A.M. Williams. *Analysis of Chemical Warfare Agents and Their Chemical Attribution Signatures in Complex Food and Environmental Matrices*. 2013. American Chemical Society.

156. Giannoukos, S., et al., *Chemical Sniffing Instrumentation for Security Applications.* Chemical Reviews, 2016. **116**(14): p. 8146-8172.

157. Gałuszka, A., Z.M. Migaszewski, and J. Namieśnik, *Moving Your Laboratories to the Field – Advantages and Limitations of the Use of Field Portable Instruments in Environmental Sample Analysis.* Environmental Research, 2015. **140**: p. 593-603.

158. Bowerbank, C.R., et al., *Rapid Field Detection of Chemical Warfare Agents, Simulants, by-Products, and Precursors Using Solid Phase Microextraction and Portable Gc-Tms.* LCGC North Am., 2009(Suppl.): p. 61.

159. Saeidian, H., et al., *Mass Spectrometric Study on O(S)-Alkyl N,N-Dimethylamino Alkylphosphonates (Alkylphosphonothiolates) for Chemical Weapons Convention Verification Purposes.* International Journal of Mass Spectrometry, 2012. **319–320**: p. 9-16.

160. Saeidian, H., et al., *Unambiguous Mass Spectral Characterization of Vx and Its Six Other Structural Isomers Using Gas Chromatography–Mass Spectrometry.* International Journal of Mass Spectrometry, 2016. **396**: p. 5-12.

161. Popiel, S. and M. Sankowska, *Determination of Chemical Warfare Agents and Related Compounds in Environmental Samples by Solid-Phase Microextraction with Gas Chromatography.* Journal of Chromatography A, 2011. **1218**(47): p. 8457-8479.

162. Tsuge, K. and Y. Seto, *Mass Spectrometric Identification of Chemical Warfare Agent Adducts with Biological Macromolecule for Verification of Their Exposure.* J. Health Sci., 2009. **55**(6): p. 879-886.

163. John, H., et al., *Optimized Verification Method for Detection of an Albumin-Sulfur Mustard Adduct at Cys(34) Using a Hybrid Quadrupole Time-of-Flight Tandem Mass Spectrometer after Direct Plasma Proteolysis.* Toxicol Lett, 2016. **244**: p. 103-111.

164. Stephenson, R.M., S. Malanowski, and D. Ambrose, *Handbook of the Thermodynamics of Organic Compounds*. 1987: Elsevier.

165. Birdi, K.S., D.T. Vu, and A. Winter, *A Study of the Evaporation Rates of Small Water Drops Placed on a Solid Surface.* The Journal of Physical Chemistry, 1989. **93**(9): p. 3702-3703.

166. Charlesworth, D.H. and W.R. Marshall, *Evaporation from Drops Containing Dissolved Solids.* AIChE Journal, 1960. **6**(1): p. 9-23.

167. Melnikov, N.N., *Residue Reviews : Residues of Pesticides and Other Foreign Chemicals in Foods and Feeds. 40.1971. With Cumulative Table of Subjects Covered, Detailed Subject-Matter Index, and Author Index of Volumes 31 - 40*, ed. F.E. Gunther and J.D. Gunther. 1971, Berlin: Springer.

168. Emel'yanenko, V.N. and S.P. Verevkin, *Benchmark Thermodynamic Properties of 1,3-Propanediol: Comprehensive Experimental and Theoretical Study.* The Journal of Chemical Thermodynamics, 2015. **85**: p. 111-119.

169. Verevkin, S.P., et al., *Thermochemistry of Halogen-Substituted Methylbenzenes.* Journal of Chemical & Engineering Data, 2015. **60**(1): p. 89-103.

170. Verevkin, S.P., *2 Phase Changes in Purecomponent Systems: Liquids and Gases*, in *Experimental Thermodynamics*, R.D. Weir and T.W.D. Loos, Editors. 2005, Elsevier. p. 5-30.

171. Rimpel, L.Y., et al., *Chemical Defense Equipment*, in *Medical Aspects of Chemical and Bioligical Warfare*, R. Brigadier General Zajtchuk, MC, U.S. Army and F.R. Colonel Bellamy, M.D., MC U.S. Army, Editors. 2008.

172. Pacsial-Ong, E.J. and Z.P. Aguilar, *Chemical Warfare Agent Detection: A Review of Current Trends and Future Perspectives.* Frontiers in Bioscience, Scholar, 2013. **5**: p. 516-543.

173. Thoraval, D., et al., *Development of Paper, Chemical Agent Detector, 3-Way Liquid Containing Non-Mutagenig Dyes. I-Replacement of the Yellow Dye Thiodiphenyl-4,4-Diazo-Bis-Salicylic Acid (A2)*, D.R. Establishment, Editor. 1988: Ottawa.

174. Labor, U.S.D.o. *Otm Section Ii Chapter 3 - Onsite Measurements*. OSHA Technical Manual (OTM) 2016 [cited 2016 2016-05-16]; Available from: https://www.osha.gov/dts/osta/otm/otm_ii/pdfs/otmii_chpt3_appb.pdf.

175. Dräger, *Dräger-Tubes & Cms Handbook; Soil, Water and Air Investigations as Well as Technical Gas Analysis*. 16 ed. 2011, Lübeck: Dräger Safety AG & Co. KGaA.

176. Harris, D.C., G. Werner, and T. Werner, *Lehrbuch Der Quantitativen Analyse*. 2014: Springer Berlin Heidelberg.

177. Longworth, T.L., J.M. Baranoski, and h.w.e.a.m. Edgewood Chemical Biological Center, *Domestic Preparedness Program: Evaluation of the Raid-M (Bruker Saxonia Analytik Gmbh Rapid Alarm and Identification Device - Monitor) against Chemical Warfare Agents: Summary Report*, R. Directorate and Technology, Editors. 2003, Edgewood Chemical Biological Center.

178. Vautz, W., et al., *Ion Characterisation by Comparison of Ion Mobility Spectrometry and Mass Spectrometry Data.* International Journal for Ion Mobility Spectrometry, 2010. **13**(3): p. 121-129.

179. Price, S.E., *Ion Mobility and Mass Spectrometric Investigations of Organophosphates Related to Chemical Warfare Agents and Pesticides*, in *School of Physics and Astronomy*. 2010, The University of Birmingham: Birmingham. p. 116.

180. Hill, H.H., W.F. Siems, and R.H. St. Louis, *Ion Mobility Spectrometry.* Analytical Chemistry, 1990. **62**(23): p. 1201A-1209A.

181. Eiceman, G.A., Z. Karpas, and H.H. Hill Jr, *Ion Mobility Spectrometry*. 2013: CRC press.

182. Borsdorf, H. and G.A. Eiceman, *Ion Mobility Spectrometry: Principles and Applications.* Applied Spectroscopy Reviews, 2006. **41**(4): p. 323-375.

183. Kanu, A.B., et al., *Ion Mobility–Mass Spectrometry.* Journal of Mass Spectrometry, 2008. **43**(1): p. 1-22.

184. McDaniel, W., *Collision Phenomena in Ionized Gases*. 1964: Wiley.

185. McDaniel, W. and E.A. Mason, *The Mobility and Diffusion of Ions in Gases*. 1973: Wiley.

186. Keller, T., *Ionenmobilitätsspektrometrie: Etablierung Einer Neuen Analysentechnik in Der Forensischen Toxikologie an Der Gerichtsmedizin Der Universität Salzburg*. 2005: wvb, Wiss. Verlag.

187. US Department of Commerce, N. *Primary Radioactivity Standardization of Ni-63*. 2015 2015-08-12; Available from: http://www.nist.gov/pml/div682/grp04/ni63.cfm.

188. Proengin, *Operating Instructions Uc Ap4c, M910 E00 003*, Proengin, Editor. 2016, Proengin: Paris.

189. Gross, J.H. and P. Roepstorff, *Mass Spectrometry: A Textbook*. 2011: Springer Berlin Heidelberg.

190. Lee, M.S., *Mass Spectrometry Handbook*. 2012: Wiley.

191. Hübschmann, H.J., *Handbook of Gc/Ms: Fundamentals and Applications*. 2009: Wiley.

192. Kováts, E., *Gas-Chromatographische Charakterisierung Organischer Verbindungen. Teil 1: Retentionsindices Aliphatischer Halogenide, Alkohole, Aldehyde Und Ketone.* Helvetica Chimica Acta, 1958. **41**(7): p. 1915-1932.

193. Lee, M.L., D.L. Vassilaros, and C.M. White, *Retention Indices for Programmed-Temperature Capillary-Column Gas Chromatography of Polycyclic Aromatic Hydrocarbons.* Analytical Chemistry, 1979. **51**(6): p. 768-773.

194. Holleman, A.F., E. Wiberg, and N. Wiberg, *Lehrbuch Der Anorganischen Chemie*. 2007: Walter de Gruyter.

195. Otto, M., *Analytische Chemie*. 2011: Wiley-VCH.

196. Dempster, A.J., *A New Method of Positive Ray Analysis.* Physical Review, 1918. **11**(4): p. 316-325.

197. Budzikiewicz, H., C. Djerassi, and D.H. Williams, *Mass Spectrometry of Organic Compounds*. 1964: Holden-Day.

198. Munson, M.S.B. and F.H. Field, *Chemical Ionization Mass Spectrometry. I. General Introduction.* Journal of the American Chemical Society, 1966. **88**(12): p. 2621-2630.

199. Böcker, J., *Spektroskopie: Instrumentelle Analytik Mit Atom- Und Molekülspektrometrie*. 1997: Vogel.

200. de Hoffmann, E., *Tandem Mass Spectrometry: A Primer.* Journal of Mass Spectrometry, 1996. **31**(2): p. 129-137.

201. Bell, A.J., et al., *Fragmentation and Reactions of Organophosphate Ions Produced by Electrospray Ionization.* International Journal of Mass Spectrometry and Ion Processes, 1997. **165–166**: p. 533-550.

202. Bell, A.J., et al., *Fragmentation and Reactions of Two Isomeric O-Alkyl S-(2-Dialkylamino)Ethyl Methylphosphonothiolates Studied by Electrospray Ionization/Ion Trap Mass Spectrometry.* Journal of the American Society for Mass Spectrometry, 2001. **12**(8): p. 902-910.

203. Housman, K.J., A.T. Swift, and J.M. Oyler, *Fragmentation Pathways and Structural Characterization of 14 Nerve Agent Compounds by Electrospray Ionization Tandem Mass Spectrometry.* Journal of Analytical Toxicology, 2014.

204. Barr, J.D., et al., *Fragmentations and Reactions of Some Isotopically Labelled Dimethyl Methyl Phosphono and Trimethyl Phosphoro Thiolates and Thionates Studied by Electrospray Ionisation Ion Trap Mass Spectrometry.* International Journal of Mass Spectrometry, 2005. **244**(1): p. 29-40.

205. Weissberg, A., N. Tzanani, and S. Dagan, *Specificity Enhancement by Electrospray Ionization Multistage Mass Spectrometry – a Valuable Tool for Differentiation and Identification of 'V'-Type Chemical Warfare Agents.* Journal of Mass Spectrometry, 2013. **48**(12): p. 1340-1348.

206. Ellis-Steinborner, S., A. Ramachandran, and S.J. Blanksby, *The Fragmentation Pathways of Protonated Amiton in the Gas Phase: Towards the Structural Characterisation of Organophosphorus Chemical Warfare Agents by Electrospray Ionisation Tandem Mass Spectrometry.* Rapid Communications in Mass Spectrometry, 2006. **20**(12): p. 1939-1948.

207. Barr, J.D., et al., *Fragmentations and Reactions of the Organophosphate Insecticide Diazinon and Its Oxygen Analog Diazoxon Studied by Electrospray Ionization Ion Trap Mass Spectrometry.* Journal of the American Society for Mass Spectrometry, 2005. **16**(4): p. 515-523.

208. Rohrbaugh, D.K., *Mass Spectral Fragmentation of Vx*, U.S.A.R.D. Ecbc and C. Engineering, Editors. 2008, US Army: Aberdeen Proving Ground, MD. p. 31.

209. Granoth, I., *Topics in Phosphorus Chemistry*, M. Grayson and E.J. Griffith, Editors. 1976, Interscience Publishers. p. 41-98.

210. Rouessac, F. and A. Rouessac, *Chemical Analysis: Modern Instrumentation Methods and Techniques*. 2013: Wiley.

211. Budzikiewicz, H. and M. Schäfer, *Massenspektrometrie*. 2011: Wiley.

212. Karaghiosoff, K., *Phosphorus-31 Nmr*, in *Emagres*. 2007, John Wiley & Sons, Ltd.

213. Halmann, M.M., *Analytical Chemistry of Phosphorus Compounds*. 1972: Wiley-Interscience.

214. Borrett, V.T., et al., *Gas Chromatographic Mass Spectrometric Characterisation of Amiton and the Recovery of Amiton from Concrete, Paint, Rubber and Soil Matrices.* Journal of Chromatography A, 2003. **1003**(1-2): p. 143-155.

215. Metcalf, R.L., et al., *The Systemic Behavior of O,O-Diethyl S-2-(Diethylamino)Ethyl Phosphorothiolate and Its Salts.* Journal of Economic Entomology, 1957. **50**(2): p. 205-210.

216. Friedrich, H.D. and K.D. Egon, *O,O-Dialkyl Thiophosphoric Acid Salts Intermeds for - Insecticides*. 1970: DE 1805159A1.

217. Danner, A., *Thiophosphorsäureester*, in *Fakultöt für Chemie und Pharmazie*. 2014, Ludwig-Maximillians Universität: Munich.

218. Pawliszyn, J., *Handbook of Solid Phase Microextraction*. 2011: Elsevier.

219. Pawliszyn, J.B., *Method and Device for Solid Phase Microextraction and Desorption*. 1997: US5691206.

220. Pragney, D. and U.V.R. Vijaya Saradhi, *Sample-Preparation Techniques for the Analysis of Chemical-Warfare Agents and Related Degradation Products.* TrAC Trends in Analytical Chemistry, 2012. **37**: p. 73-82.

221. Spietelun, A., et al., *Current Trends in Solid-Phase Microextraction (Spme) Fibre Coatings.* Chemical Society Reviews, 2010. **39**(11): p. 4524-4537.

222. Lord, H.L., et al., *In Vivo Solid-Phase Microextraction for Monitoring Intravenous Concentrations of Drugs and Metabolites.* Nat Protoc, 2011. **6**(6): p. 896-924.

223. Bojko, B. and J. Pawliszyn, *In Vivo and Ex Vivo Spme: A Low Invasive Sampling and Sample Preparation Tool in Clinical Bioanalysis.* Bioanalysis, 2014. **6**(9): p. 1227-1239.

224. Risticevic, S., et al., *Protocol for Solid-Phase Microextraction Method Development.* Nature Protocols, 2010. **5**(1): p. 122-139.

225. Risticevic, S., et al., *Protocol for the Development of Automated High-Throughput Spme-Gc Methods for the Analysis of Volatile and Semivolatile Constituents in Wine Samples.* Nature Protocols, 2010. **5**(1): p. 162-176.

226. Bartelt, R.J., *Calibration of a Commercial Solid-Phase Microextraction Device for Measuring Headspace Concentrations of Organic Volatiles.* Analytical Chemistry, 1997. **69**(3): p. 364-372.

227. Ouyang, G., et al., *Standard-Free Kinetic Calibration for Rapid on-Site Analysis by Solid-Phase Microextraction.* Journal of Separation Science, 2008. **31**(6-7): p. 1167-1172.

228. Ouyang, G. and J. Pawliszyn, *A Critical Review in Calibration Methods for Solid-Phase Microextraction.* Analytica Chimica Acta, 2008. **627**(2): p. 184-197.

229. Doong, R.A. and S.M. Chang, *Determination of Distribution Coefficients of Priority Polycyclic Aromatic Hydrocarbons Using Solid-Phase Microextraction.* Analytical Chemistry, 2000. **72**(15): p. 3647-3652.

230. Liu, X., et al., *Elimination of Matrix Effects in the Determination of Bisphenol a in Milk by Solid-Phase Microextraction–High-Performance Liquid Chromatography.* Food Additives & Contaminants: Part A, 2008. **25**(6): p. 772-778.

231. Souza-Silva, É.A. and J. Pawliszyn, *Direct Immersion Solid-Phase Microextraction with Matrix-Compatible Fiber Coating for Multiresidue Pesticide Analysis of Grapes by Gas Chromatography–Time-of-Flight Mass Spectrometry (Di-Spme-Gc-Tofms).* Journal of Agricultural and Food Chemistry, 2015. **63**(18): p. 4464-4477.

232. Vanninen, P., *Recommended Operating Procedures for Analysis in the Verification of Chemical Disarmament, 2011 Edition*, ed. P. Vanninen. 2011, Helsinki, Finland: University of Helsinki.

233. Lakso, H.A. and W.F. Ng, *Determination of Chemical Warfare Agents in Natural Water Samples by Solid-Phase Microextraction.* Analytical Chemistry, 1997. **69**(10): p. 1866-1872.

234. Hook, G.L., et al., *Detection of Vx Contamination in Soil through Solid-Phase Microextraction Sampling and Gas Chromatography/Mass Spectrometry of the Vx Degradation Product Bis(Diisopropylaminoethyl)Disulfide.* Journal of Chromatography A, 2003. **992**(1-2): p. 1-9.

235. Harvey, S.D., et al., *Selective Stationary Phase for Solid-Phase Microextraction Analysis of Sarin (Gb).* Journal of Chromatography A, 2002. **954**(1-2): p. 217-225.

236. Zygmunt, B., et al., *Solid Phase Microextraction Combined with Gas Chromatography - a Powerful Tool for the Determination of Chemical Warfare Agents and Related Compounds.* Curr. Org. Chem., 2007. **11**(3): p. 241-253.

237. Rearden, P. and P.B. Harrington, *Rapid Screening of Precursor and Degradation Products of Chemical Warfare Agents in Soil by Solid-Phase Microextraction Ion Mobility Spectrometry (Spme–Ims).* Analytica Chimica Acta, 2005. **545**(1): p. 13-20.

238. Zygmunt, B., A. Jastrzecbska, and J. Namiesnik, *Solid Phase Microextraction — a Convenient Tool for the Determination of Organic Pollutants in Environmental Matrices.* Critical Reviews in Analytical Chemistry, 2001. **31**(1): p. 1-18.

239. Zhang, Z.Y., J. Poerschmann, and J. Pawliszyn, *Direct Solid Phase Microextraction of Complex Aqueous Samples with Hollow Fibre Membrane Protection.* Analytical Communications, 1996. **33**(7): p. 219-221.

240. Silva, E.A.S. and J. Pawliszyn, *Optimization of Fiber Coating Structure Enables Direct Immersion Solid Phase Microextraction and High-Throughput Determination of Complex Samples.* Analytical Chemistry, 2012. **84**(16): p. 6933-6938.

241. Volante, M., et al., *A Spme-Gc-Ms Approach for Antivarroa and Pesticide Residues Analysis in Honey.* Chromatographia, 2001. **54**(3-4): p. 241-246.

242. Natangelo, M., S. Tavazzi, and E. Benfenati, *Evaluation of Solid Phase Microextraction-Gas Chromatography in the Analysis of Some Pesticides with Different Mass Spectrometric Techniques: Application to Environmental Waters and Food Samples.* Analytical Letters, 2002. **35**(2): p. 327-338.

243. Stenerson, K.K., et al., *Application of Spme Using an Overcoated Pdms-Dvb Fiber to the Extraction of Pesticides from Spaghetti Sauce: Method Evaluation and Comparison to Quechers.* Lc Gc North America, 2016. **34**(7): p. 500-509.

244. Silva, É.A.S., V. Lopez-Avila, and J. Pawliszyn, *Fast and Robust Direct Immersion Solid Phase Microextraction Coupled with Gas Chromatography–Time-of-Flight Mass Spectrometry Method Employing a Matrix Compatible Fiber for Determination of Triazole Fungicides in Fruits.* Journal of Chromatography A, 2013. **1313**: p. 139-146.

245. Souza-Silva, É.A., E. Gionfriddo, and J. Pawliszyn, *A Critical Review of the State of the Art of Solid-Phase Microextraction of Complex Matrices Ii. Food Analysis.* TrAC Trends in Analytical Chemistry, 2015. **71**: p. 236-248.

246. Souza-Silva, É.A., et al., *Methodical Evaluation and Improvement of Matrix Compatible Pdms-Overcoated Coating for Direct Immersion Solid Phase Microextraction Gas Chromatography (Di-Spme-Gc)-Based Applications.* Analytica Chimica Acta, 2016. **920**: p. 54-62.

247. Searles, S. and V.P. Gregory, *The Reaction of Trimethylene Oxide with Amines*. Journal of the American Chemical Society, 1954. **76**(10): p. 2789-2790.

248. Blicke, F.F. and J.H. Biel, *Aminolysis Products of 1-Chloro-2-Hydroxy-3-Butene, 1-Hydroxy-2-Chloro-3-Butene and 1,2-Epoxy-3-Butene.* Journal of the American Chemical Society, 1957. **79**(20): p. 5508-5512.

249. Magidson, O.J. and I.T. Strukow, *Die Derivate Des 8-Aminochinolins Als Antimalariapräparate. Mitteilung Ii: Der Einfluß Der Länge Der Kette in Stellung 8*. Archiv der Pharmazie, 1933. **271**(9): p. 569-580.

250. Doyle, F.P. and E.R. Stove, *Improvements in or Relating to Sulphonium Compounds*. 1955, Beecham Res Lab: GB 800963A.

251. Barbry, D. and B. Hasiak, *Study of Interactions between Alcohol and Amine Functions - Thermal Evolution of Hydroxides and of D'omega-Trialkylammonium 1-Alkanol Salts*. Collection of Czechoslovak Chemical Communications, 1983. **48**(6): p. 1734-1744.

252. Oppenländer, K., *Verfahren Zur Herstellung Von N,N'-Diarylaminoalkanolen*. 1966: DE15433335B1.

253. Hinsberg, O. and J. Kessler, *Ueber Die Trennung Der Primären Und Secundären Aminbasen.* Berichte der deutschen chemischen Gesellschaft, 1905. **38**(1): p. 906-911.

254. Hinsberg, O., *Ueber Die Bildung Von Säureestern Und Säureamiden Bei Gegenwart Von Wasser Und Alkali.* Berichte der deutschen chemischen Gesellschaft, 1890. **23**(2): p. 2962-2965.

255. Adams, R. and J.B. Segur, *Beta-Arylamino Ethanols.* Journal of the American Chemical Society, 1923. **45**(3): p. 785-790.

256. Socrates, G., *Infrared and Raman Characteristic Group Frequencies: Tables and Charts*. 2004: Wiley.

257. Silverstein, R.M., et al., *Spectrometric Identification of Organic Compounds*. 2014: Wiley.

258. Cadogan, J.I.G., *Reactivity of Organophosphorus Compounds .11. High-Temperature Decomposition of S-2-Diethylaminoethyl Diethyl Phosphorothioate (Amiton).* Journal of the Chemical Society, 1962(JAN): p. 18-&.

259. *Houben-Weyl Methods of Organic Chemistry Vol. Ii, 3rd Edition: Oxidation, Reduction, Special Topics*. 2014: Thieme.

260. Quin, L.D. and A.J. Williams, *Practical Interpretation of P-31 Nmr Spectra and Computer-Assisted Structure Verification*. 2004: Advanced Chemistry Development.

261. Breitmaier, E., *Vom Nmr-Spektrum Zur Strukturformel Organischer Verbindungen*. 2012: Wiley.

262. Research, M., *Mestrenovao Manual 9.0.1*. 2014.

263. Williamson, M.P. and C.E. Griffin, *Three- and Four-Bond Phosphorus-31-Proton Coupling Constants and Geminal Proton Nonequivalence in Ethyl Esters of Phosphorus Acids.* The Journal of Physical Chemistry, 1968. **72**(12): p. 4043-4047.

264. Karplus, M. and D.H. Anderson, *Valence-Bond Interpretation of Electron-Coupled Nuclear Spin Interactions; Application to Methane.* The Journal of Chemical Physics, 1959. **30**(1): p. 6-10.

265. Friebolin, H., *Ein- Und Zweidimensionale Nmr-Spektroskopie: Eine Einführung*. 2013: Wiley VCH Verlag GmbH.

266. Mizrahi, D.M. and I. Columbus, *31p Mas Nmr: A Useful Tool for the Evaluation of Vx Natural Weathering in Various Urban Matrixes.* Environ Sci Technol, 2005. **39**(22): p. 8931-8935.

267. Mayer, B.P., et al., *31p-Edited Diffusion-Ordered 1h Nmr Spectroscopy for the Spectral Isolation and Identification of Organophosphorus Compounds Related to Chemical Weapons Agents and Their Degradation Products.* Analytical Chemistry, 2012. **84**(23): p. 10478-10484.

268. Koskela, H., *Use of Nmr Techniques for Toxic Organophosphorus Compound Profiling.* J. Chromatogr. B: Anal. Technol. Biomed. Life Sci., 2010. **878**(17-18): p. 1365-1381.

269. Eyring, H., *The Activated Complex in Chemical Reactions.* The Journal of Chemical Physics, 1935. **3**(2): p. 107-115.

270. Moore, W.J. and D.O. Hummel, *Physikalische Chemie*. 1986: de Gruyter.

271. Barrow, G.M. and G.W.B. von Herzog, *Physikalische Chemie: Gesamtausgabe*. 1984: Vieweg+Teubner Verlag.

272. Markowska, A., T. Nowicki, and W. Reimschussel, *Kinetics of Pishchimuka Reaction.* Chemische Berichte-Recueil, 1975. **108**(7): p. 2465-2468.

273. Calderbank, A. and R. Ghosh, *131. The Preparation and Isomerization of Some Basic Esters of Oo[Prime or Minute]-Diethyl Hydrogen Phosphorothioate.* Journal of the Chemical Society (Resumed), 1960(0): p. 637-642.

274. Akahori, Y. and S. Fukushima, *Studies on Isotopic Acyl Exchange. I. Kinetics and Mechanism of Acyl Exchange Reaction of P-Nitrophenyl Acetate.* CHEMICAL & PHARMACEUTICAL BULLETIN, 1964. **12**(2): p. 166-175.

275. Brandenburg, K., *Diamond*. 2014, Crystal Impact GbR: Bonn, Germany.

276. Gunasekaran, S. and B. Anita, *Spectral Investigation and Normal Coordinate Analysis of Piperazine.* Indian Journal of Pure & Applied Physics, 2008. **46**(12): p. 833-8388.

277. Tilley, R.J.D., *Understanding Solids: The Science of Materials*. 2005: Wiley.

278. Clarke, E.C.W. and D.N. Glew, *Evaluation of Thermodynamic Functions from Equilibrium Constants.* Transactions of the Faraday Society, 1966. **62**(0): p. 539-547.

279. Hurst, J.E. and B. Keith Harrison, *Estimation of Liquid and Solid Heat Capacities Using a Modified Kopp's Rule.* Chemical Engineering Communications, 1992. **112**(1): p. 21-30.

280. Acree, W. and J.S. Chickos, *Phase Transition Enthalpy Measurementsof Organic and Organometallic Compounds. Sublimation, Vaporizationand Fusion Enthalpies from 1880 to 2010.* Journal of Physical and Chemical Reference Data, 2010. **39**(4): p. 043101.

281. Baldit, G.L., *Amiton—a New Acaricide and Scalicide.* Journal of the Science of Food and Agriculture, 1958. **9**(8): p. 516-524.

282. Zhuang, X.-M., et al., *Contribution of Carboxylesterase and Cytochrome P450 to the Bioactivation and Detoxification of Isocarbophos and Its Enantiomers in Human Liver Microsomes.* Toxicological Sciences, 2014. **140**(1): p. 40-48.

283. Dravnicks, A., R. Brabets, and T.A. Stanley, *Evaluating Sensitivity Requirements of Explosive Vapor Detector Systems*. 1972, IIT Research Institute Technology Center: Chicago Illinois.

284. Bird, R.B., W.E. Stewart, and E.N. Lightfoot, *Transport Phenomena*. 2002, New Jork: John Wiley & Sons, Inc.

285. Vogel, A.I. and D.M. Cowan, *8. Physical Properties and Chemical Constitution. Part Vii. Alkyl Sulphides, Disulphides, Sulphites, Sulphates, and Orthophosphates.* Journal of the Chemical Society (Resumed), 1943(0): p. 16-24.

286. Malinovskii, M.S., Z.F. Solomko, and L.M. Yurilina, *Reaction of Dialkylaminoethanols with Esters of Phosphoric and Thiophosphoric Acids.* Zh. Obshch. Khim., 1960. **30**: p. 3454-3456.

287. Althoff, M.A., et al., *Application of Headspace and Direct Immersion Solid-Phase Microextraction in the Analysis of Organothiophosphates Related to the Chemical Weapons Convention from Water and Complex Matrices.* Talanta, 2017. **174**: p. 295-300.

288. Kromidas, S. and H.J. Kuss, *Chromatogramme Richtig Integrieren Und Bewerten: Ein Praxishandbuch Für Die Hplc Und Gc*. 2012: Wiley.

289. *Trinkwasseranalyse Der Stadt Sonthofen*, Stadtwerke_Sonthofen, Editor. 2015: Sonthofen.

290. Klappa, P., *Kinetics for Bioscientist*. 2009: Bookboon.

291. Rogers, D.F. and J.A. Adams, *Mathematical Elements for Computer Graphics*. 1990: McGraw-Hill.

292. Yung-Chi, C. and W.H. Prusoff, *Relationship between the Inhibition Constant (Ki) and the Concentration of Inhibitor Which Causes 50 Per Cent Inhibition (I50) of an Enzymatic Reaction.* Biochemical Pharmacology, 1973. **22**(23): p. 3099-3108.

293. Lazareno, S. and N.J. Birdsall, *Estimation of Competitive Antagonist Affinity from Functional Inhibition Curves Using the Gaddum, Schild and Cheng-Prusoff Equations.* British Journal of Pharmacology, 1993. **109**(4): p. 1110-1119.

294. Varo, P., *Pesticide Chemistry–3: Third International Congress of Pesticide Chemistry Including the Symposium on Dispersion Dynamics of Pollutants in the Environment*. 2013: Elsevier Science.

295. Main, A.R., *Kinetic Evidence of Multiple Reversible Cholinesterases Based on Inhibition by Organophosphates.* The Journal of Biological Chemistry, 1969. **244**: p. 829-840.

296. Otoguro, K., F. Kuno, and S. Omura, *Arisugacins, Selective Acetylcholinesterase Inhibitors of Microbial Origin.* Pharmacol Ther, 1997. **76**(1-3): p. 45-54.

297. Kapková, P., *Biologische Untersuchungen Zu Inhibitoren Der Acetylcholinesterase Und Erzeugung Von Neuen Leitstrukturen Mittels „Random Chemistry“*. 2004, University of Würzburg: Würzburg.

298. Reddy, T.J., et al., *Mass Spectral Studies of N,N-Dialkylaminoethanols.* Rapid Communications in Mass Spectrometry, 2003. **17**(7): p. 746-752.

299. McLafferty, F.W., F. Turecek, and B. Schenk, *Interpretation Von Massenspektren*. 2013: Springer Berlin Heidelberg.

300. Lias, S.G., *Ionization Energy Evauation*, in *Nist Chemistry Webbook, Nist Standard Reference Database Number 69*, P.J. Linstrom and W.G. Mallard, Editors.: Gaithersburg MD, 20899.

301. Fraas, *Calculation Algorithm of the Bruker Xims Nt 3.0 Software*. 2016, Bruker Daltonik GmbH: unpublished.

302. Eiceman, G.A., et al., *Fragmentation of Butyl Acetate Isomers in the Drift Region of an Ion Mobility Spectrometer.* International Journal of Mass Spectrometry and Ion Processes, 1988. **85**(3): p. 265-275.

303. Gunzer, F., *Mercury-Induced Fragmentation of N-Decane and N-Undecane in Positive Mode Ion Mobility Spectrometry.* Analyst, 2015. **140**(18): p. 6379-6385.

304. Karasek, F.W., D.W. Denney, and E.H. DeDecker, *Plasma Chromatography of Normal Alkanes and Its Relation to Chemical Ionization Mass Spectrometry.* Analytical Chemistry, 1974. **46**(8): p. 970-973.

305. *Crysalis Ccd*. 2005, Oxford Diffraction Ltd.

306. *Crysalis Red*. 2005, Oxford Diffraction Ltd.

307. *Scale3 Abspack - an Oxford Diffraction Programm*. 2005, Oxford Diffraction Ltd.

308. Sheldrick, G.M., *Shelxs-97: Program for Crystal Structure Solution*. 1997, University of Göttingen: Göttingen, Germany.

309. Sheldrick, G.M., *Shelxl-97: Program for the Refinement of Crystal Structures*. 1997, University of Göttingen: Göttingen, Germany.

310. Sheldrick, G.M., *Crystal Structure Refinement with Shelxl.* Acta Crystallographica: Section C, Structural Chemistry, 2015. **71**(1): p. 3-8.

311. Altomare, A., et al., *Completion and Refinement of Crystal Structures with Sir92.* Journal of Applied Crystallography, 1993. **26**(3): p. 343-350.

312. Altomare, A., et al., *Sir97: A New Tool for Crystal Structure Determination and Refinement.* Journal of Applied Crystallography, 1999. **32**(1): p. 115-119.

313. Farrugia, L., *Wingx and Ortep for Windows: An Update.* Journal of Applied Crystallography, 2012. **45**(4): p. 849-854.

314. Macrae, C.F., et al., *Mercury Csd 2.0– New Features for the Visualization and Investigation of Crystal Structures.* Journal of Applied Crystallography, 2008. **41**(2): p. 466-470.

315. de Zeeuw, J., et al., *Simplifying the Setup for Vacuum-Outlet Gc: Using a Restriction inside the Injection Port.* Journal of Separation Science, 2009. **32**(11): p. 1849-1857.

316. Boeker, P., T. Haas, and P. Schulze Lammers, *Theory and Practice of a Variable Dome Splitter for Gas Chromatography-Olfactometry.* Journal of Chromatography A, 2013. **1286**: p. 200-207.

317. Althoff, M.A., et al., *Application of the Transpiration Method to Determine the Vapor Pressure and Related Physico-Chemical Data of Low Volatile, Thermolabile, and Toxic Organo(Thio)Phosphates.* The Journal of Physical Chemistry A, 2017. **121**(13): p. 2603-2609.

318. *Din 32645:2008-11; Chemische Analytik - Nachweis-, Erfassungs- Und Bestimmungsgrenze Unter Wiederholbedingungen - Begriffe, Verfahren, Auswertung*, ed. D.I.f. Normung. Vol. 2008-11. 2008, Germany: Deutsches Institut für Normung.

D List of Publications

- ***New Aspects of the Detection and Analysis of Organo(thio)phosphates related to the Chemical Weapons Convention.***
  Althoff, M.A., Bertsch, A., Metzulat, M., Kalthoff, O., Karaghiosoff, K.L., Phosphorus, Sulfur, Silicon and the Related Elements, 2017, Vol. 192, No. 2, 149-156, http://dx.doi.org/10.1080/10426507.2016.1259237

- ***Vapor Pressure Measurements of Amiton (VG) and Related Derivatives by the Transpiration Method Approach***
  Althoff, M.A., Grieger, K. Härtel, M.A.C., Karaghiosoff, K.L. Klapötke, T.M. Metzulat, M., J Chrom. A, 2017, 121(13), 2603-2609.
  http://pubs.acs.org/doi/abs/10.1021/acs.jpca.7b01177

- ***Application of Headspace and Direct Immersion Solid-Phase Microextraction (SPME) in the Analysis of Organothiophosphates related to the Chemical Weapons Convention (CWC) from Water and Complex Matrices.***
  Althoff, M.A., Bertsch, A., Metzulat, M., Klapötke, T.M. and Karaghiosoff, K.L
  Talanta 174 (2017) 295-300,
  https://doi.org/10.1016/j.talanta.2017.05.024

- ***SPME Application and Method Development Options with the TriPlus RSH***
  Althoff, M.A., Bolliger, R., Preiswerk, T., Böhm, G.
  Ingenious News, Issue 4, December 2017
  www.palsystem.com

- ***O,O-Diethyl O-[2-(dimethylamino)ethyl] phosphorothioate: "Hard" Evidence of the decomposition product and its oxalte salt***
  Althoff M.A., Martens J., Reichel M., Metzulat M., Klapötke T.M., Karaghiosoff K.L.
  Status: in submission process of Zeitschrift für Kristallographie

- ***Acetylcholinesterase (AChE) and Butyrylcholinesterase (BuChE) inhibition comparative study of Amiton and several structural isomers closely related to the Chemical Weapons Convention (CWC)***
  Althoff M.A., Metzulat, M., Klapötke, T.M. and Karaghiosoff, K.L
  Status: in preparation for J. Forensic Toxicology

E Presentations at Conferences and Meetings

- 13th European Workshop on Phosphorus Chemistry, Berlin, Germany, March 7th – March 9th, 2016, *oral presentation: "*Synthesis and Characterization of Organo(thio)phosphates related to the Chemical Weapons Convention"

- 3rd Interdisciplinary PhD-Candidate Seminar of the German Working Group for Analytical Spectroscopy, Ulm, Germany, April 6th – April 8th 2016, *oral presentation*: "Analytics and Detection of Amiton and Related Compounds"

- 12th International Symposium on Protection against Chemical and Biological Warfare Agents, Stockholm, Sweden, June 8th – June 10th 2016, *oral presentation:* "Analytical Challenges in the on-site Detection and Characterization of Chemicals in Asymmetric Scenarios".

- 18th International Symposium on Advances in Extraction Technologies & 22nd International Symposium on Separation Sciences, Torun, Poland, July 3rd – July 6th, 2016, *poster presentation*: "Application of HS- and DI-SPME in the Analysis of Organo(thio)phosphates related to the Chemical Weapons Convention."

- Advanced training for platoon leaders of hazard defense management units at the federal state of Rhineland-Palatinate fire brigade training facility in Andernach, Germany, July 9th, 2016, *invited speaker:* "Chemische Kampf- und Gefahrstoffe – Arten, Einsatz, Schutz und Nachweis".

- 27th International Symposium on Organic Chemistry of Sulphur, Jena, Germany, July 24th – July 29th, 2016, *oral presentation:* "New Aspects of the Detection and Analysis of Organothiophosphates related to the Chemical Weapons Convention".

- Thermo Fisher Scientific Chromatography Tour, Munich Germany, March 14th 2017, *invited speaker:* "Solid-phase Microextraction (SPME) with the TriPlusRSH autosampler".

- 1st Hexal Symposium: Fachübergreifende modern Analytik – Innovative Nutzung analytischer Verfahren, July 28th 2017, *invited speaker*: "SPME-Methodenentwicklung für die Extraktion von Kampfstoffen aus komplexer Matrix".

F Guest Visits at other Institutes

Period	Institute
24.02. – 28.02.14	Central Institute of the Bundeswehr Medical Corps, Munich, Training Course on Chemical Warfare Agents Analytics I
04.04. – 18.04.14	Georgia Institute of Technology, School of Chemistry and Biochemistry, Atlanta, USA, inhibition kinetic studies, group of Prof. Dr. Lyon
19.05. – 23.05.14	Central Institute of the Bundeswehr Medical Corps, Munster, Training Course on Chemical Warfare Agents Analytics II
27.06. – 11.07.14	Georgia Institute of Technology, School of Chemistry and Biochemistry, Atlanta, USA, inhibition kinetic studies, group of Prof. Dr. Lyon
02.02. – 06.02.15	LMU, department of pharmaceutics, inhibition kinetic studies, group of Prof. Dr. Wanner
30.04. – 08.05.15	University of Waterloo, Waterloo, Canada, Training Course on solid-phase micro extraction, group of Prof. Dr. Pawliszyn
07.11. – 11.11.16	University Clinic Ulm, department of pharmaceutics and toxicology, inhibition kinetic studies, group of Prof. Dr. Barth

G Acknowledgement

First of all, I would like to thank all officials of the German Bundeswehr who made effort in promoting the necessity of conducting this thesis and granted permission to start this (ad)venture beside of my regular job. Particularly, the two most important players herby were Colonel Neumann, Commander of the CBRN Defence Command of the Bundeswehr and Dr. Metzulat, who, as Head of the Chemistry Section of the CBRN Defence and Environmental Protection School, also had relevant influence on the direction of the thesis. Furthermore, Dr. Metzulat was my first reference partner with an outstanding range of expertise in the field of Analytical Chemistry and Chemical Warfare Agents. Thank you for your faith, advice and the almost unrestricted freedom in performing this thesis.

Coinstantaneous, I would like to thank Prof. Karaghiosoff for his great enthusiasm in this difficile topic, his well-accepted ideas on experiments and his never ending interest in the progress of this work. Conny, thank you very much for being more than just a supervisor to me! Thank you for the advice and the challenging topic of this thesis.

Furthermore, I have to thank my co-workers at the chemistry lab in Sonthofen for supporting me in my efforts. May it have been by taking over lectures, to run errands or by simply remembering me to join sports and other social activities in the evenings. Especially, I would like to thank Miss Fink for always preparing clean glass ware and handling thousands of other small and big jobs in daily business. Additionally, I have to acknowledge the support of SFC Bertsch, particularly in the last steps of this work. Andi, with your excellent support in, e.g. operating the HPLC-MS instrument and running countless measurements on the GC's, important projects could be successfully finalized You are also a great sparring partner at our Taekwondo training and have become a true friend to me.

However, I also have to thank all members of the groups of Prof. Klapötke and Prof. Karaghiosoff at LMU. I was always welcome with open arms at any time with any request I had. That was a great experience to me. To be highlighted are Marco, Jörn and Martin who always made big efforts to support me. Finally, our close collaboration paid off and resulted in two joint publications. Jörn especially helped in solving the single crystal structures.

Last but not least I have to apologize to my wife and family who shared the burden of writing a thesis on top of the regular job and showed great respect. They always supported this project unconditionally. I really appreciate it! Nicole, thank you for your love and your excellent advice not only in chemistry issues, I could not have done it without you! Sorry for the little time I could spare in family activities or weekend trips.

Finally, I did it! Thank you all!